Qiang Liao
Jo-shu Chang
Christiane Herrmann
Ao Xia *Editors*

Bioreactors for Microbial Biomass and Energy Conversion

Springer

Green Energy and Technology

Climate change, environmental impact and the limited natural resources urge scientific research and novel technical solutions. The monograph series Green Energy and Technology serves as a publishing platform for scientific and technological approaches to "green"—i.e. environmentally friendly and sustainable—technologies. While a focus lies on energy and power supply, it also covers "green" solutions in industrial engineering and engineering design. Green Energy and Technology addresses researchers, advanced students, technical consultants as well as decision makers in industries and politics. Hence, the level of presentation spans from instructional to highly technical.

More information about this series at http://www.springer.com/series/8059

Qiang Liao · Jo-shu Chang
Christiane Herrmann · Ao Xia
Editors

Bioreactors for Microbial Biomass and Energy Conversion

🐎 Springer

Editors
Qiang Liao
College of Power Engineering
Chongqing University
Chongqing
China

Jo-shu Chang
Department of Chemical Engineering
National Cheng Kung University
Tainan
Taiwan

Christiane Herrmann
Leibniz Institute for Agricultural
    Engineering Potsdam-Bornim e.V.
Potsdam
Germany

Ao Xia
College of Power Engineering
Chongqing University
Chongqing
China

Preface

Bioenergy derived from biomass may play a significant role in future energy systems due to its renewability and sustainability. The wide distribution of biomass provides rich sources of raw materials, while the significant development in bioenergy conversion technology has improved its competitiveness. Bioenergy, which is used to produce biofuel, heat, and electricity, may be generated via various routes such as thermo-chemical, biological, and bio-electrochemical processes. Bioenergy systems should be optimized to ensure their sustainability, maximize their efficiency, and minimize costs.

The bioreactor is a critical unit in the microbial conversion process, since it provides a suitable, stable place for microbial growth and metabolism by controlling the operating conditions. The performance of bioreactors is greatly influenced by many other factors, such as the bioreactor's structure and size, mixing and transfer characteristics, and means of feed introduction and product removal. There are complex multiphase flow patterns that exist in bioreactors that can vary the heat and mass transfer characteristics in the bioreactors and affect the microbial conversion processes. This book discusses the fundamentals of biomass energy systems, as well as the recent trends and developments in the microbial conversion process, with a particular focus on bioreactors. It combines the most current understanding of microbial conversion with the multiphase flow and mass transfer and provides an alternative perspective for the understanding of the microbial biomass and energy production process, as well as enhancement strategies.

This book contains 4 parts and 11 chapters, with contributions from leading scientists in the bioenergy field. Part I presents an overview of bioenergy and bioreactors, with a focus on the current state of the art. Chapter 1 provides an introduction to the basics and developments in biomass and bioenergy technologies. A large variety of bioenergy conversion pathways, such as thermo-chemical, biological, and bio-electrochemical, are introduced and compared. Biomass pre-treatment and biofuel upgrading technologies are also outlined. Chapter 2 reviews the function and role of bioreactors in the applications of bioenergy conversion technologies, including microbial biomass production, microbial

biofuels conversion, and microbial electrochemical conversion systems. It comprehensively discusses the mass and heat transfer in bioreactors.

Part II covers bioreactors for the biomass production of phototrophic and heterotrophic microalgae. Chapter 3 deals with the phototrophic cultivation of microalgae in open and closed photo-bioreactors. It provides a comprehensive discussion on the photo-bioreactors and their enhancement strategies from the aspects of light and mass transfer. This chapter includes the potential approaches for autotrophic microalgal cell concentrating and conversion to biofuels. Chapter 4 discusses the heterotrophic metabolism of microalgae in detail, the factors affecting heterotrophic cultivation, and commercial value-added products. It presents some future perspectives for heterotrophic cultivation as a potential solution for obtaining large-scale microalgal biomass.

Part III deals with bioreactors for gaseous and liquid biofuel conversion processes. Chapter 5 presents an overview of the fundamentals of biogas production and bioreactor configurations for the production of biogas. It investigates different enhancement strategies related to bioreactor design for the conversion of organic biomass to methane during the anaerobic digestion with various solid contents. Chapter 6 presents the basic concepts of hydrogen production by dark fermentation. The main operational parameters, such as the inoculum source and pre-treatment, organic substrate used, reactor operation and type, temperature, pH, and hydraulic retention time, are comprehensively reviewed. The integration of the dark fermentation bioprocesses into the concept of an environmental biorefinery is outlined. Chapter 7 provides an overview of photo-fermentative hydrogen production by purple non-sulfur bacteria. It reviews the key enzyme system involved in the fermentation, factors affecting the fermentation, and hydrogen production from industrial wastes, wastewater, and agricultural biomass. Both the suspension and immobilized cultures for various types of photo-bioreactors are discussed in detail. The fluid flow and mass transfer in bioreactors using the lattice Boltzmann simulation are presented. Chapter 8 presents the key principles of bioreactor design for the production of alcohols by the fermentation of sugar and syngas. It analyzes the hydrodynamics inside the units, bubble columns or stirred tank reactors, gas–liquid mass transfer rates, implications in the heat transfer for jacketed reactors, and kinetic mechanisms for microbial reactions. Chapter 9 reviews the sources of microbial lipids, factors that affect microbial lipid production, and the technologies and bioreactors used for microbial lipid conversion into biofuels. Alternative and innovative techniques for biofuel production and the life cycle impact of biofuel production from microbial lipids are discussed in detail.

Part IV defines the role of bioreactors in microbial electrochemical systems. Chapter 10 focuses on microbial fuel cells for electricity production in light of the fundamental principles, electrode materials and construction methods, architectures, cell stack, and feasibility in practical power generation. The applications of such a technology are also discussed. Chapter 11 reviews the recent developments in microbial electrolysis cells and microbial electrosynthesis cells for gaseous biofuel production. It includes the recent developments in the electrode materials,

configurations, electron transfer manners, microbial ecosystems, and applications in bio-electrochemical systems.

We would like to thank all the contributors to this book. We also wish to express our appreciation to the editorial team from Springer for their support and assistance. We hope this book will be helpful for students, researchers, engineers, policy makers, and economists in the fields of renewable energy, engineering, and biotechnology.

Chongqing, China   Qiang Liao
Tainan, Taiwan   Jo-shu Chang
Potsdam, Germany   Christiane Herrmann
Chongqing, China   Ao Xia
December 2017

Contents

Editors and Contributors

About the Editors

Qiang Liao is a Professor in College of Power Engineering at Chongqing University. He is also the Dean of College of Power Engineering, Director of Key Laboratory of Low-grade Energy Utilization Technologies and Systems of Ministry of Education, and Director of Institute of Engineering Thermophysics at Chongqing University. His research focuses on bioenergy, bioreactors, and heat and mass transfer. He has more than 350 peer-reviewed journal papers and has a number of conference presentations. According to Scopus, his work has been cited nearly 3000 times in peer-reviewed press. He serves as the Guest Editor for *International Journal of Hydrogen Energy* and *International Journal of Green Energy* and is on the editorial board of 12 journals such as *Energy*, *Fuel* and *Applied Thermal Engineering*. He has served as temporal Representative of China in International Energy Agency (IEA) Hydrogen Implementing Agreement (HIA) Task 34. He has co-authored "*Development Strategy Report for Engineering Thermophysics and Energy Utilization* (2006–2010 and 2011–2020)." He has chaired the 2012 Asian Biohydrogen and Bioproducts Symposium and served on the organizing committee of 16 international conferences. He has been awarded as Distinguished Professor of Chang Jiang Scholars from the Ministry of Education and Distinguished Young Scholar from the National Natural Science Foundation of China.

Jo-shu Chang is Deputy Director of Research Center for Energy Technology and Strategy and University Chair Professor of Department of Chemical Engineering at National Cheng Kung University, Taiwan. He received his Ph.D. degree from University of California, Irvine (USA), in 1993. His research interests cover biochemical engineering, environmental biotechnology, and applied microbiology with a recent focus on microalgae-based CO_2 reutilization, biofuels production, and biorefineries. He plays an important role in Taiwan's biomass energy R&D and policy making. Since July 2006, he has served as Member of National Bioethanol Standard Committee for Bureau of National Standard, Ministry of Economical Affairs, Taiwan. He is the leading PI of National Energy Project working on flue

gas CO_2 fixation by microalgae with the subsequent biofuels and bio-based chemical production. He is Fellow of American Institute of Medical and Biological Engineering (AIMBE) and has received numerous prestigious domestic and international academic awards. He has published nearly 350 SCI-indexed journal papers (including 12 ISI Hi-Ci papers) with a total citation of over 10,000 times and an h-index (Web of Science) of 53. He also authored 7 books and owns more than 40 patents. He is now the editor, associate editor, guest editor, and editorial board member of 12 SCI-indexed journals. He also serves as executive committee member of Asia Federation of Biotechnology (AFOB).

Christiane Herrmann is a Research Scientist in the Department of Bioengineering at the Leibniz Institute for Agricultural Engineering Potsdam-Bornim (ATB). She received her Ph.D. degree from the Humboldt University of Berlin (Germany) in 2010 and was awarded for the best doctoral graduation at the ATB (2009–2011). From 2014 to 2015, she worked as a Senior PostDoctoral researcher in the Environmental Research Institute (ERI) at University College Cork (UCC) in Ireland. Her research focuses on anaerobic digestion, bioprocess engineering, bioenergy production, biomass supply and algae. She has published 25 peer-reviewed journal articles and has delivered more than 20 conference presentations. She is Associate Editor of the journal *Renewable Energy and Environmental Sustainability* and serves as reviewer for more than 20 peer-reviewed journals. Since 2012, she acts as a Member of the guideline committee "VDI 4630—Fermentation of organic materials" of the Association of German Engineers.

Ao Xia is an Assistant Professor in College of Power Engineering at Chongqing University. He completed his Ph.D. research in 2013 in Energy Engineering from Zhejiang University. He was awarded the Chu Kochen Scholarship for the highest honors at Zhejiang University. He worked as a PostDoctoral Researcher in the Environmental Research Institute at University College Cork during 2014–2016. His research interests include algae, biofuels, biogas, fermentation, and anaerobic digestion. He has over 60 papers published in peer-reviewed journals such as *Trends in Biotechnology*, *Applied Energy*, *Bioresource Technology*, *Energy*, and *Biotechnology Advances*. He has authored a chapter in the Springer Major Reference Works "*Encyclopedia of Sustainability Science and Technology*" and co-authored an IEA publication "*A perspective on algal biogas.*" As per Google Scholar, his current h-index of publications is 20. He is the Guest Editor and Editorial Board Member of *Frontiers in Bioengineering and Biotechnology* and *Frontiers in Energy Research*. He also serves as a referee on 20 peer-reviewed journals, such as *Applied Energy*, *Energy*, *Bioresource Technology*, *Algal Research*, and *Energy & Fuels*, and has received the Top Reviewer Award from *Bioresource Technology* (2015).

Contributors

Nicolas Bernet LBE, INRA, Univ Montpellier, Narbonne, France

Gabriel Capson-Tojo LBE, INRA, Univ Montpellier, Narbonne, France; CIRSEE, Suez, Le Pecq, France

Haixing Chang School of Chemistry and Chemical Engineering, Chongqing University of Technology, Chongqing, China

Jo-shu Chang Department of Chemical Engineering, National Cheng Kung University, Tainan, Taiwan; Research Center for Energy Technology and Strategy, National Cheng Kung University, Tainan, Taiwan

Rong Chen Key Laboratory of Low-Grade Energy Utilization Technologies and Systems, Chongqing University, Ministry of Education, Chongqing, China; Institute of Engineering Thermophysics, Chongqing University, Chongqing, China

Lucile Chatellard LBE, INRA, Univ Montpellier, Narbonne, France

Kit Wayne Chew Faculty of Engineering, Department of Chemical and Environmental Engineering, University of Nottingham Malaysia Campus, Semenyih, Selangor Darul Ehsan, Malaysia

Shir Reen Chia Faculty of Engineering, Department of Mechanical Engineering, University of Malaya, Kuala Lumpur, Malaysia

Yudong Ding Key Laboratory of Low-Grade Energy Utilization Technologies and Systems, Chongqing University, Ministry of Education, Chongqing, China; Institute of Engineering Thermophysics, Chongqing University, Chongqing, China

Qian Fu Key Laboratory of Low-grade Energy Utilization Technologies and Systems, Chongqing University, Ministry of Education, Chongqing, China; Institute of Engineering Thermophysics, Chongqing University, Chongqing, China

Christiane Herrmann Department of Bioengineering, Leibniz Institute for Agricultural Engineering and Bioeconomy (ATB), Potsdam, Germany

Yun Huang Key Laboratory of Low-Grade Energy Utilization Technologies and Systems, Chongqing University, Ministry of Education, Chongqing, China; Institute of Engineering Thermophysics, Chongqing University, Chongqing, China

Antônio Djalma Nunes Ferraz Júnior LBE, INRA, Univ Montpellier, Narbonne, France; Brazilian Bioethanol Science and Technology Laboratory (CTBE), Brazilian Center for Research in Energy and Materials (CNPEM), Campinas, São Paulo, Brazil

Hajime Kobayashi Department of Systems Innovation, Graduate School of Engineering, The University of Tokyo, Tokyo, Japan

Gopalakrishnan Kumar Green Processing, Bioremediation and Alternative Energies Research Group, Faculty of Environment and Labour Safety, Ton Duc Thang University, Ho Chi Minh City, Viet Nam

Duu-Jong Lee Department of Chemical Engineering, National Taiwan University, Taipei, Taiwan

Jun Li Key Laboratory of Low-Grade Energy Utilization Technologies and Systems, Chongqing University, Chongqing, China; Institute of Engineering Thermophysics, Chongqing University, Chongqing, China

Zhuo Li Key Laboratory of Low-grade Energy Utilization Technologies and Systems, Chongqing University, Ministry of Education, Chongqing, China; Institute of Engineering Thermophysics, Chongqing University, Chongqing, China

Qiang Liao Key Laboratory of Low-Grade Energy Utilization Technologies and Systems, Chongqing University, Chongqing, China; Institute of Engineering Thermophysics, Chongqing University, Chongqing, China

Tau Chuan Ling Institute of Biological Sciences, University of Malaya, Kuala Lumpur, Malaysia

Antonella Marone LBE, INRA, Univ Montpellier, Narbonne, France

Gregory J. O. Martin Department of Chemical Engineering, Melbourne School of Engineering, The University of Melbourne, Melbourne, VIC, Australia

Mariano Martín Departamento de Ingeniería Química y textil, University of Salamanca, Salamanca, Spain

Jerry D. Murphy MaREI Centre, Environmental Research Institute, School of Engineering, University College Cork, Cork, Ireland

Dillirani Nagarajan Department of Chemical Engineering, National Cheng Kung University, Tainan, Taiwan; Department of Chemical Engineering, National Taiwan University, Taipei, Taiwan

Shiqi Ou Oak Ridge National Laboratory, Knoxville, TN, USA

Florian Paillet CIRSEE, Suez, Le Pecq, France; TRIFYL, Labessiere-Candeil, France

Patrice Ramm Department of Bioengineering, Leibniz Institute for Agricultural Engineering and Bioeconomy (ATB), Potsdam, Germany

Alissara Reungsang Faculty of Technology, Department of Biotechnology, Khon Kaen University, Khon Kaen, Thailand; Research Group for Development of Microbial Hydrogen Production Process from Biomass, Khon Kaen University, A. Muang, Khon Kaen, Thailand

Pau Loke Show Faculty of Engineering, Department of Chemical and Environmental Engineering, University of Nottingham Malaysia Campus, Semenyih, Selangor Darul Ehsan, Malaysia

Sureewan Sittijunda Faculty of Environment and Resource Studies, Mahidol University, Nakhon Pathom, Thailand

Chihe Sun Key Laboratory of Low-grade Energy Utilization Technologies and Systems, Chongqing University, Ministry of Education, Chongqing, China; Institute of Engineering Thermophysics, Chongqing University, Chongqing, China

Yahui Sun Key Laboratory of Low-Grade Energy Utilization Technologies and Systems, Chongqing University, Ministry of Education, Chongqing, China; Institute of Engineering Thermophysics, Chongqing University, Chongqing, China

Antonio Sánchez Departamento de Ingeniería Química y textil, University of Salamanca, Salamanca, Spain

Javiera Toledo-Alarcón LBE, INRA, Univ Montpellier, Narbonne, France

Eric Trably LBE, INRA, Univ Montpellier, Narbonne, France

Hong Wang Key Laboratory of Low-Grade Energy Utilization Technologies and Systems, Chongqing University, Ministry of Education, Chongqing, China; Institute of Engineering Thermophysics, Chongqing University, Chongqing, China

John M. Woodley Department of Chemical and Biochemical Engineering, Technical University of Denmark, Copenhagen, Denmark

Ao Xia Key Laboratory of Low-grade Energy Utilization Technologies and Systems, Chongqing University, Ministry of Education, Chongqing, China; Institute of Engineering Thermophysics, Chongqing University, Chongqing, China

Shuai Xiao Key Laboratory of Low-grade Energy Utilization Technologies and Systems, Chongqing University, Ministry of Education, Chongqing, China; Institute of Engineering Thermophysics, Chongqing University, Chongqing, China

Wei Yang Key Laboratory of Low-Grade Energy Utilization Technologies and Systems, Chongqing University, Chongqing, China; Institute of Engineering Thermophysics, Chongqing University, Chongqing, China

Yanxia Yang Thermal Engineering Department, School of Electrical and Power Engineering, Taiyuan University of Technology, Taiyuan, Shanxi, China

Dingding Ye Key Laboratory of Low-Grade Energy Utilization Technologies and Systems, Chongqing University, Chongqing, China; Institute of Engineering Thermophysics, Chongqing University, Chongqing, China

Biao Zhang Key Laboratory of Low-Grade Energy Utilization Technologies and Systems, Chongqing University, Chongqing, China; Institute of Engineering Thermophysics, Chongqing University, Chongqing, China

Liang Zhang Key Laboratory of Low-Grade Energy Utilization Technologies and Systems, Chongqing University, Ministry of Education, Chongqing, China; Institute of Engineering Thermophysics, Chongqing University, Chongqing, China

Nianbing Zhong Chongqing Key Laboratory of Fiber Optic Sensor and Photodetector, Chongqing Key Laboratory of Modern Photoelectric Detection Technology and Instrument, Chongqing University of Technology, Chongqing, China

Xun Zhu Key Laboratory of Low-Grade Energy Utilization Technologies and Systems, Chongqing University, Chongqing, China; Institute of Engineering Thermophysics, Chongqing University, Chongqing, China

Part I
Introduction

Chapter 1
Biomass and Bioenergy: Current State

Chihe Sun, Ao Xia, Qiang Liao, Gopalakrishnan Kumar and Jerry D. Murphy

1 Energy and Environment

1.1 Energy Demand

Energy sources are ubiquitous. Potential for energy is found within fossil fuels, in the light of sun, in forests, in water, wind, and even in geologic activity. Our modern society depends on these forms of energy in many aspects, including chemical and medical production, food processing, illumination, and heating [1].

Increase of global energy demand is associated with world economy development and population growth [2]. The average growth in population is 3.4% per year with more than 2 billion people in poverty [3]. Global energy demand is forecasted to continuously grow over the next two decades with economy and population. However growth rate of energy demand is slower than in the past, expected to be 1.3% per annum in the time frame 2015–2035 as opposed to 2.2% per annum in the

C. Sun · A. Xia (✉) · Q. Liao
Key Laboratory of Low-grade Energy Utilization Technologies and Systems,
Chongqing University, Ministry of Education, Chongqing 400030, China
e-mail: aoxia@cqu.edu.cn

C. Sun · A. Xia · Q. Liao
Institute of Engineering Thermophysics, Chongqing University,
Chongqing 400030, China

G. Kumar
Green Processing, Bioremediation and Alternative Energies Research Group, Faculty of Environment and Labour Safety, Ton Duc Thang University, Ho Chi Minh City, Viet Nam
e-mail: gopalakrishnankumar@tdt.edu.vn

J. D. Murphy
MaREI Centre, Environmental Research Institute, University College Cork, Cork, Ireland

J. D. Murphy
School of Engineering, University College Cork, Cork, Ireland

years 1995–2015. This phenomenon is mainly attributed to the changes of economy form and energy structure. The major increase of energy demand is driven by fast-growing emerging economies, particularly in China and India (accounting for more than half of the increase) [3]. In contrast, the energy demand is relatively stagnant in developed areas, such as America and Europe.

In 2014, fossil fuels, which include for oil, coal, and natural gas, still played a significant role in the global energy supply (Fig. 1) [4]. Among these fossil fuels, the consumption of oil is largest (31.3%), followed by coal (28.6%) and natural gas (21.2%).

Coal and natural gas, are still the dominant energy source for power generation (62.4%). Additionally, the world primary energy consumption in 2015 increased to 552.2 EJ, which is equivalent to 13,147 Mtoe, leading to a 20.2% increase compared with 2005 [5]. This has led to often extreme environment pollution in particular in China and India, especially in air quality. It is absolutely necessary to convert energy systems to alternative energy sources, which are sustainable and clean. There is a huge interest and growing production in renewable energy [6, 7]. For example, the world power generation from renewable energy is forecasted to increase to 25% in 2040, while the coal-fired share would decrease to 36% [8]. Renewable energy has an average annual growth rate of 2.5% [8].

China consumed 3,069 Mtoe of energy and generated 5,716 TWh of power in 2014, 22.4% of the global energy consumption and 24.0% of the global power generation, respectively [4]. The increases in energy supply and power generation were 1.6% and 4.3%, respectively, compared to 2013 [9]. However, energy demand is projected to grow by less than 2% per year in the next few years as compared with 6% over the past 20 years [10]. This is driven by the transformation of society from an energy-intensive industry infrastructure to a more low-energy consumption society [10]. Government policies also drive further improvements in energy conversion efficiency. Fossil fuel combustion and pollution are also problematic elsewhere. Power generation in the Organisation for Economic Co-operation and Development (OECD) is nearly twice that of China [4]. It is essential that all countries play a role in devising a more prosperous and sustainable planet.

1.2   Environmental Sustainability

Excessive greenhouse gas (GHG) emissions derived from the utilization of fossil fuels increase the earth's temperature, leads to the water acidification, and climate change [11, 12]. To reduce GHG emissions, over 40 countries have established carbon taxes [13]. In 2014, global CO_2 emissions were 32,381 Mt which only increased about 0.6% compared to that in 2013 (32,190 Mt) [4, 9]. The growth rate of carbon emissions is considered to be slowing as compared to past decades; however, it still falls below the target of total carbon emissions set at COP21 in Paris. Global CO_2 emissions from energy in 2014 are mainly attributed to the use of coal, followed by oil and natural gas (see Fig. 1c). As coal accounted for more than
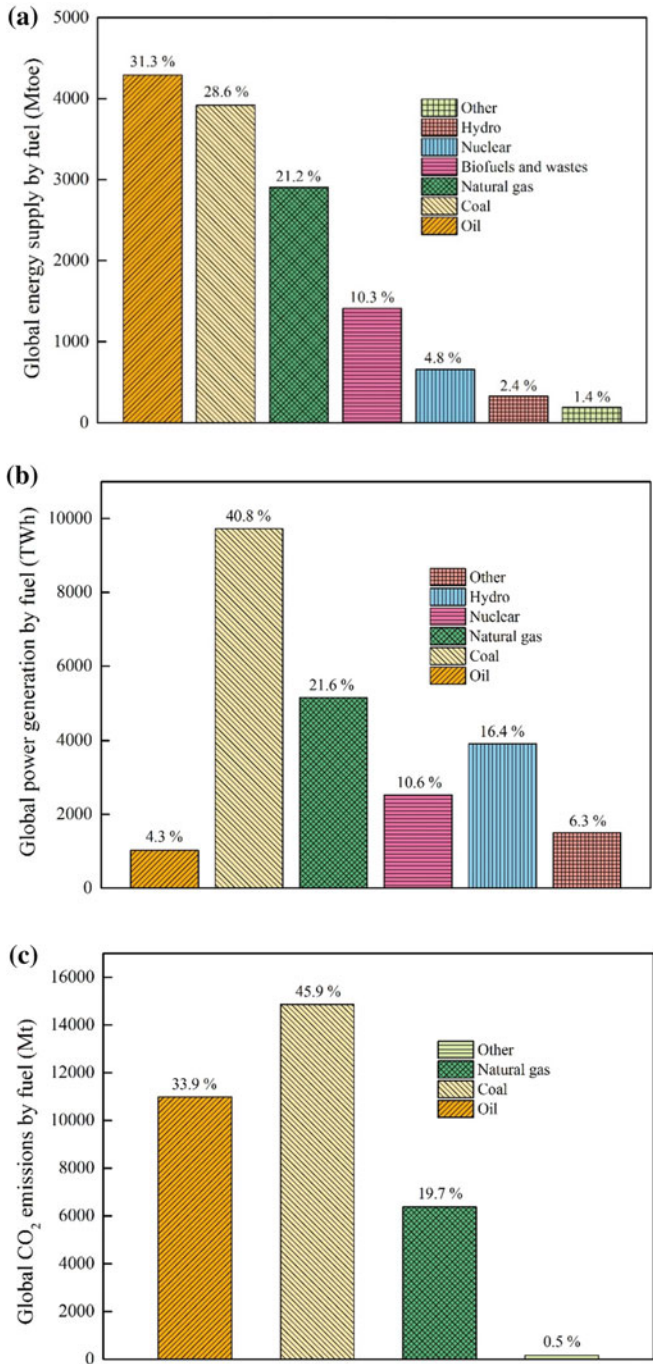
Fig. 1 Global energy supply (**a**) power generation (**b**) and CO_2 emissions (**c**) by fuel in 2014. (Data collected from [4])

40% of total power generation, the abatement of CO_2 emissions depends on decarbonizing the power sector. To limit global temperature rise to 2 °C on the pre-industrial times, global CO_2 emissions in 2035 should be decreased by 32% compared to that in 2015 [14].

In 2014, China produced 28.2% of global CO_2 emissions (9,131 Mt) [4]. China's 13th Five-Year Plan for national economic and social development stated that the government should pay more attention to changing the structure of energy supply, introducing feasible policies, and moving to cleaner and lower carbon fuels [15]. Due to the development of renewable and nuclear energy, total CO_2 emissions in China are on a deceleration pathway. The increase of total CO_2 emissions was only 1.3% from 2013 to 2014, which is equivalent to 117.8 Mt [4, 9]. It is forecasted that the coal consumption in China will reach a steady-state, while more renewable power will be produced during the next 20 years. This should facilitate significant deceleration of growth in total CO_2 emissions in China [10].

Probably a bigger driver in China is tackling air quality and the concerns for public health [16]. The production and consumption of oil and gas contributes to serious air pollution. Burning large amounts of fossil fuels for power generation emits excessive air pollutants, such as nitrous oxides (NO_x), sulphur oxides (SO_x), and particulate matter (PM) [5].

Exploration, production and refining of fossil fuels such as natural gas and oil consume about 1% of global freshwater sources. Water requirement may be much higher in some developing economies due to the relatively underdeveloped technology and poor government regulation [17]. Additionally, in countries with water shortages, such as Egypt, Saudi Arabia, Kuwait, Jordan, and Yemen, the limitation in supply of potable water has significant impact on quality of life and industrial output.

1.3 Renewable Energy

Many countries have committed to the development of renewable energy. Renewable energy is produced from natural resources that can be sustainably reused in the foreseeable future; it can be classified into various types, such as geothermal energy, wind energy, hydro-energy, tidal energy, ocean energy, solar energy, and bioenergy [18].

In 2016 China produced the largest amounts of wind electricity of any country, followed by the United States, Germany, India, and Brazil [19]. China is also the largest hydroelectricity-generating country. Electricity produced through photovoltaic (PV) technology has developed rapidly in the past decades [20]. In 2035, the total production of electricity obtained through solar PV is expected to reach 740 TWh, which is over 35 times higher than in 2011 [21].

Table 1 Biofuel production in major countries around the world during 2012 to 2016. (Data collected from [23])

Countries	2012	2013	2014	2015	2016
United States	29.8	31.1	32.9	33.8	35.8
Brazil	14.7	17.1	18.0	19.3	18.6
Germany	3.0	2.8	3.5	3.2	3.2
Argentina	2.3	2.0	2.6	2.0	2.8
Indonesia	1.4	1.8	2.5	1.4	2.5
France	2.1	2.3	2.5	2.5	2.2
China	2.1	2.3	2.6	2.7	2.1
Total world	66.9	72.3	79.7	80.0	82.3

The unit of biofuel production is million tonnes oil equivalent (Mtoe)

Bioenergy is a broader energy vector with a numerous sources and many applications. It is not possible to compare bioenergy across the entire production and use system to a wind turbine. Bioenergy can be readily adapted to provide heat, electricity for industrial and residential application and a source for the production of transport fuels [18, 22]. In 2015 petroleum provided the major energy source in the transport sector (more than 90%), whereas biofuels shared only around 4% of global transport fuel.

As shown in Table 1, global biofuel production was 82.3 Mtoe in 2016, nearly two times more than 2006 [23]. The United States (35.8 Mtoe) and Brazil (18.6 Mtoe) are two major biofuel-producing countries, accounted for more than 60% of global production. Over the past ten years, Belgium had the fastest average growth rate (89.9%), followed by Netherlands (87.5%), Portugal (79.7%), and Argentina (71.7%).

Different regions have large differences in the annual yield and growth rate of biofuels. For example, the annual productivity of biofuels in China in 2015 showed negative growth (of −22.8%); this was the first contraction since 2005 [23] and can be attributed to the changes of strategic direction on energy and economic development, as well as the fundamental realities of China. In 2016, due to falling bio-ethanol production in Brazil, the global bio-ethanol production only increased by 0.7%. Bio-oil production rose by 6.5% with Indonesia providing more than half of the increment. As a result, Indonesia had the largest increase in biofuel production in 2016 (about 84.3%), whereas Brazil has a decline (about −4.3%) [23].

According to the International Energy Agency (IEA) [24], bioenergy accounts for approximately 11% of the total world primary energy supply. However, almost two-thirds of bioenergy has been used in rural areas of developing countries for cooking and heating. In 2015 around 6% of the global heat supply was from bioenergy, which is equivalent to 13 EJ. Heat energy obtained from biomass is widely used in the pulp and paper industry as well as in city heating schemes. Additionally, around 2% of the global power generation was also from bioenergy, equivalent to 474 TWh.

1.4   Source, Resource and Benefits of Bioenergy

Energy is stored in biomass in the form of chemical energy, which is converted from solar energy by photosynthesis. Solar energy enters the atmosphere as light and is radiated by the earth's surface as heat. Only a small portion of this solar energy, is available to humans. Most of the solar energy is stored in the atmosphere (such as wind) and other substances (such as water) in the earth. Since solar energy can be effectively absorbed and stored through the photosynthesis of biomass, it becomes the ultimate source of bioenergy [25].

Biomass, as the sole renewable carbon source, is widely distributed in most regions of the earth; it can be continuously converted to bioenergy with little influence on climate change [26, 27]. A recent IEA publication states there is 63 EJ of bioenergy in current use with a sustainable resource estimated between 100–300 EJ per annum [28]. In many developing areas, the use of bioenergy can effectively boost the industrialization of countries through stimulation of economic development by creating employment opportunities [29]. For example, the United Nations Environment Program (UNEP) states that the bioenergy industry may offer about 12 million jobs by 2030, which is equivalent to more than 50% of total jobs obtained from the renewable energy industry. The Chinese government has provided many preferential policies for companies to develop the bioenergy industry such as tax incentives and electricity subsidies over the past two decades [30]. Correspondingly, these companies offered employment. Using bioenergy can also obviously reduce the national dependence on imported energy resources and mitigate the issue of energy security. Bioenergy has advantages for political strategy, economic development, and social construction [31].

2   Generation of Biomass Feedstock

2.1   First Generation Feedstock

The first generation feedstock is starch-based and oilseed-based biomass feedstock (Table 2). Since starch-based biomass contains a high content of carbohydrates (excess of 60% of the total dry weight), they are ready for fermentation conversion and are considered as the major resources for bio-ethanol and bio-methane production during the last decade [32]. If 1 kg of starch or sucrose can produce about 0.5 kg of bio-ethanol at an overall conversion efficiency of 90%, the yields of bio-ethanol produced from corn, cassava, and sweet potato are about 1.7, 2.3, and 1.2 t/ha, respectively. The energy yields of these crops are 374, 522, and 258 gasoline gallon equivalent (GGE) per hectare [33]. Due to the variation of the annual yield of starch-based biomass and the relations between food supply and demand in different regions, the source of biomass feedstock may be significantly different. For instances, the annual yield of cassava is much higher in Nigeria,

Table 2 Comparison of different generation biofuels for bioenergy conversion (adapted and reprinted from [11], Copyright 2016, with permission from Elsevier)

	First generation	Second generation	Third generation
Compositions	• Starch-based biomass such as corn, wheat, barley, rice, millet, sorghum, potato, cassava, and sweet potato • Oilseed-based biomass such as soybean, safflower, peanut, rapeseed, sesame, jartropha, and oil palm	• Lignocellulose-based biomass such as crop residues, woody crops, and forest biomass • Perennial rye grass • Waste streams such as food waste, waste sludge, household garbage, and animal dung	• Macroalgae such as *Saccharima latissima, Himanthalia elongate, Gracilaria verrucosa,* and *Codium tomentosum* • Microalgae such as *Chlorella* sp., *Scenedesmus* sp., *Nannochloris* sp., and *Dunaliella* sp.
Advantages	• Mature conversion techniques • Low cost	• No food crop competition • Reuse and recycling of waste • Environment benefit of waste treatment • Non-arable land for energy crop cultivation	• No food crop competition • High growth rate and yield • Non-arable land for energy crop cultivation • Independent of fresh water • Environment benefit of waste water and flue gas treatment • Various bioenergy products
Disadvantages	• High arable land requirement • High fertilizer consumption • High fresh water input • High economic cost • Food fuel debate	• High energy consumption in pre-treatment and conversion • Requirement of advanced technology for cost-effective conversion	• High economic cost in cultivation • High energy consumption in harvesting • Easily contaminated

Thailand, and Indonesia. As a result, cassava is usually used for bio-ethanol production in these countries. However, corn is the dominant biomass feedstock for bio-ethanol in USA, which is the largest corn producer [33].

Additionally, the differences in growth conditions, such as light, temperature, and water, in different regions can significant change the bio-chemical compositions of starch-based biomass, thereby affecting bio-ethanol production. Ziska et al. found that sweet potato planted in Maryland exhibited a greater potential for bio-ethanol production than corn due to its high starch content [34].

The major sources of oilseed-based biomass feedstock are oil plants (see Table 2). Oil plants contain large amounts of lipids ranged from 20 to 50% [35], resulting in a high potential for bio-oil production [36, 37]. Similar to the

starch-based biomass, the species of oil plants used for bio-oil production also depends on the climate and economic conditions. In tropical regions, such as Malaysia and Indonesia, palm is the major oil plant, and these two countries produce more than 70% of the global palm oil. USA is the largest soybean producing country, followed by Brazil and Argentina. Oilseed rape is largely grown in the European Union (EU), Canada, and China [38].

Starch-based and oilseed-based biomass feedstock have been widely used for bioenergy production on a large-scale; however, there still exists a number of drawbacks [39]. Excessive production of bio-ethanol from starch-based feedstock such as rice, wheat, and corn can significantly increase food prices [40]. Expanding growth of oil plants reduces the available arable land areas, which may lead to food riots in some countries [11]. Also, food crops planted in large monocultures over large areas of land may increase deforestation, upsetting biological diversity and ecological balance. Furthermore, large quantities of freshwater would be consumed during crop cultivation causing water shortages in some water-deficient regions. The large use of chemicals in several processes, such as fertilizer production, can have adverse impacts on the environment. Fertilizer runoff can lead to eutrophication and soil hardening. The first generation feedstock has caused critical debates on food and energy.

The European Union (EU) legislation states that bioenergy obtained from crops should not exceed 6% of total energy consumption in transport by 2020 [11]. In China, the 13th Five-Year Plan for energy development requires that bio-ethanol and bio-oil produced from non-food crops should be at levels of production of 400 and 200 Mt, respectively by 2020 [41]. To avoid the food and energy competition caused by the first generation feedstock, bioenergy derived from other biomass sources should be carefully considered.

2.2 Second Generation Feedstock

The second generation feedstock mainly includes lignocellulose-based biomass, grasses and waste streams (see Table 2). Compared with the first generation feedstock, using second generation feedstock can effectively reduce the food fuel competition, while decreasing the energy input in ploughing, fertilizing, and harvesting processes.

Lignocellulose-based biomass is considered as the major feedstock for bioenergy production; it is one of the most abundant resources around the world, with an annual global energy potential ranged from 100 to 270 EJ [33]. In the US, more than 1.3 billion tons of lignocellulose-based biomass can be used [42]. Forest biomass, as the main resource of lignocellulose-based biomass, alone contributes more than 40% of total global biomass [43]. In China, the yield of primary forest biomass was around 72.2 million cubic meters in 2015 [44]. Thus, abundant biomass resources if sustainable managed can provide feedstock for bioenergy production. However, traditional conversion techniques of lignocellulosic biomass are

not energy efficient and have caused environmental problems. For example, in many rural areas of developing countries, forest biomass is usually used for heating and cooking, whereas waste crop residues such as rice and wheat straw are burned in the fields. This can cause serious air pollution. Advanced bioenergy technology is required to improve the energy efficiency whilst reducing the environmental risk.

Lignocellulose-based biomass is primarily composed of cellulose, hemicellulose, and lignin. Cellulose surrounded with lignin and hemicellulose leads to a compact and complex cell structure, which effectively protects biomass from the damage of extreme environment. Comprehensive pre-treatment is required to break down the lignocellulosic structure for efficient bioenergy conversion. Thus, bioenergy produced from the second generation feedstock may not be commercially available by 2020, either because of techniques or costs [35].

2.3 Third Generation Feedstock

Third generation feedstock is mainly sourced from aquatic algae (macroalgae and microalgae). As the oldest plant in the world, algae are commonly present in fresh water and seawater. Algae can use light (natural light or artificial light) and inorganics (water, inorganic salt and carbon dioxide) as an energy source for photosynthesis to produce organics.

Generally, the physiological and morphological characteristics of algae vary. Depending on the compositions and contents of the intracellular pigments, macroalgae can be classified as brown, red, and green macroalgae [45]. Additionally, macroalgae that grow in the intertidal zones (between high and low water of tides) or the sub-tidal zones (submerged most of the time) also need to be differentiated [46]. Due to the difficulty of harvesting of algae, the amounts and values of macroalgae from the sub-tidal zone are frequently underestimated.

Microalgae can also be divided into several major species according to the abundance of the intracellular pigments, such as red, green, golden, and blue microalgae. Unlike macroalgae, microalgae are microscopically small, and the average cell diameter generally ranges from 3 to 20 μm [47]. Although most microalgae are single-celled organisms, they can still form microbial colonies through bio-sorption [35]. The colonies with different shapes can be used to differentiate the species of microalgae. For instance, the colonies formed by *Mougeotia* sp. are filamentous, while the colonies formed by *Chlorella* sp. are simple spherical. Since the concentration of microalgae in the cultivation system is low and the density of microalgae is close to water, microalgae in the cultivation system are even more difficult to harvest compared to macroalgae [35]. The harvesting process is energy intensive and expensive, and is an unavoidable bottleneck for bioenergy production from microalgae.

Algae with different chemical compositions can be widely applied in distinct fields, such as feed/food and bioenergy production. In terms of bioenergy production, researchers usually apply different cultivation conditions, including

temperature, pH, illumination, CO_2 and nutrient supply, to directionally change the chemical composition of algae. For example, Illman et al. found that nutrient limiting condition in the steady-phase was effective for improving the algae's lipid content [48]. Besides, high light intensity may also promote the accumulation of lipids [7].

Due to the high photosynthesis efficiency and growth rate, the cultivation area requirements of algae are lower than other biomass feedstock. Most of all, algae cultivation combining with waste water and flue gas treatment can significant decrease the pollutant emissions [11]. Nevertheless, algae grown in the open raceway ponds (ORPs) may be easily contaminated by other microorganisms, resulting in a low biomass yield. The economic cost in building closed photo-bioreactors is also quite high [11]. Commercially viable bioenergy production from algae depends on the effective strategies. High-volume and low-cost bioenergy coupled with high-value by-products is the ambition of future development [11, 49]. Table 2 shows a comparison of different generation feedstock for bioenergy conversion.

3   Production Technology of Bioenergy

The production technology of the bioenergy system with different operational parameters and reaction mechanisms has a critical impact on the bioenergy yield, energy balance, environmental impact, and economic cost. Over the past decades, significant efforts have been devoted to develop various conversion technologies in lab-scale, pilot-scale, as well as large-scale. Figure 2 shows the relationships of various technologies based on final bioenergy products.

3.1   Thermo-Chemical Conversion Technology

Various types of bioenergy can be obtained through thermo-chemical conversion technologies, including heat and electricity produced via combustion of biomass, liquid biofuels produced via trasesterification, hydrothermal liquefaction (HTL) and pyrolysis, and gaseous biofuels produced via gasification. Table 3 compares the advantages and disadvantages of different thermo-chemical conversion technologies.

3.1.1   Combustion

Biomass combustion generally comprises four stages; drying, pyrolysis, volatile combustion, and char combustion [50–52]. At the drying and pyrolysis stages, biomass is firstly heated from ambient temperature to initial pyrolysis temperature
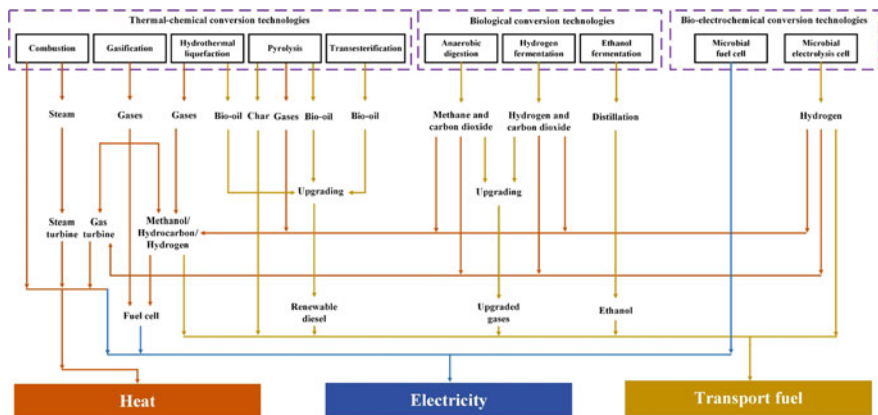
Fig. 2 Relationships of various production technologies based on final bioenergy products

Table 3 Comparison of different thermo-chemical conversion technologies

Methods	Advantages	Disadvantages
Combustion	• Low economic cost • Heat and power generation • Simple operation • Mature conversion technology	• High air pollutant emission • Low conversion efficiency
Gasification	• High thermal efficiency • Less secondary pollution • Synthesis gas production • Heat and power generation	• High energy consumption • Strong peculiar smell • Large amounts of tar
Pyrolysis	• Process hazardous substance • Less secondary pollution • Various bioenergy products	• Require biomass drying process • Low quality of bio-oil • High energy consumption
Hydrothermal liquefaction	• Process biomass with high water content • Less secondary pollution • Flexible biomass feeding model • Bio-oil production	• High energy consumption • Low quality of bio-oil
Transesterification	• Low economic cost • Low energy consumption • Simple operation • Less secondary pollution • Bio-oil production	• Depend on the catalytic activity • Require large amounts of organic solvents • High quality of bio-oil

(about 200–225 °C), and then devolatilized into condensable and non-condensable gases (about 200 to 400 °C). The decomposition mechanisms of different biomass composition may vary at the pyrolysis stage. For example, cellulose and hemi-cellulose can be decomposed through the damage of glycosidic bonds at a

temperature between 200 and 350 °C, whereas lignin can be degraded between 350 and 500 °C [50].

Biomass combustion has been inextricably linked to human civilizations. Although much of the recent focus has shifted to liquid and gaseous biofuel production, biomass combustion is still widely used for heat and power generation. In recent years, excess of 75% of the primary energy supply is derived from biomass combustion in many developing countries [33]. However, serious air pollution caused by the incomplete combustion urgently needs to be addressed [53, 54]. Developing high-performance biomass combustion furnace with pollutant control units is very important for highly efficient and environmentally friendly biomass combustion.

3.1.2 Gasification

Gasification is usually carried out under a high temperature (around 700–1400 °C) and an oxygen-limited environment [33, 55]. In such a process, the major products include synthesis gases such as hydrogen, methane, carbon dioxide and carbon monoxide. To facilitate biomass conversion, oxygen can be supplied in various forms, such as pure oxygen, air, steam, and mixtures of the foregoing. Gasification can handle biomass with high water content; however, the energy that is supplied to heat water is still higher than other conversion technologies, such as transesterification and HTL.

3.1.3 Transesterification

Transesterification is one of the most common technologies to produce bio-oil and glycerine from biomass, in which triglycerides are reacted with a short chain alcohols (such as methanol or ethanol) with the aid of alkaline or acidic catalyst [56, 57]. It is a relatively eco-friendly process compared to biomass combustion. Meanwhile, compared to HTL and pyrolysis, the physical characteristics of bio-oil products are closer to diesel fuel [55]. Prior to transesterification, the raw lipid contained in the biomass feedstock should be extracted through organic solvents (such as ethanol/n-hexane and chloroform/methanol). Hence, lipid extraction is a necessary step for bio-oil production [58]. Due to the compact cell structure of biomass, the process of lipid extraction usually requires large amounts of organic solvents and long reaction time. As transesterification cannot convert proteins or carbohydrates to lipids, the extraction performance is limited by the lipid content of biomass [59, 60].

The reaction rate of transesterification is closely linked to the catalytic activity. To avoid the adverse impacts on environment and the high economic costs in catalyst recovery, heterogeneous catalysts with high catalytic activity, reusability, and separability are promising alternative catalysts for homogenous acids or alkalis [61]. Besides, many studies focus on a one-step method, in which lipid extraction

and transesterification can be carried out in the same reactor [58, 62, 63]. It not only reduces the production units, but also lowers the economy costs and reaction time for bio-oil production.

3.1.4 Hydrothermal Liquefaction (HTL) and Pyrolysis

As HTL and pyrolysis can produce bio-oil not only from lipids but also from carbohydrates and proteins, they are also considered as effective technologies for bio-oil production [12]. However, the reaction conditions of these two thermo-chemical processes are harsher than transesterification, resulting in a high energy input. Meanwhile, the quality of bio-oil is also lower. Based on the lifecycle assessments (LCA) of bio-oil production from microalgae, the energy consumption of transesterification, HTL, and pyrolysis are 3.7, 6.6, and 4.1 MJ/kg dry microalgae, respectively.

HTL is an effective method for converting biomass that contains a high water content to bio-oil in sub-critical water at temperatures from 200 to 350 °C and pressures from 15 to 20 MPa [64, 65]. Differently, pyrolysis is more suitable for dried biomass (with less than 20% water content). Water must be removed before being heated to high temperatures (approximately 400–600 °C) under ambient pressure [66]. Thus, the energy consumption is usually quite high. This process would be more competitive if a waste heat source is available.

3.2 Biological Conversion Technology

Biological conversion technology, such as anaerobic digestion (AD), fermentation, bio-photolysis, usually operates under ambient temperature and pressure. It is considered as an energy-efficient and eco-friendly approach, especially when organic wastes are used as substrates. In this process, various soluble and gaseous metabolites, including alcohols, volatile fatty acids (VFAs), methane, carbon dioxide and hydrogen, can be produced through pure or complex microorganisms [67].

3.2.1 Anaerobic Digestion (AD)

AD, as a well-known approach for bio-methane production, is composed of four stages; hydrolysis, acidogenesis, acetogenesis, and methanogenesis [11, 68]. High-molecular-weight organic macromolecules can be degraded into low-molecular-weight monomers at the hydrolysis stage. These monomers are further converted to soluble (such as acetate, propionate, butyrate, and, ethanol) and gaseous products (such as hydrogen, and carbon dioxide) at the acidogenesis stage. Afterwards, the soluble products are converted to acetic acid. Notably, acetic acid

can be also produced from hydrogen and carbon dioxide through homoacetogenesis. At the final stage, methane can be produced not only from acetic acid but also from hydrogen and carbon dioxide. Due to the complex structure of biomass cells, the whole process of AD is limited by the hydrolysis stage [69]. Although biomass cells can be completely disrupted and intracellular metabolites can be successfully released by pre-treatment, it is still difficult to rapidly convert several types of organic macromolecules to monomers, such as cellulose and triglyceride. This unfavourable result would also limit bio-methane production.

AD can be carried out at the mesophilic (ranged from 20 to 45 °C) and thermophilic (ranged from 45 to 60 °C) conditions [70, 71]. Compared to the mesophilic condition, the thermophilic condition with higher degradation rate can significantly reduce the activity of harmful microorganisms [72–74]. However, without effectively surplus heat utilization, high temperature would increase the energy input of fermentation. Besides, many other factors, including hydraulic retention time (HRT), organic loading rate (OLR), and substrates, can also affect the fermentation performance. For example, substrates containing excessive inhibitors such as ammonia, sulphide, metals, and organics may make the fermentation process more instable, resulting in a low yield of bio-methane [75]. Short HRT may lead to a risk of washout of microbial communities [11, 74]. Meanwhile, high OLR would boost the acidogenesis stage of easily degradable substrates and the excessive accumulation of VFAs may further inhibit the activity of microorganisms [76, 77].

3.2.2 Hydrogen Fermentation and Bio-photolysis

Hydrogen is a potential alternative energy source due to its cleanliness and high energy density by mass [78]. It can be produced by various routes through using different types of microorganisms, including dark fermentation (DF) via hydrogen producing bacteria (HPB), photo fermentation (PF) via photosynthetic bacteria (PSB), direct bio-photolysis via green microalgae, and indirect bio-photolysis via cyanobacteria. DF can be considered as a sub-process derived from AD, in which the methanogenesis stage is hindered by the inactivation of methanogenic archaea [79].

In terms of PF, PSB can degrade low-molecular weight organics including sugars, alcohols, and VFAs to hydrogen and carbon dioxide under an anaerobic environment [80, 81]. Unlike DF and AD, this process is driven by light. Generally, the light penetration depth is inversely related to the concentration of PSB. With increasing growth of PSB, the distribution of light may be heterogeneous [82]. An efficient photo-bioreactor with high illumination surface area to volume ratio is usually required in PF. However, this design would increase the economic costs in equipment construction. The use of artificial light is expensive and increases energy consumption [83]; sunlight, as a cheap and abundant light source, may be a relatively good option. When using sunlight as the energy source, the uncontrolled temperature caused by the discontinuous sunlight should be avoided. Besides, PF is

also more sensitive to the accumulation of ammonium [84]. Effective methods of ammonium removal need to be applied for the large-scale industrial bio-hydrogen production.

For direct bio-photolysis, water can be converted into hydrogen and oxygen by green microalgae [85]. However, the gas mixture may be potentially explosive due to the inseparability of hydrogen and oxygen [86]. Meanwhile, the increasing oxygen content may limit the metabolic process of hydrogen generation, resulting in a low hydrogen yield. An indirect bio-photolysis using cyanobacteria can solve these problems to some extent; photosynthesis and fermentation are carried out in separate bioreactors [87, 88]. Notably, hydrogen produced via indirect bio-photolysis usually contains complex operational sub-processes, leading to high costs in time, energy, and economy.

3.2.3 Ethanol Fermentation

Bio-ethanol can be produced through microbial fermentation. The microbial community of ethanol production mainly includes two groups [89]. One group is used to degrade complicate substrates to simple compounds (such as sugars) through the catalysis of hydrolytic enzymes at the stage of saccharification (or hydrolysis). The other group is used to convert metabolic sugars to ethanol and carbon dioxide at the stage of fermentation.

Generally, saccharification and fermentation can be operated in the same or separate bioreactors [90, 91]. The use of enzymes and the culture conditions of microbes (such as pH and temperature) in different stages need to be differentiated [89]. Compared with separate hydrolysis and fermentation (SHF), the limitation of cellobiose and glucose can be significantly reduced in simultaneous saccharification and fermentation (SSF) [92]. However, a low cellulose hydrolysis rate in SSF still hinders its development. Lignocellulose-based biomass is commonly used as the fermentative substrate for ethanol production [93, 94]. It should be noted that only a few microorganisms can readily ferment xylose, which is the major component of hydrolyzates derived from cellulose and hemicellulose [95]. Thus, recombinant microorganisms should be developed and used in the xylose rich hydrolyzates.

In recent years, some advanced technologies have been widely used to improve the fermentation performance. For substrate improvements, algae has been considered as promising biomass for microbial fermentation due to the high growth rate and high content of easily degradable compounds [96–98]. For inoculum improvements, efficient and stable metabolic engineering has been applied, such as genetic engineering and high-throughput screening [99]. Genetic engineering can not only provide the overexpression of genes encoding for the rapid and sufficient use of substrate, but also can active the pathway regulating carbon flux towards desired products through blocking the formation of by-products [100–102]. For process improvements, immobilization cultures have been developed to reduce washout of microbial cells and eliminate inhibition caused by high substrate concentration [89].

3.3   Bio-electrochemical Conversion Technology

3.3.1   Microbial Fuel Cell (MFC)

MFC, as a typical bio-electrochemical conversion technology, can directly convert chemical energy that is stored in the organic matters of biomass to electrical energy through the catalytic effect of electrogenic bacteria [103–105]. Generally, a simple MFC includes an anode chamber and a cathode chamber, split by a separator (such as a proton exchange membrane). Electrogenic bacteria in the anode chamber oxidize organic matters to release electron and protons under an anaerobic condition. Afterwards, protons enter the cathode chamber through the separator. The electrons flow through the external circuit to the cathode chamber and combine with oxygen and protons to form water, resulting in electricity production [106]. The use of electrogenic bacteria makes MFCs more suitable compared with the conventional fuel cells that use precious metal catalysts. MFCs can also take advantages of using low-cost substrates (such as organic waste) and environmentally available electron acceptors (such as oxygen) [33, 107, 108].

Although MFCs have a certain potential to produce electricity, there still exists several technical challenges that need to be solved, such as the economic investments, electrochemically active bacteria and electrode materials [109–111]. In recent years, a series of advanced methods have been studied for improving the viability of MFC technologies. For bacteria improvements, high electrochemically active bacteria has been successfully achieved through artificial screening [112, 113]. For oxidizing agent improvements, air used in the cathode chamber has been considered as an alternative chemical agent due to high conversion efficiencies and desirable environmental impacts [114, 115]. For electrode material improvements, using carbonaceous materials (such as waste paper, algae, and bamboo) can decrease the economic cost whilst enhancing the biological compatibility [104, 116]. For bioreactor configuration improvements, single-chamber construction was used to reduce the ohmic resistance between the anode chamber and cathode chamber [117]. For process improvements, the concept of microbial electrochemical system has been extended to other applications, including the electrochemical treatment of contaminants and microbial electro-synthesis of valuable chemicals [109, 115].

3.3.2   Microbial Electrolysis Cell (MEC)

Generally, the reactions occurred in the anodes of MEC are similar to MFC, and the same materials used for anodes in MFC (such as carbon cloth, carbon paper, graphite felt, and graphite granules) can also be employed in MEC [117]. Nevertheless, MEC utilizes metals or microorganisms attached to the cathode as catalysts to convert chemical energy in biomass into hydrogen, or to electrosynthesize versatile carbon fuel (such as methane and alcohols) and valuable chemicals (such as formate,

acetate, and hydrogen peroxide) from CO_2 by using electricity [118, 119]. The process of bio-electrochemistry in such a system cannot occur spontaneously. A small power supply generally ranged from 0.2 to 0.8 V should be supplied between the two electrodes, thereby reducing the thermodynamic barrier [120]. Considering the extra energy consumption of the external power supply, renewable energy sources such as wind and solar can be applied in such a system [120].

3.4 Biomass Pre-treatment for Bioenergy Conversion

Pre-treatment of biomass prior to bioenergy conversion is shown to be an effective method for improving bioenergy production. The major pre-treatment methods are comprised of four different technologies, i.e., physical, mechanical, chemical, and biological technologies (see Table 4) [121]. Notably, an ideal pre-treatment should contain the following qualities. First of all, the cell wall structure of biomass should be effectively destroyed with high reaction rates, low energy requirements, and low toxic wastes. Secondly, when the hydrolysates are used for biological conversion, they should contain large amounts of degradable substrates (such as carbohydrate and protein) and little toxic by-products (such as furan and phenols). Thirdly, the process of pre-treatment should be easily operated for the large-scale bioenergy production with low economic investments.

3.4.1 Physical Pre-treatment

Physical pre-treatments mainly include microwave, thermal, hydrothermal, steam explosion, freeze drying, and osmotic shock. Microwave is commonly used to extract intracellular organic matters at lab scale. The frequency of microwave is around 2.5 GHz. When a polar or dielectric material is put in a rapidly oscillating electric field, heat would be generated by the frictional forces from the inter-molecular and intramolecular movements [122, 123]. With the increase of energy, the intracellular water would be heated to a boiling state. Afterwards, water vapour can disrupt biomass cells in situ. This physical energy can cause the rotation of molecular dipole through disrupting the weak hydrogen bonds [124]. However, it is still too weak to break the chemical bonds.

Thermal, hydrothermal, and steam explosion pre-treatment methods have been long used for disrupting the cell wall structure and decomposing the intracellular metabolites in large-scale industrial production [69, 121, 125]. Generally, thermal and hydrothermal pre-treatment are operated in a heating reactor without obvious pressure changes. However, steam explosion pre-treatment can be described as a process of sudden pressure drop [126, 127]. Biomass is firstly placed in a sealed vessel, and generated steam is kept at a high temperature (more than 160 °C) and pressure (no less than 6 bars) for about 10 to 30 min [128, 129]. Afterwards, steam is rapidly discharged, and biomass is cooled down in another vessel. The biomass

Table 4 Comparison of major pre-treatment methods (adapted from [121], Copyright 2014, with permission from Elsevier)

Pre-treatment	Advantages	Disadvantages
Thermal (below 100 °C)	• Low energy demand • Non-chemical contamination • Simple operation • Scalability	• Long reaction time • Low hydrolysis performance
Hydrothermal (above 100 °C)	• Non-chemical contamination • Simple operation • Scalability	• High energy demand • Risk of formation of inhibitors
Steam explosion (above 100 °C)	• Non-chemical contamination • Scalability	• High energy demand • Risk of formation of inhibitors • High investment cost
Microwave	• Non-chemical contamination • High hydrolysis performance • Short reaction time	• High energy demand • High investment cost
Sonication	• Non-chemical contamination • Simple operation • Scalability	• High energy demand • Low hydrolysis performance • High investment cost
Chemical	• Low energy demand • High hydrolysis performance • Short reaction time	• Chemical contamination • Risk of formation of inhibitors • High economic cost
Enzymatic	• Low energy demand • Non-chemical contamination • High hydrolysis performance	• Long reaction time • High sensitivity to reaction conditions • High economic cost

structure can be effectively destroyed due to this rapid change of pressure. The heating temperature of hydrothermal pre-treatment without or with steam explosion (from 110 to 270 °C) is higher than conventional thermal pre-treatment (from 50 to 100 °C) [121]. It is also dependent on the characteristics of biomass. Cellulose surrounded by hemicellulose and lignin cannot be easily destroyed, resulting in the requirement for a high pre-treatment temperature (above 180 °C) during pre-treatment. In terms of microalgae or other waste organic substrates (such as food waste and sewage sludge), temperatures above 180 °C may cause formation of toxic by-products and reduce the anaerobic biodegradability of biomass [130].

Freeze drying is a process of ice crystal sublimation. Biomass is firstly frozen at a temperature below −40 °C and then subjected to a low pressure around 1 kPa [123, 131]. Due to the growth of ice crystals, the cell wall of biomass can be punctured and become more porous. Additionally, biomass should be allowed to freeze slowly in order to form large intracellular ice crystals. A quick supply of heat

energy may cause localized melting and structural deformations [123]. Although freeze drying can effectively enhance the extraction performance, some disadvantages still hinder its fast development, including for high energy input and long reaction time.

Osmotic shock using salt solution or other neutral polymers (such as polyethylene glycol and dextran) is considered as a simple pre-treatment method for a wide range of biomass [132, 133]. This method can cause a sudden reduction in the concentration of water across the cell membrane. The rapid change of intracellular pressure can lead to the disruption of biomass cells. Nevertheless, it usually consumes large amounts of chemicals, resulting in adverse environmental impacts and high economic costs. It also requires a long reaction time to successfully disrupt cells. As for these reasons, freeze drying and osmotic shock have not yet been applied for biomass pre-treatment at a large scale.

3.4.2 Mechanical Pre-treatment

The major mechanical pre-treatments consist of bead milling, homogenization, and sonication. Among these methods, bead milling and homogenization have been proven to be more promising technologies for large-scale biomass disruption, especially in high biomass concentration applications (50–200 kg/m^3) [132]. However, the energy requirements of such methods are higher than sonication. A bead beater composed of either a vertical or a horizontal cylindrical compartment is commonly used for bead milling. In the compartment, biomass and glass or steel beads are mixed under a high speed spin condition [132, 134]. The disruption degree mostly depends on the contact area between biomass and beads, the size, shape and composition of the beads, and the strength of the biomass cell wall [135–137].

The reactor of homogenization includes one or two positive displacement pumps; this design can force biomass suspension through an orifice to collide against a valve seat under a pressure from 150 to 400 MPa [123, 138, 139]. The impingement of biomass on the surfaces of valve seats and impact rings can cause a sudden drop of pressure, leading to an increase of gas bubbles in biomass cells. With the decrease of flow velocities, these gas bubbles may collapse and a series of cavitation bubbles would emerge. Many studies propose that cavitation bubbles have a closely link to cell disruption [134, 140, 141].

The mechanism of cell disruption caused by sonication is similar to homogenization. For sonication, the micro-bubble cavitation can provide chemical and mechanical energy to disrupt the cell wall structure of biomass [142]. To obtain a good pre-treatment performance, high output power should be applied; whereas a low output power may only provide a small amount of cavitation, resulting in an undesirable damage of biomass cells.

3.4.3   Chemical Pre-treatment

Chemical pre-treatments mainly include acids, alkalis, organic solvents, ionic liquids, and supercritical fluids. Alkali and acid reagents are commonly applied in the pre-treatment of lignin rich biomass. Alkalis have significant effects on lignin removal, whereas acids are proven to be efficient in the solubilization of cellulose and hemicellulose [33, 143, 144]. Additionally, alkalis can decrease the crystallinity of lignocellulose-based biomass, leading to an increase of the porosity and internal surface area [69, 132]. A certain amount of alkali residues remaining in the biomass hydrolysates may be helpful to prevent the rapid reduction of pH during the acidogenesis process of AD [69]. Alkaline and acid pre-treatment can be conducted by diluted or concentrated solution. Diluted solution pre-treatment is usually combined with other pre-treatment methods, such as sonication and microwave [76, 145, 146]. With a good synergistic effect, this combined method can increase the degradation degree of biomass and obtain a high yield of biogas. Concentrated solutions are more effective than dilute solutions for cellulose and hemicellulose hydrolysis. However, the reliability of operation and the formation of by-products are the main factors limiting large scale application. Additionally, due to a heavy use of toxic and corrosive chemicals, post-treatment is required to reduce the environment impact.

Organic solvents are conventional reagents that are used to improve the performance of lipid extraction. Polar solvents such as ethanol or methanol have the ability to disrupt the vander Waals interactions in the cell membrane, which are formed by the hydrogen bonds and proteins [147]. Non-polar solvents (such as n-hexane) or weak-polar solvents (such as chloroform) can successfully penetrate into the cells and extract the crude lipids presented in the cytoplasm. As this method requires large amounts of solvents and long reaction time, cell wall disruption and lipid extraction are commonly conducted in the ionic liquids or supercritical fluids. Ionic liquids are composed of relatively large asymmetric organic cations and small inorganic or organic anions [148–150]. Similar to the effects of polar solvents, the hydrogen bonds on the cell wall can also be disrupted by the ions. A strong change of cell morphology can increase the extraction yield of crude lipids [151]. It should be noted that even today the economic cost of ionic liquid production is still very high.

Supercritical fluids generally have the properties of liquid and gas [132, 152]. In other words, they can effuse through solids like gases and dissolve materials like liquids [153]. Compared to other chemical pre-treatment methods, this method can effectively extract intracellular materials in a short time without using toxic organic solvents. As a result, using supercritical fluids is considered as a promising technology for biomass pre-treatment. High economic cost in equipment investment and maintenance is the major challenge for realizing its commercial utilization.

3.4.4 Biological Pre-treatment

Enzymes, as the biological catalysts, can catalyse a large number of reactions in biological systems, especially the biological degradation of organic compounds. For biological pre-treatment, the hydrolytic enzymes can effectively convert the macromolecular substrates (such as cellulose and hemicellulose) to low molecular compounds (such as oligosaccharide or monosaccharide) [33]. Most of all, biological pre-treatment does not produce large amounts of toxic inhibitors in the subsequent bioenergy production. Since the reaction conditions are mild, it is also considered as a promising method to replace high energy-consuming pre-treatments. Notably, the operability of this method depends largely on the activity and the specificity of hydrolytic enzymes. A slight change of the reaction conditions including temperature and pH may significantly reduce the pre-treatment performance. The high economic costs in enzyme extraction may also limit its development.

4 Biofuel Upgrading and Utilization

4.1 Biofuel Upgrading

Bio-oil and biogas are common biofuel products that can be widely used in the transport sector. Raw bio-oil is composed of several hundred organic compounds such as acids, alcohols, aldehydes, esters, ketones, and phenols [153–155]. Extreme amounts of unwanted organic compounds would result in negative impacts, such as low heating value and high viscosity [12, 156]. The metallic elements remaining in the aqueous phase may also affect the normal engine operation and reduce its lifetime. Additionally, high water and ash content may limit the utilization of bio-oil. Thus, a bio-oil upgrading process is required to remove the impurities and to improve the heating values before utilization.

Raw biogas mainly comprises of abundant methane (40–75%) and carbon dioxide (15–60%). Besides, trace amounts of other gaseous components such as water vapour, nitrogen, oxygen, hydrogen sulphide, ammonia and carbon monoxide still remain in raw biogas [11]. To make the use of biogas more effective and clean, carbon dioxide and trace components also should be removed.

4.1.1 Bio-oil Upgrading Technology

The bio-oil upgrading technologies mainly include hydrogenation, supercritical fluids, esterification, emulsification, and steam reforming [153]. Table 5 shows the advantages and disadvantages of different bio-oil upgrading technologies.

Table 5 Comparison of different bio-oil upgrading technologies (adapted and reprinted from [153], Copyright 2012, with permission from Elsevier)

Methods	Reaction conditions	Advantages	Disadvantages
Hydro-treating	Temperature: around 500 °C; Pressure: atmospheric pressure; Requires catalysts	• Mature conversion technology	• High amounts of char, coke, and tar • Reactor clogging • Catalyst deactivation
Hydro-cracking	Temperature: above 350 °C; Pressure: 0.7–13.8 Mpa; Requires catalysts	• Mature conversion technology • Large quantities of light products	• High energy consumption and economic cost • Reactor clogging • Catalyst deactivation
Supercritical liquids	Temperature: mild; Supercritical state; Requires organic solvents	• High bio-oil yield • High quality of bio-oil	• High economic cost for the use of organic solvent • High energy consumption
Esterification	Temperature: mild; Pressure: atmospheric pressure; Requires organic solvents	• Simple operation • Low energy consumption and economic cost • Mature conversion technology • High quality of bio-oil	• Adverse environmental impacts caused by homogeneous catalysts • Low reusability of heterogeneous catalysts • High economic cost for the use of organic solvent
Emulsification	Temperature: mild; Pressure: atmospheric pressure; Require surfactants	• Simple operation • Low energy input • Low corrosive	• High economic cost for surfactant production • Not a long-term method
Steam reforming	Temperature: 800–900 °C; Pressure: low; Require catalysts	• Produces synthesis gases, including hydrogen production;	• High energy consumption and economic cost • Complex reaction system

Hydrogenation consists of hydro-treating and hydro-cracking and is most commonly used in industrial refineries. With increase in hydrogen content, excessive oxygen in the raw bio-oils can be successfully removed and the quality of fuel products can be significantly improved. To realize hydrogenation reactions,

catalysts are usually required [157]. Comparing these two different hydrogenation processes, hydro-treating can be used to convert aromatics to naphthenes at around 500 °C under atmospheric pressure [153, 154, 158]. A constant high pressure ranged from 0.7 to 13.8 MPa is needed for hydro-cracking. Table 5 shows the advantages and limitations when hydrogenation is applied for bio-oil upgrading. Large amounts of by-products such as char, coke, and tar produced by hydro-treating would cause catalyst deactivation and reactor clogging. Meanwhile, high pressure and temperature used in hydro-cracking would also increase the energy consumption and investment cost [156, 157].

Steam reforming is considered as an effective method to upgrade raw pyrolysis bio-oils through increasing the octane numbers at the temperature from 800 to 900 °C [153]. Since various chemical reactions including cracking, dehydrogenation, and isomerisation would simultaneously occur at such a high temperature, a dependable and steady reaction process is necessary for steam reforming [153]. On the other hand, these uncertain reactions also increase the complexities of reactor design.

Supercritical fluids can promote the gasification and liquefaction reactions via dissolving liquid or gaseous insoluble materials [153, 159] Many organic solvents such as ethanol, methanol, butanol, and propanol have been adopted to improve the performance of bio-oil upgrading [159]. In such a process, the final bio-oil products usually exhibit a high heating value with a low viscosity. Whereas, the heavy use of organic solvents would also make it economically unfeasible on an industrial scale. Many advanced approaches have been employed to solve these problems in recent years. Bennion et al. reported a detailed process that used near-critical propane for bio-oil upgrading [12]. The bio-oil upgrading process includes four sub-processes, in which four extractors are operated at 23 °C under the pressure of 3.5, 3, 2, and 0.2 MPa, respectively. Besides extracting oil products for biofuel production, some of the chemical absorbents can be also used to extract derivative products, such as phenols, pyrroles and alkanes [160]. Esterification is defined as the reaction between organic acids and short chain alcohol (such as methanol or ethanol) in the presence of catalyst. This method can not only reduce the acidity and viscosity of raw bio-oil, but also improve its volatility and heating value [161, 162]. Adding emulsifier such as octanol to raw bio-oil can also improve its ignition property [153]. In addition, mixing bio-oil with other fuel sources such as diesel fuels is widely adopted due to the simpler operation and lower economy costs [163].

4.1.2 Biogas Upgrading Technology

The current technologies for biogas upgrading mainly include water scrubbing, physical absorption, chemical absorption, pressure swing adsorption, cryogenic separation, and membrane separation. Table 6 shows a comparison of several major biogas upgrading technologies. Considering the potential for inexpensive heat associated with power plants and electricity availability, different countries may choose different upgrading technologies [11]. The energy consumption and

Table 6 Comparison of biogas upgrading technologies (adapted and reprinted from [11], Copyright 2016, with permission from Elsevier)

Methods	Reaction parameters	Advantages	Disadvantages
Water scrubbing	Temperature: ambient; Pressure: 0.8–2.0 Mpa; Material: water	• High gas quality • Less CH_4 losses • No deep desulfurization • No heat energy supplement	• Complex operation • High investment cost • Scrubber clogging caused by microorganism growth • Require dry process • Require large amounts of water
Physical absorption	Temperature: mild; Pressure: 0.7–0.8 Mpa; Material: propylene carbonate, polyethylene glycol dimethyl ether, etc.	• High gas quality • Less CH_4 losses • No deep desulfurization	• Require large amounts of solvents • Solvent losses caused by volatilization • Chemical contamination
Chemical absorption	Temperature: around 160 °C; Pressure: around 0.1 Mpa; Material: monoethanolamine, diethanolamine, etc.	• High gas quality • Less CH_4 losses • Compact process	• High investment cost • High energy consumption • Require large amounts of solvents • Require deep desulfurization • Chemical contamination • Waste water disposal
Pressure swing adsorption	Temperature: ambient; Pressure: 0.6–0.8 Mpa; Material: activated carbon, carbon molecular sieve, etc.	• High gas quality • No process water demand • Partial removal of N_2 and O_2 • No waste water	• Complex operation • High investment cost • CH_4 content not stable • Require deep desulfurization • Require 3–4 parallel sheets
Cryogenic separation	Temperature: around −60 °C; Pressure: 1.8–2.5 Mpa	• High gas quality • Less CH_4 losses • No chemicals • No deep desulfurization • Low extra energy cost for liquid CH_4	• Complex operation • High investment cost • High energy consumption
Membrane separation	Temperature: ambient; Pressure: 0.6–0.8 Mpa; Material: polyimide membrane, polysulfone membrane, etc.	• Fast installation and start-up • Flexible production output • Low mechanical abrasion • Possible re-use of CO_2 • Compact process	• Complex operation • Low CH_4 recovery • High investment cost • Unstable long-term operation • Require deep desulfurization

economic cost are also closely related to the size of biogas plant; they significantly decrease through increasing the capacity of biogas plant [164].

For transport fuels, upgraded biogas should contain a high content of methane (more than 97%) and a low content of carbon dioxide (less than 3%) [165]. Carbon dioxide removal is the most important process for biogas upgrading. However, current biogas upgrading technologies are not considered complete carbon dioxide absorption; the released carbon dioxide can still lead to some GHG emissions and reduce the sustainability of the bio-methane. For this reason, exploring alternative biogas upgrading technology and associated carbon capture is necessary to optimize sustainability.

Methanation using hydrogen sourced from surplus electricity sourced from renewables such as wind, solar, and tide provides a good sustainable option for biogas upgrading and carbon capture. Water can be converted to hydrogen and oxygen via electrolysis; hydrogen and carbon dioxide can be used to produce methane and water through the catalytic or biological methanation [166, 167].

Furthermore, since carbon dioxide is commonly used as a carbon source in the microalgae cultivation, biogas can also be effectively upgraded through microalgae photosynthesis. When raw biogas is directly pumped into the microalgae suspension, the increased oxygen content may make the gas mixture potentially explosive [168]. Separating oxygen and methane would still consume large amounts of energy and is expensive. Many advanced technologies focused on consuming the produced oxygen [169] or separating the process of microalgae cultivation and carbon dioxide absorption [11].

4.2 Biofuel Utilization

Compared to the conventional fossil fuels, the use of biofuels have many benefits, including readily available sources and technologies, renewability, high combustion efficiency, low sulphuric and aromatic content, and biodegradability [170]. Co-combustion of biofuel and conventional diesel fuels in the same engine or boiler usually results in low flue gas emissions of carbon monoxide (CO), unburned HCs, sulphide, and PM; it can further reduce adverse environmental impacts such as air pollution, acid rain, and soil acidification [171]. For instances, when adding 20% soybean-based bio-oil to diesel fuels, the total emissions of PM, unburned HCs, and CO would decrease by 10.1%, 21.1%, and 11%, respectively [172]. When burning of ethanol-diesel blend fuel, the mass of PM can decrease by 11.7–26.9% [173]. Nevertheless, emissions of nitrogen oxide (NO_x) would increase via co-combusting of these blended fuels [172]. This is attributed to the high oxygen content of bio-oil and bio-ethanol. A series of reasonable modifications, such as lowering the reaction temperature, reducing the oxygen supply, and decreasing the burning time can overcome this unfavourable issue.

Due to the effective absorption of CO_2 by biomass photosynthesis, global warming can also be mitigated to some extent [12, 174–176]. The compatibility of

bioenergy vectors with existing industrial production can decrease the economic cost in technical improvement [177]. High value by-products (such as pitch, paraffin, and lubricating oil) can be produced during the biofuel production, thereby promoting the formation of bio-chemical production system.

Biogas can be regarded as a clean gaseous biofuel. The use of biogas as a vehicle fuel can significant decrease the exhaust emissions that are caused by diesel-powered vehicles; the total emissions may be even lower compared with those of using bio-oil or bio-ethanol [178]. Nevertheless, to date, most of the produced biogas is used for heat and/or power generation. The development of biogas as a transport biofuel is hampered by several factors, such as the complex oil engine modification, the limited biogas filling stations, and the high economy costs of dual-fuel vehicles [179]. Stimulating policies would be very beneficial for the use of biogas as a vehicle fuel. It must be stated that these problems can be overcome as exemplified by the widespread use of bio-methane as a transport fuel in Sweden.

5 Conclusion

Biomass, which is considered as the sole renewable carbon source, is widely distributed across the planet. Bioenergy derived from biomass will play an important role in the future as a clean energy supply, especially for the transport sector. There are a number of existing techniques to realize bioenergy production from various types of biomass. However, no single bioenergy conversion route is suitable for all biomass feedstock. It is very important to combine suitable biomass substrate with the cost-effective bioenergy conversion pathway to improve the energy efficiency and the economic feasibility. Advanced techniques for high efficient bioenergy conversion using non-food based biomass, such as lignocellulosic biomass and aquatic algae, needs to be developed urgently. Bioenergy in all its complexity and variety is constantly scrutinised for its sustainability. Evidence of sustainability must be shown through detailed analyses of energy flows, economic feasibility and environmental impacts in biomass cultivation, harvesting, and conversion.

References

1. Lior N (2010) Energy resources and use: the present situation and possible sustainable paths to the future. Energy 35(6):2631–26387
2. Destek MA, Aslan A (2017) Renewable and non-renewable energy consumption and economic growth in emerging economies: evidence from bootstrap panel causality. Renew Energy 111:757–763
3. BP (2017) Energy outlook 2017. http://www.bp.com/. Accessed 17 Aug 2017
4. IEA (2016) Key world energy statistics 2016. http://www.iea.org/statistics/. Accessed 21 Aug 2017
5. BP (2016) Statistical review of world energy 2016. http://www.bp.com/. Accessed 17 Aug 2017
6. Conti J, Holtberg P, Diefenderfer J, Larose A, Turnure JT, Westfall L (2016) International energy outlook 2016 with projections to 2040. Accessed 17 Aug 2017
7. Liao Q, Sun Y, Huang Y, Xia A, Fu Q, Zhu X (2017) Simultaneous enhancement of *Chlorella vulgaris* growth and lipid accumulation through the synergy effect between light and nitrate in a planar waveguide flat-plate photobioreactor. Bioresour Technol 243:528–538
8. EIA (2013) International energy outlook 2013. http://www.eia.gov/forecasts/ieo/pdf/0484 (2013).pdf. Accessed 10 Apr 2017
9. IEA (2015) Key world energy statistics 2015. http://www.iea.org/statistics/. Accessed 21 Aug 2017
10. BP (2016) BP China's changing energy landscape 2016. http://www.bp.com/. Accessed 17 Aug 2017
11. Xia A, Cheng J, Murphy JD (2016) Innovation in biological production and upgrading of methane and hydrogen for use as gaseous transport biofuel. Biotechnol Adv 34(5):451–472
12. Bennion EP, Ginosar DM, Moses J, Agblevor F, Quinn JC (2015) Lifecycle assessment of microalgae to biofuel: comparison of thermochemical processing pathways. Appl Energy 154:1062–1071
13. BP (2016) BP sustainability report 2016. http://www.bp.com/content/dam/bp/en/corporate/ pdf/sustainability-report/group-reports/bp-sustainability-report-2016.pdf. Accessed 5 Aug 2017
14. BP (2016) BP Key uncertainty—paths to a lower carbon world. http://www.bp.com/. Accessed 10 Aug 2017
15. The outline of China's 13th Five-Year Plan for national economic and social development (2016). http://www.gov.cn/xinwen/2016-03/17/content_5054992.htm. (In Chineses). Accessed 30 Oct 2017
16. BP (2017) Sustainability: air quality. http://www.bp.com/. Accessed 10 Aug 2017
17. BP (2016) BP managing local environmental impacts 2016. http://www.bp.com/. Accessed 17 Aug 2017
18. Jha S (2017) Renewable energy: Present research and future scope of Artificial Intelligence. Renew Sustain Energy Rev 77:297–317
19. GWEC (2017) Global wind report 2016. http://gwec.net/. Accessed 30 Oct 2017
20. Metayer M, Breyer C, Fell HJ (2015) The projections for the future and quality in the past of the World Energy Outlook for solar PV and other renewable energy technologies. 31st EU PVSEC
21. IEA (2011) World energy outlook 2011. http://www.enecho.meti.go.jp/committee/council/ basic_problem_committee/004/pdf/4-12.pdf. Accessed 30 Apr 2016
22. He Y, Bagley DM, Leung KT, Liss SN, Liao BQ (2012) Recent advances in membrane technologies for biorefining and bioenergy production. Biotechnol Adv 30(4):817–858
23. BP (2017) Statistical review of world energy 2017. http://www.bp.com/content/dam/bp/en/ corporate/pdf/energy-economics/statistical-review-2017/bp-statistical-review-of-world-energy- 2017-full-report.pdf. Accessed 27 Aug 2017

24. IEA (2016) IEA topics of bioenergy and biofuels. http://www.iea.org/. Accessed 20 Aug 2017

25. Rittmann BE (2008) Opportunities for renewable bioenergy using microorganisms. Biotechnol Bioeng 100(2):203–212

26. Prasertsan S, Sajjakulnukit B (2006) Biomass and biogas energy in Thailand: potential, opportunity and barriers. Renew Energy 31(5):599–610

27. Liu J, Wu J, Liu F, Han X (2012) Quantitative assessment of bioenergy from crop stalk resources in Inner Mongolia. China Appl Energy 93(5):305–318

28. IEA (2017) Energy technology perspectives 2017. www.iea.org/etp2017/. Accessed 30 Oct 2017

29. UNEP (2011) Green economy report. http://www.unep.org/greeneconomy/sites/unep.org. greeneconomy/files/field/image/green_economyreport_final_dec2011.pdf. Accessed 15 Aug 2017

30. Baidu Encyclopedia (2017) Biomass. http://baike.baidu.com/. (In Chinese). Accessed 30 Oct 2017

31. Beringer T, Lucht W, Schaphoff S (2011) Bioenergy production potential of global biomass plantations under environmental and agricultural constraints. Oxford University Press

32. Martin MA, Potrykus I, Ammann K (2010) First generation biofuels compete. New Biotechnol 27(5):596–608

33. Li Y, Khanal S (2015) Bioenergy: principles and applications. Wiley

34. Ziska LH, Runion GB, Tomecek M, Prior SA, Torbet HA, Sicher R (2009) An evaluation of cassava, sweet potato and field corn as potential carbohydrate sources for bioethanol production in Alabama and Maryland. Biomass Bioenergy 33(11):1503–1508

35. Murphy JD, Drosg B, Allen E, Jerney J, Xia A, Herrmann C (2015) A perspective on algal biogas. IEA Bioenergy 1–38

36. Chisti Y (2007) Biodiesel from microalgae. Biotechnol Adv 25(3):294–306

37. Collet P, Hélias A, Lardon L, Steyer JP, Bernard O, Chiaramonti D, Maniatis K, Tredici MR, Verdelho V, Yan J (2015) Recommendations for life cycle assessment of algal fuels. Appl Energy 154:1089–1102

38. FAO (2016) Food outlook–Biannual report on global food markets, June 2016. Accessed 20 Aug 2017

39. Kiran B, Kumar R, Deshmukh D (2014) Perspectives of microalgal biofuels as a renewable source of energy. Energy Convers Manage 88(2):1228–1244

40. Nigam PS, Singh A (2011) Production of liquid biofuels from renewable resources. Prog Energy Combust 37(1):52–68

41. (2016) Outline of the 13th five-year plan for national economic and social development of the People's Republic of China

42. DOE (2017) Department of energy: bioenergy. https://www.energy.gov/. Accessed 20 Aug 2017

43. Skytte K, Meibom P, Henriksen TC (2006) Electricity from biomass in the European Union—with or without biomass import. Biomass Bioenergy 30(5):385–392

44. NBSC (2016) National bureau of statistics of China: forest production. http://data.stats.gov. cn/easyquery.htm?cn=C01&zb=A0D0N&sj=2015. Accessed 10 May 2017

45. Jard G, Marfaing H, Carrère H, Delgenes JP, Steyer JP, Dumas C (2013) French Brittany macroalgae screening: composition and methane potential for potential alternative sources of energy and products. Bioresour Technol 144(6):492–498

46. Hughes AD, Black KD, Campbell I, Heymans JJ, Orr KK, Stanley MS, Kelly MS (2013) Comments on prospects for the use of macroalgae for fuel in Ireland and UK: an overview of marine management issues. Mar Policy 38(38):554–556

47. Becker EW (1995) Microalgae, biotechnology and microbiology. Cambridge University Press

48. Illman AM, Scragg AH, Shales SW (2000) Increase in *Chlorella* strains calorific values when grown in low nitrogen medium. Enzyme Microb Tech 27(8):631–635

49. Xia A, Herrmann C, Murphy JD (2015) How do we optimize third-generation algal biofuels? Biofuel Bioprod Bior 9(4):358–367
50. Tillman DA, Rossi AJ, Kitto WD (1981) Wood combustion. Principles, processes, and economics. Elsevier Press
51. Bridgwater AV, Bridgwater AV (2012) Review of fast pyrolysis of biomass and product upgrading. Biomass Bioenergy 38(2):68–94
52. Mohan D, Pittman CU, Steele PH (2006) Pyrolysis of wood/biomass for bio-oil: a critical review. Energy Fuel 20(3):848–889
53. Demirbas A (2005) Potential applications of renewable energy sources, biomass combustion problems in boiler power systems and combustion related environmental issues. Prog Energy Combust 31(2):171–192
54. Jenkins BM, Baxter LL, M TR Jr, Miles TR (1998) Combustion properties of biomass. Fuel Process Technol 54(1–3):17–46
55. Pragya N, Pandey KK, Sahoo PK (2013) A review on harvesting, oil extraction and biofuels production technologies from microalgae. Renew Sustain Energy Rev 24(10):159–171
56. Mankee L, Keatteong L, Mohamed AR (2010) Homogeneous, heterogeneous and enzymatic catalysis for transesterification of high free fatty acid oil (waste cooking oil) to biodiesel: a review. Biotechnol Adv 28(4):500–518
57. Man KL, Lee KT (2012) Microalgae biofuels: A critical review of issues, problems and the way forward. Biotechnol Adv 30(3):673–690
58. Cheng J, Huang R, Li T, Zhou J, Cen K (2014) Biodiesel from wet microalgae: extraction with hexane after the microwave-assisted transesterification of lipids. Bioresour Technol 170 (5):69–75
59. Meher LC, Sagar DV, Naik SN (2006) Technical aspects of biodiesel production by transesterification—a review. Renew Sust Energy Rev 10(3):248–268
60. Schuchardt UlfSercheli, RicardoVargas Matheus R (1998) Transesterification of vegetable oils: a review. J Brazil Chem Soc 9(3):199–210
61. Helwani Z, Othman MR, Aziz N, Kim J, Fernando WJN (2009) Solid heterogeneous catalysts for transesterification of triglycerides with methanol: a review. Appl Catal A Gen 363(1):1–10
62. Guo F, Fang Z, Tian XF, Long YD, Jiang LQ (2013) One-step production of biodiesel from *Jatropha* oil with high-acid value in ionic liquids. Bioresource Technol 140(11):447–450
63. Li Y, Lian S, Tong D, Song R, Yang W, Fan Y, Qing R, Hu C (2011) One-step production of biodiesel from *Nannochloropsis* sp. on solid base Mg–Zr catalyst. Appl. Energy 88 (10):3313–3317
64. Frank ED, Elgowainy A, Han J, Wang Z (2013) Life cycle comparison of hydrothermal liquefaction and lipid extraction pathways to renewable diesel from algae. Mitig Adapt Strat GL 18(1):137–158
65. Vardon DR, Sharma BK, Blazina GV, Rajagopalan K, Strathmann TJ (2012) Thermochemical conversion of raw and defatted algal biomass via hydrothermal liquefaction and slow pyrolysis. Bioresour Technol 109(109):178–187
66. Sanchez-Silva L, López-González D, Garcia-Minguillan AM, Valverde JL (2013) Pyrolysis, combustion and gasification characteristics of Nannochloropsis gaditana microalgae. Bioresour Technol 130(1):321–331
67. Long L, Yu Z, Li Y (2017) Sequential batch thermophilic solid-state anaerobic digestion of lignocellulosic biomass via recirculating digestate as inoculum—part II: microbial diversity and succession. Bioresour Technol 241:1027–1035
68. Manchala KR, Sun Y, Zhang D, Wang ZW (2017) Anaerobic digestion modelling. Adv Bioenergy 2:69–141
69. Rodriguez C, Alaswad A, Mooney J, Prescott T, Olabi AG (2015) Pre-treatment techniques used for anaerobic digestion of algae. Fuel Process Technol 138:765–779
70. Nguyen DD, Chang SW, Jeong SY, Jeung J, Kim S, Guo W, Ngo HH (2016) Dry thermophilic semi-continuous anaerobic digestion of food waste: performance evaluation,

modified Gompertz model analysis, and energy balance. Energy Convers Manag 128:
203–210

71. Nguyen DD, Chang SW, Cha JH, Jeong SY, Yong SY, Lee SJ, Tran MC, Ngo HH (2017)
Dry semi-continuous anaerobic digestion of food waste in the mesophilic and thermophilic
modes: new aspects of sustainable management and energy recovery in South Korea. Energy
Convers Manag 135:445–452

72. Fu SF, Wang F, Yuan XZ, Yang ZM, Luo SJ, Wang CS, Guo RB, Fu SF, Wang F, Yuan XZ
(2016) The thermophilic (55 degrees C) microaerobic pretreatment of corn straw for
anaerobic digestion. Bioresour Technol 204(1):213

73. Kim JK, Oh BR, Chun YN, Kim SW (2006) Effects of temperature and hydraulic retention
time on anaerobic digestion of food waste. J Biosci Bioeng 102(4):328–332

74. Weiland P (2010) Biogas production: current state and perspectives. Appl Microbiol Biot 85
(4):849–860

75. Chen Y, Cheng J, Creamer K (2008) Inhibition of anaerobic digestion process: a review.
Bioresour Technol 99(10):4044–4064

76. Xia A, Cheng J, Ding LK, Lin RC, Song WL, Su HB, Zhou JH, Cen KF (2015) Substrate
consumption and hydrogen production via co-fermentation of monomers derived from
carbohydrates and proteins in biomass wastes. Appl Energ 139:9–16

77. Xia A, Cheng J, Song W, Su H, Ding L, Lin R, Lu H, Liu J, Zhou J, Cen K (2015)
Fermentative hydrogen production using algal biomass as feedstock. Renew Sustain Energy
Rev 51:209–230

78. Verhelst S, Wallner T (2009) Hydrogen-fueled internal combustion engines. Prog Energy
Combust 35(6):490–527

79. Ding L, Cheng J, Xia A, Jacob A, Voelklein M, Murphy JD (2016) Co-generation of
biohydrogen and biomethane through two-stage batch co-fermentation of macro- and
micro-algal biomass. Bioresour Technol 218:224–231

80. Liao Q, Liu DM, Ye DD, Zhu X, Lee DJ (2011) Mathematical modeling of two-phase
flow and transport in an immobilized-cell photobioreactor. Int J Hydrog Energy 36(21):
13939–13948

81. Zhu X, Guo CL, Wang YZ, Liao Q, Chen R, Lee DJ (2012) A feasibility study on
unsaturated flow bioreactor using optical fiber illumination for photo-hydrogen production.
Int J Hydrog Energy 37(20):15666–15671

82. Imaizumi Y, Nagao N, Yusoff FM, Taguchi S, Toda T (2014) Estimation of optimum
specific light intensity per cell on a high-cell-density continuous culture of *Chlorella
zofingiensis* not limited by nutrients or CO_2. Bioresour Technol 162:53–59

83. Androga DD, Ozgur E, Gunduz U, Yucel M, Eroglu I (2011) Factors affecting the longterm
stability of biomass and hydrogen productivity in outdoor photofermentation. Int J Hydrog
Energy 36(17):11369–11378

84. Koku H, Eroğlu İ, Gündüz U, Yücel M, Türker L (2002) Aspects of the metabolism of
hydrogen production by *Rhodobacter sphaeroides*. Int J Hydrog Energy 27(11–12):1315–
1329

85. Ghirardi ML, Zhang L, Lee JW, Flynn T, Seibert M, Greenbaum E, Melis A (2000)
Microalgae: a green source of renewable H_2. Trends Biotechnol 18(12):506–511

86. Holladay JD, Hu J, King DL, Wang Y (2009) An overview of hydrogen production
technologies. Catal Today 139(4):244–260

87. Carrieri D, Momot D, Brasg IA, Ananyev G, Lenz O, Bryant DA, Dismukes GC (2010)
Boosting autofermentation rates and product yields with sodium stress cycling: application
to production of renewable fuels by *Cyanobacteria*. Appl Environ Microb 76(19):
6455–6462

88. Dutta D, De D, Chaudhuri S, Bhattacharya SK (2005) Hydrogen production by
cyanobacteria. Microb Cell Fact 4(1):1–11

89. Lin Y, Tanaka S (2006) Ethanol fermentation from biomass resources: current state and
prospects. Appl Microbiol Biotechnol 69(6):627–642

90. Alfani F, Gallifuoco A, Saporosi A, Spera A, Cantarella M (2000) Comparison of SHF and SSF processes for the bioconversion of steam-exploded wheat straw. J Ind Microbiol Biotechnol 25(4):184–192

91. Wingren A, Galbe M, Zacchi G (2003) Techno-economic evaluation of producing ethanol from softwood: comparison of SSF and SHF and identification of bottlenecks. Biotechnol Progr 19(4):1109–1117

92. Mcmillan JD, Newman MM, Templeton DW, Mohagheghi A (1999) Simultaneous saccharification and cofermentation of dilute-acid pretreated yellow poplar hardwood to ethanol using xylose-fermenting *Zymomonas mobilis*. Appl Biochem Biotech 79(1–3): 649–665

93. Katahira S, Mizuike A, Fukuda H, Kondo A (2006) Ethanol fermentation from lignocellulosic hydrolysate by a recombinant xylose- and cellooligosaccharide-assimilating yeast strain. Appl Microbiol Biotechnol 72(6):1136–1143

94. Bai FWAWA, Mooyoung M (2008) Ethanol fermentation technologies from sugar and starch feedstocks. Biotechnol Adv 26(1):89–105

95. Jeffries TW, Shi NQ (1999) Genetic engineering for improved xylose fermentation by yeasts. Adv Biochem Eng Biotechnol 65:117–161

96. Ayala-Parra P, Liu Y, Field JA, Sierra-Alvarez R (2017) Nutrient recovery and biogas generation from the anaerobic digestion of waste biomass from algal biofuel production. Renew Energy 108:410–416

97. Ghimire A, Kumar G, Sivagurunathan P, Shobana S, Saratale GD, Kim HW, Luongo V, Esposito G, Munoz R (2017) Bio-hythane production from microalgae biomass: Key challenges and potential opportunities for algal bio-refineries. Bioresour Technol 241: 525–536

98. Jankowska E, Sahu AK, Oleskowicz-Popiel P (2016) Biogas from microalgae: review on microalgae's cultivation, harvesting and pretreatment for anaerobic digestion. Renew Sustain Energy Rev 75:692–709

99. Jang YS, Park JM, Choi S, Yong JC, Seung DY, Cho JH, Sang YL (2012) Engineering of microorganisms for the production of biofuels and perspectives based on systems metabolic engineering approaches. Biotechnol Adv 30(5):989–1000

100. Abo-Hashesh M, Wang R, Hallenbeck PC (2011) Metabolic engineering in dark fermentative hydrogen production; theory and practice. Bioresour Technol 102(18): 8414–8422

101. Cai G, Jin B, Monis P, Saint C (2011) Metabolic flux network and analysis of fermentative hydrogen production. Biotechnol Adv 29(4):375–387

102. Song W, Cheng J, Zhao J, Carrieri D, Zhang C, Zhou J, Cen K (2011) Improvement of hydrogen production by over-expression of a hydrogen-promoting protein gene in Enterobacter cloacae. Int J Hydrog Energy 36(11):6609–6615

103. Zhang L, Zhu X, Li J, Fu Q, Liao Q, Li Y, Li Y (2017) A self-recirculation electrolyte system for unbuffered microbial fuel cells with an aerated cathode. Bioresour Technol 241:1173–1177

104. Yang W, Li J, Fu Q, Zhang L, Zhu X, Liao Q (2017) A simple method for preparing a binder-free paper-based air cathode for microbial fuel cells. Bioresour Technol 241:325–331

105. Li J, Hu L, Liang Z, Ye DD, Xun Z, Qiang L (2017) Uneven biofilm and current distribution in three-dimensional macroporous anodes of bio-electrochemical systems composed of graphite electrode arrays. Bioresour Technol 228:25–30

106. Allen RM, Bennetto HP (1993) Microbial fuel-cells. Appl Biochem Biotech 39–40(1):27–40

107. Mikhail G, Ibrahim D, Rosen MA (2006) Economic and environmental comparison of conventional, hybrid, electric and hydrogen fuel cell vehicles. J Power Sour 159(2): 1186–1193

108. Daalkhaijav U (2012) Removal of ammonia (nitrification) in conventional and microbial fuel cell type bioreactors, Doctoral Dissertation

109. Logan BE, Regan JM (2006) Microbial fuel cells—challenges and applications. Environ Sci Technol 40(17):5172–5180

110. Logan BE (2010) Scaling up microbial fuel cells and other bioelectrochemical systems. Appl Microbiol Biotechnol 85(6):1665–1671
111. Logan BE, Regan JM (2006) Electricity-producing bacterial communities in microbial fuel cells. Trends Microbiol 14(12):512–518
112. Biffinger J, Ribbens M, Ringeisen B, Pietron J, Finkel S, Nealson K (2010) Characterization of electrochemically active bacteria utilizing a high-throughput voltage-based screening assay. Biotechnol Bioeng 102(2):436–444
113. Commault AS, Laczka O, Siboni N, Tamburic B, Crosswell JR, Seymour JR, Ralph PJ (2017) Electricity and biomass production in a bacteria- *Chlorella* based microbial fuel cell treating wastewater. J Power Sour 356:299–309
114. Liu H, Logan BE (2004) Electricity generation using an air-cathode single chamber microbial fuel cell in the presence and absence of a proton exchange membrane. Environ Sci Technol 38(14):4040–4046
115. Mohamed HO, Obaid M, Sayed ET, Liu Y, Lee J, Park M, Nam B, Kim HY (2017) Electricity generation from real industrial wastewater using a single-chamber air cathode microbial fuel cell with an activated carbon anode. Bioproc Biosyst Eng 40:1151–1161
116. Yang W, Li J, Ye D, Zhu X, Liao Q (2017) Bamboo charcoal as a cost-effective catalyst for an air-cathode of microbial fuel cells. Electrochim Acta 224:585–592
117. Logan BE, Call D, Cheng S, Hamelers HVM, Sleutels THJA, Jeremiasse AW, Rozendal RA (2008) Microbial electrolysis cells for high yield hydrogen gas production from organic matter. Environ Sci Technol 42(23):8630–8640
118. Cheng S, Xing D, Call DF, Logan BE (2009) Direct biological conversion of electrical current into methane by electromethanogenesis. Environ Sci Technol 43(10):3953–3958
119. Rabaey K, Rozendal RA (2010) Microbial electrosynthesis—revisiting the electrical route for microbial production. Nat Rev Microbiol 8(10):706–716
120. Zhen G, Lu X, Kumar G, Bakonyi P, Xu K, Zhao Y (2017) Microbial electrolysis cell platform for simultaneous waste biorefinery and clean electrofuels generation: Current situation, challenges and future perspectives. Prog Energ Combust 63:119–145
121. Passos F, Uggetti E, Carrère H, Ferrer I (2014) Pretreatment of microalgae to improve biogas production: A review. Bioresour Technol 172:403–412
122. Amarni F, Kadi H (2010) Kinetics study of microwave-assisted solvent extraction of oil from olive cake using hexane: Comparison with the conventional extraction. Innov Food Sci Emerg 11(2):322–327
123. Lee AK, Lewis DM, Ashman PJ (2012) Disruption of microalgal cells for the extraction of lipids for biofuels: processes and specific energy requirements. Biomass Bioenergy 46 (1):89–101
124. Guldhe A, Singh B, Rawat I, Ramluckan K, Bux F (2014) Efficacy of drying and cell disruption techniques on lipid recovery from microalgae for biodiesel production. Fuel 128 (28):46–52
125. Ding L, Cheng J, Dan Q, Yue L, Li YY, Zhou J, Cen K (2017) Investigating hydrothermal pretreatment of food waste for two-stage fermentative hydrogen and methane co-production. Bioresour Technol 241:491–499
126. Brownell HH, Yu EK, Saddler JN (2010) Steam-explosion pretreatment of wood: Effect of chip size, acid, moisture content and pressure drop. Biotechnol Bioeng 28(6):792–801
127. Datar R, Huang J, Maness PC, Mohagheghi A, Czernik S, Chornet E (2007) Hydrogen production from the fermentation of corn stover biomass pretreated with a steam-explosion process. Int J Hydrog Energy 32(8):932–939
128. Hendriks AT, Zeeman G (2009) Pretreatments to enhance the digestibility of lignocellulosic biomass. Bioresour Technol 100(1):10–18
129. Keymer P, Ruffell I, Pratt S, Lant P (2013) High pressure thermal hydrolysis as pre-treatment to increase the methane yield during anaerobic digestion of microalgae. Bioresour Technol 131(2):128–133
130. Wilson CA, Novak JT (2009) Hydrolysis of macromolecular components of primary and secondary wastewater sludge by thermal hydrolytic pretreatment. Water Res 43(18):4489

131. Nolan P, Luostarinen S, Doyle EM, O'Kiely P (2016) Anaerobic digestion of perennial ryegrass prepared by cryogenic freezing versus thermal drying methods, using contrasting invitro batch digestion systems. Renew Energy 87:273–278
132. Show KY, Lee DJ, Tay JH, Lee TM, Chang JS (2015) Microalgal drying and cell disruption–recent advances. Bioresour Technol 184:258–266
133. Chisti Y, Moo-Young M (1986) Disruption of microbial cells for intracellular products. Enzyme Microb Tech 8(4):194–204
134. Lee SJ, Yoon BD, Oh HM (1998) Rapid method for the determination of lipid from the green alga *Botryococcus braunii*. Biotechnol Tech 12(7):553–556
135. Schütte H, Kula M (1990) Separation processes in biotechnology. Bead mill disruption. Bioprocess Technol 9:107–141
136. Mcgarvey J (2011) Prion extraction methods: comparison of bead beating, ultrasonic disruption, and repeated freeze-thaw methodologies for the recovery of functional renilla-prion fusion protein from bacteria. Arch Intern Med 171(21):1920–1927
137. Meullemiestre A, Breil C, Abertvian M, Chemat F (2016) Microwave, ultrasound, thermal treatments, and bead milling as intensification techniques for extraction of lipids from oleaginous Yarrowia lipolytica yeast for a biojetfuel application. Bioresour Technol 211:190–199
138. Günerken E, D'Hondt E, Eppink MHM, Garciagonzalez L, Elst K, Wijffels RH (2015) Cell disruption for microalgae biorefineries. Biotechnol Adv 33(2):243–260
139. Halim R, Harun R, Danquah MK, Webley PA (2012) Microalgal cell disruption for biofuel development. Appl Energy 91(1):116–121
140. Follows M, Heterington PJ, Dunnill P, Lilly MD (1971) Release of enzymes from bakers' yeast by disruption in an industrial homogenizer. Biotechnol Bioeng 13(4):549–560
141. Floury J, Legrand J, Desrumaux A (2004) Analysis of a new type of high pressure homogeniser. Part B. Study of droplet break-up and recoalescence phenomena. Chem Eng Sci 59(6):1285–1294
142. Mendes-Pinto MM, Raposo MFJ, Bowen J, Young AJ, Morais R (2001) Evaluation of different cell disruption processes on encysted cells of *Haematococcus pluvialis*: Effects on astaxanthin recovery and implications for bio-availability. J Appl Phycol 13(1):19–24
143. Cho S, Park S, Seon J, Yu J, Lee T (2013) Evaluation of thermal, ultrasonic and alkali pretreatments on mixed-microalgal biomass to enhance anaerobic methane production. Bioresour Technol 143(17):330–336
144. Mendez L, Mahdy A, Timmers RA, Ballesteros M, Gonzálezfernández C (2013) Enhancing methane production of Chlorella vulgaris via thermochemical pretreatments. Bioresour Technol 149(4):136–141
145. Xia A, Cheng J, Lin R, Liu J, Zhou J, Cen K (2013) Sequential generation of hydrogen and methane from glutamic acid through combined photo-fermentation and methanogenesis. Bioresour Technol 131:146–151
146. Xia A, Cheng J, Lin R, Lu H, Zhou J, Cen K (2013) Comparison in dark hydrogen fermentation followed by photo hydrogen fermentation and methanogenesis between protein and carbohydrate compositions in *Nannochloropsis oceanica* biomass. Bioresour Technol 138(6):204–213
147. Halim R, Gladman B, Danquah MK, Webley PA (2011) Oil extraction from microalgae for biodiesel production. Bioresource Technol 102(1):178–185
148. Fred VR, Sheldon RA (2007) Biocatalysis in ionic liquids. Chem Rev 107(6):2757–2785
149. Marsh KN, Boxall JA, Lichtenthaler R (2004) Room temperature ionic liquids and their mixtures—a review. Fluid Phase Equilibr 219(1):93–98
150. Rantwijk FV, Sheldon RA (2007) Biocatalysis in ionic liquids. The Royal Society of Chemistry
151. Suna C, Youkwan O, Minji J, Seungwook K, Jinsuk L, Jiyeon P (2014) Effects of ionic liquid mixtures on lipid extraction from *Chlorella vulgaris*. Renew Energy 65(5):169–174

152. Rui LM, Reis AD, Palavra AF (2006) Supercritical CO_2 extraction of γ-linolenic acid and other lipids from *Arthrospira (Spirulina) maxima:* Comparison with organic solvent extraction. Food Chem 99(1):57–63

153. Xiu S, Shahbazi A (2012) Bio-oil production and upgrading research: a review. Renew Sust Energ Rev 16(7):4406–4414

154. Mortensen PM, Grunwaldt JD, Jensen PA, Knudsen KG, Jensen AD (2011) A review of catalytic upgrading of bio-oil to engine fuels. Appl Catal A Gen 407(1):1–19

155. Fisk CA, Morgan T, Ji Y, Crocker M, Crofcheck C, Lewis SA (2009) Bio-oil upgrading over platinum catalysts using in situ generated hydrogen. Appl Catal A Gen 358(2):150–156

156. Tang Z, Lu Q, Zhang Y, Zhu X, Guo Q (2009) One step bio-oil upgrading through hydrotreatment, esterification, and cracking. Ind Eng Chem Res 48(15):6923–6929

157. Nava R, Pawelec B, Castaño P, Álvarez-Galván MC, Loricera CV, Fierro JLG (2009) Upgrading of bio-liquids on different mesoporous silica-supported CoMo catalysts. Appl Catal B Environ 92(1):154–167

158. Kandiyoti R (2016) Hydroprocessing of heavy oils and residua. J Energ Inst 2007(3):184

159. Liu ZG, Zhang FS (2008) Effects of various solvents on the liquefaction of biomass to produce fuels and chemical feedstocks. Energy Convers Manag 49(12):3498–3504

160. Ross AB, Biller P, Kubacki ML, Li H, Lea-Langton A, Jones JM (2010) Hydrothermal processing of microalgae using alkali and organic acids. Fuel 89(9):2234–2243

161. And AO, Czernik Stefan (1999) Fuel oil quality of biomass pyrolysis oils state of the art for the end users. Fuel Energy Abs 41(4):914–921

162. Tang Y, Yu W, Mo L, Lou H, Zheng X (2015) One-step hydrogenation − esterification of aldehyde and acid to ester over bifunctional Pt catalysts: A model reaction as novel route for catalytic upgrading of fast pyrolysis bio-oil. Energy Fuel 22(5):3484–3488

163. Ikura M, Stanciulescu M, Hogan E (2003) Emulsification of pyrolysis derived bio-oil in diesel fuel. Biomass Bioenergy 24(3):221–232

164. Chaemchuen S, Kabir NA, Zhou K, Verpoort F (2013) Metal-organic frameworks for upgrading biogas via CO_2 adsorption to biogas green energy. Chem Soc Rev 42(24): 9304–9332

165. Ryckebosch E, Drouillon M, Vervaeren H (2011) Techniques for transformation of biogas to biomethane. Biomass Bioenerg 35(5):1633–1645

166. Yasin NHM, Maeda T, Hu AY, Yu CP, Wood TK (2015) CO_2 sequestration by methanogens in activated sludge for methane production. Appl Energy 142:426–434

167. Vandewalle J, Bruninx K, D'Haeseleer W (2015) Effects of large-scale power to gas conversion on the power, gas and carbon sectors and their interactions. Energy Convers Manage 94(7):28–39

168. Mann G, Schlegel M, Schumann R, Sakalauskas A (2009) Biogas-conditioning with microalgae. Agron Res 7:33–38

169. Bahr M, Díaz I, Dominguez A, González Sánchez A, Muñoz R (2014) Microalgal-biotechnology as a platform for an integral biogas upgrading and nutrient removal from anaerobic effluents. Environ Sci Technol 48(1):573–581

170. Demirbas A (2006) Theoretical heating values and impacts of pure compounds and fuels. Energy Sour Part A 28(5):459–467

171. Cofala J, Bertok I, Borkenkleefeld J, Heyes C, Klimont Z, Rafaj P, Sander R, Schoepp W, Amann M (2012) Emissions of air pollutants for the world energy outlook 2012 energy scenarios. International Institute for Applied Systems Analysis, Schlossplatz, p 1

172. Demirbas A (2009) Political, economic and environmental impacts of biofuels: a review. Appl Energy 86(11):S108–S117

173. Kim H, Choi B (2008) Effect of ethanol–diesel blend fuels on emission and particle size distribution in a common-rail direct injection diesel engine with warm-up catalytic converter. Renew Energy 33(10):2222–2228

174. Frank ED, Elgowainy A, Han JW, Wang ZC (2013) Life cycle comparison of hydrothermal liquefaction and lipid extraction pathways to renewable diesel from algae. Mitig Adapt Strat G 18(1):137–158

175. Liu X, Saydah B, Eranki P, Colosi LM, Mitchell BG, Rhodes J, Clarens AF (2013) Pilot-scale data provide enhanced estimates of the life cycle energy and emissions profile of algae biofuels produced via hydrothermal liquefaction. Bioresour Technol 148(8):163–171
176. Lokesh K, Sethi V, Nikolaidis T, Goodger E, Nalianda D (2015) Life cycle greenhouse gas analysis of biojet fuels with a technical investigation into their impact onjet engine performance. Biomass Bioenergy 77:26–44
177. Muench S, Guenther E (2013) A systematic review of bioenergy life cycle assessments. Appl Energy 112(4):257–273
178. Mariani A, Prati MV, Unich A, Morrone B (2013) Combustion analysis of a spark ignition i. c. engine fuelled alternatively with natural gas and hydrogen-natural gas blends. Int J Hydrog Energy 38(3):1616–1623
179. Börjesson P, Mattiasson B (2008) Biogas as a resource-efficient vehicle fuel. Trends Biotechnol 26(1):7–13

Chapter 2
Role of Bioreactors in Microbial Biomass and Energy Conversion

Liang Zhang, Biao Zhang, Xun Zhu, Haixing Chang, Shiqi Ou and Hong Wang

1 Introduction

In recent decades, the global energy crisis and widespread environmental destruction caused by over-exploitation of traditional, petroleum-based energy sources have put forward a pressing need to develop renewable and sustainable energy. Renewable sources of energy, including biomass, hydropower, geothermal, solar, wind and marine energy, have become important and promising parts of the energy infrastructure. Among the different types of renewable energy, bioenergy is a widely available source that supplies combustion for motor fuels, electricity power, and other domains. Bioreactors are the principal devices that provide a suitable environment for the biochemical reactions involved in microbial biomass cultivation and energy conversion. Bioreactor technology attracts great interest in processes such as microbial biomass cultivation, microbial biofuel conversion, and microbial electrochemical systems because of its simplicity, moderate reaction, sustainability, low energy and raw material input, and minimal carbon footprint. Undoubtedly, bioreactor technology is one of the most promising approaches for microbial biomass production and energy conversion, and plays a significant role in

L. Zhang · B. Zhang · X. Zhu (✉) · H. Wang
Key Laboratory of Low-Grade Energy Utilization Technologies and Systems,
Chongqing University, Ministry of Education, Chongqing 400030, China
e-mail: zhuxun@cqu.edu.cn

L. Zhang · B. Zhang · X. Zhu · H. Wang
Institute of Engineering Thermophysics, Chongqing University,
Chongqing 400030, China

H. Chang
School of Chemistry and Chemical Engineering, Chongqing University of Technology,
Chongqing 400030, China

S. Ou
Oak Ridge National Laboratory, 2360 Cherahala Blvd, Knoxville, TN 37932, USA

this bioprocess. In this chapter, the role of bioreactors is reviewed with respect to its application in microbial biomass cultivation, microbial biofuel conversion, and microbial electrochemical systems. In addition, fundamental aspects and noteworthy functions of bioreactors are outlined within each of these applications.

2 Bioreactors in Microbial Biomass Cultivation

It is well known that microbial energy conversion technology is an effective and eco-friendly solution to global energy problems. Within this technology, cultivation of microbial biomass such as microalgae is one of the most promising. The lipid productivity of microalgae is ten times higher than that of terrestrial crops like soybean and sunflower. Additionally, microalgae have many other advantages like high photosynthetic efficiency, low water footprint, and the ability to grow on non-arable land using nutrients from wastewater. The microbial energy conversion process is usually conducted in a bioreactor, which provides a suitable environment for microbial cells. Therefore, bioreactors play a significant role in the cultivation of microbial biomass and can promote the widespread use of bioenergy.

2.1 Application in Microbial Biomass Cultivation

As one of the main methods of producing microbial biomass, microalgae cultivation can be divided into photoautotrophic, heterotrophic and mixotrophic cultivation depending on the type of carbon and energy source.

In photoautotrophic cultivation, microalgae use photosynthesis to convert light and inorganic carbons (e.g., CO_2 and HCO_3^-) into high-value organic matter, which is nature's most primitive way of converting carbon into biomass. The synthetic intracellular organic matter produced by microalgae in photoautotrophic cultivation can be made into biodiesel, cosmetics, and food. Additionally, photoautotrophic cultivation is suited to large-scale production due to its easy, low-cost operation and maintenance. However, photoautotrophic culture medium impedes light penetration, thereby greatly restricting high-density microalgae cultivation. At present, the microalgae concentration in small photobioreactors can reach 5–6 g/L, but the concentration in outdoor ponds only reaches 1–1.5 g/L. The low density of microalgae makes it difficult to separate the useful biomass from excess bulk and limits the large-scale cultivation of microalgae in bioreactors.

In heterotrophic cultivation, microalgae utilize organic carbon sources present in the culture medium (like glucose and acetic acid) to synthesize intracellular macromolecules like chlorophyll, proteins, and carbohydrates, without the need for light energy [1]. Heterotrophic microalgae cultivation can produce a relatively high biomass concentration since it directly utilizes organic matter in the medium as the energy source, thereby avoiding the growth limitations caused by insufficient light

penetration in photoautotrophic cultivation. It is reported that the biomass concentration of heterotrophic cultivation can easily reach 100 g/L. Therefore, in terms of high-density accumulation of biomass, heterotrophic cultivation of microalgae in bioreactors is superior to photoautotrophic cultivation [2]. However, there is an increased risk of bacterial contamination in heterotrophic cultivation, requiring the culture medium to undergo a thorough sterilization process prior to use. Additionally, the cost of replenishing the culture medium is also an important factor hindering commercial heterotrophic production of microalgae biomass [3].

In mixotrophic cultivation, microalgae cells are capable of reproducing under both photoautotrophic and heterotrophic conditions, using both inorganic and organic carbons as their energy source for growth [4]. Although mixotrophic cultivation can partially reduce the photo-limitation effect present in photoautotrophic cultivation and the bacterial contamination risk present in heterotrophic cultivation, it is rarely used in large-scale microalgae biomass and biofuel production due to operating complexity.

2.2 Bioreactors in Microbial Biomass Cultivation: The Fundamentals

A bioreactor refers to any manufactured or engineered system that supports a biologically active environment [5]. A photobioreactor (PBR) is a type of bioreactor that incorporates a light source (natural sunlight or artificial illumination). The success of mass production of microalgae for biodiesel depends greatly on the design and performance of PBRs [6].

2.2.1 Configurations

As shown in Fig. 1, bioreactors for microalgae cultivation can be categorized into open ponds (raceway pond) and closed PBRs (flat-plate, column, and tubular PBRs) [7].

Open ponds can be subdivided into natural waters (lakes, lagoons, and ponds), artificial ponds, and containers [8]. Because of their low cost, convenient maintenance, and large-scale suitability, open ponds are widely used in commercial production. Taking raceway ponds as an example, the depth of microalgae suspension is about 15–30 cm, with circulating flow driven by a pump. This water circulation keeps the cells in suspension, generating enough velocity to prevent cells from settling or aggregating via flocculation. However, the major limitations in open ponds include poor productivity, the need for large tracts of land, the restriction to certain microalgae strains, poor light utilization, and constant loss of water via evaporation [9]. Raceway ponds can typically yield a biomass concentration of 1 $g_{dryweight}$/L and reach a productivity level of 100 $mg_{dry\ weight}$/L/d [10].
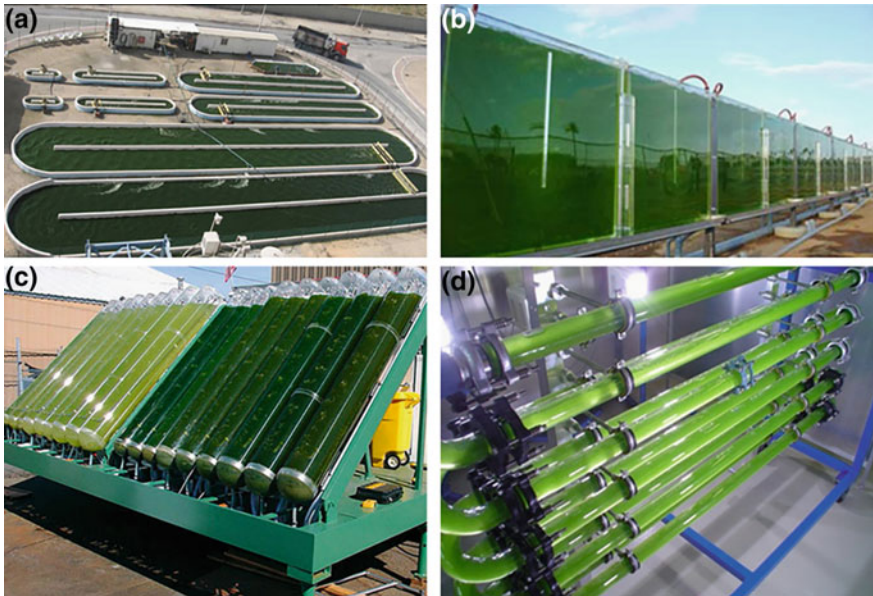
Fig. 1 Raceway pond (**a**), flat-plate photobioreactor (**b**), column photobioreactor (**c**) and tubular photobioreactor (**d**) (adapted and reprinted from [7], Copyright 2011, with permission from Elsevier)

A closed PBR is generally made of glass, plastic, or some other transparent material [11]. Since the culture conditions (like temperature, humidity, and flow parameter) are easy to control, this kind of bioreactor has some advantages over open ponds, such as large illuminated surface area per unit volume, long gas residence time, high growth rate, and high biomass concentration. In addition, the closed PBR is less likely to cause environmental pollution. Therefore, extensive research is focused on optimizing the closed PBR. In terms of structure, closed PBRs can be divided into three types: the flat-plate, the column, and the tubular PBR [7]. Flat-plate PBRs have attracted particular interest for the cultivation of photosynthetic microorganisms due to their large illuminated surface to volume ratio and their modular design that is convenient for scaling up. For example, Pulz et al. [12] reported an optimized, large-scale, flat-plate PBR module of 6000 L, and Tredici et al. [13] developed a vertical alveolar panel (2.2 m^2) based on the same material. In column PBRs, CO_2 gas is bubbled into the microalgae suspension through a gas distributor to provide the carbon source for growth. The force of the rising bubbles keeps the microalgae suspension circulating. The advantages of column PBRs include efficient mass transfer, good mixing with low shear stress and low energy consumption [9]. Tubular PBRs are usually made of transparent materials and are placed under natural sunlight or an artificial light source. The mixing of the microalgae suspension in this type of bioreactor is driven by a pump or airlift system. Some disadvantages include high manufacturing cost,

poor circulation, and accumulation of dissolved oxygen [14]. Nevertheless, tubular PBRs are currently the most widely used type of closed bioreactor for large-scale cultivation of microalgae due to their large illuminated surface to volume ratio and relatively high biomass productivity.

2.2.2 Functions

There are four main applications of bioreactors in microalgae cultivation [15]:

(1) Bioreactors are used to cultivate small phototrophic organisms, such as cyanobacteria, algae, or moss plants for biodiesel and other liquid fuels [16]. For example, microalgae open pond systems were used for biofuel production between 1980 and 1996 by the United States (U.S.) Department of Energy's ASP plan [17].
(2) Bioreactors can be used to generate microalgae biomass and other high-value metabolites. The nutrient composition of algal biomass has proved to be a superior alternative in animal feed supplements [18]. For example, the most common *Chlorella* sp. and *Spirulina* sp. can be used as food, food additives, and feed supplement in the form of algal biomass powder.
(3) Bioreactors are also designed to treat exhaust gas and wastewater [19]. Since CO_2 is efficiently absorbed by microalgae in bioreactors, flue gas and other industrial waste gases can be used to provide their carbon source. Microalgae cultivated in bioreactors are used to absorb nitrogen, phosphorus, heavy metals, and other toxic substances present in wastewater [9].
(4) Bioreactors are used in manned space exploration programs as bioregenerative technology like the Controlled Ecological Life Support System.

2.2.3 Influencing Factors

Light is used as an energy source in microalgae photosynthesis, and light intensity is one of the most important factors in this process [20]. There are three aspects of light that influence the growth of microalgae: light intensity, optical wavelength, and photoperiod. Light is the driving force of photosynthetic electron transfer, and the electron transfer rate is improved with increased light intensity. An increased electron transfer rate in turn enhances the rate of photosynthesis. However, light intensities above the light saturation point can inhibit the growth of microalgae [21]. Therefore, in the process of microalgae cultivation, light intensity should be maintained as close to the light saturation point as possible.

CO_2 is the main carbon source for microalgae photosynthesis, and the CO_2 transfer process directly affects photosynthesis, especially the dark reactions of photosynthesis. According to the two-film theory, CO_2 molecules in the gaseous phase are utilized by microalgae cells in two main stages. In the first stage, CO_2 molecules transfer from the gaseous phase to the liquid phase. In the second stage,

this liquid form of inorganic carbon is converted into organic carbon in the microalgal cell [22]. Microalgae cultivation in an airlift PBR uses a typical carbon-capture process in which CO_2 is bubbled into the reactor via a gas distributor. As the gas rises up through the reactor, the CO_2 molecules diffuse across the gas-liquid interface and dissolve into the surrounding microalgae suspension. Afterwards, the dissolved CO_2 is consumed by microalgae cells to produce organic matter through photosynthesis [6, 23]. In the above-mentioned process, the efficiency of CO_2 delivery can significantly affect microalgae growth, bio-oil accumulation, and CO_2 fixation in the PBR.

Temperature is another important factor influencing microalgae metabolism by affecting enzyme activity. The optimum temperature range for microalgae growth varies by strain. In general, the ideal temperature for microalgae cultivation ranges from 20 to 24 °C. The most commonly used microalgae species can tolerate temperatures between 16 and 27 °C. Temperatures lower than 16 °C will attenuate the growth of microalgae, whereas temperatures higher than 35 °C are lethal for a number of species [24].

The pH of the culture medium has a large impact on microalgae growth and other physiological processes. The pH can affect the dissolution and diffusion of CO_2 in the liquid phase, thus affecting the efficiency of photosynthetic carbon fixation. In addition, the pH can influence microalgae respiration rate, ion absorption, metabolism, and distribution of algal cells in the bioreactor [25–27]. Different species of microalgae prefer different pH values. Additionally, the pH of a microalgae suspension tends to increase during the cultivation process, which hinders the enzymatic activity of the microalgae and in turn inhibits growth. Therefore, it is important to actively maintain the pH of the culture medium at the optimum range by adding acetic acid or hydrochloric acid to the medium during cultivation.

2.3 The Importance of Bioreactors in Microbial Biomass Cultivation

2.3.1 Ideal Site for Microbial Growth and Metabolic Reactions

Bioreactors are the primary devices that provide a suitable environment for the biochemical reactions mediated by microorganisms. Almost all microbial metabolic processes are carried out in bioreactors. Growing microorganisms in bioreactors reduces the risk of contamination, improves the reproducibility of cultivation conditions, provides controlled hydrodynamics, temperature, and substratum, and allows appropriate technical design [28]. Bioreactors provide favorable physical and chemical environments for biological metabolism, allowing microorganisms to grow and metabolize at relatively high rates. In the biological engineering industry, the bioreactants, substrate, enzyme, catalyst, and nutrients are added to the bioreactor to undergo biochemical reactions aided by microbial cells. Then, these microbial cells

proliferate and synthesize various metabolic products. Bioreactors provide the necessary mixing, mass transfer, and physical containment to guarantee a controlled environment for the organism to produce the desired biological product [29].

During the past few decades, bioreactors have been applied in many fields for biomass cultivation and metabolite production. Chinnasamy et al. [30] used open and closed bioreactors for microalgae biomass accumulation. Lehr and Posten [31] employed PBRs to produce biofuel. Zhang et al. [32] analyzed the performance of a groove-type PBR for hydrogen production by immobilized photosynthetic bacteria. Pen et al. [33] designed an innovative membrane bioreactor for methane biohydroxylation. Furthermore, bioreactors have been widely used in many fields such as the chemical, pharmaceutical, material, environmental protection, and metallurgy industries. The development and optimization of bioreactors and their operating parameters are therefore a key focus of biochemical engineering.

Microbial biomass production involves a series of complex biochemical reactions that call for specific physicochemical properties of the reactants and appropriate transfer characteristics of light, mass, and heat [34]. A high solid liquid ratio is conducive to the mass and heat transfer process in microbial systems. The viscosity, turbidity, and homogeneity of the reaction liquid inside the bioreactor, as well as its physical properties (temperature, light intensity, pH, etc.), have important influences on the biomass production process. In other words, flow pattern, light penetration properties, as well as heat and mass transfer characteristics of the reaction liquid directly influence the microbial biomass production process.

2.3.2 Multiphase Flow

For the optimal design and operation of bioreactors, turbulent mixing of multiphase flows have been recognized as an important factor in determining the overall performance of the bioreactor [35]. In a well-mixed bioreactor, local turbulences can position the microorganism's cells randomly throughout the container and near the substratum sources. As a result, each individual cell is exposed to a suitable growth environment. A well-mixed bioreactor is also necessary to prevent cells from settling or attaching to the reactor walls. Free-floating cells allow for maximal gas exchange and prevent accumulation of excess metabolites that could inhibit growth. However, intense mixing can inhibit growth by causing high levels of shear stress and physical damage to the cells [36]. Therefore, appropriately controlled circulation is a key factor for the optimal design and operation of a bioreactor.

Several studies have investigated the optimum circulation dynamics of different types of bioreactors. Ninno and Power [37] investigated turbulent multiphase flows in a flat-panel bioreactor and their consequent effects on microalgae cultivation using Computational Fluid Dynamics (CFD) simulation and Particle Image Velocimetry (PIV). Liao et al. [38] conducted Lattice Boltzmann simulation on liquid flow and mass transfer in a bioreactor with a cylinder bundle for hydrogen production. Sikula et al. [39] developed a fermentation model in an internal loop

airlift bioreactor to enhance fermentation efficiency. Zhang et al. [40] studied multiphase flow in an anaerobic bioreactor with a multi-scale approach.

2.3.3 Heat and Mass Transfer

Heat and mass transfer in a bioreactor mainly include the transfer of light, heat, organic or inorganic matter, and metabolites. Most bioreactions are sensitive to temperature. Hence, it is essential to analyze the thermal dynamics of the microbial biomass production process and regulate heat transfer to achieve efficient biomass production.

Laukevics et al. [41] reported that steric hindrance, which encompasses the effects of geometry, mass transfer, and substrate availability, was partially responsible for limited microbial growth in the void spaces of the substrate bed. Rathbun and Shuler [42] reported that steep temperature gradients (reaching 50 °C in the reactor bed) inside the static bioreactor were sufficient to prevent the growth of microorganisms. The interaction between the complex phenomena of heat and mass transfer often leads to the development of steep concentration and temperature gradients, resulting in non-homogeneous conditions in the bioreactor and subsequent low efficiency. In addition, Rajagopalan and Modak [43] modeled the heat and mass transfer for solid-state fermentation (SSF) in a tray bioreactor. The extent of growth restriction due to inefficient heat and/or mass transfer was analyzed during different stages of fermentation. It is expected that this model can lead to a better understanding of the transport processes in SSF, thereby allowing optimization of bioreactor design for SSF. A different study by Valiorgue et al. [44] investigated CO_2 mass transfer and conversion to improve microalgae biomass accumulation in a horizontal gas-liquid PBR.

2.3.4 Energy Conversion

The potential for the production of biofuels or other valuable byproducts from biomass has recently been intensively investigated. However, many bottlenecks still exist and most of these processes are considered cost-prohibitive [45]. Open PBR systems like raceway ponds have proven to be the most cost-effective method to produce microbial biomass on a large scale but closed PBR technologies are still necessary to provide inoculum cultures for the large-scale systems [46]. Even for the production of high-value products, the cost of manufacturing and operating closed bioreactors can be restrictive. Therefore, there is much ongoing research examining and optimizing the cost-benefit ratio of PBRs. Jacoblopes et al. [47] investigated the biotransformation of carbon dioxide (CO_2) in PBRs. Murphy [48] designed an artificial leaf for biofuel production and improved the energy conversion efficiency in the bioreactor system. Moreover, many researchers have investigated the light energy conversion process and designed many kinds of novel bioreactors to improve the efficiency of energy conversion [49–52].

3   Bioreactors in Microbial Biofuel Conversion

Over-utilization of traditional fossil fuels has caused severe energy shortages and environmental damage. The combustion products of fossil fuels, like SO_2, NO_x, CO, CO_2, etc., are harmful to the environment. It is therefore necessary to develop renewable and environment-friendly energy sources [53]. Microbial biofuels are promising energy alternatives owing to prevalent raw materials, mild operation conditions, and clean combustion products. Currently, increasing efforts are being made to improve biofuel production using this promising approach. In order to maximize biofuel production, microbial cells require an optimal environment for growth. To maintain such favorable conditions for microbial growth and metabolism, bioreactors play an indispensable role.

Bioreactors, especially closed bioreactors, can provide the ideal milieu for microbial growth and metabolism. Microbial biofuel conversion is mainly divided into an upstream treatment process that includes fermentation for microbial growth and product generation, and a downstream treatment process that includes product purification, isolation, and collection [54]. In order to improve energy conversion efficiency, the specifications of the bioreactor should integrate not only the correct structural configuration but also precise operational control for optimized multiphase flow as well as heat and mass transfer in the reaction solution.

3.1   Application in Microbial Biofuel Conversion

Due to their adaptable operating conditions, bioreactors are widely used in different types of microbial biofuel conversion processes, such as biogas production by anaerobic digestion, hydrogen production by photo-fermentation or dark-fermentation, alcohol production by fermentation, and fatty acid production by microalgae. Microbes utilize a variety of substrates (cellulose, hemicellulose, starch, glucose, xylose, etc.) to produce biofuels. During the biofuel conversion processes, microbial cells are sensitive to variations in their surroundings, and any instability is detrimental to their growth and product synthesis. In bioreactors, the environmental parameters (temperature, pH, medium composition, retention time, mass and heat transfer rate, etc.) can be maintained at near-optimal ranges to enhance microorganism growth and product accumulation.

Anaerobic digestion is a biological process in which microbes metabolize organic substrates in the absence of oxygen to produce biogas [55]. This biogas is composed of a mixture of compounds, with methane and CO_2 as major contributors. Fermentative hydrogen production is an anaerobic reaction that has received substantial attention in recent years owing to advantages such as rapid hydrogen production rate, mild production conditions, and ease of operation. There are two

types of fermentative hydrogen production: photo-fermentative production and dark-fermentative production. Photo-fermentative hydrogen production is mainly catalyzed by photosynthetic bacteria, whereas dark-fermentative hydrogen production is mainly catalyzed by anaerobic bacteria. Alcohols and fatty acids can also be produced via anaerobic fermentation processes. Both alcohols and fatty acids are potential substitutes for petroleum-derived fuel as they have comparable properties to those of gasoline [56]. Types of alcohols that can be generated by fermentation include short-chain alcohols like ethanol and several higher alcohols like 1-butanol, isobutanol, 2-methyl-1-butanol and 3-methyl-1-butanol [56]. The most widely used form of alcohol is ethanol; however, being highly corrosive and hygroscopic, it is not conducive to the existing fuel storage and distribution equipment [57]. On the contrary, n-butanol, isobutanol, and other higher alcohols have a lower hygroscopicity compared to ethanol, with an energy density (27 MJ/L) close to that of gasoline (32 MJ/L) [58]. In addition, these higher alcohols are compatible with the existing fuel storage and distribution infrastructure. Fatty acids can be classified into three groups by the length of their carbon chains, i.e., short-chain fatty acids (less than 6 carbon atoms), mid-chain fatty acids (6–12 carbon atoms) and long-chain fatty acids (more than 12 carbon atoms) [59].

3.2 Bioreactors in Microbial Biofuel Conversion: The Fundamentals

A bioreactor represents the equipment in which biological reactions and microbial cell reproduction occur using enzymes or living cells as biocatalysts. The bioreactors can simulate the biological characteristics and physiological functions of microbial cells and tissues to synthesize target products. They are widely used in a variety of fields, like food and agriculture, health and medicine, energy, and environmental protection. In particular, bioreactors play an important role in microbial biofuel conversion where microbial catalysts generate biofuels like biohydrogen, biogas, alcohols and fatty acids. Research has developed various configurations of bioreactors with optimized operating conditions to maximize biofuel output [60]. The merits and limitations of each type of bioreactor are discussed below.

3.2.1 Configurations

Microbial biofuel conversion is a complex biochemical process that is greatly dependent on the configuration of the bioreactor where it occurs. Bioreactor design is usually conducted on an experimental basis, taking into consideration influencing factors like gas-liquid-gas multiphase flow, mass and heat transfer balance, and energy conversion efficiency. A bioreactor with superior performance requires a

watertight structure, high heat and mass transfer efficiency, good mixing performance, low energy investment, and high product output. Thus far, the most commonly used configurations include: (i) conventional anaerobic reactors such as the anaerobic sequencing batch reactor, the continuous stirred tank reactor, and the anaerobic plug-flow reactor; (ii) sludge retention reactors such as the anaerobic contact reactor, the up-flow anaerobic sludge bed reactor, the up-flow anaerobic solid-state reactor, the anaerobic baffled reactor, and the internal circulation reactor; and (iii) anaerobic membrane reactors such as the anaerobic filter reactor, the anaerobic fluidized bed reactor, and the expanded granular sludge blanket.

The conventional anaerobic reactor is a single-tank system that utilizes the same tank for substrate treatment and fermentation [61]. All steps of microbial biofuel conversion take place in a single tank, which means that downstream treatment processes as well as the intermediate byproducts can have significant negative influences on the upstream treatment processes. Thus, efficient approaches to avoid the interactive effects of different reactions are essential to enhance bioreactor performance.

The configuration of sludge retention reactors is relatively complex compared to the conventional reactors. Sludge retention reactors usually contain two main components: the liquid-phase reaction module and the solid-phase recycling or gathering module. For example, the anaerobic contact reactor contains an agitated reactor module and a solid phase setting module to recycle the microorganisms, whereas the up-flow anaerobic sludge bed reactor contains the liquid-phase reaction module at the top of the reactor and a dense sludge bed located at the bottom of the reactor. Sludge retention reactors provide good contact between wastewater and biomass, which prevents washout of microorganisms. They are often used to process effluents containing high concentrations of suspended solids.

Anaerobic membrane reactors are constructed with a supporting membrane to enhance contact between wastewater and the bacterial microorganism. The bacterial biofilm accumulates and grows on this supporting membrane, causing a separation between bacterial biomass and the wastewater in the reactor. For example, the anaerobic filter reactor contains a filter on which the bacterial biofilm grows. In the anaerobic fluidized bed reactor, inert particles like fine sand and alumina are provided for the thin bacterial biofilm to grow on. The configurations of anaerobic membrane reactors enhance the resistance of the microbes to inhibitors, thereby improving biofuel production.

3.2.2 Functions

In the microbial biofuel conversion process, bioreactors provide fine control of operating conditions for microorganism growth, metabolism, and product synthesis, thus improving biofuel production. For example, the pH can be maintained at suitable levels by adding buffer solutions, the temperature can be controlled by a thermostatic water bath, and the hydraulic retention time (HRT) of wastewater can be controlled by regulating the inward feeding rate. The structural configuration of a

bioreactor closely aligns with its functional advantages. Different structural characteristics are required for different applications of a bioreactor. For example, the leakage resistance of a bioreactor is critical when applied to biogas production. The function of conventional anaerobic reactors is to supply relatively stable operating conditions in an established temporal sequence. Owing to its simple structure, the sequencing anaerobic reactor has advantages of operational simplicity and low cost. However, the self-immobilization of the conventional anaerobic reactor is poor, and the channeling and clogging effects severe. These disadvantages limit reactor performance and biofuel conversion efficiency. The major function of sludge retention reactors is recycling of microbial biomass, thus avoiding biomass washout. These reactors rapidly achieve steady-state due to short hydraulic retention time [62]. In addition, some configurations of sludge retention reactors can have special functions. For example, in the anaerobic baffled reactor, the flow patterns of waste influents can be regulated by arranging the baffles, serving to separate acidogenesis and methanogenesis along the vertical axis of the reactor and allowing different bacterial communities to develop under independently suited conditions [63]. The function of the anaerobic membrane reactor is based on the supporting membrane material used for microbial biofilm formation, which serves to separate influents from microbial biomass. By generating this microbial biofilm, biomass washout can be avoided and the microbes have a longer retention time than the hydraulic retention time. As a result, the mechanical mixing and sludge settling that occur in sludge retention reactors can be avoided in anaerobic membrane reactors [64].

3.2.3   Influencing Factors

During the microbial biofuel conversion process, product yields are affected by many factors including temperature, pH, nutrient content, organic loading rate, type of reactor, hydraulic retention time and solids retention time [61, 65, 66]. In particular, bioreactor design is important for applications of biochemical engineering. The design of a bioreactor includes determination of operating conditions, reactor size, mixing and mass transfer capabilities, temperature and sterility conditions, the means of feed introduction and product removal, and control of operating variables such as pH, oxygen concentration, and illumination [67]. Reactor size and shape usually influence biofuel output capacity. Increasing the size of the container can improve biofuel production to some extent, but can also cause biomass concentration gradients in the reactors, which hinders biofuel production. Bioreactors operated at low temperature are less prone to thermal instability and degradation. However, since some thermophilic bacteria prefer high ambient temperatures of up to 65 °C, bioreactors must maintain the standard for thermotolerance. Generated byproducts can dissolve and accumulate in the bioreactor over time, inhibiting microbial growth and metabolism. Thus, in order to maximize the efficiency of microbial biofuel conversion, bioreactor design must incorporate some mechanism to quickly remove such byproducts.

3.3 The Importance of Bioreactors in Microbial Biofuel Conversion

3.3.1 Ideal Site for Microbial Metabolic Reactions

By appropriately controlling the operating conditions, bioreactors provide a near-optimal environment for biofuel conversion reactions. Inside the bioreactor, biogas is produced via the degradation of organic substrates, cycling consecutively through hydrolysis, acidogenesis, acetogenesis, and methanogenesis [68]. Firstly, the fermentative microbes excrete hydrolytic enzymes that break down complex carbohydrates, lipids, and proteins into soluble monomers and oligomers, long-chain fatty acids, and amino acids, respectively. Then, these soluble molecules are converted into volatile fatty acids, CO_2, alcohols, and hydrogen by acidogenic microbes. Next, the volatile fatty acids and alcohols are converted into acetic acid and hydrogen via acetogenesis. Finally, the acetic acid, CO_2, and hydrogen are converted into methane through acetotrophic, hydrogenotrophic, and methanogenic reactions [69]. A bioreactor designed to incorporate the physiological requirements of several different microbial communities (acidogenic bacteria, acetogenic bacteria, and methanogenic bacteria) is necessary to maximize biogas production from anaerobic digestion.

In photo-fermentative hydrogen production, the degradation of organic substrates generate electrons that need to be eliminated to maintain electrical neutrality of the system [70]. Surrounding protons act as electron acceptors, thereby generating hydrogen (H_2). Fermentative hydrogen production can be described by Eq. (1) when microorganisms use glucose as the organic substrate. The glucose is first converted to pyruvate and NADH (the reduced state of nicotinamide adenine dinucleotide) via the glycolytic pathway. Then, the pyruvate is converted to acetyl coenzyme A (acetyl-CoA), CO_2 and H_2 by pyruvate-ferredoxin oxide-reductase and hydrogenase enzymes [65, 66].

$$C_6H_{12}O_6 + 6H_2O \rightarrow 6CO_2 + 12H_2 \qquad (1)$$
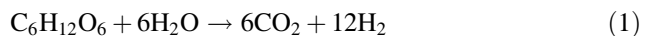
To produce alcohols, microorganisms first reduce primary metabolites like acetyl-CoA and pyruvate and then elongate them into electron-rich compounds like higher carbon acyl-CoA and 2-keto acids. Then the electron-rich compounds are further reduced into higher alcohols by microbial metabolism and secreted into the medium [58]. Similarly, fatty acids are produced through an anaerobic process involving hydrolysis and acidogenesis. During hydrolysis, complex organic polymers are broken down into simple monomers by specific enzymes. Subsequently, during acidogenesis, acidogens ferment the monomers into fatty acids (acetic acid, propionic acid, butyric acid, etc.). Fatty acids can also be produced by photosynthetic bacteria (like algae and cyanobacteria) through photosynthesis. All these microbial biofuel conversion reactions are conducted in bioreactors and are discussed in the following text.

3.3.2   Biomass Cultivation

Another important role of the bioreactor is to provide a suitable environment for microbial reproduction, namely microbial biomass cultivation. Biofuel production is collectively determined by both microbial biomass concentration and specific biofuel production capacity. A bioreactor with high biofuel production requires high biomass concentration as well as high specific biofuel productivity. However, the robust growth of microbes and high specific biofuel productivity are mutually exclusive, especially for microalgal lipid production [71]. When microalgae are cultivated in optimal conditions for growth, the lipid content in the cells is usually poor [72]. Conversely, when microalgae are cultivated in optimal conditions for lipid synthesis, microalgae growth is usually slow. As a result, overall lipid productivity is rarely improved.

3.3.3   Multiphase Flow

Microbial biofuel conversion requires a typical multiphase flow system in which all three phases (gas, liquid and solid) coexist. The gases present in the bioreactor are mainly H_2, CO_2, and O_2 produced by the metabolism of microbes and algae, the liquid phase consists primarily of influents like wastewater, and the solid phase consists of the microbial biomass and particles suspended in the influents. The gases produced by microbial metabolism exist in the reaction solution as bubbles and rise to the top of the bioreactor by the force of buoyancy. The rising bubbles create a constant flow of the liquid solution and the microbial biomass, and the flow patterns are influenced by bioreactor shape and size. For example, the up-flow anaerobic sludge bed reactor permits upward circulation, whereas the anaerobic baffled reactor allows alteration of this flow pattern by adjusting the position of the baffles. Aside from the structural configuration of the bioreactor, mixing method can also alter multiphase flow characteristics of the system. An efficient mixing method is particularly important in photo-fermentative hydrogen production since mixing is beneficial for the effusion of hydrogen from the reaction solution and can prevent the inhibitory effect caused by hydrogen dissolution in the reaction liquid [73]. In conclusion, the flow characteristics and rheological properties of multiphase flow systems can significantly influence mixing and contact between the microbes and the liquid solution. They can also influence the heat and mass transfer between different phases in the bioreactor, which are important factors affecting the growth and metabolism of the microorganism.

3.3.4   Heat and Mass Transfer

Inside a bioreactor, heat and mass transfer characteristics of the reaction solution directly influence the microbial biofuel conversion processes. For example, dissolved hydrogen concentration (i.e., hydrogen partial pressure) negatively affects

the metabolism of photosynthetic bacteria by decreasing the mass transfer efficiency of hydrogen. In other words, when hydrogen concentration in the reaction solution is high, the mass transfer efficiency of hydrogen is reduced, hindering the productivity of the microbes [34]. Thus, removal of dissolved hydrogen from the reaction liquid by adjusting the operating conditions (temperature, pressure, etc.) is important to enhance mass transfer and subsequent hydrogen yield. Temperature and pressure can affect mass transfer characteristics by influencing the physical and chemical properties of the reaction solution. The surface tension of the reaction solution, density, viscosity, diffusion coefficient of the solute, and the individual properties of reaction byproducts also influence the mass transfer characteristics of the system [34, 74]. In general, mixing is the simplest way to enhance mass transfer efficiency, but the shear effect of the mixing wheels and the heat generated in the reaction liquid have a negative impact on microbial metabolism. Therefore, reduction of the shear effect and improvement of heat transfer are essential. There are many factors that influence the heat transfer efficiency of a bioreactor: the physical and chemical properties (thermal conductivity, specific heat, etc.) of the solution, the rheological properties (i.e., viscosity) of the reaction solution, flow characteristics of the solution, and ambient conditions (temperature, light intensity, etc.) [75]. Along with the running of the bioreactor itself, the heat produced by exothermic biochemical reactions gradually increase the internal temperature of the bioreactor. Thus, strategies to dissipate this accumulated heat by enhancing heat transfer and evaporative heat loss are important to keep the reaction solution at a temperature range conducive to maximal bacterial activity.

3.3.5   Energy Conversion

Transformation of energy sources (like organic substrates and light) to energy-containing products (biogas, hydrogen, fatty acids, alcohols, etc.) is a key purpose of a bioreactor. Researchers have explored several strategies to improve the conversion efficiency of the substrate or light energy. Maximal exploitation of the energy source is necessary to enhance energy conversion efficiency. For example, high light intensity, large illuminated surface area, and reasonable light distribution in bioreactors are effective methods to improve light conversion efficiency in the photo-fermentative hydrogen production process [34, 76]. However, excess light exposure significantly reduces light energy conversion efficiency by dissipating the light [77]. In theory, the highest light energy conversion efficiencies that can be achieved from microalgae biomass in the photo-fermentative hydrogen production process and in the lipid production process are 10% and 12%, respectively [78, 79]. But in reality, the actual efficiencies are very low due to light shading and scattering effects, which stand at about 8% in photo-fermentative hydrogen production [80] and 6% in lipid production via microalgae cultivation [81]. Similarly, the energy conversion efficiency of most fermentation processes is poor because the structure and composition of the fermentative substrates (with cellulose and hemicellulose components) are very complex. The conversion of cellulosic substrates to biofuels

requires deconstructing the robust outer structure to release the interior mass for further fermentation, and this step is a key limiting factor for high-energy conversion efficiency. Thus, researchers have proposed that cellulosic substrates undergo pretreatment methods to increase their surface area and porosity, while decreasing cellulose crystallinity and polymerization [82]. Commonly used pretreatment strategies include mechanical methods like milling and extrusion, thermochemical methods like pyrolysis, steam explosion, high pressure, and ammonia fiber explosion, physicochemical methods like alkali treatment, acid treatment, and gas oxidizing treatments, and biological methods like microbial deconstruction and enzymatic deconstruction [83]. Results from testing such methods showed that pretreatment of substrates can effectively improve substrate accessibility for energy conversion. For example, Dale et al. [84] demonstrated that hydrolysis yields in the reduction of sugar reached 90% of the theoretical yields after using the ammonia fiber explosion method to pretreat the lignocellulose substrate.

4 Bioreactors in Microbial Electrochemical Systems

Microbial electrochemical systems (MESs) exploit the metabolism of microorganisms to bio-electrochemically convert low-grade chemical energy stored in biodegradable substrates to high-grade energy (i.e., electricity) and value-added chemicals like hydrogen and methane [85]. As a rapidly evolving technology, MESs have been successfully implemented to treat wastewater for electricity generation (using microbial fuel cells; MFCs) and in biorefinery facilities (using microbial electrolysis cellss; MECs and microbial electrosynthesis; MEs). Specific applications include wastewater treatment [86, 87], power sources for remote sensors [88], research platforms for electrode-bacteria interaction [85, 89], and value-added component production [90–93]. Compared with other biological processes, MESs show higher versatility and lower sludge production [94], making them very promising in practical applications.

The substrates used in MESs can vary greatly from glucose, acetate, lactate, and dyes to domestic wastewater containing complex species [95]. Typically, these biodegradable substrates are electro-oxidized at the anode via bacterial metabolism to produce electrons and protons. Then, the electrons are conducted to the cathode and are accepted by oxygen, nitrate, or metal ions. After decades of research and development, the performance and stability of MESs have approached industry standards. It is predicted that MFCs can potentially produce 23.3 and 40 TWh of electricity from wastewater in India by 2025 and 2050, respectively [96]. Their long-term operational stability has also been verified. Zhang et al. [97] installed and operated two MFCs in a municipal wastewater treatment plant for over 400 days. The two MFCs showed great durability in COD (chemical oxygen demand) removal and fluctuation tolerance, demonstrating the long-term effectiveness of this technology outside the laboratory.

At the heart of an MES lies the bioreactor, where biodegradable substrates are converted to electrical current. The current is utilized directly (in MFCs) or conducted to the cathode for further reaction (in MECs). Therefore, the performance of an MES is dictated by the performance of the bioreactor within, where scientific disciplines like microorganism ecology, biomaterials science, mechanical engineering, and control strategy meet multiphysics phenomena like biofilm formation, multiphase flow, heat/mass transfer, and bio-electrochemical conversion.

This section aims to provide a fundamental and comprehensive overview of the bioreactors used in MESs, detailing principles in each transport phenomenon that play an important role in overall system performance. Perspectives on future development and optimization will also be discussed.

4.1 Application in Microbial Electrochemical Systems

For a typical wastewater treatment plant, about 45–75% of the energy needed is consumed by aeration treatment step [98]. In 2006, nearly 3% of all the electrical power produced in the U.S. ($\sim$110 TWh per year) was consumed by wastewater treatment [99]. Similarly, wastewater treatment constitutes up to 3–5% of the United Kingdom's national electricity consumption [100]. This demand is expected to increase further due to growing human population and higher environmental protection standards. If aspiring to the profitable operation of MESs, the energy cost has to be significantly reduced. On the contrary, wastewater has great potential for energy recovery; a report in 2004 indicated that domestic, industrial, and animal wastewater together contain $\sim$1.50 TWh of potential energy output in the U.S., which is higher than the power required for wastewater treatment [101]. Additionally, the energy-consuming aeration step can be replaced by MEs treatment; this would entirely eliminate aeration power consumption and allow the net power produced (10–20% of the aeration power) to be recycled for other processes within the MES. This strategy could make wastewater treatment commercially competitive.

Recently, Wang et al. reviewed the diverse applications of MESs, assessing 47 different functions and system configurations [85]. Figure 2 shows the basic principles of four typical MESs. Among these, MFCs are the most common application of MESs, converting the chemical energy stored in both the electron donor (i.e., the substrate) and electron acceptor (i.e., the oxidant) into electricity (Fig. 1a). A typical MFC consists of two chambers: the anaerobic anode chamber where microorganisms generate electrons via electro-oxidation of organic substrates and the aerobic cathode chamber where the reduction reaction takes place with oxygen or other chemicals. These two chambers are separated by an ion exchange membrane or a salt bridge to allow ion transport. Electrons produced by microorganisms are transferred to the anode by direct or indirect extracellular electron transport and
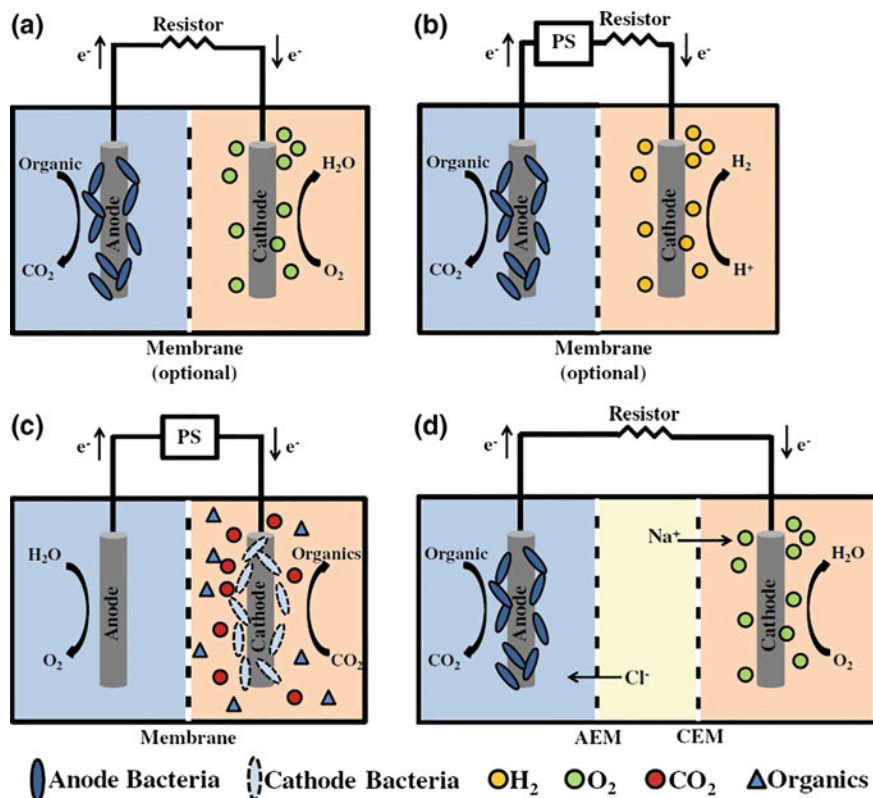
Fig. 2 Principles of four typical MESs (left chamber: anode; right chamber: cathode). **a** Electricity generation in air-cathode microbial fuel cells (MFCs); **b** hydrogen generation with external power supply in microbial electrolysis cells (MECs); **c** chemical production by microbial electrosynthesis (MES); **d** middle chamber desalination in microbial desalination cells (MDCs). (adapted and reprinted from [85], Copyright 2013, with permission from Elsevier)

are conducted to the cathode through an external circuit. Protons and other ions migrate through the membrane to complete the circuit. When an external power source is applied to increase the cathode voltage (0.6–1.0 V) for hydrogen production, the MFC is transformed into an MEC (Fig. 1b), where the mobile H^+ in the cathode chamber is reduced by the cathode to form H_2 or hydrogen gas [102]. This strategy provides a fundamentally new approach to hydrogen production that outperforms the traditional water-split (requiring a voltage higher than 1.2 V) and dark-fermentation methods in terms of power consumption and production rate. It was also noted that the produced H_2 can be further consumed by methanogenesis to produced methane (Fig. 1c) [102–104], especially in a single-chambered MES. In addition, the inner electrical field between the anode and cathode can be utilized to drive water desalination. For this application, the conventional ion exchange membrane is replaced by a thin chamber, sandwiched by an anion exchange

membrane (AEM) and a cation exchange membrane (CEM). Upon operation, the inner electrical field drives the anions (e.g., Cl^-) and cations (e.g., Na^+ and Ca^{2+}) to migrate through the AEM and CEM towards the anode and cathode, respectively, thereby desalinating the salt water present in the thin chamber (Fig. 1d). Cao et al. [105] were the first to describe this novel approach. A high desalination efficiency of 90% was achieved in a single cycle, outperforming traditional, energy-intensive water desalination technology.

The energy source of MEs systems comes from microbial metabolism at the anode. Limited by the activity and conversion efficiency of these microorganisms, MESs are more suitable for treatment of domestic wastewater than for treatment of industrial wastewater that contains heavy metal ions and chemical toxicants. In order to meet the strict environmental standards for domestic wastewater treatment, the concentration of organic components and nutrients like nitrogen and phosphorus need to be reduced. Numerous studies have shown excellent MEs performance in decreasing organic components (99% acetate removal was achieved in [106]), but the removal of nutrients requires aerobic conditions not compatible with the anaerobic conditions at the anode [86]. Wang et al. [107] developed a novel electrochemical membrane bioreactor, in which wastewater was treated by the microorganisms at the anode and then filtered at the cathode, releasing a final effluent of high quality. This study highlighted the possibility of simultaneous wastewater treatment and net energy production in an MES. Kelly and He [86] reviewed the influencing factors and challenges for nutrient removal and recovery in various MESs including MFCs and MECs. In addition, Nam et al. [108] demonstrated that a high nutrient concentration can negatively affect power generation by MFCs; specifically, an initial concentration of TAN (total ammonia nitrogen) over 500 mg N L^{-1} strongly decreased electricity production in MFCs by inhibiting the anode-attached bacteria. The peak power density dropped by 59% when the initial TAN increased from 500 to 4000 mg N L^{-1}. For simultaneous COD and nutrient removal, configuration innovation and system integration are needed. Gao et al. [109] proposed an integrated system that combined an MFC and an electric membrane bioreactor. In this configuration, the effluent from the MFC was driven to flow through an air-contact oxidation bed and trickling filter to enhance TAN removal by leveraging the aeration effect. The efficiency of both COD and TAN removal exceeded 93% in this system.

Although significant strides have been made in the development of MESs, their performance (in terms of power density) is still lower than the industry standard of 1 kW m^{-3}. Exceptions to this do exist in several microscale bioreactors that have achieved industry-level values for power density [86, 94]. Factors that have potential for improvement include the following: (i) biomass and microorganism catalytic activity; (ii) mass transport between bulk and reactive region; (iii) electron transport between microorganisms and solid electrodes; and (iv) material conductivity and durability.

4.2   Bioreactors in Microbial Electrochemical Systems: The Fundamentals

MESs employ the electrochemical activity of certain microorganisms that oxidize organic or inorganic (e.g., sulfides) substrates to produce electrons during their anaerobic respiration. These electrons are transferred to solid electrodes either directly via membrane-bound protein structures such as nanowire and c-type cytochrome, or indirectly using mobile redox electron shuttles [85]. As a result, a negative anode potential of about −0.2 V versus SHE (Standard Hydrogen Electrode) is obtained. Meanwhile, due to the sluggish reaction kinetics with non-precious metal catalysts, the cathode potential can only reach about +0.3 V, together providing an open circuit voltage of +0.5 V [101]. The efficiencies of the reaction at the anode and of electron transport are the cornerstones of the MES, and they are currently the limiting factors of overall system performance [94]. It should be mentioned that an exhaustive electron transfer mechanism remains to be established, and the interactions between direct and indirect electron transfer methods still need further investigation. Both the anode and cathode reactions are usually conducted in different chambers of the bioreactor, at least one of which is catalyzed by microorganisms. Therefore, the bioreactor plays a significant role in the bio-electrochemical reaction rate and electricity production.

4.2.1   Configurations

As described above, a typical MES consists of two chambers: the anode chamber for electron production and the cathode chamber to close the circuit and yield the final products. MESs have evolved from typical two-chamber configurations to single-chamber and hybrid designs. Novel modes of operation like the up-flow mode have also been developed. In a two-chamber MES, aqueous and gaseous substrates are bio-electrochemically degraded to produce electrons in the anode. These electrons are transferred to the cathode, resulting in electricity production or product generation. The first single-chamber MFC was described by Liu et al. [110] as shown in Fig. 3a. They demonstrated that atmospheric oxygen can passively diffuse into and react with the porous hydrophobic cathode. Plain anode and cathode can also be used to form a single-chamber MES bioreactor (Fig. 3b). Single-chamber MFCs are capable of treating wastewater with a high concentration of nitrogen [106], although ammonia inhibition was still observed. The maximum power density decreased from 6.1 to 1.4 W/m^3 when TAN concentration increased from 3500 to 10,000 mg/L. One concern for the single-chamber MFC is that a large percentage of the organic substrate is lost without contributing to electricity production [110].

From a geometric perspective, both the single- and double-chamber MESs can be engineered to form a tubular configuration. This configuration is considered very promising due to increased sludge retention time and reduced hydraulic retention
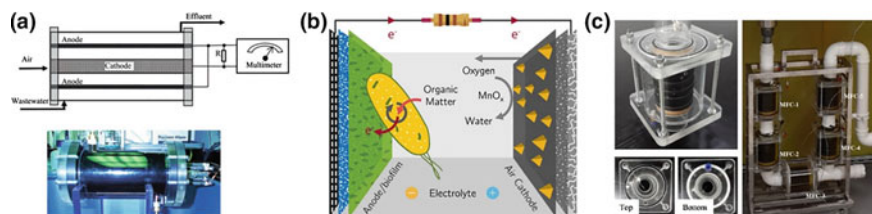
Fig. 3 Configurations of microbial electrochemical systems (MESs). **a** Schematic and prototype of the first single-chamber MFC (adapted and reprinted from [110], Copyright 2004, with permission from American Chemical Society), **b** Schematic illustration of a single-chamber MFC with plain anode and cathode (adapted and reprinted from [111], Copyright 2016, with permission from Elsevier), **c** Tubular two-chamber MFC, and 5 MFCs were connected to form a stack and integrated into a sink drain pipe (adapted and reprinted from [112], Copyright 2016, with permission from Springer)

time. More importantly, tubular MESs can be readily integrated to fit into existing facilities [100]. Rabaey et al. [113] proposed a tubular single-chamber MFC using packed granular graphite as the anode and a woven graphite mat as the cathode. Ye et al. [112] developed tubular two-chambered MFCs using PMMA (Polymethyl Methacrylate) tubes of different diameters; the inner tube and the interspace served as the anodic and cathodic chambers, respectively. Five of these MFCs were integrated into a sink drainpipe for kitchen wastewater treatment (Fig. 3c). The flushing process was found to disturb the performance of the MFC, but only for a few minutes. On the contrary, an irreversible drop in MFC performance was observed after flushing the substrate at 50 °C. Conventional tubular two-chamber MFCs usually have a concentric cylinder configuration (Fig. 3c), where a cation exchange membrane covers the inner cylinder to segregate the anode and cathode chambers and to allow proton transport. However, many other configurations have also been developed. Li et al. [114] proposed a single-chamber MFC with a cathode on either side of the anode chamber. Their results showed that the volumetric power density was positively correlated with the ratio between cathode surface area and anode volume, implying that a larger cathode surface area can lead to better performance.

Recently, the unique advantages of miniaturized platforms (i.e., microfluidics and lab-on-a-chip devices) in microbial research have been recognized. These methods provide better microenvironment manipulation for cell and biofilm culturing, as well as high-throughput and time-effective approaches for characterization [89, 115–118]. In addition, by leveraging advanced microscopy technologies as a powerful research tool, microfluidic chips enable real-time and in situ imaging even at a single-cell level [119]. Qian et al. [120] developed a two-chamber MFC with an anode chamber volume of 1.5 μL to investigate microbe-anode interaction, and succeeded in enhancing biofilm growth on the anode electrode. Qian et al. [121] also developed a PDMS (Polydimethylsiloxane)-fabricated MFC with a chamber volume of 4 μL. This MFC showed faster start-up and higher power density. Their results suggested the volumetric power density was inversely

correlated with chamber volume. However, one major challenge that still hinders the application of miniaturized platforms is the clogging that results from the growth and aggregation of microorganisms over time [122].

4.2.2 System Integration

The output of a single bioreactor is usually insufficient for most applications. One promising approach to this problem is to combine several bioreactors to form a stack, which improves productivity and efficiency. For example, several MFCs can be hydraulically and electrically connected to form an MFC stack. This approach does not affect the coulombic efficiency of individual fuel cells but can increase the total power output and COD removal efficiency [123]. Ledezma et al. [124] demonstrated the first self-sustainable MFC stack that is not only self-sufficient (in terms of feeding, hydration, sensing, and reporting), but can also produce sufficient net power output to run peristaltic pumps. Research has revealed that MFC configuration, as well as the hydraulic and electric connections in stacked MFCs, have to be properly engineered to avoid short-circuiting and to fulfill the requirements of the desired application. One major challenge for MFC stacks is voltage reversal (where one or more MFCs reverse polarity), which results in severe deterioration of the MFC system as a whole. Oh and Logan [125] investigated voltage reversal in two air-cathode MFCs connected in series. They found that the MFC voltage can reverse under conditions of low fuel or in the absence of bacterial activity. They suggested the development of a control strategy that isolates the reversed MFC while still maintaining power output from the remainder of the stack. In order to avoid voltage reversal of any one fuel cell, all the cells in the MFC stack need to have exceptionally consistent performance characteristics. This is quite challenging in practice, especially when the cells are hydraulically connected in series. Alternatively, electrical engineering approaches can be utilized to mitigate voltage reversal. For instance, capacitors can be integrated into a serially connected MFC stack to accumulate charge, which would prevent voltage reversal and enhance power output [126, 127]. Kim et al. [127] integrated an MFC stack with two sets of multiple capacitors, which were alternately charged and discharged at a frequency of 1 Hz. The capacitors were charged in parallel to avoid voltage reversal of the MFC stack but were discharged in series to increase the voltage output ($\sim$2.5 V). Wu et al. [128] developed a DC/DC booster circuit to increase the voltage of an MFC stack to more than 3 V. However, one commonly ignored issue is that an MFC stack is merely a composite of single or double-chamber MFCs, and therefore suffers from the same disadvantages as individual cells. For example, single-chamber MFCs suffer from decreased coulombic efficiency [129]. Double-chamber MFCs suffer from anode chamber acidification, which is amplified when multiple two-chamber MFCs are hydraulically connected in series due to the gradual accumulation of protons in downstream cells [130, 131]. Yang et al. [132] found that the aerobic oxidation of acetate by the microbial biofilm at the cathode of the single-chamber MFC was able to remove accumulated H^+ in the medium. Therefore, they proposed a hybrid MFC stack that combined single- and
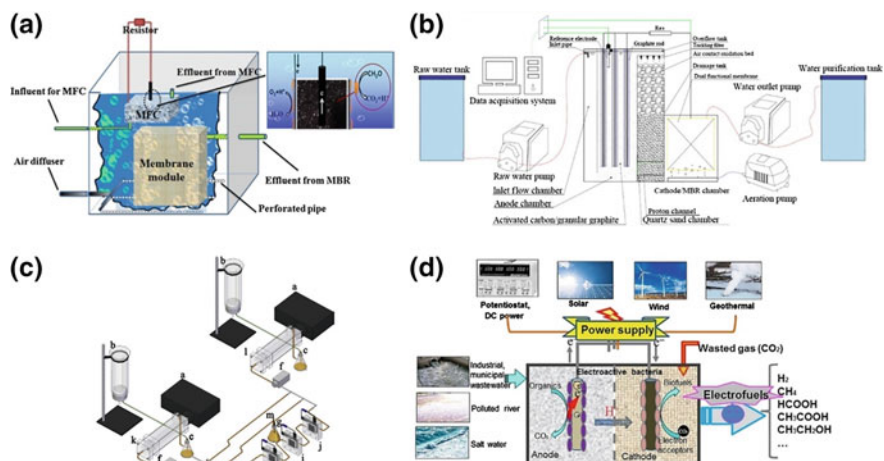
Fig. 4 Schematic illustration of typical integrated MESs. **a** An integrated MFC-membrane bioreactor (MBR) system. The oxygen in the MBR aeration tank was further utilized by MFC for electricity generation and more efficient treatment (adapted and reprinted from [134], Copyright 2012, with permission from Elsevier), **b** a combined system with MFC and electric membrane bioreactor (EMBR). This system exploited the hydraulic pressure difference between the anode and cathode chambers to drive the MFC effluent to flow through an air contact oxidation bed and trickling filter for enhanced nitrogen removal (adapted and reprinted from [109], Copyright 2017, with permission from Elsevier), **c** a combined MFC and photosynthetic biohydrogen reactor (PBR) system. The effluent from upstream PBR was treated by MFCs to remove inhibitory byproducts and protons, enhancing the performance of downstream PBR (adapted and reprinted from [135], Copyright 2013, with permission from Elsevier), **d** MESs can also be integrated with renewable energy systems to maximize the energy efficiency (adapted and reprinted from [136], Copyright 2017, with permission from Elsevier)

double-chamber MFCs to achieve self-sustaining pH control and avoid anodic acidification.

Bioreactors do not serve as stand-alone devices; they need to be integrated with other MESs and even other energy systems for maximum performance and energy efficiency. Liu et al. [133] proposed an integrated MFC-SBR (sequencing batch reactor) for the activated sludge process. The MFC was submerged into the SBR, synthetic wastewater was fed to the MFC first, and the resulting effluent was processed by the SBR. The oxygen for the aeration process was shared by the MFC biocathode to further recover electrical energy and reduce the cost of operation. Wang et al. [134] integrated an MFC and a membrane bioreactor (MBR) to develop a hybrid system (Fig. 4a) where the excess oxygen in the aeration chamber of the MBR was used to enhance the cathode performance of the MFC and the electricity produced by the MFC partially offset the overall energy cost. Gao et al. [109] proposed an integrated system with an MFC and an electric MBR. The conventional proton exchange membrane was replaced with a quartz sand chamber (Fig. 4b). The effluent from the MFC was run through an air-contact oxidation bed

and trickling filter to exploit the aeration reaction for nitrogen removal. This hybrid system achieved >93% efficiency in COD and TAN removal, and 50% efficiency in phosphorus removal. Li et al. [135] integrated two photosynthetic biohydrogen reactors (PBR) with three MFCs to form a PBR1-MFCs-PBR2 system to produce additional hydrogen from PBR2 (Fig. 4c). The idea was to utilize the MFC to degrade soluble intermediate products (e.g., lactate, propionate, and butyrate) generated from PBR1 thereby (i) removing excess H^+ for pH adjustment and (ii) changing the volatile fatty acid composition to facilitate hydrogen production in downstream PBR2. The results showed that this configuration outperformed traditional series-connected PBR systems (PBR1-PBR2) by reaching a 15-fold increase in hydrogen production rate, and also surpassed conventional pH adjustment methods (PBR-pH regulation-PBR2) by achieving a fourfold improvement in hydrogen production rate.

MESs can also be coupled to renewable energy sources (e.g., solar, wind, and geothermal energy) to maximize the energy production of the entire system (Fig. 4e). These renewable energy sources are naturally intermittent and their power output is not as stable as conventional power plants, which leads to big fluctuations and potential risks for the electric grid [137–139]. Alternatively, the electricity produced by these renewable sources can be used to power MESs, within which reactions are mild and can easily be started or stopped. Before successful execution of this strategy, the electrical and material (e.g., substrate and oxygen) flux at both the bioreactor and system levels should be properly distributed and regulated for safe and efficient operation.

4.2.3   Influencing Factors

Since MES performance is dominated by bio-electrochemical reactions, it is expected that factors affecting reaction kinetics such as external resistance, operation mode, and environmental elements will have a significant influence on MES performance. Aelterman et al. [140] studied the electrochemical performance of MFCs with different three-dimensional electrodes. Their results showed that lowering the external resistance from 50 to 10.5 Ω increased the kinetic capacity of the microbes in the bioreactor and caused a threefold increase in electricity generation. The authors suggested that an MFC should be operated at an external resistance closely matching its internal resistance, in order to increase COD loading rate and subsequent electricity production. Zhang et al. [141] performed a detailed investigation of the effect of external resistances on biofilm formation and electricity production in MFCs. When external resistance was decreased from 1000 to 50 Ω, the maximum power density increased by $\sim 181\%$. On the contrary, an even lower external resistance of 10 Ω caused a decrease in MFC performance due to low biomass activity and high extracellular polymer content in the biofilm. This study demonstrated that biofilm structure plays a crucial role in MFC performance.

Continuous and batch modes are the two typical modes of operation for MESs. In continuous mode, the substrate and catholyte are fed into the MES continuously,

whereas in batch mode, they are fed in all at once and then stored in the MES chamber for subsequent treatment. Although it is still unclear whether continuous mode outperforms batch mode in terms of performance and energy efficiency, the continuous mode of operation does have the advantage of being more productive, less labor-intensive, readily regulatable, and easier to control [96]. Kim et al. [106] compared the performance of a single-chamber MFC operated in either continuous or batch mode. They found that the MFC operated in continuous mode showed much higher TAN tolerance and sustained a 6.5-fold increase in TAN concentration when compared to the MFC in batch mode. However, a relatively long acclimation period of 40 days was required to achieve optimal electricity production in continuous mode.

Zhang et al. [142] investigated the effect of anolyte recirculation in MFCs with a floating air-cathode. Their work suggested that recirculation rate has a significant influence on proton transfer, fuel cell performance, and coulombic efficiency. Patil et al. [143] investigated the effect of temperature on biofilm formation and performance in MESs. They found that high temperatures not only accelerate biofilm formation but also increase biofilm activity. On the contrary, when the operating temperature was low, biofilms grown at low temperatures outperformed those grown at higher temperatures, implying the existence of a compensatory biological mechanism that accommodates environmental factors like temperature. The same study also found that the temperature limit for biofilm growth was approximately 0–50 °C, in which range the biofilm can adjust reversibly to temperature fluctuations.

4.3 The Importance of Bioreactors in Microbial Electrochemical Systems

4.3.1 Biomass Cultivation

The functionality of MESs relies on the anode reaction, which means that their performance is dominated by the metabolic activity of microorganisms [94]. A strong correlation between microbial metabolic rate and growth rate has been observed [96], implying that growth rate can be used as an indicator to predict biofilm performance. The stability of the microbial biofilm is dictated by substrate transport and the chemical signaling between multiple species [144]. Bhattacharjee et al. [144] fabricated surfaces with different topographies to regulate biofilm growth. Biofilm morphology was found to strongly correlate with the topography of the membrane material. Fluid flow is known to affect the three-dimensional morphology and bacterial communities forming the biofilm by generating shear stress and regulating molecular transport. Thomen et al. [145] developed a microfluidic platform that enabled hydrodynamic control and in situ observation of biofilm development. They determined the shear stress threshold for biofilm formation.

Hydrodynamic shear stress was found to regulate biofilm growth by controlling oxygen distribution.

Proton transport between the reaction solution and the biofilm also has a significant influence on the performance of the microbial biofilm. It has been shown that the protons accumulated inside the microbial biofilm can induce acidification, which severely inhibits biofilm metabolic activity [130]. Several methods have been proposed to mitigate this acidification, either by operating the bioreactor in continuous mode or by adding a buffer to regulate the pH of the surrounding milieu. Li et al. [146] proposed a new method to overcome acidification by periodically reversing the polarity of the MFC, thereby neutralizing the accumulated protons and hydroxyl groups. In addition, they showed that polarity reversal further enhanced the anode and cathode performance. Long-term stability (>4 months) with an ultra-low phosphate buffer concentration of 5 mM was also demonstrated. Yang et al. [132] proposed a hybrid MFC stack that utilized single-chamber MFCs to remove the accumulated H^+ produced by the double-chamber MFCs. Liao et al. [147] proposed to operate an MFC in alkaline media, as they found that the MFC operated with a repeating pH sequence (pH 7-8-9-8-7) achieved the highest performance. Electrochemical and biological analyses confirmed that the enhanced fuel cell performance was induced by the synergistic effects of highly active biomass and low internal resistance.

In addition to the reactions at the anode, the biomass in the cathode chamber can also contribute to enhancing reaction kinetics and producing bio-product. Park et al. [148] showed that the cathodic biofilm contributed to removal of organic components and nitrogen. Commault et al. [149] demonstrated that microalgae at the cathode can generate oxygen via photosynthesis to improve cathode reaction kinetics, resulting in a 100% increase in maximum power density. In addition, the cathodic microalgae also contributed to ammonium removal and algal biomass production. However, it was noted that the cathode biofilm can induce irreversible alkalization by inhibiting clearance of hydroxyls, also known as air-cathode biofouling [150]. Since cathode biofouling can be compensated by gradually increasing anode performance, it cannot be directly detected from the polarization curve [151]. Oliot et al. [151] developed a novel MFC enabling easy air-cathode replacement. Their results suggested that replacing the air-cathode can enhance fuel cell performance by 108% and 180% for anode areas of 9 and 50 cm^2, respectively. This study acknowledged the existence of biofouling and proposed a promising solution.

Significant effort was focused on increasing biomass production and enriching specific microorganisms that directly contribute to electron generation; however, little is known about the competition and evolution of microorganisms after inoculum [100]. As a result, one can only tune the system's performance using empirical correlations, which are quite apparent and facility-dependent. There is a long-standing debate over whether mixed microorganism cultures can outperform pure cultures. Increasing evidence points toward the mixed microorganism cultures, which show higher productivity and better tolerance to environmental impacts [152, 153]. Other benefits include substrate flexibility and less maintenance.

Conversely, mixed cultures normally involve several competitive bio-electrochemical processes and the electrosynthesis production efficiency exhibits considerable fluctuations [154, 155]. In order to target practical applications like the treatment of real waste materials (e.g., municipal and industrial wastewater, and biomass wastes), at least two types of microorganisms should be cultured in the MESs: one to break down complex polymers like cellulose and another to convert the resulting small molecules into electrons.

4.3.2 Mass Transport

Transport phenomena are crucial for MES performance, from the biofilm level (intracellular transport of biomolecules and extracellular transport of electrons/signal molecules) to the electrode level (substrate/product transport near the electrodes) and even at the bioreactor level (two-phase transport inside the anode and cathode chambers). In this section, we will focus mainly on the electrode and bioreactor levels.

As mentioned above, MES performance is not intrinsically limited by the microorganisms themselves, but by the biofilm microenvironment that is suboptimal for every bacterium. One can slightly enhance mass replenishment by increasing the reactant flow rate. However, this strategy is limited by uneven flow as well as increased power consumption. More importantly, the shear stress at high flow rates can destroy up to 50% of the microbial biomass and induce structural changes in the biofilm [156].

At the electrode level, the electrode configuration and material properties greatly affect biomass transport and enrichment. Conventional electrodes used in MESs were based on only graphite/carbon-based materials like graphite plate and carbon cloth. It has been demonstrated that biofilm distribution was not uniform and tilted towards the inlet end due to the continuous consumption of substrate and development of concentration boundary layer. Ye et al. [157] developed a microfluidic MFC and observed that biofilm thickness gradually decreased along the microchannel due to the severe diffusive mixing of the catholyte downstream. Compared to planar electrodes, the three-dimensional electrode can provide a larger surface area for microorganism attachment, and more importantly, can enhance mass transport by breaking the continuous development of concentration boundary layer. Cheng et al. [158] proposed a novel MFC in which the substrate was driven to penetrate a porous, carbon cloth-based anode in the through-plane direction. Although this approach could cause clogging, the maximum power density was improved by 17% as compared to the flow-over MFC configuration (substrate moving in plane with the anode). Recently, the unique advantages of three-dimensional electrodes (e.g., porous electrode, graphite rod array, and graphite granules) have been recognized. Jiang et al. [159] reported an MFC where the substrate was driven to flow through a 3D grapheme foam anode in the in-plane direction. Because of the convective mass transport and rapid replenishment of substrate inside the anode, this MFC yielded a volume power density of 745 $\mu W/cm^3$, which is higher than that of other devices.

Additionally, the consumption of culture medium and response time of this MFC were reduced by over 16-fold and fourfold, respectively, compared to non-flow-through devices. Graphite granules were also used to form a packed-bed anode for MFC operation. Rabaey et al. [160] found that packed-bed anodes made of granules can lead to a two-fold increase in MFC voltage, as compared to a plate anode. Additionally, fuel cell voltage can be further improved by inducing a cross-flow in the granular bed using baffles. However, other studies suggested that the graphite granules have a higher electrical resistance compared to graphite and carbon felt, and therefore decrease performance [140]. Recently, novel electrode materials with multi-scale porous structures were invented. Xie et al. [161] proposed a novel strategy to boost the effective anolyte-biofilm-anode reaction area by employing a unique, two-scale porous anode material made of carbon nanotube-textile (CNT-textile) composite. This two-scale porous structure featured (i) intertwined CNT-textile fibers that form a macroscale three-dimensional space for efficient substrate transport and microorganism colonization, and (ii) a microscale porous CNT-textile layer for enhanced electron transfer from biofilm to electrode. The MFC equipped with this CNT-textile composite outperformed the one with traditional carbon cloth; the maximum current density and power density were increased by 157% and 68%, respectively. In summary, an optimal electrode configuration for MESs should fulfill the following requirements: porous framework and biocompatible surface for microorganism attachment, large pore size for efficient mass transport inside the electrode, exceptional electrical conductivity, great corrosion resistance, convective replenishment for reaction depletion, and rapid product removal.

At the bioreactor level, several strategies to enhance mass transport have been reported. Li et al. [114] placed two baffles in the anode chamber to enhance the mixing of wastewater and active sludge (Fig. 5a). Jiang et al. [159] proposed a microfluidic MFC equipped with a flow-through porous anode (Fig. 5b). The interconnected pores of this graphene foam anode allowed convective enhancement of the electrochemical interactions between the microbes and the substrate. In addition, the unique scaffold structure of the graphene foam anode also enabled efficient diffusive nutrient transport to the biofilm. Compared with non-flow-through configurations, this flow-through MFC achieved 16-fold lower consumption of the culture medium and fourfold lower response time for electricity generation. Liao et al. [162] enhanced substrate transfer by rotating the carbon-brush anode (Fig. 5c). Compared with the non-rotating anode, the MFC with a rotating anode yielded 1.4 and 2.7 times higher peak power density and current density, respectively. It should be noted that external power was needed to drive the motor, which is not favorable for maximum system efficiency. Generally, buffers like phosphate or bicarbonate are added to the substrate to maintain the pH and facilitate proton transport to the cathode. Operating the system without buffering usually slows down proton transfer rate, thereby limiting the performance of the bioreactor. However, in practical applications, the use of buffers have to be minimized or eliminated, as they not only increase cost but also induce secondary
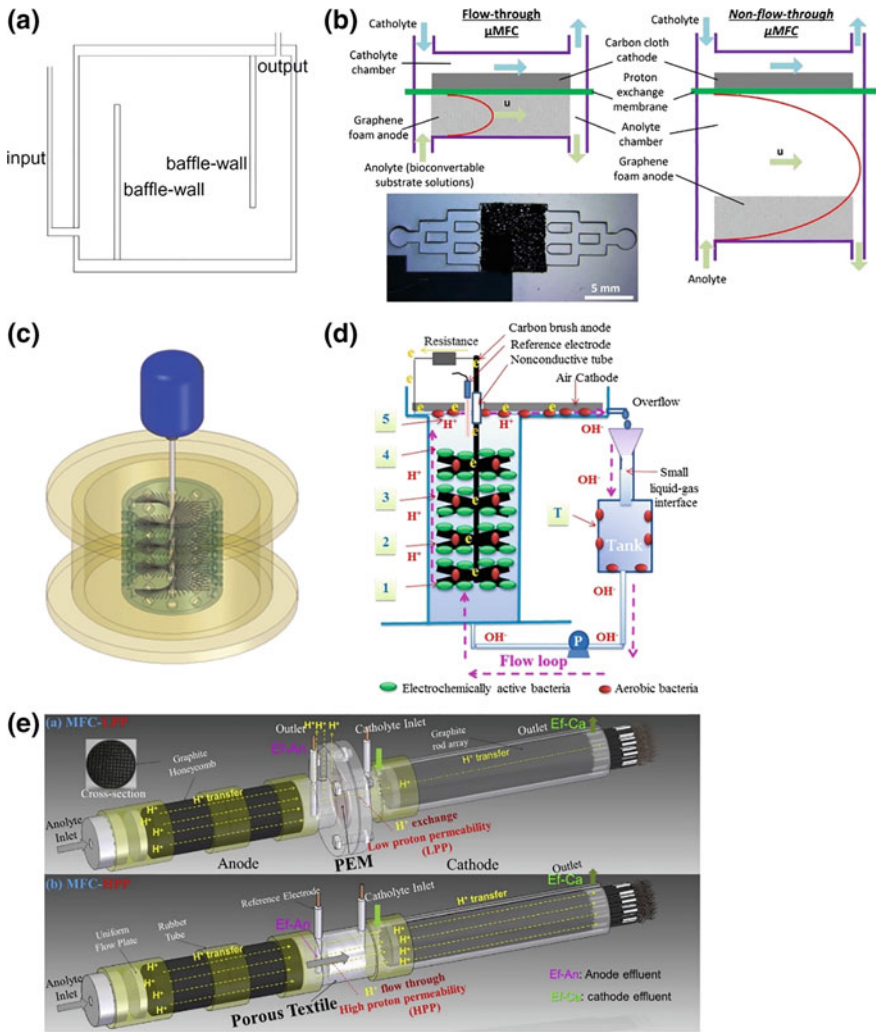
Fig. 5 Typical mass transport enhancement methods in the area of MESs. **a** Baffles were inserted in the anode chamber to enhance the mixing of wastewater and active sludge (adapted and reprinted from [114], Copyright 2008, with permission from Elsevier), **b** the substrate was driven to flow-through porous anode to convectively enhance mass transport (adapted and reprinted from [159], Copyright 2017, with permission from Springer), **c** a rotating brush anode was introduced to enhance substrate transfer (adapted and reprinted from [162], Copyright 2015, with permission from Elsevier), **d** The anolyte was recirculated to enhance the proton transport (adapted and reprinted from [142], Copyright 2008, with permission from Elsevier), **e** schematic of the continuous-flow tubular MFC with PEM and porous textile. The proton transfer and cell performance can be enhanced by flowing the anode effluent through the cathode electrodes (adapted and reprinted from [163], Copyright 2015, with permission from Elsevier)

contamination and/or eutrophication [163]. Zhang et al. [142] proposed a novel MFC with a floating air-cathode that allowed anolyte recirculation to enhance proton transport in buffer-free conditions (Fig. 5d), resulting in higher voltage output and higher coulombic efficiency. However, this recirculation strategy for effective proton transfer also causes excess oxygen transport into the anode, and the latter was found to deteriorate fuel cell performance at recirculation rates above 0.35 mL/min. In this study, the feasibility of enhancing the performance of unbuffered MFC via anolyte recirculation was also demonstrated. Zhang et al. [163] proposed another novel method to enhance proton transport by directly running the anode effluent through the cathode electrodes (Fig. 5e). Compared to membrane-segregated MFCs, this method improved the maximum power density by 125%. Further analysis indicated that the enhanced proton transport and increased catholyte conductivity contributed 51% and ∼40%, respectively, to total performance improvement.

4.3.3 Energy Conversion

Energy conversion in MESs is a relatively complicated process that needs comprehensive analysis. For instance, the commonly reported performance metrics (i.e., cell voltage, current and power density, coulombic efficiency) only assess electrical energy, while ignoring chemical energy like methane [109, 123] and biomass production [149, 164–167]. He [88] suggested using metrics like energy density (kWh/m^3) or COD removal (kWh/kg) to properly estimate the energy conversion from organic substrate to electricity and better assess MFC performance. He also performed an energy balance analysis, which suggested that the electricity produced by MFCs hardly compensate for their power consumption in a wastewater treatment plant or generate net energy output at the system level. Following this analysis, the major promotion for the implementation of MFC in the wastewater treatment process should be reduced power consumption and less sludge production, as compared to conventional aeration treatment.

Besides electricity, MESs also hold great potential in the production of value-added chemicals and biomass. Yu et al. [90] utilized MFCs and MECs to treat wastewater from a high-strength soybean edible oil refinery (SEOR) while simultaneously producing electricity and methane. The methane was produced at an efficiency of 45.4 ± 1.1 L/kg-COD and a rate of 0.133 ± 0.005 m^3/(m^3 d), which was higher than that obtained in non-electrochemical anaerobic digestion. Zhou et al. [167] integrated an algal biocathode with a dual-chamber MFC to provide oxygen to the MFC cathode via the photosynthetic activity of the algae. The CO_2 produced at the anode was further converted to biomass at the cathode, enabling simultaneous wastewater treatment, electricity generation, and biomass production. Commault et al. [149] developed an MFC equipped with a photo-cathode, in which the wastewater was pretreated by anodic bacteria and then further treated by cathodic microalgae to produce electricity and algal biomass. Ma et al. [164] reported a photosynthetic MFC that also used microalgae-mediated oxygen

production to enhance the oxygen reduction reaction at the cathode. The energy flow analysis of this system suggested that the production of algal biomass took a majority of the recovered energy, and the net electricity production did not meet expectations.

Another issue regarding energy conversion by different types of MESs is the metric used for quantification and comparison. Current density based on the projected surface area is the most commonly reported parameter. However, the widely used porous electrode materials usually have a much larger inner surface area than the projected surface area, causing the current density calculation to overestimate system performance. Sharma et al. [168] published a critical review about the key parameters for assessing MESs, and provided guidelines to correct current and exchange current densities based on different surface areas (e.g., biofilm covered area, electrochemically active surface area) of the electrodes. In addition, the authors also suggested including the robustness of electrochemically active biofilms as a performance indicator.

5 Conclusions

Microbial energy conversion technology is a promising approach to relieve the burden on fossil fuels and decrease environmental pollution. Bioreactors play a very important role in microbial biomass production and energy conversion. This chapter presents a fundamental understanding of the functions, configurations and influencing factors of bioreactors with respect to their application in microbial biomass cultivation, microbial biofuel conversion, and microbial electrochemical systems. Bioreactors can provide a suitable and stable place for microbial growth and metabolism by appropriately controlling their operating conditions. In addition to the operating conditions, the performance of a bioreactor is greatly influenced by many other factors like structure and size, mixing and transfer characteristics, means of feed introduction and product removal. In particular, bioreactors exhibit complex multiphase flow patterns that result in varying heat and mass transfer characteristics in microbial biomass and energy conversion. However, the mass and heat transfer efficiency in bioreactors is low, leading to a poor biomass and biofuel productivity. The economic viability and competitiveness of microbial energy conversion in bioreactors are much lower than that of petroleum-based energy sources. As a result, the energy conversion efficiencies of bioreactors are poor and unstable. Further optimization of bioreactor structure and operating conditions, mass and heat transfer, as well as reactant activity should be conducted.

In conclusion, bioreactor-based microbial energy conversion is a very promising technology and holds great potential for commercialization as a sustainable energy source. Bioreactor development and system integration are already underway, and several field tests have been reported. However, further studies to improve performance, scalability, and reliability are needed to make bioreactor-based microbial energy conversion a commercially applicable energy source.

References

1. Zhu YH, Jiang JG (2008) Continuous cultivation of Dunaliella salina in photobioreactor for the production of β-carotene. Eur Food Res Technol 227(3):953–959
2. Yongmanltchal W, Ward OP (1992) Growth and eicosapentaenoic acid production by Phaeodactylum tricornutum in batch and continuous culture systems. J Am Oil Chem Soc 69(6):584–590
3. Turpin DH (1991) Effects of inorganic N availability on algal photosynthesis and carbon metabolism. J Phycol 27(1):14–20
4. Sánchez JF, Fernández JM, Acién FG, Rueda A, Pérez-Parra J, Molina E (2008) Influence of culture conditions on the productivity and lutein content of the new strain Scenedesmus almeriensis. Process Biochem 43(4):398–405
5. McNaught AD, Wilkinson A (2006) IUPAC compendium of chemical terminology. Encyclopedic dictionary of polymers
6. Bitog JPP, Lee IB, Oh HM, Hong SW, Seo IH, Kwon KS (2014) Optimised hydrodynamic parameters for the design of photobioreactors using computational fluid dynamics and experimental validation. Biosyst Eng 122(3):42–61
7. Bitog JP, Lee IB, Lee CG, Kim KS, Hwang HS, Hong SW, Seo IH, Kwon KS, Mostafa E (2011) Application of computational fluid dynamics for modeling and designing photobioreactors for microalgae production: a review. Comput Electron Agr 76(2):131–147
8. Hase R, Oikawa H, Sasao C, Morita M, Watanabe Y (2000) Photosynthetic production of microalgal biomass in a raceway system under greenhouse conditions in Sendai city. J Biosci Bioeng 89(2):157–163
9. Ugwu CU, Aoyagi H, Uchiyama H (2008) Photobioreactors for mass cultivation of algae. Bioresour Technol 99(10):4021–4028
10. Razzak SA, Hossain MM, Lucky RA, Bassi AS, Lasa HD (2013) Integrated CO_2 capture, wastewater treatment and biofuel production by microalgae culturing—a review. Renew Sustain Energy Rev 27(6):622–653
11. Zhang K, Kurano N, Miyachi S (2002) Optimized aeration by carbon dioxide gas for microalgal production and mass transfer characterization in a vertical flat-plate photobioreactor. Bioprocess Biosyst Eng 25(2):97–101
12. Pulzl O, Gerbsch N, Buchholz R (1995) Light energy supply in plate-type and light diffusing optical fiber bioreactors. J Appl Phycol 7(2):145–149
13. Tredici MR, Carlozzi P, Zittelli GC, Materassi R (1991) A vertical alveolar panel (VAP) for outdoor mass cultivation of microalgae and cyanobacteria. Bioresour Technol 38(2–3): 153–159
14. Rubio FC, Fernandez FG, Perez JA, Camacho FG, Grima EM (2015) Prediction of dissolved oxygen and carbon dioxide concentration profiles in tubular photobioreactors for microalgal culture. Biotechnol Bioeng 62(1):71–86
15. CY C, KL Y, R A, DJ L, JS C (2011) Cultivation, photobioreactor design and harvesting of microalgae for biodiesel production: a critical review. Bioresour Technol 102(1):71–81
16. Decker EL, Reski R (2008) Current achievements in the production of complex biopharmaceuticals with moss bioreactors. Bioprocess Biosyst Eng 31(1):3–9

17. Weissman JC, Goebel RP (1987) Design and analysis of microalgal open pond systems for the purpose of producing fuels. Energy 98

18. Becker W (2004) Microalgae in human and animal nutrition. Blackwell Publishing Ltd

19. Spolaore P, Joannis-Cassan C, Duran E, Isambert A (2006) Commercial applications of microalgae. J Biosci Bioeng 101(2):87–96

20. Oncel S, Sukan FV (2008) Comparison of two different pneumatically mixed column photobioreactors for the cultivation of Artrospira platensis (Spirulina platensis). Bioresour Technol 99(11):4755–4760

21. Fan LH, Zhang YT, Cheng LH, Zhang L, Tang DS, Chen HL (2010) Optimization of carbon dioxide fixation by Chlorella vulgaris cultivated in a membrane-photobioreactor. Chem Eng Technol 30(8):1094–1099

22. Ap C, La M, Fx M (2006) Microalgal reactors: a review of enclosed system designs and performances. Biotechnol Prog 22(6):1490–1506

23. Pirouzi A, Nosrati M, Shojaosadati SA, Shakhesi S (2014) Improvement of mixing time, mass transfer, and power consumption in an external loop airlift photobioreactor for microalgae cultures. Biochem Eng J 87(12):25–32

24. Mehlitz TH (2014) Temperature influence and heat management requirements of microalgae cultivation in photobioreactors

25. Vogel M, Günther A, Rossberg A, Li B, Bernhard G, Raff J (2010) Biosorption of U(VI) by the green algae Chlorella vulgaris in dependence of pH value and cell activity. Sci Total Environ 409(2):384–395

26. Maagd GJD, Hendriks AJ, Seinen W, Sijm DTHM (1999) pH-dependent hydrophobicity of the cyanobacteria toxin microcystin-LR. Water Res 33(3):677–680

27. Chiswell RK, Shaw GR, Eaglesham G, Smith MJ, Norris RL, Seawright AA, Moore MR (2015) Stability of cylindrospermopsin, the toxin from the cyanobacterium, Cylindrospermopsis raciborskii: effect of pH, temperature, and sunlight on decomposition. Environ Toxicol 14(1):155–161

28. Pulz O (2001) Photobioreactors: production systems for phototrophic microorganisms. Appl Microbiol Biotechnol 57(3):287–293

29. Chang H, Fu Q, Huang Y, Xia A, Liao Q, Zhu X (2017) Improvement of microalgae lipid productivity and quality in an ion-exchange-membrane photobioreactor using real municipal wastewater. Int J Agr Biol Eng 10:97–106

30. Chinnasamy S, Bhatnagar A, Claxton R, Das KC (2010) Biomass and bioenergy production potential of microalgae consortium in open and closed bioreactors using untreated carpet industry effluent as growth medium. Bioresour Technol 101(17):6751–6760

31. Lehr F, Posten C (2009) Closed photo-bioreactors as tools for biofuel production. Curr Opin Biotechnol 20(3):280–285

32. Zhang C, Zhu X, Liao Q, Wang Y, Li J, Ding Y, Wang H (2010) Performance of a groove-type photobioreactor for hydrogen production by immobilized photosynthetic bacteria. Int J Hydrog Energy 35(11):5284–52923

33. Pen N, Soussan L, Belleville MP, Sanchez J, Charmette C, Paoluccijeanjean D (2014) An innovative membrane bioreactor for methane biohydroxylation. Bioresour Technol 174(174):42–52

34. Zhang Z, Zhou X, Hu J, Zhang T, Zhu S, Zhang Q (2017) Photo-bioreactor structure and light-heat-mass transfer properties in photo-fermentative bio-hydrogen production system: a mini review. Int J Hydrog Energy

35. Hu Q, Richmond A (1996) Productivity and photosynthetic efficiency of Spirulina platensis as affected by light intensity, cell density and rate of mixing in a flat plate photobioreactor. J Appl Phycol 8:139–145; J Appl Phycol 8(2):139–145

36. Schultz MP (2000) Turbulent boundary layers on surfaces covered with filamentous algae. J Fluid Eng 122(2):357–363

37. Ninno D, Power M (2012) Investigation of turbulent multiphase flows in a flat panel photobioreactor and consequent effects on microalgae cultivation; using computational fluid

dynamics (CFD) simulation and particle image velocimetry (PIV) measurement. Dissertations and theses—gradworks

38. Liao Q, Yang YX, Zhu X, Wang H, Ding YD (2015) Lattice Boltzmann simulation on liquid flow and mass transport in a bioreactor with cylinder bundle for hydrogen production. Heat Mass Transf 51(6):859–873

39. Sikula I, Juraščík M, Markoš J (2007) Modeling of fermentation in an internal loop airlift bioreactor. Chem Eng Sci 62(18):5216–5221

40. Zhang JB, Poncin S, Wu J, Li HZ (2011) A multiscale approach for studying an anaerobic multiphase bioreactor. Chem Eng Sci 66(14):3423–3431

41. Laukevics JJ, Apsite AF, Viesturs US, Tengerdy RP (1985) Steric hindrance of growth of filamentous fungi in solid substrate fermentation of wheat straw. Biotechnol Bioeng 27(12): 1687–1691

42. Rathbun BL, Shuler ML (1983) Heat and mass transfer effect in static solid- substrate fermentation, design of fermentation chambers. Biotechnol Bioeng 25(4):929–938

43. Rajagopalan S, Modak JM (1995) Modeling of heat and mass transfer for solid state fermentation process in tray bioreactor. Biotechnol Bioprocess E 13(3):161–169

44. Valiorgue P, Hadid HB, Hajem ME, Rimbaud L, Muller-Feuga A, Champagne JY (2014) CO_2 mass transfer and conversion to biomass in a horizontal gas–liquid photobioreactor. Chem Eng Res Des 92(10):1891–1897

45. Borowitzka MA (2013) High-value products from microalgae—their development and commercialisation. J Appl Phycol 25(3):743–756

46. Delrue F, Setier PA, Sahut C, Cournac L, Roubaud A, Peltier G, Froment AK (2012) An economic, sustainability, and energetic model of biodiesel production from microalgae. Bioresour Technol 111(3):191–200

47. Jacoblopes E, Scoparo CHG, Queiroz MI, Franco TT (2010) Biotransformations of carbon dioxide in photobioreactors. Energy Convers Manag 51(5):894–900

48. Murphy TE (2013) Artificial leaf for biofuel production and harvesting: transport phenomena and energy conversion

49. Akkerman I, Janssen M, Rocha J, Wijffels RH (2002) Photobiological hydrogen production: photochemical efficiency and bioreactor design. Int J Hydrog Energy 27(11–12):1195–1208

50. Markov SA, Bazin MJ, Hall DO (1996) Efficiency of light energy conversion in hydrogen production by cyanobacterium Anabaena variabilis. J Mar Biotechnol 4(1):57–60

51. Cui QF, Jin YR, Ma C, Wu YN (2014) Continuous hydrogen production in a novel photo-bioreactor with high light conversion efficiency. Adv Mater Res 953–954:970–973

52. Tredici MR, Zittelli GC, Benemann JR (1998) A tubular integral gas exchange photobioreactor for biological hydrogen production. Biohydrogen

53. Das D, Veziroğlu TN (2001) Hydrogen production by biological processes: a survey of literature. Int J Hydrog Energy 26(1):13–28

54. Pörtner R, Barradas OP, Frahm B, Hass VC (2017) Advanced process and control strategies for bioreactors

55. Zhang Quanguo, Jianjun Hu, Lee D-J (2016) Biogas from anaerobic digestion processes: research updates. Renew Energy 98:108–119

56. Gonçalves AL, Simões M (2017) Metabolic engineering of Escherichia coli for higher alcohols production: an environmentally friendly alternative to fossil fuels. Renew Sustain Energy Rev 77:580–589

57. Atsumi S, Liao JC (2008) Metabolic engineering for advanced biofuels production from Escherichia coli. Curr Opin Biotechnol 19(5):414–419

58. Lan EI, Liao JC (2012) Microbial synthesis of n-butanol, isobutanol, and other higher alcohols from diverse resources. Bioresour Technol 135(2):339–349

59. Walter WG (1971) Standard methods for the examination of water and wastewater. APHA

60. Adessi A, De Philippis R (2014) Photobioreactor design and illumination systems for H_2 production with anoxygenic photosynthetic bacteria: a review. Int J Hydrog Energy 39(7): 3127–3141

61. Chunlan Mao, Yongzhong Feng, Xiaojiao Wang, Guangxin R (2015) Review on research achievements of biogas from anaerobic digestion. Renew Sustain Energy Rev 45:540–555
62. Şentürk E, İnce M, EngiN GO (2012) The effect of transient loading on the performance of a mesophilic anaerobic contact reactor at constant feed strength. J Biotechnol 164(2):232
63. Tauseef SM, Abbasi T, Abbasi SA (2013) Energy recovery from wastewaters with high-rate anaerobic digesters. Renew Sustain Energy Rev 19(1):704–741
64. Bodkhe S (2008) Development of an improved anaerobic filter for municipal wastewater treatment. 99(1):222–226
65. Wang J, Wan W (2009) Factors influencing fermentative hydrogen production: a review. Int J Hydrog Energy 34(2):799–811
66. Hawkes F, Hussy I, Kyazze G, Dinsdale R, Hawkes D (2007) Continuous dark fermentative hydrogen production by mesophilic microflora: principles and progress. Int J Hydrog Energy 32(2):172–184
67. Mcduffie NG (1991) Bioreactor design fundamentals. Butterworth-Heinemann
68. Nguyen D, Gadhamshetty V, Nitayavardhana S, Khanal SK (2015) Automatic process control in anaerobic digestion technology: a critical review. Bioresour Technol 193:513–522
69. Khanal S, Giri B, Nitayavardhana S, Gadhamshetty V (2016) Anaerobic bioreactors/digesters: design and development. Curr Dev Biotechnol Bioeng: Biol Treat Ind Effl 261
70. Das D, Veziroglu TN (2008) Advances in biological hydrogen production processes. Int J Hydrog Energy 33(21):6046–6057
71. Haixing C, Qiang L, Qian F, Yun H, Ao X, Yaping Z, Yahui S, Xun Z (2017) Phase-feeding strategy for Chlorella vulgaris to enhance biomass and lipid productivity. Int J Agr Biol Eng 10(2):205–215
72. Chang H-X, Fu Q, Huang Y, Xia A, Liao Q, Zhu X, Zheng Y-P, Sun C-H (2016) An annular photobioreactor with ion-exchange-membrane for non-touch microalgae cultivation with wastewater. Bioresour Technol 219:668–676
73. Clark IC, Zhang RH, Upadhyaya SK (2012) The effect of low pressure and mixing on biological hydrogen production via anaerobic fermentation. Int J Hydrog Energy 37 (15):11504–11513
74. Soccol CR (2017) Recent developments and innovations in solid state fermentation. Biotechnol Res Innov
75. Chen CY, Liu CH, Lo YC, Chang JS (2011) Perspectives on cultivation strategies and photobioreactor designs for photo-fermentative hydrogen production. Bioresour Technol 102(18):8484–8492
76. Duu-Jong L, Jo-Shu C, Juin-Yih L (2015) Microalgae-microbial fuel cell: a mini review. Bioresour Technol 198:891–895
77. Nakada E, Asada Y, Arai T, Miyake J (1995) Light penetration into cell suspensions of photosynthetic bacteria and relatioin to hydrogen production. J Ferment Bioeng 80(1):53–57
78. Akkerman I, Janssen M, Rocha J, Wijffels RH (2002) Photobiological hydrogen production: photochemical efficiency and bioreactor design. Int J Hydrog Energy 27(11–12):1195–1208
79. Ooms MD, Cao TD, Sargent EH, Sinton D (2016) Photon management for augmented photosynthesis. Nat Commun 7:12699
80. Miyake J, Wakayama T, Schnackenberg J, Arai T, Asada Y (1999) Simulation of the daily sunlight illumination pattern for bacterial photo-hydrogen production. J Biosci Bioeng 88 (6):659
81. Carlozzi P (2000) Hydrodynamic aspects and Arthrospira growth in two outdoor tubular undulating row photobioreactors. Appl Microbiol Biotechnol 54(1):14–22
82. Alvira P, Tomás-Pejó E, Ballesteros M, Negro MJ (2010) Pretreatment technologies for an efficient bioethanol production process based on enzymatic hydrolysis: a review. Bioresour Technol 101(13):4851
83. Alfenore S, Molina-Jouve C (2016) Current status and future prospects of conversion of lignocellulosic resources to biofuels using yeasts and bacteria. Process Biochem 51(11): 1747–1756

84. Dale BE, Leong CK, Pham TK, Esquivel VM, Rios I, Latimer VM (1996) Hydrolysis of lignocellulosics at low enzyme levels: application of the AFEX process. Bioresour Technol 56(1):111–116

85. Wang H, Ren ZJ (2013) A comprehensive review of microbial electrochemical systems as a platform technology. Biotechnol Adv 31(8):1796–1807

86. Kelly PT, He Z (2014) Nutrients removal and recovery in bioelectrochemical systems: a review. Bioresour Technol 153:351–360

87. Rozendal RA, Hamelers HVM, Rabaey K, Keller J, Buisman CJN (2008) Towards practical implementation of bioelectrochemical wastewater treatment. Trends Biotechnol 26(8):450–459

88. He Z (2013) Microbial fuel cells: now let us talk about energy. Environ Sci Technol 47 (1):332–333

89. Han A, Hou H, Li L, Kim HS, de Figueiredo P (2013) Microfabricated devices in microbial bioenergy sciences. Trends Biotechnol 31(4):225–232

90. Yu N, Xing D, Li W, Yang Y, Li Z, Li Y, Ren N (2017) Electricity and methane production from soybean edible oil refinery wastewater using microbial electrochemical systems. Int J Hydrog Energy 42(1):96–102

91. Geppert F, Liu D, van Eerten-Jansen M, Weidner E, Buisman C, ter Heijne A (2016) Bioelectrochemical power-to-gas: state of the art and future perspectives. Trends Biotechnol 34(11):879–894

92. Cai W, Han T, Guo Z, Varrone C, Wang A, Liu W (2016) Methane production enhancement by an independent cathode in integrated anaerobic reactor with microbial electrolysis. Bioresour Technol 208:13–18

93. Feng Q, Song Y-C (2016) Surface modification of a graphite fiber fabric anode for enhanced bioelectrochemical methane production. Energy Fuel 30(8):6467–6474

94. Pham TH, Aelterman P, Verstraete W (2009) Bioanode performance in bioelectrochemical systems: recent improvements and prospects. Trends Biotechnol 27(3):168–178

95. Pandey P, Shinde VN, Deopurkar RL, Kale SP, Patil SA, Pant D (2016) Recent advances in the use of different substrates in microbial fuel cells toward wastewater treatment and simultaneous energy recovery. Appl Energy 168:706–723

96. Khan MD, Khan N, Sultana S, Joshi R, Ahmed S, Yu E, Scott K, Ahmad A, Khan MZ (2017) Bioelectrochemical conversion of waste to energy using microbial fuel cell technology. Process Biochem 57:141–158

97. Zhang F, Ge Z, Grimaud J, Hurst J, He Z (2013) Long-term performance of liter-scale microbial fuel cells treating primary effluent installed in a municipal wastewater treatment facility. Environ Sci Technol 47(9):4941–4948

98. Huggins T, Fallgren P, Jin S, Ren Z (2013) Energy and performance comparison of microbial fuel cell and conventional aeration treating of wastewater. J Microb Biochem Technol S 6(2)

99. EPA Office of Water (2006) Wastewater Management Fact Sheet, Energy Conservation, EPA 832-F-06–024. U.S. Environmental Protection Agency: Washington DC, p 7

100. Oh ST, Kim JR, Premier GC, Lee TH, Kim C, Sloan WT (2010) Sustainable wastewater treatment: how might microbial fuel cells contribute. Biotechnol Adv 28(6):871–881

101. Logan BE (2004) Extracting hydrogen and electricity from renewable resources. Environ Sci Technol 38(9):160A–167A

102. Liu H, Hu H, Chignell J, Fan Y (2010) Microbial electrolysis: novel technology for hydrogen production from biomass. Biofuels 1(1):129–142

103. van Eerten-Jansen MCAA, Jansen NC, Plugge CM, de Wilde V, Buisman CJN, ter Heijne A (2015) Analysis of the mechanisms of bioelectrochemical methane production by mixed cultures. J Chem Technol Biot 90(5):963–970

104. Gajaraj S, Huang Y, Zheng P, Hu Z (2017) Methane production improvement and associated methanogenic assemblages in bioelectrochemically assisted anaerobic digestion. Biochem Eng J Part B 117:105–112

105. Cao X, Huang X, Liang P, Xiao K, Zhou Y, Zhang X, Logan BE (2009) A new method for water desalination using microbial desalination cells. Environ Sci Technol 43(18):7148–7152
106. Kim H-W, Nam J-Y, Shin H-S (2011) Ammonia inhibition and microbial adaptation in continuous single-chamber microbial fuel cells. J Power Sources 196(15):6210–6213
107. Wang Y-K, Sheng G-P, Shi B-J, Li W-W, Yu H-Q (2013) A novel electrochemical membrane bioreactor as a potential net energy producer for sustainable wastewater treatment. Sci Rep 3:1864
108. Nam J-Y, Kim H-W, Shin H-S (2010) Ammonia inhibition of electricity generation in single-chambered microbial fuel cells. J Power Sources 195(19):6428–6433
109. Gao C, Liu L, Yang F (2017) Development of a novel proton exchange membrane-free integrated MFC system with electric membrane bioreactor and air contact oxidation bed for efficient and energy-saving wastewater treatment. Bioresour Technol 238:472–483
110. Liu H, Ramnarayanan R, Logan BE (2004) Production of electricity during wastewater treatment using a single chamber microbial fuel cell. Environ Sci Technol 38(7):2281–2285
111. Najafabadi AT, Ng N, Gyenge E (2016) Electrochemically exfoliated graphene anodes with enhanced biocurrent production in single-chamber air-breathing microbial fuel cells. Biosens Bioelectron 81:103–110
112. Ye D, Deng B, Li J, Zou W, Ke C, Yuan Z, Zhu X, Liao Q (2016) Electricity production of a microbial fuel cell stack integrated into a sink drain pipe. Res Chem Intermed 42:1–12
113. Rabaey K, Clauwaert P, Aelterman P, Verstraete W (2005) Tubular microbial fuel cells for efficient electricity generation. Environ Sci Technol 39(20):8077–8082
114. Li Z, Yao L, Kong L, Liu H (2008) Electricity generation using a baffled microbial fuel cell convenient for stacking. Bioresour Technol 99(6):1650–1655
115. Jiang X, Hu J, Petersen ER, Fitzgerald LA, Jackan CS, Lieber AM, Ringeisen BR, Lieber CM, Biffinger JC (2013) Probing single- to multi-cell level charge transport in Geobacter sulfurreducens DL-1. Nat Commun 4:2751
116. Kim BJ, Chu I, Jusuf S, Kuo T, TerAvest MA, Angenent LT, Wu M (2016) Oxygen tension and riboflavin gradients cooperatively regulate the migration of Shewanella oneidensis MR-1 revealed by a hydrogel-based microfluidic device. Front Microbiol 7:1438
117. Humphries J, Xiong L, Liu J, Prindle A, Yuan F, Arjes HA, Tsimring L, Süel GM (2017) Species-independent attraction to biofilms through electrical signaling. Cell 168(1–2):200–209.e212
118. Liu J, Martinez-Corral R, Prindle A, D-yD Lee, Larkin J, Gabalda-Sagarra M, Garcia-Ojalvo J, Süel GM (2017) Coupling between distant biofilms and emergence of nutrient time-sharing. Science 356(6338):638
119. Massalha H, Korenblum E, Malitsky S, Shapiro OH, Aharoni A (2017) Live imaging of root–bacteria interactions in a microfluidics setup. Proc Natl Acad Sci USA 114(17):4549–4554
120. Qian F, Baum M, Gu Q, Morse DE (2009) A 1.5 [small micro]L microbial fuel cell for on-chip bioelectricity generation. Lab Chip 9(21):3076–3081
121. Qian F, He Z, Thelen MP, Li Y (2011) A microfluidic microbial fuel cell fabricated by soft lithography. Bioresour Technol 102(10):5836–5840
122. Dressaire E, Sauret A (2017) Clogging of microfluidic systems. Soft Matter 13(1):37–48
123. Liu H, Leng F, Guan Y, Yao Y, Li Y, Xu S (2017) Simultaneous pollutant removal and electricity generation in a combined ABR-MFC-MEC system treating fecal wastewater. Water Air Soil Pollut 228(5):179
124. Ledezma P, Stinchcombe A, Greenman J, Ieropoulos I (2013) The first self-sustainable microbial fuel cell stack. Phys Chem Chem Phys 15(7):2278–2281
125. Oh SE, Logan BE (2007) Voltage reversal during microbial fuel cell stack operation. J Power Sources 167(1):11–17
126. Liang P, Wu W, Wei J, Yuan L, Xia X, Huang X (2011) Alternate charging and discharging of capacitor to enhance the electron production of bioelectrochemical systems. Environ Sci Technol 45(15):6647–6653

127. Kim Y, Hatzell MC, Hutchinson AJ, Logan BE (2011) Capturing power at higher voltages from arrays of microbial fuel cells without voltage reversal. Energy Environ Sci 4(11):4662–4667

128. Wu PK, Biffinger JC, Fitzgerald LA, Ringeisen BR (2012) A low power DC/DC booster circuit designed for microbial fuel cells. Process Biochem 47(11):1620–1626

129. Dong H, Yu H, Wang X (2012) Catalysis kinetics and porous analysis of rolling activated carbon-PTFE air-cathode in microbial fuel cells. Environ Sci Technol 46(23):13009–13015

130. Yuan Y, Zhao B, Zhou S, Zhong S, Zhuang L (2011) Electrocatalytic activity of anodic biofilm responses to pH changes in microbial fuel cells. Bioresour Technol 102(13):6887–6891

131. Sun M, Zhai L-F, Li W-W, Yu H-Q (2016) Harvest and utilization of chemical energy in wastes by microbial fuel cells. Chem Soc Rev 45(10):2847–2870

132. Yang W, Li J, Ye D, Zhang L, Zhu X, Liao Q (2016) A hybrid microbial fuel cell stack based on single and double chamber microbial fuel cells for self-sustaining pH control. J Power Sources 306:685–691

133. Liu XW, Wang YP, Huang YX, Sun XF, Sheng GP, Zeng RJ, Li F, Dong F, Wang SG, Tong ZH (2011) Integration of a microbial fuel cell with activated sludge process for energy-saving wastewater treatment: taking a sequencing batch reactor as an example. Biotechnol Bioeng 108(6):1260–1267

134. Wang Y-P, Liu X-W, Li W-W, Li F, Wang Y-K, Sheng G-P, Zeng RJ, Yu H-Q (2012) A microbial fuel cell–membrane bioreactor integrated system for cost-effective wastewater treatment. Appl Energy 98:230–235

135. Li J, Zou W, Xu Z, Ye D, Zhu X, Liao Q (2013) Improved hydrogen production of the downstream bioreactor by coupling single chamber microbial fuel cells between series-connected photosynthetic biohydrogen reactors. Int J Hydrog Energy 38(35):15613–15619

136. Kumar G, Saratale RG, Kadier A, Sivagurunathan P, Zhen G, Kim S-H, Saratale GD (2017) A review on bio-electrochemical systems (BESs) for the syngas and value added biochemicals production. Chemosphere 177:84–92

137. Khare V, Nema S, Baredar P (2016) Solar–wind hybrid renewable energy system: a review. Renew Sustain Energy Rev 58:23–33

138. Archer CL, Simão HP, Kempton W, Powell WB, Dvorak MJ (2017) The challenge of integrating offshore wind power in the U.S. electric grid. Part I: Wind forecast error. Renew Energy 103:346–360

139. Wang ZL (2017) New wave power. Nature 542:159–160

140. Aelterman P, Versichele M, Marzorati M, Boon N, Verstraete W (2008) Loading rate and external resistance control the electricity generation of microbial fuel cells with different three-dimensional anodes. Bioresour Technol 99(18):8895–8902

141. Zhang L, Zhu X, Li J, Liao Q, Ye D (2011) Biofilm formation and electricity generation of a microbial fuel cell started up under different external resistances. J Power Sources 196 (15):6029–6035

142. Zhang L, Zhu X, Kashima H, Li J, D-d Ye, Liao Q, Regan JM (2015) Anolyte recirculation effects in buffered and unbuffered single-chamber air-cathode microbial fuel cells. Bioresour Technol 179:26–34

143. Patil SA, Harnisch F, Kapadnis B, Schröder U (2010) Electroactive mixed culture biofilms in microbial bioelectrochemical systems: the role of temperature for biofilm formation and performance. Biosens Bioelectron 26(2):803–808

144. Bhattacharjee A, Khan M, Kleiman M, Hochbaum AI (2017) Effects of growth surface topography on bacterial signaling in coculture biofilms. ACS Appl Mater Inter 9(22):18531–18539

145. Thomen P, Robert J, Monmeyran A, Bitbol A-F, Douarche C, Henry N (2017) Bacterial biofilm under flow: first a physical struggle to stay, then a matter of breathing. PLoS ONE 12 (4):e0175197

146. Li W, Sun J, Hu Y, Zhang Y, Deng F, Chen J (2014) Simultaneous pH self-neutralization and bioelectricity generation in a dual bioelectrode microbial fuel cell under periodic reversion of polarity. J Power Sources 268:287–293
147. Liao Q, Zhang J, Li J, Ye D, Zhu X, Zheng J, Zhang B (2014) Electricity generation and COD removal of microbial fuel cells (MFCs) operated with alkaline substrates. Int J Hydrog Energy 39(33):19349–19354
148. Park Y, Park S, Nguyen VK, Yu J, Torres CI, Rittmann BE, Lee T (2017) Complete nitrogen removal by simultaneous nitrification and denitrification in flat-panel air-cathode microbial fuel cells treating domestic wastewater. Chem Eng J 316:673–679
149. Commault AS, Laczka O, Siboni N, Tamburic B, Crosswell JR, Seymour JR, Ralph PJ (2017) Electricity and biomass production in a bacteria-Chlorella based microbial fuel cell treating wastewater. J Power Sources 356:299–309
150. Ma J, Wang Z, Suor D, Liu S, Li J, Wu Z (2014) Temporal variations of cathode performance in air-cathode single-chamber microbial fuel cells with different separators. J Power Sources 272:24–33
151. Oliot M, Etcheverry L, Bergel A (2016) Removable air-cathode to overcome cathode biofouling in microbial fuel cells. Bioresour Technol 221:691–696
152. Zhang B, Hao L, Tian C, Yuan S, Feng C, Ni J, Borthwick AGL (2015) Microbial reduction and precipitation of vanadium (V) in groundwater by immobilized mixed anaerobic culture. Bioresour Technol 192:410–417
153. Bajracharya S, Yuliasni R, Vanbroekhoven K, Buisman CJN, Strik DPBTB, Pant D (2017) Long-term operation of microbial electrosynthesis cell reducing CO_2 to multi-carbon chemicals with a mixed culture avoiding methanogenesis. Bioelectrochemistry 113:26–34
154. Bajracharya S, ter Heijne A, Dominguez Benetton X, Vanbroekhoven K, Buisman CJN, Strik DPBTB, Pant D (2015) Carbon dioxide reduction by mixed and pure cultures in microbial electrosynthesis using an assembly of graphite felt and stainless steel as a cathode. Bioresour Technol 195:14–24
155. Xiao L, He Z (2014) Applications and perspectives of phototrophic microorganisms for electricity generation from organic compounds in microbial fuel cells. Renew Sustain Energy Rev 37:550–559
156. Zarabadi MP, Paquet-Mercier F, Charette SJ, Greener J (2017) Hydrodynamic effects on biofilms at the biointerface using a microfluidic electrochemical cell: case study of Pseudomonas sp. Langmuir 33(8):2041–2049
157. Ye D, Yang Y, Li J, Zhu X, Liao Q, Deng B, Chen R (2013) Performance of a microfluidic microbial fuel cell based on graphite electrodes. Int J Hydrog Energy 38(35):15710–15715
158. Cheng S, Liu H, Logan BE (2006) Increased power generation in a continuous flow MFC with advective flow through the porous anode and reduced electrode spacing. Environ Sci Technol 40(7):2426–2432
159. Jiang H, Ali MA, Xu Z, Halverson LJ, Dong L (2017) Integrated microfluidic flow-through microbial fuel cells. Sci Rep 7:41208
160. Rabaey K, Ossieur W, Verhaege M, Verstraete W (2005) Continuous microbial fuel cells convert carbohydratesto electricity. Water Sci Technol 52(1–2):515–523
161. Xie X, Hu L, Pasta M, Wells GF, Kong D, Criddle CS, Cui Y (2011) Three-dimensional carbon nanotube−textile anode for high-performance microbial fuel cells. Nano Lett 11 (1):291–296
162. Liao Q, Zhang J, Li J, Ye D, Zhu X, Zhang B (2015) Increased performance of a tubular microbial fuel cell with a rotating carbon-brush anode. Biosens Bioelectron 63:558–561
163. Zhang L, Li J, Zhu X, D-d Ye, Liao Q (2015) Effect of proton transfer on the performance of unbuffered tubular microbial fuel cells in continuous flow mode. Int J Hydrog Energy 40 (10):3953–3960
164. Ma J, Wang Z, Zhang J, Waite TD, Wu Z (2017) Cost-effective Chlorella biomass production from dilute wastewater using a novel photosynthetic microbial fuel cell (PMFC). Water Res 108:356–364

165. Jadhav DA, Jain SC, Ghangrekar MM (2017) Simultaneous wastewater treatment, algal biomass production and electricity generation in clayware microbial carbon capture cells. Appl Biochem Biotechnol 1–17
166. Saba B, Christy AD, Yu Z, Co AC (2017) Sustainable power generation from bacterio-algal microbial fuel cells (MFCs): an overview. Renew Sustain Energy Rev 73:75–84
167. Zhou M, He H, Jin T, Wang H (2012) Power generation enhancement in novel microbial carbon capture cells with immobilized Chlorella vulgaris. J Power Sources 214:216–219
168. Sharma M, Bajracharya S, Gildemyn S, Patil SA, Alvarez-Gallego Y, Pant D, Rabaey K, Dominguez-Benetton X (2014) A critical revisit of the key parameters used to describe microbial electrochemical systems. Electrochim Acta 140:191–208

Part II
Bioreactors for Microalgal Biomass Production

Chapter 3
Photoautotrophic Microalgal Cultivation and Conversion

Yahui Sun, Yun Huang, Gregory J. O. Martin, Rong Chen and Yudong Ding

1 Introduction of Microalgae

Microalgae are photosynthetic microorganisms characterized by unicellular and simple multi-cellular structures that commonly exist in freshwater habitats and marine systems living in both water columns and sediments [1]. Owing to the wide varieties of microalgal species, their sizes generally range from a few micrometers to dozens of micrometers. Specifically, they can be categorized into prokaryotic microalgae (i.e. cyanobacteria *Chloroxybacteria*), and eukaryotic microalgae (e.g. green algae *Chlorophyta*, red algae *Rhodophyta*, and diatoms *Bacillariophta*). With regard to their cellular chemical compositions, microalgal cells are mainly composed of proteins (40–60%), carbohydrates (8–30%), lipids (5–60%), and other valuable components, such as pigments, antioxidants, vitamins, etc. [2]. As compared to terrestrial plants, microalgae exhibit the advantages of a rapid growth rate, higher lipid content, wide environmental adaptability, etc. In particular, they can be grown without competition with conventional crops using non-arable land, oceans, lakes, alkali lakes, and marshes [3].

Photoautotrophic microalgal growth refers to the process of converting CO_2 and water directly to chemicals through photosynthesis. Under this kind of sunlight-driven cultivation mode, microalgal cells can absorb CO_2 from industrial waste gas or the atmosphere and utilize nitrate and phosphate in industrial and

Y. Sun · Y. Huang (✉) · R. Chen · Y. Ding
Key Laboratory of Low-Grade Energy Utilization Technologies and Systems,
Chongqing University, Ministry of Education, Chongqing 400044, China
e-mail: yunhuang@cqu.edu.cn

Y. Sun · Y. Huang · R. Chen · Y. Ding
Institute of Engineering Thermophysics, Chongqing University, Chongqing 400044, China

G. J. O. Martin
Department of Chemical Engineering, Melbourne School of Engineering,
The University of Melbourne, Melbourne, VIC 3010, Australia

agricultural wastewater as nutrients and eventually convert them into organic matter, which can be used to produce biodiesel, cosmetics, nutrition, etc. [4]. Photoautotrophic, heterotrophic, mixotrophic, and photoheterotrophic cultivation are the four dominating microalgal cultivation modes. Among them, photoautotrophic cultivation is recognized as the most environmental and only economically feasible method of microalgal cultivation when targeting biomass production at the commercial scale [5]. Additionally, photoautotrophic cultivation provides a promising and effective solution to global warming, wastewater pollution, and fossil energy crisis.

2 Photosynthetic Mechanism of Microalgae

2.1 Microalgal Photoautotrophic Cultivation

As for microalgal photoautotrophic cultivation, microalgal cells utilize light (natural sunlight or artificial light) and inorganics (H_2O, inorganic salt, and CO_2) as the energy and mass sources for photosynthesis to produce organics [6, 7], which is the most commonly adopted cultivation mode for microalgal growth [8]. The overall equation for photosynthesis is shown as follows:

$$nCO_2 + nH_2O + light \rightarrow (CH_2O)_n + nO_2 \tag{1}$$
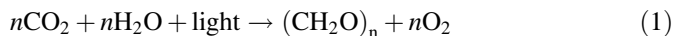
To be specific, the entire photosynthesis process consists of two stages, i.e., light-dependent reactions and light-independent reactions (also named carbon reactions), as illustrated in Fig. 1. In light-dependent reactions, H_2O is photo-decomposed into reducing hydrogen in the chloroplast thylakoid. Meanwhile, O_2 is released and adenosine triphosphate (ATP) is produced. In light-independent reactions, ATP and CO_2 are used to produce organics in the chloroplast stroma. As a consequence, it can be concluded from the process of photosynthesis that light, CO_2, and inorganic nutrients are the three critical factors affecting microalgal photoautotrophic growth. Moreover, the combination of CO_2 and inorganic nutrients transfer with O_2 releasing also have a significant impact on photosynthetic efficiency.

2.2 Factors Affecting Microalgal Photoautotrophic Cultivation

2.2.1 Light

Light, as the energy source of photosynthesis, plays an important role in chloroplast development and chlorophyll synthesis. Light is essential for the process of photosynthesis, especially during light-dependent reactions. When light penetrates the
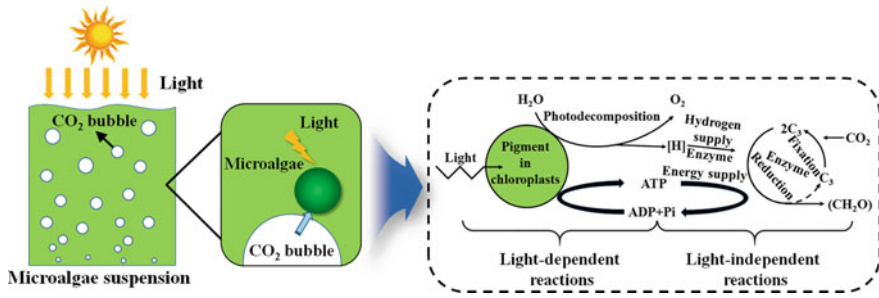
Fig. 1 Schematic diagram for the process of photosynthesis

microalgal suspension, one part is absorbed by the microalgal suspension and other is reflected and scattered back to the surrounding environment by microalgal cells and CO_2 bubbles. The remainder of the light goes into the depths of the microalgal suspension. With the growth of microalgae, the concentration of microalgal biomass increases, whereas the light penetrability within microalgal culture rapidly declines, thereby resulting in the serious attenuation of light intensity along with the direction of the light path (Fig. 2). Consequently, in terms of the local light intensity microalgal cells are exposed to, the whole microalgal suspension volume can be divided into three regions, namely the photoinhibition, light-limited, and stagnation regions, as depicted in Fig. 2. Microalgal cells in the light-limited and stagnation regions do not receive enough light and thus hinder the further accumulation of microalgal biomass. In comparison, microalgal cells in photoinhibition regions close to light incident surfaces are exposed to excess light, thereby arousing serious photoinhibition destruction in the photosystem II (PSII) complexes of the cells, both of which are detrimental to microalgal growth [9]. In this regard, increasing the disturbance degree within the microalgal suspension, i.e., forcing the microalgal cells to circulate periodically between the light and dark regions, is beneficial as it helps the microalgal cells receive uniform illumination and hence improves the yield of microalgal biomass [10].
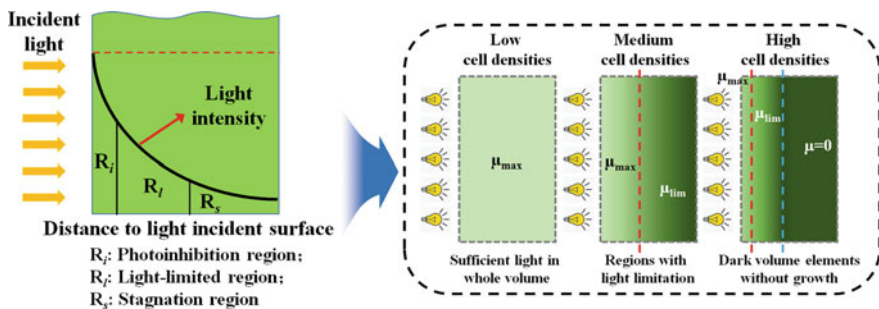
Fig. 2 Light intensity distribution characteristics within microalgal suspension

More specifically, when microalgal cells encounter light, photons are captured by the light-trapping apparatuses in the cells, which provide energy for the subsequent photosynthesis process. Photon-trapping apparatuses mainly consist of peripheral antennae, pigments, nuclei, and reaction centers. Chlorophyll b is characterized as the primary peripheral antenna pigment, as well as chlorophyll a and other accessory pigments, such as carotenoids and phycobiliproteins. These pigments absorb light with different wavelengths, thereby allowing the efficient utilization of solar energy [11]. The peripheral antenna pigments capture photons and transfer the activation energy to the interior closely linked pigment core (chlorophyll a cluster). Subsequently, the activation energy undergoes further migration and transfers to the reaction center where it undergoes electron separation.

The electrons transmitted from PSII to photosystem I (PSI) are combined with nicotinamide adenine dinucleotide phosphate (NADP+) to form NADPH under the action of the ferredoxin-NADP enzyme [12]. At the same time, protons released from water molecules and the transition from PQH_2 to PQ forms an electrochemical proton potential on both sides of the thylakoid, which drives adenosine diphosphate (ADP) and Pi to synthesize ATP [13]. Finally, NADPH and ATP participate in the immobilization of CO_2 and the synthesis of carbohydrates in the light-independent reactions [14].

2.2.2 CO_2

CO_2 is the primary carbon source for photosynthesis [6]. Its transportation process directly affects the photosynthetic process, especially light-independent reactions. When CO_2 is injected into the microalgal suspension, CO_2 forms a concentration gradient between the gas and liquid phases due to microalgal cell-driven CO_2 absorption. According to the double film layer theory, the transmission of CO_2 molecules from the gas phase to microalgal cells mainly occurs via two stages [15]. The first stage is the transportation of CO_2 molecules from the gas phase to the liquid phase, as presented in Fig. 3. To be concrete, CO_2 molecules are transferred
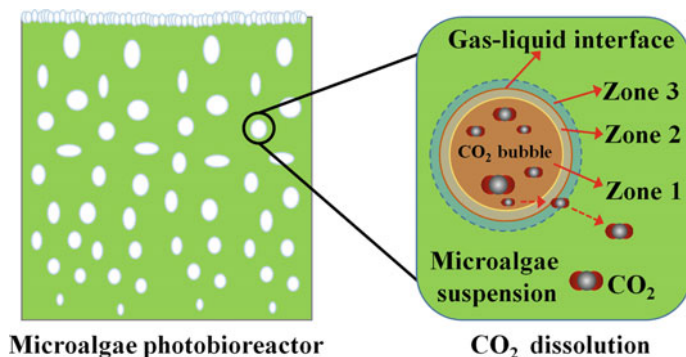
Fig. 3 Transmission of CO_2 in microalgal suspension

from the gas phase (Zone 1) to the thin gas film region (Zone 2) close to the gas-liquid interface, after which it is diffused from the thin gas film to the liquid film (Zone 3) close to the gas-liquid interface. Finally, the molecules are transferred from the thin liquid film region to the liquid phase.

In general, inorganic carbon is present as H_2CO_3, CO_2 (aq), HCO_3^-, and CO_3^{2-} in aqueous solutions and exhibits a dynamic balance between them [16, 17]. The relative content of each inorganic carbon form is mainly controlled by the pH and is also affected by salinity and temperature. The total dynamic balance equations are defined as follows:

$$CO_2 + H_2O \rightleftarrows H_2CO_3 \rightleftarrows HCO_3^- + H^+ \tag{2}$$

$$HCO_3^- \rightleftarrows CO_3^{2-} + H^+ \tag{3}$$

The second stage is the transportation of CO_2 molecules from the liquid phase to the microalgal cells. First, CO_2 molecules are transferred from the liquid phase to the thin liquid film region near the cell wall, after which it is diffused through the thin liquid film and passed into the cells as the carbon source for microalgal photosynthesis. Consequently, the transmission process can be enhanced by increasing the disturbance of the liquid phase, gas phase, and the fluctuation of the gas-liquid interface. In addition, an increase in the direct contact between microalgal cells with gaseous CO_2 molecules decreases the transportation time the molecules spend in the liquid phase, which plays a certain role in promoting the transmission and consumption of CO_2. Furthermore, smaller gas bubbles are characterized by higher surface areas for mass transfer and longer residence time within microalgal suspension due to their reduced buoyancy as compared to larger bubbles, which provide promising ways to facilitate CO_2 transfer and thus enhances microalgal growth.

When CO_2 molecules are diffused into microalgal cells, they are fixed by RuBisCo and converted to organic carbon by the Calvin-Benson cycle. These molecules are eventually converted into complex biomolecules, such as carbohydrates, fats, and proteins.

2.2.3 Inorganic Nutrients

With the exception of carbon, nitrogen (N) and phosphorus (P) are the other two dominating components in microalgal cells, thereby indicating that the supply of N and P also have a significant influence on microalgal photoautotrophic growth [18]. Inorganic nitrogen forms, such as nitrates, nitrites, and ammonia, are currently the most commonly used nitrogen sources for microalgal phototrophic cultivation, among which nitrates are the most frequently adopted. Nitrogen is mainly used for the synthesis of amino acids, purines, pyrimidines, amino sugars, amines, and chlorophyll as it has an important effect on the metabolism and fission of microalgae [19]. When the N concentration is too low, the total chlorophyll content

of microalgal cells decreases and the demand for light and CO_2 is reduced, which adversely affects the photosynthesis of microalgae. However, when the N concentration is too high, the microalgal growth can be inhibited.

The P sources that are commonly employed in microalgal photoautotrophic cultivation include biphosphate and dihydric phosphate [20]. For microalgal cellular metabolism, P is used to produce ATP, guanosine triphosphate (GTP), nucleic acids, phospholipids, and coenzymes. Moreover, P mainly exists in the protoplasm and nucleus of unicellular microalgal cells and acts as the substrate or regulator that is directly involved in all of the aspects of photosynthesis, including the absorption of light energy, the formation of assimilative force, the Calvin-Benson cycle, the transportation of assimilation products, and the regulation of some key enzymes. In this way, P directly affects the metabolism of carbohydrates, proteins, fats, and other metabolic processes as well as the synthesis of phospholipids, nucleic acids, and some coenzymes in microalgal cells [21]. Generally, the exogenous inorganic phosphorus that is absorbed by microalgae is transported into the microalgal cells via active transportation. The majority of the phosphorus is present as soluble phosphorus in the cytoplasm, of which the residual is converted to polyphosphate for energy storage, for the synthesis of phospholipids, or for other cellular components.

2.2.4 Other Environmental Parameters

Microalgal photoautotrophic growth is also affected by temperature given that temperature can influence the activity of enzymes during photosynthesis and thus affects the metabolism of microalgae [22, 23]. In addition, the pH of the culture medium also has a significant impact on the physiological processes (i.e., growth and metabolism) of microalgae as it influences the activity of enzymes that are crucial for photosynthesis. However, the pH value affects the dissolution and diffusion of CO_2 within the microalgal suspension. Furthermore, the pH value also plays an important role in the respiration of microalgal cells, absorption of ions, the ups and downs of microalgal cellular metabolism, and the associated metabolite production [24].

3 Photobioreactors for Microalgal Photoautotrophic Cultivation

As mentioned in Sect. 2, microalgal photoautotrophic growth is executed through photosynthesis, which is primary influenced by light availability, CO_2 transfer, and nutrients supply. In practice, microalgal photoautotrophic cultivation is realized in open or closed growth systems called photobioreactors (PBRs), which can provide appropriate growth conditions, such as pH, temperature, light, CO_2, and inorganic

nutrients, for the proliferation of microalgal cells [25]. To date, according to the motion state of microalgal cells during cultivation, PBRs for microalgal photoautotrophic cultivation are classified into aqua-suspended PBRs, biofilm PBRs, and PBRs with integrated aqua-suspension and biofilm. The detailed instructions of these PBRs are presented as follows.

3.1 Aqua-suspended PBRs

Aqua-suspended PBRs are currently the dominating microalgal photoautotrophic cultivation devices which cultivate microalgal cells as planktonic cells, suspended in liquid nutrient media in PBRs [25]. Light, CO_2, and inorganic nutrients are the three primary factors that affect microalgal photoautotrophic growth. Hence, for an efficient aqua-suspended PBR, the adequate presence of light, CO_2, and inorganic nutrients should be guaranteed for microalgal cells suspended in culture media. However, due to an inherent property in aqua-suspended PBRs, water accounts for over 95% of the proportion of the total volume [26]. With such large volumes of water, the efficient transfer of light, CO_2, and inorganic nutrients from the surrounding environment to the microalgal cells in culture media is crucial for an aqua-suspended PBR. In this section, we will summarize the recent advances on aqua-suspended PBRs with elevated microalgal growth from the aspects of light, CO_2, and inorganic nutrients transfer enhancement, respectively.

3.1.1 Improving Light Availability of Microalgal Cells in Aqua-suspended PBRs

For microalgal photoautotrophic proliferation, light is indispensable since it is the fundamental driving force for microalgal cells to synthesize chemical energy through photosynthesis [6]. Therefore, light availability is one of the most important factors affecting microalgal growth in any photoautotrophic cultivation system. However, due to strong mutual shading effects between microalgal cells, microalgal cultures in aqua-suspended PBRs are characterized by exponential light attenuation along with the light path [27, 28]. As a consequence, microalgal cells in regions close to the illumination surfaces are generally exposed to excessive light, thereby resulting in harmful photoinhibition. Conversely, most of the cells in the interior regions receive inadequate or no light at all to sustain their growth, both of which are unfavorable for biomass accumulation [28]. In this regard, maintaining an optimal light environment inside the PBR is a key challenge for an efficient high-density aqua-suspended PBR. Intensive efforts have been devoted to address the adverse effects of heterogeneous light distribution on microalgal growth, including bringing light to microalgal cells by employing light-guiding materials, enhancing the circulation of microalgal cells along the light gradient direction by

installing novel static mixers, and improving light penetrability within the microalgal suspension by periodically pre-harvesting microalgal cells with recycled culture medium.

Optimization of Light Distribution by Employing Light-Guiding Materials

According to the relative position between the light source and microalgal cells, the transfer of light to microalgal cells by employing light-guiding materials is an effective approach to homogenize the light distribution within the microalgal culture, thereby alleviating the adverse effect of light attenuation on microalgal growth. Optical fiber excited by artificial lights or sunlight is a means to improve the light distribution within the microalgal culture. When the surface of the end-light illuminated optical fiber is polished mechanically or chemically, light is emitted from the lateral surface of the core, thereby producing the so-called side-light optical fiber. Side-light optical fibers are expected to remarkably enhance the light conversion efficiency of PBRs since they can provide uniform light distribution within the microalgal suspension, thereby resulting in a higher illumination surface area-to-volume ratio [29].

Side-light optical fibers can be directly immersed into the microalgal suspension to serve as internal light sources to achieve efficient light energy transfer without heat generation. For instance, Chen et al. [7] proposed a solar-energy-excited optical fiber PBR system with an internal light source (an optical fiber excited by a sunlight collecting system), as shown in Fig. 4a. In such a system, side-light optical fibers were inserted into the PBR as internal light sources to illuminate the microalgal culture. Specifically, sunlight was collected by Fresnel lenses and transferred via end-light optical fibers to the side-light optical fibers submerged in a microalgal suspension. Subsequently, light was emitted from the rough surfaces of the optical fibers to provide internal illumination for microalgal photoautotrophic growth. Xue et al. [30] developed a novel PBR structure adopting optical fibers as the inner light source to fulfill the flashing light effect of microalgae, thereby achieving a higher light conversion efficiency. As depicted in Fig. 4b, sunlight was collected and transmitted through the end-light optical fibers into a PBR and diffused from the circumference surfaces of light-diffusing optical fibers to illuminate the vicinal regions. Notably, light-diffusing optical fibers were in parallel arrangement inside the PBR and the microalgal suspension was controlled to flow vertically across the light-diffusing optical fibers (Fig. 4b), thereby periodically exposing microalgal cells to illumination conditions. The experimental results indicated the attainment of light/dark frequencies reached over 10 Hz and *Spirulina platensis* and *Scenedesmus dimorphus* microalgal productivities were elevated by 43% and 38% relative to that of the control in the PBR, respectively. However, the high initial investment costs of optical fibers together with the complicated structure of the reactor have largely hindered the further development of this type of PBR.

As an alternative to expensive light-diffusing optical fibers, Hsieh and Wu [31] introduced transparent rectangular chambers (TRCs) made of transparent acrylic
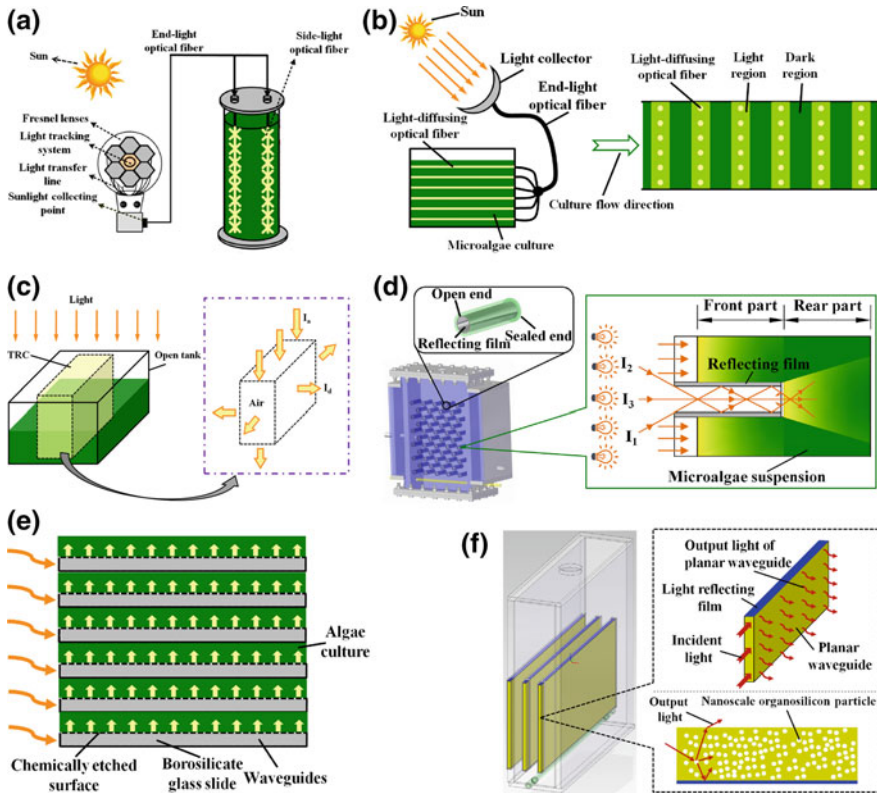
Fig. 4 **a** A solar-energy-excited optical fiber PBR system, adapted from [7], Copyright 2011, with permission from Elsevier, **b** PBR employing optical fibers as inner light source to fulfill flashing light effects of microalgae, **c** an open tank PBR containing transparent rectangular chambers (TRCs) to conduct light deep into the PBR, **d** PBR embedded with hollow light guides, **e** a 10-stack PBR with integrated borosilicate glass slides with chemically etched surfaces, **f** PBR with integrated industrially manufactured planar waveguides doped with light scattering nanoparticles

into an open tank PBR with the aim of conducting light deep into the PBR, especially at high microalgal biomass concentrations (Fig. 4c). As shown in Fig. 4c, a portion of the incident light I_a irradiated into the TRC was diffused from the side surfaces of the TRC (i.e., I_d in Fig. 4c) into the microalgal suspension. Conversely, the rest of the incident light was emitted from the bottom surface of the TRC to provide light for the microalgal cells with deep depths in the reactor. In this way, local light intensities in the microalgal suspension were given by the sum of the incident light flux on the surface and the diffused light flux from the edge surfaces of the TRCs. Large areas of illumination resulted in improved light energy utilization efficiency in this PBR and a 56% increase in the total biomass production as compared to the PBR without TRCs after 13 days of cultivation. Recently, Sun et al. [32] embedded hollow polymethyl methacrylate (PMMA) tubes into a

flat-plate PBR to serve as the light guide to mitigate the adverse effects of poor light penetrability on microalgal growth (Fig. 4d). In particular, aluminum-coated polyethylene terephthalate (PET) films with high reflectivity were adhered onto the inner surfaces of the hollow PMMA tubes (Fig. 4d). In this way, a fraction of the incident light was transmitted and emitted to the interior of the PBR, thereby providing a secondary light source for microalgal cells in light-deficient regions (i.e., the rear part of the PBR). Specifically, when light irradiates onto the open end of the tube, a part of the incident light is transmitted forward via its total reflection on the reflecting film (light paths I_1 and I_2 in Fig. 4d) and the residual fraction is transmitted forward directly through the air (light path I_3 in Fig. 4d). Afterwards, the transmitted light is directly emitted from the sealed end of the tube and irradiates the microalgal cells in the rear part of the PBR. Eventually, the average light intensity of the interior regions that were 3–6 cm from the light incident surfaces was enhanced about 2- to 6.5-fold after 3.5 days cultivation, thereby resulting in a 23.4% improvement in the biomass production relative to that obtained in the control PBR without PMMA tubes under an incident light intensity of 70 μmol m^{-2} s^{-1}. Nevertheless, the introduction of these transparent rectangular chambers and hollow PMMA tubes occupied too much of the effective volumes of the PBRs. Besides, the light distribution characteristics of regions near the light incident surfaces were not optimized and may exhibit harmful photoinhibition.

To improve the light distribution throughout the entire volume of the PBR, Jung et al. [33] designed a 10-stack PBR with integrated slab waveguides for microalgae-based ethylene production, as displayed in Fig. 4e. Borosilicate glass slides with chemically etched surfaces served as waveguides to allow the light within the waveguide to escape (Fig. 4e). In particular, the adjacent stacks exhibited spacing of 2 mm to leverage the advantages of the short-light path design. The experimental results demonstrated that the PBR exhibited the ability to sustain uniform biomass growth throughout the bioreactor for three weeks and exhibited an eight-fold enhancement in biomass productivity. In other words, the stacked architecture design reduced the requirement of intense culture mixing for optimum light distribution due to the optimized light distribution throughout the whole microalgal suspension in the PBR, thereby potentially decreasing the operational costs. However, the secondary processing of the glass slides to form chemically etched surfaces was complicated, hard to control, and difficult to scale-up.

Sun et al. [34] introduced industrially manufactured planar waveguides doped with light scattering nanoparticles to dilute and more uniformly redistribute intense incident light within the microalgal suspension, of which a flat-plate PBR with a width of 25 cm was employed to alleviate the adverse effect of heterogeneous light distribution resulting from the serious light attenuation on microalgal growth (denoted as PW-PBR), as shown in Fig. 4f. Different from the slab waveguides with etched surfaces [33, 35], engineered surface scatterers [36] and wedge-shaped waveguides with notched surfaces [37] which were reported in previous studies, wherein nanoscale organosilicon particles were doped inside the planar waveguides to serve as light scattering media (as depicted in Fig. 4f) and no secondary processing was required when using these planar waveguides. The planar waveguides

doped with light scattering nanoparticles have the advantages of lower cost, longer lifespan, higher luminance uniformity, conveniently able to be cut to any size with no need for secondary processing, etc. When incident light irradiates into the planar waveguide from its edge and is transmitted forward within it, some of the light rays encounter nanoscale organosilicon particles and are then scattered to various directions. Subsequently, the scattered light rays that no longer satisfy the total reflection condition are emitted out from the waveguide surface (Fig. 4f). It is worth noting that from the left side wall of the PW-PBR (Fig. 4f), three adjacent regions separated by the planar waveguides constituted a module and the PW-PBR was scaled-up by increasing the module number. During the entire cultivation period, the illuminated volume fractions in the proposed PBR were 21.4–410% higher over those in the flat-plate PBR without waveguides, thereby resulting in a 220% improvement in the biomass production relative to that in the flat-plate PBR without waveguides. Thereafter, PW-PBRs with different intervals between adjacent waveguides were constructed to determine the optimal configuration of the reactor and the responses of microalgal growth and lipid productivity in the optimized PW-PBR to various initial nitrate concentrations and light intensities emitted from planar waveguide surfaces were investigated [38]. The experimental data demonstrated the effective illuminated volume fraction of the microalgal cells in the regions between the adjacent waveguides under an interval of 10 mm reached 100%. Furthermore, the microalgal growth and lipid accumulation were synchronously enhanced with the rising light intensities emitted from the planar waveguide surface, thereby resulting in a maximum lipid content of 41.7% and a lipid yield of 2200 mg L^{-1} under 560 μmol m^{-2} s^{-1}. Hence, the PW-PBR exhibited great potential in microalgae-based lipid production when operated cost effectively at a large scale. Thereafter, although the use of light-guiding materials has been an emerging effective approach to eliminate the adverse effect of poor light penetrability on microalgal growth in closed PBRs, the integration of light-guiding materials into the open raceway ponds (ORPs) to homogenize light distribution and hence boost microalgal growth has been rarely reported. To fulfill this gap, Sun et al. [39] constructed a lab-scale ORP with built-in planar waveguide modules as light-guiding materials (herein referred to as PWM-ORP) for *Nannochloropsis oculata* cultivation. The light distribution characteristics within the *Nannochloropsis oculata* suspension were significantly improved due to the integration of the planar waveguide modules and the superior light distribution characteristics in the proposed ORP contributed to the 193.33% and 443.71% enhancement in the biomass concentration and lipid yield as compared to those achieved in the conventional ORP, respectively. Meanwhile, the biodiesel obtained in the PWM-ORPs also exhibited better properties over the conventional ORP due to higher monounsaturated fatty acids (MUFAs) and C18:1 component proportions. Notably, the newly-designed PWM-ORP exhibited a promising perspective for its industrial application because both planar waveguides and ORPs have been commercially used. With respect to the scaling up of the PWM-ORP, linear Fresnel lenses or trough solar collectors can be adopted to replace the energy-intensive LED light bars, thereby decreasing the cultivation cost to a further extent.

Enhanced Movement of Microalgal Cells Along the Light Gradient by
Installing Novel Static Mixers

Vigorous mixing is essential for an aqua-suspended PBR as it keeps microalgal
cells in suspension, eliminates thermal stratification, allows even nutrients distri-
bution, enhances gas-liquid mass transfer to prevent oxygen accumulation, etc.
[25]. In addition, proper mixing can shuttle microalgal cells between the light zone
near the illumination surfaces and the dark-interior regions, thereby resulting in
mixing-induced periodic light/dark cycles, which are beneficial for microalgal
growth [40]. Given that microalgal cultures in aqua-suspended PBRs are charac-
terized by exponential light intensity attenuation along with the light path length, a
light intensity gradient was observed along the light path. It has been reported than
microalgal cellular transfer between light and dark regions at a suitable frequency
elevated both the light energy utilization and photosynthetic efficiency of the
microalgal cells [41]. Therefore, the enhanced movement of microalgal cells along
the light gradient is more favorable for microalgal growth as compared to random
mixing. On account of this, the installation of static mixers in PBRs can effectively
facilitate the movement of microalgal cells along the light gradient. As a result,
various attempts have been conducted from this point of view to boost microalgal
growth.

   For instance, Degen et al. [42] developed a novel flat-plate airlift PBR with
baffles to induce regular light cycling in the microalgal suspension, and hence
enhance the microalgal growth via the flashing light effect, as shown in Fig. 5a. To
be specific, the proposed PBR consists of two parts, i.e., the downcomer and riser
zones. Moreover, the riser zone was further subdivided into interconnected
chambers by horizontal baffles that were alternately attached to the front and back
of the larger flat faces of the PBR. When compressed air was injected into the riser
zone, the microalgal suspension fluid inside the chambers circulated, thereby
resulting in the periodic cell movement between the narrow illuminated and deeper
dark zones. Eventually, *Chlorella vulgaris* biomass productivity was 1.7-fold
higher than that attained in a randomly mixing bubble column with identical
dimensions. Similarly, Wang et al. [43] designed a flat-plate PBR with horizontal
baffles alternately attached to the front and back of the PBR, whereas the small
downcomer zone designed in Degen et al. [42] was omitted to improve the scal-
ability of the PBR. By using computational fluid dynamics, the effect of the aeration
intensity, aeration site, and baffle structural parameters on the flow and mixing
performance of PBR were investigated. The experimental data indicated that the
maximum biomass productivity in the optimized PBR was 1.88-fold higher than
that of the control PBR without baffles. To enhance the mixing degree along the
light gradient in a flat-plate PBR characterized by a larger light path of 15 cm,
Huang et al. [44] proposed novel mixers characterized by trapezoidal chambers that
consisted of inclined baffles to promote microalgal culture mixing along the light
gradient (Fig. 5b). Notably, these novel mixers were independent of the PBR to
allow easy removal and cleaning. The flow field and cell trajectories of the PBRs
with these novel mixers were numerically investigated through computational fluid

dynamics (CFD). The results indicated that these novel static mixers significantly enhanced the liquid mixing degree along the light gradient as compared to those in the control PBR without mixers and a 42.9% increase in biomass production was achieved relative to the control PBR without mixers. Yang et al. [45] introduced horizontal tubes and triangular prism (HTTP) baffles that can generate flow vortices into a flat-plate PBR to elevate the solution velocity between the dark and light regions, thereby improving microalgal growth, as depicted in Fig. 5c. The solution velocity, mass-transfer coefficient, and mixing time were measured, of which the results demonstrated that the solution velocity between the dark and light regions increased from ca. 0.9 to 3.5 cm s^{-1}, which is equivalent to a four-fold decrease in the dark/light cycle period, thereby resulting in a 70% improvement in the biomass yield as compared to that in the control PBR.

In addition to the flat-plate PBRs, intensive efforts also have been devoted to enhance the vertical microalgal suspension velocity between the bottom dark and top light zones in ORPs by installing static mixers. Cheng et al. [46] proposed an ORP with built-in up-down chute baffles that can sequentially generate clockwise and anticlockwise liquid vortexes (Fig. 5d). The vertical velocity of the microalgal suspension was measured using a particle imaging velocimeter. The results indicated that the up-down chute baffles accelerated the mixing process, thereby enhancing the vertical liquid velocity and microalgal growth rate. Consequently, the vertical liquid velocity was improved from ca. 0.5 to 6.1 cm s^{-1}, thereby resulting in a 32.6% increase in biomass production as compared to that in the control ORP without baffles.
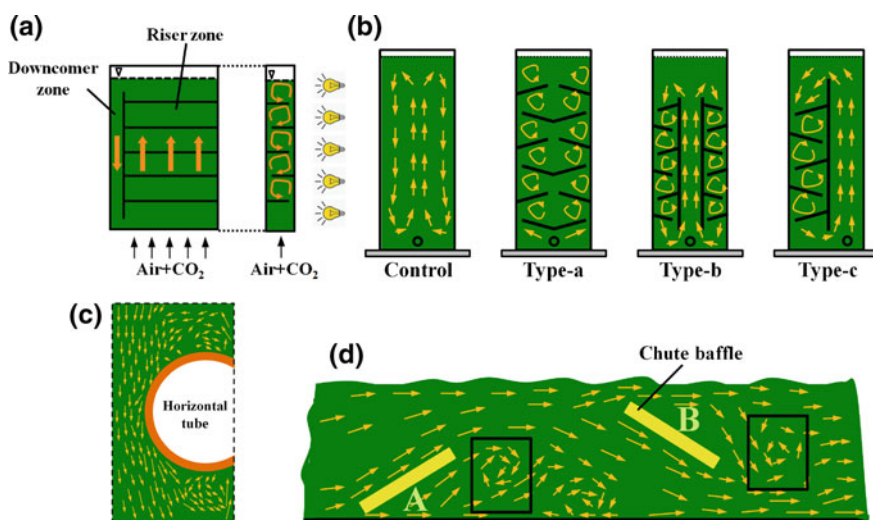
Fig. 5 **a** A flat-plate airlift PBR with baffles to induce a regular light cycling of microalgae, **b** PBR with novel mixers characterized by trapezoidal chambers, **c** flat-plate PBR with new horizontal tubes and triangular prism (HTTP) baffles, **d** an open raceway pond with built-in up-down chute baffles

With the purpose of reducing the dead zone and enhancing the flashing light effect, Zhang et al. [47] developed a novel ORP with flow deflectors and wing baffles. The configurations of the proposed wing baffles were similar to airplane wings, and significant swirling flow was produced in the ORP with built-in wing baffles, whereas no swirling flow was observed in the control pond. When microalgal suspension flowed over the baffles, a pressure difference was created under the wing baffles. At the tips of the wing baffles, the microalgal suspension flowed from the high-pressure region below the foil to the low-pressure region above the foil, thereby creating a vortex off each tip of the baffle. The results demonstrated that the installation of optimized flow deflectors and built-in wing baffles in the raceway pond generated a decrease in the dead zone area of 60.4% and the average light/dark cycle period decreased from 14.0 to 4.4 s. Finally, the *Chlorella* sp. biomass concentration in the wing-baffled raceway pond was 30% higher than that in the control pond. Similarly, Huang et al. [48] proposed the installation of sloping baffles and flow deflectors in the ORP. The results indicated that the newly-designed ORP fitted with the sloping baffles and flow deflectors promoted a 93% increase in the velocity along the light attenuation direction, and the cultivation experiments demonstrated the combination of sloping baffles and flow deflectors significantly improved microalgal productivity.

However, light penetrability decreased exponentially following an increase in biomass concentration, thereby indicating that light distribution characteristics in aqua-suspended PBRs are primarily determined by the biomass concentration in the PBR. As a result, the rational control of the biomass concentration in an aqua-suspended PBR can enhance the light penetrability within the microalgal suspension and thus improves the microalgal growth rate. From this point, Huang et al. [49] put forward a cultivation mode that involves periodically pre-harvesting partial of microalgal cells from the suspension with culture medium recycling. In particular, no additional nutrients were replenished during the culture medium recycling. The results indicated that the daily pre-harvesting of 30% of the microalgal cells from the suspension enhanced the average light intensity in the PBR by 27–122%, thereby contributing to a 46% increase in the total biomass production relative to that cultivated in batch cultivation without pre-harvesting.

3.1.2 Enhancing the CO_2 Transfer in Aqua-suspended PBRs

For microalgal photoautotrophic growth, carbon is one of the most important nutrients as it represents almost 50% of the microalgal biomass dry weight. For an aqua-suspended PBR, CO_2 gas is generally pumped into the microalgal culture in the form of bubbles to provide a carbon source for microalgal photosynthesis. However, the low mass transfer coefficient of CO_2 has been a main limitation in the transfer of CO_2 from the gaseous to the liquid phase as it can greatly limit microalgal growth [15, 50]. Various approaches have been proposed to enhance CO_2 transfer in aqua-suspended PBRs and thus boost microalgal growth.

The enlargement of the gas-liquid contacting area by reducing the size of the gas bubbles that are aerated into the PBRs has been recognized as one of the most effective ways to increase the overall mass transfer coefficient of CO_2. From this point of view, Cheng et al. [51] constructed a PBR integrated with a hollow fiber membrane module to remove CO_2 from air using microalgae (Fig. 6a). Specifically, the gas outlet of the hollow fiber membrane module was sealed, and the module was connected to the PBR. The microalgal suspension was driven to circulate between the membrane module and PBR by a peristaltic pump, and CO_2 was permeated into the microalgal culture through a hollow fiber membrane tube contained in the membrane module. In this way, the retention time of the smaller and more uniform gas bubbles in the new membrane-PBR increased from 2 to more than 20 s, thereby resulting in an improved CO_2 fixation rate from 80 to 260 mg L^{-1} h^{-1}. Hollow fiber membranes have demonstrated their ease and effectivity in supplying CO_2 into the microalgal culture. Similarly, to enhance the mass transfer of CO_2 from the gaseous to the liquid phase, Fan et al. [52] designed a membrane-sparged helical tubular PBR, which consisted of a cylindrical-shaped light receiver and a mass transfer system, as illustrated in Fig. 6b. Specifically, for the mass transfer system, hollow fiber membranes were uniformly fitted inside the reactor to function as the gas sparger and to generate small bubbles. The experimental results demonstrated improvement in microalgae-based CO_2 biofixation following the introduction of the membrane sparger. Recently, Kim et al. [53] proposed an advanced material PBR, i.e., the direct membrane-carbonation PBR (DMCPBR) in which a membrane carbonation (MC) module of hollow fiber membranes was directly submerged inside the DMCPBR. By matching the CO_2 flux to the carbon demand of photoautotrophic microalgal growth, over 90% of the supplied CO_2 was utilized by the DMCPBR, which exhibited an opportunity to improve the CO_2 delivery efficiency for microalgal cultivation. Zheng et al. [54] designed a novel membrane system to directly deliver CO_2 to microalgae from CO_2 capture solvents. To be specific, CO_2 was first absorbed by the potassium carbonate solvent and then the CO_2 gas was desorbed directly into the microalgal medium through a non-porous polydimethylsiloxane (PDMS) hollow fiber membrane submerged inside microalgal ponds or a bioreactor (Fig. 6c). In this way, Chlorella sp. exhibited elevated growth as compared to the control PBR, and the maximum volumetric productivity and biomass concentration reached 0.38 g L^{-1} d^{-1} and 1.8 g L^{-1}, respectively, by completely avoiding carbon limitation in the culture.

Another way to enhance the transfer of CO_2 into microalgal suspension is to prolong the retention time of the CO_2-enriched bubbles within the microalgal culture. Based on this point, Ketheesan and Nirmalakhandan [55] developed a pilot-scale airlift-driven raceway pond consisting of a raceway section and an airlift section, as illustrated in Fig. 6d. The airlift section was composed of plexiglass pipe with a built-in central partition to serve as a U-tube, thereby forming the downcomer and riser. Air was aerated into the pond from the bottom of the riser side of the U-tube to create fine bubbles. The microalgal suspension was driven around the raceway pond due to the density difference between the downcomer and riser (Fig. 6d). Supplemental CO_2 was injected at the mid-depth of the downcomer to

(a) Hollow fiber membrane tube, Hollow fiber membrane module, Fluorescent lamp, Microalgae culture, CO_2+N_2, Peristaltic pump

(b) Light receiver, Microalgae culture, Hollow fiber membranes, Mass transfer system, Gas inlet, Peristaltic pump

(c) CO_2 depleted gas, Lean solvent, Microalgae ponds or bioreactor, Microalgae culture, Raw flue gas, Load solvent, Pump, HCO_3^-, $CO_2 \rightarrow CO_2$, $CO_2 \leftarrow CO_2$, CO_3^{2-}

(d) Flow direction, Air-lift section, Central partition, Microalgae culture, CO_2, Air, Sparger

(e) H-shaped cover, Side wall, Microalgae culture, Flow direction, Paddle wheel, Water clapboard

(f) Flow trajectory of microalgae solution, Gas bubbles, Oscillating baffle, Compressed gas, Oscillating gas aerator, Pumped water, Microalgae suspension

(g) Oscillating baffle, Flow trajectory of microalgae solution, Gas bubbles, Swing gas aerator, Microalgae suspension

◄**Fig. 6** **a** A PBR integrated with a hollow fiber membrane module to remove CO_2 from air by using microalgae, **b** a membrane-sparged helical tubular PBR, **c** a novel membrane system used for delivering CO_2 to microalgae directly from CO_2 capture solvents, **d** a pilot-scale airlift-driven raceway reactor consisted of the raceway section and the airlift section, **e** an open raceway pond covered with specially designed transparent cover, **f** an open raceway pond integrated with a novel oscillating gas aerator combined with an oscillating baffle to generate smaller aeration bubbles and thus enhance solution mass transfer and **g** an open raceway pond integrated with a swing gas aerator

allow the downward flow of the suspension in the downcomer to retain the rising CO_2 bubbles for a longer period and carry them towards the riser, thereby improving the transfer of CO_2 into the microalgal culture and generating a maximum CO_2 utilization efficiency of 33%. However, with the aim of preventing CO_2 from directly escaping into the atmosphere and thus prolonging the retention time of CO_2 in the ORP, Li et al. [56] covered the ORP with a specially designed transparent cover that was in direct contact with the surface of the microalgal culture, as shown in Fig. 6e. The CO_2 mass transfer and CO_2 fixation efficiency of the microalgae in the closed ORP were investigated. Notably, CO_2 reached a fixation efficiency of 95% under intermittent gas sparging.

Furthermore, gas aerators play an important role in microalgal photoautotrophic cultivation given that smaller bubbles provide larger gas-solution interfacial areas and higher mass transfer coefficients. From this point, Yang et al. [57] proposed a novel oscillating gas aerator combined with an oscillating baffle to generate smaller aeration bubbles and thus enhance CO_2 mass transfer, as depicted in Fig. 6f. In the proposed oscillating gas aerator, the shearing lift force played a major role in removing generated bubbles from the aerator orifice in the presence of cross flow velocity. As such, the compressed gas was broken into smaller bubbles due to the enhanced shearing lift force that resulted from the intensively oscillating pumped solution inside the gas aerator (Fig. 6f). The results indicated that the optimized oscillating gas aerator decreased the bubble diameter and bubble generation time by 25% and 58% relative to a horizontal tubular gas aerator, respectively. In addition, the CO_2 mass transfer coefficient was increased by 15%, thereby resulting in a 19% improvement in the microalgal biomass yield. Thereafter, Yang et al. [58] replaced the oscillating gas aerator with a swing gas aerator made of a rubber hose with the length of 15 mm, as displayed in Fig. 6g. When the swing gas aerator was operated within the microalgal culture, small bubbles were generated due to the enhanced shearing lift force. In this way, the CO_2 mass transfer coefficient exhibited an improvement of 25% and an increase of 18% in biomass production. In addition, when CO_2 bubbles rise due to buoyancy within the microalgal suspension, the dynamic behaviors of the CO_2 bubbles significantly affect CO_2 mass transfer and thus arouse uneven distribution of the microalgal cells inside the PBR due to the bubble carrying effect. In consideration of this, Huang et al. [59] recently designed a gas distributor with an optimized vent hole diameter and arrangement. When microalgal cells were cultivated using the gas distributor with a hole diameter of 0.5 mm and an inner hole spacing distance of 1.5 mm, the microalgal cells

exhibited the highest growth rate and carbon sequestration ability, thereby demonstrating that the dynamic behaviors of the CO_2 bubbles indeed provided important theoretical guidance for the optimization of the subsequent PBR design and operating conditions.

3.1.3 Enhancing Inorganic Nutrients Transfer Within the Microalgal Culture in Aqua-suspended PBRs

In addition to light and CO_2, N and P are two essential inorganic nutrients for microalgal photoautotrophic growth. As N is a major element of nucleic acids and proteins, the starvation of N can hinder microalgal growth. P is a critical component of organic molecules, including nucleic acids (DNA and RNA), ATP, and membrane phospholipids, that are essential for microalgal metabolism [60]. Under the P-deficient condition, various aspects of intracellular metabolism, including nitrate transportation and protein synthesis (N needed), can be downregulated due to the limitation of adenylate and plasmalemma H^+-ATPase activity. In this regard, sufficient N and P are crucial for the accumulation of the microalgal biomass. Nevertheless, an excess of N and P nutrients can inhibit microalgal growth. In addition, deliberate N and P limitation is an often adopted to trigger lipid accumulation in microalgal cells for the production of biofuels. From this point of view, Fu et al. [61] proposed a self-adaptive microalgal PBR in which anion exchange membranes were introduced (Fig. 7a). To be specific, the anion exchange membrane is a kind of organic polymer membrane characterized by certain active groups on the surface, which shows selectivity for the permeation of different anions. As for the designed PBR, N and P can be continuously transferred from the feeding medium inside the feeding chamber to the microalgal suspension inside the cultivating chamber by the driving force of the ion concentration gradient, which not only provides adequate nutrients for microalgal growth but also avoids any adverse effects caused by the excessive nutrients that were initially added in the batch cultivation. The experimental data exhibited a 129% improvement in biomass
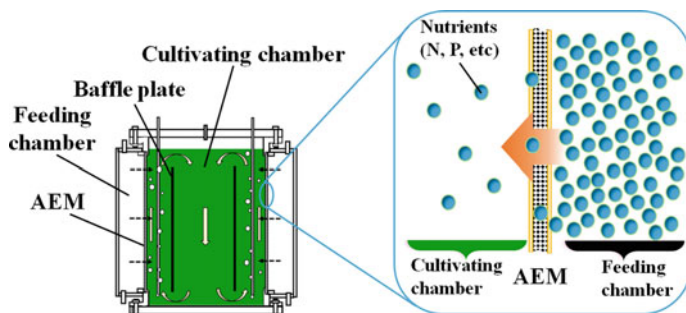
Fig. 7 A self-adaptive microalgae PBR with anion exchange membranes

production as compared to that obtained in the control PBR with all of the nitrogen added in the culture medium at the beginning of the batch growth. Thereafter, an annular PBR with an ion exchange membrane for microalgal cultivation together with wastewater treatment (denoted as IEM-PBR) was designed [62]. Particularly, the IEM-PBR avoided the direct mixing of the microalgal suspension with wastewater by means of separating them into two chambers. Nutrients (mainly N and P) contained in the wastewater were continuously permeated into microalgal suspension across the ion exchange membrane to enable microalgal growth, whereas the pollutants hardly permeated into the microalgal suspension. In this way, the negative impacts of the pollutants in the wastewater on the microalgal growth were greatly reduced. The results indicated that microalgal growth under the wastewater characterized by excess nutrients, high turbidity, and excess heavy metals exhibited significant improvements in the maximum microalgal biomass concentrations from 2.34, 2.15, and 0 g L^{-1} in the conventional PBR to 4.24, 3.13, and 2.04 g L^{-1} in the IEM-PBR, respectively. That is to say, the newly designed annular IEM-PBR provided a promising approach to exploit nutrients in wastewater for microalgal photoautotrophic cultivation.

3.2 Microalgal Attached Biofilm Cultivation PBRs

Although aqua-suspended PBRs are currently the predominant systems for microalgal photoautotrophic cultivation, many inherent disadvantages of these aqua-suspended PBRs are hard to overcome, such as huge water requirements, high energy costs in biomass harvesting, poor biomass productivity, difficulty in scaling up, susceptibility to contamination, etc. [63]. In recent years, microalgal attached biofilm cultivation has been regarded as a promising alternative to aqua-suspended PBRs. Generally, microalgal cells were directly inoculated onto the surfaces of supporting materials in the form of high-density nutrient-fed biofilm, also termed as biofilm cultivation. As compared to aqua-suspended cultivation, this method has the advantages of reduced water requirements, easier harvesting, better contamination control, and simpler scale-up. Moreover, Huang et al. [64] also validated that the effective illumination portion of the cells in the biofilm was much higher than that in the aqua-suspended microalgal culture. In addition, microalgal cells in biofilm appeared more amiable to CO_2 than those in aqua-suspended microalgal culture. Consequently, the enhanced CO_2 and light transmission within microalgal biofilm exhibited an improved light energy conversion efficiency and microalgal biomass productivity.

As examples of these microalgal attached biofilm cultivation PBRs, Ozkan et al. [65] reported a microalgal biofilm PBR consisting of a biofilm growth surface, a nutrient medium recirculation system, and an illumination device, as depicted in Fig. 8a. To be specific, the biofilm growth surface was a concrete substrate layer placed over a wood supporting flat plate. For the nutrient medium recirculation

system, the culture medium was delivered by dripping nozzles located right above the concrete substrate layer. In particular, the microalgal growth surface was tilted by 0.2° with respect to the horizontal line to enable gravity-driven nutrient medium flow over the microalgal biofilm. According to the results, the required water to produce per kilogram of microalgal biomass was reduced by 45% and the dewatering energy requirement was correspondingly decreased by 99.7%. Thereafter, Liu et al. [66] proposed a novel microalgal biofilm cultivation method in which microalgal cells were evenly filtered onto a cellulose acetate/nitrate membrane to form a microalgal 'disk'. In addition, each microalgal 'disk' was placed onto an artificial substratum material composed of a piece of filter paper, after which the filter paper was attached onto a rigid glass flat plate (Fig. 8b). The culture medium was dripped down from a perforated nylon tubing placed on the top brim of the glass flat plate into the interval between the filter paper and glass flat plate, thereby maintaining the wetness of the filter paper, cellulose membranes, and microalgal 'disks' as the culture medium flowed down under gravitational effects. Given that the aqua-medium and microalgal cells were largely separated, the disadvantages caused by the huge water proportion could be significantly neutralized. In general, the merits of the proposed microalgal attached biofilm cultivation method included water savings, high microalgal biomass productivity, and highly efficient harvesting. Additionally, each of the glass flat plate together with the attached microalgal biofilm 'disks' could be regarded as a 'cultivation module'. In addition, this type of microalgal attached biofilm cultivation PBR can be scaled up by increasing the corresponding module number. Notably, the microalgal cells must cover the entire surface of the filter paper in the subsequent practice applications. On the basis of this cultivation method, *Scenedesmus obliquus* exhibited an outdoor cultivation biomass productivity of 50–80 g m^{-2} d$^{-1,}$ which corresponds to a photosynthetic efficiency of 5.2–8.3% (total solar radiation). Afterwards, Zhang et al. [67] constructed a small-scale outdoor attached biofilm cultivation PBR for *Spirulina platensis* growth characterized by daily harvesting for 10 days, the results of which exhibited an average microalgal productivity of 60 g m^{-2} d^{-1} (Fig. 8c). Microalgal attached biofilm cultivation has also been applied in wastewater treatment. As depicted in Fig. 8d, Shi et al. [68] immobilized *Halochlorella rubescens* onto sheet-like surfaces in a vertical arrangement and operated the system employing the primary and secondary municipal wastewater as nutrient sources for microalgal cultivation. According to the results, microalgal growth was not impaired by the suspended solids or bacteria throughout the entire growth process.

3.3 PBRs with Integrated Aqua-suspended and Attached Biofilm Cultivation

Except for the aqua-suspended PBRs and attached biofilm PBRs for microalgal cultivation, PBRs with integrated aqua-suspended and attached biofilm cultivation
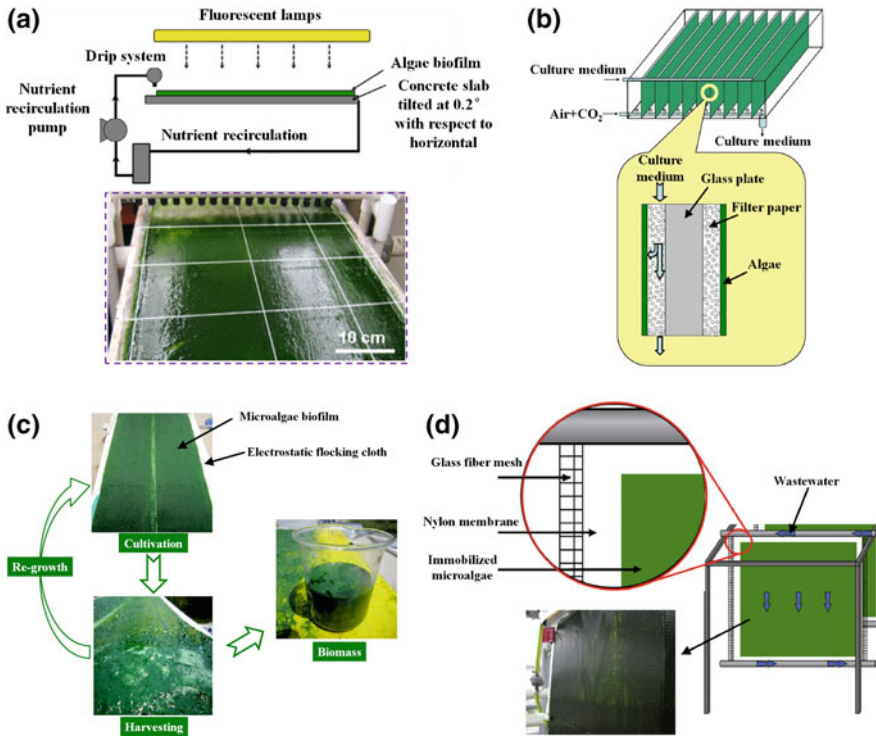
Fig. 8 **a** A microalgal biofilm PBR, adapted from [65], Copyright 2012, with permission from Elsevier, **b** a novel microalgal attached biofilm cultivation method, adapted from [66], Copyright 2013, with permission from Elsevier, **c** an outdoor microalgal attached biofilm cultivation bench-scale PBR for *Spirulina platensis* cultivation, adapted from [67], Copyright 2015, with permission from Elsevier, and **d** microalgal attached biofilm cultivation applied for wastewater treatment, adapted from [68], Copyright 2014, with permission from Elsevier

have also been proposed and have exhibited promising prospects. For example, Zhuang et al. [69] established a suspended-solid phase PBR (referred as ssPBR) in which solid carriers were added and kept suspended via bubble aeration (Fig. 9a). In the process of microalgal growth, some microalgal cells attached onto the suspended-solid phase carriers. Thereafter, when the quantity of the microalgal biomass attached onto the suspended-solid carriers reached a certain amount, the suspended carriers attached to the high-density microalgal biofilm were easily removed from the ssPBR for biomass harvesting. Notably, these suspended-solid carriers could be put back into the ssPBR for recycling following the harvesting of the microalgal biomass attached onto the carriers. The experimental results demonstrated a 30% increase in biomass production in the ssPBR as compared to that in the control PBR. Similarly, Gao et al. [70] proposed a microalgal attached biofilm membrane PBR (denoted as BMPBR) equipped with solid carriers and a

submerged membrane module, as depicted in Fig. 9b. In the designed BMPBR, the submerged membrane module functioned as a solid-liquid separator that could completely separate the suspended microalgal cells from the culture medium, whereas the solid carriers made of flexible fiber bundles served as the supporting material for attachment of the suspended microalgal biomass.

On the other hand, Gross et al. [71] designed a rotating algal attached biofilm (RAB) cultivation PBR (Fig. 9c). To be concrete, a flexible cell attachment material was stretched around the three shafts in the form of a triangular configuration. In particular, the lowest elevated corner of the triangular configuration was submerged within a nutrient-rich medium reservoir for nutrients feeding, whereas the rest of the attachment material was directly exposed to the surrounding atmospheric conditions. In terms of the working process of the RAB cultivation PBR, the flexible cell attachment material was rotated, thereby periodically exposing the microalgal cells to the nutrient-rich liquid phase and CO_2-rich gas phase. As a consequence, the microalgal biofilm attached on the material alternatively accessed nutrients and CO_2
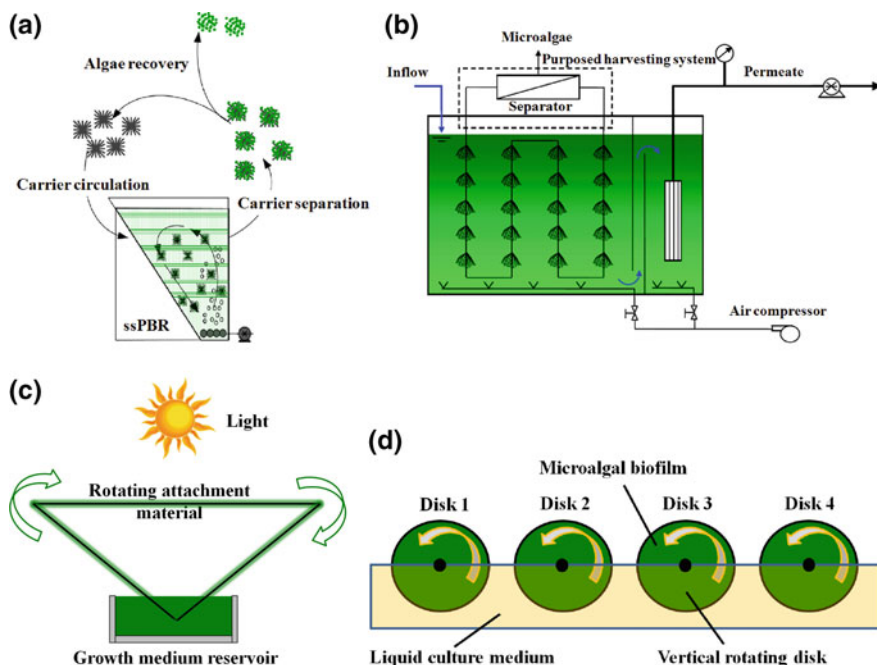
Fig. 9 **a** A suspended-solid phase PBR (named as ssPBR) in which suspended-solid carriers were added and kept suspended by bubble aeration, adapted from [69], Copyright 2014, with permission from Elsevier, **b** a microalgal biofilm membrane PBR (referred as BMPBR) integrated with solid carriers and submerged membrane module, adapted from [70], Copyright 2015, with permission from Elsevier, **c** a rotating microalgal biofilm (RAB) cultivation system and **d** a PBR based on a rotating biological contactor

to sustain their growth. After a few days of growth, a thick microalgal biofilm was formed on the attaching material. At that time, the high-density microalgal biomass was easily harvested by scraping the biofilm with a rubber knife. In the meantime, the residual microalgal cells remaining on the material served as the inoculum for the next microalgal biofilm growth cycle. Eventually, the RAB system was experimentally demonstrated as an efficient microalgal photoautotrophic cultivation system due to its easier biomass harvesting process and its elevated biomass productivity.

Thereafter, Blanken et al. [72] constructed a PBR based on a rotating biological contactor (RBC), which is referred to as Algadisk. In the proposed PBR, microalgal cells grew in the form of biofilm attached onto the vertical rotating disks that were partially submerged within a liquid culture medium (Fig. 9d). When the microalgal biomass attached on the rotating disk reached a certain amount, the corresponding microalgal attached biofilm was conveniently harvested by scraping. Afterwards, the microalgal cells attached onto the rotating disk regrew in the form of biofilm from the microalgal biomass that remained on the disk surface. The experimental results indicated that the proposed cultivation system was stable for over 21 weeks and a disk diameter of at least 1.5 m was observed for practice applications.

4 Potential Technologies for Photoautotrophic Microalgal Biomass Conversion

Microalgal photoautotrophic cultivation has four characteristics. The first and foremost is the dilute nature of the microalgal suspension (generally the microalgal biomass concentrations are lower than 6 g L^{-1}), thereby deeming it necessary to concentrate and harvest microalgal biomass from the culture medium prior to the downstream energy conversion of the microalgal biomass [73]. Second, the density of microalgal cells is close to the water (1070–1140 kg m^{-3}), thereby indicating the ineffectiveness of gravity sedimentation (i.e., the easiest method for solid-liquid separation) on microalgal biomass harvesting [74]. Third, the small size of the microalgal cells with diameters ranging from 2 to 20 μm challenged the harvesting of microalgal biomass via filtration [75]. Lastly, the surfaces of the microalgal cells are generally electronegatively charged with an intensity within a range of −10 mV for *Chlorella* to −35 mV for *Scenedesmus* over a wide pH range [76]. The electrostatic repulsion effects between the microalgal cells resulted in the suspended stability of the microalgal cells within the culture medium, which further increases the difficulty in microalgal biomass harvesting. However, the downstream utilization of the microalgal biomass for energy conversion is primarily dependent on the high-density concentrated microalgal biomass. In this regard, the dewatering process for microalgal suspension is essential and is of vital importance.

4.1 Microalgal Suspension Dewatering and Biomass Harvesting

To date, the prevailing microalgal biomass harvesting methods consist of flocculation, flotation, centrifugation, filtration, or a combination of them, as summarized in Table 1. Nevertheless, on account of the high energy consumption, it is unfeasible to apply centrifugation and filtration in large-scale applications without prior pre-concentration [77, 78]. Moreover, the filtration process requires relatively higher operating and maintenance costs, and frequent membrane replacements caused by continuous fouling make it more complicated to operate [77]. Although flotation is generally adopted in the field of wastewater treatment and is often preceded by flocculation, it is much more effective than flocculation [79]. However, added chemical flocculation agents are always difficult to remove and an excess of added flocculants is harmful to microalgal cells. For example, the application of ferric salts has been proved to induce brown-yellow coloration in microalgal cells, and cytolysis was observed following the addition of aluminium salts [80, 81]. Furthermore, the cost of the microalgal harvesting process was estimated to account for 20–30% of the total cost of microalgae-based biofuel production [73].

Hence, an ideal microalgal biomass harvesting method should be applicable to many different microalgae strains, convenient to achieve high biomass concentrations and recovery efficiencies, and require only moderate costs of operation [85]. Generally, two microalgal biomass harvesting strategies, i.e., the single-step concentrating process and the two-step concentrating process, have been employed. The two-step concentrating process consists of a primary harvesting step to produce 2–7% total suspended solids (TSS), followed by a thickening step to generate 15–25% TSS [82]. In other words, the two-step concentrating process for microalgal harvesting is comprised of the two-stage concentrating process, i.e., the primary harvesting and subsequent thickening steps [73]. The two-step concentrating

Table 1 Comparisons of the prevailing microalgal biomass harvesting methods

	Costs	Biomass recovery efficiency (%)	Concentration range (% solids)	Disadvantages	Refs.
Flocculation	Low	40–95	1–5	Contamination issues and slow process	[74]
Centrifugation	High	80–90	10–25	High energy input	[82]
Filtration	Medium-high	70–90	5–15	Slow process and high operating costs	[83]
Flotation	Low–medium	80–90	2–6	Contamination issues and high costs	[84]

process can reduce the overall cost given that the thickening step, which is much more energy-intensive than the primarily harvesting step, can be conducted on concentrated microalgal suspension [86, 87]. In particular, for microalgal photoautotrophic cultivation, the most feasible scheme for large-scale microalgal biomass harvesting is the adoption of flocculation or flotation as the primarily harvesting step, followed by centrifugation or filtration to further thicken the microalgal suspension.

4.2 Biomass Conversion

Given that the major compositions of microalgal biomass, proteins, carbohydrates, and lipids contain reduced carbon that can be oxidized exothermically, these all represent potential energy sources. Although energy is important, it is not necessarily the best product that can be produced from the different components. In particular, protein is not an ideal feedstock for energy production as it has greater utility as a nutrient (e.g., for animal or aquaculture applications) [88]. Similarly, pigments, carotenoids, and lipids that contain omega-3 fatty acids are much more valuable as nutritional supplements than as energy feedstocks [89].

Most microalgae have the ability to store energy in the form of intracellular oil droplets or starch granules. These are the compounds that are most readily convertible into fuels and the most suitable feedstocks for energy production. However, the cost of producing only biofuels from microalgal biomass is not competitive with petroleum-based fuels [90, 91]. The most economically sensible approach to obtain energy from microalgal biomass is to produce energy from oils or carbohydrates while retaining the value of proteins and other components in a so-called 'biorefinery'.

In recent years, many studies have focused on methods for extracting lipids from microalgal cells. However, many of these methods, such as Soxhlet, Kochert, liquid-liquid extraction, and supercritical fluid extraction [92–94], are only suitable for laboratory or small-scale applications as these require drying, which necessitates prohibitive amounts of energy [95, 96]. For the conversion of microalgal biomass obtained from photoautotrophic cultivation, it is more economical and effective to adopt the methods that can be applied to wet, concentrated microalgal slurries. These include hydrothermal liquefaction, dilute acid hydrolysis, and lipid extraction.

4.2.1 Hydrothermal Liquefaction

Hydrothermal liquefaction is a process in which the macromolecular constituents of wet biomass are hydrolyzed into smaller organics during exposure to subcritical water (200–400 °C and 10–40 MPa) [97]. This results in the production of a liquid biocrude (or bio-oil) fuel precursor, as well as aqueous, gaseous, and solid

by-products [98]. While nitrogen- and phosphorus-containing nutrients can potentially be recycled back to the microalgal cultures following sufficient dilution [99], nitrogen can remain as a contaminant in the biocrude oil [98]. An additional drawback is that the value of the protein is at best degraded back into a low-grade nutrient, which disregards the added value provided by the conversion of low-grade nitrogen into a protein by the microalgae. An alternative to processing the whole biomass is the adoption of a 'biorefinery' approach, wherein proteins and/or lipids are first fractionated from the residual biomass, which can then be separately subjected to hydrothermal liquefaction [100].

4.2.2 Dilute Acid Hydrolysis

Dilute acid hydrolysis is another thermochemical process for obtaining biofuels from microalgal biomass. During this approach, fermentable sugars (e.g., glucose) are released from the cellulosic and starch components of the microalgal cells through acid-catalyzed hydrolysis. These sugars are then fermented into ethanol and the lipids and proteins are recovered separately [101]. Slurries of 15% w/v biomass have been processed using acid concentrations of up to 4% and temperatures in the range of 120–170 °C [102]. At these temperatures, proteins are denatured and they are likely to undergo some chemical degradation, including via the Maillard reaction [103].

This process breaks down the cell walls, thereby eliminating the requirement of cell rupture by high-pressure homogenization. However, to obtain ethanol from carbohydrates, additional unit operations of fermentation and ethanol distillation are required. These can be costly if only dilute sugar solutions are obtained that produce low titers of ethanol.

4.2.3 Lipid Extraction

Oils (i.e., TAGs) recovered from microalgal biomass are an alternative feedstock for biodiesel that can be produced with greatly reduced demands for arable land and fresh water. TAGs are hydrophobic. As a result, they can be selectively recovered from other biomass components using organic solvents [95]. Although polar solvents, such as ethanol and isopropyl alcohol, can be effective, they are miscible in water which necessitates energy-intensive thermal distillation for their recovery. Therefore, the energy-efficient recovery of lipids from wet microalgal biomass requires the use of immiscible solvents that can be physically separated [104, 105], such as hexane, which is used extensively for soybean oil extraction [106]. Effective lipid recovery can be achieved by employing immiscible solvents after the cells have undergone mechanical rupture by high-pressure homogenization [105].

As compared to hydrothermal liquefaction and dilute acid hydrolysis, lipid extraction can be performed at sufficiently low temperatures (<60 °C) [107] to avoid protein denaturation and any possible chemical degradation of the protein or

nutraceutical components. In addition, non-polar solvents are selective to TAG, thereby allowing the omega-3 fatty acid-rich polar membrane lipids to remain in the delipidated biomass [108]. A key requirement for energy efficiency is to reduce the amount of solvent used in relation to the TAG recovered [104]. While most of the lipid-containing solvent can be physically recovered from the microalgal biomass, the solvent must be recovered from the lipid. At present, this proceeds via thermal evaporation. While this process can be sufficiently energy efficient [104], there is potential for further improvement if novel technologies, such as the use of switchable solvents [109, 110] or membrane-based solvent-lipid separation [111] can be successfully developed. However, the challenge of fully recovering of lipid-rich hexane via centrifugation has yet to be resolved. It has been shown that the separation process is limited by barriers to coalescence presented by the strongly emulsifying properties of the ruptured cells [112].

4.2.4 Conversion of Lipids to Fuels

As mentioned above, the TAG derived from microalgal biomass can be converted to biodiesel. This is achieved by transesterification, which converts the triacylglyceride into glycerol and three fatty acid methyl (if methanol is used) esters (FAME). Base-catalyzed transesterification is the most economical. However, acid catalysis and enzymatic transesterification are alternative methods that are currently being investigated. The TAG recovered from microalgae have other components, including some polar lipids, sterols, and pigments, which should be removed via degumming. The fatty acid profile of the TAG obtained from the microalgal biomass must also be considered as it directly affects the functional properties of the biodiesel, such as cold flow, oxidative stability, etc. [113, 114]. Alternatively, microalgae-based TAG can be converted into biojet fuel through the hydrotreatment process, in which the partially oxidized organics are catalytically reduced using hydrogen [115, 116].

4.2.5 Comparison of the Technologies

Each of the three technologies discussed here have unique advantages and disadvantages. Ultimately, the adoption of these methods significantly depends on the economics. In this regard, there are a number of thorough and instructive technoeconomic assessments [90]. However, these are inherently limited by the lack of full-scale data and large uncertainty in the markets (i.e., the market prices of protein, fuel, nutrients, etc. must be extrapolated over multiple decades). This makes it difficult to predict with any certainty which technology will be favored. Nonetheless, a comparison of certain key differences between the technologies can be instructive. In particular, differences in the utilization of the various microalgal

Table 2 Comparative summary of processing options for producing liquid fuels from microalgal biomass

	Hydrothermal liquefaction	Dilute acid hydrolysis	Lipid extraction
Fuel type	Biocrude—long range transportation after conversion	Ethanol—petroleum substitute/blend; and biodiesel or biojet—long range transportation	Biodiesel or biojet fuel—long range transportation
Biomass processing temperature	200–400 °C	120–170 °C	<60 °C
Fate of protein	Fully degraded into contaminants and recyclable nutrients	Recoverable, but denatured and likely with some chemical degradation—likely suitable for animal or aquaculture feed depending on extent of degradation	Recoverable with minimal denaturation and no chemical degradation or reactions—suitable for animal or aquaculture feed after desolventisation
Fate of TAGs	Converted to biocrude, gas, solids, aqueous	Converted to biodiesel or biojet if combined with solvent extraction	Converted to biodiesel of biojet fuel
Fate of carbohydrates	Converted to biocrude, gas, solids, aqueous	Converted to ethanol	Recoverable for inclusion in animal/aquaculture feed
Fate of nutraceuticals[a]	Converted to biocrude, gas, solids, aqueous	Recoverable but likely to undergo some chemical degradation	Recoverable with no chemical degradation
Technical challenges	Yield and quality of biocrude	Low ethanol titres	Physical separation of solvent

[a]Omega-3 fatty acids, pigments and carotenoids

components are important and inherent to each process (Table 2). Major technical challenges have also been identified (Table 2) that may be minimized through continuous research and development. By targeting these issues, these technologies can advance and their costs can reduce over time.

5   Perspectives

Although many effective methods have been proposed to improve microalgal photoautotrophic cultivation, most of them were conducted at the laboratory scale. To produce abundant amounts of microalgal biomass, future work must scale up these PBRs to the commercial scale. However, PBR scaling up presents many obstacles. First, for commercial scale PBRs, sunlight must be employed as the

primary light source for microalgal photoautotrophic cultivation rather than artificial light sources to reduce cultivation costs. In this regard, the structures of the PBRs must be adjusted during scaling up. Second, biomass production in aqua-suspended PBRs must be further improved through the optimization of light distribution within the microalgal culture. Third, for microalgal attached biofilm PBRs, cheap supporting substratum material should be selected and convenient approaches to inoculate microalgal cells onto supporting substratum materials should be proposed. For microalgal biomass harvesting, novel pathways with lower energy consumption, lower costs, and higher efficiency need to be developed. To increase microalgae-based lipid productivity, cultivation that simultaneously enhances microalgal growth and lipid accumulation should be exploited. Furthermore, given the high-energy consumption of during microalgal biomass, the development of cost-effective biofuel conversion methods using wet microalgal biomass are urgently required.

References

1. Sambusiti C, Bellucci M, Zabaniotou A, Beneduce L, Monlau F (2015) Algae as promising feedstocks for fermentative biohydrogen production according to a biorefinery approach: a comprehensive review. Renew Sustain Energy Rev 44:20–36
2. Uggetti E, Sialve B, Trably E, Steyer JP (2014) Integrating microalgae production with anaerobic digestion: a biorefinery approach. Biofuels Bioprod Biorefin 8(4):516–529
3. Chisti Y (2013) Constraints to commercialization of algal fuels. J Biotechnol 167(3):201–214
4. Zhang L, Xu CC, Champagne P (2010) Overview of recent advances in thermo-chemical conversion of biomass. Energy Convers Manag 51(5):969–982
5. Lam MK, Lee KT, Mohamed AR (2012) Current status and challenges on microalgae-based carbon capture. Int J Greenh Gas Control 10:456–469
6. Huang G, Chen F, Wei D, Zhang X, Chen G (2010) Biodiesel production by microalgal biotechnology. Appl Energy 87(1):38–46
7. Chen CY, Yeh KL, Aisyah R, Lee DJ, Chang JS (2011) Cultivation, photobioreactor design and harvesting of microalgae for biodiesel production: a critical review. Bioresour Technol 102(1):71–81
8. Yoo C, Jun SY, Lee JY, Ahn CY, Oh HM (2010) Selection of microalgae for lipid production under high levels carbon dioxide. Bioresour Technol 101(1):S71–S74
9. Peers G, Truong TB, Ostendorf E, Busch A, Elrad D, Grossman AR et al (2009) An ancient light-harvesting protein is critical for the regulation of algal photosynthesis. Nature 462 (7272):518–521
10. Wahidin S, Idris A, Shaleh SRM (2013) The influence of light intensity and photoperiod on the growth and lipid content of microalgae *Nannochloropsis* sp. Bioresour Technol 129:7–11

11. Kim TH, Lee Y, Han SH, Hwang SJ (2013) The effects of wavelength and wavelength mixing ratios on microalgae growth and nitrogen, phosphorus removal using *Scenedesmus* sp. for wastewater treatment. Bioresour Technol 130:75–80

12. Cardol P, Forti G, Finazzi G (2011) Regulation of electron transport in microalgae. Biochim Biophys Acta (BBA)-Bioenerg 1807(8):912–918

13. Wobbe L, Bassi R, Kruse O (2016) Multi-level light capture control in plants and green algae. Trends Plant Sci 21(1):55–68

14. Ho SH, Chen CY, Lee DJ, Chang JS (2011) Perspectives on microalgal CO_2-emission mitigation systems—a review. Biotechnol Adv 29(2):189–198

15. Carvalho AP, Meireles LA, Malcata FX (2006) Microalgal reactors: a review of enclosed system designs and performances. Biotechnol Prog 22(6):1490–1506

16. Mattos ER, Singh M, Cabrera ML, Das KC (2012) Effects of inoculum physiological stage on the growth characteristics of *Chlorella sorokiniana* cultivated under different CO_2 concentrations. Appl Biochem Biotech 168(3):519–530

17. Shene C, Chisti Y, Bustamante M, Rubilar M (2016) Effect of CO_2 in the aeration gas on cultivation of the microalga Nannochloropsis oculata: experimental study and mathematical modeling of CO_2 assimilation. Algal Res 13:16–29

18. Juneja A, Ceballos RM, Murthy GS (2013) Effects of environmental factors and nutrient availability on the biochemical composition of algae for biofuels production: a review. Energies 6(9):4607–4638

19. Peccia J, Haznedaroglu B, Gutierrez J, Zimmerman JB (2013) Nitrogen supply is an important driver of sustainable microalgae biofuel production. Trends Biotechnol 31(3):134–138

20. Xu Z, Zou D, Gao K (2010) Effects of elevated CO_2 and phosphorus supply on growth, photosynthesis and nutrient uptake in the marine macroalga *Gracilaria lemaneiformis* (Rhodophyta). Bot Mar 53(2):123–129

21. Li X, Hu HY, Gan K, Sun YX (2010) Effects of different nitrogen and phosphorus concentrations on the growth, nutrient uptake, and lipid accumulation of a freshwater microalga *Scenedesmus* sp. Bioresour Technol 101(14):5494–5500

22. Van Wagenen J, Miller TW, Hobbs S, Hook P, Crowe B, Huesemann M (2012) Effects of light and temperature on fatty acid production in *Nannochloropsis salina*. Energies 5(3):731–740

23. Béchet Q, Shilton A, Guieysse B (2013) Modeling the effects of light and temperature on algae growth: state of the art and critical assessment for productivity prediction during outdoor cultivation. Biotechnol Adv 31(8):1648–1663

24. Guedes A, Amaro HM, Pereira RD, Malcata FX (2011) Effects of temperature and pH on growth and antioxidant content of the microalga *Scenedesmus obliquus*. Biotechnol Prog 27(5):1218–1224

25. Ugwu C, Aoyagi H, Uchiyama H (2008) Photobioreactors for mass cultivation of algae. Bioresour Technol 99(10):4021–4028

26. Olivieri G, Salatino P, Marzocchella A (2014) Advances in photobioreactors for intensive microalgal production: configurations, operating strategies and applications. J Chem Technol Biotechnol 89(2):178–195

27. Kim ZH, Kim SH, Lee HS, Lee CG (2006) Enhanced production of astaxanthin by flashing light using *Haematococcus pluvialis*. Enzyme Microb Technol 39(3):414–419

28. Wang SK, Stiles AR, Guo C, Liu CZ (2014) Microalgae cultivation in photobioreactors: an overview of light characteristics. Eng Life Sci 14(6):550–559

29. Lee KH, Kim BW (1998) Enhanced microbial removal of H_2S using *Chlorobium* in an optical-fiber bioreactor. Biotechnol Lett 20(5):525–529

30. Xue S, Zhang Q, Wu X, Yan C, Cong W (2013) A novel photobioreactor structure using optical fibers as inner light source to fulfill flashing light effects of microalgae. Bioresour Technol 138:141–147

31. Hsieh CH, Wu WT (2009) A novel photobioreactor with transparent rectangular chambers for cultivation of microalgae. Biochem Eng J 46(3):300–305

32. Sun YH, Huang Y, Liao Q, Fu Q, Zhu X (2016) Enhancement of microalgae production by embedding hollow light guides to a flat-plate photobioreactor. Bioresour Technol 207:31–38
33. Jung EE, Jain A, Voulis N, Doud DF, Angenent LT, Erickson D (2014) Stacked optical waveguide photobioreactor for high density algal cultures. Bioresour Technol 171:495–499
34. Sun YH, Liao Q, Huang Y, Xia A, Fu Q, Zhu X, Zheng YP (2016) Integrating planar waveguides doped with light scattering nanoparticles into a flat-plate photobioreactor to improve light distribution and microalgae growth. Bioresour Technol 220:215–224
35. Jain A, Voulis N, Jung EE, Doud DF, Miller WB, Angenent LT, Erickson D (2015) Optimal intensity and biomass density for biofuel production in a thin-light-path photobioreactor. Environ Sci Technol 49(10):6327–6334
36. Ahsan SS, Pereyra B, Jung EE, Erickson D (2014) Engineered surface scatterers in edge-lit slab waveguides to improve light delivery in algae cultivation. Opt Express 22(106): A1526–A1537
37. Genin SN, Aitchison JS, Allen DG (2015) Novel waveguide reactor design for enhancing algal biofilm growth. Algal Res 12:529–538
38. Liao Q, Sun YH, Huang Y, Xia A, Fu Q, Zhu X (2017) Simultaneous enhancement of *Chlorella vulgaris* growth and lipid accumulation through the synergy effect between light and nitrate in a planar waveguide flat-plate photobioreactor. Bioresour Technol 243:528–538
39. Sun YH, Huang Y, Liao Q, Xia A, Fu Q, Zhu X, Fu JW (2018) Boosting *Nannochloropsis oculata* growth and lipid accumulation in a lab-scale open raceway pond characterized by improved light distributions employing built-in planar waveguide modules. Bioresour Technol 249:880–889
40. Qiang H, Richmond A (1996) Productivity and photosynthetic efficiency of *Spirulina platensis* as affected by light intensity, algal density and rate of mixing in a flat plate photobioreactor. J Appl Phycol 8(2):139–145
41. Oncel S, Sabankay M (2012) Microalgal biohydrogen production considering light energy and mixing time as the two key features for scale-up. Bioresour Technol 121:228–234
42. Degen J, Uebele A, Retze A, Schmid-Staiger U, Trösch W (2001) A novel airlift photobioreactor with baffles for improved light utilization through the flashing light effect. J Biotechnol 92(2):89–94
43. Wang LL, Tao Y, Mao XZ (2014) A novel flat plate algal bioreactor with horizontal baffles: Structural optimization and cultivation performance. Bioresour Technol 164:20–27
44. Huang JK, Li YG, Wan MX, Yan Y, Feng F, Qu XX, Wang J, Shen GM, Li W, Fan JH, Wang WL (2014) Novel flat-plate photobioreactors for microalgae cultivation with special mixers to promote mixing along the light gradient. Bioresour Technol 159:8–16
45. Yang Z, Cheng J, Xu X, Zhou J, Cen K (2016) Enhanced solution velocity between dark and light areas with horizontal tubes and triangular prism baffles to improve microalgal growth in a flat-panel photo-bioreactor. Bioresour Technol 211:519–526
46. Cheng J, Yang Z, Ye Q, Zhou J, Cen K (2015) Enhanced flashing light effect with up-down chute baffles to improve microalgal growth in a raceway pond. Bioresour Technol 190: 29–35
47. Zhang Q, Xue S, Yan C, Wu X, Wen S, Cong W (2015) Installation of flow deflectors and wing baffles to reduce dead zone and enhance flashing light effect in an open raceway pond. Bioresour Technol 198:150–156
48. Huang JK, Qu XX, Wan MX, Ying JG, Li YG, Zhu FC, Wang J, Shen GM, Chen JP, Li W (2015) Investigation on the performance of raceway ponds with internal structures by the means of CFD simulations and experiments. Algal Res 10:64–71
49. Huang Y, Sun YH, Liao Q, Fu Q, Xia A, Zhu X (2016) Improvement on light penetrability and microalgae biomass production by periodically pre-harvesting *Chlorella vulgaris* cells with culture medium recycling. Bioresour Technol 216:669–676
50. Fernández FA, Sevilla JF, Grima EM (2013) Photobioreactors for the production of microalgae. Rev Environ Sci Biotechnol 12(2):131–151
51. Cheng L, Zhang L, Chen H, Gao C (2006) Carbon dioxide removal from air by microalgae cultured in a membrane-photobioreactor. Sep Purif Technol 50(3):324–329

52. Fan LH, Zhang YT, Zhang L, Chen HL (2008) Evaluation of a membrane-sparged helical tubular photobioreactor for carbon dioxide biofixation by *Chlorella vulgaris*. J Membr Sci 325(1):336–345

53. Kim HW, Cheng J, Rittmann BE (2016) Direct membrane-carbonation photobioreactor producing photoautotrophic biomass via carbon dioxide transfer and nutrient removal. Bioresour Technol 204:32–37

54. Zheng Q, Martin GJ, Kentish SE (2016) Energy efficient transfer of carbon dioxide from flue gases to microalgal systems. Energy Environ Sci 9(3):1074–1082

55. Ketheesan B, Nirmalakhandan N (2012) Feasibility of microalgal cultivation in a pilot-scale airlift-driven raceway reactor. Bioresour Technol 108:196–202

56. Li S, Luo S, Guo R (2013) Efficiency of CO_2 fixation by microalgae in a closed raceway pond. Bioresour Technol 136:267–272

57. Yang Z, Cheng J, Lin R, Zhou J, Cen K (2016) Improving microalgal growth with reduced diameters of aeration bubbles and enhanced mass transfer of solution in an oscillating flow field. Bioresour Technol 211:429–434

58. Yang Z, Cheng J, Liu J, Zhou J, Cen K (2016) Improving microalgal growth with small bubbles in a raceway pond with swing gas aerators. Bioresour Technol 216:267–272

59. Huang Y, Zhao S, Ding YD, Liao Q, Huang Y, Zhu X (2017) Optimizing the gas distributor based on CO_2 bubble dynamic behaviors to improve microalgal biomass production in an air-lift photo-bioreactor. Bioresour Technol 233:84–91

60. Beuckels A, Smolders E, Muylaert K (2015) Nitrogen availability influences phosphorus removal in microalgae-based wastewater treatment. Water Res 77:98–106

61. Fu Q, Chang HX, Huang Y, Liao Q, Zhu X, Xia A, Sun YH (2016) A novel self-adaptive microalgae photobioreactor using anion exchange membranes for continuous supply of nutrients. Bioresour Technol 214:629–636

62. Chang HX, Fu Q, Huang Y, Xia A, Liao Q, Zhu X, Zheng YP, Sun CH (2016) An annular photobioreactor with ion-exchange-membrane for non-touch microalgae cultivation with wastewater. Bioresour Technol 219:668–676

63. Wang JF, Liu W, Liu TZ (2017) Biofilm based attached cultivation technology for microalgal biorefineries—a review. Bioresour Technol 244(2):1245–1253

64. Huang Y, Xiong W, Liao Q, Fu Q, Xia A, Zhu X, Sun YH (2016) Comparison of *Chlorella vulgaris* biomass productivity cultivated in biofilm and suspension from the aspect of light transmission and microalgae affinity to carbon dioxide. Bioresour Technol 222:367–373

65. Ozkan A, Kinney K, Katz L, Berberoglu H (2012) Reduction of water and energy requirement of algae cultivation using an algae biofilm photobioreactor. Bioresour Technol 114:542–548

66. Liu TZ, Wang JF, Hu Q, Cheng PF, Ji B, Liu JL, Chen Y, Zhang W, Chen XL, Chen L, Gao LL, Ji CL, Wang H (2013) Attached cultivation technology of microalgae for efficient biomass feedstock production. Bioresour Technol 127:216–222

67. Zhang LL, Chen L, Wang JF, Chen Y, Gao X, Zhang ZH, Liu TZ (2015) Attached cultivation for improving the biomass productivity of *Spirulina platensis*. Bioresour Technol 181:136–142

68. Shi J, Podola B, Melkonian M (2014) Application of a prototype-scale Twin-Layer photobioreactor for effective N and P removal from different process stages of municipal wastewater by immobilized microalgae. Bioresour Technol 154:260–266

69. Zhuang LL, Hu HY, Wu YH, Wang T, Zhang TY (2014) A novel suspended-solid phase photobioreactor to improve biomass production and separation of microalgae. Bioresour Technol 153:399–402

70. Gao F, Yang ZH, Li C, Zeng GM, Ma DH, Zhou L (2015) A novel algal biofilm membrane photobioreactor for attached microalgae growth and nutrients removal from secondary effluent. Bioresour Technol 179:8–12

71. Gross M, Henry W, Michael C, Wen Z (2013) Development of a rotating algal biofilm growth system for attached microalgae growth with in situ biomass harvest. Bioresour Technol 150:195–201

72. Blanken W, Janssen M, Cuaresma M, Libor Z, Bhaiji T, Wijffels R (2014) Biofilm growth of *Chlorella sorokiniana* in a rotating biological contactor based photobioreactor. Biotechnol Bioeng 111(12):2436–2445

73. Barros AI, Gonçalves AL, Simões M, Pires JC (2015) Harvesting techniques applied to microalgae: a review. Renew Sustain Energy Rev 41:1489–1500

74. Henderson R, Parsons SA, Jefferson B (2008) The impact of algal properties and pre-oxidation on solid-liquid separation of algae. Water Res 42(8):1827–1845

75. Wang SK, Stiles AR, Guo C, Liu CZ (2015) Harvesting microalgae by magnetic separation: a review. Algal Res 9:178–185

76. Ozkan A, Berberoglu H (2013) Physico-chemical surface properties of microalgae. Colloid Surfaces B 112:287–293

77. Christenson L, Sims R (2011) Production and harvesting of microalgae for wastewater treatment, biofuels, and bioproducts. Biotechnol Adv 29(6):686–702

78. Rawat I, Kumar RR, Mutanda T, Bux F (2011) Dual role of microalgae: phycoremediation of domestic wastewater and biomass production for sustainable biofuels production. Appl Energy 88(10):3411–3424

79. Rubio J, Souza M, Smith R (2002) Overview of flotation as a wastewater treatment technique. Miner Eng 15(3):139–155

80. Farooq W, Moon M, Ryu BG, Suh WI, Shrivastav A, Park MS, Mishra SK, Yang JW (2015) Effect of harvesting methods on the reusability of water for cultivation of *Chlorella vulgaris*, its lipid productivity and biodiesel quality. Algal Res 8:1–7

81. Papazi A, Makridis P, Divanach P (2010) Harvesting *Chlorella minutissima* using cell coagulants. J Appl Phycol 22(3):349–355

82. Uduman N, Qi Y, Danquah MK, Forde GM, Hoadley A (2010) Dewatering of microalgal cultures: a major bottleneck to algae-based fuels. J Renew Sustain Energy 2(1):012701

83. Bilad M, Arafat HA, Vankelecom IF (2014) Membrane technology in microalgae cultivation and harvesting: a review. Biotechnol Adv 32(7):1283–1300

84. Ndikubwimana T, Chang J, Xiao Z, Shao W, Zeng X, Ng IS, Lu YH (2016) Flotation: a promising microalgae harvesting and dewatering technology for biofuels production. Biotechnol J 11(3):315–326

85. Danquah MK, Gladman B, Moheimani N, Forde GM (2009) Microalgal growth characteristics and subsequent influence on dewatering efficiency. Chem Eng J 151(1):73–78

86. Pragya N, Pandey KK, Sahoo P (2013) A review on harvesting, oil extraction and biofuels production technologies from microalgae. Renew Sustain Energy Rev 24:159–171

87. Schlesinger A, Eisenstadt D, Bar GA, Carmely H, Einbinder S, Gressel J (2012) Inexpensive non-toxic flocculation of microalgae contradicts theories; overcoming a major hurdle to bulk algal production. Biotechnol Adv 30(5):1023–1030

88. Becker E (2007) Micro-algae as a source of protein. Biotechnol Adv 25(2):207–210

89. Ryckebosch E, Bruneel C, Termote VR, Goiris K, Muylaert K, Foubert I (2014) Nutritional evaluation of microalgae oils rich in omega-3 long chain polyunsaturated fatty acids as an alternative for fish oil. Food Chem 160:393–400

90. Quinn JC, Davis R (2015) The potentials and challenges of algae based biofuels: a review of the techno-economic, life cycle, and resource assessment modeling. Bioresour Technol 184:444–452

91. Sun A, Davis R, Starbuck M, Ben-Amotz A, Pate R, Pienkos PT (2011) Comparative cost analysis of algal oil production for biofuels. Energy 36(8):5169–5179

92. Hernández D, Solana M, Riaño B, García GM, Bertucco A (2014) Biofuels from microalgae: lipid extraction and methane production from the residual biomass in a biorefinery approach. Bioresour Technol 170:370–378

93. de Souza Silva APF, Costa MC, Lopes AC, Neto EFA, Leitão RC, Mota CR, dos Santos AB (2014) Comparison of pretreatment methods for total lipids extraction from mixed microalgae. Renew Energy 63:762–766

94. Taher H, Al ZS, Al MAH, Haik Y, Farid M (2014) Effective extraction of microalgae lipids from wet biomass for biodiesel production. Biomass Bioenergy 66:159–167

95. Cooney M, Young G, Nagle N (2009) Extraction of bio-oils from microalgae. Sep Purif Rev 38(4):291–325
96. Lardon L, Helias A, Sialve B, Steyer JP, Bernard O (2009) Life-cycle assessment of biodiesel production from microalgae. ACS Publications
97. Sheehan JD, Savage PE (2017) Modeling the effects of microalga biochemical content on the kinetics and biocrude yields from hydrothermal liquefaction. Bioresour Technol 239: 144–150
98. Barreiro DL, Prins W, Ronsse F, Brilman W (2013) Hydrothermal liquefaction (HTL) of microalgae for biofuel production: state of the art review and future prospects. Biomass Bioenergy 53:113–127
99. Biller P, Ross AB, Skill S, Lea-Langton A, Balasundaram B, Hall C, Riley R, Llewellyn CA (2012) Nutrient recycling of aqueous phase for microalgae cultivation from the hydrothermal liquefaction process. Algal Res 1(1):70–76
100. Garcia AL, Torri C, Samorì C, van der Spek J, Fabbri D, Kersten SR, Brilman DWF (2011) Hydrothermal treatment (HTT) of microalgae: evaluation of the process as conversion method in an algae biorefinery concept. Energy Fuel 26(1):642–657
101. Laurens L, Nagle N, Davis R, Sweeney N, Van WS, Lowell A, Pienkos PT (2015) Acid-catalyzed algal biomass pretreatment for integrated lipid and carbohydrate-based biofuels production. Green Chem 17(2):1145–1158
102. Dong T, Van WS, Nagle N, Pienkos PT, Laurens LM (2016) Impact of biochemical composition on susceptibility of algal biomass to acid-catalyzed pretreatment for sugar and lipid recovery. Algal Res 18:69–77
103. Van BM (2001) Kinetic aspects of the Maillard reaction: a critical review. Mol Nutr Food Res 45(3):150–159
104. Martin GJ (2016) Energy requirements for wet solvent extraction of lipids from microalgal biomass. Bioresour Technol 205:40–47
105. Yap BH, Crawford SA, Dumsday GJ, Scales PJ, Martin GJ (2014) A mechanistic study of algal cell disruption and its effect on lipid recovery by solvent extraction. Algal Res 5: 112–120
106. Johnson LA, Lusas E (1983) Comparison of alternative solvents for oils extraction. J Am Oil Chem Soc 60(2):229–242
107. Olmstead IL, Kentish SE, Scales PJ, Martin GJ (2013) Low solvent, low temperature method for extracting biodiesel lipids from concentrated microalgal biomass. Bioresour Technol 148:615–619
108. Halim R, Webley PA, Martin GJ (2016) The CIDES process: fractionation of concentrated microalgal paste for co-production of biofuel, nutraceuticals, and high-grade protein feed. Algal Res 19:299–306
109. Du Y, Schuur B, Samorì C, Tagliavini E, Brilman DWF (2013) Secondary amines as switchable solvents for lipid extraction from non-broken microalgae. Bioresour Technol 149:253–260
110. Samorì C, Barreiro DL, Vet R, Pezzolesi L, Brilman DW, Galletti P, Tagliavini E (2013) Effective lipid extraction from algae cultures using switchable solvents. Green Chem 15(2):353–356
111. de Melo JR, Tres MV, Steffens J, Oliveira JV, Di Luccio M (2015) Desolventizing organic solvent-soybean oil miscella using ultrafiltration ceramic membranes. J Membr Sci 475: 357–366
112. Law SQ, Chen B, Scales PJ, Martin GJ (2017) Centrifugal recovery of solvent after biphasic wet extraction of lipids from a concentrated slurry of *Nannochloropsis* sp. biomass. Algal Res 24:299–308
113. Knothe G (2009) Improving biodiesel fuel properties by modifying fatty ester composition. Energy Environ Sci 2(7):759–766
114. Olmstead IL, Hill DR, Dias DA, Jayasinghe NS, Callahan DL, Kentish SE, Scales PJ, Martin GJO (2013) A quantitative analysis of microalgal lipids for optimization of biodiesel and omega-3 production. Biotechnol Bioeng 110(8):2096–2104

115. Anand M, Farooqui SA, Kumar R, Joshi R, Kumar R, Sibi MG, Singh H, Sinha AK (2016) Optimizing renewable oil hydrocracking conditions for aviation bio-kerosene production. Fuel Process Technol 151:50–58
116. Trivedi J, Aila M, Bangwal D, Kaul S, Garg M (2015) Algae based biorefinery—how to make sense? Renew Sustain Energy Rev 47:295–307

Chapter 4
Heterotrophic Microalgal Cultivation

Dillirani Nagarajan, Duu-Jong Lee and Jo-shu Chang

1 Introduction

Global population is on the rise, and coupled with economic development, energy demands continue to rise. The energy demand will rise over 85% by 2040 [1]. Fossil fuels are still the major source of our primary energy, but they are finite and dwindling. Incessant use of fossil fuels has led to severe concerns, leading to anthropogenic climate change because of a considerable increase in greenhouse gases in the past century [2]. The current atmospheric CO_2 level is at 406 ppm, and it has risen from 400 ppm in the past two years (https://climate.nasa.gov/vital-signs/carbon-dioxide/). There is a pressing need for sustainable alternative energy resources to overcome the shortage of fossil fuels and concomitant decarbonization of the energy sector. In the current scenario, there is a gradual transition in the energy mix and increasing amounts of nuclear, hydro and renewable energies are being included. Renewable energy (wind, solar, geothermal, biomass, and biofuels) is the fastest growing energy sector, banking a major 10% in the primary energy pool by 2035 (BP Global energy outlook, 2017). Microalgae are increasingly recognized as the alternative feedstock for renewable and sustainable biofuel production, as they are natural sources of energy rich compounds like carbohydrates and lipids.

Microalgae are the primary producers and the most primitive photosynthetic organisms on earth. The term "microalgae" comprises of both prokaryotic and

D. Nagarajan · J. Chang (✉)
Department of Chemical Engineering, National Cheng Kung University, Tainan, Taiwan
e-mail: changjs@mail.ncku.edu.tw

D. Nagarajan · D.-J. Lee
Department of Chemical Engineering, National Taiwan University, Taipei, Taiwan

J. Chang
Research Center for Energy Technology and Strategy, National Cheng Kung University, Tainan, Taiwan

eukaryotic photosynthetic microorganisms with a wealth of about 200,000 to 800,000 species and only about 40,000 species have been identified and classified [3]. They are extremely diverse, both physiologically and phylogenetically, and has been classified into at least 10 major groups including green algae, cyanobacteria and diatoms [4]. The major metabolic modes used for the cultivation of microalgae are photoautotrophic, heterotrophic, mixotrophic and photoheterotrophic cultivation. Microalgae are capable of fixing atmospheric CO_2 by photosynthesis with sunlight as energy source and convert it into organic biomass, which forms the basic photoautotrophic mode of microalgal metabolism. They are also capable of using organic carbon sources like glucose and acetate as a source of energy and carbon, in the heterotrophic mode of metabolism [5]. Mixotrophic mode requires sunlight as the energy source, but can incorporate both organic and inorganic carbon into the biomass, highlighting the ability of the microalgae to live under both autotrophic and heterotrophic conditions. Photoheterotrophic mode, in contrast to photoautotrophic mode, does not require inorganic carbon, but requires sunlight to metabolize organic carbon [5]. Of all these cultivation modes, mixotrophic mode is believed to yield higher biomass, combining the benefits of both photoautotrophic and heterotrophic modes of cultivation but not commonly used in commercial cultivation purposes.

Photoautotrophic mode of cultivation is the most commonly used mode of cultivation, and can be done so in open systems like circular ponds, raceway ponds or in closed systems using specially designed photobioreactors (PBRs). Open systems are currently the major mode of cultivation of microalgae, making use of sunlight as energy source and atmospheric CO_2 as carbon source, but limited to a few sturdy and extreme microalgae like *Arthrospira, Dunaliella* and *Chlorella* [6]. The cultures are grown in open ponds and often mixed to prevent sedimentation of algae; in circular ponds this is carried out by a pivotal arm and in raceway ponds a special paddlewheel is installed for mixing. Decreased cost associated with installation and operation and reduced requirement of skilled personnel makes photoautotrophic cultivation economically feasible. The use of arid lands and non-potable water for cultivation ensures that the land use controversies and competition with food crops can be avoided [7]. But open systems for microalgal cultivation suffer from several challenges: very few microalgae could be cultivated, highly prone to contamination by weed algae and grazers, light penetration limits the pond depth to 15–20 cm, inefficient use of incident sunlight and CO_2, low biomass productivity and associated high costs of harvesting, requirement of large areas of land, and evaporation losses of water [8]. On the other hand, closed systems like PBRs offer all the advantages of a conventional fermenter: good control over process parameters like pH, temperature and illumination, control over contamination as the system is sealed off the environment, and higher biomass productivity compared to open systems. However, the issue of efficient distribution of light for the cultures still needs to be addressed, as light penetration decreases with increase in cell density. Also, cells often move into unilluminated dark zones leading to respiratory biomass losses, similar to night biomass loss in photoautotrophic cultivation [7]. PBR design is not versatile or universal and oftentimes a

PBR is specially built and installed for a particular strain with a product of interest, thus it comes with high installation and operating costs.

Heterotrophic cultivation of microalgae is very similar to heterotrophic bacterial cultivation and can be carried out in a conventional bacterial fermenter without any illumination under dark conditions. Thus, the major problem faced in photoautotrophic cultivation, the efficient supply of optimal light intensity is overcome in heterotrophic cultivation. Many microalgal species are capable of growing under dark conditions utilizing an organic carbon source like glucose as a source of energy and carbon. Many species of *Chlorella, Scenedesmus, Neochloris*, and *Tetraselmis* are capable of heterotrophic growth in the presence of glucose under dark conditions. Very high cell densities of the order of 25–100 g/L can be achieved for *Chlorella* using process engineering strategies and cultivation modes like continuous and fed-batch cultivation [9]. The major characteristics required for heterotrophic microalgae were summarized earlier and are as follows: the ability to grow and metabolize in the absence of light, the ability to utilize organic carbon as a source of energy and carbon, the ability to grow on inexpensive sterilized media, the ability to withstand the high hydrodynamic shear associated with vigorous mixing in fermenters, and the ability to adapt to harsh environmental conditions [10]. The major advantages of heterotrophic microalgal cultivation is illustrated in Fig. 1. In this work, we discuss in detail the metabolism of microalgae based on the utilization of carbon sources, the factors affecting heterotrophic cultivation of microalgae, including the carbon and nitrogen sources. Also, commercially important products of interest that can be obtained by heterotrophic cultivation of microalgae are reviewed. The challenges faced in heterotrophic cultivation of microalgae is discussed in detail and the future perspectives are presented.
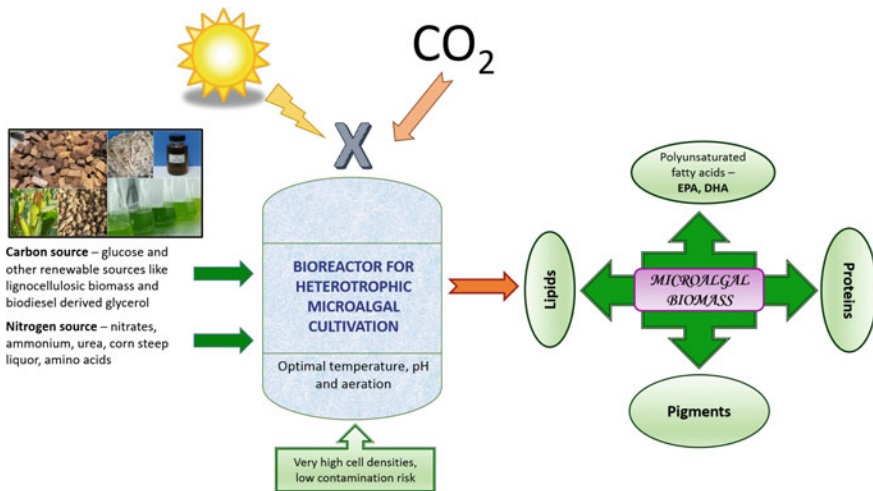
Fig. 1 The advantages of heterotrophic cultivation of microalgae and the products of interest

2   Microalgal Metabolism and Heterotrophy

All organisms have a central carbohydrate metabolism pathway. Even in photo-synthetic organisms, the atmospheric CO_2 is fixed as the carbohydrate molecule phosphoglycerate, which is then polymerized to sucrose or starch based on the metabolic requirements of the cell. Photosynthesis occurs in the thylakoid mem-branes of the chloroplast and it is divided into 4 stages. The first three steps occur exclusively in the presence of light and are called light reactions and the last step can be performed in the absence of light utilizing the metabolites derived from light reaction, hence called dark reaction. The four steps are as follows: (1) the absorption of incident light by photosynthetic pigments present in the light har-vesting center of the photosystem II, (2) excitation of the chlorophyll molecules, and the resultant electron flow from PSII to PSI via the plastoquinone, and the reduction of $NADP^+$ to NADPH, (3) generation of ATP by the membrane bound ATP synthase, (4) the actual fixation of CO_2 by the enzyme Ribulose bisphosphate carboxylase/oxygenase (often dubbed as Rubisco) [11]. For each molecule of CO_2 fixed, 2 molecules of NADPH and three molecules of ATP are required. Hence the overall reaction that generates a six-carbon sugar like glucose from CO_2 can be described as follows:

$$6CO_2 + 18ATP + 12NADPH + 12H_2O$$
$$\rightarrow C_6H_{12}O_6 + 18ADP + 18Pi + 12NADP^+ + 6H^+$$

The fixation of CO_2 by RubisCo is the rate limiting step in photosynthesis and the ribulose phosphate which is used as the substrate and to which CO_2 is added is regenerated in a series of steps first characterized by Andrew Benson and Melvin Calvin and hence called the Calvin-Benson cycle. The fixed carbohydrate can be converted to starch by the enzymes present in chloroplast, while synthesis of sucrose for metabolic needs of non-photosynthetic cells occurs in the cytosol [12]. However, it is intriguing to note that despite the presence of a central carbon metabolic pathway, most microalgae are incapable of growth in the dark with an organic carbon as the carbon source.

The inability of certain microalgae to utilize any organic carbon as a source of carbon and energy is attributed to the absence of transporters for the specific sugars. All living cells, both prokaryotic and eukaryotic, are covered by a double layered lipid cell membrane which monitors the traffic across the membrane. Transport of sugars across this cell membrane requires specific transporters, which are absent in many microalgae. The exogenous expression of one such transporter, the human erythrocyte glucose transporter GluT1 in an obligate photosynthetic diatom *Phaeodactylum tricornutum* enabled the diatom to grow in the dark utilizing glucose as a carbon source [13]. The sugar transporters have been earlier characterized in the heterotrophic *Chlorella kessleri* and it was found to be a glucose/H+ symporter that simultaneously transports one molecule of glucose and a proton at the expense of one molecule of ATP

[14]. The transporter is induced in the presence of glucose and a minimum time of 15–18 min is required for the expression of the *hup1* gene (Hexose uptake protein gene) as accomplished by enhanced glucose uptake and increased amount of membrane proteins [15, 16]. The gene is named as hexose transporter as it was induced in the presence of hexoses like D-glucose, D-fructose and D-galactose, while pentoses, sucrose, mannose and other disaccharides and sugar alcohols could not induce the expression of the protein [17] and it was observed that a set of amino acid transporters were co-induced facilitating the transport of amino acids including glycine, L-alanine, L-proline, L-serine, L-arginine L-lysine and proline [18] gathering organic nutrients for heterotrophic growth. In *Chlamydomonas*, a glucose transport phenomenon was reported which could be saturated at a glucose concentration of 5 mg/L [19]. A similar hexose transporter has been reported for *Neochloris oeloabundans* UTEX 1185, where the glucose uptake was blocked by an ionophore that worked as proton gradient decoupler and growth was not supported by xylose, arabinose, fructose, sucrose, lactose, glycerol or acetic acid indicating that the transporter is specific for hexoses [20]. A hexose inducible xylose transporter was reported in *Chlorella sorokiniana* UTEX 1602 and xylose transport was inhibited in the presence of glucose or galactose. The xylose was further metabolized to xylitol, but resulted in decreased biomass and growth rate compared to glucose [21]. Even though there are genome encoded sugar transporters in microalgae [22], the expression levels of these might be too low to support efficient growth or by evolution these genes could not be expressed in a phototrophic organism where ATP is needed for obtaining organic carbon, while CO_2 could simply diffuse across the membrane. The only organic carbon substrate that can be obtained by diffusion microalgae is glycerol [23]. Glycerol is an important constituent of many microalgae growing in high osmolarity conditions like seawater or saline ponds, where it acts as an osmoticum balancing the osmotic equilibrium of the microalgal cells [9].

Another important reason for obligate heterotrophy could be an incomplete carbohydrate metabolic pathway, where sufficient energy and reducing equivalents are obtained just for the maintenance of metabolism but cannot sustain growth or cell division [24]. In obligate heterotrophs like the marine *Thraustochytrids*, the organism has lost the photosynthetic capacity in evolution and was left with a rudimentary chloroplast which functions as the storage place for the fatty acids [25]. It has been previously reported that the industrial yeast *Saccharomyces cerevisiae* could not utilize xylose mainly because the xylose utilization enzymes are expressed at a very low level to promote growth and metabolism of the yeast [26]. An incomplete tricarboxylic acid cycle has been reported for certain obligate autotrophic cyanobacteria, restricting the organic carbon assimilation only to certain amino acids but not any carbohydrates. It was shown that only 10% of the organic carbon was incorporated into new carbon molecules, whereas in chemoautotrophs the rate is as high as 40% [27]. The lesion was particularly identified as the absence of the enzyme α-ketoglutarate dehydrogenase, and very low level expression levels of succinate and malate dehydrogenase insufficient to support biomass growth with the supply of carbon skeletons required for anabolism [27].

Like many other chemotrophic microorganisms, glucose is predicted as the preferred carbon source. The central metabolic pathway for glucose, the EMP pathway is constitutively expressed in microalgae as some of the steps are interconnected with gluconeogenesis and starch synthesis, and it has been reported that the presence of glucose inhibits the uptake of other reducing sugars. Under photoautotrophic conditions, the reserve starch is hydrolyzed by amylases and starch phosphorylases in the chloroplast and the glucose is released as glucose phosphate [28]. In heterotrophic conditions, external glucose is transported via the glucose/H+ symporter at the expense of an ATP molecule and phosphorylated by a cytoplasmic kinase, yielding Glucose-6-phosphate that would enter one of the two metabolic pathways: (i) the Embden-Meyerhoff-Parnas pathway, EMP (ii) the oxidative pentose phosphate pathway, OPPP [29]. The alternative Entner–Doudoroff pathway (ED) has been reported in both prokaryotic cyanobacteria [30] and eukaryotic microalgae [31] and their role in metabolism is still unclear. In *Synechocystis* sp. PCC 6803, ED pathway was shown to be physiologically significant in mixotrophic conditions or during dark periods in day-night cycles, with low protein costs and higher ATP yields than the EMP pathway reflecting the low nutrient conditions in the cells [30]. In *Chlamydomonas reinhardtii*, the glycolysis enzymes are compartmentalized: the upper half or the preparatory phase for the conversion of glucose to Glyceraldehyde-3-phosphate occurs in the chloroplast, while the payoff phase or the conversion of GAP to pyruvate occurs in the cytosol with ATP production from where it can be easily supplied to the flagella [32]. The OPP pathway, the essential supplier of precursors for nucleic acid synthesis and reducing equivalents for fatty acid synthesis, are co-localized with the Calvin-Benson cycle in the plastids, closely linking the two cycles and tightly regulated to avoid futile cycling [33]. The flux of glucose via the EMP pathway or the OPPP pathway is determined by illumination: under light conditions the EMP pathway remains highly active while the OPP is slightly toned down [9], and under dark conditions the OPPP pathway takes over with a slight turndown of the major glycolytic enzymes [34]. Thus, in green algae the conversion of glucose to pyruvate can occur via any one of the above mentioned pathways distributed among the chloroplast and cytosol. The interconnectivity of these pathways in the cytosol and chloroplast is accomplished by the presence of a number of transporters for sugar derivatives on the organelle membranes including ion channels, primary and secondary transporters [35].

The fate of pyruvate depends on the oxidation potential of the cells. Under aerobic conditions, the glucose is directly channeled via EMP, pyruvate oxidation, tricarboxylic acid cycle (TCA) and oxidative phosphorylation in the mitochondria generating ATP. Under anaerobic conditions, the pyruvate is completely fermented to acetate. *C. reinhardtii* is endowed with the complete set of enzymes for the fermentation of pyruvate to acetate in the cytosol and fermentation is associated with the evolution of hydrogen gas as the hydrogenases are induced under anoxic conditions [36]. Dark respiration is regarded as maintenance respiration to meet the energy demands of maintaining macromolecular turnover and maintenance of the gradient across cell membranes in solution supplying alongside the necessary ATP, carbon skeletons and reducing equivalents [37, 38]. Hence, aerobic conditions or

sufficient aeration of the cultures heterotrophically grown on glucose is an important parameter determining growth and biomass production. Under aerobic conditions in heterotrophic cultivation the respiration efficiency is very close to theoretical maximum, while under dark conditions the efficiency is reduced to a mere 40% [9].

Acetate is the second most commonly used carbon source in heterotrophic and mixotrophic cultivation of microalgae. Acetate is transported into the cells by an ATP dependent monocarboxylic acid/proton transporter protein and it is converted into acetyl CoA. In *C. reinhardtii*, acetyl CoA synthetase is present in cytosol, chloroplast and the mitochondria assisting growth on acetate [39], while the phosphotrannsacetylase-acetate kinase cycle (PTA-ACK cycle) in the cytosol and mitochondria that interconverts acetate and acetyl CoA determines the availability of acetyl CoA for synthesis of fatty acids and isoprenoids [33]. Acetyl CoA can also be metabolized via the glyoxylate cycle in the cytosol or enter TCA cycle and oxidative phosphorylation in the mitochondria. Glyoxylate cycle eliminates the release of carbon as CO_2 and is more efficient in assimilating the acquired carbon, with succinate, fumarate, malate, and oxaloacetate as the byproducts. Oxaloacetate can be converted to phosphoenol pyruvate and eventually to glucose via gluconeogenesis, thus connecting glyoxylate cycle and gluconeogenesis [39]. Glyoxylate cycle is functional in some cyanobacteria [40], although it is absent in *Synechocystis* sp. [41]. Knockdown of glyoxylate cycle enzyme isocitrate lyase in *C. reinhardtii* redirects the carbon flow towards lipid accumulation by decreased glyoxylate cycle activity, decreased gluconeogenesis and decreased β-oxidation of fatty acids. The enhanced TCA cycle activity and the resultant oxidative stress is managed by an increased levels of superoxide dismutase and ascorbate peroxidase [42]. Glycerol, now considered as a renewable carbon source as it is the abundant byproduct of biodiesel production process, can be easily used by microalgae. Glycerol is taken up by microalgae by passive diffusion across the cell membrane and then it is further metabolized to enter the central carbohydrate pathway. Glycerol is first phosphorylated by glycerol kinase using one molecule of ATP and then it is oxidized to the glyceraldehyde-3-phosphate or glycerate which are intermediates of the EMP pathway, then further metabolized to pyruvate and enters TCA cycle [23]. However, glycerol can be metabolized in the presence of light and the absence of inorganic carbon source by photoheterotrophy [9].

3 Factors Affecting Heterotrophic Cultivation

The nutritional requirements of microalgae in heterotrophic cultivation is very similar to autotrophic cultivation, the exception being the requirement of light. In photoautotrophic growth, light is used as a source of energy and atmospheric CO_2 is used as a carbon source, while the cultivation medium provides nitrogen in the form of inorganic nitrate most of the times. Heterotrophic cultivation eliminates the

requirement of light, organic carbon source is provided and the nitrogen source can be organic or inorganic depending upon the strain used. The major macronutrients to be provided for microalgal growth are carbon, nitrogen, phosphorus and potassium. Carbon is the most important nutrient to build biomass and carbon content of the biomass vary between 17 and 65% depending upon the microalga and the cultivation conditions and an average of 50% is usually seen [43]. Carbon provides the basic skeleton for all the functional biomolecules like carbohydrates, lipids and proteins, and in heterotrophic cultivation it is a source of energy. The second most important nutrition is nitrogen, and it accounts for about 5–10% of the biomass content. Nitrogen is an integral component of amino acids, nucleic acids, and pigments [44]. Also, nitrogen deprivation is an important cultivation strategy used for the accumulation of lipids or carbohydrates in microalgae. Next, phosphorus is an essential requirement in microalgal cultures, up to 3.3% of biomass and it is involved in the synthesis of the energy rich compound ATP and forms the backbone of nucleic acids and is also involved in various regulatory mechanisms maintained by the phosphorylation state of signaling molecules. Potassium is required for the maintenance of the osmotic potential of the cells and as the activator for many enzymes it is involved in the regulation of many biological processes [44]. The micronutrients essential for the cellular metabolism are magnesium, sulfur, calcium, sodium and iron. Trace elements are usually provided in the culture medium, which include Boron, Copper, Manganese, Zinc, Molybdenum, Cobalt, Vanadium, and Selinium. Vitamins are added as a vitamin solution and silica is required for the cultivation of diatoms [43]. Fresh water and seawater are used for the cultivation of freshwater and marine algae. In this section, the important factors affecting the heterotrophic cultivation like carbon, nitrogen, oxygen requirement and other cultivation parameters are discussed in detail.

3.1 Carbon Source and Availability

Organic carbon source is provided for heterotrophic cultivation, which needs to be transported into the cell for further metabolism and the import is energy dependent. The optimal carbon source for the heterotrophy of microalgae is mainly influenced by the strain used, the type of sugar transporters present on the cell that will facilitate the sugar import and the metabolic potential of the cell. As previously discussed in Sect. 2, certain algae has metabolic lesions that prevents them from utilizing a certain carbon source [24]. Various monosaccharides like glucose, galactose, mannose, sugar alcohols like mannitol, carboxylic acids like acetate, disaccharides like sucrose and lactose can be applied as the carbon source to support microalgal growth in dark. Sugar transporters have been reported for hexose sugars in green algae, but not for pentoses like xylose. A glucose inducible xylose transport system has been previously reported in *C. sorokiniana* [21] but the specificity of the transport system for a particular pentose has not been established.

Thus, the isolation of a strain capable of heterotrophic growth should be accompanied by optimizing the preferred carbon source for the strain.

C. zofingensis was tested for its ability to utilize various simple sugars and disaccharides like lactose, galactose, sucrose, fructose, mannose and glucose [45]. Of these, glucose as a carbon source yielded high biomass and lipid productivity followed by slightly lower productivity in mannose, fructose, and sucrose medium. Galactose and lactose did not provide sufficient biomass or lipids. The lipid content and yield with glucose as the carbon source was obtained as 0.52 g/g biomass and 5.72 g/L [45]. A newly isolated heterotrophic *Scenedesmus* sp. R-16 was tested for its efficiency in utilizing different carbon sources using fructose, maltose, glucose, acetate, propionate, butyrate and sucrose. Glucose was able to achieve the highest biomass and lipid content 3.46 g/L and 43.4% respectively [46]. Both the above mentioned studies report that the organism was not able to utilize sucrose as a carbon source. *C. protothecoides* however could utilize the sucrose present in waste molasses for growth and lipid production with a biomass of 8.8 g/L, and with hydrolysis of the molasses and the presence of glucose and fructose as monomers doubled the cell density to 16.9 g/L. The nitrogen content of the molasses hydrolysate seems to be higher to initiate lipid accumulation [47]. The Phycocyanin producing red alga *Galdieria sulphuraria* was able to utilize sucrose and sucrose rich sugar beet molasses as a sole carbon source without hydrolysis, with a phycocyanin production of 350 mg/L [48]. The marine Thraustochytrid *Schizochytrium limacinum* SR21 was grown on different carbon sources like glucose, fructose, sucrose, maltose, lactose, glycerol, starch, oleic acid and linseed oil. The optimal biomass production and DHA levels were obtained with glucose, fructose and glycerol, with a maximum of 43.1% of DHA with glycerol. Oleic acid and linseed oil produced good biomass but the DHA levels were lower compared to the other carbon sources [49]. *Botryococcus braunii*, the highest lipid and hydrocarbon accumulating green alga was tested for heterotrophic growth using various carbon sources like glucose, mannose, fructose, galactose, sucrose, ethanol, lactic acid, ribose, glycerol, mannitol, sorbitol, sodium acetate and sodium bicarbonate [50]. The alga could grow in the dark with glucose and mannose as carbon sources, while mixotrophic mode was much more effective than autotrophic mode. This study opens new possibilities of exploiting the heterotrophic growth of *B. braunii* for oil/lipid production, but no other study was reported. Sodium acetate was a preferred carbon source for the production astaxanthin in *H. pluvialis*. It was observed that the addition of acetate could induce the formation of the pigment accumulating resting stage and enhance carotenogenesis [51]. The DHA producing marine dinoflagellate *Crypthecodinium cohnii* is obligate heterotroph, and it can use ethanol as a carbon source for the production of DHA. In fed-batch cultures, up to 15 g/L ethanol could be used as the carbon source, with biomass content of 83 g/L, 35 g/L of total lipids, 11.7 g/L DHA and lipid productivity of 53 mg/L/d [52]. Of all these carbon sources, glucose is the most preferred carbon source, although other carbon sources can be used if it gives exceptional productivity. In addition to serving as a carbon source, the presence of glucose seems to favor the production of lipids and some carotenoids. When molasses was used as a carbon source for the

production of lipids and astaxanthin in *C. zofingensis*, increasing concentrations of glucose present in the medium enhanced biomass production and lipid accumulation. The glucose concentration of 30 g/L was found to be optimal and at this concentration, TAGs were preferably accumulated with their percentage as high as 75% of the total lipids and over 90% of the neutral lipids [53]. Also, the fatty acid composition varied based on the initial sugar concentrations. At higher initial sugar concentrations, the percentage of C18:1 increased, while at lower initial sugar concentrations, the percentage of C18:3 increased [53]. And it has also been shown in *C. zofingiensis* (ATCC30412) that the import of glucose and its subsequent phosphorylation leads to the up regulation of BKT (β-Carotenoid ketolase) and CHYb (β-Carotenoid hydroxylase), the genes responsible for the synthesis of astaxanthin. The mitochondrial alternative pathway could be involved in the synthesis of astaxanthin in *C. zofingensis* [54]. In contrast, the presence of glucose in nitrogen limited medium markedly reduced the content of lutein and chlorophyll in *C. pyrenoidosa*, referred as glucose bleaching. Lutein and chlorophyll are nitrogen rich compounds and the synthesis could be down regulated in nitrogen limiting conditions, and the presence of glucose enhances the effect. Even in the presence of sufficient nitrogen, lutein content was decreased [55]. And hence the selection of suitable carbon source for growth is crucial. As it can be seen from the Tables 1, 2 and 3, various renewable or waste carbon sources rich in glucose like sweet

Table 1 Heterotrophic production of lipids from various microalgae

Microalga	Cultivation mode, carbon source	Lipid content (% dry cell weight)	Lipid productivity	References
Neochloris oleoabundans UTEX 1185	Exponential fed-batch, nitrogen limited, glucose	53.8%	1.9 g/L/d	[57]
Chlorella protothecoides UTEX 25	Fed batch, pure glycerol	36%	1.18 g/L/d	[58]
	Semi-continuous, pure glycerol	50%	4.3 g/L/d	[58]
C. protothecoides UTEX 256	Batch, whey permeate	42%	–	[59]
	Fed batch, whey permeate	20%	–	[59]
	SSF, whey permeate	50%	–	[59]
C. protothecoides	Fed batch, sugarcane hydrolysate	53%		[60]
C. protothecoides	Batch, sweet sorghum juice	52.5%	586.8 mg/L/d	[61]
C. protothecoides sp. 0710	Fed-batch, SSF, cassava starch	54.6%	–	[62]
C. saccharophila UTEX 247	Batch, glucose	54%	–	[63]

(continued)

Table 1 (continued)

Microalga	Cultivation mode, carbon source	Lipid content (% dry cell weight)	Lipid productivity	References
C. protothecoides UTEX 256	Fed batch, pure glycerol	23 g/L	2.8 g/L/d	[64]
	Fed batch, biodiesel derived crude glycerol	24.6 g/L	2.99 g/L/d	[64]
C. protothecoides	Batch, Jerusalem artichoke hydrolysate	46%	1.6 g/L/d	[65]
C. protothecoides	Batch, waste molasses hydrolysate	57.6%	–	[47]
Chlorella protothecoides	Batch, glucose	57.8%	–	[66]
Chlorella protothecoides	Batch, corn powder hydrolysate	55%	–	[67]
Chlorella vulgaris NIES-227	Batch, glucose, nitrogen limited	89%	126.8 mg/L/d	[68]
C. vulgaris CCTCC M 209256	Batch, enzyme hydrolysate of lipid extracted microalgal residue	35%	116 mg/L/d	[69]
Chlorella sp.	Batch, molasses hydrolysate, lipid extracted microalgal residue hydrolysate	45%	335 mg/L/d	[70]
C. protothecoides	Fed-batch, sugarcane bagasse hydrolysate	34%	1.19 g/L/d	[71]
Scenedesmus obliquus NIES-2280	Batch, acetate, nitrogen limited	47%	56 mg/L/d	[72]
Chlorella vulgaris NIES-227	Batch, acetate, N-limited	56%	66 mg/L/d	[73]
Chlorella vulgaris #259	Batch, acetate, N-limited	36%	29 mg/L/d	[74]
Chlorella vulgaris #259	Batch, glucose	23%	35 mg/L/d	[74]
Chlorella vulgaris #259	Batch, glycerol	34%	31 mg/L/d	[74]
C. kessleri CGMCC No. 4917	Batch, glucose	47.67%	–	[75]
Monoraphidium sp. QLY-1	Batch, glucose, NaCl, glycine betaine	48.54%	–	[76]

Table 2 Heterotrophic production of polyunsaturated fatty acids from various microalgae

Microalga used	PUFA	Cultivation mode, carbon source	PUFA content	PUFA yield	References
Thraustochytrium striatum KF9	EPA	Batch, 60 g/L glucose	23.3%	–	[77]
		Batch, 10 g/L okara (soybean residue)	1.7% TFA	–	[77]
Ulkenia sp. KF13	EPA	Batch, 60 g/L glucose	1.7% TFA	–	[77]
		Batch, 10 g/L okara (soybean residue)	1.3% TFA	–	[77]
Monodus subterraneus UTEX 151	EPA	Batch, 60 g/L glucose	3.8% TFA	96.3 mg/L	[78]
Phaeodactylum tricornutum UTEX 642	EPA	Batch, 60 g/L glucose	2.2% TFA	43.4 mg/L	[78]
Chlorella minutissima UTEX 2341	EPA	Batch, 60 g/L glucose	3.7% TFA	36.7 mg/L	[78]
Porphyridium cruentum UTEX 161	EPA	Batch, 60 g/L glucose	1.9% TFA	17.9 mg/L	[78]
Nannochloropsis sp.	EPA	Batch, 30 mM glucose	3.1% TFA	10.1 mg/L	[79]
		Batch, 30 mM ethanol	3.8% TFA	10.1 mg/L	[79]
Nannochloropsis salina	EPA	Batch, 8 g/L glucose, 1.46 g/L sodium acetate	30.54%	–	[80]
Nitzschia laevis 2047	EPA	Batch, 10 g/L glucose	1.7% TFA	0.017 g/g DW	[81]
N. laevis UTEX 2047	EPA	Perfusion culture, 50 g/L glucose	2.84% TFA	1112 g/L	[82]
Crypthecodinium cohnii ATCC 30772	DHA	Batch, 7% rapeseed meal hydrolysate and 1–9% waste molasses	22–34%	8.72 mg/L	[83]
C. cohnii ATCC 30772	DHA	Fed-batch, 50% glucose	–	1.7 g/L	[84]
		Fed-batch, 50% acetic acid	–	8 g/L	[84]

Table 2 (continued)

Microalga used	PUFA	Cultivation mode, carbon source	PUFA content	PUFA yield	References
Crypthecodinium cohnii CCMP 316	DHA	Fed-batch fermentation with diluted carob pulp syrup	4.4% TFA	1.9 g/l	[85]
Schizochytrium sp. KH105,	DHA	Batch, 80 g/L glucose, Shochu distillery wastewater for 2 g/L total nitrogen	–	3.4 g/l	[86]
Schizochytrium mangrovei Sk-02	DHA	Batch, 60 g/L glucose in 100% coconut water	20.7% TFA	5.7 g/L	[87]
Schizochytrium limacinum SR21	DHA	Continuous, 90 g/L crude glycerol and 5 g/L corn steep solid	148.2 mg/g biomass	90 g/L	[88]
Schizochytrium sp. *CCTCC M209059.*	DHA	Batch, 40 g/L glucose	42.10% TFA	0.12 g/g	[89]
Schizochytrium sp. *HX-308 M,* mutant	DHA	Batch, 40 g/L glucose	58.25% TFA	0.23 g/g	[89]
Thraustochytriidae sp. AS4-A1	DHA	Batch, liquid residues from food industry (Potato chip processing and brewery), supplemented with nitrogen and vitamins	10–24% TFA	2698 ± 132 mg/L	[90]
Aurantiochytrium sp. KRS101	DHA	Fed-batch, 60 g/L glucose, 10 g/L corn steep solid	40% TFA	8.8 g/L	[91]
Aurantiochytrium sp. *SW1*	DHA	Batch, glucose	50% of TFA	1.12 g/L	[92]
Aurantiochytrium sp. *SW1*	DHA	5L fermenter, 60 g/L glucose	47.87% TFA	4.5 g/L	[93]
Thraustochytrium sp. ONCT18	DHA	Batch, 5 g/L glucose	31.4%	4.6 g/L	[94]

Table 3 Heterotrophic production of various pigments from microalgae

Microalgae used	Pigment produced	Cultivation mode, carbon source	Pigment content	References
Chlorella prototecoides CS-41	Lutein	Batch, Basal medium, glucose 9 g/L	16 mg/L, 4.6 mg/g	[95]
	Lutein	Batch, Kuhl medium, glucose 6 g/L	14.8 mg/L, 4.4 mg/g	[95]
	Lutein	Batch, Basal medium, glucose 36 g/L, 30L fermenter	66.3 mg/L, 4.9 mg/g	[95]
Chlorella prototecoides CS-41	Lutein	Batch, 3.7 L fermenter, glucose 40 g/L Urea 1.7 g/L	4.58 mg/g, 83.81 g/L	[96]
Chlorella prototecoides CS-41	Lutein	30 L fermenter, fed batch, N-limited, glucose 40 g/L Urea 3.6 g/L	5.35 mg/g, 209 mg/L	[97]
Chlorella pyrenoidosa 15-2070	Lutein	Initial glucose 10 g/L, fed-batch with 400 g/L glucose	178 mg/L	[98]
Chlorella pyrenoidosa 15-2070	Lutein	Batch, glucose 40 g/L	2.5 mg/g	[99]
Chlorella prototecoides UTEX 29	Lutein	Batch, glucose, NaClO, H_2O_2, Fe^{2+} as inducers	1.98 mg/g, 31.4 mg/L	[100]
Haematococcus pluvialis Flotow NIES-144	Astaxanthin	Batch, NaCl stress, 45 mM acetate	30 pg/cell (9 µg/ml)	[51]
C. zofingiensis ATCC 30412	Astaxanthin	Batch, 50 g/L glucose,	10.3 mg/L	[101]
	Astaxanthin	Batch, 30 g/L glucose, 10 mM H_2O_2, 0.5 mM NaClO	12.58 mg/L	[102]
	Astaxanthin	Batch, 30 g/L glucose, 1 mM peroxynitrite	11.78 mg/L	[103]
	Astaxanthin	Batch, 30 g/L glucose, nitryl chloride	10.99 mg/L	[103]
C. zofingiensis ATCC 30412	Astaxanthin	Batch, 30 g/L pretreated molasses	1 mg/g	[53]
C. zofingensis Mutant E17	Astaxanthin	Batch, 20 g/L glucose	1.21 mg/g	[104]
	Astaxanthin	Batch, 20 g/L fructose	1.17 mg/g	[104]
	Astaxanthin	Batch, 20 g/L sucrose	1.23 mg/g	[104]
	Astaxanthin	Batch, 20 g/L sugar mixture	1.18 mg/g	[104]
Chlorococcum sp.	Astaxanthin	Batch, 44 g/L glucose, 0.1 mM H_2O_2	1.8 mg/g	[105]
Galdieria sulphuraria 074G	Phycocyanin	Batch, molasses 7.5 g/L plus glucose 45 g/L	11.2 mg/g	[48]
	Phycocyanin	Sugar beet molasses sucrose 50 g/L, total sugar up to 750 g/L	350 mg/L	[48]

(continued)

Table 3 (continued)

Microalgae used	Pigment produced	Cultivation mode, carbon source	Pigment content	References
G. sulphuraria 074G	Phycocyanin	Batch, glucose, fructose, glycerol 5 g/L	2–4 mg/g	[106]
	Phycocyanin	Batch, glucose, fructose, glycerol 5 g/L, carbon limited, nitrogen replete	8–12 mg/g	[106]
G. sulphuraria 074G	Phycocyanin	Batch, glucose 5 g/L	18 mg/g	[107]
	Phycocyanin	Batch, restaurant waste with glucose 5 g/L	20 mg/g	[107]
	Phycocyanin	Batch, bakery waste with glucose 5 g/L	21.8 mg/g	[107]
G. sulphuraria strain 074G	Phycocyanin	Batch, glucose 5 g/L	25–30 mg/g	[108]

sorghum juice, molasses, cassava hydrolysate and other waste resources like biodiesel derived crude glycerol has been used successfully for the production of biomass and desired products. It has been estimated that in the current scenario, the feedstock price in case of biodiesel production from various oils contributes to around 85% of the production costs [56]. Assuming that microalgal biomass is used as the feedstock, utilization of cheap or waste carbon sources can help reduce the feedstock price dramatically, hence assisting in cost competitive biofuel production.

3.2 Nitrogen Source and Availability

Nitrogen is the second most important nutrient for microalgal cultivation and is often supplied as organic and inorganic nitrogen based on the requirements of the microalga. Most commonly used nitrogen sources are ammonium, nitrate salts, nitrite salts, yeast extract and urea. Microalgae transport ammonium, nitrate and nitrite across the cell membranes with specific transporters. The *C. reinhardtii* genome has about 8 ammonium transporters and 13 putative nitrate/nitrite transporters [109]. Once inside the cells, the nitrogen sources are assimilated into biomass by various enzymatic reactions. Ammonium assimilation is catalyzed by two different pathways: (i) the GS/GOGAT pathway, comprising the enzymes glutamine synthetase and glutamate synthase, resulting in the formation of α-ketoglutarate. Or (ii) the GDH pathway catalyzed by glutamate dehydrogenase, and ammonium is incorporated into glutamate to form α-ketoglutarate [9]. The nitrogen in the form of glutamate is then converted to aspartate or asparagine by the action of aspartate aminotransferase and asparagine synthetase [110]. These four

amino acids are the nitrogen suppliers for all other metabolic processes. Nitrate and nitrate are transported into the cells and are ultimately converted to ammonium by the combined action of nitrate reductase and nitrite reductase [109]. The other nitrogen source that is commonly used for heterotrophic cultivation of microalgae is urea. Urea is utilized by microalgae by splitting it into ammonium and bicarbonate by the action of two different enzymes urease and urea amidolyase, and most microalgae metabolize urea by urea amidolyase [9]. Based on the ease of assimilation, ammonium seems to be the best nitrogen source followed by nitrate and nitrite. Urea is most commonly used in heterotrophic or mixotrophic cultivation, rather than autotrophic cultivation. The use of ammonia in cultivation medium leads to a decrease in pH, hence this might affect microalgal strains that are sensitive to pH [96]. Therefore, ammonium should be used as a nitrogen source in pH-stat cultivations.

The preference for nitrogen source varies with each microalgal strain and the nitrogen source is usually optimized for maximal biomass production. Nitrogen sources tested for a newly isolated *Scenedesmus* sp. R-16 include beef extract, urea, peptone, ammonium, sodium nitrate, yeast extract, sodium glutamate and L-cysteine [46]. Highest biomass concentration was observed in nitrate medium, while highest lipid content of 45% was obtained in peptone medium and it was suggested that inefficient utilization of peptone as a nitrogen source simulating nitrogen limitation might have led to enhanced lipid accumulation. *Schizochytrium limacinum* SR21 was used for the production of DHA and various organic and inorganic nitrogen sources were tested [49]. Yeast extract, polypeptone, tryptone, corn steep liquor, urea, ammonium acetate, ammonium sulfate, ammonium nitrate, and sodium nitrate were applied for fermentation. Corn steep liquor was determined as the best organic nitrogen source with a DHA content of 1.7 g/L and ammonium acetate was the best inorganic nitrogen source [49]. Addition of non-conventional nitrogen sources like arginine, tryptophan and tyrosine was also shown to improve fatty acid accumulation by *Schizochytrium limacinum* SR21 [111]. Lutein production by *C. protothecoides* was enhanced by the addition of urea as a nitrogen source and a maximum biomass of 19.6 g/L and lutein yield of 83.81 mg/L was obtained [96]. The marine alga *Nannochloropsis salina* was cultivated heterotrophically for biomass and lipid production using various nitrogen sources including peptone, yeast extract, malt extract, meat extract, urea, sodium nitrate and ammonium nitrate. Optimal biomass production and lipid accumulation was obtained with peptone as a carbon source [80]. Nitrogen as a nutrient also plays an important role in the accumulation of carbohydrates or lipids based on the microalgal strain used. The nutrient deficient strategy accomplished by nitrogen starvation is the most widely used strategy for the accumulation of carbohydrates/lipids and the mechanisms involved are discussed in detail in Sects. 4.1 and 4.2. It should be noted that a majority of wastewaters are rich in nitrogen and this needs to be removed before environmental release to prevent the growth of harmful algal blooms. Bioremediation by microalgae is an excellent option for nutrient removal in wastewater, particularly nitrogen. Based on the analysis of different wastewaters, it

was observed that the total nitrogen, ammonia and nitrate levels of wastewaters were in the range of 35.7–7,300 mg/L, 3.3–4,800 mg/L and 0.74–195.2 mg/L respectively [112]. Wastewater also contain a high amount of volatile organic acids like acetic acid, propionic acid, butyric acid, and valeric acids providing organic carbon sources. Wastewater generated form swine farms are particularly rich in ammonia and could be a potential source of nitrogen for the cultivation of microalgae. *Chlorella vulgaris* JSC-6 was cultivated heterotrophically in swine wastewater and the nutrient removal potential was evaluated. Highly efficient nutrient removal was achieved with ammonium removal and COD removal at 64.2% and 74.3% respectively, a biomass concentration of 2.35 g/L and the strain accumulated carbohydrates at 54% dry cell weight [113]. Heterotrophic *Chlorella sorokiniana* was able to efficiently remove nitrate and phosphate when ammonium was used as a nitrogen source instead of nitrate, implying that wastewaters rich in ammonium enhances nitrogen removal [114]. Addition of an organic carbon source like acetate or glucose might improve the nitrogen removal efficiency of heterotrophic microalgae [115].

3.3   Aeration and Agitation

When all the nutrients are supplied in optimal conditions and the cultivation conditions are maintained, aeration of the culture and agitation can solely influence the biomass production in heterotrophic microalgal cultivation. Heterotrophy in microalgae is an aerobic process, and in high cell density fermentation supply of optimal oxygen concentration for the cells is critical [9]. Agitation is a way of evenly distributing the supplied oxygen; aeration and agitation should be optimized with respect to each other to maintain a constant dissolved oxygen concentration. In photoautotrophic cultivation, mixing of the cultures or agitation is mainly to prevent sedimentation of the cells, even distribution of nutrients and prevent prolonged exposure of cells to dark zones of the photobioreactor. In heterotrophic cultivation, oxygen is required for the metabolism of organic carbon sources and is a key factor of fermentation. The cultivation medium is loaded with organic and inorganic nutrients and the solubility of gaseous oxygen is low, requiring a continuous supply. The oxygen mass transfer rate describes the oxygen requirements of the culture in a quantifiable way and the maintenance of this rate is essential to maintain the biomass production [116]. It has been reported that the limitation of oxygen supply can markedly decrease the growth rate and biomass productivity of heterotrophic *Chlorella*. The optimal dissolved oxygen concentration set for most heterotrophic microalgal fermentation is 50%. Cell lysis might occur under high aeration conditions and insufficiency of oxygen also affects the metabolic potentials of the cells. The diatom *Cyclotella cryptica* was cultivated heterotrophically and the effect of aeration and agitation was investigated separately. It was found that increased aeration rate (0.42 vvm) increased maximum specific growth rate, and agitated vessels shows increased growth rate than aerated culture vessels [117].

Similarly, agitation increased the biomass productivity of *A. microscopica Nägeli* (RSMan92) when the culture was agitated at 200 rpm without aeration [118]. In contrast, the biomass production and fatty acid profile of *Chlorella* sp. TISTR 8990 was unaffected by agitation speed in the range of 100–200 rpm, but it was mainly influenced by the C/N ratio maintained in the culture medium [119].

The oxygen concentration of the medium and aeration is significant for the production of PUFAs by Thraustochytrids, as the desaturase enzyme responsible for the production of PUFAs are dependent on molecular oxygen for their activity [120]. It was shown that a high oxygen mass transfer coefficient $k_L a$ enhanced the biomass production, fatty acid composition, and fatty acid yield in *Schizochytrium* sp. S31. In fed batch cultivation with glycerol and yeast extract, a high $k_L a$ of 180/h resulted in the highest DHA concentration, productivity and yield of 28.93 g/L, 301 mg/L/h and 0.44 ± 0.02 g/g respectively [121]. Maintaining the volumetric mass transfer coefficient is an important parameter for scale-up of the culture. *Schizochytrium* sp. CCTCC M209059 fermentation for the production of DHA was scaled up from 10, 50, 1500 and 7000 L, and $k_L a$ was maintained at 88.9/h. The DHA concentration was maintained at around 14 g/L for all the scale of bioreactors, and the maximum DHA content of 19.72 g/L was obtained in 7000 L fermenters [122]. Oxygen independent fatty acid synthesis mechanisms has been proposed in *Schizochytrium* sp. ATCC 20888 [123]. The alga possess an oxygen independent polyketide synthase like fatty acid synthesis mechanism. Hence, oxygen limitation seems to enhance the PUFA content of the alga. However, decreased oxygen levels affect biomass content and productivity. Therefore a two stage cultivation strategy, where initial biomass was obtained with higher oxygen content, followed by a lipid accumulation stage with low oxygen content was devised for the cultivation of *Aurantiochytrium* sp. By applying this strategy, the fatty acid content increased from 29% in well oxygenated cells to 54% in O-limited cells [123]. Similar two stage cultivation strategy with shifting oxygen levels has been successfully employed for enhanced PUFA and lipid production in different *Schizochytrium* sp. [124–126].

3.4 Other Operational Parameters

3.4.1 The C/N Ratio of the Cultivation Medium

Microalgal heterotrophic cultivation is generally carried out in conventional bacterial fermenters and a good control over process parameters are provided, compared to open pond systems. Heterotrophic cultivation is also much suited for lipid accumulation, because of the high carbon content supplied in the media and assimilated. The C/N ratio plays a key role in lipid accumulation of microalgal cultures and it is known that a high C/N ratio and decreased nitrogen concentration can enhance lipid accumulation. For the microbial production of lipids, the ratio as high as 700:1 is considered optimal to obtain a high fat coefficient of 25 [127].

C. prototheocoides was grown using sugar cane juice hydrolysate as a carbon source and yeast extract as a nitrogen source [60]. It was observed that highest lipid accumulation of 53% was obtained when the C/N ratio was set at 26.9 and 0.6 g/L of yeast extract. In the coculture of *Chlorella vulgaris* and the blue green alga *Leptolyngbya* sp., with C/N ratios of 15:1 and 13:1, higher lipid accumulation and productivity was achieved at the low C/N ratio of 15:1 as opposed to the higher ratio in mixotrophic mode. The lipid production was much lower in heterotrophic mode [128]. This implies that the optimal C/N ratio depends on the microalgal strain cultivated and the mode of cultivation. For cyanobacteria, the C/N ratio could be lower. The blue green alga *A. microscopica Nägeli* (RSMan92) was grown heterotrophically with cassava and corn starch as carbon source and sodium nitrate as nitrogen source. Maintaining a constant C/N ratio of 20, the concentrations of carbon and nitrogen were varied and it was observed that increase in nitrogen concentration significantly affected lipid accumulation and maximum lipid production was obtained at the C/N concentrations of 5,000/250. An increase in the C/N concentration to 10,000/500 increased biomass productivity but decreased lipid accumulation [118]. The effect of C/N ratio on the heterotrophic growth and fatty acid accumulation of *Chlorella* sp. TISTR 8990 was evaluated using glucose as a carbon source, potassium nitrate as the nitrogen source and different C/N ratios of 29:1, 63:1 and 95:1 [119]. The maximum biomass production was obtained at C/N ratio of 29:1, with biomass productivity and yield coefficient from glucose as 0.68 g/L/d and 0.62 g/g respectively. The C/N ratios of 63:1 and 95:1 resulted in maximum fatty acids productivity of 186 mg/L/d and lower C/N ratio decreased the fatty acid content of the biomass [119]. Hence, C/N ratio is a crucial parameter that has to be optimized carefully for heterotrophic lipid accumulation. Increase in C/N ratio can also increase pigment production during heterotrophic cultivation of microalgae. The biomass and astaxanthin content of *C. zofingensis* almost doubled and attained 10.29 mg/L when the glucose concentration was increased from 5 g/L to 50 g/L [101]. Similar results were observed with *C. prototheocoides*, where the intracellular lutein content increased from 19.39 to 76.56 mg/L when the glucose concentration was increased from 10 to 40 g/L [129].

3.4.2 Culture Temperature

Temperature of the culture is an important parameter when microalgae are cultivated for the accumulation of PUFAs. It has been shown that higher temperature increased the saturated fatty acid (SFA) content and a decrease in temperature increased the unsaturated fatty acid (UFA) content. Cultivation of *S. limacinum* OUC88 in increasing temperatures from 10 to 40 °C resulted in a change of the fatty acid composition, even though there was no significant change in the total fatty acid content. The SFA/UFA ratio increased from 1.13 to 1.45 when the temperature was increased from 16 to 35 °C [130]. *C. minutissima* UTEX 2341 achieved higher lipid content when the temperature was at 20 °C, even though there was no significant change in biomass between 15 and 25 °C [131]. Higher

unsaturation in phosphatidyl choline fraction of the phospholipids and increase in EPA fraction was obtained at 15 °C for *Nitzschia laevis*, while maximum biomass content was achieved at 23 °C [132]. When *C. protothecoides* was grown heterotrophically for the production of lutein, the effect of different temperatures (24, 26, 28, 30, 35, and 40 °C) were tested for maximal biomass content, lutein content and lutein productivity. The maximum biomass content of 10.7 g/L and maximum lutein of 74.29 mg/L was obtained at 28 °C, while higher cellular lutein content of 4.59 mg/g was obtained at 35 °C [133].

3.4.3 Salt Stress or Changes in Salinity of the Medium

Salt stress or changes in the salinity of the medium is an important factor governing the cellular mechanisms and the resulting stress responses in microalgae. In marine microalgae, both the decrease and increase in salinity other than the adapted level might induce stress, while in freshwater algae the presence of high amounts of salts in the medium might lead to changes in osmolarity of the medium and leading to osmotic stress. Salt stress is known to affect the membrane fluidity of the cells, change the ion permeability of the membranes and disrupt the ionic potential, induce ion toxicity by the excess Na^+ and Cl^- ions and cause osmotic stress [134]. *C. protothecoides*, when subjected to salt stress accumulated higher lipid content of 41.2% when cultivated in the presence of 30 g/L NaCl and it was shown that salt stress is superior to osmotic stress by producing more ROS by the ionic effect [135]. The salinity of the medium is often optimized for the enhanced production of the desired product and certain microalga are tolerant to high salinity levels. *C. protothecoides* 249 could tolerate very high NaCl concentration of up to 35 g/L and change in salinity does not drastically change the lipid content of the alga. However, a slight increase in lipid content could be observed when the salinity increases from 17.5 to 35 g/L [136]. In contrast, *C. minutissima* had a very low tolerance to NaCl with growth severely inhibited at 20 g/L. However, when salt stress was induced after biomass production in salt free media, 40 g/L NaCl concentration resulted in maximal lipid accumulation and lipid yield of 31.82% and 2.38 g/L respectively [131]. The diatom *Nitzschia laevis* also had a very low tolerance to salinity, with growth inhibited at NaCl concentrations of 10 g/L and above. The degree of unsaturation of polar and neutral lipids decreased with increase in salinity from 10 to 20 g/L and maximum total fatty acids and EPA were obtained at 20 g/L NaCl [134]. However, the EPA was allocated with polar lipids when subject to salt stress, similar to temperature stress [132]. The increase in phospholipid content and the increase in the UFAs in polar lipids reveals that under stress conditions, *N. laevis* stores polar lipids that will aid them in rapid revival, cell growth and division upon return to favorable conditions with an enhanced supply of polar lipids for membrane synthesis. *S. limacinum* was cultivated for lipid accumulation and when salinity decreased from 3.6% (w/v) to 0.9% (w/v), the SFAs decreased from 59 to 53%, accompanied by a change in the DHA/DPA ratio [130]. Salt stress is also applied as a carotenogenesis inducer for *H. pluvialis* [51, 137].

3.4.4 The pH of the Cultivation Medium

The pH of the medium strongly influences the metabolic processes of the cell, as the membrane potential and transport across cell membranes are governed by external pH which in turn governs the internal pH of the cells. *C. cohnii* ATCC 30556 could grow well over a wide pH range of 5.5–9, however extreme pH like 4 or 10 severely inhibited biomass growth. Highest fatty acid content of 56.8% was obtained when the pH of the medium was maintained at 7.2 [138]. *Schizochytrium* sp. S31 was cultivated under different pH conditions of 5–8. Optimal biomass growth was obtained at the neutral pH 7, while at pH 8 growth was completely inhibited, and pH 5 and 6 supported sub optimal biomass growth. The lipid content and DHA content obtained at pH 7 were 40% and 13% respectively [139]. *C. minutissima* UTEX 2341 grew well over a pH range of 4–8, but biomass and lipid content were drastically decreased when the pH increased to 9 and above. Maximum biomass content of 8.67 g/L was obtained at pH 7 and maximum lipid yield of 1.16 g/L was achieved at pH 6 [131]. *C. protothecoides* was cultivated in the pH range of 5–8 for optimal biomass and lutein production. Optimal pH was found to be 6.6, with maximal biomass production, cellular lutein content and total lutein yield as 18.2 g/L, 4.75 mg/g dry cells and 77.92 mg/L respectively [129].

4 Products of Commercial Interest from Heterotrophic Algae

4.1 Lipids/Oils

Lipids are one of the most important biopolymers seen in any living organism; the basic structure of any living cell is the presence of a lipid membrane enclosed cytoplasm and nucleus. All the membranes present in both prokaryotic and eukaryotic cells are made of lipids or fats and lipids are often stored as an energy reservoir in microorganisms, plants and animals. In microalgae, lipids can be of two types based on their function: structural lipids and storage lipids. Structural lipids include (i) phospholipids, which are the most abundant accounting for about 20% of the structural lipids and is the major extra-chloroplast membrane lipid, (ii) glycolipids which are the major constituents of the chloroplast membrane, (iii) betaines seen in some microalgae, and (iv) some special lipids like squalene seen in very specific microalgae [140]. The most important category of lipids in the renewable energy sector are the storage lipids—the non-polar glycolipids or neutral lipids. Triacylglycerol (TAG) is the most commonly stored neutral lipid in oleaginous microalgae and lipid accumulation occurs during adverse conditions, serving as a source of energy or precursors for fatty acid synthesis during rejuvenation. TAG is the fatty acid ester of three fatty acid molecules with glycerol, and the diversity of TAG is derived from different combinations of the three component fatty acids, the

chain length of the component fatty acids and the degree of saturation [141]. Polyunsaturated fatty acids (PUFA) are generally seen in marine microalgae and are discussed in detail in Sect. 4.3. The lipid content in oleaginous algae vary from 10 to 70% depending on the microalgal species and the strain [142]. The lipid content of microalgae in their natural environment could be affected by seasonal variation, with higher PUFAs in winter and higher TAGs in summer. However, under laboratory cultivation many factors like light intensity, pH, carbon availability, nutrient composition of the medium, salinity of the medium might affect lipid content and productivity [142]. The pivotal point in selecting a microalgal strain for lipid production is the high biomass productivity and high lipid content of the strain chosen and with the aid of cultivation strategies, maximum lipid accumulation can be achieved.

Oleaginous algae are incapable of accumulating carbohydrates and only accumulate lipids. Well known oleaginous algae are from Eustigmatophyceae and Bacillariophyceae, and are mostly marine. Green algae or Chlorophyta can accumulate lipids or carbohydrates based on the strain and it can be seen that marine green algae preferentially accumulate lipids [143]. A screening of a total of 175 strains for higher total fatty acid accumulation revealed that the top lipid accumulators were from the genera *Nannochloropsis*, marine *Chlorella* and *Dunaliella* [144]. This holds true based on the literature and the most common lipid accumulators are from the genera *Porphyridium, Dunaliella, Isochrysis, Nannochloropsis, Tetraselmis, Phaeodactylum, Chlorella* and *Schizochytrium* [141] with the lipid content varying between 20 and 50%. Carbon flux between lipids and carbohydrates has been poorly understood in microalgae, with both sharing the same precursors. Starch is the primary storage product is algae, both from photosynthesis and from assimilation of organic carbon sources. Starch is mobilized from the chloroplast and utilized for cell growth and maintenance during dark survival in photoautotrophic algae and in even in lipid accumulating algae starch is accumulated in the initial stages of nutrient deprivation [143]. Nutrient deprivation, mainly nitrogen deprivation can reduce protein synthesis in microalgae. Proteins are the essential cellular machinery for cell division and metabolism cell division is arrested under nitrogen deprivation conditions. Hence, the carbon available is metabolized and funneled into storage reserves like lipids, which upon return to a nutrient replete medium is mobilized for cell growth and division [145]. Transcriptional analyses of lipid accumulating *C. reinhardtii* gene expression under nitrogen limited conditions revealed that within 10–15 min of nutrient deprivation, the cell growth is arrested by the expression of a specific set of genes and the metabolism is remodeled further to favor TAG accumulation. It was also shown that this cascade of events are controlled by 17 transcriptional regulators and the same set of regulators are functional during sulfur deprivation, but phosphorus deprivation unleashes a new set of regulatory elements [146]. Lipids are the most reduced from of carbon and the energy input for lipid synthesis is higher: the energy cost for storage of a single carbon in lipids is 53% greater than storage in starch [147] and thus the energy returns from lipids are higher than carbohydrates.

The cultivation of microalgae under heterotrophic conditions and their lipid accumulation potential are summarized in Table 1. It can be seen that *Chlorella* sp. dominates the scene as a promising heterotrophic microalgal strain for lipid/oil production, which can be further converted to biofuels based on the fatty acid composition. Biodiesel, aviation fuels or jet fuels and biocrude oils can be obtained from microalgal oils based on the conversion process. Biodiesel production from Chlorella biomass seems to be a feasible option for commercial scale. The heterotrophic *C. protothecoides* has been previously cultivated successfully in large scale up to 11,000 L bioreactors with a biomass yield of 14.2 g/L and lipid content of 44.3% dry weight [148]. The lipids were extracted using Soxhlet extractor method and transesterified using immobilized Candida lipase with a conversion rate of 98.15% and biodiesel yield of 6.24 g/L in the commercial scale cultivation. Heterotrophic cultivation of microalgae has the potential to be the microalgal biomass supplier for large scale biodiesel production, but the cost of installation and operation of bioreactors might hinder the economics. It was estimated that in a 7500 m^2 plant, 10,000 tons of biodiesel can be produced per year, with cost cutting measures like selling the residues as feed, using the crude glycerol for cultivation, extraction of other valuable products from the residual biomass, application of a microalgal strain with higher biomass yield and anaerobic digestion of the residues for methane production [149]. It was also suggested that algal biodiesel production facilities should be co-localized with industries which could supply the raw materials to sustain the microalgal cultivation and both industries rely symbiotically on each other for energy and other resources [150]. Dewatering and drying of the biomass and the subsequent lipid extraction for biodiesel production is another energy and cost intensive process in biofuel production process. Direct transesterification of wet microalgal biomass with 90% of water content has been attempted with success [151]. *Schizochytrium limacinum* was cultivated heterotrophically on biodiesel derived crude glycerol with a lipid yield of 51%. Direct transesterification of the wet biomass with chloroform, petroleum ether or hexane resulted in a biodiesel yield of around 55–65%, while the two step lipid extraction and transesterification yielded only 57% of crude biodiesel [151]. Thus, microalgal biomass obtained by heterotrophic cultivation of microalgae is a potential source for biodiesel production. Screening of the Peking University Algae Collection for heterotrophic algae suitable for biodiesel production led to the isolation of *Chlorella* sp. PKUAC 102 with a lipid content of around 50% and a fatty acid profile suitable for biodiesel production [152]. Heterotrophy of microalgae is the most untapped potential for successful microalgal biomass production and it can be used for cost effective biodiesel production.

4.2 Carbohydrates

Carbohydrates are the essential components of any living cell, as they are the source of energy and carbon skeletons for growth and cell division. The central metabolic

pathway is conserved in most living organisms that uses organic carbon and the glucose utilization pathway, glycolysis is also universal. Microalgae are rich in carbohydrates as they serve two functions, as the energy reserves and as structural components in cell walls. Microalgal cell walls are composed of two layers, an inner layer and an outer layer both composed of cellulose and hemicellulose. Most aquatic algae are devoid of rigid cell walls as they are buoyant in their natural environment without any prerequisite for tough cell structures [153]. Microalgal cell wall structure is devoid of lignin as opposed to higher plants, as lignin renders the biomass recalcitrant to mild treatment conditions and requires very harsh pre-treatment methods for cell wall disruption and the release of respective reducing sugars. Even present, lignin is generally seen in macroalgae in very less quantities (<3%) [154], the presence of lignin is considered more in the evolutionary sense for the development of terrestrial plants from aquatic algae [155]. The storage polysaccharides of microalgae are generally starch and glycogen [5] and the storage polysaccharide vary widely in macroalgae: glucans and sulfated polysaccharides like ulvan in green macroalgae; agar, agarose, agaropectin and carrageenan in red macroalgae; mannitol, alginate, fucoidan and laminarin in brown macroalgae [156]. Upon hydrolysis, microalgae releases simple sugars like glucose, mannose, xylose and arabinose [5], while the macroalgal sugars are rich in glucose, galactose, mannitol, and some pentoses like xylose and arabinose [157]. These sugars serve as efficient feedstock in microbial fermentations for the production of biofuels like bioethanol, biobutanol and biohydrogen. Microalgal hydrolysate are also rich in free alpha amino nitrogen (FAAN) or organic nitrogen and hence it can be used to reduce or replace organic nitrogen sources in bacterial fermentations [158]. Other renewable feedstock like lignocellulosic biomass are very low in nitrogen content with a very high C/N ratio, often requiring the addition of expensive nitrogen sources in fermentation. Microalgae can serve as both nitrogen and carbon source for heterotrophic bacteria in biofuel or alcoholic fermentations. The hydrolysis of microalgae does not release any potential fermentation inhibitors like furfural and the efficiency of the fermentation remains unaffected.

Some green algae tend to accumulate high amounts of carbohydrates and the carbohydrate content can vary between 20 and 77% [5, 159]. Carbohydrate accumulation in microalgae is triggered by nutrient deprivation, and sulfur deprivation is the most efficient strategy for inducing carbohydrate accumulation [143]. Molecular analysis of carbon flux in nitrogen deprived *Dunaliella teraticola* revealed an up regulation in starch synthesis and tricarboxylic acid cycle enzymes for the continued supply of carbon skeleton, and a down regulation of enzymes involved in fatty acid and TAG synthesis [160]. This gene expression mechanism in different from the lipid accumulation mechanism mentioned earlier [146] and is unique to starch accumulating algae. An increase in photosynthetic efficiency in case of photoautotrophic algae is also an inducer for increased carbohydrate accumulation [5]. Under heterotrophic conditions, algae accumulate carbohydrates by the same mechanism as autotrophic algae, the metabolic carbon feed is funneled into storage polysaccharides in adverse conditions. It has been reported very early that algae that are incapable of cell division in the dark can utilize the organic carbon and

accumulate very high quantities of carbohydrates [161]. This works in the similar fashion of nutrient deprivation, cell division is blocked because they are incapable of cell division in the absence of light, while in nutrient deprivation conditions cell division is blocked because of the turn down in protein synthesis in the absence of sufficient nutrients. The carbon that is metabolized is stored as reserve polysaccharides leading to an increase in cellular carbohydrate content [161]. This strategy has been applied in an innovative two stage microalgal cultivation system where the initial biomass was obtained by photoautotrophic culture and upon incubation with a carbon source in dark conditions, carbohydrate accumulation occurs [162].

Heterotrophic cultivation has been applied to enhance starch accumulation in microalgae. The oleaginous microalga *Neochloris oleoabundans* UTEX 1185 was cultivated under heterotrophic conditions in the presence of glucose as a carbon source. When cultivated in batch mode with a C/N ratio of 278 and N-limitation, lipid accumulation occurred resulting in 52% dry weight lipid accumulation. When cultivated in fed-batch mode, C/N ratio of 278 and pulsed addition of N, carbohydrate accumulation ensued resulting in a 54% dry cell weight of starch [57]. *Chlorella vulgaris* and *Chlorella sorokiniana* accumulated higher quantities of starch under heterotrophic conditions with glucose as a carbon source when co-immobilized with the plant growth promoting bacteria *Azospirillum brasilense* [163]. The carbohydrate yield and carbohydrate productivity were enhanced for both *C. vulgaris* and *C. sorokiniana* when co-immobilize with *A. brasiliense* than when they were immobilized separately. Some extracellular polysaccharides or EPS have been reported in heterotrophic algae. The Function of EPS could be to protect the alga from adverse conditions, while carbohydrates with high viscosity has applications in food and pharmaceutical industries as viscosity enhancer [164] and in enhanced oil recovery applications (EOR) in petrochemical industries [165]. Most recently, EPS has received much attention for their immune modulation and antibacterial, anti-oxidative, and anticancer properties and has new found applications in pharmaceutical industries [166]. The oleaginous alga *Crypthecodinium cohnii* ATCC 30772 secreted large amounts of EPS rich in glucose, galactose and mannose, which resulted in increased viscosity and decreased oxygen transfer efficiency in the bioreactor [164]. *Arthrospira platensis* is capable of producing EPS but the productivity and yield under heterotrophic conditions were very less compared to photoautotrophic and mixotrophic conditions. The EPS content and productivity for photoautotrophic and heterotrophic conditions were 219.6 g/L and 433.62 mg/g/d and 30.3 g/L and 38.33 mg/g/d respectively [167]. However, the oleaginous alga *N. oleoabundans* was incapable of any EPS production under heterotrophic conditions but it produced EPS under mixotrophic conditions from glucose and lactose [165].

4.3 Polyunsaturated Fatty Acids (PUFA)

The second class of lipids of importance in microalgae are the polyunsaturated fatty acids or PUFAs. The fatty acids with chain length C20 or greater are suitable fatty acids for health supplement purposes with their unsaturated bonds, while fatty acids with chain length of less than C20 are most suitable for biofuel purposes [168]. In general, the chain length of fatty acids and the degree of unsaturation is higher in microalgal lipids than lipids of higher plants owing to their natural habitats. In animals and humans, PUFAs, especially ω-3 and ω-6 PUFAs like Docasahexaneoic acid (DHA) and Eicosapentaneoic acid (EPA) cannot be synthesized as the precursor fatty acids α-linoleic (ALA) acid and cis-linoleic acid (LA) are not synthesized de novo. Thus animals are dependent on the dietary intake of these fatty acids, hence the name essential fatty acids. The efficiency of conversion of ALA and LA to the subsequent PUFAs is very low in humans, in men the conversion of ALA to EPA is about 8% while it is much higher in women at 21% owing to the requirements of a developing infant in the form of breast milk [169]. Nonetheless, supplementation of these essential fatty acids, particularly ALA, EPA and DHA is considered and the recommended daily dietary intake is set at a minimum of 250 mg/day [170]. Essential fatty acids are the precursors for the synthesis of eicosanoids, the signaling molecules comprising of thromboxanes, prostaglandins and prostacyclins which are involved in homeostasis and inflammation [171]. The regular supplement of PUFA rich foods are known to impart health benefits including cardio-protective effects, lower blood cholesterol, can positively impact low-grade systemic inflammation involved in conditions like Coronary heart disease, stroke, diabetes mellitus, hypertension, cancer, depression, schizophrenia, and Alzheimer's disease [172]. Most importantly, DHA is essential for proper development of nervous system and brain in infants and hence DHA is an additive in infant formula and health drinks for pregnant women [173]. Most plant based oils like soybean oil, mustard oil, sunflower oil, safflower oil, nuts like walnuts and sunflower seeds, whole grains, eggs and poultry are natural sources of essential fatty acids. For commercial purposes, fish oil was a major source, but in recent times concerns about increased mercury content of marine fish and unregulated fishing processes leading to marine fish depletion has led to the search of alternative sources of PUFAs [169].

Microalgae are being recognized as an important source of PUFAs as some oleaginous algae are capable of accumulating very high quantities of PUFA in their neutral lipid reserve. The storage of very long chain PUFAs in marine algae seems to implicate the necessity of reserve PUFAs for the rapid reconstruction of chloroplast rich in PUFAs for survival after low temperatures stress [174] or revival after nitrogen limiting conditions. The heterotrophic microalgae capable of accumulating very high amounts of PUFAs are summarized in Table 2. The marine heterotrophic algae of the class Thraustochytrids, including the species *Schizochytrium, Thraustochytrium* and *Aurantiochytrium* are capable of accumulating high quantities of lipids under heterotrophic conditions, up to 50% with the

majority of them being PUFAs [175]. These marine protists accumulate PUFAs and in addition some of these are potential sources of pigments like astaxanthin. The taxonomical status of these organisms are quiet unclear. The Thraustochytrids have acquired chloroplast by an endosymbiotic event, but have lost photosynthetic capacity in evolution, leaving behind a nonfunctional chloroplast and the ability to synthesize and store high quantities of VLC-PUFAs [25]. Thraustochytrids, mainly the genus *Schizochytrium* is currently the unrivalled commercial source of PUFA production, mainly because of the various advantages: the ability to grow in high cell densities in fermenters, the ability to accumulate as high as 90% of TFA as PUFAs [176], the ability to partition the PUFAs in the TAG reserve instead of cytoplasmic phosphorylated derivatives, high resistance to mechanical stirring in bioreactor, and high resistance to salinity [177]. Other heterotrophic algae of the genus *Crypthecodinium* are also used for the commercial production of DHA. The major companies involved are Aurora Algae, AlgaeBio, DSM-NP life, Lonza and GCI Nutrients [177]. And it can be seen from Table 2 that a variety of waste resources has been used as a carbon source without compromising on the fermentation performance of the algae: carob pulp [85], distillery wastewater [86], crude glycerol [88], corn steep solids [91], food industry waste [90], rapeseed meal hydrolysate and waste molasses [83]. Utilization of such alternative carbon sources can bring down the production cost associated with PUFAs and also valorize the waste in an efficient manner.

4.4 Pigments

Pigments are an integral part of the photosynthetic machinery of microalgae. The major pigment chlorophyll, responsible for the green color seen in leafy plants, is present in the photosynthetic apparatus of both microalgae and higher plants, actively taking part in photosynthesis [11]. Several accessory pigments called carotenoids help in photosynthesis, acting as light harvesting pigments or as anti-oxidants protecting the photosystems from oxidative damage under high light intensity. Carotenoids are tetraterpenoid lipophilic C40 compounds, with an extended conjugate double bond system and terminal π electron systems aiding in light absorption and anti-oxidant activity [178]. The variation in the structure of carotenoids is brought about by the number and position of the double bonds, oxygenation of the backbone and cyclization at one or both ends [179]. The hydrocarbon derivatives are called carotenes while the oxygenated version are called xanthophylls. Animals and humans are incapable of synthesizing carotenes and are totally dependent on the dietary intake for nutritional purposes. Carotenoids are also considered as important nutritional supplements because of their many capabilities endowed by their strong anti-oxidant activity—anti-ageing, anti-inflammatory, anti-angiogenic, anti-obesity, anti-tumorigenic, cardio protective and hepato-protective properties [180]. The global carotenoid market is estimated to be at US$ 1.24 Billion in 2016 and is expected to rise to US$ 5.3 billion by 2021,

with a CAGR of about 3.78% between 2016 and 2021. Microalgae is currently being the preferred source of carotenoids over the synthetic ones, mainly due to the rising consumer awareness towards natural products. Currently, astaxanthin from *Hamatococcus pluvialis*, β-carotene from *Dunaliella* are the commercially important microalgae and their carotenes in the market [181]. Astaxanthin is most important as a supplement in aquaculture feed for the bright pink color seen in salmonid fishes and shrimp, while it is also beneficial for humans because of their anti-oxidative properties [182]. Lutein, along with zeaxanthin, is an important pigment associated with eye health as it accumulates in the macula of the eye, protecting the eye from blue light damage, improving visual acuity and increased lutein intake has been reported to delay age related macular degeneration [183]. The current market source of commercial lutein is the petals of marigold flower, but the difficulties in the availability of the petals and the requirement of manual labor for processing has led to the search of alternative sustainable sources [183].

Astaxanthin has been produced by heterotrophic cultivation of certain *H. pluvialis* strains, mainly by using *H. pluvialis* Flowtow [184]. The heterotrophic growth capability of *Haematococcus* was reported much earlier, but was not pursued because of low biomass yields. The use of acetate as a carbon source supported heterotrophic growth, stimulated carotenogenesis which was usually delayed in the absence of acetate [184, 185]. *Chlorella zofingensis* is another promising microalgae for the heterotrophic production of astaxanthin, which can utilize glucose, sucrose and fructose as a carbon source [186]. For lutein, species of the genera *Chlorella* are considered good sources for heterotrophic cultivation, including *C. protothecoides*, *C. sorokiniana* and *C. pyrenoidosa*. Glucose has been used as the carbon source for heterotrophic cultivation of *C. protothecoides* [97, 100] and *C. pyreniodosa* [187], while acetate is the preferred carbon source for the mixotrophic and heterotrophic growth of *C. sorokiniana* [188, 189]. Pigment production or carotenogenesis is mainly a protective mechanism of microalgae against high light intensity, as the photosystems can be irreversibly damaged under high light intensity. However, under dark heterotrophic growth, several chemicals that induce oxidative stress have been used to trigger carotenogenesis. Ferrous ions are known to produce reactive oxygen species by the Fentons reactions and has been used to trigger carotenogenesis is *H. pluvialis* [184]. Chemical agents that are known to produce similar reactive oxygen species have been used to stimulate astaxanthin and lutein synthesis in microalgae: sodium hypochlorite [100], hydrogen peroxide [102], peroxynitrite and nitryl chloride that generate reactive nitrogen species similar to reactive oxygen species [103] and methyl viologen [190]. Salt stress has also been used to stimulate astaxanthin production in *H. pluvialis* [51].

Phycocyanin, a phycobiliprotein present mainly in cyanobacteria and red algae, is an important pigment for biomedical applications in quantitative assays as a biological coloring agent [191]. Phycocyanin absorbs orange and red light at 620 nm and emits fluorescence at 650 nm, and hence is mainly used in immunological assays [181]. Currently, photoautotrophic cultivation of the cyanobacteria *Arthrospira* is the main source of Phycocyanin. However, the heterotrophic red alga

Galdieria sulphuraria is receiving attention as a potential source of phycocyanin. The alga is endolithic in nature and is capable of heterotrophic growth in dark, and is endowed with a strong repertoire of sugar transporters that can transport a substantial 27 different sugars and sugar alcohols and utilize them for heterotrophic and mixotrophic growth. This makes the alga unique and the sugar utilization system is highly efficient is *G. sulphuraria* [192] Phycocyanin yield from varies between 8 and 20 mg/g based on the carbon source used and cultivation mode, making it a potential commercial source of Phycocyanin (Table 3).

5 Bioreactors for Microalgal Cultivation

Microalgae can be cultivated in conventional microbial fermentor, both in the presence and absence of light [193]. Cultivation of microalgae in fermentor has many added advantages like the vast knowledge about the long existing process, global availability of equipment and the accompanying software for convenient operation and a relatively lower operating cost compared to photobioreactors (PBRs) used for photoautotrophic cultivation [194]. In addition to the already existing designs, special concern should be given for the aeration of the microalgal cultures. Sufficient and optimal supply of oxygen is a crucial parameter in heterotrophic microalgal cultures, as the organic carbon supplied will be assimilated by oxidative metabolism [9]. Aeration is the single most important parameter that could severely affect the outcome of the microalgal fermentation process. Agitation spreads the supplied air to the entire culture medium determining the dissolved oxygen concentration, and hence baffles and impellers are essential. The design and the speed of the agitation devices is determined depending on the shear sensitivity of the microalgal strain grown. Reduction in the speed of impellers can significantly reduce the shear stress [194]. Other options are air-lift and bubble column methods for aeration and agitation of the culture in the bioreactor. However, the choice is heavily dependent on the microalgal strain to be cultivated, their mass and specific gravity as determined by the biomass composition (oleaginous algae float while other heavy algae tend to settle easily) and the rheological status of the culture (high cell density cultures are highly viscous) [194].

In photoautotrophic cultivation, the harvesting cost accounts for about 30% of the production costs owing to the low cell densities achieved in outdoor cultivation or PBRs. The harvesting costs could go down considerably if microalgae are cultivated in large scale in fermentors, as high-cell density cultures can be achieved with optimized process parameters, such as like temperature, pH, salinity, aeration as well as engineering strategies, such as fed-batch and continuous fermentation systems. Fed-batch fermentation seems to be more suitable for microalgal cultivation for the production of high-value products [195] and has already been applied for the production of lutein from *C. protothecoides* [97], DHA from *C. cohinii* [52], *G. sulphuraria* for the production of PC [196] and DHA from *Schizochytrium* sp. [122]. Heterotrophic cultivation of microalgae in commercial scale has long

been established. *Chlorella* spp. can be successfully cultivated in large-scale fermentors in a working volume of up to 11,000 L with a cell concentration of 14.2 g/L and a lipid content of around 45% and the algal biomass was subsequently used as the feedstock for biodiesel production [148]. Renewable carbon source like rice straw hydrolysate has also been used and with in situ transesterification over 99% methyl ester content and about 95% biodiesel yield were obtained [197]. In Japan, *Chlorella* spp. has been produced heterotrophically as a health food since the early 1990s and several countries in the Asian region like India, Taiwan and China are pioneers in cultivation of microalgae [198]. *Tetraselmis suecica* has been cultivated as an aquaculture feed in heterotrophic mode in 50,000 L scale and the replacement of live alga with the dried algal powder in the aquacultural feed did not affect the yield of the molluscs tested [199]. Commercial scale heterotrophic cultivation of *Crypthecodinium cohnii* and *Schizochytrium* sp. is well established for the production of DHA. The detailed cultivation methods and the downstream processes can be found in a recent review article [200]. The available knowledge about the heterotrophic cultivation should be extrapolated to other strains with products of interest to reduce production costs and achieve high yield of the desired products.

6 Challenges in Heterotrophic Cultivation of Microalgae and Future Perspectives

Heterotrophic cultivation of microalgae has numerous advantages, compared to photoautotrophic cultivation. High cell density culture can be achieved due to higher fast growth rates obtained in fermenters, and the culture conditions and process parameters like temperature and pH can be controlled to suit the microalgal strain cultivated. Also, the problem of supplying optimal light intensity has also been overcome in heterotrophic cultivation as growth occurs in the dark [9]. Different process engineering strategies like fed-batch and continuous cultures can be employed to enhance biomass yield further, thus reducing the costs associated with harvesting the biomass, as harvesting can contribute up to one third of the biomass production costs. Also, bioremediation of wastewater by microalgae is best performed under dark conditions, as the wastewater are often rich is suspended particulate matter affecting the penetration of light for efficient photoautotrophic cultivation [201]. Having said all these, heterotrophic cultivation of microalgae is not the method of choice for the production of microalgal biomass, as it is challenged by several issues that needs to be addressed to realize the potential of heterotrophic cultivation of microalgae for the economic production of biofuels.

The primary challenge for the success of a commercial heterotrophic cultivation system is the dearth of heterotrophic microalgal strains that can produce industrial products of interest. The primary isolation and identification of potential microalgal strains of commercial interest is performed under photoautotrophic conditions, and the culture collection centers does not have any heterotrophic strains [202]. But, it

must be noted that all microalgal strains are not obligate photoautotrophs, but are capable of dark heterotrophic growth as well. In the search of heterotrophic microalgal strains as aquaculture feed so that the feed was cultivated easily, Glaude and Maxley screened around 120 microalgal strains for heterotrophic growth with organic carbon source and it was found that 52 strains could utilize glucose and grow in the dark, while some of them were capable of utilizing acetate and glycerol [203]. Similarly, the screening of a laboratory collection of 35 strains of *Spirulina* for heterotrophic growth revealed that 34 of them could grow on glucose in dark and 24 could grow using fructose, revealing the rich source of heterotrophic strains in laboratory collections [204]. Recently, heterotrophic microalgal strains are isolated in particular for the production of biodiesel grade lipids [152] and wastewater treatment [205]. There has already been success in the use of obligate heterotrophs like Thraustochytrids for the production of poly unsaturated fatty acids for nutraceutical and pharmaceutical applications [175]. Thus, the potential of heterotrophic microalgal cultivation is slowly gaining momentum with the isolation of several heterotrophic microalgal strains.

The heterotrophic growth of microalgal strains is mainly due to the presence of a glucose transporter, as described previously in Sect. 2. The *Chlorella kessleri* glucose transport protein Hup1 has been characterized and studied completely [14] Similar other uncharacterized glucose transport systems has been reported for *Chlamydomonas*, *Scenedesmus obliquus* [206] and *Neochloris oleoabundans* [20]. Genome survey of *Chlorella protothecoides* sp. 0710 revealed the presence of three homologues of *hup1* and many other putative uncharacterized sugar transporters but none of them were characterized [22]. The only microalga identified till now with as many sugar transporters as any heterotrophic bacterium is the red alga *Galdieria sulphuraria*. The alga has at least 14 functional sugar transporters and can transport a variety of sugars, sugar alcohols and carboxylic acids [207], and the genome analysis revealed the presence of at least 28 putative sugar transporters reflecting the natural niche of the bacterium [208]. The analysis of the genome of available microalgae can indicate the presence of putative sugar transporters, and hence the capacity for heterotrophic growth aiding in isolation of heterotrophic microalgae.

The major advantage of photoautotrophic cultivation is the minimal cultural requirements in outdoor systems, as atmospheric CO_2 and sunlight can be used for cultivation. In heterotrophic cultivation, expensive nutritional media needs to be sterilized and used, along with energy intensive fermenter operation for axenic cultures. It must be noted that the existing technology for bacterial fermentation can be utilized for the heterotrophic cultivation of microalgae without much modifications and the use of these fermenters for the cultivation of axenic cultures of pharmaceutical interest can justify the enhanced product price as required for the quality and purity of the product. Glucose, acetate and glycerol are the most commonly used carbon sources for the heterotrophic cultivation of microalgae and obtaining fermentation grade carbon source can increase the production costs. There are numerous ingenious ways to utilize these carbon sources from other resources. Waste agricultural and lignocellulosic biomass are a rich source of reducing sugars, and the hydrolysis and breakdown of these complex components

has been optimized to be used in industrial scale recently. Glycerol is the abundant by product of the biodiesel industry, whereas acetate can be seen in increased amounts in numerous wastewaters. Also, there are increasing reports of heterotrophic microalgae capable of growth and metabolism in various renewable carbon sources like waste molasses [47, 53], biodiesel derived crude glycerol [88, 209], sweet sorghum [61, 210], phenolic compounds [211] and even certain unconventional nutritional sources like anaerobic digested dairy manure [212] and restaurant/bakery waste [107]. Lohrey and Kochergin suggested the co-location of microalgal culture facilities with sugar mills in an interesting design of microalgal biorefinery. The cane molasses can be utilized for the heterotrophic growth of microalgae, or the bagasse can be incinerated to release energy and CO_2, which can be used for the growth of microalgae and support the energy intensive harvesting and drying of microalgal biomass. The benefits of integrating a 10,000 ton/d cane sugar mill with an algal production facility includes the sustenance of a 530 ha algal farm, reduction in the GHG emissions of the mill by 15%, reduction in the use of fossil fuels by the mill, and if the microalgal farm cultivated oil rich microalga, a biodiesel production capacity of 5.8 million L of biodiesel/year can be obtained with a net energy ratio of 1.5 [150].

Another important problem with heterotrophic cultivation of microalgae is the overgrowth of contaminating heterotrophic bacteria which could grow easier compared to the target strain, leading to crash of the system. In photobioreactors which are similar closed systems like fermenters, the microalgae have a photosynthetic advantage in the absence of organic carbon and hence prevents the outgrowth of heterotrophic bacteria. Antibiotics have been used for the maintenance of axenic microalgal cultures [213] and there are several reports that indicate that periodic cleansing of the microalgal culture to maintain their axenic status is of importance when coming to ascertain the purity of the product in concern [214–216]. The antibiotic used for a particular microalgal strain should be optimized prior to the antibiotic cleansing, as certain antibiotics can be toxic to microalgae at higher concentrations. The choice of the antibiotic to be used depends on the microalgal strain and their physiological and biochemical characteristics. The disc diffusion test most commonly used to determine the antibiotic susceptibility of bacteria can be used for microalgae as well. A particular microalgal strain can be made axenic by treating with antibiotic before being attempted to be cultured in heterotrophic conditions. A *Tetraselmis suecica* strain has been purified by several steps: partial removal of all adherent bacteria cells by extensive centrifugation and washing, mild sonication, and treatment with a combination of antibiotics 5 mg/mL vancomycine and 10 mg/mL neomycine as in this case yielded a pure culture of the strain suitable for heterotrophic cultivation [217].

Microalgal biotechnology is on the rise over the past decade and is looking for solutions in the field of renewable energy. The genomes of many model microalgae has been sequenced, much advanced molecular tools are being available for the manipulation of the microalgal genome and genetic engineering of microalgae can be used to obtain the microalgal strain with desired properties. As discussed previously, the capacity of a microalga for dark growth is associated with the presence

of sugar transporters that help in the transport of sugars into the microalgal cell, aiding metabolism and growth. An obligate photoautotrophic diatom *Phaeodactylum tricornutum* has been engineered to be a heterotroph by the expression of a glucose transporter gene, GluT1 from human erythrocytes [13]. With the innate ability to metabolize organic carbon, this photoautotroph turned heterotroph used glucose as a carbon source for growth and metabolism. Similarly, when the glucose transporter of *Chlorella kessleri hup1* was expressed in *Chlamydomonas reinhardtii*, the mutant could grow in the dark utilizing glucose and showed enhanced photo biological hydrogen production (150%) [218]. Hence, trophic conversion of algae can increase the heterotrophic counterpart of commercial algae and high cell density cultures can be obtained in fermenters.

7 Conclusions

This chapter discusses the heterotrophic potential of microalgae to be successfully grown as the feedstock for biofuel production or valuable fine chemicals. At this point, it is imperative to reassess the photoautotrophic cultivation of microalgae in terms of biomass obtained and production costs. The economic methods like open pond systems suffer from low biomass productivity, which leads to energy intensive harvesting increasing the cost associated. Culturing in specially designed photo-bioreactors can only be justified for the production of low-volume, high value products like nutraceuticals and pharmaceuticals. Heterotrophic cultivation can be easily adapted for commercial scale production making use of the existing facilities for bacterial or yeast fermentation with a little remodeling to suit the cultivation of microalgae. Solazyme, now renamed Terravia, together with the Department of Energy, has successfully set up a pilot scale integrated biorefinery for the production of algae based oils from lignocellulosic feedstock. The carbon capture and photosynthesis are separated from the microalgal cultivation and hence it is economically viable. Heterotrophic microalgae are cultivated in the dark in commercial scale, with up to 75% lipid accumulation (https://www.osti.gov/scitech/servlets/purl/1166003). The commercial scale biofuels available from the facility include the biodiesel Soladiesel$_{BD}$® an ASTM D6751 biodiesel; Soladiesel$_{RD}$®, an ASTM D975 renewable diesel; Solajet™, an ASTM 7566 Aviation Turbine Fuel; and renewable diesel and renewable jet fuel that meet the Navy's HRD76 and HRJ5 specifications. Algal cooking oils rich in unsaturated fatty acids are in the market and are serving health conscious consumers. Commercial success has been achieved for the production of *Chlorella* based single cell proteins and nutritional supplements, the cultivation of *Crypthecodinium cohinii* and *Schizochytrium* for the production of DHA and EPA respectively. Heterotrophic *Chlorella* are versatile in their product profile: *C. zofingensis* for astaxanthin, *C. sorokiniana* and *C. minutissima* for lutein, and *C. protothecoides* is the most widely used microalga for the production of lipids and lutein. In the near future, potential and robust heterotrophic algae should be screened for and isolated, a culture collection for

heterotrophic algae needs to be established. Normalization methods needs to be agreed upon to assess successful heterotrophic cultivation products from all over the world. Microalgae can effortlessly replace the other biofuel feedstock if their untapped heterotrophic potential could be unleashed.

References

1. Ravindran B, Gupta KS, Cho WM, Kim KJ, Lee RS, Jeong KH, Lee JD, Choi HC (2016) Microalgae potential and multiple roles—current progress and future prospects—an overview. Sustainability 8(12):1215
2. Höök M, Tang X (2013) Depletion of fossil fuels and anthropogenic climate change—a review. Energy Policy 52:797–809
3. Han SF, Jin WB, Tu RJ, Wu WM (2015) Biofuel production from microalgae as feedstock: current status and potential. Crit Rev Biotechnol 35(2):255–268
4. Hu Q, Sommerfeld M, Jarvis E, Ghirardi M, Posewitz M, Seibert M, Darzins A (2008) Microalgal triacylglycerols as feedstocks for biofuel production: perspectives and advances. Plant J 54(4):621–639
5. Chen CY, Zhao XQ, Yen HW, Ho SH, Cheng CL, Lee DJ, Bai FW, Chang JS (2013) Microalgae-based carbohydrates for biofuel production. Biochem Eng J 78:1–10
6. Borowitzka MA, Moheimani NR (2013) Open pond culture systems. In: Borowitzka MA, Moheimani NR (eds) Algae for Biofuels and Energy. Springer Netherlands, Dordrecht
7. Kunjapur AM, Eldridge RB (2010) Photobioreactor design for commercial biofuel production from microalgae. Ind Eng Chem Res 49(8):3516–3526
8. Lee YK (2001) Microalgal mass culture systems and methods: their limitation and potential. J Appl Phycol 13(4):307–315
9. Perez-Garcia O, Escalante FME, de-Bashan LE, Bashan Y (2011) Heterotrophic cultures of microalgae: metabolism and potential products. Water Res 45(1):11–36
10. Chen GQ, Chen F (2006) Growing phototrophic cells without light. Biotechnol Lett 28 (9):607–616
11. Masojídek J, Torzillo G, Koblížek M (2013) Photosynthesis in microalgae. In: Handbook of microalgal culture. Wiley
12. Pereró J (2014) Calvin-Benson Cycle. In: Amils R, Gargaud M, Cernicharo Quintanilla J et al (eds) Encyclopedia of astrobiology. Springer, Berlin, Heidelberg
13. Zaslavskaia LA, Lippmeier JC, Shih C, Ehrhardt D, Grossman AR, Apt KE (2001) Trophic conversion of an obligate photoautotrophic organism through metabolic engineering. Science 292(5524):2073–2075
14. Tanner W (2000) The *Chlorella* hexose/H$^+$-symporters. Int Rev Cytol 200:101–141
15. Haass D, Tanner W (1974) Regulation of hexose transport in *Chlorella vulgaris*: characteristics of induction and turnover. Plant Physiol 53(1):14–20
16. Komor E, Tanner W (1974) The hexose-proton symport system of *Chlorella vulgaris*. Specificity, stoichiometry and energetics of sugar-induced proton uptake. Eur J Biochem 44 (1):219–223
17. Komor E, Schobert C, Cho BH (1985) Sugar specificity and sugar-proton interaction for the hexose-proton-symport system of *Chlorella*. Eur J Biochem 146(3):649–656
18. Cho BH, Sauer N, Komor E, Tanner W (1981) Glucose induces two amino acid transport systems in *Chlorella*. Proc Natl Acad Sci USA 78(6):3591–3594
19. Bennett ME, Hobbie JE (1972) The uptake of glucose by *Chlamydomonas* sp.12. J Phycol 8 (4):392–398
20. Morales SD, Tinoco VR, Kyndt J, Martinez A (2013) Heterotrophic growth of *Neochloris oleoabundans* using glucose as a carbon source. Biotechnol Biofuels 6(1):100

21. Zheng Y, Yu X, Li T, Xiong X, Chen S (2014) Induction of D-xylose uptake and expression of NAD(P)H-linked xylose reductase and NADP$^+$-linked xylitol dehydrogenase in the oleaginous microalga Chlorella sorokiniana. Biotechnol Biofuels 7:125

22. Gao C, Wang Y, Shen Y, Yan D, He X, Dai J, Wu Q (2014) Oil accumulation mechanisms of the oleaginous microalga *Chlorella protothecoides* revealed through its genome, transcriptomes, and proteomes. BMC Genomics 15:582

23. Neilson AH, Lewin RA (1974) The uptake and utilization of organic carbon by algae: an essay in comparative biochemistry. Phycologia 13(3):227–264

24. Wood AP, Aurikko JP, Kelly DP (2004) A challenge for 21st century molecular biology and biochemistry: what are the causes of obligate autotrophy and methanotrophy? FEMS Microbiol Rev 28(3):335–352

25. Mishra G (2015) Polyunsaturated fatty acids from algae. In: Sahoo D, Seckbach J (eds) The algae world. Springer Netherlands, Dordrecht

26. Hahn HB, Wahlbom CF, Gardonyi M, van Zyl WH, Cordero Otero RR, Jonsson LJ (2001) Metabolic engineering of Saccharomyces cerevisiae for xylose utilization. Adv Biochem Eng/Biotechnol 73:53–84

27. Smith AJ, London J, Stanier RY (1967) Biochemical basis of obligate autotrophy in blue-green algae and thiobacilli. J Bacteriol 94(4):972–983

28. Johnson X, Alric J (2013) Central carbon metabolism and electron transport in *Chlamydomonas reinhardtii*: metabolic constraints for carbon partitioning between oil and starch. Eukaryot Cell 12(6):776–793

29. Boyle NR, Morgan JA (2009) Flux balance analysis of primary metabolism in *Chlamydomonas reinhardtii*. BMC Syst Biol 3:4

30. Chen X, Schreiber K, Appel J, Makowka A, Fahnrich B, Roettger M, Hajirezaei MR, Sonnichsen FD, Schonheit P, Martin WF, Gutekunst K (2016) The Entner-Doudoroff pathway is an overlooked glycolytic route in cyanobacteria and plants. Proc Natl Acad Sci USA 113(19):5441–5446

31. Fabris M, Matthijs M, Rombauts S, Vyverman W, Goossens A, Baart GJ (2012) The metabolic blueprint of Phaeodactylum tricornutum reveals a eukaryotic Entner-Doudoroff glycolytic pathway. Plant J 70(6):1004–1014

32. Klein U (1986) Compartmentation of glycolysis and of the oxidative pentose-phosphate pathway in *Chlamydomonas reinhardii*. Planta 167(1):81–86

33. Hildebrand M, Abbriano RM, Polle JEW, Traller JC, Trentacoste EM, Smith SR, Davis AK (2013) Metabolic and cellular organization in evolutionarily diverse microalgae as related to biofuels production. Curr Opin Chem Biol 17(3):506–514

34. Yang C, Hua Q, Shimizu K (2000) Energetics and carbon metabolism during growth of microalgal cells under photoautotrophic, mixotrophic and cyclic light-autotrophic/dark-heterotrophic conditions. Biochem Eng J 6(2):87–102

35. Fischer K (2011) The import and export business in plastids: transport processes across the inner envelope membrane. Plant Physiol 155(4):1511

36. Melis A (2007) Photosynthetic H_2 metabolism in *Chlamydomonas reinhardtii* (unicellular green algae). Planta 226(5):1075–1086

37. Raven JA (1976) The quantitative role of 'Dark' respiratory processes in heterotrophic and photolithotrophic plant growth. Ann Bot 40(3):587–602

38. Geider RJ, Osborne BA (1989) Respiration and microalgal growth: a review of the quantitative relationship between dark respiration and growth. New Phytol 112(3):327–341

39. Johnson X, Alric J (2012) Interaction between starch breakdown, acetate assimilation, and photosynthetic cyclic electron flow in *Chlamydomonas reinhardtii*. J Biol Chem 287 (31):26445–26452

40. Zhang S, Bryant DA (2015) Biochemical validation of the glyoxylate cycle in the *Cyanobacterium Chlorogloeopsis fritschii* strain PCC 9212. J Biol Chem 290(22):14019–14030

41. Knoop H, Grundel M, Zilliges Y, Lehmann R, Hoffmann S, Lockau W, Steuer R (2013) Flux balance analysis of cyanobacterial metabolism: the metabolic network of *Synechocystis* sp. PCC 6803. PLoS Comput Biol 9(6):e1003081

42. Plancke C, Vigeolas H, Hohner R, Roberty S, Emonds AB, Larosa V, Willamme R, Duby F, Onga Dhali D, Thonart P, Hiligsmann S, Franck F, Eppe G, Cardol P, Hippler M, Remacle C (2014) Lack of isocitrate lyase in *Chlamydomonas* leads to changes in carbon metabolism and in the response to oxidative stress under mixotrophic growth. Plant J 77(3):404–417

43. Grobbelaar JU (2007) Algal nutrition—mineral nutrition. In: Handbook of microalgal culture. Blackwell Publishing Ltd

44. Markou G, Vandamme D, Muylaert K (2014) Microalgal and cyanobacterial cultivation: the supply of nutrients. Water Res 65:186–202

45. Liu J, Huang J, Fan KW, Jiang Y, Zhong Y, Sun Z, Chen F (2010) Production potential of *Chlorella zofingienesis* as a feedstock for biodiesel. Bioresour Technol 101(22):8658–8663

46. Ren HY, Liu BF, Ma C, Zhao L, Ren NQ (2013) A new lipid-rich microalga *Scenedesmus* sp. strain R-16 isolated using Nile red staining: effects of carbon and nitrogen sources and initial pH on the biomass and lipid production. Biotechnol Biofuels 6(1):143

47. Yan D, Lu Y, Chen YF, Wu Q (2011) Waste molasses alone displaces glucose-based medium for microalgal fermentation towards cost-saving biodiesel production. Bioresour Technol 102(11):6487–6493

48. Schmidt RA, Wiebe MG, Eriksen NT (2005) Heterotrophic high cell-density fed-batch cultures of the phycocyanin-producing red alga *Galdieria sulphuraria*. Biotechnol Bioeng 90(1):77–84

49. Yokochi T, Honda D, Higashihara T, Nakahara T (1998) Optimization of docosahexaenoic acid production by *Schizochytrium limacinum* SR21. Appl Microbiol Biotechnol 49(1):72–76

50. Tanoi T, Kawachi M, Watanabe MM (2011) Effects of carbon source on growth and morphology of *Botryococcus braunii*. J Appl Phycol 23(1):25–33

51. Kobayashi M, Kurimura Y, Tsuji Y (1997) Light-independent, astaxanthin production by the green microalga *Haematococcus pluvialis* under salt stress. Biotechnol Lett 19(6):507–509

52. de Swaaf ME, Pronk JT, Sijtsma L (2003) Fed-batch cultivation of the docosahexaenoic-acid-producing marine alga *Crypthecodinium cohnii* on ethanol. Appl Microbiol Biotechnol 61(1):40–43

53. Liu J, Huang J, Jiang Y, Chen F (2012) Molasses-based growth and production of oil and astaxanthin by *Chlorella zofingiensis*. Bioresour Technol 107:393–398

54. Li Y, Huang J, Sandmann G, Chen F (2008) Glucose sensing and the mitochondrial alternative pathway are involved in the regulation of astaxanthin biosynthesis in the dark-grown *Chlorella zofingiensis* (*Chlorophyceae*). Planta 228(5):735–743

55. Li T, Liu YH, Lu FP, Jiang Y (2014) Effects of glucose assimilation on lutein and chlorophyll biosyntheses in the green alga *Chlorella pyrenoidosa*. In: Zhang T-C, Ouyang P, Kaplan S, Skarnes B (eds) Proceedings of the 2012 international conference on applied biotechnology (ICAB 2012), vol 2. Springer, Berlin, Heidelberg

56. Canakci M, Sanli H (2008) Biodiesel production from various feedstocks and their effects on the fuel properties. J Ind Microbiol Biotechnol 35(5):431–441

57. Morales SD, Tinoco VR, Caro BMA, Martinez A (2014) Culturing *Neochloris oleoabundans* microalga in a nitrogen-limited, heterotrophic fed-batch system to enhance lipid and carbohydrate accumulation. Algal Res 5:61–69

58. Cerón GMC, Macías SMD, Sánchez MA, García CF, Molina GE (2013) A process for biodiesel production involving the heterotrophic fermentation of *Chlorella protothecoides* with glycerol as the carbon source. Appl Energy 103:341–349

59. Espinosa GI, Parashar A, Bressler DC (2014) Heterotrophic growth and lipid accumulation of *Chlorella protothecoides* in whey permeate, a dairy by-product stream, for biofuel production. Bioresour Technol 155:170–176

60. Cheng Y, Lu Y, Gao C, Wu Q (2009) Alga-based biodiesel production and optimization using sugar cane as the feedstock. Energy Fuels 23(8):4166–4173

61. Gao C, Zhai Y, Ding Y, Wu Q (2010) Application of sweet sorghum for biodiesel production by heterotrophic microalga *Chlorella protothecoides*. Appl Energy 87(3): 756–761

62. Lu Y, Ding Y, Wu Q (2011) Simultaneous saccharification of cassava starch and fermentation of algae for biodiesel production. J Appl Phycol 23(1):115–121

63. Isleten Hosoglu M, Gultepe I, Elibol M (2012) Optimization of carbon and nitrogen sources for biomass and lipid production by *Chlorella saccharophila* under heterotrophic conditions and development of Nile red fluorescence based method for quantification of its neutral lipid content. Biochem Eng J 61:11–19

64. Chen YH, Walker TH (2011) Biomass and lipid production of heterotrophic microalgae *Chlorella protothecoides* by using biodiesel-derived crude glycerol. Biotechnol Lett 33(10):1973–1983

65. Cheng Y, Zhou W, Gao C, Lan K, Gao Y, Wu Q (2009) Biodiesel production from Jerusalem artichoke (Helianthus Tuberosus L.) tuber by heterotrophic microalgae *Chlorella protothecoides*. J Chem Technol Biotechnol 84(5):777–781

66. Xiong W, Li X, Xiang J, Wu Q (2008) High-density fermentation of microalga *Chlorella protothecoides* in bioreactor for microbio-diesel production. Appl Microbiol Biotechnol 78(1):29–36

67. Xu H, Miao X, Wu Q (2006) High quality biodiesel production from a microalga *Chlorella protothecoides* by heterotrophic growth in fermenters. J Biotechnol 126(4):499–507

68. Shen XF, Chu FF, Lam PK, Zeng RJ (2015) Biosynthesis of high yield fatty acids from *Chlorella vulgaris* NIES-227 under nitrogen starvation stress during heterotrophic cultivation. Water Res 81:294–300

69. Zheng H, Gao Z, Yin F, Ji X, Huang H (2012) Lipid production of *Chlorella vulgaris* from lipid-extracted microalgal biomass residues through two-step enzymatic hydrolysis. Bioresour Technol 117:1–6

70. Zheng H, Ma X, Gao Z, Wan Y, Min M, Zhou W, Li Y, Liu Y, Huang H, Chen P, Ruan R (2015) Lipid production of heterotrophic *Chlorella* sp. from hydrolysate mixtures of lipid-extracted microalgal biomass residues and molasses. Appl Biochem Biotechnol 177(3):662–674

71. Mu J, Li S, Chen D, Xu H, Han F, Feng B, Li Y (2015) Enhanced biomass and oil production from sugarcane bagasse hydrolysate (SBH) by heterotrophic oleaginous microalga *Chlorella protothecoides*. Bioresour Technol 185:99–105

72. Shen XF, Liu JJ, Chu FF, Lam PKS, Zeng RJ (2015) Enhancement of FAME productivity of *Scenedesmus obliquus* by combining nitrogen deficiency with sufficient phosphorus supply in heterotrophic cultivation. Appl Energy 158:348–354

73. Shen XF, Liu JJ, Chauhan AS, Hu H, Ma LL, Lam PKS, Zeng RJ (2016) Combining nitrogen starvation with sufficient phosphorus supply for enhanced biodiesel productivity of *Chlorella vulgaris* fed on acetate. Algal Res 17:261–267

74. Liang Y, Sarkany N, Cui Y (2009) Biomass and lipid productivities of *Chlorella vulgaris* under autotrophic, heterotrophic and mixotrophic growth conditions. Biotechnol Lett 31(7):1043–1049

75. Wang Y, Chen T, Qin S (2012) Heterotrophic cultivation of *Chlorella kessleri* for fatty acids production by carbon and nitrogen supplements. Biomass Bioenergy 47:402–409

76. Zhao Y, Li D, Ding K, Che R, Xu JW, Zhao P, Li T, Ma H, Yu X (2016) Production of biomass and lipids by the oleaginous microalgae *Monoraphidium* sp. QLY-1 through heterotrophic cultivation and photo-chemical modulator induction. Bioresour Technol 211:669–676

77. Fan KW, Chen F, Jones EB, Vrijmoed LL (2001) Eicosapentaenoic and docosahexaenoic acids production by and okara-utilizing potential of thraustochytrids. J Ind Microbiol Biotechnol 27(4):199–202

78. Vazhappilly R, Chen F (1998) Eicosapentaenoic acid and docosahexaenoic acid production potential of microalgae and their heterotrophic growth. J Am Oil Chem Soc 75(3):393–397

79. Fang X, Wei C, Zhao LC, Fan O (2004) Effects of organic carbon sources on cell growth and eicosapentaenoic acid content of *Nannochloropsis* sp. J Appl Phycol 16(6):499–503
80. Marudhupandi T, Sathishkumar R, Kumar TTA (2016) Heterotrophic cultivation of *Nannochloropsis salina* for enhancing biomass and lipid production. Biotechnol Rep 10:8–16
81. Tan CK, Johns MR (1996) Screening of diatoms for heterotrophic eicosapentaenoic acid production. J Appl Phycol 8(1):59–64
82. Wen ZY, Chen F (2002) Perfusion culture of the diatom *Nitzschia laevis* for ultra-high yield of eicosapentaenoic acid. Process Biochem 38(4):523–529
83. Gong Y, Liu J, Jiang M, Liang Z, Jin H, Hu X, Wan X, Hu C (2015) Improvement of omega-3 docosahexaenoic acid production by marine dinoflagellate crypthecodinium cohnii using rapeseed meal hydrolysate and waste molasses as feedstock. PLoS One 10(5): e0125368
84. De Swaaf ME, Sijtsma L, Pronk JT (2003) High-cell-density fed-batch cultivation of the docosahexaenoic acid producing marine alga *Crypthecodinium cohnii*. Biotechnol Bioeng 81(6):666–672
85. Mendes A, Guerra P, Madeira V, Ruano F, Lopes da Silva T, Reis A (2007) Study of docosahexaenoic acid production by the heterotrophic microalga *Crypthecodinium cohnii* CCMP 316 using carob pulp as a promising carbon source. World J Microbiol Biotechnol 23(9):1209–1215
86. Yamasaki T, Aki T, Shinozaki M, Taguchi M, Kawamoto S, Ono K (2006) Utilization of Shochu distillery wastewater for production of polyunsaturated fatty acids and xanthophylls using thraustochytrid. J Biosci Bioeng 102(4):323–327
87. Unagul P, Assantachai C, Phadungruengluij S, Suphantharika M, Tanticharoen M, Verduyn C (2007) Coconut water as a medium additive for the production of docosahexaenoic acid (C22:6 n3) by *Schizochytrium mangrovei* Sk-02. Bioresour Technol 98(2): 281–287
88. Ethier S, Woisard K, Vaughan D, Wen Z (2011) Continuous culture of the microalgae *Schizochytrium limacinum* on biodiesel-derived crude glycerol for producing docosahexaenoic acid. Bioresour Technol 102(1):88–93
89. Lian M, Huang H, Ren L, Ji X, Zhu J, Jin L (2010) Increase of docosahexaenoic acid production by *Schizochytrium* sp. through mutagenesis and enzyme assay. Appl Biochem Biotechnol 162(4):935–941
90. Quilodrán B, Hinzpeter I, Hormazabal E, Quiroz A, Shene C (2010) Docosahexaenoic acid (C22:6n−3, DHA) and astaxanthin production by *Thraustochytriidae* sp. AS4-A1 a native strain with high similitude to *Ulkenia* sp.: evaluation of liquid residues from food industry as nutrient sources. Enzyme Microb Technol 47(1):24–30
91. Hong WK, Rairakhwada D, Seo PS, Park SY, Hur BK, Kim CH, Seo JW (2011) Production of lipids containing high levels of docosahexaenoic acid by a newly isolated microalga, *Aurantiochytrium* sp. KRS101. Appl Biochem Biotechnol 164(8):1468–1480
92. Manikan V, Nazir MYM, Kalil MS, Isa MHM, Kader AJA, Yusoff WMW, Hamid AA (2015) A new strain of docosahexaenoic acid producing microalga from Malaysian coastal waters. Algal Res 9:40–47
93. Manikan V, Kalil MS, Hamid AA (2015) Response surface optimization of culture medium for enhanced docosahexaenoic acid production by a Malaysian thraustochytrid. Sci Rep 5:8611
94. Burja AM, Radianingtyas H, Windust A, Barrow CJ (2006) Isolation and characterization of polyunsaturated fatty acid producing Thraustochytrium species: screening of strains and optimization of omega-3 production. Appl Microbiol Biotechnol 72(6):1161–1169
95. Shi XM, Chen F, Yuan JP, Chen H (1997) Heterotrophic production of lutein by selected *Chlorella* strains. J Appl Phycol 9(5):445–450
96. Shi X, Zhang X, Chen F (2000) Heterotrophic production of biomass and lutein by *Chlorella prototheocoides* on various nitrogen sources. Enzyme Microb Technol 27(3–5):312–318

97. Shi XM, Jiang Y, Chen F (2002) High-yield production of lutein by the green microalga *Chlorella protothecoides* in heterotrophic fed-batch culture. Biotechnol Prog 18(4):723–727

98. Wu Z, Wu S, Shi X (2007) Supercritical fluid extraction and determination of lutein in heterotrophically cultivated *Chlorella pyrenoidosa*. J Food Process Eng 30(2):174–185

99. Wu ZY, Qu CB, Shi XM (2009) Biochemical system analysis of lutein production by heterotrophic *Chlorella pyrenoidosa* in a fermentor. Food Technol Biotechnol 47(4): 450–455

100. Wei D, Chen F, Chen G, Zhang X, Liu L, Zhang H (2008) Enhanced production of lutein in heterotrophic *Chlorella protothecoides* by oxidative stress. Sci China Ser C Life Sci 51 (12):1088–1093

101. Ip PF, Chen F (2005) Production of astaxanthin by the green microalga *Chlorella zofingiensis* in the dark. Process Biochem 40(2):733–738

102. Ip PF, Chen F (2005) Employment of reactive oxygen species to enhance astaxanthin formation in *Chlorella zofingiensis* in heterotrophic culture. Process Biochem 40(11): 3491–3496

103. Ip PF, Chen F (2005) Peroxynitrite and nitryl chloride enhance astaxanthin production by the green microalga *Chlorella zofingiensis* in heterotrophic culture. Process Biochem 40 (11):3595–3599

104. Liu J, Sun Z, Zhong Y, Gerken H, Huang J, Chen F (2013) Utilization of cane molasses towards cost-saving astaxanthin production by a *Chlorella zofingiensis* mutant. J Appl Phycol 25(5):1447–1456

105. Ma RYN, Chen F (2001) Enhanced production of free trans-astaxanthin by oxidative stress in the cultures of the green microalga *Chlorococcum* sp. Process Biochem 36(12): 1175–1179

106. Sloth JK, Wiebe MG, Eriksen NT (2006) Accumulation of phycocyanin in heterotrophic and mixotrophic cultures of the acidophilic red alga *Galdieria sulphuraria*. Enzyme Microb Technol 38(1):168–175

107. Sloth JK, Jensen HC, Pleissner D, Eriksen NT (2017) Growth and phycocyanin synthesis in the heterotrophic microalga *Galdieria sulphuraria* on substrates made of food waste from restaurants and bakeries. Bioresour Technol 238:296–305

108. Sorensen L, Hantke A, Eriksen NT (2013) Purification of the photosynthetic pigment C-phycocyanin from heterotrophic *Galdieria sulphuraria*. J Sci Food Agric 93(12): 2933–2938

109. Fernandez E, Galvan A (2007) Inorganic nitrogen assimilation in *Chlamydomonas*. J Exp Bot 58(9):2279–2287

110. Inokuchi R, Kuma KI, Miyata T, Okada M (2002) Nitrogen-assimilating enzymes in land plants and algae: phylogenic and physiological perspectives. Physiol Plant 116(1):1–11

111. Patil KP, Gogate PR (2015) Improved synthesis of docosahexaenoic acid (DHA) using *Schizochytrium limacinum* SR21 and sustainable media. Chem Eng J 268:187–196

112. Lowrey J, Brooks MS, McGinn PJ (2015) Heterotrophic and mixotrophic cultivation of microalgae for biodiesel production in agricultural wastewaters and associated challenges—a critical review. J Appl Phycol 27(4):1485–1498

113. Wang Y, Guo W, Yen HW, Ho SH, Lo YC, Cheng CL, Ren N, Chang JS (2015) Cultivation of *Chlorella vulgaris* JSC-6 with swine wastewater for simultaneous nutrient/COD removal and carbohydrate production. Bioresour Technol 198:619–625

114. Kim S, Lee Y, Hwang SJ (2013) Removal of nitrogen and phosphorus by *Chlorella sorokiniana* cultured heterotrophically in ammonia and nitrate. Int Biodeterior Biodegrad 85:511–516

115. Perez GO, Bashan Y, Esther Puente M (2011) Organic carbon supplementation of sterilized municipal wastewater is essential for heterotrophic growth and removing ammonium by the microalga *Chlorella vulgaris*. J Phycol 47(1):190–199

116. Garcia OF, Gomez E (2009) Bioreactor scale-up and oxygen transfer rate in microbial processes: an overview. Biotechnol Adv 27(2):153–176

117. Pahl SL, Lewis DM, Chen F, King KD (2010) Growth dynamics and the proximate biochemical composition and fatty acid profile of the heterotrophically grown diatom *Cyclotella cryptica*. J Appl Phycol 22(2):165–171

118. Meireles DSA, Vieira KR, Basso SR, Meireles DSA, Queiroz MI, Queiroz ZL, Jacob LE (2017) Heterotrophic cultivation of *Cyanobacteria*: study of effect of exogenous sources of organic carbon, absolute amount of nutrients, and stirring speed on biomass and lipid productivity. Front Bioeng Biotechnol 5:12

119. Singhasuwan S, Choorit W, Sirisansaneeyakul S, Kokkaew N, Chisti Y (2015) Carbon-to-nitrogen ratio affects the biomass composition and the fatty acid profile of heterotrophically grown *Chlorella* sp. TISTR 8990 for biodiesel production. J Biotechnol 216:169–177

120. Chen F, Johns MR (1991) Effect of C/N ratio and aeration on the fatty acid composition of heterotrophic *Chlorella sorokiniana*. J Appl Phycol 3(3):203–209

121. Chang G, Gao N, Tian G, Wu Q, Chang M, Wang X (2013) Improvement of docosahexaenoic acid production on glycerol by *Schizochytrium* sp. S31 with constantly high oxygen transfer coefficient. Bioresour Technol 142:400–406

122. Qu L, Ren LJ, Huang H (2013) Scale-up of docosahexaenoic acid production in fed-batch fermentation by *Schizochytrium* sp. based on volumetric oxygen-transfer coefficient. Biochem Eng J 77:82–87

123. Jakobsen AN, Aasen IM, Josefsen KD, Strom AR (2008) Accumulation of docosahexaenoic acid-rich lipid in thraustochytrid *Aurantiochytrium* sp. strain T66: effects of N and P starvation and O_2 limitation. Appl Microbiol Biotechnol 80(2):297–306

124. Qu L, Ji XJ, Ren LJ, Nie ZK, Feng Y, Wu WJ, Ouyang PK, Huang H (2011) Enhancement of docosahexaenoic acid production by *Schizochytrium* sp. using a two-stage oxygen supply control strategy based on oxygen transfer coefficient. Lett Appl Microbiol 52(1):22–27

125. Ren LJ, Ji XJ, Huang H, Qu L, Feng Y, Tong QQ, Ouyang PK (2010) Development of a stepwise aeration control strategy for efficient docosahexaenoic acid production by *Schizochytrium* sp. Appl Microbiol Biotechnol 87(5):1649–1656

126. Chi Z, Liu Y, Frear C, Chen S (2009) Study of a two-stage growth of DHA-producing marine algae *Schizochytrium limacinum* SR21 with shifting dissolved oxygen level. Appl Microbiol Biotechnol 81(6):1141–1148

127. Sattur AP, Karanth NG (1989) Production of microbial lipids: II. Influence of C/N ratio—model prediction. Biotechnol Bioeng 34(6):868–871

128. Silaban A, Bai R, Gutierrez WMT, Negulescu II, Rusch KA (2014) Effect of organic carbon, C:N ratio and light on the growth and lipid productivity of microalgae/cyanobacteria coculture. Eng Life Sci 14(1):47–56

129. Shi XM, Liu HJ, Zhang XW, Chen F (1999) Production of biomass and lutein by *Chlorella protothecoides* at various glucose concentrations in heterotrophic cultures. Process Biochem 34(4):341–347

130. Zhu L, Zhang X, Ji L, Song X, Kuang C (2007) Changes of lipid content and fatty acid composition of *Schizochytrium limacinum* in response to different temperatures and salinities. Process Biochem 42(2):210–214

131. Cao J, Yuan H, Li B, Yang J (2014) Significance evaluation of the effects of environmental factors on the lipid accumulation of *Chlorella minutissima* UTEX 2341 under low-nutrition heterotrophic condition. Bioresour Technol 152:177–184

132. Chen GQ, Jiang Y, Chen F (2008) Variation of lipid class composition in *Nitzschia laevis* as a response to growth temperature change. Food Chem 109(1):88–94

133. Shi X, Wu Z, Chen F (2006) Kinetic modeling of lutein production by heterotrophic *Chlorella* at various pH and temperatures. Mol Nutr Food Res 50(8):763–768

134. Chen GQ, Jiang Y, Chen F (2008) Salt-induced alterations in lipid composition of diatom *Nitzschia laevis* (bacillariophyceae) under heterotrophic culture condition. J Phycol 44 (5):1309–1314

135. Wang T, Ge H, Liu T, Tian X, Wang Z, Guo M, Chu J, Zhuang Y (2016) Salt stress induced lipid accumulation in heterotrophic culture cells of *Chlorella protothecoides*: mechanisms

based on the multi-level analysis of oxidative response, key enzyme activity and biochemical alteration. J Biotechnol 228:18–27

136. Heredia AT, Wei W, Hu B (2010) Oil accumulation via heterotrophic/mixotrophic *Chlorella protothecoides*. Appl Biochem Biotechnol 162(7):1978–1995

137. Sarada R, Tripathi U, Ravishankar GA (2002) Influence of stress on astaxanthin production in *Haematococcus pluvialis* grown under different culture conditions. Process Biochem 37(6):623–627

138. Jiang Y, Chen F (2000) Effects of medium glucose concentration and pH on docosahexaenoic acid content of heterotrophic *Crypthecodinium cohnii*. Process Biochem 35 (10):1205–1209

139. Wu ST, Yu ST, Lin LP (2005) Effect of culture conditions on docosahexaenoic acid production by *Schizochytrium* sp. S31. Process Biochem 40(9):3103–3108

140. Kumari P, Kumar M, Reddy CRK, Jha B (2013) Algal lipids, fatty acids and sterols Domínguez, Herminia. In: Functional ingredients from algae for foods and nutraceuticals. Woodhead Publishing

141. Bellou S, Baeshen MN, Elazzazy AM, Aggeli D, Sayegh F, Aggelis G (2014) Microalgal lipids biochemistry and biotechnological perspectives. Biotechnol Adv 32(8):1476–1493

142. Chen CY, Yeh KL, Aisyah R, Lee DJ, Chang JS (2011) Cultivation, photobioreactor design and harvesting of microalgae for biodiesel production: a critical review. Bioresour Technol 102(1):71–81

143. Vitova M, Bisova K, Kawano S, Zachleder V (2015) Accumulation of energy reserves in algae: from cell cycles to biotechnological applications. Biotechnol Adv 33:1204–1218

144. Slocombe S, Zhang Q, Ross M, Anderson A, Thomas NJ, Lapresa Á, Rad MC, Campbell C, Black K, Stanley M, Day J (2015) Unlocking nature's treasure-chest: screening for oleaginous algae. Sci Rep 9:9844

145. Meng X, Yang J, Xu X, Zhang L, Nie Q, Xian M (2009) Biodiesel production from oleaginous microorganisms. Renew Energy 34(1):1–5

146. García López, de Lomana A, Schäuble S, Valenzuela J, Imam S, Carter W, Bilgin DD, Yohn CB, Turkarslan S, Reiss DJ, Orellana MV, Price ND, Baliga NS (2015) Transcriptional program for nitrogen starvation-induced lipid accumulation in *Chlamydomonas reinhardtii*. Biotechnol Biofuels 8(1):207

147. Subramanian S, Barry AN, Pieris S, Sayre RT (2013) Comparative energetics and kinetics of autotrophic lipid and starch metabolism in chlorophytic microalgae: implications for biomass and biofuel production. Biotechnol Biofuels 6(1):150

148. Li X, Xu H, Wu Q (2007) Large-scale biodiesel production from microalga *Chlorella protothecoides* through heterotrophic cultivation in bioreactors. Biotechnol Bioeng 98 (4):764–771

149. Tabernero A, Martín del Valle EM, Galán MA (2012) Evaluating the industrial potential of biodiesel from a microalgae heterotrophic culture: scale-up and economics. Biochem Eng J 63:104–115

150. Lohrey C, Kochergin V (2012) Biodiesel production from microalgae: co-location with sugar mills. Bioresour Technol 108:76–82

151. Johnson MB, Wen Z (2009) Production of biodiesel fuel from the microalga *Schizochytrium limacinum* by direct transesterification of algal biomass. Energy Fuels 23(10):5179–5183

152. Jia Z, Liu Y, Daroch M, Geng S, Cheng JJ (2014) Screening, growth medium optimisation and heterotrophic cultivation of microalgae for biodiesel production. Appl Biochem Biotechnol 173(7):1667–1679

153. John RP, Anisha GS, Nampoothiri KM, Pandey A (2011) Micro and macroalgal biomass: a renewable source for bioethanol. Bioresour Technol 102(1):186–193

154. Özçimen D, İnan B (2015) An overview of bioethanol production from algae. In: Biernat K (ed) Biofuels-status and perspective. InTech, Rijeka

155. Martone PT, Estevez JM, Lu F, Ruel K, Denny MW, Somerville C, Ralph J (2009) Discovery of lignin in seaweed reveals convergent evolution of cell-wall architecture. Curr Biol: CB 19(2):169–175

156. Jung KA, Lim SR, Kim Y, Park JM (2013) Potentials of macroalgae as feedstocks for biorefinery. Bioresour Technol 135:182–190
157. Wei N, Quarterman J, Jin YS (2013) Marine macroalgae: an untapped resource for producing fuels and chemicals. Trends Biotechnol 31(2):70–77
158. Nguyen CM, Kim JS, Hwang HJ, Park MS, Choi GJ, Choi YH, Jang KS, Kim JC (2012) Production of l-lactic acid from a green microalga, *Hydrodictyon reticulum*, by *Lactobacillus paracasei* LA104 isolated from the traditional Korean food, makgeolli. Bioresour Technol 110:552–559
159. Cheng D, Li D, Yuan Y, Zhou L, Li X, Wu T, Wang L, Zhao Q, Wei W, Sun Y (2017) Improving carbohydrate and starch accumulation in *Chlorella* sp. AE10 by a novel two-stage process with cell dilution. Biotechnol Biofuels 10(1):75
160. Tan KW, Lin H, Shen H, Lee YK (2016) Nitrogen-induced metabolic changes and molecular determinants of carbon allocation in *Dunaliella tertiolecta*. Sci Rep 6:37235
161. Griffiths DJ (1965) The accumulation of carbohydrate in *Chlorella vulgaris* under heterotrophic conditions. Ann Bot 29(3):347–357
162. Di Caprio F, Visca A, Altimari P, Toro L, Masciocchi B, Iaquaniello G, Pagnanelli F (2016) Two stage process of microalgae cultivation for starch and carotenoid production. In: Chemical engineering transactions. Italian Association of Chemical Engineering-AIDIC
163. Choix FJ, de Bashan LE, Bashan Y (2012) Enhanced accumulation of starch and total carbohydrates in alginate-immobilized *Chlorella* sp. induced by *Azospirillum brasilense*: II. Heterotrophic conditions. Enzyme Microb Technol 51(5):300–309
164. Swaaf M, Grobben G, Eggink G, Rijk T, Meer P, Sijtsma L (2001) Characterisation of extracellular polysaccharides produced by *Crypthecodinium cohnii*. Appl Microbiol Biotechnol 57(3):395–400
165. Wu N, Li Y, Lan CQ (2011) Production and rheological studies of microalgal extracellular biopolymer from lactose using the green alga *Neochloris oleoabundans*. J Polym Environ 19(4):935–942
166. Liu L, Pohnert G, Wei D (2016) Extracellular metabolites from industrial microalgae and their biotechnological potential. Mar Drugs 14(10):191
167. Trabelsi L, Ben Ouada H, Zili F, Mazhoud N, Ammar J (2013) Evaluation of *Arthrospira platensis* extracellular polymeric substances production in photoautotrophic, heterotrophic and mixotrophic conditions. Folia Microbiol 58(1):39–45
168. Minhas AK, Hodgson P, Barrow CJ, Adholeya A (2016) A review on the assessment of stress conditions for simultaneous production of microalgal lipids and carotenoids. Front Microbiol 7:546
169. Das UN (2006) Essential fatty acids: biochemistry, physiology and pathology. Biotechnol J 1(4):420–439
170. Ryckebosch E, Bruneel C, Muylaert K, Foubert I (2012) Microalgae as an alternative source of omega-3 long chain polyunsaturated fatty acids. Lipid Technol 24(6):128–130
171. Funk CD (2001) Prostaglandins and leukotrienes: advances in eicosanoid biology. Science 294(5548):1871–1875
172. Das UN (2008) Can essential fatty acids reduce the burden of diseases? Lipids Health Dis 7:9
173. Kaur N, Chugh V, Gupta AK (2014) Essential fatty acids as functional components of foods- a review. J Food Sci Technol 51(10):2289–2303
174. Bigogno C, Khozin GI, Cohen Z (2002) Accumulation of arachidonic acid-rich triacylglycerols in the microalga *Parietochloris incisa* (Trebuxiophyceae, Chlorophyta). Phytochemistry 60(2):135–143
175. Raghukumar S (2008) Thraustochytrid marine protists: production of PUFAs and other emerging technologies. Mar Biotechnol 10(6):631–640
176. Ward OP, Singh A (2005) Omega-3/6 fatty acids: alternative sources of production. Process Biochem 40(12):3627–3652

177. Martins DA, Custódio L, Barreira L, Pereira H, Ben HR, Varela J, Abu SKM (2013) Alternative sources of n-3 long-chain polyunsaturated fatty acids in marine microalgae. Mar Drugs 11(7):2259–2281
178. Varela JC, Pereira H, Vila M, Leon R (2015) Production of carotenoids by microalgae: achievements and challenges. Photosynth Res 125(3):423–436
179. Britton G (1995) Structure and properties of carotenoids in relation to function. FASEB J: Off Publ Fed Am Soc Exp Biol 9(15):1551–1558
180. Gong M, Bassi A (2016) Carotenoids from microalgae: a review of recent developments. Biotechnol Adv 34(8):1396–1412
181. Spolaore P, Joannis CC, Duran E, Isambert A (2006) Commercial applications of microalgae. J Biosci Bioeng 101(2):87–96
182. Lim KC, Yusoff FM, Shariff M, Kamarudin MS (2017) Astaxanthin as feed supplement in aquatic animals. Rev Aquac 0:1–36
183. Lin JH, Lee DJ, Chang JS (2015) Lutein production from biomass: marigold flowers versus microalgae. Bioresour Technol 184:421–428
184. Kobayashi M, Kakizono T, Nagai S (1991) Astaxanthin production by a green alga, *Haematococcus pluvialis* accompanied with morphological changes in acetate media. J Ferment Bioeng 71(5):335–339
185. Choi YE, Yun YS, Park JM (2002) Evaluation of factors promoting astaxanthin production by a unicellular green alga, *Haematococcus pluvialis*, with fractional factorial design. Biotechnol Prog 18(6):1170–1175
186. Liu J, Sun Z, Gerken H, Liu Z, Jiang Y, Chen F (2014) *Chlorella zofingiensis* as an alternative microalgal producer of astaxanthin: biology and industrial potential. Mar Drugs 12(6):3487–3515
187. Zheng YW, Chun BQ, Xian MS (2009) Biochemical system analysis of lutein production by heterotrophic *Chlorella pyrenoidosa* in a fermentor. Food Technol Biotechnol 47(4):450–455
188. Chen CY, Ho SH, Liu CC, Chang JS (2017) Enhancing lutein production with *Chlorella sorokiniana* Mb-1 by optimizing acetate and nitrate concentrations under mixotrophic growth. J Taiwan Inst Chem Eng 79:88–96
189. Cordero BF, Obraztsova I, Couso I, Leon R, Vargas MA, Rodriguez H (2011) Enhancement of lutein production in *Chlorella sorokiniana* (*Chorophyta*) by improvement of culture conditions and random mutagenesis. Mar Drugs 9(9):1607–1624
190. Yin NMR, Chen F (2001) Induction of astaxanthin formation by reactive oxygen species in mixotrophic culture of *Chlorococcum* sp. Biotechnol Lett 23(7):519–523
191. Eriksen NT (2008) Production of phycocyanin–a pigment with applications in biology, biotechnology, foods and medicine. Appl Microbiol Biotechnol 80(1):1–14
192. Gross W, Schnarrenberger C (1995) Heterotrophic growth of two strains of the acido-thermophilic red alga *Galdieria sulphuraria*. Plant Cell Physiol 36(4):633–638
193. Theriault RJ (1965) Heterotrophic growth and production of xanthophylls by *Chlorella pyrenoidosa*. Appl Microbiol 13:402–416
194. Behrens PW (2005) Photobioreactor and fermentors: the light and the dark sides of the growing algae. In: Algal culturing techniques, pp 189–204
195. Bumbak F, Cook S, Zachleder V, Hauser S, Kovar K (2011) Best practices in heterotrophic high-cell-density microalgal processes: achievements, potential and possible limitations. Appl Microbiol Biotechnol 91(1):31–46
196. Graverholt OS, Eriksen NT (2007) Heterotrophic high-cell-density fed-batch and continuous-flow cultures of *Galdieria sulphuraria* and production of phycocyanin. Appl Microbiol Biotechnol 77(1):69–75
197. Li P, Miao X, Li R, Zhong J (2011) In situ biodiesel production from fast-growing and high oil content *Chlorella pyrenoidosa* in rice straw hydrolysate. J Biomed Biotechnol 2011:8
198. Lee YK (1997) Commercial production of microalgae in the Asia-Pacific rim. J Appl Phycol 9(5):403–411

199. Day JD, Edwards AP, Rodgers GA (1991) Development of an industrial-scale process for the heterotrophic production of a micro-algal mollusc feed. Bioresour Technol 38(2):245–249

200. Barclay W, Weaver C, Metz J, Hansen J (2010) Development of a docosahexaenoic acid production technology using schizochytrium: historical perspective and update. In: Single cell oils, 2nd edn. AOCS Press

201. Christenson L, Sims R (2011) Production and harvesting of microalgae for wastewater treatment, biofuels, and bioproducts. Biotechnol Adv 29(6):686–702

202. Lee YK (2007) Algal nutrition—heterotrophic carbon nutrition. In: Handbook of microalgal culture. Blackwell Publishing Ltd

203. Gladue RM, Maxey JE (1994) Microalgal feeds for aquaculture. J Appl Phycol 6(2):131–141

204. Mühling M, Belay A, Whitton BA (2005) Screening *Arthrospira* (*Spirulina*) strains for heterotrophy. J Appl Phycol 17(2):129–135

205. Tian YZ, Yin HW, Lin LZ, Xiao XW, Hong YH (2014) Screening heterotrophic microalgal strains by using the biolog method for biofuel production from organic wastewater. Algal Res 6:175–179

206. Abeliovich A, Weisman D (1978) Role of heterotrophic nutrition in growth of the alga *Scenedesmus obliquus* in high-rate oxidation ponds. Appl Environ Microbiol 35(1):32–37

207. Schilling S, Oesterhelt C (2007) Structurally reduced monosaccharide transporters in an evolutionarily conserved red alga. Biochem J 406(2):325–331

208. Barbier G, Oesterhelt C, Larson MD, Halgren RG, Wilkerson C, Garavito RM, Benning C, Weber AP (2005) Comparative genomics of two closely related unicellular thermo-acidophilic red algae, *Galdieria sulphuraria* and *Cyanidioschyzon merolae*, reveals the molecular basis of the metabolic flexibility of Galdieria sulphuraria and significant differences in carbohydrate metabolism of both algae. Plant Physiol 137(2):460–474

209. Lung YT, Tan CH, Show PL, Ling TC, Lan JCW, Lam HL, Chang JS (2016) Docosahexaenoic acid production from crude glycerol by *Schizochytrium limacinum* SR21. Clean Technol Environ Policy 18(7):2209–2216

210. Liang Y, Sarkany N, Cui Y, Yesuf J, Trushenski J, Blackburn JW (2010) Use of sweet sorghum juice for lipid production by *Schizochytrium limacinum* SR21. Bioresour Technol 101(10):3623–3627

211. Semple KT (1998) Heterotrophic growth on phenolic mixtures by *Ochromonas danica*. Res Microbiol 149(1):65–72

212. Wang L, Li Y, Chen P, Min M, Chen Y, Zhu J, Ruan RR (2010) Anaerobic digested dairy manure as a nutrient supplement for cultivation of oil-rich green microalgae *Chlorella* sp. Bioresour Technol 101(8):2623–2628

213. Jones A, Rhodes ME, Evans SC (1973) The use of antibiotics to obtain axenic cultures of algae. Br Phycol J 8(2):185–196

214. Han J, Wang S, Zhang L, Yang G, Zhao L, Pan K (2016) A method of batch-purifying microalgae with multiple antibiotics at extremely high concentrations. Chin J Oceanol Limnol 34(1):79–85

215. Choi GG, Bae MS, Ahn CY, Oh HM (2008) Induction of axenic culture of *Arthrospira* (*Spirulina*) platensis based on antibiotic sensitivity of contaminating bacteria. Biotechnol Lett 30(1):87–92

216. Cho JY, Choi JS, Kong IS, Park SI, Kerr RG, Hong YK (2002) A procedure for axenic isolation of the marine microalga *Isochrysis galbana* from heavily contaminated mass cultures. J Appl Phycol 14(5):385–390

217. Azma M, Mohamad R, Abdul Rahim R, Ariff A (2010) Improved protocol for the preparation of tetraselmis suecica axenic culture and adaptation to heterotrophic cultivation. Open Biotechnol J 4:36–46

218. Doebbe A, Rupprecht J, Beckmann J, Mussgnug JH, Hallmann A, Hankamer B, Kruse O (2007) Functional integration of the HUP1 hexose symporter gene into the genome of *C. reinhardtii*: impacts on biological H_2 production. J Biotechnol 131(1):27–33

Part III
Bioreactors for Microbial Biofuels Conversion

Chapter 5
The Relationship Between Bioreactor Design and Feedstock for Optimal Biogas Production

Christiane Herrmann, Patrice Ramm and Jerry D. Murphy

Nomenclature

ABR	Anaerobic baffled reactor
ACR	Anaerobic contact reactor
AD	Anaerobic digestion
AFBR	Anaerobic fluidized bed reactor
AFR	Anaerobic filter reactor
AHR	Anaerobic hybrid reactor
AMBR	Anaerobic membrane bioreactor
APFR	Anaerobic plug-flow reactor
ASBR	Anaerobic sequencing batch reactor
COD	Chemical oxygen demand
CSTR	Continuously stirred tank reactor
EGSB	Expanded granular sludge blanket
FBDR	Fixed bed disc reactor
FBR	Floating bed reactor
HIT	Half-submerged two-phase reactor
HRT	Hydraulic retention time
ICR	Internal circulation reactor
LBR	Leach bed reactor
ME-ADR	Microbial electrolysis anaerobic digestion reactor
OFMSW	Organic fraction of municipal solid waste
OLR	Organic loading rate
Q	Daily added volume of feedstock
SRT	Solid retention time

C. Herrmann (✉) · P. Ramm
Department of Bioengineering, Leibniz Institute for Agricultural Engineering
and Bioeconomy (ATB), Max-Eyth-Allee 100, 14469 Potsdam, Germany
e-mail: cherrmann@atb-potsdam.de

J. D. Murphy
MaREI Centre, Environmental Research Institute, School of Engineering,
University College Cork, Cork, Ireland

SSSAR   Spiral symmetry stream anaerobic reactor
TBR   Trickle-bed reactor
TPAD   Temperature phased anaerobic digestion
TS   Total solids
UASB   Up-flow anaerobic sludge blanket
UASS   Up-flow anaerobic solid state reactor
VFA   Volatile fatty acid
V_R Working volume of the reactor
VS   Volatile solids
VSS   Volatile suspended solids

1 Fundamentals of Biogas Production Through Anaerobic Microbial Communities

Anaerobic digestion is a process in which in the absence of oxygen complex organic substances are degraded and biogas is formed as gaseous product, mainly consisting of methane (50–75%) and carbon dioxide (CO_2) (25–50%). The anaerobic degradation of biopolymers, (i.e. carbohydrates, fats and proteins) involves a consortium of hydrolytic/fermentative, acetogenic and methanogenic microbes (Fig. 1). Their sequential metabolic reactions eventually lead to the conversion of biomass to biogas. In the first step of the conversion chain (hydrolysis), biopolymers (fats, proteins, carbohydrates) are degraded into soluble oligo- and monomers by

Steps	Hydrolysis	Acidogenesis	Acetogenesis	Methanogenesis
Microbes	e.g. Streptococcus, Peptococcus, Micrococcus, Clostridium	e.g. Bacteroides, Clostridium, Butyribacterium, Propionibacterium, Pseudomonas, Ruminococcus	e.g. Syntrophomonas, Syntrophobacter, Acetobacterium, Clostridium	e.g. Methanosaeta, Methanosarcina, Methano-bacterium, Methanospirillum, Methanobrevibactor, Methanothermobacter
Doubling time	0.5 – 1.8 days	0.5 – 1.8 days	2.5 – 10 days	0.5 – 9 days
Main metabolites	Sugar mono- and dimers, peptides, amino acids, glycerin, fatty acids	Acetate, Propionate, Butyrate, Lactate, Ethanol, Formate, H_2, CO_2	Acetate, H_2, CO_2	CH_4, CO_2, H_2O
Optimal conditions	pH 5.2 – 6.3 redox potential +400 – -300 mV C:N ratio 10 – 45 C:N:P:S =500:15:5:3		pH 6.5 – 8 redox potential < -250 mV C:N ratio 20 – 30 C:N:P:S 600:15:5:3	

Fig. 1 Overview of the anaerobic digestion process [1, 3, 4]

exo-enzymes of hydrolytic bacteria. In the second step (acidogenesis) soluble monomers are incorporated by fermentative bacteria and converted into organic acids, alcohols, CO_2 and H_2, depending on the H_2 partial pressure. At low H_2 partial pressure mainly CO_2, H_2 and acetate are produced whereas at high H_2 partial pressure volatile fatty acids (VFA) such as propionic, butyric or valeric acid and alcohols are formed [1]. Degradation of the VFAs and alcohols require the third step (acetogenesis), in which these substrates are further oxidized to acetate, H_2 and CO_2 by acetogenic microorganisms. A precondition for acetogenesis is a very low H_2 partial pressure, which is achieved by conversion of H_2 and CO_2 to methane by H_2-consuming (hydrogenotrophic) methanogens in the last step of the conversion chain (methanogenesis). Thus, acetogens need to live in syntrophy with hydrogenotrophic methanogens, with the interspecies H_2-transfer optimized by close proximity of H_2-producing and H_2-consuming microbes [2]. Methanogenesis is carried out by strict anaerobe methanogenic archaea, which can be categorized according to their metabolized substrates into hydrogenotrophic, methylotrophic and acetoclastic methanogens. Only a few species can utilize acetate or methanol whereas almost all methanogens can metabolize H_2 and CO_2 [1]. As the microbes of the first and second step and also of the third and fourth step are closely linked and have similar optimal living conditions (Fig. 1), separation of the AD process into two stages (hydrolysis/acidogenesis and acetogenesis/methanogenesis) is possible.

For a successful overall AD process, maintenance of the balance between the different groups of microorganisms and their metabolic activity is essential. Any imbalance reduces the process efficiency and may lead to process failure. Over-loading of organic feedstock results in excess VFA formation, which can inhibit methanogenesis. If VFAs are not further degraded they will accumulate within the reactor. VFA concentrations that exceed the buffering capacity of the system can reduce the pH value below the appropriate range and cause acidification [5]. Besides VFAs, ammonia and hydrogen sulphide are other degradation products that can inhibit methane formation. In general, the undissociated form of these substances is more inhibitory than the dissociated form as it can easier diffuse through microbial cell membranes [1].

The nutrient requirements of microbes of the AD process are low, thus, C:N:P:S ratios of 600:15:5:3 are sufficient [3]. C:N ratios below 20 are unfavourable as degradation of such feedstocks can result in excess ammonia formation and process inhibition. In addition, micro-nutrients such as nickel, cobalt, selenium, molybdenum, and tungsten at about 0.05–0.06 mg L^{-1}, and iron at concentrations of 1–10 mg L^{-1} are necessary [5].

The methane production from acetate is usually the rate-limiting step of the AD of soluble substrates due to its low conversion rate, whereas hydrolysis is more time demanding and rate-limiting during AD of solid feedstocks. Hydrolysis of soluble carbohydrates occurs within a few hours whereas hydrolysis of compounds such as cellulose, proteins and lipids requires several days [5]. In order to ensure an efficient AD process, bioreactor design and process operation generally need to be adapted to feedstock characteristics.

Although the microbial groups and metabolic pathways involved in biogas production through anaerobic digestion are basically understood, the predominant part of the highly diverse anaerobic microbiome has not been precisely identified and characterized yet, and detailed functions and the multiple interactions under varying environmental conditions are still largely unknown [6]. Research efforts are currently undertaken to identify key players of anaerobic digestion microbial communities and their functional and ecological role [7]. The establishment of microbial indicators could assist in determination of the process state, indication of process imbalance or deficiencies, and enhanced process control [8]. Expanded knowledge of the anaerobic digestion microbiome could help to provide optimal environmental conditions for improved process performance and to optimally design and manage anaerobic digesters.

2 Main Parameters of Reactor Operation

2.1 Organic Loading Rate

The daily amount of organic biomass that is fed into the biogas plant per unit of working volume of the bioreactor is determined by the organic loading rate (OLR) (Eq. 1):

$$\text{OLR} \ (\text{kg}_{vs} \ \text{m}^{-3} \ \text{d}^{-1} \ \text{or} \ \text{kg}_{COD} \ \text{m}^{-3} \ \text{d}^{-1}) = \frac{Q \times c}{V_R} \tag{1}$$

where Q is the daily added volume of feedstock ($\text{m}^3 \ \text{d}^{-1}$), c is the concentration of volatile solids ($\text{kg}_{VS} \ \text{m}^{-3}$ or $\text{kg}_{COD} \ \text{m}^{-3}$), and V_R is the working volume of the reactor (m^3). The volume of biogas production per unit time increases with increasing OLR, but overloading leads to excessive formation of VFAs, process disturbance and eventually to irreversible process failure. The maximum bearable OLR is a highly relevant parameter that mainly depends on feedstock composition, reactor design and process temperature. It can be regarded as a measure for the conversion capacity of an AD system [2].

2.2 Hydraulic Retention Time

The average time the feedstock remains within the reactor until it is discharged as digestate is defined as the hydraulic retention time (HRT). Simplified, it is calculated according to Eq. (2).

$$\text{HRT (d)} = \frac{V_R}{Q} \qquad (2)$$

where V_R is the working volume of the reactor (m^3), and Q is the daily added volume of feedstock $(m^3\,d^{-1})$. The HRT is an important parameter to decide on the size of the bioreactor. The retention time is related to the growth rate of the microbes and should be long enough to ensure the development of a balanced microbial community that is capable of sufficient feedstock degradation. The necessary HRT depends on the feedstock composition, the process temperature and the OLR. A short HRT can lead to accumulation of organic acids caused by microbial washout if more microbes are removed than can regrow. Therefore, choosing a long HRT and a low OLR provides a safe strategy for high methane yields and process stability [9]. However, this may also result in inadequate reactor utilization. For efficient reactor operation and high methane production rates, short retention times and, at the same time, high methane yields are desired. Some reactor configurations decouple the solid and liquid retention (Sects. 3.1.1.2–3.1.1.4). The solid retention time (SRT) then describes the average time the solid biomass resides within the reactor [9].

2.3   Temperature

The process temperature is one of the basic parameters that influence microbial activity and thus, methane formation during anaerobic digestion. In general, three different temperature ranges are in use for operation of bioreactors for AD: psychrophilic (<10–20 °C), mesophilic (20–45 °C) and thermophilic (55–60 °C).

Temperatures in the mesophilic range are the most commonly applied process temperatures in biogas plants, whereas comparatively few biogas plants are operated under thermophilic temperature conditions [5]. Since reaction and metabolic growth rates increase with higher process temperature, thermophilic AD is usually associated with higher productivity and faster feedstock degradation compared with mesophilic AD [10]. Lignocellulosic feedstocks mainly consist of cellulose, hemicellulose and lignin, which can form a recalcitrant structure resistant to anaerobic degradation. High temperatures particularly promote hydrolysis of lignocellulose by loosening its structure, which results in a better accessibility for microbes, and acceleration of enzymatic reactions [11]. Higher methane yields are often reported under thermophilic conditions. Furthermore, thermophilic temperatures assist in feedstock sanitation and can produce pathogen-free digestate. The major drawback of operation at thermophilic temperatures is their adverse effect on process stability, with methanogens being more sensitive than hydrolytic or acidogenic microbes. This can be attributed to a decreasing diversity and an increasing susceptibility of methanogens to inhibitory metabolites and environmental changes at higher temperatures. Thermophilic processes are very sensitive to sudden

temperature changes while mesophilic microbes tolerate short-term temperature fluctuations of about ± 3 °C [5]. At thermophilic conditions, the solubility of hydrogen (H_2) decreases which makes it less available as substrate to hydrogenotrophic methanogens, and the risk of ammonia inhibition rises due to a shift of the free to ionized ammonia ratio towards the more toxic free ammonia [12]. Thus, reducing the process temperature is one option to overcome ammonia inhibition in AD reactors [12]. The overall effect of thermophilic versus mesophilic process temperature on methane formation depends on the process state, i.e. the pH and presence of inhibitory metabolites. Higher energy input necessary to establish and maintain thermophilic temperature conditions also need to be taken into account.

Psychrophilic AD can be an option especially in regions of cold climates where intensive heating is required for reactor operation at mesophilic temperatures, which leads to a marginal overall energy yield. AD at ambient temperatures does not require extra heat supply but results in low methane yields and unsteady temperature conditions. It was shown that methane in psychrophilic microbial communities is almost exclusively formed from acetate. The use of special psychrophilic microbial consortia adapted to low temperatures can aid in increasing the efficiency of psychrophilic AD [13].

Hyperthermophilic (60–70 °C) AD has also been tested in few studies. It was reported to be beneficial in terms of COD solubilisation when applied to the first stage of a two-stage system [14]. Temperature-phased AD (TPAD) with individual temperatures of different process stages is considered as another possibility to optimize the process performance and feedstock degradation [9] (Sects. 3.1.2 and 3.2.2).

2.4 Digestate Recirculation

The recirculation of digestate is another option to influence the process performance of an AD system. Digestate recirculation can have diverging effects. It can support biomass degradation and biogas formation, and enhance process stability, mainly through dilution effects of toxic or inhibiting substances and increased buffering. This can result in higher possible OLRs as compared to an AD process without digestate recycling [15]. Furthermore, it recycles active biomass, i.e. microorganisms that are actively involved in the digestion process, and enhances the contact between feedstock and microbes. This is especially important in high-solids AD systems where mixing inside the reactors is limited. On the other hand, digestate recirculation increases the amount of hydraulic dead space of the reactor and the loss of solids, and can reduce the HRT and overall reactor efficiency. In staged reactor systems such as the anaerobic baffled reactor (ABR), it can further involve the return to a single-stage system, associated with the loss of advantages of the stage separation [16]. The overall benefit of digestate recirculation depends on the

type of feedstock, on process parameters and the type of reactor system. Positive effects are likely to be achieved at high OLRs and with significant amounts of inhibiting substances in the feedstock.

3   Overview of Bioreactor Concepts

A number of different bioreactor concepts have been developed and are in use for biogas production from anaerobic digestion. The efficient bioreactor aims at high methane production rates and methane yields, at a maximum OLR and minimum HRT, and allows for substantial VS removal at a low parasitic energy demand and low capital and operational costs. The achievement of an optimal reactor performance is, in turn, influenced by several feedstock, operational and process parameters as depicted in Fig. 2.

For selection of an optimal reactor design the consideration of feedstock characteristics is essential. Bioreactors can broadly be divided into reactors for liquid or low solids content and high-solid AD. More recently, biological methanation of gases has been considered [17]. The main challenge of liquid AD is the retention of active biomass within the reactor for prevention of microbial washout. This has been implemented in bioreactor design through different measures of biomass immobilization (Fig. 3). The main challenge of high-solid AD is the handling of
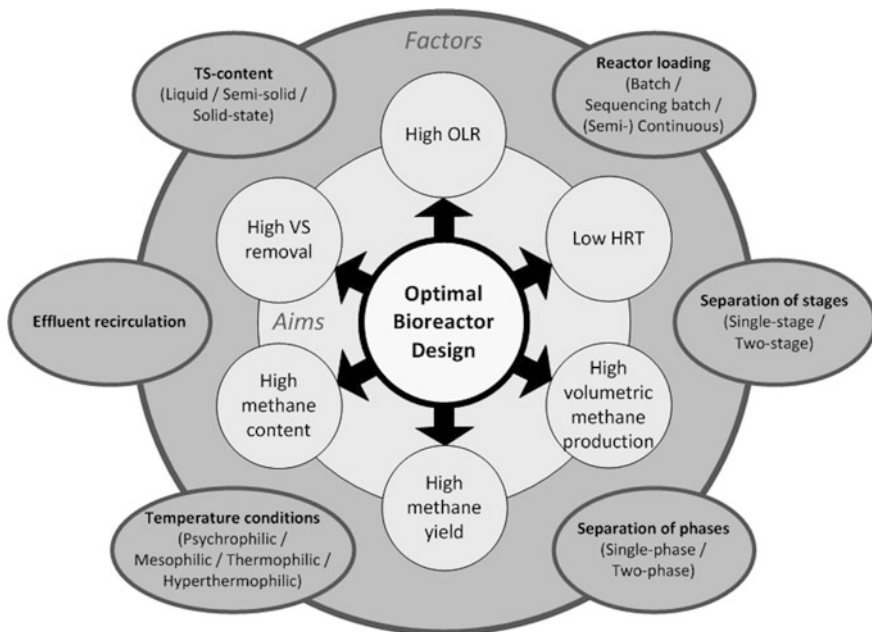
Fig. 2   Aims of optimal bioreactor design and major factors of reactor categorization
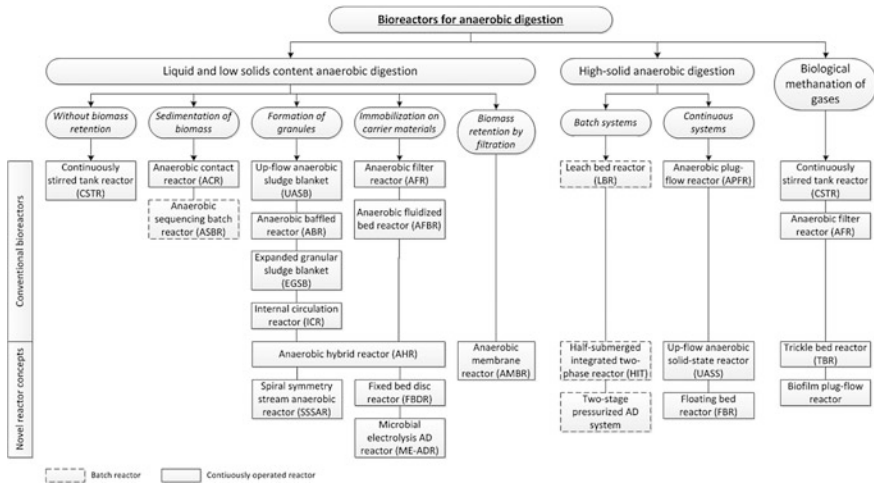
Fig. 3 Categorization of bioreactors for anaerobic digestion

high solids biomass and to overcome mass transfer limitations while the methanation of gases is mainly restricted by gas-liquid mass transfer. Figure 3 gives an overview of bioreactor concepts for conversion of liquid, solid and gaseous feedstocks, which are further described in the following sections.

3.1 Bioreactors for Liquid or Low Solids Content Anaerobic Digestion

Anaerobic digestion processes with total solids (TS) concentrations of up to 10% are regarded as liquid or low solids content AD [5, 18]. However, this criteria is not definite and AD processes with TS concentrations up to 15% are also sometimes defined as liquid or low solids content AD [19]. Feedstocks for liquid AD mainly include different types of industrial and agricultural wastewaters such as from paper and pulp industry, food producing and processing industry or chemical and pharmaceutical industry. Low solids content would include for sewage sludge, liquid animal manure and co-digestion of manure with fractions of energy crops or residues in agricultural biogas plants.

The low solids content in these AD processes allows for easy pumping, homogenization and mixing of the reactor influent and reactor content. This enables good biogas release and intense contact between substrate and microorganisms. However, the low solids content of the reactor influent is also associated with a risk of microbial wash-out attributed to low HRTs at higher organic loading. Thus, the OLR is usually restricted to <7 kg$_{VS}$ m^{-3} d^{-1} [20]. AD is a bioprocess that involves slow-growing microbes such as syntrophic acetogens and acetoclastic methanogens

with doubling times of up to 10 days (Fig. 1). If the retention time is lower than the doubling time of some of the microbes, these microorganisms will eventually be lost. This leads to an imbalance between different groups of microorganisms resulting in process instability, decreasing degradation rates and methane production, or complete process failure. Retaining sufficient active biomass within the reactor is imperative for efficient AD. An effective option to avoid microbial wash-out is the enrichment of biomass within the reactor, independently of the influent flow. Approaches to enrich active biomass include sedimentation within the reactor or outside the reactor with biomass recirculation, the retention of granules that form through self-aggregation, or the immobilization of microbes on the surface of carrier materials [1]. A solids retention time of at least 16 [21] to 20 days [4] is required to prevent microbial wash-out.

Another advantage of the growth of microbes in granules or biofilms besides the retention of active biomass within the reactor is the close physical proximity of H_2 producing acetogens and H_2 utilizing methanogens. This enables an optimal syntrophic performance due to an effective transfer of H_2 over short distances leading to a quick conversion into methane [1].

Numerous different types of bioreactors have been developed for liquid and low solid content AD, mainly for the treatment of wastewaters. The aim of wastewater treatment is usually the avoidance of environmental pollution and production of a good quality effluent with low organic matter rather than the production of biofuels or bioenergy. Some of the more prominent reactor types for liquid or low solids content AD are described in Sect. 3.1.1, while more sophisticated and novel reactor concepts are described in Sects. 3.1.2 and 3.1.3. Examples for the performance of different reactor systems for liquid or low solids content AD are shown in Table 1.

3.1.1 Conventional Bioreactors for Liquid and Low Solids Content Anaerobic Digestion

Reactors Without Biomass Retention

The **Continuously Stirred Tank Reactor (CSTR)** is the most widely applied reactor configuration for liquid or low solids content AD, mainly because of its simplicity and ease of operation, and its ability to treat feedstocks in a wide TS range of about 2–12% [49]. The majority (>90%) of agricultural biogas plants comprise CSTRs [5]. The CSTR is a continuously operated, vertical reactor in which feedstocks enter from the bottom and digestate is withdrawn at the reactor top. A characteristic feature is the complete agitation of the reactor content through mechanical, hydraulic or pneumatic mixing. The most commonly employed mixing systems are mechanical motor propeller stirrers; several stirrers can be installed in one CSTR to prevent stratification, scum layers and deposition of solid biomass [5]. Active stirring provides good contact between substrate and microorganisms and facilitates mass transfer. However, stirring-induced shearing forces can also disturb the symbiotic relation between H_2-producing acetogens and H_2-consuming

Table 1 Examples for the performance of different types of bioreactors for liquid and low solids content anaerobic digestion

Reactor	Feedstock	Feedstock concentration	Reactor size	Temperature °C	OLR kg$_{VS/COD}$ m^{-3} d^{-1}	HRT d	Methane rate m^3 m^{-3} d^{-1}	Methane yield m^3 kg$_{VS/COD}$$^{-1}$	Methane content %	VS/COD removal efficiency %	Source
CSTR	Waste activated sludge, source sorted biowaste	70–80 g$_{TS}$ kg^{-1}	2000 m^3	55	1.28[a]	22	0.42[d]	0.33[a, d]	60	47.2[a]	[22]
CSTR	Cattle manure, maize silage	64 g$_{VS}$ kg^{-1}	3000 m^3	37.8	3.2[a]	60	1.21	0.379[a]	52.8	72[a]	[23]
ACR	Fermented olive mill wastewater	30 g$_{COD}$ L^{-1}	10 L	35	2[b]	15	n.r.	0.15[c]	59–68	43–51[b]	[24]
ACR	Food-processing wastewater	5.25–5.75 g$_{COD}$ L^{-1}	33 L	35	5[b]	1.06	1.09[d]	0.272[b, d]	80	78[b]	[25]
ASBR	Brewery wastewater	22.5–32.5 g$_{COD}$ L^{-1}	45 L	33	5[b]	1	1.62[d]	0.326[b, d]	68	>90[b]	[26]
ASBR	Municipal landfill leachate	14.5 g$_{COD}$ L^{-1}	2 L	35	9.43[b]	1.5	1.85	0.2[b]	63	72[b]	[27]
UASB	Vinasses from hydrous ethanol	121 g$_{COD}$ L^{-1}	3 L	30	17.05[b]	7.5	n.r.	0.263[b]	84	69[b]	[28]
UASB	Microalgae	26 g$_{VS}$ L^{-1}	3.5 L	35	3.57[a]	7.29	0.626	0.17[a]	65.6	n.r.	[29]
EGSB	Leachate from municipal solid waste	65 g$_{COD}$ L^{-1}	6 L	35	22.5[b]	2.83	6.0	0.28[b]	60–80	94–96[b]	[30]
ICR	Molasses wastewater (synthetic)	12.5 g$_{COD}$ L^{-1}	24 L	35	18.94[b]	0.66	4.49	n.r.	50–60	85[b]	[31]
ICR	Dyeing wastewater	3 g$_{COD}$ L^{-1}	20 L	35	15[b]	0.21	4.9[d]	n.r.	n.r.	87[b]	[32]
ABR	Baker's yeast manufacturing wastewater	15 g$_{COD}$ L^{-1}	14.5 L	28	7.5[b]	2	n.r.	0.45[c]	75.3	95[b]	[33]

(continued)

Table 1 (continued)

Reactor	Feedstock	Feedstock concentration	Reactor size	Temperature °C	OLR kgVS/COD m^{-3} d^{-1}	HRT d	Methane rate m^3 m^{-3} d^{-1}	Methane yield m^3 kgVS/COD^{-1}	Methane content %	VS/COD removal efficiency %	Source
ABR	Municipal wastewater	0.35–0.45 g$_{COD}$ L^{-1}	37 L	35	1.6[b]	0.25	n.r.	0.34[c]	67	84[b]	[34]
AFR	Fermented olive mill wastewater	30 g$_{COD}$ L^{-1}	3.5 L	35	2[b]	15	n.r.	0.33[c]	73–84	59–63[b]	[24]
AFR	Sewage sludge	38.4 g$_{COD}$ L^{-1}	9 L	25–31	4.7[b]	7	0.95[d]	0.28[c]	77	73.4[b]	[35]
AFR	Complex dairy wastewater	8.67 g$_{COD}$ L^{-1}	12 m^3	35–37	4.7[b]	1.85	3.79[d]	n.r.	68	90.9[b]	[36]
AFBR	Distillery wastewater	9.3 g$_{COD}$ L^{-1}	5.9 L	30	20[b]	0.46	n.r.	0.29[c]	n.r.	80[b]	[37]
AFBR	Primary sludge	39 g$_{COD}$ L^{-1}	16 L	37	18[b]	2.2	n.r.	0.28[c]	n.r.	62[b]	[38]
Two-stage CSTR + CSTR	Dairy slurry	45.7 g$_{VS}$ kg^{-1}	0.4 L + 1.6 L	36	11.5[a]	2 + 8	0.382[d, e]	0.150[a, e]	n.r.	54–71[b]	[39]
Two-stage CSTR + UASB	Waste from food processing industry	78 g$_{VS}$ kg^{-1}	3 L + 2.25 L	55 + 34	8[a]	3 + 2.25	n.r.	0.46[a]	n.r.	86.2[b]	[40]
AMBR	Molasses wastewater (synthetic)	23.9 g$_{COD}$ L^{-1}	9 L	55	12[b]	2	~2.6[d]	n.r.	55–65	61[b]	[41]
AMBR	Municipal wastewater	0.275 g$_{COD}$ L^{-1}	60 L	35	3.0[b]	0.09	n.r.	0.12[c]	50–70	87[b]	[42]
AHR	Distillery - spent wash	90–130 g$_{COD}$ L^{-1}	11.78 L	n.r.	8.7[b]	5	3.5	0.33[b]	n.r.	79[b]	[43]
AHR	Olive mill effluent	80.8 g$_{COD}$ L^{-1}	20 L	35	32[b]	2.5	4.9	n.r.	70–75	51[b]	[44]
SSSAR	Synthetic wastewater	24.1 g$_{COD}$ L^{-1}	18.7 L	35	361.5[b]	0.07	73	0.265[c]	n.r.	63.4[b]	[45]

(continued)

Table 1 (continued)

Reactor	Feedstock	Feedstock concentration	Reactor size	Temperature °C	OLR $kg_{VS/COD}$ m^{-3} d^{-1}	HRT d	Methane rate m^3 m^{-3} d^{-1}	Methane yield m^3 $kg_{VS/COD}^{-1}$	Methane content %	VS/COD removal efficiency %	Source
FBDR	Sugar beet silage	87.3 g_{VS} kg^{-1}	57 L	37	4^a	22	1.81	0.449^a	56	n.r.	[46]
ME-ADR	Waste activated sludge	17.5 g_{COD} L^{-1}	0.65 L	20–25	n.r.	45 (batch)	0.138	$0.175^{d,\,f}$	n.r.	48^f	[47]
ME-ADR	High-strength wastewater (synthetic)	6.06 g_{COD} L^{-1}	3.5 L	35	15.5^b	0.25–0.5	4.60	0.27^c	66	77^b	[48]

[a]Based on VS; [b]Based on COD; [c]Based on $COD_{removed}$; [d]Own calculation based on presented data; [e]Biogas; [f]Based on volatile suspended solids (VSS)

OLR: Organic Loading Rate, HRT: Hydraulic Retention Time, TS: Total Solids, VS: Volatile Solids, COD: Chemical Oxygen Demand, CSTR: Continuously Stirred Tank Reactor, ACR: Anaerobic Contact Reactor, ASBR: Anaerobic Sequencing Batch Reactor, UASB: Up-flow Anaerobic Sludge Blanket, EGSB: Expanded Granular Sludge Blanket, ICR: Internal Circulation Reactor, ABR: Anaerobic Baffled Reactor, AFR: Anaerobic Filter Reactor, AFBR: Anaerobic Fluidized Bed Reactor, AMBR: Anaerobic Membrane Bioreactor, AHR: Anaerobic hybrid reactor, SSSAR: Spiral Symmetry Stream Anaerobic Reactor, FBDR: Fixed Bed Disc Reactor, ME-ADR: Microbial Electrolysis Anaerobic Digestion Reactor, n.r.: not reported

methanogens. Thus, gentle but effective stirring is desired. Complete reactor agitation is beneficial as it provides an even distribution of feedstocks and temperature within the reactor, dilutes inhibitory substances and supports the upflow and escape of biogas bubbles from the liquid. Yet, it is also energy-intensive and leads to a comparatively high parasitic energy demand.

The CSTR does not enable specific retention or enrichment of active biomass within the system. The HRT equals the retention time of solids and microorganisms. In order to keep the process stable, the number of regrown microbes needs to be at least as high as the numbers of microbes that are flushed out with the digestate. A sufficiently high HRT is necessary to prevent microbial wash-out. Long HRTs of 30–60 days are often chosen for operation of CSTRs [4] (Table 1). Retention times even reach 100–150 days in CSTRs for co-digestion of manure and crop feedstocks in agricultural biogas plants in order to fully exploit the methane potential [5]. Consequently, the OLR typically lies in a lower range of 1–4 kg_{VS} m^{-3} d^{-1}. Altogether, the CSTR represents a simple technology available at comparatively low capital costs but with restricted efficiency [9].

One recent approach to enhance the retention of microbes in CSTRs is the addition of magnetic foam glass particles to the reactor, which can serve as carriers for biofilm formation [50]. The magnetic particles are recovered from the digestate by means of a magnetic separator and recycled back to the reactor. The magnetic biofilm carriers were shown to increase methane yield, methane production rate and possible OLR of the CSTR [50].

Reactors with Biomass Retention by Sedimentation of Biomass

One approach to retain microbes in completely stirred systems is to couple the CSTR with an additional gravity sedimentation tank in series. This reactor system is referred to as **Anaerobic Contact Reactor** (**ACR**). Effluent from the reactor is conveyed to a sedimentation tank, biomass settles inside the tank and is recycled back to the reactor in order to seed the influent. ACRs tolerate higher OLRs and feature enhanced methane production and process stability as compared with the CSTR, but additional equipment and energy input are required [4].

The **Anaerobic Sequencing Batch Reactor (ASBR)** in contrast comprises of only one single tank with solid/liquid separation by sedimentation, which is operated in batch or fed-batch mode. The operation of the ASBR is characterized by a continuously repeated process cycle that includes a series of consecutive steps: filling with influent; reacting with active biomass that is present inside the reactor; sedimentation of biomass; and discharge of digestate (supernatant) [51]. Each step is effected for a defined period of time. During the reaction step the reactor is mixed to enable intense contact between feedstock and microorganisms. Afterwards, mixing is stopped to allow biomass to settle to the bottom of the reactor before a defined volume of supernatant is removed from the liquid surface of the reactor and the process cycle starts again. Settling of the biomass facilitates an extended SRT and retains a more abundant and diverse microbial population within the reactor.

The performance of the system is dependent on the successful sedimentation of the biomass.

The main benefit of the ASBR lies in its flexibility. The ASBR can treat a wide range of influent volumes [51]. The duration of the process steps can be adjusted as required by feedstock characteristics. The mode of operation can be optimized with regard to: the total cycle time; the fill time to cycle time ratio; or the volumetric exchange ratio [52]. At higher OLRs a short fill time can cause acidification problems while a higher fill time to cycle time ratio and a small volumetric exchange ratio can avoid substrate inhibition [51]. The cycle times can be performed as fixed times or may be changed in real-time, adjusted to the influent composition. If feedstock is unavailable, the ASBR can even stay dormant. Besides its flexibility, the ASBR enables high gas yields and methanogenic activity and good process control and efficiency at comparatively low energy input and mechanical requirements and low costs [9]. Disadvantages of the system concern the organic loading which is limited due to the operation strategy [52], resulting in low methane production rates. Furthermore, dead zones might occur within the ASBR, and a long start-up period of the reactor and long settle times within the process cycle might be necessary [53]. The knowledge of appropriate agitation and feeding strategies for different feedstocks is still limited [53].

Reactors with Biomass Retention by Formation of Granules

The principle of several reactor configurations is based on the ability of some of the microorganisms that are involved in AD to form flocs or granules. Due to the dense form of these granules, they possess good settling properties and can be enriched within the reactor. In the lower part of the **Up-flow Anaerobic Sludge Blanket (UASB) reactor** granules consisting of self-immobilized microbial biomass add up to a blanket of sludge of about 1–3 m [21]. The reactor is fed from the bottom, and mixing and substrate distribution occurs by the up-flowing influent and by rising biogas bubbles. A three-phase separator at the reactor top enables the discharge of the produced biogas to the gas storage and forces up-flowing granules to sink down to the reactor bottom again.

The UASB reactor can treat medium-strength wastewaters such as from pulp and paper, brewery, food-processing, or bioethanol industry; however, its ability to digest larger amounts of suspended solids is limited [4]. HRTs can be as low as <24 h and OLRs typically lie in the range of 8–15 kg_{COD} m^{-3} d^{-1} [21]. It is one of the most commonly used types of bioreactors for anaerobic wastewater treatment, and can be applied as a second stage reactor in two-stage processes (Sect. 3.1.2). The technology of the UASB reactor is compact and comparatively inexpensive showing low reactor volume and no digestate recycling requirements [9]. Furthermore, the system is robust as it contains no moving parts such as stirrers inside the reactor. It provides enhanced process stability due to a less susceptible microbial population grown in granules. However, the performance of an UASB reactor strongly depends on the successful formation of granules, which requires

adequate and stable process temperature, a stable neutral pH, and the presence of adequate nutrients and metals, and on granule quality, which varies with feedstock strength and composition [54]. Long start-up periods ($\sim$4–16 months) might be necessary, and a risk of wash-out of granules exist. The system requires skilled operation [9, 55].

The **Expanded Granular Sludge Blanket** (**EGSB**) **reactor** represents an advanced version of the UASB reactor. It differs from the UASB reactor by an expanded sludge bed, which is achieved through higher up-flow velocities and can reach up to 60% of the reactor height [21]. Increased organic loadings of typically 10–25 kg_{COD} m^{-3} d^{-1} (with corresponding HRTs of 2–3 h) are possible due to improved mixing, mass transfer and microbial activity. The EGSB reactor can also treat low- and high-strength wastewaters and is more resistant against inhibitory compounds than the UASB reactor, but removal of suspended solids is limited. TS concentration of the influent should lie below a maximum of 300–500 mg_{TS} L^{-1} [21].

The **Internal Circulation Reactor (ICR)** is another development based on the UASB reactor. In principle, it comprises of two UASB reactors arranged one on top of the other. Biogas which is produced and collected in the lower compartment rises to the reactor top in a rise pipe and creates an internal circulation by causing a return flow of effluent from the upper compartment in a down pipe. No energy input is required for the internal circulation. Feedstock is added at the bottom of the ICR and mixed with the internally recirculated effluent before it is equally distributed to the sludge bed of the lower compartment. High up-flow velocities result in an almost complete mixing of the lower compartment accompanied by intense contact between feedstock and granules, optimal mass transfer and high biomass activity. Most of the biomass conversion occurs in the lower compartment before the wastewater reaches the upper compartment where residual biogas production continues. Up-flow velocity and sludge concentration in the upper compartment are low, allowing for good recovery of floating granules and compensation of peak loads. Thus, the ICR system features a high degradation capacity, high possible OLRs of up to 35 kg_{COD} m^{-3} d^{-1}, high process stability and resistance against shock loads [9, 21].

The **Anaerobic Baffled Reactor (ABR)** can be described as a number of UASBs connected in series in a horizontal reactor [4]. Baffles are used to force the influent to pass a series of compartments with sludge beds, towards the reactor outlet. Active biomass within the compartments gently rises and settles, caused by the liquid flow and biogas production [16]. Flow characteristics and the degree of mixing affect the contact between feedstock and microbes, thus controlling mass transfer and reactor performance. The design of the ABR is variable and can be adapted to special feedstock characteristics or degradation needs by rearrangement of the baffles, by different compartment sizes or by additional solids settling chambers [16].

The main advantage of the ABR is the possibility to spatially separate acidogenesis and methanogenesis in different compartments down the reactor. Hydrolytic and acidogenic bacteria, that grow faster and tolerate higher substrate levels and

lower pH-values, will dominate in the front compartments, while slower growing syntrophic acetogens and methanogens will establish towards the reactor end [16]. Thus, a two-stage system is created without additional reactor and equipment requirements. Combined with an enhanced SRT, this results in an efficient reactor system with good COD removal capability, OLRs of up to 20 kg_{COD} m^{-3} d^{-1}, and high tolerance to inhibitory compounds and shock loads [9, 16]. The ABR can be used to treat wastewater of any strength, but the digestion of feedstock with higher TS content is limited as the solids can accumulate in the first compartment leading to a displacement of active biomass within the reactor [16]. Further difficulties associated with the operation of the ABR regard an uneven distribution of the influent, inadequate mixing that can be caused by insufficient liquid and gas up-flow velocities, and insufficient sedimentation of granules which can lead to biomass wash-out [9]. In contrast to the UASB reactor, the EGSB reactor and the ICR, the ABR is rarely applied at commercial scale.

Reactors with Biomass Retention by Immobilization on Carrier Materials

If a suitable carrier material is provided, AD microorganisms tend to grow and attach to the surface of the carriers as biofilms. Microbes attached to the carrier surface build up complex aggregates with high cell densities and beneficial conditions for syntrophic interactions. Moreover, a matrix of extracellular polymeric substances is formed which protects microbial biofilm growth as it acts as a barrier that prevents wash-out of extracellular enzymes and penetration of harmful substances [56]. Thus, biofilm formation supports feedstock degradation, process stability and resistance to environmental changes.

The **Anaerobic Filter Reactor (AFR)** is a vertical reactor with typically 70% of the reactor volume filled with biofilm carriers [21]. Today, plastic carrier materials are usually used which provide large specific surface areas, high stability and low weight. The AFR can be operated in up-flow or down-flow mode. Up-flow operation is more common as it enables higher biomass concentrations within the reactor, although the risk of clogging of the carriers is increased as compared with down-flow conditions [21]. Retention of microorganisms in biofilms on carrier materials inside the AFR is a simple and effective solution for prevention of biomass wash-out. It allows for enrichment of specialized microbes and a high degree of adaptation to complex feedstocks, high COD loads or inhibitory substances [9]. OLRs of 5–15 kg_{COD} m^{-3} d^{-1} can usually be reached [21]. Owing to the biofilm formation, the AFR is robust against load fluctuations and varying influent composition. The AFR can treat high- and low-strength wastewaters, however, feedstocks should contain low amounts of suspended solids since otherwise the suspended solids can cause clogging of the packing material [57]. Furthermore, a risk of short-circuiting exists for AFRs. Longer start-up periods for biofilm formation ($\sim$3–4 months) might be necessary, and the use of high-quality carrier materials can result in high investment costs for the ABR system.

Another reactor configuration, which uses support materials for the attachment of microbes is the **Anaerobic Fluidized Bed Reactor** (**AFBR**). Within the AFBR, most of the active biomass grows attached to small, mobile carrier particles, which are fluidized by a high up-flow velocity of the influent and recycled effluent. Materials such as sand, pumice stone, activated carbon or plastics are used as biofilm carriers. The high flow velocity results in intense movement of the particles and facilitates nutrient distribution and mass transfer which leads to high biomass activities. Thus, operation of the AFBR at high OLRs of 15–35 kg_{COD} m^{-3} d^{-1} is possible [21]. The AFBR is effective for the treatment of low- to high-strength wastewaters, and can degrade feedstocks with comparatively high content of suspended solids of up to 10% [4]. The risk of reactor clogging is significantly reduced compared to the AFR. However, the range of an appropriate up-flow velocity to keep carrier particles fluidized but prevent wash-out of carriers is often small. Thus, active biomass can be lost as a result of inadequate or changing flow rates or particle densities. The AFBR also requires longer start-up periods for biofilm formation, and additional costs are incurred for carrier materials and reactor operation, especially for the fluidization of the carrier particles. Up-scaling of the AFBR is difficult and large-scale applications are limited [4].

3.1.2 Two-Stage Reactor Systems

The different microbes, which are involved in the four stages of anaerobic digestion have varying needs for an optimal growth regarding nutrients, feedstock concentration and pH-value (Fig. 1). Microorganisms of the hydrolysis and acidogenesis steps generally grow faster and are more tolerant to variations in environmental conditions. In contrast, acetogens and methanogens show a slower growth, are susceptible to environmental changes and require close proximity for effective H_2 transfer. Spatial separation of the hydrolysis/acidogenesis and acetogenesis/methanogenesis processes in two-stage reactor systems provides an opportunity to individually fulfill the different requirements of the respective microbes of these AD steps and thus, to enhance process performance and control. Two-stage liquid or low solids content AD systems typically comprise of a CSTR for hydrolysis and acidogenesis where a liquid effluent enriched with VFAs is produced, followed by a CSTR, UASB reactor or AFR for acetogenesis and methanogenesis where these intermediates are converted into methane, but other reactor combinations are also possible [9, 57]. It has been stated that two-stage operation can remarkably increase the acidogenic and methanogenic activity [16]. A large number of studies compared two-stage and single-stage liquid and low solids content AD and found higher methane yields, enhanced reduction of VS or COD, increased process stability, higher possible OLRs and shorter HRTs in the two-stage reactor configuration for a variety of feedstocks such as food processing waste, industrial wastewaters, and dairy manure [39, 40, 58]. However, advantages of two-stage over single-stage AD depend on feedstock type and composition and might vary to a large extent [59]. Besides, the construction of two reactors instead of one is more cost-intensive, but

enhanced methanogenic performance and process stability might be able to compensate for extra costs.

An opportunity to optimize methane production in two-stage systems is the so-called temperature-phased anaerobic digestion (TPAD) where the hydrolysis and the methanogenesis reactor are operated at different temperatures. A thermophilic hydrolysis stage is usually connected to a mesophilic methanogenic stage. The thermophilic temperature in the first stage accelerates the metabolism for hydrolysis, while the mesophilic temperature in the second stage protects microbes, such as syntrophic acetogens and methanogens that are more sensitive to inhibitors at elevated temperatures [11]. TPAD has been reported to outperform two-stage mesophilic AD and single-stage mesophilic and thermophilic AD in terms of VS removal, methane yield and process stability [11]. It can reduce pathogens that might be present in some feedstock. TPAD is still under research and further knowledge regarding the effects on digestion of different feedstocks is necessary to support its implementation at commercial scale.

3.1.3 Novel Reactor Concepts for Liquid and Low Solids Content Anaerobic Digestion

In more recent years, numerous advanced reactor concepts have been developed for liquid/low solids content AD with the aim to further enhance retention of active biomass, increase the process stability and possible OLR, enable effective AD of feedstocks with high amounts of particulate matter, and increase methane production. Some examples are briefly discussed in this section. Membrane reactors and anaerobic hybrid reactors already exist at pilot or commercial scale while the spiral symmetry stream anaerobic reactor, the fixed bed disc reactor and microbial electrolysis AD reactors are some examples for bioreactor configurations that are still under development.

In **Anaerobic Membrane BioReactors (AMBR)** microbes are retained within the AD process by micro- or ultrafiltration using membranes. Membranes can be included in the AMBR system either as an external unit, or submerged within the main reactor or in a separate reactor. Advantage of AMBRs is the capability to almost completely retain active biomass within the system. Applied membranes are of polymeric, metallic or ceramic material and have pore sizes in the range of 0.3–1.0 µm which is below the size of most microbes or flocs involved in AD [60]. Consequently, high biomass concentrations, optimal metabolic conversion and effluent quality, and a high degree of adaptation to feedstock properties can be reached. The AMBR only requires short start-up periods and can handle all types of wastewater as well as fluctuating influent qualities [60]. However, the major obstacle in the use of AMBRs for AD is membrane fouling. This term describes deposition of (organic and inorganic) materials and pore-blocking which leads to loss of permeability of the membranes. Membrane fouling can be reduced or removed by cleaning techniques such as membrane relaxation or membrane backflushing, but this is accompanied by higher energy requirements and can

diminish the lifespan of the membrane [60]. An enhanced AMBR system is proposed which prevents fouling by biogas bubbling through the membrane surface [57]. Nevertheless, AMBRs currently have high capital costs and costs for operation and maintenance. Fields of application are suggested for AD under extreme conditions, such as high temperature, salt content, toxic compounds or for the AD of extremely high-strength wastewater [21].

Anaerobic Hybrid Reactors (AHR) combine a sludge blanket with granules in the lower part and a packed zone with biofilm carriers in the upper part of a vertical reactor. This can be a combination of an EGSB or UASB reactor and an AFR. Reactor influent is added and evenly distributed at the bottom, passes the lower and upper zones, and finally digestate is discharged at the reactor top. The combination of the two zones is beneficial as the fixed bed of the upper zone additionally retains active biomass in the lower compartment and reduces microbial wash-out even at high up-flow velocities. This allows for enhanced mixing and mass transfer. Furthermore, a specialized microbial community can develop in the fixed bed which aids in the degradation of complex or toxic wastewaters, as has been shown in several studies [43, 44, 61]. Since a higher acidogenic activity is noticed in the lower zone, and a higher methanogenic activity occurs in the upper zone, the AHR presents a transition towards stage separation [62].

Several novel reactor configurations aim at increasing the possible OLR for reduced reactor volume requirements. A **Spiral Symmetry Stream Anaerobic Reactor** (**SSSAR**) developed by Chen et al. [45] is reported to operate at an OLR of up to 361.5 kg_{COD} m^{-3} d^{-1} and an HRT of 1.6 h at laboratory scale. The SSSAR is a slim vertical vessel with influent addition and distribution at the bottom, a reaction zone filled with granular sludge in the middle and a three-phase separator at the reactor top. The reaction zone contains three elliptic plates arranged 120° spirally and symmetrically which create three separate chambers. Biogas is collected by gas collection pipes underneath each elliptic plate [45]. The high performance of the SSSAR is attributed to the intense mixing conditions generated by a spiral up-flow that increase with decreasing HRTs and reduce mass transfer resistance. Active biomass retention is supported by gas entrapment and diversion with the elliptic plates and gas collection pipes [45]. So far, the reactor has only been investigated at laboratory scale.

A reactor solution for AD of liquid feedstock with high content of suspended solids or particulate matter is presented by Terboven et al. [46]. The **Fixed Bed Disc Reactor** (**FBDR**) contains carrier materials attached to the lower side of the discs of a specially developed disc stirrer to prevent microbial wash-out. Intense contact between microorganisms and feedstock is provided by up-flow operation and an offset arrangement of the discs. Thus, this special stirrer allows for improved retention of active biomass, intense agitation for equal distribution of nutrients, and digestion of particulate suspensions eliminating the risk of clogging. The FBDR has been reported to be suitable for demand-driven biogas production by flexible feeding [46]. Demand-driven biogas production has recently received attention against the background of compensating intermittent and fluctuating power supply from other renewable sources such as wind and solar [63]. Biogas is produced and/

or utilized in combined heat and power units only in times of positive balancing power demand. The FBDR showed high process stability at varying feeding patterns, resistance against shock-loads and the ability to notably alter biogas production within a very short time span of about 15 min and, thus, high flexibility for methane formation on demand [46].

Another novel approach to enhance methane production in AD bioreactors is the integration of microbial electrolysis. This is implemented by placing a pair of electrodes inside an AD reactor, and by applying external voltage. Anode and cathode can be employed in a single chamber, or can be positioned in two chambers separated by a cation or anion exchange membrane. Carbon, graphite (partly Pt-coated) or stainless steel are typically used as electrode materials [64]. **Microbial** **Electrolysis** **AD** **Reactors** (**ME-ADR**) have been demonstrated to notably enhance methane production rates, methane yields and COD removal efficiency. Oxidation of carbon is promoted on the anode, and increased hydrolysis of biopolymers as well as positive effects of micro-aerobic conditions due to formation of small amounts of oxygen are observed [48]. H_2 is supplied at the cathode and stimulates the growth of hydrogenotrophic methanogens, leading to additional methane production and increased methane concentrations within the biogas through CO_2 reduction [47, 65]. Furthermore, active biomass is immobilized on the electrodes, which can improve process stability [66]. Additional methane formation might cover costs for energy input of the microbial electrolysis system [67]. However, ME-ADRs are still in their early stage and extensive research is necessary for industrial applicability [64].

3.2 Bioreactors for High-Solid Anaerobic Digestion

Anaerobic digestion of high-solid organic feedstock may be categorized into semi-solid AD, which takes place at a TS contents of 10–20%, and solid-state AD operated at TS contents above 20% up to approx. 40% [18, 20]. Typical feedstocks that have been used for high-solid AD applications comprise agricultural residues such as corn stover or straw, solid livestock manures such as solid pig or cattle manure, food and municipal wastes such as the organic fraction of municipal solid waste (OFMSW), garden waste or fruits and vegetable waste, energy crops and grasses such as maize or perennial ryegrass, and macro-algae. These feedstocks mainly have TS contents of about 10–50% and are digested with little or no addition of water.

High-solid AD exhibits several advantages over liquid or low solids content AD. Due to the higher TS content less reactor volume is required, and high volumetric methane productivity can be achieved. High-solids bioreactors can be operated at higher organic loading; OLRs of 7 up to 15 kg_{VS} m^{-3} d^{-1} are possible [20]. The lower reactor volume further results in less thermal energy input required for heating of the reactor content. Besides, less mixing is usually applied, which may lead to a lower energy demand for reactor operation. Few moving parts inside the

reactor are also beneficial with regard to a reduced risk of short circuiting and operational problems. Extraneous materials and impurities, which, for example, might be present in OFMSW, are less damaging. Owing to the lower water content of digestate of high-solid AD systems, the digestate is easier to handle, and digestate transport and management are associated with lower costs [2].

On the other hand, the elevated TS concentration of feedstock and reactor content in high-solid AD systems is linked to challenges regarding process efficiency, stability and reactor design. High-solid AD systems are more sensitive to the accumulation of inhibitory or toxic substances, and high solids input can cause excessive VFA formation followed by a drop in pH-value and process failure [2, 18]. It was found that TS concentrations above 30% lead to limitations of the gas-liquid mass transfer resulting in an accumulation of dissolved CO_2, methane and H_2 within the digestion media [68]. Locally increased CO_2 concentrations cause acidification and, thus, inhibition of methanogenesis. Elevated H_2 partial pressure can inhibit H_2 producing acetogens. Decreasing methane yields, methane production rates and specific methanogenic activity are observed at increasing TS contents above 10% due to reduced hydrolysis rates and a slower mass transfer between feedstock and microorganisms [68–70]. High-solid digestion systems are often slightly mixed or not mixed. Thus, convective transfer within the digestion media is negligible while diffusive transfer governs mobility of substrates [71]. A reduced water content drastically reduces diffusion in high-solid AD media, presumably due to a markedly higher viscosity [71]. In consequence, high-solid AD in conventional reactors often suffers from low VS reduction (less than 50%) low methane yields and inhomogeneity. Inoculation of feedstock with a high share of digestate is usually applied to avoid the risk of AD failure and ensure enhanced process kinetics and feedstock degradation within a manageable retention time [72]. However, high amounts of inoculum reduce the reactor volume available for feedstock digestion. Besides, high-solid reactor systems often require sophisticated pumping equipment [20].

Bioreactors applied for high-solid AD are either batch-operated leach bed reactor systems or continuous plug-flow reactor systems. However, there is still large potential for enhancement of process efficiency and economy through innovative reactor design. The leach bed and plug-flow reactor system are described in Sect. 3.2.1, while more sophisticated and novel reactor concepts for high-solid AD are described in Sects. 3.2.2 and 3.2.3. Some examples for the performance of reactors for high-solid AD are listed in Table 2.

3.2.1 Conventional Bioreactors for High-Solid Anaerobic Digestion

Leach Bed Reactor (LBR)

Leach Bed Reactors (LBR) are used for discontinuous high-solid AD. A mixture of solid substrate and about 40–60% of recycled digestate is filled batch-wise into the digester [82]. At commercial scale, reactors typically consist of gas-tight garage

Table 2 Examples for the performance of different bioreactor systems for high-solid anaerobic digestion

Reactor	Feedstock	TS %	Reactor size	Temperature °C	OLR kgVS/COD m^{-3} d^{-1}	HRT d	Methane rate m^3 m^{-3} d^{-1}	Methane yield m^3 kgVS/COD^{-1}	Methane content %	VS/COD removal efficiency %	Source
LBR	Horse dung	32.2	50 L	35	n.r.	46	0.25–0.28[d]	0.17	51.1–53.5	38–48[a]	[73]
LBR	Maize silage, poultry manure, other silages	30	4 × 480 m^3	38	2.1[a]	20	0.64	0.309	53.1	61[a]	[23]
LBR	Grass silage, solid cattle manure, hay	37	2 × 408 m^3	48	1.9[a]	18	0.29	0.155	54.3	59[a]	[23]
APFR	Manure bedded with straw	22	9.2 L	37	4.2[a]	40	n.r.	0.163	65.1	57.4[a]	[74]
APFR	Maize silage, sugar beet, rye meal	33	2080 m^3	40	3[a]	108	1.09	0.375	51.6	73[a]	[23]
LBR + UASB, two-stage	Grass silage	25.9	1 L + 1 L	35	5[b] (UASB)	55	n.r.	0.179	n.r.	55[a]	[75]
APFR + CSTR, two-stage	Maize silage, catch crop silage, rye silage	31	600 m^3 + 1800 m^3	42	3.2[a]	101	1.31	0.368	51	82[a]	[23]
HIT	Wheat straw, fruit/vegetable waste	94.5; 7.4	75 L	35	1.37[a]	10[c]	n.r.	~0.48[d]	64.9–76.7	88.8[a]	[76]
UASS + AFR	Maize silage, barley straw	34.9; 89.8	26.5 L + 79.2 L	55	17[a]	4.6	1.6	0.312	53.9	86.1[b]	[77]
UASS + AFR	Wheat straw	n.r.	37 L + 30 L	37	2.5[a]	14–21[c]	0.239 + 0.079	0.121	41.6–60.8	47.9[b]	[78]
UASS + AFR	Wheat straw	n.r.	37 L + 30 L	55	2.5[a]	14–21[c]	0.403 + 0.05	0.165	41.6–60.8	49.8[b]	[78]
FBR + AFR	Maize silage	38.2	35 L + 22 L	38	4.5[a]	158[c]	n.r.	0.339	60.7	n.r.	[79]

(continued)

Table 2 (continued)

Reactor	Feedstock	TS %	Reactor size	Temperature °C	OLR $kg_{VS/COD}$ m^{-3} d^{-1}	HRT d	Methane rate m^3 m^{-3} d^{-1}	Methane yield m^3 $kg_{VS/COD}^{-1}$	Methane content %	VS/COD removal efficiency %	Source
Two-stage pressurized (9 bar) LBR + AFR	Maize silage	31.3	3 × 50 L + 20 L	55 + 37	5.1ᵇ (AFR)	n.r.	n.r.	0.31 (AFR)	75 (AFR)	93ᵇ (AFR)	[80]
Two-stage pressurized (50 bar) LBR + AFR	Maize silage, grass silage	31.0; 34.4	4 × 50 L + 21 L	55 + 37	4.19ᵇ (AFR)	4.19 (AFR)	n.r.	0.26 (AFR)	90.45 (AFR)	80.4ᵇ (AFR)	[81]

[a]Based on VS; [b]Based on COD; [c]SRT; [d]Own calculation based on presented data

TS: Total Solids, VS: Volatile Solids, COD: Chemical Oxygen Demand, OLR: Organic Loading Rate, HRT: Hydraulic Retention Time, LBR: Leach Bed Reactor, APFR: Anaerobic Plug-Flow Reactor, UASB: Up-flow Anaerobic Sludge Blanket, CSTR: Continuously Stirred Tank Reactor, HIT: Half-submerged Integrated Two-phase Reactor, UASS: Up-flow Anaerobic Solid-State Reactor, AFR: Anaerobic Filter Reactor, FBR: Floating Bed Reactor, n.r.: not reported

type boxes, which are loaded and unloaded with wheel loaders or similar suitable agricultural equipment. Process liquid trickles to the base of the reactor, is separated from the solid reactor content by means of a perforated layer, collected and conveyed to a heated storage tank, from where it is sprinkled over the feedstock again. This recirculation of leachate facilitates contact between substrate and microorganisms, and supports the distribution of moisture and heat within the reactor. However, toxic or inhibitory substances present in the feedstock or formed during degradation can accumulate within the leachate, thus, leachate recirculation can also cause inhibition of methanogenesis and process failure. The percolation of leachate depends on the physical characteristics of the feedstock such as viscosity, particle size and spacing between feedstock particles. In general, an even distribution of microorganisms and moisture is difficult to achieve due to inhomogeneity of the feedstock and packing which may result in formation of dead zones and reduction in methane yield [18]. Packing height of the feedstock is limited to 2–3 m in order to prevent compaction of the lower feedstock layers [82]. An alternative to leachate percolation is the periodical flooding of the feedstock. Kusch et al. [73] found that a higher volumetric methane production can be achieved by flooding compared to leachate percolation since no mixing with solid digestate is required while degradation and methane yield are equal. Yet, the flooded process bears the risk of floating of solid feedstock.

The main advantage of the leach bed reactor system is its simplicity, which makes it easy to maintain and results in low capital and operating costs [10]. However, the batch operation mode requires a recurrent, labour-intensive procedure comprising reactor opening and restarting of the AD process. Special safety appliances are necessary as explosive gas mixtures can occur. Methane as a highly potent greenhouse gas can be lost and emitted at reactor opening [82]. Furthermore, the batch-wise operation leads to a fluctuating gas production with varying biogas quality. Thus, in order to achieve a more constant gas production, at least 3–4 reactors are usually operated in a sequential batch mode in which leachate from a mature reactor can be used for start-up of the new reactor [5]. The LBR can also be deployed as the first stage in two-stage high-solid AD reactor systems (Sect. 3.2.2).

Anaerobic Plug-Flow Reactor (APFR)

Anaerobic Plug-Flow Reactors (APFR) are applied for continuous high-solid AD. APFRs are predominantly horizontal reactors although vertical reactor systems also exist. In APFRs the feedstock is continuously introduced and moves through the digester as a "plug", i.e. with lateral agitation but restricted mixing in axial direction. Horizontal APFRs are typically equipped with slowly rotating axial mixers or paddle mixers that are integrated across the flow direction of the reactor content and generate local agitation only [5]. Mixing provides enhanced contact between substrate and microorganisms and facilitates degassing of the highly-viscous reactor content. Vertical APFRs are long cylindrical reactors that lack any internal agitation system. Fresh feedstock is introduced at the top and digestate is withdrawn at the

conical bottom of the reactor [82]. Similar to the LBR, a large share of digestate of up to 80% is recycled for feedstock inoculation and prevention of process failure in the APFR. Recycling of digestate enables bioconversion at high OLR but largely reduces the reactor volume available for feedstock digestion.

The APFR has higher application potential in practice as compared with batch-operated high-solid AD systems. It is usually operated at TS contents below 30% and has been successfully applied or tested for AD of OFMSW, energy crop mixtures with high portions of maize silage, grass silage and similar feedstocks (Table 2). The APFR combines robustness and high methanogenic performance with relatively low complexity and expenditure for investment, operation and maintenance. Main drawbacks of the APFR are the requirement for large amounts of recycled digestate, and for heavy process equipment and energy to agitate and handle dry, viscous material.

3.2.2 Two-Stage Two-Phase Reactor Systems

Similar to the two-stage systems for liquid and low solids content AD (Sect. 3.1.2), high-solid AD can also be split into two stages. The term "two-stage" reactor system describes the division of the AD process into the hydrolysis/acidogenesis and the acetogenesis/methanogenesis steps, while "two-phase" means the separation of fluid and solid phases. In two-stage two-phase reactor systems, hydrolysis and acidogenesis take place in the first stage where solid organic matter with high TS content is degraded and a liquid phase enriched with organic acids and other intermediates is formed. The liquid phase is separated and conveyed to a second stage reactor where the acetogenesis and methanogenesis steps occur and methane is produced from acids and intermediates. As hydrolysis is often the rate-limiting step in anaerobic digestion of solid biomass, decoupling and separate optimization of the hydrolysis and methanogenesis steps in high-solid AD systems can be of special benefit [18].

Leach bed reactors are usually used as first stage reactors for high-solid two-stage AD with the leachate being subsequently pumped to a second stage where reactors used in liquid AD are applied (UASB or AFR) [79, 83]. Two-stage high-solid AD has been shown to considerably enhance methane production compared with single-stage processes. For example, a threefold increase in methane yield was achieved for anaerobic digestion of grass silage in a combined leach bed and UASB two-stage system as compared with digestion in a LBR without a second stage [75]. Browne et al. [84] reported an almost 60% increase in VS removal for food waste by connecting an UASB to a sequential LBR at a suitable recirculation rate of effluent. An up to twofold higher methane yield, a more stable operation and toleration of higher OLR, and an improved biogas quality was found for corn straw digestion when combining an Up-flow Anaerobic Solid State (UASS) reactor with an AFR as compared with a single-stage UASS system [85]. Since a larger share of CO_2 is produced in the separated hydrolysis/acidogenesis step, higher methane

content is usually reported for the second stage of two-stage two-phase AD systems [86].

Separation of acid and methane producing microorganisms allows for a better control of the exposure of methanogens to potentially inhibiting intermediates. Thus, negative impacts of fermentative inhibitors such as VFAs or ammonia, and of changes in pH are reduced. In addition, agglomerated microbes in biofilms or granules of AFR or UASB reactors are more robust against unfavourable conditions and might tolerate higher inhibitor concentrations [20]. This leads to an improved process stability of two-stage high-solid AD systems.

Another advantage of two-stage two-phase systems is its particular suitability for demand-driven biogas production (as described for the FBDR in Sect. 3.1.3). The leachate from the first-stage reactor can be stored and fed to the second-stage reactor for an adapted methane production on demand [83]. As the leachate contains quickly convertible organic substances, the methane rate of the second-stage reactor can be varied within few hours via flexible feeding [87]. Owing to the biofilm formation on carrier materials, fixed bed reactors such as the AFR can be easily kept dormant during times of low energy demand, and can be quickly restarted when methane is required [87]. An extended system, the so-called "ReBi-process", is proposed for demand-driven biogas production where hydrolysate from a first-stage reactor is separated into a liquid and a solid fraction with a screw press. The solid fraction is used for continuous basic load methane production in a CSTR while the liquid fraction is stored and fed to an AFR on demand [87].

Two-stage high-solid AD systems can further be operated as TPAD systems by combining reactors with different process temperature as described in Sect. 3.1.2. A thermophilic hydrolysis/acidogenesis stage can further enhance the rate-limiting hydrolysis step for digestion of lignocellulosic biomass. Despite numerous advantages, the number of commercially operated two-stage AD systems is low and rather limited to liquid or low solids content AD systems [82]. The main reason is presumably the higher expenditure for construction and operation, accompanied by higher costs for investment, operation and maintenance [20]. Furthermore, the exact separation of hydrolysis and methanogenesis is difficult to maintain in large scale [88].

3.2.3 Novel Reactor Concepts for High-Solid Anaerobic Digestion

Advanced reactor concepts for high-solid AD are comparatively scarce. Developments aim at efficient and easily manageable systems that are robust despite the high solids input. Some novel approaches are described below.

The **Half-submerged Integrated Two-phase (HIT) reactor** system separates the hydrolysis/acidogenesis and acetogenesis/methanogenesis stages within one reactor [76]. It consists of a slowly rotating (3–30 rpm) perforated roller in the reactor head, which is half-submerged in a lower methanogenic liquid zone [76]. Solid biomass is fed batch-wise to the roller for hydrolysis. Organic acids and other

intermediates of the hydrolysis diffuse into the liquid zone. An inner recycling system further pumps the hydrolysate from the top to the bottom of the liquid zone in order to prevent VFA accumulation and enhance mass transfer. The methanogenic unit is filled with granular sludge for efficient methane production. The HIT reactor system has been successfully applied to biogas production from a mixture of wheat straw and fruit/vegetable waste (Table 2). An advantage of this system over traditional two-stage systems might be the improved mass transfer and syntrophic interaction [76]. However, similar to other batch systems, operation of the HIT reactor results in fluctuating gas production.

The **U**p-flow **A**naerobic **S**olid-**S**tate reactor (**UASS**) is a continuously fed vertical reactor, which is operated on the basis of a spontaneous solid-liquid separation due to differences in densities [78]. Solid biomass is fed to the bottom of the reactor filled with liquid inoculum, and solid digestate is withdrawn at the top of the reactor. Produced microgas bubbles, which adhere to solid biomass particles, promote the ascent of the feedstock in the liquor and the formation of a solid-state bed [77]. Thus, the reactor is divided into three different zones; a lower and an upper liquid zone at the bottom and head of the reactor, and the solid-state bed in between. A perforated layer below the liquid surface in the reactor head keeps the solid-state bed in the liquor. The liquid phase is recirculated from the top to the bottom and distributes microorganisms within the reactor. An AFR can be connected to the UASS for conversion of metabolites such as organic acids, which are enriched in the liquid medium. The UASS combined with an AFR cascade was tested for digestion of a mixture of maize silage and barley straw with an OLR up to 17 kg_{VS} m^{-3} d^{-1}; the methanogenic performance which was amongst the highest reported for solid biomass thus far (Table 2) [77]. This system provides high process efficiency at a low parasitic energy consumption and a comparatively simple operation and management [9, 78]. Yet, it is not suitable for digestion of colloidal substrates as this might result in compaction and clogging of the solid-state bed [77]. Up-scaling of the UASS system is still to be implemented.

The **F**loating **B**ed **R**eactor (**FBR**) is a horizontal, continuously fed leach bed reactor, which is especially suitable for digestion of stalky biomass [79]. Added solid biomass naturally floats on top of a liquid phase inside the reactor and forms a floating bed. The floating bed provides favorable conditions for microorganisms of the anaerobic digestion process as microbial communities can grow on the fibrous material and form biofilms, which protect sensitive methanogens from environmental changes. The liquid is periodically pumped from the bottom of the digester and sprinkled over the floating bed. This results in a gentle mixing and moistening of the floating bed, and makes nutrients available to the microorganisms. Due to the natural separation of the solid and liquid phases within the reactor, the liquid phase can be easily withdrawn and sent to a connected AFR for efficient methane production from organic acids and other intermediates, which accumulate in the liquid.

The FBR connected to an AFR has been stably operated with high methane yields from maize silage and a mixture of grass and foliage silage at an OLR of 4.5 and 5.5 kg_{VS} m^{-3} d^{-1}, respectively (Table 2) [79, 89]. This system was further

shown to be suitable for demand-driven biogas production, at which a change in methane production by 50–60% per day was achieved through variable loading [79]. Advances of this system are its high reliability and robustness against inhibitors or environmental changes, its low energy input and absence of internal mixing devices. No recirculation of solid digestate is necessary. However, a precondition for successful application of the FBR system is the characteristic of the solid feedstock to form a stable floating bed. Suitability of the system for the anaerobic digestion of different solid feedstocks still needs to be investigated and proven.

A **Two-stage Pressurized Anaerobic Digestion System** is proposed for simultaneous biogas production, biogas upgrading and compression, which can significantly reduce expenditure for subsequent injection of biomethane into the gas grid as natural gas substitute or its use as biofuel for transportation [80, 81, 90]. A sequencing leach bed reactor for hydrolysis/acidogenesis is coupled with a pressurized AFR for acetogenesis/methanogenesis [80]. Elevated pressure inside the AFR is auto-generated by the produced biogas, which is retained within the reactor until the desired pressure is reached. The elevated pressure results in an intensified solution of CO_2 in the liquid phase while less soluble methane remains in the gas phase. Pressurization of the AFR up to 50 bar has been successfully tested which resulted in an increase in methane content of the produced biogas up to 90% (Table 2) [81]. The main challenge for operation of the methanogenic reactor under high pressure is a reduction in pH as a result of formation of carbonic acid from dissolved CO_2. Thus, the pH value drops below the optimum pH range for methanogenesis, which can reduce the process efficiency and counteract the high solubility of CO_2. An effective method to maintain the pH level in the pressurized AFR still needs to be developed [81].

3.3 Bioreactors for Biological Methanation of Gases

Besides the biomethanation of liquid and solid biomass, the biological conversion of CO_2 and H_2 to methane has recently received attention. Biological methanation of these gases can be integrated into Power-to-Gas process chains where H_2 is produced by electrolysis of water, preferably using surplus energy from renewable sources (e.g. excess wind energy), and is thereafter combined with CO_2 to produce methane, which can be injected into the natural gas grid or be used as biofuel for transportation [91]. CO_2 and H_2 are converted into methane and water by hydrogenotrophic methanogens [17], strictly anaerobic microbes that are involved in the last step of the AD process (Fig. 1).

The technical implementation of the biological methanation of CO_2 and H_2 is currently under development. In general, this process can take place directly within an existing biogas plant (in situ) or in an external reactor (ex situ). The ex situ process is more flexible in terms of the use of variable CO_2 sources and the

adaptability of the process design to the requirements of the hydrogenotrophic methanogens [92]. CSTRs have been applied for in situ and ex situ biological methanation of the gases. Increased partial pressure of H_2 following H_2 injection into the biogas plant in the "in situ" process can lead to process inhibition [93]. However, existing reactor systems can be used and the methane content of the biogas can be enriched. High methane formation rates, i.e. 1.4–28.7 m^3 CH_4 m^{-3} h^{-1}, can be reached in ex situ CSTRs, but this is accompanied by a wide range of methane contents in the output gas [94–96]. AFRs have been shown to be suitable for ex situ biological methanation of CO_2 and H_2. Immobilization of active biomass on carrier materials enables the development of specialized microbes that are optimally adapted to the gaseous feedstocks [93]. Methane formation rates of up to 0.26 m^3 CH_4 m^{-3} h^{-1} and methane contents of up to 90% were reached in a reactor system with two AFRs in series filled with vermiculite shales and granular perlite as packing material [97]. Burkhardt et al. [98] developed a **Trickle Bed Reactor** (**TBR**), which is based on the AFR system but minimizes the liquid phase. Process liquid is kept below the fixed bed and is sprinkled over the biofilm carriers. High concentration gradients and short diffusion paths in the biofilm improve mass transfer and the productivity of this system [98]. The TBR can produce output gas with high product quality of 98% methane. A methane formation rate of 0.06–0.64 m^3 CH_4 m^{-3} h^{-1} is achieved with this reactor concept [98, 99].

Another bioreactor configuration with a reduced liquid and increased gas phase is the **Biofilm Plug-flow Reactor** proposed by Savvas et al. [100]. This reactor consists of a horizontally arranged tube with a very high ratio of length to diameter of 54, which is filled with biofilm carriers. The biofilm is wetted in short intervals by adding small amounts of liquid media. The liquid is transported through the tube by the gas flow as short discs due to adhesion effects caused by the small tube diameter (13 mm) [100]. The biofilm plug-flow reactor enables an intense gas-liquid surface contact and long retention time of the gas within the reactor due to the special geometry at a low parasitic energy demand. Methane formation rates of up to 1.67 m^3 CH_4 m^{-3} h^{-1} were measured [100].

Since the methanation reaction takes place in the liquid phase and H_2 has poor solubility, namely 23 times less than CO_2 [92], the gas-liquid mass transfer and availability of H_2 to the microorganisms is the major bottleneck for the increase of productivity for all applied reactor concepts. Intensified mechanical agitation in CSTRs has been mainly applied as a means to enhance the mass transfer [92, 96], however, intensive stirring requires high energy input. In addition the effects of reactor geometry, shaking of the reactor, the use of hollow membrane diffuser for gas supply, recirculation of gas and active biomass, and pressurization of reactors were investigated (e.g. [93, 94, 96, 101, 102]). A major challenge lies in the up-scaling of the developed reactor systems and technologies to commercial scale, at which energy requirements for gas-liquid mass transfer enhancement and maintenance efforts need to be considered.

4 Conclusions

Biogas production through anaerobic digestion is unique in that it can efficiently convert a considerable variety of feedstocks, thus, allowing for simultaneous biofuel supply and treatment of wastewaters or solid wastes, or the utilization of biomasses and CO_2 streams. Continuously stirred reactors, a technique that is simple, reliable and versatile but limited in loading rate depending on feedstock, are the widespread conversion technology. However, a large choice of other bioreactor configurations suitable for different types of feedstocks exists. The application of feedstock-adapted reactor systems can considerably enhance conversion efficiency although each of these systems has special advantages and disadvantages. Continued progress in reactor development and implementation of new technologies will further improve methane formation, biomass conversion and process stability and flexibility, and will make anaerobic digestion more cost-effective in the future. Furthermore, an ongoing advancement in identification and understanding of the microbial community and interplay can aid in the development of improved prospective digestion technologies.

References

1. Gallert C, Winter J, Svardal K (2015) Grundlagen anaerober Prozesse. In: Rosenwinkel KH, Kroiss H, Dichtl N, Seyfried CF, Weiland P (eds) Anaerobtechnik, 3rd edn. Springer Vieweg, Berlin Heidelberg, Germany, pp 19–79
2. Karthikeyan OP, Visvanathan C (2013) Bio-energy recovery from high-solid organic substrates by dry anaerobic bio-conversion processes: a review. Rev Environ Sci Biotechnol 12(3):257–284
3. Weiland P (2001) Grundlagen der Methangärung - Biologie and Substrate. VDI-Tagung "Biogas als regenerative Energie—Stand and Perspektiven". VDI-Berichte Nr. 1620, Hannover, Germany, 19–20 June 2001, pp 19–32
4. Yu Z, Morrison M, Schanbacher FL (2010) Production and utilization of methane biogas as renewable fuel. In: Vertés AA, Qureshi N, Blaschek HP, Yukawa H (eds) Biomass to biofuels: strategies for global industries. Wiley, Chichester, United Kingdom, pp 403–433
5. Weiland P (2010) Biogas production: current state and perspectives. Appl Microbiol Biotechnol 85(4):849–860
6. Rivière D, Desvignes V, Pelletier E, Chaussonnerie S, Guermazi S, Weissenbach J, Li T, Camacho P, Sghir A (2009) Towards the definition of a core of microorganisms involved in anaerobic digestion of sludge. ISME J 3(6):700–714
7. Theuerl S, Kohrs F, Benndorf D, Maus I, Wibberg D, Schlüter A, Kausmann R, Heiermann M, Rapp E, Reichl U, Pühler A, Klocke M (2015) Community shifts in a well-operating agricultural biogas plant: how process variations are handled by the microbiome. Appl Microbiol Biotechnol 99(18):7791–7803
8. Carballa M, Regueiro L, Lema JM (2015) Microbial management of anaerobic digestion: exploiting the microbiome-functionality nexus. Curr Opin Biotechnol 33:103–111
9. Mao C, Feng Y, Wang X, Ren G (2015) Review on research achievements of biogas from anaerobic digestion. Renew Sustain Energy Rev 45:540–555
10. Ge X, Xu F, Li Y (2016) Solid-state anaerobic digestion of lignocellulosic biomass: recent progress and perspectives. Bioresour Technol 205:239–249

11. Lv W, Schanbacher FL, Yu Z (2010) Putting microbes to work in sequence: recent advances in temperature-phased anaerobic digestion processes. Bioresour Technol 101(24):9409–9414

12. Angelidaki I, Ahring BK (1994) Anaerobic thermophilic digestion of manure at different ammonia loads: effect of temperature. Water Res 28(3):727–731

13. Dhaked RK, Singh P, Singh L (2010) Biomethanation under psychrophilic conditions. Waste Manage 30(12):2490–2496

14. Lee M, Hidaka T, Tsuno H (2009) Two-phased hyperthermophilic anaerobic co-digestion of waste activated sludge with kitchen garbage. J Biosci Bioeng 108(5):408–413

15. Nges IA, Wang B, Cui Z, Liu J (2015) Digestate liquor recycle in minimal nutrients-supplemented anaerobic digestion of wheat straw. Biochem Eng J 94:106–114

16. Barber WP, Stuckey DC (1999) The use of the anaerobic baffled reactor (ABR) for wastewater treatment: a review. Water Res 33(7):1559–1578

17. Jacob Guneratnam A, Ahern E, Fitzgerald J, Jackson S, Xia A, Dobson A, Murphy JD (2017) Study of the performance of a thermophilic biological methanation system. Bioresour Technol 225:308–315

18. Sawatdeenarunat C, Surendra KC, Takara D, Oechsner H, Khanal SK (2015) Anaerobic digestion of lignocellulosic biomass: challenges and opportunities. Bioresour Technol 178:178–186

19. Brown D, Shi J, Li Y (2012) Comparison of solid-state to liquid anaerobic digestion of lignocellulosic feedstocks for biogas production. Bioresour Technol 124:379–386

20. Fagbohungbe MO, Dodd IC, Herbert BMJ, Li H, Ricketts L, Semple KT (2015) High solid anaerobic digestion: operational challenges and possibilities. Environ Technol Innov 4:268–284

21. Hinken L, Austermann-Haun U, Meyer H, Urban I (2015) Anaerobe Abwasserbehandlung zur Kohlenstoffelimination. In: Rosenwinkel KH, Kroiss H, Dichtl N, Seyfried CF, Weiland P (eds) Anaerobtechnik, 3rd edn. Springer Vieweg, Berlin Heidelberg, Germany, pp 283–356

22. Cavinato C, Bolzonella D, Pavan P, Fatone F, Cecchi F (2013) Mesophilic and thermophilic anaerobic co-digestion of waste activated sludge and source sorted biowaste in pilot- and full-scale reactors. Renew Energy 55:260–265

23. Gemmeke B, Rieger C, Weiland P (2009) Biogas-Messprogramm II. 61 Biogasanlagen im Vergleich. Fachagentur Nachwachsende Rohstoffe e.V. (FNR), Gülzow, Germany

24. Hamdi M, Garcia JL (1991) Comparison between anaerobic filter and anaerobic contact process for fermented olive mill wastewaters. Bioresour Technol 38(1):23–29

25. Şentürk E, İnce M, Onkal Engin G (2010) Kinetic evaluation and performance of a mesophilic anaerobic contact reactor treating medium-strength food-processing wastewater. Bioresour Technol 101(11):3970–3977

26. Shao X, Peng D, Teng Z, Ju X (2008) Treatment of brewery wastewater using anaerobic sequencing batch reactor (ASBR). Bioresour Technol 99(8):3182–3186

27. Timur H, Özturk I (1999) Anaerobic sequencing batch reactor treatment of landfill leachate. Water Res 33(15):3225–3230

28. España-Gamboa EI, Mijangos-Cortés JO, Hernández-Zárate G, Maldonado JAD, Alzate-Gaviria LM (2012) Methane production by treating vinasses from hydrous ethanol using a modified UASB reactor. Biotechnol Biofuels 5(1):82–91

29. Tartakovsky B, Lebrun FM, Guiot SR (2015) High-rate biomethane production from microalgal biomass in a UASB reactor. Algal Res 7:86–91

30. Liu J, Zhong J, Wang Y, Liu Q, Qian G, Zhong L, Guo R, Zhang P, Xu ZP (2010) Effective bio-treatment of fresh leachate from pretreated municipal solid waste in an expanded granular sludge bed bioreactor. Bioresour Technol 101(5):1447–1452

31. Luo G, Li J, Li Y, Wang Z, Li WT, Li AM (2016) Performance, kinetics behaviors and microbial community of internal circulation anaerobic reactor treating wastewater with high organic loading rate: role of external hydraulic circulation. Bioresour Technol 222:470–477

32. Wang J, Xu W, Yan J, Yu J (2014) Study on the flow characteristics and the wastewater treatment performance in modified internal circulation reactor. Chemosphere 117:631–637

33. Pirsaheb M, Rostamifar M, Mansouri AM, Zinatizadeh AAL, Sharafi K (2015) Performance of an anaerobic baffled reactor (ABR) treating high strength baker's yeast manufacturing wastewater. J Taiwan Inst Chem Eng 47:137–148

34. Bodkhe SY (2009) A modified anaerobic baffled reactor for municipal wastewater treatment. J Environ Manage 90(8):2488–2493

35. Sanchez E, Montalvo S, Travieso L, Rodriguez X (1995) Anaerobic digestion of sewage sludge in an anaerobic fixed bed digester. Biomass Bioenergy 9(6):493–495

36. Omil F, Garrido JM, Arrojo B, Méndez R (2003) Anaerobic filter reactor performance for the treatment of complex dairy wastewater at industrial scale. Water Res 37(17):4099–4108

37. Fernández N, Montalvo S, Borja R, Guerrero L, Sánchez E, Cortés I, Colmenarejo MF, Travieso L, Raposo F (2008) Performance evaluation of an anaerobic fluidized bed reactor with natural zeolite as support material when treating high-strength distillery wastewater. Renew Energy 33(11):2458–2466

38. Wang Z, Kim M, Nakhla G, Zhu J (2016) Anaerobic fluidized bed digestion of primary and thickened waste activated sludges. Chem Eng J 284:620–629

39. Demirer GN, Chen S (2005) Two-phase anaerobic digestion of unscreened dairy manure. Process Biochem 40(11):3542–3549

40. Aslanzadeh S, Rajendran K, Taherzadeh MJ (2014) A comparative study between single- and two-stage anaerobic digestion processes: effects of organic loading rate and hydraulic retention time. Int Biodeterior Biodegrad 95:181–188

41. Wijekoon KC, Visvanathan C, Abeynayaka A (2011) Effect of organic loading rate on VFA production, organic matter removal and microbial activity of a two-stage thermophilic anaerobic membrane bioreactor. Bioresour Technol 102(9):5353–5360

42. Mei X, Wang Z, Miao Y, Wu Z (2017) A pilot-scale anaerobic membrane bioreactor under short hydraulic retention time for municipal wastewater treatment: performance and microbial community identification. J Water Reuse Desalin (in press)

43. Sunil Kumar G, Gupta SK, Singh G (2007) Biodegradation of distillery spent wash in anaerobic hybrid reactor. Water Res 41(4):721–730

44. Azbar N, Tutuk F, Keskin T (2009) Biodegradation performance of an anaerobic hybrid reactor treating olive mill effluent under various organic loading rates. Int Biodeterior Biodegrad 63(6):690–698

45. Chen X, Dai R, Ni S, Luo Y, Ma P, Xiang X, Li G (2016) Super-high-rate performance and its mechanisms of a spiral symmetry stream anaerobic bioreactor. Chem Eng J 295:237–244

46. Terboven C, Ramm P, Herrmann C (2017) Demand-driven biogas production from sugar beet silage in a novel fixed bed disc reactor under mesophilic and thermophilic conditions. Bioresour Technol 241:582–592

47. Liu W, Cai W, Guo Z, Wang L, Yang C, Varrone C, Wang A (2016) Microbial electrolysis contribution to anaerobic digestion of waste activated sludge, leading to accelerated methane production. Renew Energy 91:334–339

48. Tartakovsky B, Mehta P, Bourque JS, Guiot SR (2011) Electrolysis-enhanced anaerobic digestion of wastewater. Bioresour Technol 102(10):5685–5691

49. Murphy JD, Thamsiriroj T (2013) Fundamental science and engineering of the anaerobic digestion process for biogas production. In: Wellinger A, Murphy J, Baxter D (eds) The biogas handbook. Woodhead Publishing, pp 104–130

50. Ramm P, Jost C, Neitmann E, Sohling U, Menhorn O, Weinberger K, Mumme J, Linke B (2014) Magnetic biofilm carriers: the use of novel magnetic foam glass particles in anaerobic digestion of sugar beet silage. J Renew Energy 10:68–78

51. Morgenroth E, Wilderer PA (1998) Sequencing batch reactor technology: concepts, design and experiences (Abridged). Water Environ J 12(5):314–320

52. Shizas I, Bagley DM (2002) Improving anaerobic sequencing batch reactor performance by modifying operational parameters. Water Res 36(1):363–367

53. Zaiat M, Rodrigues JAD, Ratusznei SM, de Camargo EFM, Borzani W (2001) Anaerobic sequencing batch reactors for wastewater treatment: a developing technology. Appl Microbiol Biotechnol 55(1):29–35

54. Tiwari MK, Guha S, Harendranath CS, Tripathi S (2006) Influence of extrinsic factors on granulation in UASB reactor. Appl Microbiol Biotechnol 71(2):145–154

55. Rajeshwari KV, Balakrishnan M, Kansal A, Lata K, Kishore VVN (2000) State-of-the-art of anaerobic digestion technology for industrial wastewater treatment. Renew Sustain Energy Rev 4(2):135–156

56. Langer S, Schropp D, Bengelsdorf FR, Othman M, Kazda M (2014) Dynamics of biofilm formation during anaerobic digestion of organic waste. Anaerobe 29:44–51

57. Budzianowski WM (2016) A review of potential innovations for production, conditioning and utilization of biogas with multiple-criteria assessment. Renew Sustain Energy Rev 54:1148–1171

58. Demirel B, Yenigün O (2002) Two-phase anaerobic digestion processes: a review. J Chem Technol Biotechnol 77(7):743–755

59. Lindner J, Zielonka S, Oechsner H, Lemmer A (2016) Is the continuous two-stage anaerobic digestion process well suited for all substrates? Bioresour Technol 200:470–476

60. Lin H, Peng W, Zhang M, Chen J, Hong H, Zhang Y (2013) A review on anaerobic membrane bioreactors: applications, membrane fouling and future perspectives. Desalination 314:169–188

61. Ramakrishnan A, Surampalli RY (2013) Performance of anaerobic hybrid reactors for the treatment of complex phenolic wastewaters with biogas recirculation. Bioresour Technol 129:26–32

62. Buyukkamaci N, Filibeli A (2004) Volatile fatty acid formation in an anaerobic hybrid reactor. Process Biochem 39(11):1491–1494

63. O'Shea R, Kilgallon I, Wall D, Murphy JD (2016) Quantification and location of a renewable gas industry based on digestion of wastes in Ireland. Appl Energy 175:229–239

64. Geppert F, Liu D, van Eerten-Jansen M, Weidner E, Buisman C, ter Heijne A (2016) Bioelectrochemical power-to-gas: state of the art and future perspectives. Trends Biotechnol 34(11):879–894

65. Bo T, Zhu X, Zhang L, Tao Y, He X, Li D, Yan Z (2014) A new upgraded biogas production process: coupling microbial electrolysis cell and anaerobic digestion in single-chamber, barrel-shape stainless steel reactor. Electrochem Commun 45:67–70

66. De Vrieze J, Gildemyn S, Arends JBA, Vanwonterghem I, Verbeken K, Boon N, Verstraete W, Tyson GW, Hennebel T, Rabaey K (2014) Biomass retention on electrodes rather than electrical current enhances stability in anaerobic digestion. Water Res 54: 211–221

67. Cai W, Han T, Guo Z, Varrone C, Wang A, Liu W (2016) Methane production enhancement by an independent cathode in integrated anaerobic reactor with microbial electrolysis. Bioresour Technol 208:13–18

68. Abbassi-Guendouz A, Brockmann D, Trably E, Dumas C, Delgenès JP, Steyer JP, Escudié R (2012) Total solids content drives high solid anaerobic digestion via mass transfer limitation. Bioresour Technol 111:55–61

69. Fernández J, Pérez M, Romero LI (2010) Kinetics of mesophilic anaerobic digestion of the organic fraction of municipal solid waste: influence of initial total solid concentration. Bioresour Technol 101(16):6322–6328

70. Le Hyaric R, Benbelkacem H, Bollon J, Bayard R, Escudié R, Buffière P (2012) Influence of moisture content on the specific methanogenic activity of dry mesophilic municipal solid waste digestate. J Chem Technol Biot 87(7):1032–1035

71. Bollon J, Benbelkacem H, Gourdon R, Buffière P (2013) Measurement of diffusion coefficients in dry anaerobic digestion media. Chem Eng Sci 89:115–119

72. Motte JC, Escudié R, Bernet N, Delgenes JP, Steyer JP, Dumas C (2013) Dynamic effect of total solid content, low substrate/inoculum ratio and particle size on solid-state anaerobic digestion. Bioresour Technol 144:141–148

73. Kusch S, Oechsner H, Jungbluth T (2008) Biogas production with horse dung in solid-phase digestion systems. Bioresour Technol 99(5):1280–1292

74. Patinvoh RJ, Kalantar Mehrjerdi A, Sárvári Horváth I, Taherzadeh MJ (2017) Dry fermentation of manure with straw in continuous plug flow reactor: reactor development and process stability at different loading rates. Bioresour Technol 224:197–205

75. Lehtomäki A, Huttunen S, Lehtinen TM, Rintala JA (2008) Anaerobic digestion of grass silage in batch leach bed processes for methane production. Bioresour Technol 99(8): 3267–3278

76. Xing W, Chen X, Zuo J, Wang C, Lin J, Wang K (2014) A half-submerged integrated two-phase anaerobic reactor for agricultural solid waste codigestion. Biochem Eng J 88: 19–25

77. Mumme J, Linke B, Tölle R (2010) Novel upflow anaerobic solid-state (UASS) reactor. Bioresour Technol 101(2):592–599

78. Pohl M, Mumme J, Heeg K, Nettmann E (2012) Thermo- and mesophilic anaerobic digestion of wheat straw by the upflow anaerobic solid-state (UASS) process. Bioresour Technol 124:321–327

79. Linke B, Rodríguez-Abalde Á, Jost C, Krieg A (2015) Performance of a novel two-phase continuously fed leach bed reactor for demand-based biogas production from maize silage. Bioresour Technol 177:34–40

80. Chen Y, Rößler B, Zielonka S, Lemmer A, Wonneberger AM, Jungbluth T (2014) The pressure effects on two-phase anaerobic digestion. Appl Energy 116:409–415

81. Merkle W, Baer K, Lindner J, Zielonka S, Ortloff F, Graf F, Kolb T, Jungbluth T, Lemmer A (2017) Influence of pressures up to 50 bar on two-stage anaerobic digestion. Bioresour Technol 232:72–78

82. Weiland P, Fricke K, Heußner C, Hüttner A, Turk T (2015) Anlagen zur Erzeugung von Bioenergie. In: Rosenwinkel KH, Kroiss H, Dichtl N, Seyfried CF, Weiland P (eds) Anaerobtechnik, 3rd edn. Springer Vieweg, Berlin Heidelberg, Germany, pp 603–740

83. Wall D, Allen E, O'Shea R, O'Kiely P, Murphy JD (2016) Investigating two-phase digestion of grass silage for demand-driven biogas applications: effect of particle size and rumen fluid addition. Renew Energy 86:1215–1223

84. Browne JD, Allen E, Murphy JD (2013) Improving hydrolysis of food waste in a leach bed reactor. Waste Manage 33(11):2470–2477

85. Meng Y, Jost C, Mumme J, Wang K, Linke B (2016) An analysis of single and two stage, mesophilic and thermophilic high rate systems for anaerobic digestion of corn stalk. Chem Eng J 288:79–86

86. Nizami AS, Murphy JD (2011) Optimizing the operation of a two-phase anaerobic digestion system digesting grass silage. Environ Sci Technol 45(17):7561–7569

87. Hahn H, Krautkremer B, Hartmann K, Wachendorf M (2014) Review of concepts for a demand-driven biogas supply for flexible power generation. Renew Sustain Energy Rev 29:383–393

88. Zielonka S, Lemmer A, Oechsner H, Jungbluth T (2009) Vergärung von Grassilage in einer zwei-phasigen prozessführung. Bornimer Agrartechnische Ber 68:140–152

89. Terboven C, Herrmann C, Lehmann M, Weckenmann J (2017) Biogasgewinnung aus Herbstlaub – Methanpotenziale und verfahrenstechnische Ansätze zur Prozessoptimierung. In: Biogas in der Landwirtschaft - Stand und Perspektiven, FNR/KTBL congress, Bayreuth, Germany, 26–27 September 2017

90. Lemmer A, Chen Y, Wonneberger AM, Graf F, Reimert R (2015) Integration of a water scrubbing technique and two-stage pressurized anaerobic digestion in one process. Energies 8(3):2048–2065

91. Persson T, Murphy J, Jannasch AK, Ahern E, Liebetrau J, Trommler M, Toyama J (2014) A perspective on the potential role of biogas in smart energy grids. IEA Bioenergy, Technical brochure, 27 p

92. Götz M, Lefebvre J, Mörs F, McDaniel Koch A, Graf F, Bajohr S, Reimert R, Kolb T (2016) Renewable power-to-gas: a technological and economic review. Renew Energy 85: 1371–1390
93. Lecker B, Illi L, Lemmer A, Oechsner H (2017) Biological hydrogen methanation—a review. Bioresour Technol 245:1220–1228
94. Martin MR, Fornero JJ, Stark R, Mets L, Angenen LT (2013) A Single-culture bioprocess of *Methanothermobacter thermautotrophicus* to upgrade digester biogas by CO_2-to-CH_4 conversion with H_2. Archaea 2013:11 p, Article ID 157529
95. Nishimura N, Kitaura S, Mimura A, Takahara Y (1992) Cultivation of thermophilic methanogen KN-15 on H_2-CO_2 under pressurized conditions. J Ferment Bioeng 73(6): 477–480
96. Seifert AH, Rittmann S, Herwig C (2014) Analysis of process related factors to increase volumetric productivity and quality of biomethane with methanothermobacter marburgensis. Appl Energy 132:155–162
97. Alitalo A, Niskanen M, Aura E (2015) Biocatalytic methanation of hydrogen and carbon dioxide in a fixed bed bioreactor. Bioresour Technol 196:600–605
98. Burkhardt M, Koschack T, Busch G (2015) Biocatalytic methanation of hydrogen and carbon dioxide in an anaerobic three-phase system. Bioresour Technol 178:330–333
99. Strübing D, Huber B, Lebuhn M, Drewes JE, Koch K (2017) High performance biological methanation in a thermophilic anaerobic trickle bed reactor. Bioresour Technol 245: 1176–1183
100. Savvas S, Donnelly J, Patterson T, Chong ZS, Esteves SR (2017) Biological methanation of CO_2 in a novel biofilm plug-flow reactor: a high rate and low parasitic energy process. Appl Energy 202:238–247
101. Luo G, Angelidaki I (2013) Hollow fiber membrane based H_2 diffusion for efficient in situ biogas upgrading in an anaerobic reactor. Appl Microbiol Biotechnol 97(8):3739–3744
102. Luo G, Johansson S, Boe K, Xie L, Zhou Q, Angelidaki I (2012) Simultaneous hydrogen utilization and in situ biogas upgrading in an anaerobic reactor. Biotechnol Bioeng 109(4):1088–1094

Chapter 6
Basics of Bio-hydrogen Production by Dark Fermentation

Javiera Toledo-Alarcón, Gabriel Capson-Tojo, Antonella Marone, Florian Paillet, Antônio Djalma Nunes Ferraz Júnior, Lucile Chatellard, Nicolas Bernet and Eric Trably

1 Introduction

In the recent years, a growing awareness of the environmental damage caused by the use of fossil fuels has arisen. It is well admitted that fossil fuels contribute to climate change and that their production and consumption are associated with the generation of large amounts of non-biodegradable wastes. These issues have led to a growing interest of the scientific community to seek alternative renewable energy sources. In this context, hydrogen is considered to be one of the most promising alternative fuels for the future. Other than generating only water during its combustion, its high energetic value of 120 MJ kg^{-1} (more than twice that of common natural gas or gasoline) makes this gas a cleaner and competitive alternative to common fossil fuels [1]. When compared to other energy sources and in particular those producing electricity, hydrogen presents the main advantages of being storable and generated from various renewable sources i.e., by using the surplus of electricity of wind turbines or solar panels [2]. Different scenarios of hydrogen-based energy systems have been proposed so far and, in all cases, hydrogen will supply energy for diverse applications, such as industrial, commer-

J. Toledo-Alarcón · G. Capson-Tojo · A. Marone · A. D. N. F. Júnior · L. Chatellard
N. Bernet · E. Trably (✉)
LBE, INRA, Univ Montpellier, 102 Avenue Des Etangs, 11100 Narbonne, France
e-mail: eric.trably@inra.fr

G. Capson-Tojo · F. Paillet
CIRSEE, Suez, 38 Rue Du Président Wilson, 78230 Le Pecq, France

F. Paillet
TRIFYL, Route de Sieurac, 81300 Labessiere-Candeil, France

A. D. N. F. Júnior
Brazilian Bioethanol Science and Technology Laboratory (CTBE), Brazilian
Center for Research in Energy and Materials (CNPEM), Rua Giuseppe Máximo Scolfaro,
10.000, Polo II de Alta Tecnologia, 6170, 13083-970 Campinas, São Paulo, Brazil

cial, residential or transportation activities [3]. In particular, H_2-based electro-mobility is expected to gradually replace the use of fossil fuels and special efforts will be made on renewable H_2, so-called green hydrogen.

Currently about 96% of all the hydrogen produced worldwide is based on chemical processes that use fossil materials as raw materials [4]. To stand as an environmental-friendly and renewable alternative, hydrogen must be produced using sustainable processes, such as physico-chemical techniques (e.g. water electrolysis, biomass gasification or solar thermo-chemical processes) or biological processes. These latter are based on the biological capability of some microorganisms to produce hydrogen gas by the degradation of organic matter, as found in Nature. In addition to the production of clean hydrogen, these processes can be used to treat organic wastes, converting them into more valuable products. This is the case of dark fermentation (DF), a fermentation process in which microorganisms degrade complex organic matter to simpler molecules and simultaneously generate hydrogen. The added-value co-products are mainly composed of volatile fatty acids (e.g. acetate and butyrate), other organic acids (e.g. lactate) and organic solvents (e.g. ethanol). All of these are valuable chemicals that are also used in the chemical industry. Therefore, DF appears as a promising technology that can be included in the concepts of environmental biorefinery and circular economy, where organic residues are not anymore considered as a waste but as a resource. Moreover, more than 220 billion tons of agricultural organic waste accumulate per year because of intensive agricultural production that constitute one of the most abundant renewable sources for producing H_2 by DF [5].

This chapter aims to describe the main aspects of the production of hydrogen by DF, including the bases of the microbial metabolism involved, the main operational parameters affecting the process and the different substrates that DF can accommodate. The integration of DF within the concept of environmental biorefinery will also be discussed. Finally, the current situation of hydrogen as fuel and its potential implications for the future energy systems are also assessed.

2 Dark Fermentation Microbiology and Metabolisms

Production of dark fermentative hydrogen is a ubiquitous phenomenon that occurs in most of anaerobic natural environments. It consists in an obligate cascade of reduction-oxidation (redox) reactions that must be kept in balance. Although these reactions are mostly thermodynamically favorable and spontaneous, they are also constrained by biological regulations within microorganisms and by interspecies interactions in microbial communities [6].

Dark fermentation can involve any type of organic molecules, being glucose the most common substrate investigated in literature. Many biological pathways have been proposed using glucose as model substrate (Fig. 1). The hydrogen production is a natural response of the cellular need for releasing the excess of electrons and is always coupled with volatile fatty acids and/or alcohols production. The most

common co-products in the glucose fermentation are acetate, butyrate, and formate. The hydrogen–acetate couple produces more ATP per mol of substrate than alcohols such as ethanol and butanol and is therefore the energetically "preferred" bacterial fermentation product from sugars [7]. The stoichiometric yields are 4 mol of hydrogen for each mole of glucose when acetic acid is the co-product [8] and 2 mol of hydrogen if butyric acid is produced [9–11]. In practice, the hydrogen yields are within the range of 10–20% of COD [12], which is equivalent to 1.17–2.34 mol H_2 mol glucose^{-1} [13–15]. Indeed, each molecule of glucose can potentially produce 4 mol of hydrogen if no biomass production is considered. However, the fermentation process naturally implies maximizing the cell growth and not the hydrogen production and thus the maximum hydrogen yield is rarely achieved in practice, especially with mixed microbial cultures [10, 14]. In any case, glucose is first converted into pyruvate, producing adenosine triphosphate (ATP) from adenosine diphosphate (ADP) and the reduced form of nicotinamide adenine dinucleotide (NADH) via the glycolytic pathway. Pyruvate is then converted to acetyl coenzyme A (acetyl-CoA) and carbon dioxide by pyruvate–ferredoxin oxidoreductase (PFOR) (Fig. 1b), when strict anaerobes break down glucose.
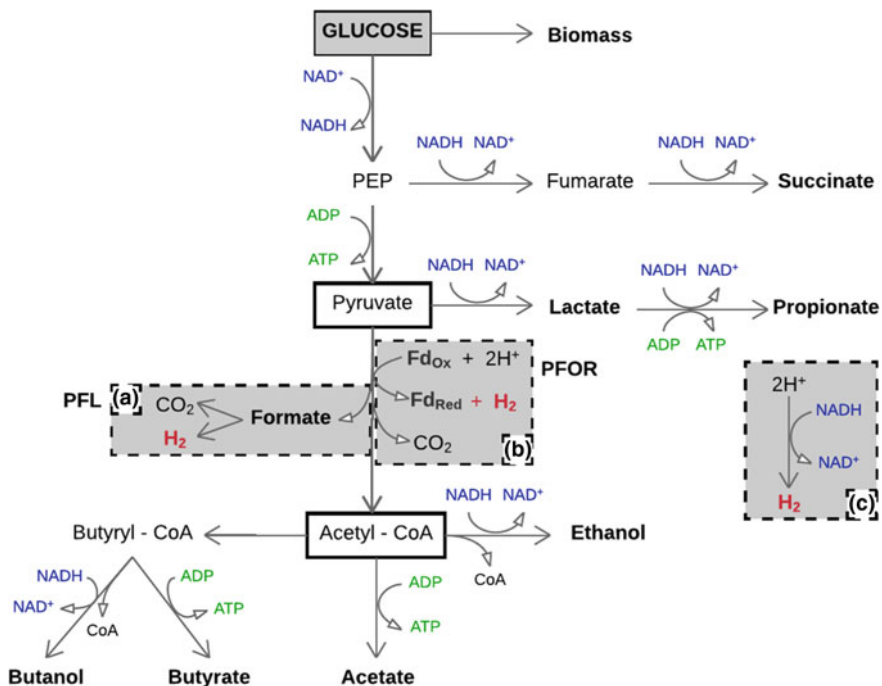
Fig. 1 Pathways for hydrogen production by dark fermentation from glucose under anaerobic conditions using mixed cultures; **a** Pyruvate formate lyase (PFL) is the common pathway in facultative anaerobes; **b** Pyruvate-ferredoxin oxidoreductase (PFOR) is the common pathway in strict anaerobes; **c** Additional hydrogen-production by hydrogenases at low hydrogen partial pressure (<60 Pa). (Adapted from [11, 16])

In contrast, facultative anaerobes convert pyruvate to acetyl-CoA and formate by pyruvate formate lyase (PFL) (Fig. 1a). In both cases acetyl-CoA is finally converted into acetate, butyrate, or ethanol, depending on the involved microorganisms and the environmental conditions [11, 16, 17].

As key parameter, the microbial inoculum used to start the DF process can substantially impact the hydrogen yields. This is because the fermentation end products are directly influenced by the type of bacterial metabolism [16]. A wide variety of obligate and/or facultative bacteria have been used for hydrogen production by DF. This includes mixed cultures and pure hydrogen-producing cultures [17, 18].

In strict anaerobes, the oxidation of pyruvate into acetyl-CoA requires the reduction of ferredoxin (Fd) by PFOR, which is then oxidized by a hydrogenase that regenerates oxidized Fd and hydrogen [18]. Additional hydrogen can be produced from the NADH excess that is generated during glycolysis (Fig. 1c). The NADH is oxidized by NADH-[FeFe] hydrogenase, but only at very low partial pressures of hydrogen (<60 Pa) [11, 16]. Some strict anaerobes are particularly efficient in producing hydrogen by DF such as *C. acetobutylicum*, *C. beijerinckii* or *C. butyricum*, among others [11, 19]. *C. butyricum* is a widely studied clostridia species, responsible for the production of butyric acid as the major product of fermentation together with acetate and hydrogen. Mostly, clostridia are identified as dominant HPB in DF operated with mesophilic mixed cultures [20].

Facultative anaerobes can grow under anaerobic and aerobic conditions. In anaerobic conditions, formate is produced to get rid of extra reducing equivalents that would have been lost through the reduction of NAD^+ under aerobic conditions. Subsequently, formate can be degraded into hydrogen and carbon dioxide under acid conditions to maintain the pH of the system and lower the formate concentration in the cell [11]. Some facultative anaerobes capable of producing hydrogen by DF include *E. coli*, *E. Cloacae*, and *E. aerogenes,* among others [11, 19].

Working with pure cultures allows detecting easily the metabolic shifts due to the low diversity of the microbial biomass. Studies employing pure cultures can reveal important information regarding the operating conditions to be applied for increasing the hydrogen yields [19]. Although relatively high hydrogen yields have been obtained with pure cultures of hydrogen-producing bacteria (HPB), their use is not always feasible when dealing with the transformation of complex substrates, providing indigenous bacterial contamination. Moreover, during the DF process, a wide consortium of microorganisms is required for hydrolyzing the complex substrates prior to fermentation of the released sugars into hydrogen. Besides, it has been argued that it is more practical and economically feasible to use mixed cultures on larger scale rather than pure cultures [21–23]. Nonetheless, the use of mixed cultures has a major constraint. Besides containing HPB, mixed microflora also consist of a wide variety of microorganisms such as hydrogen-consuming bacteria and other microorganisms that compete with HPB for organic substrates. This may eventually decrease the net hydrogen yield. These non-hydrogen producers include hydrogenotrophic methanogens, homoacetogenic bacteria (HAB), sulphate-reducing bacteria (SRB), nitrate-reducing bacteria (NRB), propionate producers, iron-reducing bacteria and lactic acid bacteria (LAB) [10, 24, 25].

Consequently, the use of mixed microflora may result in direct hydrogen consumption, lower hydrogen yields, increased formation of end products and further process inhibition [26]. The main strategy to eliminate the hydrogen-consuming microorganisms is the pretreatment of the microbial inoculum prior to DF. The different kinds of pretreatment will be discussed in the coming Sect. (3.1.1).

3   Main Operating Conditions Affecting Dark Fermentation

Several bioprocess parameters can influence the hydrogen production by DF, impacting the hydrogen yields and/or the hydrogen production rates. The main operational parameters affecting the DF process are: the inoculum source and pre-treatment, the organic substrate used, the reactor operation/type, the temperature, the pH and the hydraulic retention time (HRT) [19, 22, 27]. These parameters have been separated into two different sections: (i) parameters for reactor start-up and (ii) parameters to be monitored during DF.

3.1   Parameters for Reactor Start–up

3.1.1   Inoculum and Pre-treatments

As aforementioned, hydrogen production by DF can be performed using pure cultures (such as *Clostridium sp.*) or mixed cultures (such as anaerobic sludge) and both have their own benefits and disadvantages. However, the use of mixed cultures is more practical in terms of control, operation and may be able to degrade a broader range of feedstock, being more attractive for industrial use [28, 29], especially since sterile conditions are not necessary [30, 31]. Despite these benefits, the hydrogen yields using mixed cultures are relatively low due to the presence of hydrogen-consuming microorganisms such as methanogens (archaea) [26, 32]. Commonly, these microorganisms are inhibited and/or eliminated by both inoculum pre-treatment and adapted operating conditions. The most common pretreatment techniques reported in the literature include: heat-shock, pH shock, loading-shock, chemical pretreatment, swinging the oxidation-reduction potential (ORP) (e.g. by aeration) and combination of different methods [26, 30].

The heat shock treatment allows removing the non-spore forming microorganisms, like archaea (methanogens), thereby enriching the culture media with spore-forming bacteria, such as *Clostridium sp.*, which is a very well-known hydrogen producer [33]. The control conditions for heat-shock pretreatment usually

listed on the literature range from 90 to 100 °C, with exposure time between 15 to 60 min [28, 29, 33–38].

A pH shock consists in removing the hydrogen- consuming bacteria and the methanogens while protecting the spore-forming microorganisms [33]. Acid (lower than 6.3) or basic treatment (higher than 7.8) are efficient options for inhibiting the growth of methanogens [39]. The acid treatment is the most widely used option, using HCl 1 or 2 M at an adjusted pH of 3 maintained during 24 h [40, 41]. The base treatment is usually undertaken by adjusting the pH of the inoculum at 10 using NaOH 1 M maintained for 24 h at 25 °C [38, 41].

Chemical treatment in mixed cultures eliminates the hydrogen consuming methanogens by chemical inhibition, using molecules such as 2-bromoethanesulfonic acid (BES), iodopropane or chloroform, which are toxic to these archaea [28, 42]. BESA is a structural molecule analog to the co-enzyme M reductase complex found in methanogens and blocks this reaction. Iodopropane is a corrinoid antagonist who prevents functioning of B12 enzymes as a methyl group carrier, therefore inhibiting cell growth and hydrogen consumption for methane production [43].

However, inoculum treatment can also affect the production of hydrogen if it is not properly managed. In a batch study, Luo et al. [37] applied various pretreatment methods on mixed inocula, reaching the highest hydrogen yield without pretreatment (65.3 mL H_2 g VS^{-1}) and the lowest one after a base and heat shock (51.3 ± 1.8 and 51.4 ± 1.8 mL H_2 g VS^{-1} respectively).

3.1.2 Micro- and Macro-nutrients Requirements for Efficient DF Nutritional Requirements

When talking about substrate, this refers to the carbon and energy source (generally sugars). However, microorganisms need other elements for their growth, such as nitrogen, phosphorous and other important micronutrients. That is why, the nutritional requirements and the composition of the culture medium are important variables that directly affect the microbial metabolism during DF and therefore are critical for hydrogen production [44–46].

Concerning nitrogen, it is an important component in proteins, including enzymes, and nucleic acids, whose synthesis is crucial for the growth of bacteria. However, there are still disagreements with respect to the optimum concentration. It is known that a nitrogen excess can affect the intracellular pH and eventually inhibit the activity of nitrogenases, inhibiting also bacterial growth. High nitrogen concentrations can induce ammonification, which is not favorable for the hydrogen production [22, 44]. It has also been shown that appropriate C/N and C/P ratios are fundamental for fermentative hydrogen production. However, it exists a certain disagreement on the optimal values, because all the studies have utilized different substrates, inoculums and C/N- C/P ranges [22, 46].

Within the micronutrients, metal ions are also suspected to play an important role because they assist cell growth and both enzyme and co-enzyme activation [26]. Nonetheless, high concentrations of metal ions might lead to inhibition of the

hydrogen production. Metal ions can be classified into light metal ions (Mg^{2+}, Na^+ and Ca^{2+}) or heavy metal ions (Fe^{2+} and Ni^{2+}) [22, 26]. Among the later, Iron is the most studied, since it is required for bacterial growth and for biosynthesis of enzymes and proteins, such as hydrogenases and ferredoxins, which are critical for hydrogen production by DF [14, 26, 47].

3.1.3 Bioreactor Configuration and Operational Mode

For hydrogen production by DF, the reactors can be operated in batch or continuous mode, batch tests being more reported in the literature because of their simplicity and flexibility [19, 27]. Continuous processes are more recommended when considering industrial applications, mainly because of their economic feasibility and their practical engineering design when treating large amounts of substrates [16, 19, 25].

Different kinds of bioreactor configurations have been used for continuous hydrogen production by DF. Nowadays, the suspended-cell completely stirred tank reactor (CSTR) is the most commonly applied option. However, up-flow anaerobic sludge blanket (UASB) reactors, anaerobic membrane bioreactors and immobilized (e.g. fluidized bed) bioreactors are becoming popular due to their improved hydrogen producing potentials [30, 48]. The use of CSTRs is generally associated with relatively short start-up phase when compared to other configurations due to better mass transfer, but it also needs rigorous supervision due to the disposition of cells to be washed out at inadequate operating bioreactor regimen (e.g. HRT). This risk of wash out can be avoided by retained-biomass systems such as the membrane reactors or immobilized systems [30, 48].

3.2 Parameters to be Monitored During DF

3.2.1 pH

pH is one of the most important parameters in DF. It affects the hydrolysis of substrates (when complex), the activity of important enzymes for hydrogen production (such as hydrogenase), the predominant microbial population and their main metabolic pathways [27, 49]. The range of operational pH for hydrogen production has been reported between 4.5 and 8.0 [49, 50]. Such wide range of optimal pH can be explained by the variability of inocula and substrates [20]. Indeed, for simple substrates such as glucose, the highest hydrogen yields were reported at pH of 6.0 (1.83 mol H_2 mol^{-1}) in batch experiments [51]. When fermenting a complex substrate (food waste), maximum hydrogen yields were reported at pH 8.0 (1.92 mol H_2 mol hexose^{-1}) [52]. However, there is an agreement of the negative effect of pH values below 4.5–5.5, generally caused by the accumulation of volatile fatty acids, which can reduce the hydrogen production due

to shifts in the metabolite production pathways towards solventogenesis (acetone, butanol, ethanol) [50].

3.2.2 Temperature

Temperature plays an important role in reducing the activity of hydrogen consumers [20]. The range of operational temperature is mesophilic (35 °C), thermophilic (55 °C) and extreme thermophilic (>65 °C). Varying the temperature affects greatly the structure of the bacterial community. Lazaro et al. [53] explained that significant differences between the microbial communities at 37 °C and 55 °C exist. A shift from *Clostridium* at mesophilic conditions to *Thermoanaerobacterium* when thermophilic conditions were applied was shown. However, the hydrogen yield was not impacted by the temperature regime (2.31 and 2.23 mmol H_2 $g^{-1}COD_{influent}$ at mesophilic and thermophilic respectively) [54]. As reported by Ghimire et al. [20], the temperature also affects the metabolic pathways, thus modifying the by-products produced during DF. Consistently, the study of Valdez et al. [23] showed a significant difference on the average distribution of metabolites between thermophilic and mesophilic conditions. The predominant metabolite produced under mesophilic temperatures was butyrate, while in thermophilic conditions acetate was the main metabolite.

3.2.3 Hydraulic Retention Time

The hydraulic retention time (HRT), as defined in Eq. 1, is one of the major critical parameters affecting the continuous production of hydrogen. In suspended-cell reactors, such as CSTRs, the HRT corresponds to the inverse of the dilution rate (D). In these systems, D (and thus the HRT) will determine which microorganisms will be dominant in the reactor. Basically, if D is equal to the microbial growth rate (μ), the system reaches equilibrium, also called steady-state. If D is higher than μ_{max}, (maximum growth rate), the slow-growing microorganisms are washed out from the reactor and if D is lower than μ_{max}, slow-growers will also survive, although they could be washed out by lack of nutrients (competitive exclusion between microorganisms).

$$HRT(h) = \frac{Volume_{reactor}(L)}{Flow_{feed}(L/h)} \tag{1}$$

Therefore, to favor the emergence of certain hydrogen-producing microbial populations, it is important to know the μ_{max} of the microorganisms to further establish an adequate HRT and avoid the wash-out of the biomass from the reactor, maximizing at the same time the microbial growth and the production of desired metabolites. Indeed, unlike pure cultures, mixed cultures have a greater microbial

richness and contain different microorganisms with different μ_{max}. In this context, the HRT is a key parameter that allows the selection of the desired populations (i.e., washing-out slow-growing microorganisms from the reactors). Focusing on hydrogen producing reactors by DF, this is a good way to eliminate methanogenic microorganisms, which grow slower (HRT $\geq$ 1 d) than HPB (HRT $\leq$ 24 h). However, it is important to consider the type of substrate and the inoculum sources. As an illustration, several studies reported that in order to decrease the methanogenic activity during DF, it is sufficient to work at short HRTs (<few h) and low pH (5–5.5), in what has been called a "biokinetic control" [16, 20, 55].

4 Subtrates for Dark Fermentation: Solid Wastes and Wastewaters

Fermenting bacteria can utilize several types of substrates, mostly the ones rich in carbohydrates, such as first generation fuel crops (i.e., sugar cane, wheat, corn, and sugar beets), second generation biomass like agricultural residues as well as industrial waste and wastewaters [20]. Since DF allows coupling organic waste treatment with the production of renewable energy, the utilization of waste as substrates is particularly attractive from an environmental and economic point of view [31]. Therefore, nowadays this alternative is being widely researched, aiming to reduce the costs of organic waste treatment, while generating added-value end-products. Thus, the Table 1 shows the different main wastes and wastewaters that have been used for hydrogen production by DF.

The choice of the type of substrate is a key decision that affects greatly the hydrogen yields, the hydrogen production rates and the overall process economy. These variables are largely dependent on the carbohydrate content of the substrate (with higher hydrogen yields at higher contents of soluble carbohydrates), its bioavailability and its biodegradation rate [25, 56–58]. Substrates rich in carbohydrates have been widely used in studies focused on DF, particularly pure glucose and mixtures of sucrose and starch [20]. However, using this type of substrates at an industrial level is not economically profitable. In this context, wastewaters and solid wastes appear as perfect possibilities to generate 'green' hydrogen from renewable sources.

Recent studies have dealt with the dark fermentation of complex substrates, such as the organic fraction of municipal solid waste (OFMSW), agricultural residues (e.g. rice straw, wheat straw and corn stalks), agro-industrial wastes (e.g. olive mill wastewater or cheese whey), effluents from livestock farms or aquatic plants. Moreover, if DF is integrated within the concept of environmental biorefinery (i.e., multi-substrates to multi end-products), the co-products generated during biofuel production such as crude glycerol, de-oiled algal cake or cotton seed cake, could be further used as substrates for DF.

Table 1 Summary of main substrates used for hydrogen production by dark fermentation including wastes and wastewaters. (Adapted from [20])

Source	Waste	Type	Considerations
Agricultural residues from plant biomass waste	Lignocellulosic waste	Rice straw	Due to the complex structure of the lignocellulosic materials it is necessary to perform pre-treatments to increase its degradability
		Wheat straw	
		Barley straw	
		Corn stalk	
		Corn cobs	
	Livestock waste (manure)	Solid animal manure waste	Need to eliminate indigenous methanogenic activity. High ammonium content could inhibit hydrogen production. High concentrations of sulfates could reduce the production of hydrogen due to sulfate reducing microorganisms
		Fodder waste	
		Wastewater (urine and faeces)	
Industrial waste		Palm oil mill wastewater	
		Olive mill wastewater (OMWW)	
		Tapioca industries	
		Brewery industries	
		Dairy industries	
Municipal waste	Waste biosolids	Food wase	Pretreatments such as ultrasonication, acidification, sterilization or basification are necessary to facilitate fermentation
	Urban sludge	Organic fraction of Municipal Solid Waste (OFMSW)	

To achieve satisfactory hydrogen yields using complex organic wastes as substrates for DF, pretreatments are frequently required to facilitate the hydrolysis step, especially with substrates containing significant lignocellulosic fractions. These pretreatments increase the soluble fraction of carbohydrates, improving the hydrogen yields [20]. Among all the possible substrate pretreatments, the most relevant are: physical methods (e.g. mechanical comminution, irradiation with gamma-rays, electro-beam or microwaves, hydrothermal treatment, high pressure steaming and pyrolysis), chemicals methods (e.g. ozonolysis, acid or alkaline hydrolysis, solvent extraction and explosion with steam ammonia fiber or carbon dioxide) and even biological methods, using fungi [20]. It has been reported that it is possible to increase from 2 to 50 times the hydrogen yields by pretreating the substrates [25, 59–61]. However, economic and energetic assessments are required before application of a pretreatment.

Concerning livestock wastes, they are also suitable as DF substrates and can be categorized in: urine waste, solid manure and wastewaters from process water collection (e.g. feedlot runoff, silage juices, bedding, disinfectants and liquid manure) [62]. The proper disposal and treatment of these wastes is crucial because they can contaminate the air and natural water courses. Nutrient leaching and pathogen contamination can also cause important health problems [25]. When using this type of substrate for DF, it is necessary to include thermal pretreatment not only to eliminate the indigenous methanogenic activity but also to hygienize the wastewater, which are inherent to this waste due to the presence of native archaea and enteric pathogens [25].

Due to its high biodegradability and energy content, food industry waste has been regarded as ideal for microbial growth. In addition, this waste is commonly disposed in landfills, causing environmental problems, such as of odors, methane emissions and groundwater contamination. Therefore, its treatment and valorization by DF is clearly beneficial. Kitchen refuse [63], organic fraction of municipal waste [64], food industry co-products (such as oil mill) [65, 66], cheese whey [67] and starch-manufacturing waste [68] are representative waste of this category that have been efficiently applied for hydrogen production by DF.

In general, all the wastes aforementioned have shown a great potential as substrates for producing hydrogen by DF, with various yields mainly depending on their content in readily accessible carbohydrates. Nonetheless, hydrogen yields will not only depend on the composition of the waste, but also on the correct choice of the key operational parameters and the microbial consortium, which must be optimized for each particular DF feed since it contains its own indigenous microbial communities.

5 Dark Fermentation as Core Process in Future Environmental Biorefineries

The concept of environmental biorefinery lies on the idea of integrating different bioprocess to convert biomass into several added-value products [69]. The main aim of this approach is to obtain a global process which is self-sufficient, environmentally sustainable and economically beneficial. The integration of DF with other processes will reduce the amount of organic residues produced (and the associated disposal costs), increasing at the same time the total revenues by synthetizing added-value chemicals and improving the global energy yields [70]. In addition, the development of a comprehensive biorefinery would help to overcome two of the main bottlenecks for commercial hydrogen production from DF: the low yields of the process and the incomplete biomass conversion/stabilization.

A main advantage of DF, when compared to other processes for organic waste treatment and energy production, is the wide variety of substrates that it can accommodate. Thus, DF can be integrated within existing or novel biomass
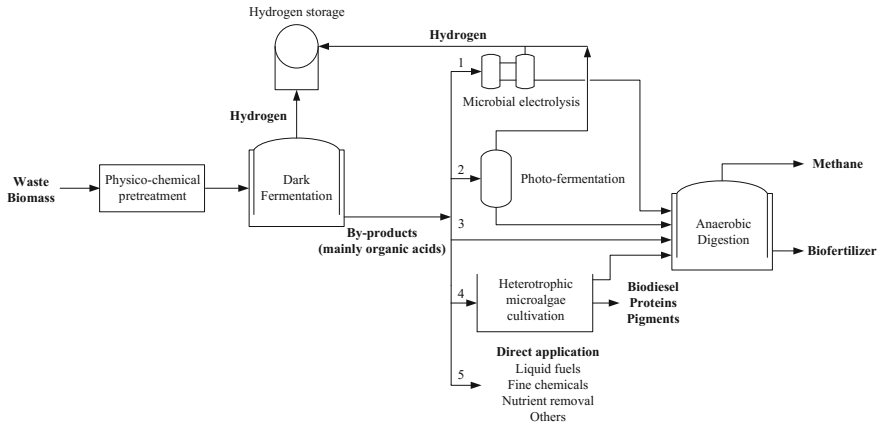
Fig. 2 Different options for coupling dark fermentation with other bio-processes in a biorefinery framework for organic waste valorization. The numbers stand for: (1) microbial electrolysis, (2) photo-fermentation, (3) anaerobic digestion, (4) microalgae cultivation and (5) direct application/recovery (Adapted from [20, 57, 73, 75, 76, 95, 96])

valorization (bio)-processes treating several substrates, such as residues from agricultural activities, forestry activities, macro- and micro-algae activities, food industry, municipal waste and bio-industrial waste [70]. In a DF-based biorefinery, these wastes could be transformed into several added-value products, such as hydrogen, methane, liquid fuels, lipids, bioplastics, electricity, fine chemicals or proteins, among others.

Several biorefinery models including DF have been proposed. These models are flexible and can be adapted to local specific conditions (geographical location, seasonal variability in substrate production, among others). Figure 2 shows a comprehensive (but not exhaustive) schematic representation of DF biorefinery frameworks. The most common one (Fig. 2, process 3) is the so-called "acidogenic model" or two-stage anaerobic digestion (AD) [71]. In this process, DF represents the first stage, producing hydrogen and different metabolites, such as alcohols and volatile fatty acids. DF metabolites, being value-added products, can be (all or some of them) extracted and purified, while the remaining organic matter in DF effluent enters the second stage, which consists in an anaerobic reactor for methane production and waste stabilization. It has been stated that this process integration could have a tremendous positive impact in the economic viability of AD processes by maximizing the substrate conversion [72]. The integration of these two stages increases the sustainability of the process, achieving at the same time a complete waste treatment. Combined DF and AD has been proved to be economically and technically feasible using a wide variety of substrates, with high yields of both hydrogen and methane [20]. Therefore, AD can clearly be applied to improve the economic performance of commercial hydrogen production by DF.

In addition to this approach, several other options exist for coupling DF with other processes which can use DF by-products. Among them, some of the most promising alternatives (Fig. 2) that have been proposed are: DF and direct recovery of value-added compounds in the effluent [73], DF and photofermentation for hydrogen production [74], DF and microbial electrolysis for hydrogen production [75] and DF and microalgae growth in the effluents for biofuel production [76]. Eventually, a final AD stage could always be included to further valorize and stabilize the residual biomass [20].

Among other biotechnologies that could utilize the metabolic by-products generated by DF processes, bio-electrochemical systems have been proposed as a technology that can be coupled with fermentative hydrogen production [77]. More specifically, microbial electrolysis cells (MECs), a recent emerging technology related to microbial fuel cells (MFCs), is a promising candidate for the improvement of classical, single-stage DF to generate hydrogen gas with a better efficiency [78]. Microbial electrolysis is accomplished in an electrochemical reactor, in which bacteria referred as exoelectrogens [79] oxidize a substrate and release electrons to the anode providing an electric current that is then used at the cathode to electrochemically produce hydrogen from water. However, this process requires a small external power supply in order to make the hydrogen production thermodynamically favorable [79]. Hydrogen from MECs is considered a very promising route with near term commercialization potential [80] and it has been recently demonstrated that coupling DF and MEC for organic waste/wastewater treatment and/or by-products transformation highly increases the hydrogen yield compared to DF alone and thus constitutes not only a suitable but also a highly promising route for producing bio-hydrogen within the scheme of an environmental biorefinery [75, 81–83].

To produce further hydrogen from DF effluents, another option that has received a lot of attention in the recent years is the coupling of DF with photo-fermentation (Fig. 2, process 2). In this process, the effluents from DF are consumed by purple non sulfur photosynthetic bacteria in a secondary anaerobic reactor. These microorganisms use light as energy source and the organic matter from DF as electron donor, converting VFA to hydrogen and carbon dioxide. A great advantage of this process is that purple non sulfur bacteria are able to use a wide range of organic acids as substrate, making photofermentation a suitable post-treatment of DF effluents. This further hydrogen production has served to increase the productions yields significantly. As reported in Ghimire et al. [20], combined hydrogen yields up to 10.25 mol H_2 mol sucrose^{-1} were achieved. In addition, from a total yield of 5.48 mol H_2 mol glucose^{-1}, 4.16 mol H_2 mol glucose^{-1} were produced in the photo-fermentation stage, indicating its importance to improve the global hydrogen yields of this process [84]. Eventually, residual organic matter from the photobioreactor can be send to an AD reactor (Fig. 2, process 3) for completing the biomass final stabilization.

Indeed, as aforementioned, AD is the most widely applied process and it can be considered as the final step of most of DF biorefinery pathways (including DF,

MEC, photofermentation and algae cultivation) to further stabilize the end products (Fig. 2).

Instead of producing further hydrogen, an interesting alternative is the production of biodiesel by using the effluents from DF as substrate for cultivation of microalgae. This is an attractive options because it allows the production of both gaseous (hydrogen by DF) and liquid (i.e., biodiesel from algal lipids) biofuels (Fig. 2, process 4). This alternative relies on the heterotrophic growth of microalgae, which can uptake the organic matter present in the DF effluents (preferably acetate) for their growth [76]. Afterwards, the lipids produced by the algal biomass could be converted into biodiesel by transesterification and the remaining biomass could be used for methane production by AD. Still on its infancy, this is clearly a process worthy to be pursued in the future.

Moreover, as mentioned before, the direct utilization of the DF effluent or the direct recovery of the most value-added compounds already present in this stream have are options that have also been considered (Fig. 2, process 5). Indeed, as listed by Ghimire et al. [20], the effluent from DF has been directly used as carbon sources for biological nutrient removal from wastewater, for sulfur and sulfide reduction and for producing phosphate solubilizing biofertilizer. In addition, depending on the DF working conditions, high concentrations of value-added co-products, such as ethanol, butyric acid, caproic acid or 1,3-propanediol in the effluent can be achieved [70, 73]. Although the direct recovery/purification of these compounds from DF effluents remains unexplored, the high prices associated with these co-products make this alternative a simple approach to improve the economic viability of DF.

Finally, some authors have pointed out the feasibility of generating other value-added products from DF effluents, such as polyhydroxyalkanoates and microbial lipids [20, 70].

In order to consolidate DF as a main technology for the future, the aforementioned biorefineries should have high energy efficiencies, generating value-added products while applying almost zero-waste production processes [71]. Holistic studies are needed to evaluate the environmental impacts and the economic feasibility of these systems and more research must be carried out to increase the yields of products.

6 Outlook of Bio-hydrogen as Energy Carrier

6.1 Hydrogen as Energetic Vector for Future Transportation

Fossil fuels are finite. No wonder that today there is a constant search for alternative sources of clean energy worldwide. And it is this quest that will determine the next "champions" of the world race for energy security in several sectors of the energy

system such as the power sector, the industry, the building sector and transportation.

The hydrogen market[1] is growing incredibly fast due to the flexibility of its production, which can be from any prevalent primary energy source (i.e., biomass, natural gas and coal). Furthermore, hydrogen can be stored in large quantities over long periods although it requires high pressurization (700 bars) and adapted materials to avoid leakages. H_2 can then be distributed in both centralized and decentralized systems as energy carrier for diverse end-use applications.

According to the International Energy Agency [85] hydrogen can be re-transformed into (i) electricity for powering buildings and industries (power-to-power); it can be mixed into (ii) the natural gas grid or converted to synthetic methane (power-to-gas); or even sold as (iii) fuel for fuel cell electric vehicle (FCEV) to the transport sector (power-to-fuel).

To date, the status of hydrogen-based technologies for the aforementioned alternatives are presented as follows: (i) Power-to-power storage systems still must to achieve the leveled cost of electricity (LCOE[2]) of USD 90 per MWh, as in the breakthrough scenario, the cost of investment attributable to both the electrolyzer (i.e., to achieve the electrolysis[3]) and the fuel cell would need to drop to around USD 400 per MWh, and efficiencies would need to increase to up to 90% for electrolyzers and 60% for fuel cells higher heating value (HHV) [85]. (ii) A low blend share of 5% hydrogen mixed with natural gas are close to the benchmark [85]; (iii) around 550 FCEV (passenger cars and buses) are running in several demonstration projects across the world. Toyota launched its Mirai ("Future") model in Japan in 2014, Hyundai is planning to begin the sale of FCEVs in the near future (the Hyundai Tucson FCEV has been available for lease since summer 2014), and Honda announced plans to launch its next generation FCEV in 2016 [85, 86].

Only focusing on improving the technology is not sufficient, new and more integrated approaches need to be applied to create viable business cases. The association of i–iii point towards a link between the different energy sectors and networks, increasing the operational flexibility of future low-carbon energy systems as illustrate in Fig. 3.

---

[1]In this section, it is important to take into consideration that hydrogen is referred to as energy carrier and not as an energy source: although hydrogen as a molecular component is abundant in nature, energy needs to be used to generate pure hydrogen which incurs a cost and suffers from thermodynamic losses.

[2]LCOE is a measure of a power source which attempts to compare different methods of electricity generation on a consistent basis. It is an economic assessment of the average total cost to build and operate a power-generating asset over its lifetime divided by the total energy output of the asset over that lifetime. The LCOE can also be regarded as the minimum cost at which electricity must be sold in order to break-even over the lifetime of the project.

[3]Electrolysis is a process of splitting water into hydrogen and oxygen by applying a direct current, converting electricity into chemical energy.
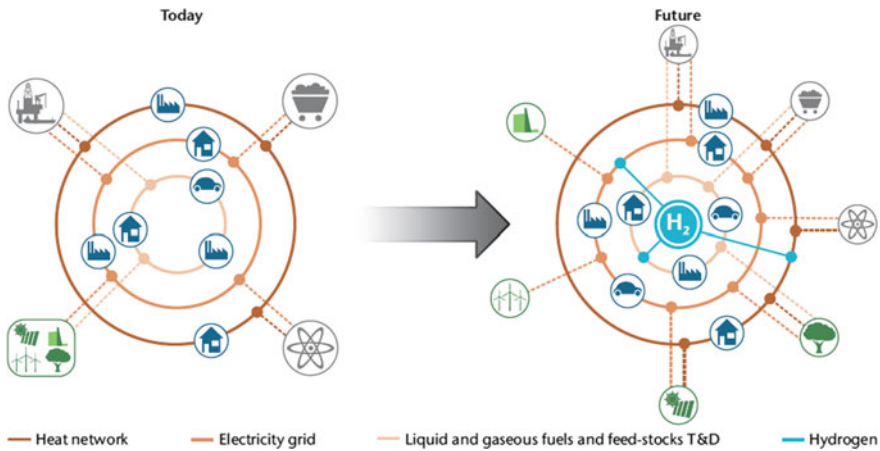
Fig. 3 Transformation of today's energy system with hydrogen as renewable energy linking different energy sectors (collected from International Energy Agency, 2015, [85])

According to Kapdan and Kargi [57], it is expected that hydrogen will account for 8–10% of the total energy market in the United States of America by 2025 with hydrogen power and transport systems available in all regions of the country by 2040. A similar trend can be observed in Germany with a remarkable concentration of activity on hydrogen-based large-scale energy storage and Japan ranking first for delivered systems due to the successful upscaling of the Ene-Farm micro co-generation power system [85].

6.2 Potential Role of Dark Fermentation in 'Green' Hydrogen Production

Undeniable progress on hydrogen and fuel cell technologies have been achieved since the first FCEV developed in the 1960s [87]. However, the adoption of renewable hydrogen is still in the early stages of commercialization and currently struggle to compete with alternative technologies (fossil-derived hydrogen with or without carbon capture and storage—CCS), including other low-carbon options, due to high costs [85].

Highlighting renewable pathways of hydrogen generation, more specifically electrolysis versus DF process, both have been supporting the hydrogen market progress and unlocking public and private funds for research, development and demonstration though electrolysis represents the only process modelled explicitly[4]

---

[4]Explicit methods calculate the state of a system at a later time from the state of the system at the current time.

and counting with 8 GW of capacity installed worldwide [85]. However, even under optimistic assumptions, in relation to the electrolyze techno-economic parameters, electrolytic hydrogen remains considerably more expensive than hydrogen from natural gas reforming, unless very low cost renewable electricity is available and carbon or natural gas prices are high [85]. Based on that, the question of how to produce the required hydrogen remains a main issue to be addressed.

The future of DF as a core technology for hydrogen generation lies within the concept of the biorefinery. In such scenario, DF process has the advantage over other pathways for ensuring the biological hydrogen generation associated with the production of value-added compounds (organic acids, solvents, etc.) or alternatively, to the treatment of residual liquid stream, when a methanogenic reactor is coupled to the fermentative system.

However, biohydrogen generation by DF is still a technological challenge for being a very sensitive process, requiring careful balancing of pH [88], temperature [89], organic loading rate [90] and specific organic loading rate [91, 92]. Moreover, the hydrogen yields in fermentative systems are mostly between 1.2–2.3 mol H_2 mol hexose^{-1} [20], representing only 30–50% of the theoretical maximum hydrogen yield (4 mol H_2 mol glucose^{-1}).

As an illustration, in Ferraz Júnior et al. [90, 93] the theoretical calculation of energy conversion for one liter of sugarcane vinasse in a two-stage system (acidogenic/methanogenic) was 45.5 W, with only 1.5 W corresponding to the hydrogen generation in the first stage. Corroborating these findings, it is expected that DF will account for no more than the 10–12% of the total hydrogen produced by 2050 [85].

Recent studies have speculated that the construction of industrial DF processes would be economically feasible. The economic viability of a DF system in a solid wastes plant depends mainly on the evolution of the biohydrogen price in the near future [94] and the cost optimization of the operational conditions (i.e., improved metabolic pathway of hydrogen at low energy costs). Economic evaluation should consider the energy costs of the process, as assessed on a thermophilic hydrogen production system with a working volume of 1947.8 m^3 and fed with sugarcane vinasses to support the investments made in system implementation within 2 years [88].

Optimistically, new alternatives are coming up to valorize biohydrogen, such as the biohythane (i.e., a fuel that blends until 20% hydrogen with 80% natural gas) [70]. Those alternatives could be interesting options to increase the calorific value in the natural gas grid, to stabilize the energy supply in rural areas where the access to the grid might be limited, and to act as backup system when other energy sources are insufficient to supply the required demand. Therefore, a strong policy, regulatory framework and finance (hydrogen-based) associated to improving the efficiency of DF systems (optimization of reactors design and operation; and most important, hydrogen productivities and yields) will guarantee the economic feasibility of waste valorization by DF.

References

1. Dutta S (2014) A review on production, storage of hydrogen and its utilization as an energy resource. J Ind Eng Chem 20(4):1148–1156
2. ADEME (2016) L'hydrogène dans la transition énergétique p 1–7
3. Marbán G, Valdés-Solís T (2007) Towards the hydrogen economy? Int J Hydrog Energy 32(12):1625–1637
4. Lin CY, Lay CH, Sen B, Chu CY, Kumar G, Chen CC, Chang JS (2012) Fermentative hydrogen production from wastewaters: a review and prognosis. Int J Hydrog Energy 37(20):15632–15642
5. Ren N, Wang A, Cao G, Xu J, Gao L (2009) Bioconversion of lignocellulosic biomass to hydrogen: potential and challenges. Biotechnol Adv 27(6):1051–1060
6. Moscoviz R, Toledo-Alarcón J, Trably E, Bernet N (2016) Electro-fermentation: How to drive fermentation using electrochemical systems. Trends Biotechnol 34(11):856–865
7. Logan BE, Oh SE, Kim IS, Van Ginkel S (2002) Biological hydrogen production measured in batch anaerobic respirometers. Environ Sci Technol 36(11):2530–2535
8. Nandi R, Sengupta S (1998) Microbial production of hydrogen: an overview. Critic Rev Microbiol 24(1):61–84
9. Hwang MH, Jang NJ, Hyun SH, Kim IS (2004) Anaerobic bio-hydrogen production from ethanol fermentation: the role of pH. J Biotechnol 111(3):297–309
10. Saady NMC (2013) Homoacetogenesis during hydrogen production by mixed cultures dark fermentation: unresolved challenge. Int J Hydrog Energy 38(30):13172–13191
11. Mathews J, Wang G (2009) Metabolic pathway engineering for enhanced biohydrogen production. Int J Hydrog Energy 34(17):7404–7416
12. Kalia VC, Purohit HJ (2008) Microbial diversity and genomics in aid of bioenergy. J Ind Microbiol Biotechnol 35(5):403–419
13. Angenent LT, Karim K, Al-Dahhan MH, Wrenn BA, Domíguez-Espinosa R (2004) Production of bioenergy and biochemicals from industrial and agricultural wastewater. Trends Biotechnol 22(9):477–485
14. Hallenbeck PC, Benemann JR (2002) Biological hydrogen production; fundamentals and limiting processes. Int J Hydrog Energy 27(11–12):1185–1193
15. Logan BE (2004) Extracting hydrogen and electricity from renewable resources. Environ Sci Technol 38(9):160–167
16. Ramírez-Morales JE, Tapia-Venegas E, Toledo-Alarcón J, Ruiz-Filippi G (2015) Simultaneous production and separation of biohydrogen in mixed culture systems by continuous dark fermentation. Water Sci Technol 71(9):1271–1285
17. Tapia-Venegas E, Ramirez-Morales JE, Silva-Illanes F, Toledo-Alarcón J, Paillet F, Escudie R, Ruiz-Filippi G (2015) Biohydrogen production by dark fermentation: scaling-up and technologies integration for a sustainable system. Rev Environ Sci Bio 14(4):761–785

18. Nath K, Das D (2004) Improvement of fermentative hydrogen production: various approaches. Appl Microbiol Biotechnol 65(5):520–529
19. Elsharnouby O, Hafez H, Nakhla G, El MH (2013) A critical literature review on biohydrogen production by pure cultures. Int J Hydrog Energy 38(12):4945–4966
20. Ghimire A, Frunzo L, Pirozzi F, Trably E, Escudie R, Lens PNL, Esposito G (2015) A review on dark fermentative biohydrogen production from organic biomass: process parameters and use of by-products. Appl Energ 144:73–95
21. Li C, Fang HHP (2007) Fermentative hydrogen production from wastewater and solid wastes by mixed cultures. Environ Sci Technol 37(1):1–39
22. Wang JL, Wan W (2009) Factors influencing fermentative hydrogen production: a review. Int J Hydrog Energy 34(2):799–811
23. Valdez-Vazquez I, Ríos-Leal E, Esparza-García F, Cecchi F, Poggi-Varaldo HM (2005) Semi-continuous solid substrate anaerobic reactors for H_2 production from organic waste: Mesophilic versus thermophilic regime. Int J Hydrog Energy 30(13–14):1383–1391
24. Valdez-Vazquez I, Poggi-Varaldo HM (2009) Hydrogen production by fermentative consortia. Renew Sustain Energy Rev 13(5):1000–1013
25. Guo XM, Trably E, Latrille E, Carrère H, Steyer JP (2010) Hydrogen production from agricultural waste by dark fermentation: a review. Int J Hydrog Energy 35(19):10660–10673
26. Bundhoo MAZ, Mohee R (2016) Inhibition of dark fermentative bio-hydrogen production: a review. Int J Hydrog Energy 41:6713–6733
27. Azwar MY, Ma Hussain, Abdul-Wahab aK (2014) Development of biohydrogen production by photobiological, fermentation and electrochemical processes: a review. Renew Sust Energy Rev 31:158–173
28. Wang JL, Wan W (2008) Comparison of different pretreatment methods for enriching hydrogen-producing bacteria from digested sludge. Int J Hydrog Energy 33(12):2934–2941
29. Kannaiah Goud R, Sarkar O, Venkata Mohan S (2014) Regulation of biohydrogen production by heat-shock pretreatment facilitates selective enrichment of Clostridium sp. Int J Hydrog Energy 39(14):7572–7586
30. Bakonyi P, Nemestóthy N, Simon V, Bélafi-Bakó K (2014) Review on the start-up experiences of continuous fermentative hydrogen producing bioreactors. Renew Sustain Energy Rev 40:806–813
31. Boboescu IZ, Ilie M, Gherman VD, Mirel I, Pap B, Negrea A, Maróti G (2014) Revealing the factors influencing a fermentative biohydrogen production process using industrial wastewater as fermentation substrate. Biotechnol Biofuels 7(1):139–149
32. Ben-yi X, Jun-xin L (2006) Effects of thermally pretreated temperature on bio-hydrogen production from sewage sludge. J Environ Sci 18(1):6–12
33. Mohan SV (2008) Fermentative hydrogen production with simultaneous wastewater treatment: Influence of pretreatment and system operating conditions. J Sci Ind Res India 67(11):950–961
34. Penteado ED, Lazaro CZ, Sakamoto IK, Zaiat M (2013) Influence of seed sludge and pretreatment method on hydrogen production in packed-bed anaerobic reactors. Int J Hydrog Energy 38(14):6137–6145
35. Cisneros-Pérez C, Carrillo-Reyes J, Celis LB, Alatriste-Mondragón F, Etchebehere C, Razo-Flores E (2015) Inoculum pretreatment promotes differences in hydrogen production performance in EGSB reactors. Int J Hydrog Energy 40(19):6329–6339
36. El-Bery H, Tawfik A, Kumari S, Bux F (2013) Effect of thermal pre-treatment on inoculum sludge to enhance bio-hydrogen production from alkali hydrolysed rice straw in a mesophilic anaerobic baffled reactor. Environ Technol 34(13):1965–1972
37. Luo G, Xie L, Zou Z, Wang W, Zhou Q (2010) Evaluation of pretreatment methods on mixed inoculum for both batch and continuous thermophilic biohydrogen production from cassava stillage. Bioresour Technol 101(3):959–964
38. Kan E (2013) Effects of pretreatments of anaerobic sludge and culture conditions on hydrogen productivity in dark anaerobic fermentation. Renew Energy 49:227–231

39. Chen CC, Lin CY, Lin MC (2002) Acid-base enrichment enhances anaerobic hydrogen production process. Appl Microbiol Biotechnol 58(2):224–228
40. Chaganti SR, Kim DH, Ja Lalman (2012) Dark fermentative hydrogen production by mixed anaerobic cultures: Effect of inoculum treatment methods on hydrogen yield. Renew Energ 48:117–121
41. Yin Y, Hu J, Wang J (2014) Enriching hydrogen-producing bacteria from digested sludge by different pretreatment methods. Int J Hydrog Energy 39(25):13550–13556
42. Zhu H, Beland M (2006) Evaluation of alternative methods of preparing hydrogen producing seeds from digested wastewater sludge. Int J Hydrog Energy 31(14):1980–1988
43. Kenealy W, Zeikus JG (1981) Influence of corrinoid antagonists on methanogen metabolism. J Bacteriol 146(1):133–140
44. Chandrasekhar K, Lee Y, Lee D (2015) Biohydrogen production: Strategies to Improve Process Efficiency through Microbial Routes. Int J Mol Sci 16(4):8266–8293
45. Lin CY, Lay CH (2005) A nutrient formulation for fermentative hydrogen production using anaerobic sewage sludge microflora. Int J Hydrog Energy 30(3):285–292
46. Lin CY, Lay CH (2004) Carbon/nitrogen-ratio effect on fermentative hydrogen production by mixed microflora. Int J Hydrog Energy 29(1):41–45
47. Das D, Veziroglu T (2008) Advances in biological hydrogen production processes. Int J Hydrog Energy 33(21):6046–6057
48. Hallenbeck PC, Ghosh D (2009) Advances in fermentative biohydrogen production: the way forward? Trends Biotechnol 27(5):287–297
49. Kim DH, Kim SH, Jung KW, Kim MS, Shin HS (2011) Effect of initial pH independent of operational pH on hydrogen fermentation of food waste. Bioresour Technol 102(18):8646–8652
50. Xie GJ, Feng LB, Ren N, Ding J, Liu C, Xing DF, Ren HY (2010) Control strategies for hydrogen production through co-culture of Ethanoligenens harbinense B49 and immobilized Rhodopseudomonas faecalis RLD-53. Int J Hydrog Energy 35(5):1929–1935
51. Li Z, Wang H, Tang Z, Wang X, Bai J (2008) Effects of pH value and substrate concentration on hydrogen production from the anaerobic fermentation of glucose. Int J Hydrogen Energ 33 (24):7413–7418
52. De Gioannis G, Friargiu M, Massi E, Muntoni A, Polettini A, Pomi R, Spiga D (2014) Biohydrogen production from dark fermentation of cheese whey: Influence of pH. Int J Hydrog Energy 39(36):20930–20941
53. Karadag D, Puhakka JA (2010) Effect of changing temperature on anaerobic hydrogen production and microbial community composition in an open-mixed culture bioreactor. Int J Hydrog Energy 35(20):10954–10959
54. Lazaro CZ, Perna V, Etchebehere C, Varesche MBA (2014) Sugarcane vinasse as substrate for fermentative hydrogen production: The effects of temperature and substrate concentration. Int J Hydrog Energy 39(12):6407–6418
55. Si B, Li J, Li B, Zhu Z, Shen R, Zhang Y, Liu Z (2015) The role of hydraulic retention time on controlling methanogenesis and homoacetogenesis in biohydrogen production using upflow anaerobic sludge blanket (UASB) reactor and packed bed reactor (PBR). Int J Hydrog Energy 40(35):11414–11421
56. Ren N, Guo W, Liu B, Cao G, Ding J (2011) Biological hydrogen production by dark fermentation: challenges and prospects towards scaled-up production. Curr Opin Biotech 22 (3):365–370
57. Kapdan IK, Kargi F (2006) Bio-hydrogen production from waste materials. Enzyme Microb Tech 38(5):569–582
58. Chong ML, Sabaratnam V, Shirai Y, Hassan MA (2009) Biohydrogen production from biomass and industrial wastes by dark fermentation. Int J Hydrog Energy 34(8):3277–3287
59. Li D, Chen H (2007) Biological hydrogen production from steam-exploded straw by simultaneous saccharification and fermentation. Int J Hydrog Energy 32(12):1742–1748

60. Zhang ML, Fan YT, Xing Y, Pan CM, Zhang GS, Lay JJ (2007) Enhanced biohydrogen production from cornstalk wastes with acidification pretreatment by mixed anaerobic cultures. Biomass Bioenerg 31(4):250–254
61. Ivanova G, Rakhely G, Kovacs KL (2009) Thermophilic biohydrogen production from energy plants by Caldicellulosiruptor saccharolyticus and comparison with related studies. Int J Hydrog Energy 34(9):3659–3670
62. Burton CH, Turner C (2003) Manure management: treatment strategies for sustainable agriculture. Silsoe Research Institute, London
63. Jayalakshmi S, Joseph K, Sukumaran V (2009) Biohydrogen generation from kitchen waste in an inclined plug flow reactor. Int J Hydrog Energy 34(21):8854–8858
64. Liu D, Liu D, Zeng RJ, Angelidaki I (2006) Hydrogen and methane production from household solid waste in the two-stage fermentation process. Water Res 40(11):2230–2236
65. Eroglu E, Erolu I, Gunduz U, Yucel M (2009) Treatment of olive mill wastewater by different physicochemical methods and utilization of their liquid effluents for biological hydrogen production. Biomass Bioenerg 33(4):701–705
66. Chookaew T, O-Thong S, Prasertsan P (2012) Fermentative production of hydrogen and soluble metabolites from crude glycerol of biodiesel plant by the newly isolated thermotolerant *Klebsiella pneumoniae* TR17. Int J Hydrog Energy 37(18):13314–13322
67. Venetsaneas N, Antonopoulou G, Stamatelatou K, Kornaros M, Lyberatos G (2009) Using cheese whey for hydrogen and methane generation in a two-stage continuous process with alternative pH controlling approaches. Bioresour Technol 100(15):3713–3717
68. Yokoi H, Maki R, Hirose J, Hayashi S (2002) Microbial production of hydrogen from starch-manufacturing wastes. Biomass Bioenerg 22(5):389–395
69. Rama Mohan S (2016) Strategy and design of innovation policy roadmapping for a waste biorefinery. Bioresour Technol 215:76–83
70. Bastidas-Oyanedel JR, Bonk F, Thomsen MH, Schmidt JE (2015) Dark fermentation biorefinery in the present and future (bio)chemical industry. Rev Environ Sci Bio 14(3):473–498
71. Venkata SM, Nikhil GN, Chiranjeevi P, Nagendranatha Reddy C, Rohit MV, Naresh Kumar A, Sarkar O (2016) Waste biorefinery models towards sustainable bioeconomy: critical review and future perspectives. Bioresour Technol 2015:2–12
72. Sawatdeenarunat C, Nguyen D, Surendra KC, Shrestha S, Rajendran K, Oechsner H, Khanal SK (2016) Anaerobic biorefinery: current status, challenges, and opportunities. Bioresour Technol 215:304–313
73. Sarma SJ, Pachapur V, Brar SK, Le Bihan Y, Buelna G (2015) Hydrogen biorefinery: potential utilization of the liquid waste from fermentative hydrogen production. Renew Sustain Energy Rev 50:942–951
74. Zong W, Yu R, Zhang P, Fan M, Zhou Z (2009) Efficient hydrogen gas production from cassava and food waste by a two-step process of dark fermentation and photo-fermentation. Biomass Bioenerg 33(10):1458–1463
75. Marone A, Ayala-Campos OR, Trably E, Carmona-Martinez AA, Moscoviz R, Latrille E, Bernet N (2016) Coupling dark fermentation and microbial electrolysis to enhance bio-hydrogen production from agro-industrial wastewaters and by-products in a bio-refinery framework. Int J Hydrog Energy 42(3):1609–1621
76. Turon V, Trably E, Fouilland E, Steyer JP (2016) Potentialities of dark fermentation effluents as substrates for microalgae growth: a review. Proc Biochem 51(11):1843–1854
77. Rozendal RA, Hamelers HVM, Euverink GJW, Metz SJ, Buisman CJN (2006) Principle and perspectives of hydrogen production through biocatalyzed electrolysis. Int J Hydrog Energ 31 (12):1632–1640
78. Kumar G, Bakonyi P, Kobayashi T, Xu K, Sivagurunathan P, Kim S, Béla K (2016) Enhancement of biofuel production via microbial augmentation: The case of dark fermentative hydrogen. Renew Sustain Energ Rev 57:879–891
79. Logan B, Regan J (2006) Electricity-producing bacterial communities in microbial fuel cells. Trends Microbiol 14:512–518

80. Lee HS, Vermaas WFJ, Rittmann BE (2010) Biological hydrogen production: prospects and challenges. Trends Biotechnol 28(5):62–271

81. Moreno R, Escapa A, Cara J, Carracedo B, Gómez X (2015) A two-stage process for hydrogen production from cheese whey: Integration of dark fermentation and biocatalyzed electrolysis. Int J Hydrog Energ 40(1):168–175

82. Dhar BR, Elbeshbishy E, Hafez H, Lee HS (2015) Hydrogen production from sugar beet juice using an integrated biohydrogen process of dark fermentation and microbial electrolysis cell. Bioresour Technol 198:223–230

83. Li XHH, Liang DWW, Bai YXX, Fan YTT, Hou HWW (2014) Enhanced H$_2$ production from corn stalk by integrating dark fermentation and single chamber microbial electrolysis cells with double anode arrangement. Int J Hydrog Energy 39(17):8977–8982

84. Su H, Cheng J, Zhou J, Song W, Cen K (2009) Combination of dark- and photo-fermentation to enhance hydrogen production and energy conversion efficiency. Int J Hydrog Energ 34(21):8846–8853

85. International Energy Agency (2015) Technology roadmap: hydrogen and fuel cells

86. The Linde Group (2017) Hydrogen energy applications

87. Chan CC (2015) Overview of electric, hybrid, and fuel cell vehicles. Encyc Autom Eng

88. Koyama MH, Araújo Júnior MM, Zaiat M, Ferraz Júnior ADN (2016) Kinetics of thermophilic acidogenesis of typical Brazilian sugarcane vinasse. Energy 116(1):1097–1103

89. Ferraz Junior ADN, Etchebehere C, Zaiat M (2015) High organic loading rate on thermophilic hydrogen production and metagenomic study at an anaerobic packed-bed reactor treating a residual liquid stream of a Brazilian biorefinery. Bioresour Technol 186:81–88

90. Ferraz Junior ADN, Wenzel J, Etchebehere C, Zaiat M (2014) Effect of organic loading rate on hydrogen production from sugarcane vinasse in thermophilic acidogenic packed bed reactors. Int J Hydrog Energy 39(30):16852–16862

91. Ferraz Junior ADN, Etchebehere C, Zaiat M (2015) Mesophilic hydrogen production in acidogenic packed-bed reactors (APBR) using raw sugarcane vinasse as substrate: influence of support materials. Anaerobe 34:94–105

92. MdelP Anzola-Rojas, da Fonseca SG, da Silva CC, de Oliveira VM, Zaiat M (2015) The use of the carbon/nitrogen ratio and specific organic loading rate as tools for improving biohydrogen production in fixed-bed reactors. Biotechnol Rep 5:46–54

93. Ferraz Júnior ADN, Koyama MH, Araújo Júnior MM, Zaiat M (2016) Thermophilic anaerobic digestion of raw sugarcane vinasse. Renew Energy 89:245–252

94. Han W, Fang J, Liu Z, Tang J (2016) Techno-economic evaluation of a combined bioprocess for fermentative hydrogen production from food waste. Bioresour Technol 202:107–112

95. Capson-Tojo G, Rouez M, Crest M, Steyer JP, Delgenès JP, Escudié R (2016) Food waste valorization via anaerobic processes: a review. Rev Environ Sci Bio 15(3):499–547

96. Redwood MD, Orozco RL, Majewski AJ, Macaskie LE (2012) An integrated biohydrogen refinery: synergy of photofermentation, extractive fermentation and hydrothermal hydrolysis of food wastes. Bioresour Technol 119:384–392

Chapter 7
Hydrogen from Photo Fermentation

**Alissara Reungsang, Nianbing Zhong, Yanxia Yang,
Sureewan Sittijunda, Ao Xia and Qiang Liao**

1 Introduction

Depletion of non-renewable energy sources and greenhouse gas emission (GHG) from its usage causes a great impact on human society [1]. Awareness to these problems leads to discovery of new sources of renewable energy such as wind, solar, hydrothermal, and biofuels [1]. Among those sources, hydrogen is a

A. Reungsang
Faculty of Technology, Department of Biotechnology, Khon Kaen University,
Khon Kaen 40002, Thailand

A. Reungsang
Research Group for Development of Microbial Hydrogen Production Process from Biomass,
Khon Kaen University, A. Muang, Khon Kaen 40002, Thailand

N. Zhong
Chongqing Key Laboratory of Fiber Optic Sensor and Photodetector,
Chongqing Key Laboratory of Modern Photoelectric Detection Technology
and Instrument, Chongqing University of Technology, Chongqing 400054, China

Y. Yang
Thermal Engineering Department, School of Electrical and Power Engineering,
Taiyuan University of Technology, No.79 Yingze West Street, Wanbailin Distinct,
Taiyuan, Shanxi 030024, China

S. Sittijunda
Faculty of Environment and Resource Studies, Mahidol University,
Nakhon Pathom 73170, Thailand

A. Xia · Q. Liao (✉)
Key Laboratory of Low-Grade Energy Utilization Technologies and Systems,
Chongqing University, Ministry of Education, Chongqing 400030, China
e-mail: lqzx@cqu.edu.cn

A. Xia · Q. Liao
Institute of Engineering Thermophysics, Chongqing University, Chongqing 400030, China

promising future fuel for transportation sector due to its advantages of absolute zero carbon emission and high energy density by mass [1]. Hydrogen production by biological pathway is attractive because it is cost-effective and can utilize various wastes as substrates in the production [2, 3]. Biological hydrogen production is possible through photofermentative route or through dark fermentation. Conversion of waste streams to hydrogen is possible by using purple non-sulfur bacteria (PNSB) through photofermentative pathway. PNSB can utilize wide ranges of substrates, such as simple sugars, volatile fatty acids (VFAs), industrial wastes and agricultural wastes, to produce hydrogen and carbon dioxide under anaerobic condition and with the presence of light. In addition, using PNSB is also an attractive option for complete conversion of organic acids presented in the effluent stream from hydrogen production using dark fermentation [4–6]. It is noticeable that by using different organic acids, different hydrogen yields (HY) are obtained. Butyric acid yields the highest theoretical HY of 10 mol H_2/mol substrate, whereas acetic acid yields the lowest value of 4 mol H_2/mol substrate.

In practical, HY from photofermentative hydrogen production using organic acids are always lower than the theoretical values. This owes to the effects of environmental factors such as substrate inhibition, temperature, pH, color of wastewater, light intensity and light wavelengths [7]. Due to the importance of these factors, many studies on factors affecting hydrogen production by photosynthetic bacteria and optimization of the factors have been carried out [7, 8]. Studies on conversion of various organic acids to hydrogen by photosynthetic bacteria have employed the pure form of these acids. However, many recent studies started to investigate the use of various waste streams in photofermentative hydrogen production such as agricultural biomass [9], crude glycerol from biodiesel production [10, 11] and industrial wastes that are rich in organic matters [12, 13].

In this chapter, overviews of photo hydrogen fermentation research are provided. It would cover the areas of PNSB and its enzyme system involved in photofermentative hydrogen production, factors affecting the fermentation, the production from industrial waste/wastewater and agricultural biomass. Both the suspension and immobilized cultures of PNSB for various types of photo bioreactors are discussed in details. Furthermore, the fluid flow and mass transfer in bioreactors using lattice Boltzmann simulation are presented. The enhancement strategies and perspectives of photofermentative hydrogen production are also outlined.

2 Photosynthetic Bacteria for Photo Fermentation

2.1 Purple Non-sulfur Photosynthetic Bacteria (PNSB)

PNSB are proteobacteria which tend to grow under anaerobic or microaerobic conditions. They do not use water as reducing agent as in plants, algae and cyanobacteria. Thus, there is no oxygen generated in the system. Unlike sulfur bacteria, PNSB use a minute concentration of sulfide as electron donor during

photoautotrophic growth; hence, it is called "non-sulfur". In comparison to the hydrogen production by algae through water splitting, PNSB require much less free energy to produce hydrogen.

Generally, PNSB are gram-negative with red colonies [14–16]. They contain carotenoids and bacteriochlorophyll pigments. Some examples of physical shapes and structures of PNSB under scanning electron microscopy (SEM) are depicted in Fig. 1. PNSB use photosynthesis to produce energy and generate ATP through the cyclic function of its single photosystem. Carbon compounds, inorganic ions such as Fe^{2+} or hydrogen can be used as the sources of electrons for its metabolic activities. PNSB can grow as photoautotrophs under the presence of light and CO_2, photoheterotrophs under the presence of light and organic compounds or chemoheterotrophs under the sole presence of organic compounds [14]. PNSB growing photoheterotrophically get electrons and carbon from reduced carbon compounds. Some species can also grow photolithoautotrophically by using S^{2-}, H_2 or Fe^{2+} as electron donors and CO_2 as the sole carbon source [19].

PNSB can use a wide variety of organic carbon compounds such as pyruvate, acetate and other organic acids, amino acids, alcohols and carbohydrates. Some species can use C1 compounds, i.e., methanol and formate as carbon source. Aromatic organic compounds such as benzoate, cinnamate, chlorobenzoate, phenylacetate and phenol can also be used as carbon sources by PNSB [20]. Organic acids that can be assimilated by PNSB include acetic acid [21], butyric acid [22], propionic acid [21], malic acid [23] and lactic acid [18]. Therefore, when using organic wastes as substrates in hydrogen production, PNSB can utilize organic acids produced during acidogenic phase of anaerobic digestion as carbon source for conversion to H_2 and CO_2. Genus of PNSB that can utilize organic acids for hydrogen production include *Rhodobacter* sp. [17], *Rhodobacter sphaeroides* [16, 18, 24–26], *Rhodobacter capsulatus* [27–29], *Rhodopseudomonas* sp. [30], *Rhodopseudomonas palustris* [31–33], *Rhodopseudomonas capsulata* [34],
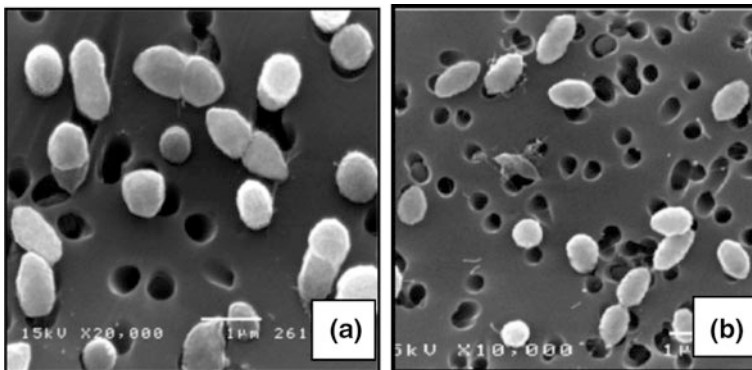
Fig. 1 Physical shapes and structures of some species of PNSB under scanning electron microscopy (SEM); **a**: *Rhodobacter* sp. KKU-PS1 (adapted from [17]); **b**: *Rhodobacter sphaeroides* KKU-PS5 (adapted from [18], Copyright 2014, with permission from Elsevier)

Rhodospirillum rubrum [35] and *Rhodovulum sulfidophilum* [36]. PNSB can use artificial light such as tungsten and luminescence type as the energy source. Previously, it was reported that light intensity exceeding the optimum level did not pose any adverse effects on PNSB growth and photo hydrogen production [37]. However, recent studies showed that high light intensity could cause partial inhibition in hydrogen production ability of PNSB [38, 39].

PNSB can be found in both aquatic environments including sediments and moist soils and wastewater treatment sites, especially those with low oxygen solubility, good light penetration and availability of organic substance [40]. Since the bacteria can grow in many modes and survive in diverse environments, they could be isolated from various sources. Some example included *Rhodobacter sphaeroides* AV1b which was isolated from the Averno lake, Naples, Italy [21]; *Rhodopseudomonas palustris* 42OL from wastewater pond of a sugar refinery [41]; *Rhodopseudomonas* sp. nov. strain A7 from sludge in a running bioreactor [30]; *Rhodobacter sphaeroides* KKU-PS1 from an effluent of up-flow anaerobic sludge blanket (UASB) reactor [17]; *Rhodobacter sphaeroides* HY01 from paddy field wastewater [42]; and *Rhodovulum sulfidophilum* P5 from a shrimp farm [36]. Lists of PNSB capable of producing hydrogen are tabulated in Table 1.

2.2 Photofermentative Hydrogen Production by Purple Non-sulfur Bacteria

Photofermentative hydrogen production involves the conversion of organic compounds into CO_2 and hydrogen in the presence of light as energy source with no oxygen evolution. Photofermentative hydrogen production can completely convert organic compounds into hydrogen even with a relatively high hydrogen partial pressure. This is because the pathways toward the production of hydrogen are supported by ATP-dependent nitrogenase and ATP is formed via photosynthesis. PNSB have been the most reported photofermentative hydrogen producers [51]. Gest and Kamen [52] reported *Rhodospirillum rubrum* as the first PNSB capable of photofermentative hydrogen production. PNSB in the genus *Rhodobacter* has been the most widely used in photo hydrogen fermentation due to its ability to use various types of substrates and flexibility in surviving and growing in diverse environments. PNSB with high hydrogen production capability under photofermentation condition include *Rhodobacter sphaeroides* KKU-PS1 [17], *Rhodopseudomonas palustris* [41], *Rhodobacter capsulatus* [47], and *Rhodospirillum rubrum* [53].

A major advantage of photofermentation is high HY. The theoretical HY from glucose is 12 mol H_2/mol following the reaction shown in Eq. (1). Other theoretical HY from various VFAs that involve in photofermentation process are tabulated in Table 2 [54, 55]. In comparison to dark fermentation process, chemical oxygen demand (COD) removal efficiency and hydrogen content of photofermentative hydrogen production are relatively high [51]. However, there are some limitations

Table 1 Purple non-sulfur photosynthetic bacteria (PNSB) capable of photofermentative hydrogen production

PNSB strain	Carbon source	Carbon source concentration	Hydrogen yield[a] (%)	Hydrogen production rate[b] (mL/L h)	References
Rhodobacter sphaeroides AV1b	Acetate	466 mg/L	42.7	NA	[22]
	Propionate	449 mg/L			
	Butyrate	1075 mg/L			
Rhodobacter sphaeroides NCIMB8253	Malate	4.66 g/L	NA	64.9	[43]
Rhodopseudomonas palustris 42OL	Malate	2 g/L	31.5	21.8	[41]
Rhodobacter sphaeroides NCIMB8253	Malate	0.75 g/L	NA	133.6	[44]
Rhodobacter sphaeroides NCIMB8253	Malate	0.75 g/L	NA	322	[23]
Rhodobacter sphaeroides NCIMB8253	Malate	4.66 g/L	NA	138.6	[45]
Rhodobacter sphaeroides NCIMB8253	Malate	4.66 g/L	NA	200.5	[46]
Rhodobacter capsulatus	Acetate	2 mM	19	19.67	[47]
	Butyrate	11 mM			
	Propionate	1.7 mM			
Rhodobacter sphaeroides AV1b	Acetate	287.9 mg/L	NA	0.42	[21]
	Butyrate	558.66 mg/L			
	Propionate	238.9 mg/L			
Mixed PNSB	Acetate	287.9 mg/L	NA	0.65	
	Butyrate	558.66 mg/L			
	Propionate	238.9 mg/L			
Mixed PNSB	Glucose	70 mM	NA	136	[48]
Rhodopseudomonas palustris PB-Z	Glucose	12.6 g/L	NA	78.7	[49]
Rhodopsuedomonas sp. nov. strain A7	Acetate	4.92 g/L	NA	1.11	[30]
Rhodopseudomonas pentothenatexigens KKU-SN1/1	Malic acid	7.6 g/L	NA	3.23	[50]
Rhodobacter sphaeroides KKU-PS1	Malic acid	0.268 g/L	65	12	[17]

[a]Percentage of hydrogen yield (HY) (mol H_2/mol substrate) in relation to the theoretical value
[b]Maximum hydrogen production rate (HPR) (mL/L h)
NA Not available

Table 2 Theoretical hydrogen yield (HY) of photofermentative hydrogen production pathways obtained from utilizing various organic acids (adapted from [54, 55])

Organic acids		Equation of biochemistry pathways	Theoretical HY[a]
Common name	Formula		
Butyric acid	$CH_3CH_2CH_2COOH$	$CH_3CH_2CH_2COOH + 6H_2O \rightarrow 10H_2 + 4CO_2$	10
Propionic acid	CH_3CH_2COOH	$CH_3CH_2COOH + 4H_2O \rightarrow 7H_2 + 3CO_2$	7
Malic acid	$COOHCH_2CHOHCOOH$	$COOHCH_2CHOHCOOH + 3H_2O \rightarrow 6H_2 + 4CO_2$	6
Succinic acid	$COOHCH_2CH_2COOH$	$COOHCH_2CH_2COOH + 4H_2O \rightarrow 7H_2 + 4CO_2$	7
Lactic acid	$CH_3CHOHCOOH$	$CH_3CHOHCOOH + 3H_2O \rightarrow 6H_2 + 3CO_2$	6
Acetic acid	CH_3COOH	$CH_3COOH + 2H_2O \rightarrow 4H_2 + 2CO_2$	4

[a]The unit of the theoretical HY is mol H_2/mol substrate

of hydrogen production from photofermentative pathway including a low hydrogen production rate (HPR), toxicity to PNSB caused by high substrate concentration and light requirement for hydrogen production [56].

$$C_6H_{12}O_6 + 12H_2O + \text{light energy} \rightarrow 12H_2 + 6CO_2 \tag{1}$$
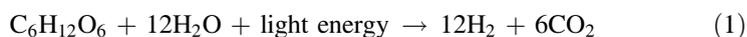
There are two different fermentation processes employed in photofermentative hydrogen production viz. single-stage and two-stage processes. In a single-stage process, range of substrates includes organic acids, sugars, industrial waste, agricultural waste and acidic effluents from hydrogen production process. Single-stage process in photofermentative hydrogen production yields a better hydrogen production than that obtained from dark fermentation. For example, hydrogen production by PNSB from glycerol resulted in a much higher HY than those obtained in dark fermentation. Theoretically, HY from crude glycerol by dark fermentation is 1 mol H_2/mol glycerol. However, HY obtained by photofermentative hydrogen production from crude glycerol by *R. palustris* CGA009 was 6.1 mol H_2/mol crude glycerol at the optimum medium containing 20 mM glycerol and 5 mM of glutamate [57].

For a two-stage photofermentative hydrogen production, dark fermentation is coupled with photofermentative hydrogen production in order to obtain a higher HY. The coupling was either by sequential (two-stage) or combined (co-cultures) dark and photo fermentation [4]. In sequential dark-photo fermentation, VFAs presented in the acidic effluent obtained from dark fermentation in the first stage are used as the substrates to produce hydrogen by PNSB in the second stage. This approach could yield a maximum theoretical HY of 12 mol H_2/mol glucose when acetic acid is the only by-product of dark fermentation [58, 59]. However, the acidic effluent can be inhibitive to photofermentative hydrogen production due to its low pH, excess of fixed nitrogen and high substrate concentration [4]. Therefore, pretreatment of the acidic effluent is required. Various pretreatment approaches could be employed such as dilution, addition of nutrients, adjustment of pH, sterilization and centrifugation [60]. Various kinds of wastes were reported in hydrogen production by sequential dark-photo fermentation such as palm oil mill effluent [61], starch wastewater [62], crude glycerol [63], amino acids from protein degradation in waste biomass [64], corn stalk [65], sugarcane bagasse [66], potato steam peels hydrolysate [67], beet molasses [60], cassava and food waste [68] and ground wheat solution [69].

In order to solve the problems caused by acidic pH and high substrate concentration of the acidic effluent from dark fermentation, the combined (co-cultures) dark and photo fermentation was investigated. This process involves co-cultures of dark and photo hydrogen producers in the same reactor [4]. VFAs produced by dark-hydrogen producer are immediately consumed by PNSB; hence acid accumulation and excess substrate that cause the inhibition were prevented. Moreover, alkalinization due to photofermentative hydrogen production can neutralize the acids from dark fermentation [4]. A maximum HY obtained by this fermentation process is 7 mol H_2/mol hexose. Since growth rates of the two microorganisms are different;

thus the environmental conditions of these two microorganisms needed to be optimized in order to achieve a maximum HY [4]. A few number of research on this approach were reported, e.g., co-cultures of *Cellulomonas fimi* and *Rhodopseudomonas palustris* in a single stage hydrogen production from cellulose [70], co-cultures of *Ethanoligenens harbinense* B49 and immobilized *Rhodopseudomonas faecalis* RLD-53 for hydrogen production from glucose [71], mixed cultures of *Clostridium butyricum* and *Rhodopseudomonas faecalis* RLD-53 for hydrogen production from glucose [72].

3 Key Enzymes Responsible for Hydrogen Production

Nitrogenase and hydrogenase are 2 key enzymes responsible for hydrogen production in PNSB. Both enzymes contain metals in their active sites (metalloproteins). Proton (H^+) is reduced to hydrogen (H_2) by the action of these enzymes.

3.1 Nitrogenase

Nitrogenase is an enzyme that governs biological nitrogen fixation to maintain the balance of global nitrogen cycle. It can be found in many bacteria and archaea [73]. Nitrogenase is the key enzyme responsible for photofermentative hydrogen production by photosynthetic bacteria [74]. It can be classified into three groups based on metal clusters at its active site. Three homologous nitrogenases are molybdenum (Mo), vanadium (V) and iron (Fe) nitrogenases [75, 76]. Among the three nitrogenases, Mo-nitrogenase is the major cluster responsible for photofermentative hydrogen production [77]. Mo-nitrogenase consists of two component proteins namely iron (Fe) protein and MoFe protein [78]. Fe protein or dinitrogenase reductase is a homodimeric protein encoded by *nifH*. Another protein called dinitrogenase contains FeMo as the heterometal cofactor at its active site. MoFe-nitrogenase consists of two protein subunits designated as alpha (or *nifD*) and beta (or *nifK*) subunits [79, 80]. In enzyme function, Fe protein (Fe4–S4 cluster) acts as electron donor while MoFe protein is electron acceptor. Electrons flow from NifH to NifDK or α- and β-subunits via P-clusters which acts as a bridge or mediator. Structure and mechanism of nitrogenase enzyme are depicted in Fig. 2.

As shown in Fig. 2, hydrogen is produced as a side product during the reduction of nitrogen to ammonia. The reduction reaction by Mo-nitrogenase requires ATP. Each electron transfer also requires two ATP molecules. Therefore, 16 ATP molecules are needed to fix one mole of nitrogen resulting in one mole of hydrogen as shown in Eq. (2). The presence of ammonia in the system decreases the activity of Mo-nitrogenase and causes product inhibition, hence the inhibition of hydrogen production [82]. In addition, ATP must be sufficiently supplied to nitrogenase complex for optimal enzyme activity. Therefore, photofermentative hydrogen

production is the most rapid under the environment that provides saturating light intensity and organic electron donors [83].

$$\text{Mo - nitrogenase:} N_2 + 8H^+ + 8e^- + 16ATP \rightarrow 2NH_3 + H_2 + 16ADP \tag{2}$$
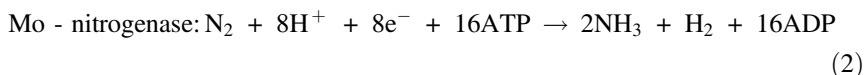
Mo-nitrogenase also catalyzes hydrogen production anaerobically under nitrogen limitation [84]. In the absence of N_2, hydrogen production occurs without formation of ammonia, as shown in Eq. (3) [82].

$$\text{Absence of } N_2 : 8H^+ + 8e^- + 4ATP \rightarrow 4H_2 + 4ADP \tag{3}$$

Hydrogen formation driven by Mo-nitrogenase is irreversible [85] which is advantageous because the hydrogen production would not be inhibited under high hydrogen partial pressure. Oxygen and ammonium are the main inhibitors for Mo-nitrogenase. Molecular oxygen damages the photo pigments needed to maintain ATP flux for Mo-nitrogenase function. Therefore, Mo-nitrogenase expression is strongly inhibited by oxygen in an irreversible manner. In the case of NH_4^+, the inhibition takes place as product inhibition and it is reversible [86]. Mo-nitrogenase activity could be recovered when ammonium ion is consumed or removed.

The "alternative nitrogenases", i.e., V-nitrogenase and Fe-nitrogenase contain vanadium and iron instead of molybdenum. Structures of these nitrogenases are similar to Mo-nitrogenase. The difference is the cofactors. V-nitrogenase features FeVa cofactor while Fe-nitrogenase features FeFe cofactor. Equations (4) and (5) show that these alternative nitrogenases require more electrons to reduce H^+ to H_2

than in the conventional Mo-nitrogenase [87]. *R. Palustris* CGA009 is the only photosynthetic bacterium that is known to contain all three nitrogenases. Expression of alternative nitrogenase was shown to be correlated with nitrogen starvation conditions [88].

$$V - nitrogenase: N_2 + 12H^+ + 12e^- + 24ATP \rightarrow 2NH_3 + 3H_2 + 24ADP \tag{4}$$

$$Fe - nitrogenase: N_2 + 24H^+ + 24e^- + 48ATP \rightarrow 2NH_3 + 9H_2 + 48ADP \tag{5}$$
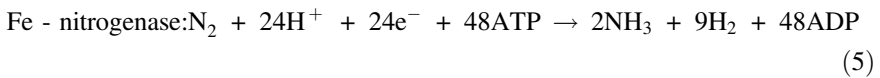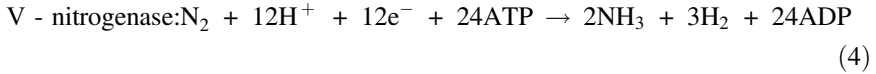
3.2 Hydrogenase

Hydrogenases are classified into three types: [NiFe]-hydrogenase, [FeFe]-hydrogenase, and [Fe]-hydrogenase, depending on metal atoms presented in their active sites [89].

[NiFe]-hydrogenase is the most common hydrogenase. It is more tolerable to CO and O_2 than [FeFe]-hydrogenase [90]. Nickel is the important cofactor that located at the enzyme's active site. Limited availability of Ni may reduce the activity of this enzyme. In general, [NiFe]-hydrogenase is hydrogen-uptake (or unidirectional) hydrogenase that is encoded by *hup* gene. This enzyme oxidizes hydrogen molecules to protons, Eq. (6). Activity of hydrogen-uptake hydrogenase poses a negative impact on the efficiency of hydrogen production both in terms of amount produced and production rate, especially in photofermentation.

$$H_2 \rightarrow 2H^+ + 2e^- \tag{6}$$

[FeFe]-hydrogenase contains Fe–S clusters in its molecule. It is encoded by *hox* gene. [Fe]-hydrogenase, a hydrogenase with similar nomenclature, contains neither nickel nor Fe-S clusters. It was initially named "metal-free hydrogenase" but it was later renamed as "iron–sulfur-cluster-free hydrogenase" or simply [Fe]-hydrogenase [91]. [FeFe]-hydrogenase often involves in hydrogen production pathways while [Fe]-hydrogenase does not have any role in hydrogen production.

Reaction driven by [FeFe]-hydrogenase is reversible (or bidirectional). Reversible hydrogenase is capable of oxidizing hydrogen into protons and also catalyzing hydrogen formation from protons as shown in Eq. (7) [92, 93]. Not only [FeFe]-hydrogenase involves in hydrogen evolution but also intrinsically biases towards this direction [94, 95].

$$H_2 \Leftrightarrow 2H^+ + 2e^- \tag{7}$$

Table 3 Comparisons of various properties between nitrogenase and hydrogenase (adapted from [92])

Property	Nitrogenase	Hydrogenase
Number of proteins	Two (Fe and MoFe proteins)	One
Metal elements	Mo, Fe	Ni, Fe
Substrates	Electrons, protons, ATP (or N_2)	H_2
Products generated	H_2 (or NH_4^+)	Electrons, protons, ATP
Stimulators	Light	H_2
Inhibitors	Oxygen, ammonia	Oxygen, Carbon monoxide, EDTA
Optimum temperature	30 °C (*Azotobacter vinelandii*)	55 °C (*Rhodospirillum rubrum*)
Optimum pH	Ranged from 7.1 to 7.3	Ranged from 6.5 to 7.5

Hydrogenase is the preferred enzyme for hydrogen production in dark fermentation due to its higher turnover rate and lower metabolic energy requirement than nitrogenase. Microbial fermentation mediated by hydrogenase theoretically generates up to 4 mol H_2/mol hexose according to the metabolic system and conditions. Minority of fermentative microorganisms (e.g., *Klebsiella* spp.) produce hydrogen via the action of nitrogenase [96]. High ATP requirement and low turnover rate of nitrogenase resulted in a much lower theoretical HY of 0.5 mol H_2/mol hexose [97].

Hydrogenase and nitrogenase are found in photoautotrophs, i.e., cyanobacteria and microalgae. In cyanobacteria, the self-sustained photofermentative hydrogen production occurs via the activity of nitrogenase which consumes ATP and re-oxidises the electron carriers. In microalgae, hydrogenase reduces $2H^+$ to H_2 without any ATP requirement [83]. PNSB produce hydrogen under photoheterotrophic conditions through nitrogenase-driven reaction [84]. Presence of hydrogen-uptake hydrogenase activity in PNSB can lower the hydrogen yield [98]. The development of hydrogen-uptake hydrogenase deficient PNSB mutants improved hydrogen production efficiency for up to 70% [99–102].

Key properties of nitrogenase and hydrogenase are summarized and compared in Table 3

4   Factors Influencing Photofermentative Hydrogen Production

4.1   Carbon Sources

Carbon source is the most important factor that affects cell growth and hydrogen production of PNSB [103, 104]. Carbon substrate is mainly used for cell growth and only a small fraction is used for hydrogen production. PNSB have an ability to utilize various substrates as carbon source including short chain organic acids (Table 1) such as malic, lactic, succinic, acetic, propionic and butyric acids [21–23, 41, 47]; glucose [48, 49]; organic waste (Table 4); industrial wastewaters such as fresh olive

mill waste [108], blackstrap molasses [28]; and agricultural waste such as corn stalk hydrolysate [65]. In addition, acidic effluent from dark hydrogen fermentation process can also be utilized by PNSB for hydrogen production [61, 109].

Type of carbon substrates affects the efficiency of photofermentative hydrogen production. This is due to variations in electron transfer capabilities in different metabolic pathways of photosynthetic microorganisms [51]. The most suitable carbon source for hydrogen production by *Rhodobacter sphaeroides* was malic acid [110, 111]. Koku et al. [92] and Basak and Das [26] reported that the absence of favored carbon sources such as malic and lactic acids was a major problem for photofermentative hydrogen production by PNSB. Some carbon sources such as

Table 4 Organic wastes used as carbon sources by purple-non-sulfur bacteria

Feedstock	Substrate concentrations	Microorganism	Substrate conversion efficiency (%)	Hydrogen production rate (mL H_2/L h)	References
Dairy wastewater	40% of waste (18.5 g COD/L)	*Rhodobacter sphaeriodes* O.U. 001	ND	49	[12]
Brewery wastewater	10% of waste (20.2 g COD/L)	*Rhodobacter sphaeriodes* O.U. 001	ND	61	[13]
Dark fermentation effluent of acid hydrolyzed wheat starch	2 g/L of TVFA	*Rhodobacter sphaeriodes* NRRL B-1727	ND	14.16[a]	[105]
Dark fermentation effluent of ground wheat strach	2 g/L of TVFA	*Rhodobacter sphaeriodes* NRRL B-1727	ND	1.13	[106]
Fermented food waste	2 g COD/L	*Rhodobacter sphaeoides* KD131	24	ND	[25]
Synthetic soluble metabolite of dark fermentation	10% of effluent (9.2 g/L of TVFA)	*Rhodopseudomonas palustris* WP3-5	49.9[a]	ND	[107]
Beet Molasses	1 g/L of sugar	*Rhodobacter capsulatus* JP91	87.5[a]	15.8[a]	[28]
Blackstrap molasses	1 g/L of sugar	*Rhodobacter capsulatus* JP91	66.7[a]	17.8[a]	[28]
Fresh olive mill waste	30% of waste (56.6 g COD/L)	*Rhodopseudomonas palustris* 42OL	ND	5.28	[108]
Corn stalk hydrolysate	5 g/L	*Rhodobacter sphaeroides* HY01	ND	74	[65]

[a]The values were calculated from the reported experiment
ND No reported data
TVFA Total volatile fatty acid

acetate gave HY of over 70% of the theoretical value. *Rhodopseudomonas palustris* P4 could convert acetate into hydrogen with HY of 60–70% of the theoretical yield [112]. In addition, HY of 75% was obtained when glucose was consumed by *Rhodopseudomonas palustris* WP 3-5 [113] and 53% was obtained when sucrose was consumed as carbon source by *Rhodopseudomonas capsulatus* JP91 [28]. Concentration of carbon substrate also has a major effect on hydrogen production. Suitable concentrations of VFAs for photofermentative hydrogen production were in the range of 1800–2500 mg/L [114, 115].

4.2   Nitrogen Sources

Nitrogen is required for cell synthesis and photofermentative hydrogen production. Hydrogen production by PNSB occurs through the action of nitrogenase. Type and concentration of nitrogen affect the activity of nitrogenase. Nitrogenase is inhibited in the presence of oxygen and ammonium salts [110]. Therefore, photofermentative hydrogen production requires oxygen-free and ammonia-limited conditions [116]. Hydrogen gas production by photosynthetic bacteria was low in the presence of ammonium salts. Therefore, addition of carbonate to remove ammonium salts was suggested in hydrogen production using ammonium-rich wastewater [117]. Although ammonium salt has an adverse effect on hydrogen production, other nitrogen sources such as glutamate, yeast extract, and albumin enhanced hydrogen gas production [112]. However, in the presence of high nitrogen concentration, microbial metabolism shifts from using organic substances for hydrogen production to cell synthesis [112].

The presence of NH_4^+ ions in small amounts could improve photofermentative hydrogen production [86]. However, high concentration of NH_4^+ ions inhibited nitrogenase activity [92]. Acidic effluent from dark fermentation of carbohydrate-rich wastewater usually contains large amount of NH_4^+ ions. Therefore, it is not suitable for photofermentative hydrogen production by PNSB. Glutamate is frequently used as nitrogen source for photofermentative hydrogen production [92, 118] because it shows less inhibition to nitrogenase and can be rapidly consumed by PNSB [92, 118, 119]. Addition of glutamate enhanced the hydrogen production from mixed VFAs by *R. Capsulate* [119]. However, glutamate is more expensive than NH_4Cl, using it in the process would bear a higher production cost [51]. Table 5 summarized the performance of photofermentative hydrogen production using different nitrogen sources and concentrations.

4.3   pH

pH value of culture medium affects the ionic concentration and the form of active site of nitrogenase, hence affecting its activity. It also impacts biochemical

Table 5 Hydrogen production performance of PNSB from different nitrogen types and concentrations

Nitrogen source	Nitrogen source concentration	PNSB	Substrate conversion efficiency (%)	References
Glutamate	15 mM	*Rhodopseudomonas* sp. nov. strain A7	80.5	[120]
Glutamate	224 mg/L	*Rhodobacter sphaeoides* KKU-PS1	74.5	[121]
Glutamate	1690 mg/L	*Rhodopseudomonas* sp. nov. strain A7	74.7	[122]
Glutamate	500 mg/L	*Rhodobacter capsulatus* SB1003 strain ZY29	57.8	[123]
Glutamate	600 mg/L	*Rhodobacter sphaeroides* CNT 2A	29	[124]
Glutamate	1690 mg/L	*Rhodopseudomonas* sp. nov. strain A7	63	[125]
Yeast extract	1000 mg/L	*Rhodopseudomonas palustris* CGA009 (co-culture with *Cellulomonas fimi* ATCC 484)	32	[70]
Yeast extract	500 mg/L	*Rhodobacter sphaeroides* O.U.001	49	[126]
Yeast extract	1000 mg/L	*Rhodobacter sphaeroides* O.U.001	64.2	[127]
Yeast extract	1000 mg/L	The photosynthetic bacterial consortium was made by enriching the isolated strains F1, F5, F7, F11 (all photosynthetic purple non-sulfur bacteria), L6 (*Chlorobiaceae*), S7 and S9 (purple sulfur bacteria)	77.8	[128]
Peptone	1000 mg/L	*Rhodobacter sphaeroides* O.U.001	49	[126]
Beef extract	1000 mg/L	*Rhodopseudomonas* sp. nov. strain A7	74.7	[122]
L-cysteine	500 mg/L	*Rhodopseudomonas* sp. nov. strain A7	74.7	[122]
L-cysteine	500 mg/L	*Rhodopseudomonas* sp. nov. strain A7	63	[125]
Peptone	500 mg/L	*Rhodopseudomonas* sp. nov. strain A7	74.7	[122]
NH$_4$Cl	1000 mg/L	Bacterial consortium comprised of the isolated strains F1, F5, F7, F11 (all photosynthetic purple non-sulfur bacteria), L6 (*Chlorobiaceae*), S7 and S9 (purple sulfur bacteria)	77.8	[128]
NH$_4$Cl	1000 mg/L	*Rhodopseudomonas* sp. nov. strain A7	74.7	[122]

characteristic in microbial cells during metabolism [36, 51]. Apart from its single effect, interaction between pH and nitrogen source concentration also affects hydrogen production by PNSB [129]. More acidic or alkaline pH creates an environment with low proton motive force, resulting in the lower ATP generation which in turn obstructs cell growth and reduces hydrogen production efficiency [130]. The optimum pH for nitrogenase was reported to be pH 7.1–7.3 [92] while the optimal value for photofermentative hydrogen production by PNSB is pH 7.0 [16, 18, 24]. However, the optimum pH for hydrogen production by PNSB is varied depending on the strains. Zhang et al. [123] discovered that a suitable pH for

hydrogen production from acetate by *Rhodobacter capsulatus* SB1003 ZY29 was pH 7. The same optimum pH was observed also in photosynthetic bacterium consortia (microorganisms related to the genera *Rhodobacter*, *Rhodospirillum, Rhodopseudomonas* and *Sulfurospirillum*) by Lazaro et al. [131]. Zagrodnik and Laniecki [126] reported an optimum pH of 7.5 for photofermentative hydrogen production from mixture of acetic and butyric acids by *Rhodobacter sphaeroides.* The report by Tao et al. [16] and Lazaro et al. [131] indicated that hydrogen production was inhibited when using an initial pH of 5. Therefore, it is necessary to optimize initial pH in order to achieve maximum hydrogen production. The effect of initial pH on batch photofermentative hydrogen production by different microorganisms is summarized in Table 6

4.4 Co-factors

Important co-factors for synthesis of nitrogenase are molybdenum (Mo) and iron (Fe) [92]. Addition of these metals in the medium is important for enhancing the efficiency of photofermentative hydrogen production by PNSB. Higher hydrogen production was obtained when the microelements were presented in the medium [132]. Yu and Lee [133] reported that an increase in Mo concentration alone did not increase hydrogen production. However, at an optimum concentration, Mo was

Table 6 Effect of initial pH on batch photofermentative hydrogen production by different photosynthetic bacteria

Microorganism	Substrate	Initial pH		H_{max} (mL H_2/L)	Substrate conversion efficiency (%)	References
		Range studied	Optimal value			
Rhodobacter sphaeroides CNT 2A	Acetate	4.0–9.0	8.0	739	52.50	[124]
Rhodobacter sphaeroides CNT 2A	Butyrate	4.0–9.0	8.0	1185	29.00	[124]
Rhodobacter sphaeroides CNT 2A	Glucose	4.0–9.0	9.0	289	3.83	[124]
Rhodobacter sphaeroides CNT 2A	Sucrose	4.0–9.0	9.0	314	10.00	[124]
Rhodobacter capsulatus SB1003 ZY29	Acetate	6.2–7.6	7	2312.6	51.59	[123]
Rhodobacter sphaeroides	Mixture of acetic and butyric acids	6.5–8.0	7.5	2305	64.21	[127]

found to enhance hydrogen production by *Rhodospeudomonas palustris* KU003 [134], *Rhodobacter capsulatus* [135] and *R. sphaeroides* O.U.001 [136, 137].

Iron is a major cofactor at the active site of FeMo-nitrogenase [81, 92]. Each molecule of nitrogenase contains 24 atoms of Fe [138]. An increase in Fe concentration resulted in an increase in hydrogen production [133]. The presence of Fe ehanced the efficiency of photofermentative hydrogen production by *Rhodobacter sphaeroides* O.U.001 [136] and *Rhodopseudomonas palustris* AV33 [31]. The optimal Fe concentration were varied depending on the species of PNSB such as 2.4 mg/L for *Rhodobacter sphaeroides* [139], 35 mg/L for *Rhodobacter sphaeroides* RV [140], 3.35 mg/L for *Rhodopseudomonas* BHU01 [141] and 1.68 mg/L for *Rhodobacter sphaeroides* KKU-PS5 [18]. However, iron may pose an adverse effect on activity of microbial cells by disrupting the cell surface if it was present in excess of the need for regular physiological metabolisms [139].

4.5 Light Intensity

Effective photofermentative hydrogen production requires sufficient supply of ATP and reducing power [38]. Photosynthetic bacteria generate ATP through photosynthetic system which requires light energy for the reaction, electron transport, ATP synthesis and hydrogen production. Useful wavelengths of light were 522, 805 and 850 nm [82, 118]. At the optimum light intensity, large amounts of ATP and reductive power are sufficient for supporting the activity of nitrogenase to produce hydrogen and to generate the cells [142, 143]. Further increase in light intensity above the optimal value causes a saturation effect. The effect leads to excess formation of ATP and $Fd_{(red)}$ [13] which would then dissipate as heat energy, causing damages to photosynthetic apparatus [144]. The consequence of this phenomenon is low hydrogen production. In addition, Kim et al. [145] reported that the cell could also be damaged by bleaching of bacteriochlorophyII pigment during cultivation with excess light intensity.

Low light intensity was reported also to decrease HY, total volume of hydrogen and HPR. Different PNSB requires different illumination intensity. Liu and Hallenbeck. [146] reported that a suitable light intensity for photofermentative hydrogen production from glucose by *Rhodobacter capsulatus* JP91 was 7.4 klux, whereas Yang et al. [42] found that 10 klux light intensity was effective for *R. sphaeroides* HY01. Zhang et al. [123] reported that the optimum light intensity for hydrogen production by *Rhodobacter capsulatus* ZY29 from acetate was 49 klux and 139 klux was reported for *R. sphaeroides* DSM158 [147]. The light intensity of 5 klux was optimum for hydrogen production by photosynthetic bacterium consortia that included microorganisms related to the genera *Rhodobacter*, *Rhodospirillum*, *Rhodopseudomonas* and *Sulfurospirillum* [131]. Table 7 tabulated light intensities for photofermentative hydrogen production by various PNSB.

Lighting from various sources was employed in photofermentative hydrogen production by PNSB. Some examples are halogen [25, 103], tungsten [16, 48],

Table 7 Light intensity employed in photofermentative hydrogen production by various photo-non sulfur bacteria

Microorganism	Substrate	Light intensity (klux)		H_{max} (mL H_2/L)	Substrate conversion efficiency (%)	References
		Range studied	Optimal value			
Phototrophic microbial consortium	Acetate and butyrate	3–8	5	ND	25.0	[131]
Rhodobacter sphaeroides DSM 158	Lactate	0.31–155.252	139.727	2280	32.8	[147]
Rhodobacter capsulatus ZY 29	Acetate	24.84–49.681	49.681	2591	57.8	[123]
Rhodobacter capsulatus JP91	Glucose	1.742–14.904	7.452	ND	52.0	[6]
Rhodobacter capsulatus YL1	Glucose	1.742–14.904	7.452	ND	63.0	[6]

ND No reported data

fluorescent [148], infrared [148] and light-emitting diode (LED) lamps [149, 150]. Among these lamps, LED provided high operational stability which could improve the performance of photofermentative hydrogen production [51]. The advantages of LED light sources include specific wavelengths (770–920 nm), low electricity consumption, low heat generation and long life expectancy [51, 150].

4.6 Temperature

Fermentation temperature influences hydrogen production, cell growth, HY and substrate degradation efficiency. An increase in temperature up to the optimum improves nitrogenase activity as well as proteins associated with cell growth or hydrogen production. An imbalance of incubation temperature caused the inhibition of physiological activity, intracellular enzyme activity and metabolism of cells. Unstable temperature causes bacteria to spend their energy for adaptation to changes in temperature in order to survive [60]. As a consequence, hydrogen production, HPR, HY and substrate conversion efficiency were decreased [51, 60]. Optimum growth temperatures for photosynthetic bacteria range between 30 and 40 °C [151] (Table 8). For example, the optimum growth of *Rhodopseudomonas palustris* CQK 01 occurred between 27.5 and 32.5 °C. Large decrease in hydrogen production was observed when the temperature was higher than 35 °C [153]. Basak et al. [154] reported the optimum temperature range for *Rhodobacter* sp. to be between 31 and 36 °C.

Table 8 Effect of incubation temperatures on batch photofermentative hydrogen production by different photo-non sulfur bacteria

Microorganism	Substrate	Temperature (°C)		H_{max} (mL H_2/L)	Substrate conversion efficiency (%)	References
		Range studied	Optimal value			
Rhodovulum sulfidophilum P5	Acetate	30–40	30	170	8.55	[152]
An acid tolerant mutant of *Rhodovulum sulfidophilum* P5 (An acid tolerant mutant strain TH-102)	Acetate	30–40	30	1004	50.5	[152]
Rhodobacter sp. KKU-PS1	Malic acid	22–38	25.6	1264	64.7	[17]
The mixed photoheterotrophic culture (NG07) (*Rhodopseudomonas* sp. and *Rhodobacter* sp. were predominant)	Glucose	30–50	35	2746.9	15.37	[48]

4.7 Inoculum Age and Concentration

Early stationary phase was suitable for hydrogen production by photosynthetic bacteria [155–157]. PNSB inoculum in exponential growth phase is the most suitable to enhance hydrogen production. Cultivation of cells for extended period causes the change in cell metabolism towards other pathways such as pathway that promotes polyhydroxyl butyrate (PHB) accumulation [158].

Initial cell concentration has the most important roles in influencing the culture conditions of photofermentative hydrogen production [24, 131, 159]. In batch fermentation, ratio between initial cell concentration (X_0) and initial substrate concentration (S_0) affects initial energy level of microorganisms that is required to support cell synthesis and metabolism [24]. At a high S_0/X_0 ratio, i.e., low seed concentration, microorganisms need more time to adapt to be able to utilize high substrate concentration, resulting in a delay or lag period in the fermentation [24, 131, 159]. Further increase in cell concentration to greater than the optimal level resulted in a decrease in hydrogen production [24, 131, 159]. At a low S_0/X_0 ratio, i.e., high seed concentration, substrate is insufficient to support the growth of cells [24]. In addition, excess biomass interfere the penetration of light into cultivation system due to self-shading effect. The decrease in light intensity reduces the ATP formation and eventually diminishes hydrogen production by photosynthetic bacteria. Moreover, high cell concentration may promote formation of bacterial flocs or biofilm which can hinder substrate distribution within the bioreactor system [24, 92, 118]. Different optimum inoculum levels in photofermentative hydrogen production

by PNSB were reported, such as 0.36 g cell dry weight (CDW)/L [12, 13], 0.56 g CDW/L [24], and 0.2 g volatile suspended solid (VSS)/L [131].

5 Photofermentative Hydrogen Production from Industrial Waste/Wastewater and Biomass Waste

5.1 *Industrial Wastes and Wastewaters*

A wide variety of waste streams is possible to use as substrates in biohydrogen production. Various criteria should be considered in order to assess their suitability as a possible substrate. Relative cost, overall abundance, carbohydrate content and ease of degradation contribute a significant impact on process economics. The most suitable waste streams for hydrogen production via photofermentation are those containing organic acids [4, 6]. However, availability of those wastes is scarce comparing to waste streams from other sources such as agricultural biomass. Another substrate that is rich in organic acids is the effluent obtained from hydrogen fermentation process. This effluent contains large quantities of VFAs such as acetic acid, butyric acid, propionic acid, succinic acid, lactic acid and other alcohols. These compounds are suitable for conversion to hydrogen by photosynthetic bacteria [4, 6].

Industrial wastes and wastewaters generally contain high carbon contents especially those contributed by organic acids. Therefore, these waste streams are favorable for biohydrogen production by photosynthetic bacteria. Many industrial wastes and wastewaters have been used as substrates in photofermentative hydrogen production. Examples are those from dairy industry [13], brewery [12], tofu manufacturing [160, 161], sugar industry [28], soy sauce wastewater [162], palm oil mill effluent (POME) [163], pulp and paper mills [46, 164], olive mill [136] and biodiesel industry [57, 165]. Table 9 presents some examples of waste streams used in photofermentative hydrogen production and its performance as substrates.

The use of different type of wastes as substrates in biohydrogen production resulted in a different results on hydrogen gas production (Table 9). Based on the data presented in Table 9, the important criteria for effective photofermentative hydrogen performance are type and composition of feedstocks. Feedstocks containing organic acids are favorable and easy to convert to hydrogen by photosynthetic bacteria. However, other factors must be concerned in order to achieve an effective production process. Those factors include inhibitors and toxic compounds, color of the wastewater, turbidity, light intensity and sources, initial pH, temperature, substrate concentration and reactor configuration [4, 6]. Hydrogen production via photofermentative pathway employing various industrial wastewaters is focused in this section.

Table 9 Photofermentative hydrogen production from industrial wastes and wastewaters by photo-non sulfur bacteria

Wastes and wastewaters	Type of organic acid	Organism	Light intensity	Operation	Hydrogen production	References
Brewery wastewater	ND	*Rhodobacter sphaeroides* O.U. (ATCC 4919)	116 W/m², 9 klux	Batch	2.24 L H₂/L medium, 0.22 L H₂/L waste	[12]
Non sterile dairy wastewater	Lactic acid	*Rhodobacter sphaeroides* O.U.001 (ATCC 4919)	9 klux	Batch	7.6 L H₂/L waste	[13]
Sterile dairy wastewater	Lactic acid	*Rhodobacter sphaeroides* O.U.001 (ATCC 4919)	9 klux	Batch	4.4 L H₂/L waste	[13]
Tofu wastewaters	Total volatile acid 200 mg/L	*Rhodobacter sphaeroides*	8 klux	Batch	15.87 mL H₂/L h	[160]
Tofu wastewaters	Total volatile acids 200 mg/L	Immobilized *Rhodobacter sphaeroides*	8 klux	Immobilized	0.24 mL H₂/mg carbohydrate	[160]
Tofu wastewaters	Total volatile acid 200 mg/L	Immobilized *Rhodobacter sphaeroides*	8.5 klux	Immobilized	0.39 mL H₂/mg DW h	[161]
Soy sauce wastewater	Organic acid 170 mmol/L	*Rhodobium marinum*	60 W/m²	Batch	200 mL H₂	[162]
Palm oil mill effluent and pulp and paper mill	ND	*R. sphaeroides* NCIMB8253	7 klux	Batch	8.72 mL H₂/mL medium	[164]
Palm oil mill effluent and pulp and paper mill	ND	*R. sphaeroides* NCIMB8253	7 klux	Batch	14.438 mL H₂/mL medium	[45]
Palm oil mill effluent (POME)	ND	*Rhodpseudomonas palustris* PBUM001	4 klux	Batch	1.05 mL H₂/L POME	[163]
Olive mill wastewater	Acetic, Formic, Propionic, Lactic, Butyric, Aspartic, Glutamic acids	*Rhodobacter sphaeroides* O.U.001	150 W/m²	Batch	16 L H₂/L OMW	[166]

Table 9 (continued)

Wastes and wastewaters	Type of organic acid	Organism	Light intensity	Operation	Hydrogen production	References
Clay pretreatment of olive mill wastewater	Acetic, Formic, Propionic, Lactic, Butyric, Aspartic, Glutamic acids	*Rhodobacter sphaeroides* O.U.001	150 W/m^2	Batch	31.5 L H$_2$/L OMW	[166]
Beet molasses	ND	*Rhodobacter capsulatus* JP91	200 W/m^2	Batch	10.5 mol H$_2$/mol sucrose	[28]
Black strap molasses	ND	*Rhodobacter capsulatus* JP91	200 W/m^2	Batch	8 mol H$_2$/mol sucrose	[28]
Beet molasses	Acetic, Lactic, Formic, Propionic, Malic, Fumaric, and Succinic acids	*Rhodobacter sphaeroides* O.U.001	200 W/m^2	Batch	0.5 mol H$_2$/mol sucrose, 1.01 L H$_2$/L culture	[167]
Pure glycerol	ND	*Rhodopseudomonas palustris* NCIMB 11774	150-180 μmol/m^2/s	Batch	34 mL H$_2$/g DW h	[10]
Crude glycerol	ND	*Rhodopseudomonas palustris* CGA009	200 W/m^2	Batch	6.1 mol H$_2$/mol glycerol	[57]
Crude glycerol	ND	*Rhodopseudomonas palustris*	175 W/m^2	Batch	6.69 mol H$_2$/mol glycerol	[165]

ND No reported data

5.2   Crude Glycerol

Crude glycerol is a waste stream from biodiesel production process with high organic content and expensive disposal cost [3, 168]. It is formed along with fatty acid methyl ester (FAME) from transesterification reaction of oils and fats. Production of 10 kg of biodiesel via transesterification process generates 1 kg of glycerol [3]. Crude glycerol derived from biodiesel production process contains high carbon content and impurities such as methanol, salts and soap; all of which act as inhibitors to hydrogen production [3]. Many researches have used crude glycerol as the feedstock for biofuels (e.g., hydrogen, methane, and ethanol) and chemicals (e.g., PHB) by dark and aerobic fermentation process [3, 168–170]. However, there were a few researches that focused on conversion of glycerol to hydrogen via photofermentative route.

The use of different nitrogen sources and crude glycerol concentrations resulted in different values of hydrogen produced and microbial growth rates. Ghosh et al. [57] studied the effect of nitrogen concentration and glycerol concentration on hydrogen production from crude glycerol by *R. palustris* CGA009. It was found that glutamate is a nitrogen source that supports the growth of *R. palustris* CGA009. However, no hydrogen was detected when glutamate was used as a sole carbon source. Pott et al. [10] used crude glycerol from biodiesel production process as the substrate for a photofermentative hydrogen producer, *Rhodopseudomonas palustris*. Crude glycerol was pretreated with solid $CaCl_2$ at a dosage of 25 g/L. Results showed that conversion efficiency of glycerol to hydrogen was in the range from 80 to 85%. This range of efficiency values were similar to those reported by other researchers, e.g., 96% by Ghosh et al. [57] and 75% by Sabourin-Provost and Hallenbeck [171].

The presence of saponified fatty acid in crude glycerol is inhibitive to the growth of *R. palustris*. Although *R. palustris* was shown to tolerate high concentration of glycerol, ethanol and methanol, using high concentration of crude glycerol may affect the bacterium because it may contain also significant amount of saponified fatty acid. Therefore, suitable concentration of crude glycerol is essential in this case in order to obtain a high concentration of crude glycerol with no deteriorated effect from saponified fatty acid [10]. Response surface methodology with Box-Benkhen design was used as a tool to optimize process parameters for enhanced hydrogen production from crude glycerol [165]. Three factors in the study were crude glycerol concentration, glutamate concentration, and light intensity. Results showed that light intensity and crude glycerol concentration had significant effect on HY and nitrogenase activity and a maximum HY of 6.69 mol H_2/ mol glycerol was obtained at the optimal conditions (Table 9). The conditions were 30 mM crude glycerol, 4.5 mM glutamate and light intensity of 175 W/m^2. Light intensity was the most important factor that influenced nitrogenase protein expression and the supply of energy electrons and ATP through photofermentative pathway.

5.3 Palm Oil Mill Effluent (POME)

POME is a wastewater from milling process of palm fruit and it is the most pollutant from agro-industrial sector. POME contains high concentrations of organic carbon, nitrogen, suspended solid, heavy metal, oil and greases [163]. High level of organic carbon resulted in high COD and biochemical oxygen demand (BOD) values. The COD value of POME is around 84,450 mg/L [46]. However, the dark color of POME inhibits a successful hydrogen production. Therefore, an approach to reduce the color of POME was conducted by diluting 25% (v/v) of POME with 75% (v/v) of pulp and paper mill effluent (PPME) before being used as the feedstock for photofermentative hydrogen production by *R. sphaeroides* NCIMB 8253 (Table 9) [46]. Ultrasonic pretreatment with various amplitudes and durations were applied to pretreat this combined substrate. Results suggested that ultrasonic pretreatment enhanced bioavailability of organic matters, from which hydrogen production was enhanced. Biohydrogen production was improved from 467 mL H_2 in control experiment with no ultrasonication to 827.4 mL H_2 when pretreating the substrate with ultrasonication at 70% amplitude for 45 min. The improvement was due to an increase in $COD_{soluble}/COD_{total}$ value of the substrate from 0.25 to 0.85. Ultrasonication can breakdown the organic matters in substrates, resulting in an improvement of substrate bioavailability. Moreover, dilution of POME with PPME reduced the turbidity of POME and increased the light distribution during photofermentative hydrogen production process.

5.4 Olive Mill Wastewater

Olive oil production is the most important industry in the Mediterranean region, which accounts for 95% of worldwide olive oil production [166]. Extraction of olive fruits generated olive oil as the product and the effluent from the extraction process was called olive mill wastewater (OMW). This effluent has dark color and high organic matters. It is regarded as pollutant due to its high COD and BOD values that could be up to 200 g/L and 100 g/L, respectively [166, 172]. Moreover, it contains recalcitrant compounds such as polyphenols. Release of OMW without any pretreatment is not possible. Many researchers have focused on utilization of OMW as a substrate for photofermentative hydrogen production due to its high content of organic acids such as acetic acid, aspartic acid, glutamic acid [166, 172]. An attempt has been made by Eroğlu et al. [166] to reduce biorecalcitrant compounds in OMW such as phenol and color by using clay pretreatment. The pretreatment resulted in increasing light transmission during photofermentative hydrogen production due to its high color removal efficiency (65%). It also efficiently removed phenol (81%) and COD (31%) from OMW. The clay-pretreated OMW was used as the substrate for photofermentative hydrogen production by *Rhodobacter sphaeroides* O.U.001. The maximum hydrogen production of 31.5 L

H_2/L OMW was obtained. This value was twice of that obtained using OMW without pretreatment (16.5 L H_2/L OMW). Clay may also reduce nitrogen content in the media causing low C/N ratio which led to an enhancement in nitrogenase activity and hydrogen production.

The effect of OMW compositions on photofermentative hydrogen production was investigated by Eroğlu et al. [173]. OMW from different processes were compared. The maximum hydrogen production potential of 19.9 m^3/m^3 was obtained when using raw OMW from traditional process. Highest light conversion efficiency (0.33%) was evident when using raw OMW from a process that involved centrifugation, mainly due to its brightest color. The highest hydrogen production potential was obtained from the OMW with the highest organic content (consisted mainly of acetic acid, aspartic acid and glutamic acid) and highest molar C/N ratio of 73.8. These medium characteristics favor photofermentative hydrogen production by PNSB. On the other hand, if an OMW sample had a low level of C/N ratio, supplementation with other waste stream containing high carbon content such as algae biomass or domestic wastewater, could be a good option to increase C/N ratio in order to enhance hydrogen production.

5.5 Sugar Industry Wastewater

Beet molasses and blackstrap molasses are the effluents from sugar refinery processes. Beet molasses is the byproduct obtained from refining of sugar beet and typically contains 50% (w/w) sucrose and small amount of amino acids and organic acids. Blackstrap molasses is the byproduct from sugarcane refining process. It consists of 50% sugar content, of which are 36% sucrose, 6% fructose and 3% glucose. High sugar content in beet and blackstrap molasses made it the promising substrates for biohydrogen production. The hydrogen production from beet molasses and blackstrap molasses using *Rhodobacter capsulatus* JP91 was investigated by Keskin and Hallenbeck [28]. The effect of initial sugar concentration on hydrogen production was investigated. Increase in initial sugar concentration greater than 1 g/L resulted in a decrease in hydrogen production from 64 to 27 mL H_2 when using beet molasses. Different result was observed when using blackstrap molasses where hydrogen production increased with an increase in sugar concentration from 1 to 2 g/L. At 1 g/L molasses, maximum HY of 10.5 mol H_2/mol sucrose was obtained from beet molasses. A lower maximum HY of 8 mol H_2/mol sucrose was obtained from blackstrap molasses (Table 9). This study showed that beet molasses and blackstrap molasses are the good feedstocks for photofermentative hydrogen production. However, sugar concentration in production medium should be kept below 2 g/L since higher sugar concentration appeared to be toxic to microorganisms. In addition, dilution is required to reduce the color of raw materials and to increase light penetration.

Sugar beet molasses was used as the substrate for biohydrogen and 5-aminolevulinic acid (5-ALA) using *Rhodobacter sphaeroides* O.U.001 (DSM

5864) [167]. Dilution of sugar beet molasses was necessary in order to reduce the color and viscosity of the raw material. The dilution makes the molasses suitable for photofermentative hydrogen production due to improvement in light penetration. Apart from the main composition of 50% sucrose, beet molasses also contains various organic acids including 42.24 mg/L lactic acid, 16.91 mg/L acetic acid, 9.59 mg/L formic acid, 8.7 mg/L succinic acid, 5.94 mg/L malic acid, 4.94 mg/L propionic acid and 0.61 mg/L fumaric acid. Among those acids, lactic acid and malic acid showed a positive effect on hydrogen production while succinic acid had a positive effect on 5-ALA production.

In addition to reduction in color and viscosity, dilution of raw material also reduced the level of ammonium content in beet molasses. In the study, ammonium content could be reduced to a level lower than the suppression level of 2 mM. This result suggested the benefit of dilution in alleviating the negative effect of ammonium salts on photofermentative hydrogen production. Moreover, dilution also reduced phenol content in sugar beet molasses to the level below its suppressive level. However, dilution caused the level of molybdenum (Mo^{2+}) and iron (Fe^{2+}) to be too low to support the hydrogen production and the supplementation would be required. Mo^{2+} and Fe^{2+} are required for hydrogen production because both ions are the components in the main structure of Mo-nitrogenase which is responsible for hydrogen production in *R. sphaeroides*. By using various sugar concentrations between 3 and 28 g/L, hydrogen production by *R. sphaeroides* O.U.001 increased with increasing sugar concentration. The highest hydrogen production of 1.01 L H_2/L culture was obtained at the sugar concentration of 28 g/L.

5.6 Dairy Wastewater

Wastewater from dairy industry contains high organic content with COD values ranged from 5 to 50 g O_2/L. Main compositions in waste stream are remaining milk, fat and whey [13]. Untreated waste stream is normally released directly to rivers. Although, it is degradable in the environment, it consequently drops the pH value of water surface. Therefore, conversion of dairy waste stream to value-added chemicals or biofuel is a suitable option. Photofermentative hydrogen production from dairy wastewater of various concentrations between 5 and 60% (v/v) using *Rhodobacter sphaeroides* O.U.001 (ATCC 4919) was conducted in batch mode [13]. Hydrogen production from raw diary wastewater was unsuccessful because dairy wastewater contained normal flora and its low pH (pH 4.27) suppressed the photosynthetic bacteria. Filtration and sterilization at 120 °C for 20 min were carried out to treat the raw dairy wastewater. Thermal sterilization killed normal flora that is responsible for hydrolysis of organic compounds to undesirable products. By adjusting the pH of the same dairy wastewater to almost neutral, hydrogen production was successful. Dairy wastewater concentrations of up to 60% (v/v) were applied for hydrogen production by *R. sphaeroides* O.U.001 (ATCC 4919) under 9000 lux illumination. Increase in wastewater concentration up to 40%

enhanced hydrogen production using both sterile and non-sterile wastewaters. Further increase to the highest concentration of 60% (v/v) resulted in inhibition on hydrogen production. At high wastewater concentration, nitrogen content in the form of NH_4^+ increases and causes the reduction in nitrogenase activity. The highest hydrogen production of 3.23 L H_2/L medium was obtained at 40% (v/v) wastewater, 0.36 g DW/L inoculum and 9 klux illumination.

5.7 Soy Sauce Wastewater

Soy sauce is made from fermentation of soybeans, roasted grain and brine by *Aspergillus oryzae* or *Aspergillus sojae*. Soy sauce wastewater has dark color and contains high concentration of organic matters. It contains 11.5% (w/v) glucose, 170 mmol/L organic acids, 2.1% (w/v) protein, 633.8 mg/L iron and 0.3 mg/L molybdenum. Combinations of these components make it a good biodegradable substrate [162]. Anam et al. [162] reported the photofermentative hydrogen production using *Rhodobium marinum* from soy sauce wastewater (Table 9). In this study the effect of different pretreatment methods includes dilution, neutralization, and sterilization was performed. Soy sauce wastewater was treated by dilution, neutralization and sterilization and the headspace of the fermentation was filled with N_2 gas. The maximal cumulative hydrogen production reached 200 mL H_2. Addition of nitrogen gas along with yeast extract to provide extra nitrogen source could obstruct the nitrogenase enzyme. However, carbon dioxide produced during fermentation process could expel some nitrogen out, by which reduces its obstruction to hydrogen production.

5.8 Brewery Wastewater

Brewery wastewater is an effluent from beer production process. It has high COD value ranging from 0.8 to 2.5 kg/100 L. The amount of waste stream from beer production process is enormous, i.e., approximately 300–400 L per 100 L of beer [12]. Chemical compositions of waste depend on fermentation degree and the type of beer produced. Normally, it composes of amino acids, proteins, organic acids, sugars, alcohol, as well as vitamin B [12]. All compounds can be efficiently used in biological hydrogen production [174]. Seifert et al. [13] used brewery wastewater to produce hydrogen by using *Rhodobacter sphaeroides* O.U.001 (ATCC 4919) cultivated in 12 h–12 h light-dark cycle under 9 klux illumination. Raw brewery wastewater was prepared by filtration and heat sterilization to remove yeast cells and solid sediments which helped enhancing hydrogen production. Thermal pretreatment had shown to provide better access of light in the photofermentation process using brewery wastewater and consequently resulted in better hydrogen production. Influence of nitrogen concentration on hydrogen production using 5%

(v/v) of brewery wastewater was investigated. Results showed that hydrogen production was very similar (1.5–1.7 L H_2/L medium) when using the medium containing 0–0.72 g/L sodium glutamate. These results suggested that there was sufficient nitrogen in 5% (v/v) of brewery wastewater to support the growth of the bacteria. In addition, the presented concentration did not influence the production of hydrogen.

Further investigation in varying the brewery wastewater concentration from 1 to 20% (v/v) showed that increasing the wastewater concentration for up to 10% (v/v) resulted in increases in hydrogen production from 0.86 to 2.24 L H_2/L medium and HY from 0.009 to 0.22 L H_2/L waste (Table 9). However, further increase in wastewater concentration resulted in a significant decrease in hydrogen production. At 20% (v/v) wastewater, HY reduced by half and longer lag time was observed due to an inhibition effect from nitrogen compound (1.5 mmol NH_4^+/L). Under this condition, activity of nitrogenase enzyme also dropped. The best hydrogen production was obtained when using 10% (v/v) wastewater, resulting in 2.24 L H_2/L medium, the yield of 0.22 L H_2/L waste and the light conversion efficiency of 1.7%. In the same study, effect of light-dark period was also investigated. During the dark period, there was no hydrogen production in all concentrations used but a slightly increase in biomass was observed. It was concluded that the photosynthetic bacteria strictly required light for their growth and hydrogen production while they survived under dark condition.

5.9 Tofu Wastewater

Tofu or bean curd is popular in many Asian countries. In its production process, the coagulated soy milk was pressed to obtain blocks of bean curd. Wastewater from the production usually contains reducing sugar, sucrose, starch, protein and volatile acids. COD and total organic carbon (TOC) of the wastewater are 27,400 and 8,810 mg/L, respectively. High concentration of organic contents makes it a suitable substrate for biological hydrogen production. Zhu et al. [161] studied hydrogen production from tofu wastewater using entrapped *R. sphaeroides* (Table 9). The bacterium was entrapped in agar gel to prevent inhibition by NH_4^+. The use of single culture of entrapped *R. sphaeroides* was also compared with the use of entrapped co-culture of *R. sphaeroides* and *Clostridium butyricum*. The single entrapped culture resulted in 305 mL hydrogen per cultivation vessel, while the co-culture resulted in higher production of 358 mL hydrogen. HY of the co-culture was also superior at 2.2 mL/mL wastewater, compared to 1.9 mL/mL wastewater obtained from single culture. Although superior hydrogen production was observed when using the entrapped co-culture, NH_4^+ consumption during hydrogen production was faster in entrapped *R. sphaeroides* as NH_4^+ is a preferable nitrogen source for growth of photosynthetic bacteria. The preference led to a faster growth of *R. sphaeroides* when compared with that of *C. butyricum*.

Regardless of lower hydrogen production, entrapped *R. sphaeroides* has a higher TOC removal efficiency than the entrapped co-culture (40% vs. 32%). *C. butyricum* in co-culture favors the conversion of organic compounds to volatile organic acids while *R. sphaeroides* favors the conversion of organic compounds to CO_2, hence better COD removal. Dilution of tofu wastewater for up to 50% improved both HY (4.32 mL/mL-wastewater) and TOC removal efficiency (66%) when using entrapped *R. sphaeroides*. While dilution improved the performance of entrapped single culture, TOC removal efficiency by the co-culture did not show any improvement with increasing wastewater concentrations. The result implied that inhibitory compounds in wastewater had more impact on hydrogen production by *R. sphaeroides* than did NH_4^+. Mutation of *R. sphaeroides* by deletion of glutamine synthetase gene was conducted to overcome the repressive effect of NH_4^+ on hydrogen production by repressing the activity of nitrogenase through glutamine synthetase which is the key enzyme in the assimilation of NH_4^+ [175]. The mutation process resulted in 2.79-fold decrease in glutamine synthetase activity. The mutant showed high hydrogen production activity in the presence of 15 mM NH_4^+ but no hydrogen production activity was observed in wild type. The hydrogen production by the mutant was not different from the wild type under cultivation without NH_4^+ addition.

5.10 Agricultural Biomass

Agricultural biomass is considered a major waste stream due to its abundance in nature and low cost [28]. It consists of complex carbohydrates such as cellulose and hemicellulose which can be hydrolyzed to simple C6 and C5 sugars by various methods. These simple sugars can be further converted to hydrogen by anaerobic and photosynthetic bacteria. However, the operation cost involving pretreatment and hydrolysis steps prior to biohydrogen production becomes the main concern in using agricultural biomass [7].

Types and Compositions of Agricultural Biomass
Agricultural biomass is the major renewable carbon source that can be used for energy production. It can be categorized into food crops, non-food biomass which is mainly agricultural wastes, grass, weed and animal waste. In general, all types of agricultural biomass, except food crops, are the preferred feedstocks for hydrogen production by dark fermentation process. However, some literatures have reported the potential of these feedstocks for photofermentative hydrogen production. Composition of agricultural biomass varies among different species. Some examples of chemical composition in agricultural biomass are illustrated in Table 10.

The main components in non-food biomass are cellulose and hemicellulose. Its low lignin content makes them more favorable for bioenergy production. Cellulose is a polymer of glucose linked by beta-1,4-glycosidic linkage. Hemicellulose is a branched copolymer of pentose, hexose sugars and uronic acids [185, 186].

Table 10 Chemical composition of some agricultural biomass

Agricultural biomass	Compositions			References
	Cellulose (%)	Hemicellulose (%)	Lignin (%)	
Non-food biomass				
Rice straw	32–47	19–27	5–24	[176, 177]
Wheat straw	33–38	26–32	17–19	[176, 177]
Corn stover	33–37.5	28–30	8.4	[176, 178]
Sugarcane bagasse	33–45	23–35	4.31–30	[66, 176, 179]
Oil palm trunk	30.6	33.2	3.8	[180]
Oil palm fruit bunch (OPEFB)	43	30	Not applicable	[181]
Grass and weed				
Napier grass	32–34	17.36–20	9–32.04	[182, 183]
Water hyacinth	28	39	14	[184]

Crystalline cellulose is more resistant to hydrolysis than amorphous cellulose and hemicellulose. Lignin is a polymer of aromatic alcohols and it is the most recalcitrant component of lignocellulose. Inside lignocellulose complex, cellulose retains the crystalline fibrous structure and it appears to be the core of the complex. Hemicellulose is positioned both between micro and macro fibrils of cellulose. Lignin strengthens the matrix in which cellulose and hemicellulose is embedded and acts as microbial barrier in bioenergy production process [185, 186]. Strong structure of lignocellulose makes it difficult to directly use as substrate in the bioenergy production. Pretreatment of lignocellulose would be needed to weaken the structure and improve its degradability.

Photofermentative Hydrogen Production from Agricultural Biomass

Most of photofermentative hydrogen production from agricultural biomass by PNSB involves utilization of simple sugars obtained from pretreatment of the complex biomass. Depolymerization of cellulose and hemicellulose to simple sugars, such as glucose, xylose and arabinose, is the important step for biohydrogen production from agricultural biomass. Simple sugars serve as substrates for PNSB in hydrogen production. In addition, pretreatment step also removes lignin components which prevent its inhibition on PNSB.

Pretreatment methods may be categorized into three groups: physical, chemical and biological pretreatments. Physical pretreatment aims to reduce particle size of biomass and increase the reaction surface between celllulase and crystalline cellulose. Examples of physical pretreatment include grinding, steam-explosion, extrusion, hydrothermolysis and irradiation. Common chemicals that are employed in chemical pretreatment are acids, bases and ionic liquids. Acid pretreatment degrades hemicellulose structure, resulting in soluble sugars and lignin in liquid phase. Pretreatment by alkaline promotes swelling of the biomass structure by which leads to an increase in internal surface area of the biomass. It also reduces biomass crystallinity. Biological pretreatments are those involved the use of

enzymes either as solution or pretreated with microorganisms such as fungi [187]. Biological pretreatment aims to hydrolyze polymeric component of biomass.

Pretreatment of biomass yielded end products into 2 phases; liquid hydrolysate and solid residue. Hydrolysate comprises of mainly glucose and xylose. Small amount of arabinose is also detected. These sugars are solubilized from hemicellulose fraction of the biomass [188]. Solid residue is cellulose fraction of the biomass. It can be subsequently hydrolyzed to glucose which could be used further in production of bioenergy. Pretreatment of agricultural biomass for use in hydrogen production has a focus in studies using dark fermentation pathway [189]. Fewer studies were reported on using agricultural biomass in photofermentative hydrogen production. Some examples were summarized in Table 11.

Jiang et al. [190] hydrolyzed corn stalk pith with commercial cellulase for use in photofermentation to produce hydrogen using photosynthetic microbial consortium. Maximum HY of 2.61 mol H_2/mol sugar consumed was obtained at an initial pH of 7 and biomass concentration of 0.18 g/L. In addition, hydrogen was mainly produced via acetic acid production pathway in the first 24 h. The butyric acid production pathway dominated the hydrogen production for the next 72 h. Corn stalk pith was also used as substrate in the study by Liu et al. [122]. The photofermentation from enzymatic hydrolysate was carried out in a baffled photofermentation reactor by photosynthetic bacteria HAU-M1. Increasing organic loading rate (OLR) from 3.3 to 20 g/L d resulted in an increase in HY from 64.13 to 148.65 mol/m^3 d. However, further increase of OLR above 20 g/L d caused a decrease in HY. The same bacterium (HAU-M1) was also used for hydrogen production from apple waste. The maximum specific HY (SHY) of 111.85 mL H_2/g total solid (TS) was achieved at an initial pH of 7.14, light intensity of 3029.37 lux, 30.46 °C and material to liquid ratio of 0.21 [196].

Various biomasses; corn cob, corn stover, sorghum stover, rice straw and soybean stalk, were compared for their hydrogen production potentials. They were pretreated using immobilized cellulase and the hydrolysates were used in biohydrogen production by isolated photosynthetic bacterial consortium [178]. Due to different concentrations of reducing sugar obtained from pretreatment of the biomasses which ranged between 278.4 and 505.6 mg/g, different hydrogen production was resulted. Maximum hydrogen production of 230.09 mmol/L was obtained from corn cob hydrolysate owing to the highest reducing sugar obtained from the pretreatment. Similar comparison study was also carried out by Jiang et al. [193]. Wheat straw and corn cob hydrolysates were used as substrates in hydrogen production by photosynthetic consortium. Different hydrogen production was also resulted in this study. Therefore, different composition of cellulose and hemicellulose in raw materials is a crucial factor, responsible for different sugar concentrations in the enzymatic hydrolysate in which resulted in different hydrogen production.

The photosynthetic bacterial consortium and corn cob hydrolysate from Zhang et al. [178] was also used in continuous hydrogen production in a baffled photofermentative bioreactor [195]. The results revealed that hydrogen production increased rapidly as hydraulic retention time (HRT) decreased from 72 h to 24 h.

Table 11 Photofermentative hydrogen production from various agricultural biomasses

Biomass	Pretreatment methods	Microorganism	Fermentation conditions	Hydrogen production	Substrate conversion efficiency	References
Corn stalk pith	Cellulase at 50 °C	Photosynthetic microbial consortium consisted of *Rhodospirillum rubrum*, *Rhodopseudomonas capsulata*, *Rhodopseudomonas palustris*, *Rhodobacter sphaeroides* and *Rhodobacter capsulatus*	11 g/L reducing sugar, 30 °C, pH 7 (initial), 96 h and light exposure at 2 klux using filament lamps	2.61 mol H_2/mol sugar consumed	82–94%	[190]
Corn stalk pith	Cellulase at 50 °C	Photosynthetic bacteria HAU-M1 (mixture of *Rhodospirillum rubrum*, *Rhodopseudomonas capsulata* and *Rhodopseudomonas palustris*)	20 g/L reducing sugar, OLR 20 g/L.d, pilot-scale baffled bioreactor, 30 °C, pH 7.14 (initial) and 3.029 klux illuminance	148.65 mol/m^3 d	N/A	[191]
Apple waste	Crushed and screened with 40-mesh sieve	Photosynthetic bacteria HAU-M1 (see above)	Solid-to-liquid ratio of 0.21, batch mode, 30.46 °C, pH 7.14 (initial), 3.029 klux illuminance	111.85 mL/g TS	N/A	[191]
Corn cob	Milling followed by immobilized cellulase	Photosynthetic bacteria isolated from silt sewage, pig and cow manures (*Rhodospirillum rubrum*, *Rhodopseudomonas capsulata*, *Rhodopseudomonas palustris*)	20% (v/v) mixed bacteria, 30 °C, pH 7 (initial), 3 klux illuminance	230.09 mmol/L 5.97 mmol/L h	N/A	[178]
Corn stover	Milling followed by immobilized cellulase	Photosynthetic bacteria isolated from silt sewage, pig and cow manures (see above)	20% (v/v) mixed bacteria, 30 °C, pH 7 (initial), 3 klux illuminance	145.75 mmol/L 3.95 mmol/L h	N/A	[178]
Sorghum stover	Milling followed by immobilized cellulase	Photosynthetic bacteria isolated from silt sewage, pig and cow manures (see above)	20% (v/v) mixed bacteria, 30 °C, pH 7 (initial), 3 klux illuminance	150.39 mmol/L 4.07 mmol/L h	N/A	[178]

(continued)

Table 11 (continued)

Biomass	Pretreatment methods	Microorganism	Fermentation conditions	Hydrogen production	Substrate conversion efficiency	References
Rice straw	Milling followed by immobilized cellulase	Photosynthetic bacteria isolated from silt sewage, pig and cow manures (see above)	20% (v/v) mixed bacteria, 30 °C, pH 7 (initial), 3 klux illuminance	140.26 mmol/L 3.76 mmol/L h	N/A	[178]
Soybean stalk	Milling followed by immobilized cellulase	Photosynthetic bacteria isolated from silt sewage, pig and cow manures (see above)	20% (v/v) mixed bacteria, 30 °C, pH 7 (initial), 3 klux illuminance	130.65 mmol/L 3.31 mmol/L h	N/A	[178]
Cotton stalk	Milling followed by immobilized cellulase	Photosynthetic bacteria isolated from silt sewage, pig and cow manures (see above)	20% (v/v) mixed bacteria, 30 °C, pH 7 (initial), 3 klux illuminance	119.29 mmol/L 2.74 mmol/L h	N/A	[178]
Wheat straw	H_2SO_4 (pH 3) and autoclaved at 90 °C for 15 min	*Rhodobacter sphaeroides* NRLL	5 g/L initial sugar, pH 7, 30 °C, 3 klux, shaking at 100 rpm and -200 mV ORP	115.3 mL H_2 0.9 mL H_2/h	N/A	[192]
Wheat straw	H_2SO_4 (pH 3) and autoclaved at 90 °C for 15 min	*Rhodobacter sphaeroides* DSZM	5 g/L initial sugar, pH 7, 30 °C, 3 klux, shaking at 100 rpm and -200 mV ORP	135.1 mL H_2 1.5 mL H_2/h	N/A	[192]
Wheat straw	H_2SO_4 (pH 3) and autoclaved at 90 °C for 15 min	*Rhodobacter sphaeroides* RV	5 g/L initial sugar, pH 7, 30 °C, 3 klux, shaking at 100 rpm and -200 mV ORP	178 mL H_2 3.69 mL H_2/h 1.23 mol H_2/mol glucose	N/A	[192]
Wheat straw	6% $Ca(OH)_2$, 120 °C for 2 h	Photosynthetic consortium	0.1 g cellulase/g-substrate, 50 °C for 84 h	2.1 mol/mol glucose	N/A	[193]
Corn stover	6% $Ca(OH)_2$, 120 °C for 2 h	Photosynthetic consortium	Cellulase 0.1 g/g-substrate, 50 °C for 84 h	1.9 mol/mol glucose		[193]

Table 11 (continued)

Biomass	Pretreatment methods	Microorganism	Fermentation conditions	Hydrogen production	Substrate conversion efficiency	References
Wheat straw	4% H$_2$SO$_4$ at 121 °C for 30 min	*Rhodobacter capsulatus*—PK	10% seed inoculum, 30 ± 2.0 °C, initial pH 7	254 mL/L	N/A	[9]
Wheat straw	4% H$_2$SO$_4$ at 121 °C for 30 min, detoxified the hydrolysate with Ca(OH)$_2$	*Rhodobacter capsulatus*—PK	10% seed inoculum, 30 ± 2.0 °C, initial pH 7	372 mL/L	N/A	[9]
Wheat straw	30% (v/v) ammonia at 50 °C for 24 h and Cellulase 80 FPU/g β-glucosidase 220 CbU/mol 50 °C for 24 h	*Rhodobacter capsulatus*—PK	10% seed inoculum, 30 ± 2.0 °C, initial pH 7	712 mL/L	N/A	[9]
Distillers grains with solubles (DGS)	Sterilized at 120 ° C for 20 min	*Rhodobacter sphaeroides* strain MDC6521	2-fold diluted DGS under illumination	9.71 mmol/g DW	N/A	[194]
Corn cob	30 U/mg cellulase	Photosynthetic bacteria isolated from silt sewage, pig and cow manures (*Rhodospirillum rubrum*, *Rhodopseudomonas capsulata*, *Rhodopseudomonas palustris*)	10.5 g/L reducing sugar, low-energy LED lamps, 20% (v/v) inoculum, baffled photofermentative bioreactor and 24 h HRT	589.21 mmol/L 6.98 mmol/L h	40.48%	[195]
Bagasse	4% (w/w) H$_2$SO$_4$, hydrolysate detoxified with active carbon and neutralized with NaOH	*Rhodobium marinum* NBRC 100434	Supplemented with yeast extract, 4 table lamps (60 W/m^2), 120 rpm and 30 °C in batch mode	0.55 L/L 3.64 mL/L h	N/A	[162]

Table 11 (continued)

Biomass	Pretreatment methods	Microorganism	Fermentation conditions	Hydrogen production	Substrate conversion efficiency	References
Bagasse	4% (w/w) H_2SO_4, hydrolysate detoxified with active carbon and neutralized with NaOH	*Rhodobium marinum* (Sanur)	Supplemented with yeast extract, 4 table lamps (60 W/m², 120 rpm and 30 °C in batch mode	0.005 L/L 0.02 mL/L h	N/A	[162]
Oil palm empty fruit bunch (OPEFB)	6% H_2SO_4, autoclaved at 120 °C for 15 min	*Rhodobacter sphaeroides* S10	pH 7, 35°C, 14.6 W/m² illuminance and batch mode	22.4 mL H_2/L h	N/A	[181]

N/A not available

Maximum hydrogen production of 589.21 mmol/L and hydrogen production rate (HPR) of 6.98 mmol/L.h were obtained at a HRT of 24 h. When further decreased the HRT to shorter than 24 h, hydrogen production decreased. The decrease was caused from removal of microbial biomass due to short HRT and insufficient contact time that is required for the bacteria to acclimate to the environment. Therefore, HRT is a major factor affecting the performance of continuous biohydrogen production [195].

Kapdan et al. [192] investigated hydrogen production from wheat straw hydrolysate by using *Rhodobacter sphaeroides* RV, *R. sphaeroides* NRLL, and *R. sphaeroides* DSZM. Among the three species, *R. sphaeroides* RV produced the highest hydrogen volume at 178 mL H_2 and production rate of 3.69 mL H_2/h. Significantly lower hydrogen production and yields were resulted from the other 2 strains. This study has emphasized that bacterial strain is a primary factor responsible for hydrogen production efficiency.

A study on effect of different pretreatment methods on biohydrogen production from wheat straw using *Rhodobacter capsulatus* PK was carried out by Shahzad et al. [9]. Pretreatment methods influenced the hydrogen production by the bacterium. Maximum hydrogen production of 712 mL/L was obtained when combination of ammonia pretreatment and enzyme hydrolysis was used as the pretreatment method. The use of dilute acid pretreatment with or without detoxification resulted in lower hydrogen production when compared with the combination methods. Acid pretreatment alone was inferior when compared with enzymatic pretreatment due to its low sugar contents and the presence of inhibitors such as acetic acid, hydroxymethylfurfural (HMF) and furfural. Removal of inhibitors by adding NaOH (detoxification) slightly enhanced the ability of photosynthetic bacteria to convert sugar into hydrogen. According to the results from this study, selection of pretreatment methods based on the compositions inside lignocellulosic biomass is critical for the success in photofermentative hydrogen production.

Apart from aforementioned importance of pretreatment, other concerns in hydrogen production from hydrolysate of agricultural biomass by photofermentative bacteria are the excess of fine particles, inhibitive substances and nitrogen content. The presence of inhibitors such as furfural and HMF inhibits hydrogen production via both dark and photofermentation processes [188]. However, the presence of acetic acid positively affects photofermentative hydrogen production but acts negatively in dark fermentation. Furan derivatives inhibit enzyme activity and cell growth. They cause mutation in bacteria and DNA damage affects fermentation pathways. Therefore, removal of toxic substances is required for enhanced hydrogen production. Several approaches such as alkaline and electrochemical detoxification have been applied to remove those inhibitors resulting in higher hydrogen production and yield [197].

Chemical pretreatment of agricultural biomass generates hydrolysate with fine particles. These particles have large impact on light penetration into hydrogen production medium. They reduce light penetration and cause the fouling of photobioreactor's transparent surface. Antifouling is essential for improvement of

photofermentative hydrogen production. Some agricultural biomasses contain proteins and amino acids which could be hydrolyzed to ammonium ions (NH_4^+) under anaerobic and alkaline conditions [7, 8]. Ammonium ions can inhibit the activity of nitrogenase enzyme [198]. Removal of ammonium ions by adsorption using substances such as zeolite [198] or conversion of ammonium ions to nitrate forms are needed to prevent inhibitory effect of the ions on photosynthetic bacteria during photofermentative hydrogen production.

Hydrogen production from hydrolysate of oil palm empty fruit bunch (OPEFB) by *R. sphaeroides* S10 was investigated by Pattanamanee et al. [181]. Pretreatment of OPEFB by dilute sulfuric acid at 120 °C for 15 min was carried out to release fermentable sugars. The hydrolysate of OPEFB contained primarily xylose with small amounts of acetic acid and glucose. *R. sphaeroides* S10 consumed all of three carbon sources but only glucose and xylose were used in hydrogen production. Acetic acid involved only in biomass production. Furthermore, influences of five factors (yeast extract, molybdenum, magnesium, EDTA and iron concentrations) on hydrogen production were examined statistically. All factors showed significant effect on hydrogen production. Magnesium concentration had a strong effect because it is a component in bacteriochlorophyll structure. Magnesium limitation directly influences the synthesis of bacteriochlorophyll and subsequently impacts photosynthesis and hydrogen production. Effects of molybdenum and iron on hydrogen production were due to their presence in nitrogenase structure. Yeast extract acts as the source of essential vitamins for photofermentation bacteria. EDTA is a chelator of iron ions (Fe^{+2}). Removal of iron ions by adding EDTA (iron chelation) decreases the activity of hydrogenase [199]. The optimum medium supplementation for hydrogen production in this study were 0.3 g/L yeast extract, 1.45 mg/L molybdenum, 2.46 g/L magnesium, 0.02 g/L EDTA, and 11 mg/L of iron concentrations. Under this condition, the maximum HPR was 22.4 mL H_2/L h with a specific hydrogen production rate of 7.0 mL H_2/g h and 29% substrate conversion efficiency.

6 Bioreactors for Photofermentation: Suspension Culture

A number of studies have been carried out in suspension systems. To achieve stable and continuous hydrogen production, a large number of photobioreactors have been developed. Such photobioreactors are composed of the reactor main body, an illumination system, a stirring system, a temperature control system, and a hydrogen purification and collecting system. Generally, photobioreactors are closed systems to ensure anaerobic conditions because biohydrogen is produced by photosynthetic bacteria that are very sensitive to N_2 and O_2; hence, closed systems are advantageous to maintain pure photofermentation and to collect produced hydrogen.

Closed photobioreactors are mainly divided into two categories: suspension culture photobioreactors and static culture flasks. Suspension culture

photobioreactors have several advantages over static culture photobioreactors [200–202]. First, suspension culture systems facilitate the large-scale expansion of microorganisms in a homogeneous culture environment, decreasing the risk of culture variability. Second, it is also less labor-intensive to control and monitor the culture conditions, including temperature, light intensity, pH, and substrate level. Third, suspension culture photobioreactors also facilitate cell seeding because of the stirred culture environment, which is a further advantage over the use of static culture bioreactors. Although suspension culture photobioreactor use is promising, the performance of these photobioreactors is still very poor owing to the limited light [203, 204].

Undesirable light conditions in photobioreactors are mainly due to the following: (1) Since biohydrogen production and collection need anaerobic conditions, it is a prerequisite to have an enclosed system [205, 206]. Hence, when light is incident on the outer surface of a photobioreactor (common construction materials, such as glass, polymethyl methacrylate, polycarbonate, and low-density polyethylene, are the most widely used), although there may be good light transmission efficiency, some light is reflected and scattered at the surface, and some is absorbed by the material of the reactor wall, causing a decrease of total transmitted light into the photobioreactor. (2) Photosynthetic bacteria create a self-shading effect resulting in light attenuation by substrates and products, limiting light penetration into the depths of the photobioreactor [207]. Consequently, maximum photobioreactor depth is limited and large areas have limited light. (3) The efficiency of photosynthesis is significantly affected by the light-receiving area of the cultivation apparatus; however, it is difficult to increase the light-receiving area or utilization efficiency of light per occupying area, thus the structure of the photobioreactor is very important to enhance the performance of biohydrogen production.

To enhance the light intensity in photobioreactors and improve the conversion efficiency of light energy, a promising method is to increase the ratio (A/V) of surface area (A) to volume (V) of the photobioreactor. The A/V ratio is a key factor in determining the total amount of light energy per unit volume of reactor: a high A/V can cultivate high concentrations of biomass and thus achieve a high volumetric efficiency. To obtain a high A/V ratio, different photobioreactors have been developed to increase hydrogen yield. In the last 30 years, photobioreactors for hydrogen production have included the following categories: tubular bioreactors, plate type bioreactors, optical fiber bioreactors, and other types of bioreactors.

6.1 Tubular Photobioreactors

Fully closed tubular bioreactors are potentially attractive for the large-scale culture of microorganisms free of contaminants. These photobioreactors may be the first and simplest type developed for photofermentation. A tubular reactor generally consists of one or multiple transparent tubes with inner diameters ranging from 3 to 6 cm, and lengths ranging from 10 to 100 m. To effectively capture light energy,

the structure of a tubular photobioreactor is usually designed as vertical and horizontal cylinders [208–211].

Vertical Tubular Photobioreactors. For large-scale outdoor photofermentation systems, closed photobioreactors allow greater control over the physical, chemical, and biological environment of the cultures compared with open pond systems. In closed photobioreactors, vertical and horizontal tubes are constructed from low cost, commercially available glass or polymethyl methacrylate (PMMA). Vertical tubular photobioreactors (VTPs) have the inherent advantage of allowing continuous gassing of the cultures compared to horizontal or serpentine reactors because VTPs can enhance the efficiency of gas transfer, improving culture mixing and inhibiting the adhesion of cells on the surface [212]. VTPs are mainly composed of a gas meter, gas solid separator, light source, mixer, and peristaltic pump. The photobioreactors have a hole at the bottom and two holes at the top. During reactor operation, the culture medium is pumped in through the hole at the bottom. Through the gas solid separator, the generated gas is discharged and collected by the central hole at the top, while the culture is withdrawn or drained by using the other hole at the top. A typical VTP employed to produce hydrogen by photofermentation is shown in Fig. 3.

The photobioreactor system shown in Fig. 3 consists of five vertical Pyrex glass tubes (the length and diameter are 75 cm and 2.8 cm, respectively), and the total working volume is about 1.6 L arranged in a circular sequence. The artificial light source is provided by 200 W tungsten filament lamps, and the light intensity in the middle of the circle is about 190 W/m^2. The produced hydrogen gas is collected from the top. The volume of total gas production is measured by the gas meter, and the hydrogen concentration is analyzed using a gas chromatograph. During experiments, the temperature and pH values are 31 °C and 5.5, respectively, and the
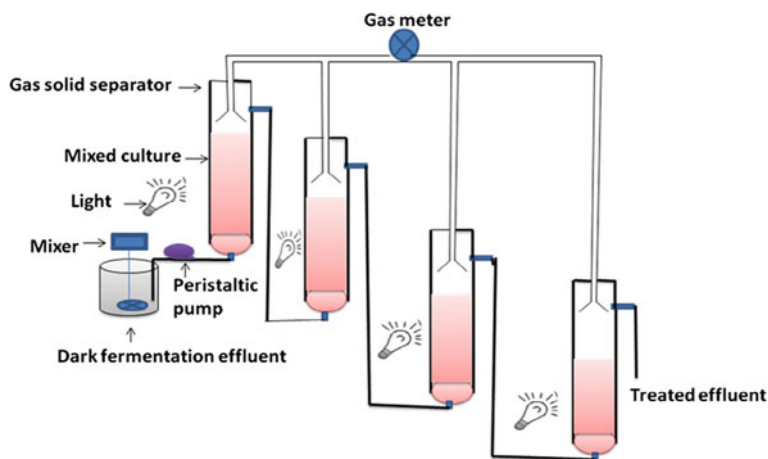
Fig. 3 Schematic diagram of the vertical tubular photobioreactor for hydrogen production (adapted from [209], Copyright 2014, with permission from Elsevier)

HRT is in a range of 0.4–4.0 h. Tawfik et al. [209] discovered that when the PNSB *Rhodopseudomonas palustris* was employed and the bioreactor was operated at a light intensity of 190 W/m^2, the HRT was 0.9–4.0 h; the hydrogen production rate significantly increased with the increasing HRT in a range of 0.9–2.5 h, and the rate increased to 3.05 ± 0.19 L/d; thereafter, the rate slightly increased when increasing the HRT up to 4.0 h.

Horizontal Tubular Photobioreactors. Although vertical tubular photobioreactors have some advantages, they have a lower photon flux density on their surface that penetrates less into the culture. Horizontal tubular photobioreactors can obtain a higher biomass concentration and hydrogen production performance because they receive a higher photon flux density. In a typical arrangement, the tubes are placed parallel to each other and are level with the ground. The solar collector tubes, which have a similar shape of the light gradient in most designs, are usually made of plastic or glass and are laid horizontally on a supporting frame to form a helical coil. To increase the number of tubes per unit area, horizontal, parallel straight tubes are arranged like a fence. The tubes are always oriented north-south because more solar energy can be received when the reactor is placed in that orientation, and the productivity is higher than that in an east-west facing orientation. A typical horizontal tubular photobioreactor used for outdoor hydrogen production is shown in Fig. 4.

Figure 4b, shows a photobioreactor reported by Scoma et al. [210] and Adessi et al. [211] that consists of 10 parallel glass tubes (length 2 m, internal diameter 4.85 cm) connected by PVC U-bends with watertight flanges, and the tubes are placed horizontally in a stainless-steel basin containing a constant temperature water bath (28 ± 0.5 °C). The illuminated area (1.52 m^2) of the photobioreactor is calculated on the basis of the tube semi-circumference, and the corresponding
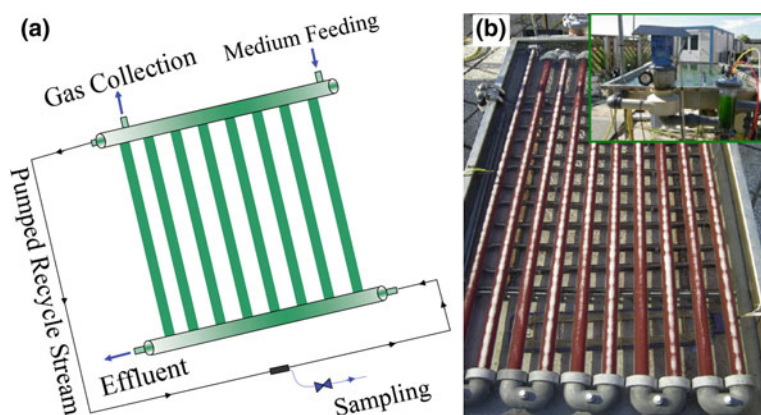
Fig. 4 Tubular photobioreactor for hydrogen production. **a** Schematic representation of horizontal tubular photobioreactor setup; **b** general view of the 50 L horizontal tubular photobioreactor, Insert: details of the PVC pump and the degasser (adapted from [210], Copyright 2012, with permission from Elsevier, and [39], Copyright 2012, with permission from Elsevier)

surface to volume ratio is about 30.45 m^{-1}. The culture medium with microorganisms is recycled by means of a centrifuge PVC pump equipped with three stainless steel flat blades with an angle of 120° to each other on the propeller shaft. The distance between the blades and the casing is 0.5 cm, the internal diameter and height of the casing are respectively 16 cm and 6.5 cm, and the net volume of the PVC pump without the impeller is about 1.1 L. The speed of the culture medium is adjustable from 0.2 to 0.8 ms^{-1}, thus yielding a Reynolds number (Re) from 12,000 to 48,000. Additional mixing of the culture medium occurs with the U bends (2 m), which can produce a frictional effect and cause lateral acceleration in the fluid; the acceleration can lead to a highly turbulent regime that persists in up to one half of the total length of the tube [213]. After a cycle has been completed (the total length of the tubular photobioreactor is about 23 m), the culture medium flows into a 2.2-L transparent PVC cylindrical degasser. The degasser contains several hose fittings for fresh medium additions, such as N$_2$ bubbling, and for culture sampling and biogas recovery. During hydrogen production experiments, the head space of the photobioreactor, i.e., the volume above the culture level, was about 0.2 L (0.4% of the total volume). The photobioreactor is placed in a north-south facing orientation; the latitude and longitude at the site where it was tested were about 43°50′ north and 11°11′ east. The mixing time is measured by filling the photobioreactor with culture medium and circulating it at a speed of 0.36 ms^{-1}, which is the same speed used for both the cell culture and hydrogen production experiments. Adessi et al. [211] discovered that the hydrogen production rate was highest at 27.2 mL/L/h, and the mean rate per illuminated surface was highest at 3.54 ± 1.53 L/m^2/d when the speed of the culture was adjusted to within 0.2 ms^{-1}, yielding a Re of 12.000. The *R. palustris* strain 42OL was employed, and the hydrogen production performance of the photosystem was unaffected by changing light irradiance during the day and maintained a high activity level over the whole period.

In summary, tubular reactors have been used both horizontally and vertically. The reactors have higher A/V ratios to allow the cells to be illuminated uniformly [214]. Moreover, tubular reactors show a high hydrogen production rate and have enhanced solid-liquid separation rates because the associated mass transfer rate between the liquid and the gas phase is high [215]. Their main drawback is their geometry, which is difficult to scale up: a single column is limited in length or height due to the increase of liquid pressure and non-optimal mixing. Increased working volumes need high energy input because of high flow resistance in the tube. These photobioreactors also suffer from difficulty in temperature control, high material cost, and low light conversion efficiency.

6.2 Flat-Panel Photobioreactors

Flat-panel photobioreactors (FPPs) were first reported in the early 1950s [216]. FPPs consist of rectangular transparent boxes and can be made from transparent materials, such as glass, plexiglass, and polycarbonate. Generally speaking, the

appropriate thickness of FPPs is 5 cm, and this exposes cells to very short mixing-induced light/dark cycles, which can increase hydrogen productivity; in particular, Gilbert et al. [217] discovered that the hydrogen production rate first increases as the thickness of the FPPs increases from 1 to 5 cm, but then decreases beyond 5 cm. The height and width of the FPPs are flexible to some extent, but in practice only panels with a height and width both smaller than 1 m have been investigated. The frames of the FPPs do not need to be transparent and can be made from sturdy materials, such as PMMA, glass, PVC, or stainless steel. The inlet-outlets are located on the sides where required. FPPs can work indoors or outdoors. In indoor conditions, illumination can be provided from both sides to enhance light penetration into the inner parts of the culture medium. However, when hydrogen production is carried out outdoors using solar irradiation, FPPs can be either vertically placed or inclined in the direction of the sun, with light conversion efficiencies (LCE) around 1%; the highest LCE (1.4%) is obtained by employing purple bacteria.

Flat-panel reactors have identical configuration potential and have been reported to be more economically feasible for the following reasons. (1) FPPs are easier to control and keep clear of contaminants [218]. (2) Hydrodynamic and mass transfer characterizations of FPPs with a high light path indicate that they are more efficient than those reported for tubular photobioreactors. Their performance is also higher than that of similar bubble column reactors under oversaturating light conditions. In particular, Zhang et al. [195] compared the performances of three different photobioreactors (tubular, bath, and FPP) with hydrolyzed corncobs, and they found that the FPP had the highest hydrogen yield (589.21 mmol/L) and exhibited higher substrate conversion efficiency (40.48%) and higher sunlight utilization efficiency than the bath reactor or tubular reactor. (3) An advantage in using FPPs is the possibility to arrange a set of reactors so that one is behind the other, at a proper distance, to increase the ground area productivity. To demonstrate the advantages and working principle of FPPs, a typical flat-panel photobioreactor is shown in Fig. 5.

As shown in Fig. 5, an FPP is manufactured of acrylic sheets at a thickness of 5 mm and has an illuminated front area of 0.2 m^2. The dimensions are 0.5 m (H) × 0.4 m (L) × 0.04 m (W). Figure 5a is a schematic diagram of the photobioreactor, and Fig. 5b shows the experimental setup for hydrogen production. The maximum culture medium that can be used is about 6.5 L in the photobioreactor system. To enhance hydrogen production, the bioreactor is inclined θ at 30° and faced south, which can improve the light collection efficiency and inhibit the adhesion of cells to the bioreactor surface. The FPP has six output ports on the top: one for collecting the gas produced by the bacteria, one for argon gas exhaust, one for argon gas flushing through a T-shaped sparger, a septum containing two ports for gas sampling, one port for inoculation of the bacteria, and a temperature sensor entrance. The reactor has four outlets in its right-side wall as follows: the first and third outlets from the top are for cooling water coming in and out, respectively, the second outlet from the top is used for the liquid sampling, and the bottom outlet is for emptying the reactor. During experiments, the FPP is illuminated with sunlight,

(a)   **(b)**
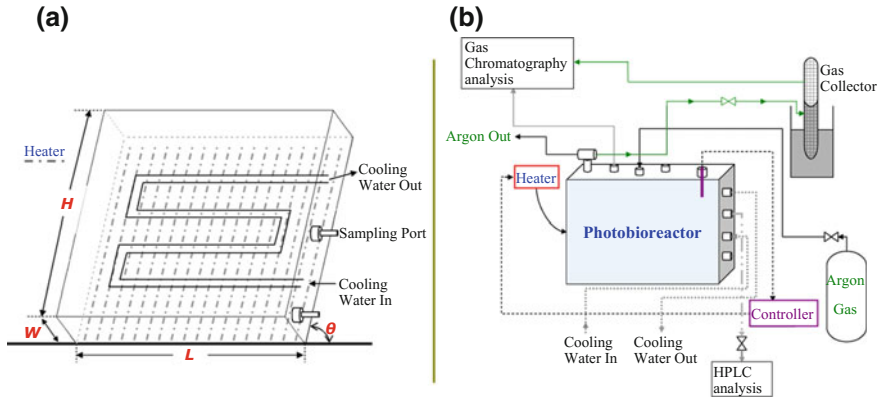
Fig. 5 Flat panel photobioreactor (adapted from [166], Copyright 2008, with permission from Elsevier); **a** Schematic drawing of the flat plate photobioreactor. **b** The photobioreactor system for outdoor hydrogen production

except during the first night when it is illuminated with a tungsten lamp at 150 W/m^2 until hydrogen production has started. Furthermore, to improve the culture temperature, a heating blanket is placed on the back face of the bioreactor and cooling water continuously flows through a coil made of a glass tube as shown in Fig. 5a. Experimental results show that the hydrogen production rate is highest (0.01 L/L/h) when malate is the carbon source and *Rhodobacter sphaeroides* O.U.001 (DSM 5864) is employed [166].

Although FPPs have a lot of advantages, such as ground area productivity, easy construction and modification, and suitability for base studies on light distribution and mixing, their hydrogen production is still unsatisfactory. The main disadvantages of FPPs are as follows: First, their light collection capacity is controlled by the material and ratio of surface area to volume. Second, low light penetration occurs via light decay along the light-path increasing as cell density grows because of a combination of photon absorption by the photosynthetic unit and cell scattering. Third, the mixing performance is undesirable due to limitations in mixing intensity, especially at high cell density, resulting in poor mixing and mass transfer rates. Thus, to further enhance hydrogen production, it is necessary to optimize the light conditions of these photobioreactors.

6.3 Optical Fiber Photobioreactors

Although photofermentation is an effective way to produce hydrogen, photofermentation systems have high power consumption and high operating costs by using artificial light sources (e.g., LED, tungsten filament lamp, halogen lamp, or metal-halide lamp). To decrease power consumption and operating costs, the

utilization of solar energy is a good choice, because sunlight is the most abundant light source on earth and contains a full spectrum of light energy. Solar radiation provides an energy flow of ca. 5.7×10^{24} J year^{-1}, which is about 10,000 times higher than the total energy consumed by human beings [219]; hence, free and natural sunlight can be employed as the energy source for photosynthetic bacteria during cultivation. Currently, most of the commercial photofermentation is carried out in flat-panel photobioreactors and tubular photobioreactors, as solar light energy is directly utilized. Although sunlight as a light source can be directly employed for photohydrogen production, the performance of photobioreactors is still unsatisfactory because of low light intensity (low light collection capacity due to low surface AV ratios) and uneven light distribution. Therefore, to enhance the light use efficiency of sunlight, increase light intensity, and improve light distribution, optical-fiber photobioreactors with sunlight collectors have been developed [220].

Optical fibers, which are made of polymer and silica and used to transmit light from one place to another, have been widely applied in photofermentation systems and illumination applications. Sunlight can be collected automatically by a sunlight collector and then transmitted by optical fibers into a photobioreactor in the laboratory. Thereafter, the light in the coated fibers is diffused from the circumference of side-light optical fibers (bare fibers) to illuminate vicinal regions. The diameter of side-light optical fibers is generally in the range of 1.5–14 mm, and a schematic is shown in Fig. 6. Side-light optical fibers are arranged parallel inside photobioreactors, and their number is determined by the working volume of the photobioreactor and the appropriate light intensity of the photosynthetic bacteria.

Optical-fiber photobioreactors with sunlight collectors can resolve four main problems for photofermentation [86, 221]. (1) The light intensity and distribution in the photobioreactor are not affected by the concentration of cells and product, but they are controlled by the number and distribution of the optical fibers. In contrast, for flat-plate and tubular photobioreactors, although they have high AV ratios, the light intensity decreases exponentially with distance from the incident surface as the concentrations of cell and product increase; uneven distribution and increased cell
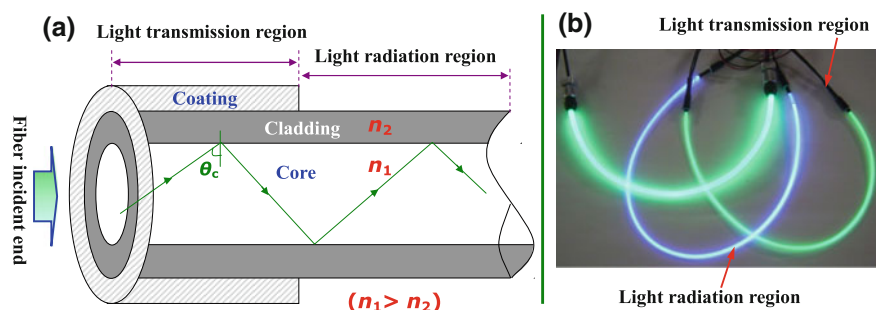
Fig. 6 Polymer side-light optical fiber; **a** schematic of the fiber; **b** the picture of the fiber; θ_c denotes the light incident angle; n_1 and n_2 are the refractive index of the fiber cladding and core, respectively

concentration also impact the light distribution. To resolve this problem, the most common methods are to increase the intensity of the light source and optimize the distance between the source and the reactor, which increases the temperature of the surface. Inappropriate temperatures may result in cell damage. However, when an optical fiber bundle is adopted, it solves the problems of light intensity, light distribution, and heat distribution. (2) Optical fibers are employed as optical transmission media and can effectively move sunlight from outdoors to indoors. Furthermore, optical fiber materials can filter most UV and IR radiation, so they are particularly suitable for photofermentation. (3) The light source is from sunlight, thus optical-fiber photobioreactors consume little energy and are very environmentally friendly. (4) Optical fibers inserted into photobioreactors can enhance the mixing of the culture medium and photosynthetic bacteria; this means that optical fibers can enhance the transfer of the substrate, product, light, and heat. To demonstrate the advantages and working principles of optical-fiber photobioreactors with sunlight collectors, a typical photobioreactor is shown in Fig. 7.

The photobioreactor shown in Fig. 7 is a 2.7 L glass vessel using *R. palustris* WP3-5. In this system, solar-energy-excited side light optical fibers (SLOFs) and an artificial light source (tungsten filament lamp) are employed. Here, sunlight is used to provide the light energy at daytime; however, when the sunlight intensity does not satisfy bacterial growth, in particular at night, artificial light sources are used. To provide high light intensity and uniform distribution for the enhancement of hydrogen production, two pieces of the optical fiber protected in a glass tube are immersed into the liquid medium inside the photobioreactor. The SLOF is made of quartz glass (the diameter and length are 11 mm and 50 cm, respectively) and
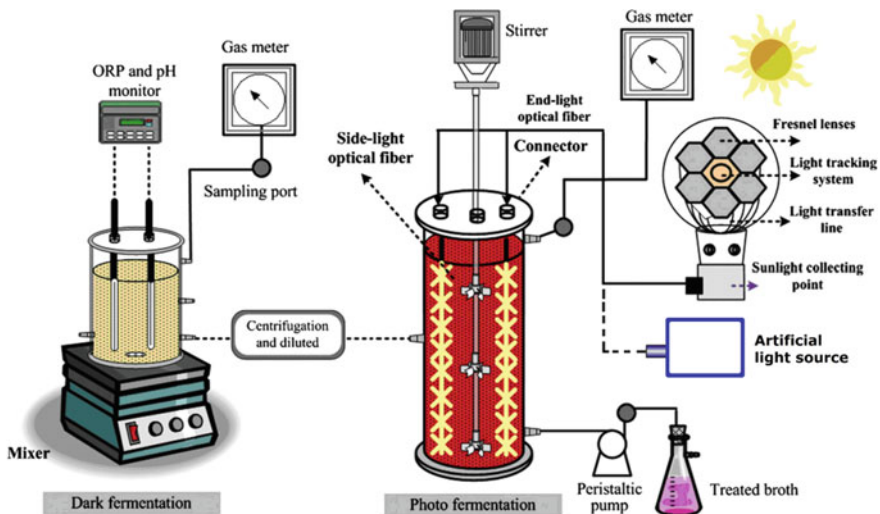
Fig. 7 Schematic description of the solar optical-fiber photobioreactors (optical fiber excited by sunlight collecting system) (adapted from [86], Copyright 2008, with permission from Elsevier)

excited by a sunlight collector or tungsten filament lamp. The sunlight is collected by using Fresnel lenses and then transmitted through the fiber incident end toward the SLOFs as shown in Fig. 6a. A light tracking system is employed to obtain the maximum light energy from sunlight during the daytime, and each Fresnel lens can be rotated toward the position of sun. In experiments, the illumination intensity of the tungsten filament lamps is set at 95 W/m^2. The solar-energy-excited SLOF has a light intensity varying from 0 to 350 W/m^2 depending on the weather and time. The cumulative hydrogen production (H, mL) of the photobioreactor is evaluated by the following Eq. (8) [86]:

$$H = H_{max} \exp\left\{ -\exp\left[\frac{R_{max} \cdot e}{H_{max}} (\lambda - t) + 1 \right] \right\} \qquad (8)$$

where, H_{max}, R_{max}, λ, and t denote the maximum cumulative hydrogen production (mL), the maximum hydrogen production rate (mL/h), the lag time required for the onset of hydrogen evolution (h), and the culture time (h), respectively.

Experimental results show that, when the initial cell concentration of WP3-5, temperature, pH, and agitation rate are respectively 0.875 g/L, 32 °C, 7.1, and 200 rpm, using both the solar-energy-excited optical fiber and tungsten filament lamps, the overall hydrogen production rate is improved to 17.86 mL/L/h. The power consumption by combining sunlight and artificial light is about 37.1% lower than using artificial light alone. This demonstrates that solar optical-fiber photobioreactors can significantly improve hydrogen production and decrease energy consumption.

6.4 Other Types of Photobioreactors

In addition to the above-mentioned three main types, various other photobioreactors have been investigated, including a fermenter type as a continuous culture device used to estimate the pathway of hydrogen evolution of *Enterobacter aerogenes* strain E.82005 [222]; a floating-type photobioreactor that continuously produced hydrogen over three months using artificial light, artificial raw wastewater, and *R. palustris* R-1 [223]; a multilayered photobioreactor in which cell suspensions and clear media layers are alternately arranged to form light paths [224]; a triple jacketed annular photobioreactor consisting of three concentric chambers used with *R. sphaeroides* OU 001 applying axial light in batch and suspension cultures [154]; and a microchannel photobioreactor to visualize the colony formation of photosynthetic bacteria, biomass growth, as well as biogas bubble behavior within the microstructure [225].

In summary, in the last few decades, many types of photobioreactors for hydrogen production in suspension culture have been exploited. The main aim of developing different photobioreactors is to increase light energy efficiency, decrease energy consumption, enhance substrate and product transfer, and optimize the

distribution of light and heat. Through constant improvements, we may obtain the high performance of hydrogen production, including a good production rate and high stability.

7 Bioreactors for Photofermentation: Immobilized Culture

Suspension cultures of PNSB for photofermentation may be constrained by low biomass concentration, as bacteria can be continuously flushed out with effluents from the reactor [226], resulting in poor hydrogen production, including low hydrogen yield and hydrogen production rate. Biofilm techniques can effectively solve this problem by immobilizing cells on the surface of support materials, which greatly increases the biomass concentration. Porous glass, reactor surfaces, activated carbon, and optical fibers have been used for PNSB immobilization. Such support materials grown with biomass have a high sedimentation rate, thereby reducing the washout of PNSB. Thus, biofilm attachment is considered a highly efficient technology for hydrogen production by photosynthetic bacteria [125, 227]. Biofilm photobioreactors (BPBRs), therefore, have attracted intense interest for their potential advantages, including high conversion yield, avoidance of biomass-liquid separation, and dual functions of wastewater biodegradation and hydrogen production. Although promising, the performance of BPBRs with PNSB still faces three critical problems: limited light, low cell concentrations, and low biofilm activity [228, 229]. To further enhance the hydrogen production performance of BPBRs, different systems have been developed. In the last 30 years, the following categories of biofilm photobioreactors for hydrogen production by immobilized cultures have been reported: flat-panel biofilm, microchannel biofilm, groove-type biofilm, optical fiber biofilm, and other types of biofilm photobioreactors.

7.1 Flat-Panel Biofilm Photobioreactors

Biofilms are composed of microbial cells and their extracellular polymer substances (EPS), and are associated with the surface of the photobioreactor wall or support material that has been inserted into the reactor [230]. Flat-panel biofilm photobioreactors, which are made of a flat plate, have been widely used in hydrogen and biomass production because of their simple structure, easy operation, large illumination surface area, and low cost. The construction material is glass, Plexiglas, plastic, or another transparent material that enables light to pass inside the biofilm because it is attached to a flat surface. Good transparency of the photobioreactor wall enhances light transmission and can be used for non-invasive diagnostics of biofilm accumulation, amount, and biofilm-cell reactivity. Flat-panel photobioreactors with
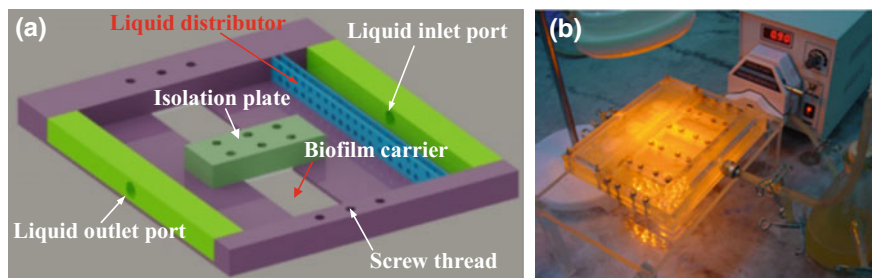
Fig. 8 Flat panel biofilm photobioreactor and experimental apparatus of system; **a** Schematic drawing of the flat plate biofilm photobioreactor. **b** Picture of the experimental apparatus for hydrogen production

good transparency are the simplest biofilm photobioreactors, and their dimensions can be compatible with a microscope for easy focus on the biofilm. To demonstrate the advantages and working principles of flat-panel biofilms for hydrogen production, a typical flat-panel biofilm photobioreactor, made of PMMA and glass slides, with immobilization of *R. palustris* on the surface, is shown in Fig. 8.

As shown in Fig. 8a, the flat-panel biofilm bioreactor is made of PMMA with a thin glass slide offering a solid-carrier surface for the adsorption and growth of bacteria (*R. palustris* CQK 01). A liquid distributor composed of a fixed-bed of glass beads (4 mm in diameter) is installed at the entrance of the reactor to obtain uniform flow distribution. The isolation plate is employed to form two flow paths that can avoid interactions between biofilm growth processes in different regions, allowing an investigation into the development of biofilms on different carriers. The flow cross-section area and working volume are 18 mm × 10 mm, and 9000 mL, respectively.

Figure 8b shows the experimental apparatus of a system consisting of a medium container, peristaltic pump, flat-panel photobioreactor, liquid/biogas separator, and gas collecting bottle. Sterile silicon hoses are used to connect the bioreactor to the medium container and liquid/biogas separator. Aside from the side wall being exposed to incident light, the external surfaces of the photobioreactor and silicone rubber hoses are covered with aluminum foil. To better understand the effects of operational parameters on biofilm structure and the hydrogen production, experiments, including the start-up stage and mature stage, are performed. In the start-up stage, which is undertaken to form the biofilm and achieve steady hydrogen production, the medium in the container is continuously pumped by the peristaltic pump to pass through the reactor and flow into the liquid/biogas separator, and then the separated liquid returns to the medium container to avoid the loss of activated PNSB cells. The solution in the container is replaced by fresh sterilized nutrient culture every 24 h until a mature biofilm is reached. A mature biofilm under fixed operating conditions is obtained when the deviations of the glucose conversion rate and biomass concentration are less than 5% over 24 h. To study the effect of start-up conditions on the structure of the PNSB biofilm, a substrate solution with

different concentrations and flow rates is supplied. The operating parameters during start-up are as follows: the flow rate is 38–1080 mL/h and the substrate concentration is 3–110 mmol/L. After the successful establishment of the biofilm, the bioreactor is mature and the culture is continuously pumped to pass through the reactor, and the separated liquid in the liquid/biogas separator is drained out of the system. Hydrogen production performance evaluations are carried out under various flow rates (30, 70, 90, and 120 mL/h) and substrate concentrations (20, 40, 60, and 80 mmol/L) during this stage. During both the start-up and mature operations, the temperature of the substrate solution is maintained at approximately 30 °C. Monochromatic LED lamps with main wavelengths of 590 nm are chosen as the light source, and the illumination intensity is adjusted to 5 klux. To maintain the anaerobic conditions, the reactor and silicone hoses are filled with substrate solution, and the headspace of the medium container is purged with argon.

The experimental results show that mature biofilms formed at a low flow rate and high substrate concentration have a looser structure, which affects the hydrogen production performance during the mature stage. Biofilms formed at a flow rate of 228 mL/h and substrate concentration of 60 mmol/L exhibit the highest dry weight and optimally porous structure, which is beneficial not only for hydrogen removal but also for glucose diffusion into the biofilm, thus significantly boosting production performance. This work serves as a guide for determining practical operating conditions for biofilm photobioreactors.

7.2   Microchannel Biofilm Photobioreactors

Although a flat-panel biofilm photobioreactor has a very simple structure and can be used for the online monitoring of biofilm development, biofilms have difficulty attaching to smooth surfaces, such as PMMA and glass. Furthermore, the hydrogen production of the immobilized bacteria (PNSB) is also limited by difficulties in light penetration and the transport of the substrate and product [149]. To maintain a high hydrogen production rate and high transfer rate of the substrate, support materials with appropriate spaces for immobilizing bacteria as well as sufficient light penetration are required. Thus, transparent gel granules, silicon chip-based microreactor photobioreactors, and polydimethylsiloxane (PDMS) microchannel photobioreactors have been developed. Transparent gel granules are a suitable solid support matrix for PNSB immobilization because many interconnected pores exist in its structure [225], forming microchannels for the supply of the substrate and the removal of products. A typical microchannel biofilm photobioreactor with immobilized *R. palustris* in polyvinyl alcohol (PVA)-boric acid gel granules is shown in Fig. 9. In Fig. 9a, b, gel granules using PVA as a solid support matrix are shown to be adequately porous, and the pores are mutually connected. There are many cells firmly attached to the surface of the solid support matrix. These stable network matrices can create a biocompatible environment that provides mechanical and chemical stability. Remarkably, the diameters of the pores are greater than the
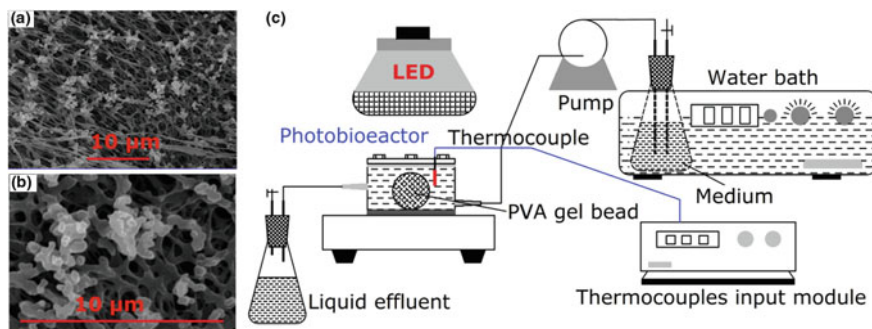
Fig. 9 Structure of the PVA-PNSB gel granules and experimental system of the biofilm photobioreactor systm (adapted from [149], Copyright 2009, with permission from Elsevier); **a** and **b** scanning electron microscope studies of the immobilized PVA-PNSB gel granules: (**a**) 3000× , (**b**) 10,000× ; (**c**) Schematic diagram of the photobioreactor system

thickness of the wall, resulting in a huge specific porosity and surface area in the PVA-PNSB gel granules. The huge porous microstructure of the gel matrices provides ample room for bacterial growth; this helps them overcome the problem of disruption caused by bacterial growth. In addition, the porous microstructure facilitates the transfer of substrate, water, and products (H_2 and CO_2). These two features make it possible to continuously operate PVA-PNSB gel granules.

Although microchannel biofilm reactors employing PVA-PNSB gel granules have many advantages as mentioned, the transport processes of the substrate and the products as well as the metabolism of the microorganisms are extremely complicated due to the complex porous microstructure and uneven distribution of cells. In a typical PVA-PNSB gel granule, PNSB consume organic substrate for their growth and metabolism while producing hydrogen and other products. Photobiohydrogen generation in the interior of the granule is a process involving the transfer of organic substrate, photons, and other products, creating a complicated microenvironment in which liquid, gaseous, and solid phases coexist. In this situation, the counter-transport of substrate, product, and protons becomes critical for the metabolism of PNSB. However, there is limited information concerning these phenomena and their mechanism in the microchannels of PVA-PNSB gel granules. This is mainly due to the difficulty in directly observing PNSB growth and hydrogen production resulting from the complexity of the immobilized granule shape and reactor structure. To understand the micro-behavior and mass transfer of PNSB in immobilized cultures and to enhance hydrogen production, it is important to develop a suitable microchannel photobioreactor. Thus, visualizable PDMS microchannel photobioreactors and visualizable silicon chip-based microreactors have been developed, and they can be used to observe the adsorption and film formation of PNSB. To demonstrate visualized colony formation, mass transfer, and biogas formation in the microstructure, a typical visualizable PDMS microchannel photobioreactor is shown in Fig. 10.
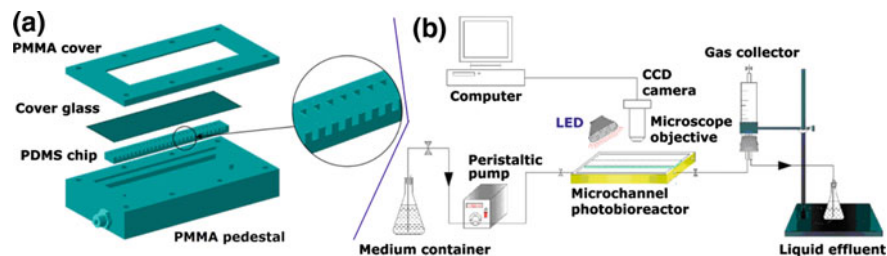
Fig. 10 Microchannel photobioreactor and experimental apparatus (adapted from [225], Copyright 2011, with permission from Elsevier); **a** Schematic of PDMS microchannel photobioreactor; **b** Schematic of the experimental apparatus

As shown in Fig. 10a, the photobioreactor consists of a PMMA cover, cover glass, PDMS chip, and PMMA pedestal; the microchannel bioreactor is made of polymethyl methacrylate (PMMA) and PDMS with a cover glass slide (24 mm 60 mm × 0.17 mm). It offers a solid carrier surface for the adsorption and growth of bacteria. PMMA and PDMS are suitable for photobiological hydrogen production due to their transparency, chemical stability, and ease of mechanical incising. To simulate the microstructures of the gel granules, 125 semi-closed microchannels are fabricated on the PDMS chip. The length, width, and height of the microchannels are 3.5 mm, 0.1 mm, and 0.1 mm, respectively. The configuration and size of the microchannels are selected according to SEM scanning images as shown in Fig. 10a, with the chosen length being the same as the radius of a real PVA-PNSB gel granule produced in our lab as shown in Fig. 10a. Based on this design, the microorganism growth and hydrogen production within the microchannels can be visualized and recorded by a charge coupled device (CCD) camera. The substrate is supplied by the channels between the PDMS chip and PMMA pedestal with a width of 6.25 mm and a height of 2.5 mm. The PMMA pedestal size is 78 mm × 42 mm × 12.3 mm.

As shown in Fig. 10b, the experimental system consists of the PDMS microchannel photobioreactor, a light source, a peristaltic pump, a substrate medium flask, an effluent flask, a gas collector, and an imaging system. The microimage system is composed of an optical microscope and a CCD camera connected to a personal computer. The photobioreactor is connected with the medium and the effluent flask using silicon hoses. LED lamps are used as the external light source and are mounted to the topside of the photobioreactor. Four monochromatic LED lamps emitting at 470, 520, 590, and 630 nm are used as light sources, and the illumination intensity can be adjusted from 1 to 9 klux by varying the distance between the LED and the reactor. The substrate solution is fed by peristaltic pumps, with the flow rate controlled by adjusting the rotation speed of the pump. The temperature of the substrate solution is maintained at approximately 30 °C during the experiments.

The experiments are conducted in two stages: the start-up stage and the continuous hydrogen production stage. Before the start-up stage, all of the experimental

equipment is completely sterilized by formalin vapor. During the first stage, 100 mL precultured suspension of PNSB is inoculated into fresh medium containing 50 mmol/L glucose, and then the solution is pumped into the photobioreactor. PNSB gradually contact with the solid surface of the PDMS microchannels and gradually adsorb through diffusion and bacterial swimming. Meanwhile, PNSB consume the substrate and excrete a large amount of EPS during its growth; the adhesiveness of EPS gradually captures other suspended PNSB to form bacterial colonies. During this stage, the volumetric flow rate of the substrate is adjusted to 1.5 mL/h. The initial light wavelength is set to 590 nm, and light intensity measured at the incident surface is adjusted to 5 klux. An optical microscope is used to observe of the formation of PNSB colonies inside the microchannel at regular time intervals. After stable colonies are formed, the photobioreactor goes into the hydrogen producing stage. The culture medium is provided by the peristaltic pump. The whole bioreactor and pipeline system are covered with foil, except for the microchannel part. During the second stage, an evaluation of the performance is conducted in a continuous flow mode at a quasi-steady-state. The quasi-steady-state is defined as a constant hydrogen production rate and constant substrate consumption rate obtained for a period of over 24 h with the designated parameters. The performance of the photobioreactor with different operation parameters is assessed mainly by the hydrogen production rate, hydrogen yield, substrate consumption rate, and substrate removal efficiency. The average hydrogen production rate, hydrogen yield, substrate consumption rate, and substrate removal efficiency are used to assess the performance of the photobioreactor in continuous hydrogen production. The average hydrogen production rate and hydrogen yield are defined as shown in Eqs. (9)–(12) [225]:

$$H_2 \ production \ rate = \frac{Cumulative \ H_2 \ production \ (mmol)}{Cell \ dry \ weight \ (g) \ \times \ H_2 \ evolution \ time \ (h)} \quad (9)$$

$$H_2 \ yield = \frac{Amount \ of \ H_2 \ produced \ (mol)}{Amount \ of \ substrate \ consumed \ (mol)} \quad (10)$$

$$Substrate \ consumption \ rate = \frac{Amount \ of \ substrate \ consumed \ (mmol)}{Cell \ dry \ weight \ (g) \ \times \ time \ (h)} \quad (11)$$

$$Substrate \ removal \ efficiency = \frac{Inlet \ substrate \ (mmol/L) - outlet \ substrate \ (mmol/L)}{Inlet \ substrate \ (mmol/L)}$$

$$(12)$$

Visualization studies show that the formation of PNSB colonies in the interior of the microchannels can be divided into four stages: bacteria absorption, bacteria reproduction, morphological transformation, and colony formation. The microchannel vents immobilized by PNSB colonies are favorable sites for the formation of hydrogen bubbles, which grow by continuous hydrogen molecule transfer across the gas-liquid interface. With the increase of substrate concentration

and flow rate, the rate and yield of hydrogen production rises first and then falls, but the substrate conversion monotonically goes up with its rate slowed down. The substrate degradation efficiency increases first and then decreases with an increase of substrate concentration, and reduces with an increase of the solution flow rate. At a higher substrate concentration and flow rate, substrate inhibition and the loss of biofilms are the main reasons for lower rates and yields of hydrogen production. Specifically, the microchannel photobioreactor has a maximal hydrogen production rate of 1.48 mmol/g CDW/h and a maximal hydrogen yield of 0.91 mol H_2/mol glucose in all of the tests at an optimal inlet flow rate of 2.8 mL/h and substrate concentration of 50 mmol/L. In addition, the microchannel photobioreactor shows an optimal performance of hydrogen production and substrate consumption at 590 nm illumination wavelength and 5 klux illumination intensity. In summary, microchannel biofilm photobioreactors,, in particular those that are visualizable, can provide important insights into the micro-behavior and mass transfer of PNSB in an immobilized culture, reveal the mechanism of PNSB biofilm growth and metabolism, and enhance hydrogen production performance.

7.3 Groove-Type Biofilm Photobioreactors

Visualization studies of the biofilm development using microscopes and online sensors have revealed that cells facing physical, chemical, and biological threats from their environment prefer to adhere to the surfaces of channels or tubes. As adherent cells grow and divide, physiological adaptations, including the secretion of EPS, are induced to create a protective matrix surrounding the cells. These dynamic communities can spread across surfaces and incorporate new planktonic cells to ultimately form a biofilm [144]. Thus, the surface features of the support materials play an important role in biofilm formation. Research on the dependence of biofilm formation on substratum materials and surface topography has revealed that rough or patterned surfaces can enrich cell adherence compared with smooth surfaces. Walker and Marsh [231] reviewed biofilm formation and its role in microbial contamination of dental unit water systems (DUWS) with narrow-bore tubing, and they concluded that DUWS are susceptible to biofilms and encourage biofilm growth. Carlén et al. [232], who studied surface characteristics and biofilm formation on unpolished and polished glass ionomers and composite resins for tooth protection, showed that higher surface roughness leads to more inorganic and better bacterial adherence. Whitehead and Verran [233] compared the experimental results of cell retention on four stainless steel surfaces used to avoid corrosion, and they found that the cells were more evenly spread across titanium-coated surfaces than fine-polished surfaces and the cell numbers were higher. In addition, the surface topography influences the pattern of cell retention. Scheuerman et al. [234] studied cell adhesion on silicon chips with etched grooves perpendicular to the flow direction. Their results showed that the maximum initial accumulation was at the bottom of the rough elements due to protection from shearing stress. Ginsburg and

Karamanev [235] investigated the roughness effect of a graphite surface on the immobilization of *Acidithiobacillus ferrooxidans* and they found that the activated carbon fibers with the largest surface area per gram led to the maximum number of immobilized microorganisms. These results show that the rough surfaces of the support materials are beneficial to PNSB immobilization and biomass enrichment in a photobioreactor. Hence, to utilize the advantages of rough surface support materials for the enhancement of hydrogen production, biofilm photobioreactors with grooved surfaces have been developed. A typical groove-type biofilm photobioreactor for continuous hydrogen production by immobilized PNSB is shown in Fig. 11a, and the experimental system is shown in Fig. 11b.

Figure 11a shows a groove-type biofilm photobioreactor, which is a sealed vessel with a working volume of $100\,(H) \times 50\,(L) \times 20\,(W)\,mm^3$ fabricated from PMMA, which is suitable for photobiological hydrogen production as mentioned above. Grooves (1 mm width and 1 mm depth) are etched with a mechanical incising technique on one vessel wall of 100 mm length and 50 mm width. Furthermore, a flat-panel photobioreactor (Fig. 11c) with the same volume (vessel walls with a smooth surface) as the groove-type one is fabricated and used as a comparison.

Figure 11b shows the schematic details of the experimental setup. The system consists of a biofilm photobioreactor, a light source, a peristaltic pump, a substrate medium flask, a liquid effluent flask, a gas-liquid separator, a gas collector, and a water container. LED lamps are used as the external light source and are mounted to face the grooved wall of the reactor. LED lamps emit wavelengths in the visible
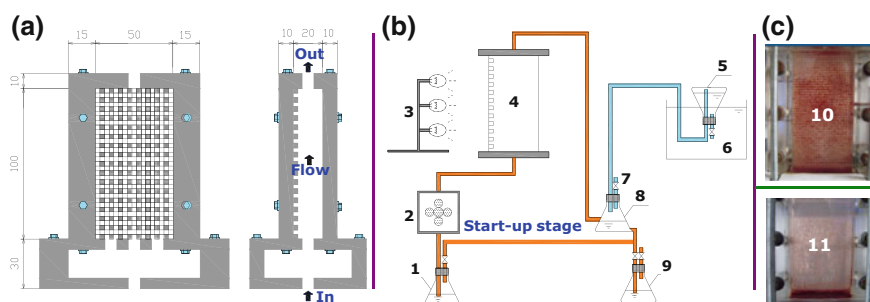
1. Glucose-based substrate flask; 2. Peristaltic pump; 3. Light source; 4. Photobioreactor; 5. Gas collector; 6. Water container; 7.Valve; 8. Gas-liquid separator; 9. Liquid effluent flask; 10. Groove-type biofilm photobioreactor; 11. Flat-panel biofilm photobioreactors.

Fig. 11 Groove-type photobioreactor, experimental apparatus and pictures of photobioreactors (adapted from [144], Copyright 2010, with permission from Elsevier); **a** Schematic of groove-type biofilm photobioreactor; **b** Schematic of the experimental apparatus; **c** Pictures of groove-type and flat-panel biofilm photobioreactors

light spectrum (400–760 nm). Incident light intensity is adjusted from 1.78 to 10.06 W/m^2 by varying the distance between the LEDs and bioreactor.

The photobioreactor operation includes two steps, i.e., the start-up stage and the continuous hydrogen production stage. During the start-up stage, 100 mL fresh medium for inoculation with an initial glucose concentration of 6 g/L is pumped into the reactor and then it circulates until the PNSB adhere and grow on the surface to form a stable biofilm. The volumetric flow rate of the substrate is adjusted to 10 mL/h. The operation temperature is controlled at 30 °C, and the initial pH of the medium is adjusted to 7.0. The initial wavelength is set to 590 nm, and light intensity measured at the incident surface is adjusted to 5.09 W/m^2. To avoid nutrient competition by suspended cells and to accelerate the formation of biofilms, half of the culture medium is discharged once the cell concentration in the liquid phase is high, and the same volume of fresh medium is then rapidly fed into the photobioreactor. When a deep red layer is evident on the transparent reactor wall as shown in Fig. 11c, this indicates that PNSB have successfully adhered to the surface and a stable biofilm has formed. The hydrogen production and glucose consumption of the groove-type photobioreactor are higher than those of the flat-panel photobioreactors during the entire start-up stage. This can be attributed to the enriched biomass obtained in the groove-type photobioreactor as shown in Fig. 11c. The etched grooves provide extra sites for bacteria immobilization, and the undulate surfaces of the groove channels act as shelters to protect cells from flow shear stress, hence being beneficial to cell adherence.

Photobioreactors go into the continuous hydrogen production stage after stable biofilms are formed. The baseline case is set under operational conditions of: 590 nm light wavelength, 6.75 W/m^2 light intensity, 10 g/L glucose concentration, 60 mL/h influent flow rate, and pH value 7.0 at 30 °C. In this stage, a series of experiments is carried out on continuous hydrogen production in the groove-type photobioreactor illuminated by monochromatic LED lights, and the performance is investigated. The effects of wavelength, light intensity, inlet glucose concentration, flow rate, and initial substrate pH are compared with those obtained in a flat-panel photobioreactor with a smooth surface. The results show that the optimum operational conditions for hydrogen production in the groove-type photobioreactor are: inlet glucose concentration 10 g/L, flow rate 60 mL/h, light intensity 6.75 W/m^2, light wavelength 590 nm, and initial substrate pH 7.0. The maximum hydrogen production rate, hydrogen yield, and light conversion efficiency in the groove-type photobioreactor are 3.816 mmol/m^2/h, 0.75 mol H^2/mol glucose, and 3.8%, respectively, which are about 75% higher than those in the flat-panel photobioreactor. The results confirm that grooved structure support materials can enrich immobilized biomass, increase specific surface area, and enhance convective mass transfer for both substrate and metabolic products of photofermentation, leading to high performance hydrogen production.

7.4 Optical Fiber Biofilm Photobioreactors

The performance of reactors with photosynthetic bacteria still faces two critical problems: limited light and low cell concentrations, even in groove-type biofilm reactors. A simple approach to improve the lighting conditions and increase the biofilm mass is by using optical fibers as the biofilm support material; such reactors are called optical fiber biofilm photobioreactors. So far, optical fiber biofilm photobioreactors have undergone three generations of development. The first is the annular fiber-illuminating photobioreactor, the second is biofilm photobioreactors using optical fibers with added rough surfaces, and the third is biofilm photobioreactors using hollow optical fibers with intrinsic rough surfaces.

First-generation Annular Fiber-illuminating Photobioreactors [236–238]. A first-generation optical fiber biofilm photobioreactor is shown in Fig. 12. The structure of the optical fiber is shown in Fig. 12a; the side-light optical fiber consists of a fiber core and cladding with the refractive index of the core being higher than that of the cladding, i.e., $n_1 > n_2$, and the fiber diameter is generally greater than 6 mm. Figure 12b shows an annular fiber-illuminating biological hydrogen reactor. One can see that the structure is very simple, and the reactor consists of a rectangular cavity fabricated from PMMA, a light source, and a side-light optical fiber. The side-light optical fiber, with the desired surface light intensity and uniform light distribution, is inserted into a sealed PMMA vessel (rectangular cavity) as an internal light source.

To test the advantages of optical fiber biofilm reactors, the experimental apparatus has been employed as shown in Fig. 13a, with continuous hydrogen
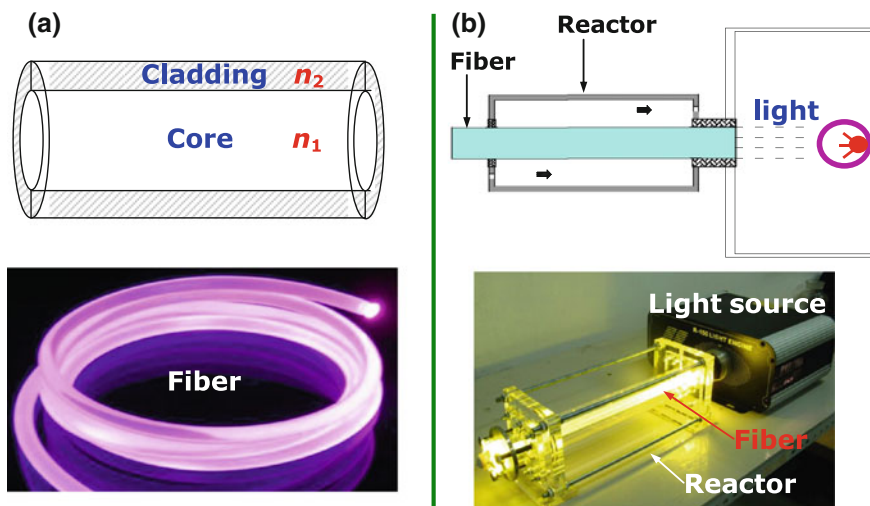
Fig. 12 Optical fiber and photobioreactor (adapted from [238]); **a** Schematic and picture of side-light optical fiber; **b** Schematic and picture of the annular fiber-illuminating photobioreactor
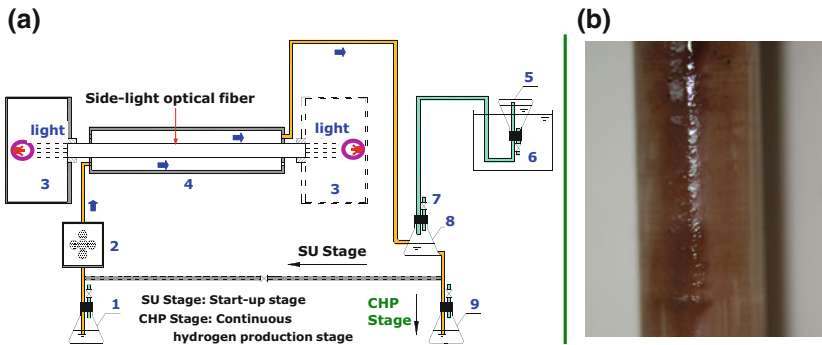
1. Glucose-based substrate container; 2. Peristaltical pump; 3. Light engine; 4.

Rectangular cavity of the bioreactor; 5. Hydorgen collector; 6. Water container; 7.

Gas sampling valve; 8. Gas-liquid separator; 9. Liquid effluent container.

Fig. 13 experimental apparatus and picture of the optical fiber attached biofilm (adapted from [238]); **a** Scheme of experimental apparatus; **b** Photograph of biofilm formation on the surface of optical fiber after start-up stage

production carried out at different light wavelengths, light intensities, inlet substrate concentrations, and flow rates. The results show that the biofilm successfully adheres and grows on the surface of the optical fiber (see Fig. 13b), and the reactor exhibits excellent performance for both hydrogen production and light energy conversion when employing *R. palustris* CQK 01. A high hydrogen production rate of 0.83 mmol/(g cell)/h and excellent light conversion efficiency of 47.9% are attained under the operational conditions of monochromatic light illumination at 530 nm, light intensity of 4.15 W/m^2, inlet substrate concentration of 10 g/L, and flow rate of 100 mL/h.

The high-performance hydrogen production using the solid optical fiber (SOF) can be attributed to the following. First, optical fibers can provide uniform light distribution with a high relative AV ratio and proximal contact with light-demanding microorganisms to achieve high light transmission efficiency. Moreover, optical fibers are easy to use and can transfer sunlight into reactors to achieve results comparable with LED, tungsten filament, and fluorescent lamps that must consume electrical energy. Although the hydrogen production capacity is significantly enhanced compared to biofilm reactors without optical fiber, the hydrogen production is still unsatisfactory and should be improved. The main reason is that the surface of the optical fiber is rather smooth so it is difficult for cells to attach and form a biofilm, leading to long biofilm formation time and low attached biomass. To resolve this problem, second-generation biofilm photobioreactors using optical fibers with added rough surfaces have been developed.

Second-generation Biofilm Photobioreactors Using Optical Fibers with Added Rough Surfaces [239]. Fibers are shown in Fig. 14a, b, and a schematic
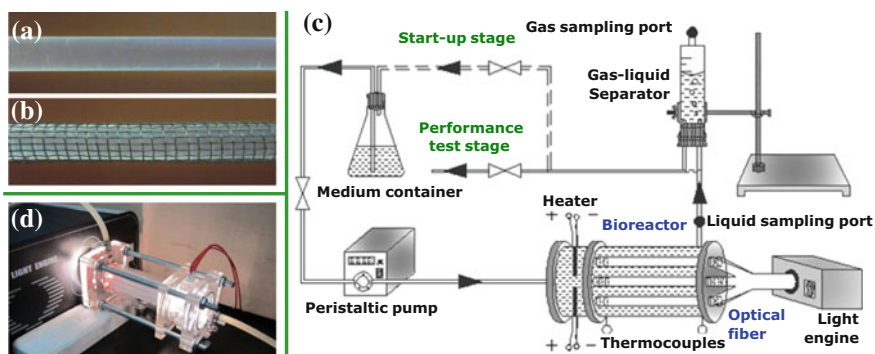
Fig. 14 Photography of the surface of optical fiber **a** prior to treatment **b** after treatment; schematic **c** and picture **d** of the experimental system (adapted from [239], Copyright 2011, with permission from Elsevier)

and picture of the experimental system are shown in Fig. 14c, d. Figure 14a shows an optical fiber with a smooth surface (composed of PMMA with a 6-mm diameter and 100-mm working length). To increase the surface roughness, 18-mesh stainless steel wire mesh is wrapped around the optical fiber, resulting in interlaced grooves (a rough surface) leading to extra available sites for PNSB attachment. A picture of the optical fiber with an added rough surface is shown in Fig. 14b.

As shown in Fig. 14c, d, the photobioreactor is a sealed vessel fabricated by PMMA with a working volume of 125 mL and seven side-light plastic-clad optical fibers with added rough surfaces. The seven modified optical fibers are excited to achieve a light intensity of ca. 12 W/m^2 by a metal-halide lamp (250 W). A heater is installed at the inlet of the reactor to maintain the desired temperature of the influent culture medium. Two T-type thermocouples are distributed at the inlet and outlet of the reactor to detect internal temperature. Finally, the photobioreactor is covered with aluminum foil to avoid the impact of outside light on the experimental results. Prior to inoculation of *R. palustris* CQK 01 with 10% inoculum, the reactor body is sterilized with formalin and rinsed three times with sterile water, and the remaining components of the experimental system are autoclaved. Experiments are conducted in two stages: the start-up stage and the continuous operation stage. During the start-up stage, medium with a flow rate of 50 mL/h is recycled to avoid the loss of activated PNSB cells in the circulating solution. In addition, 50 mL medium is discharged and 50 mL fresh nutrient medium of 30 mM is fed into the reactor every day. In this period, the hydrogen production and substrate biodegradation rates of the reactor are measured every day until constant values are attained, indicating that PNSB have been successfully immobilized to form a stable biofilm. In this system, it was found that the start-up stage of the reactor is about 25 days, after which continuous operation can be performed. In the continuous operation stage, the experimental system becomes an open loop system. The evolved biogas and effluent liquid are discharged from the outlet of the reactor and

flow into a gas-liquid separator. The biogas produced is then collected by water displacement to determine the volume and density of hydrogen. Effluent liquid samples are taken from the liquid sampling port at desired time intervals to measure residual glucose concentrations.

By using the experimental system shown in Fig. 14c, the effects of operational conditions, including the influent substrate concentration, flow rate, temperature, and influent medium pH, on the performance of hydrogen production are investigated. The results show that the optimum conditions for hydrogen production are: influent substrate concentration 60 mM, flow rate 30 mL/h, temperature 30 °C, and influent medium pH 7. Under optimal conditions, the optical fiber biofilm photo-bioreactor yields fairly good and stable long-term performance with a hydrogen production rate of 1.75 mmol/L/h, light conversion efficiency of 9.3%, and substrate degradation efficiency of 75%. This good performance is attributed to the added rough surface that greatly enhances biofilm formation and thus increases cell concentration.

Third-generation Biofilm Photobioreactors Using Hollow Optical Fibers with Intrinsic Rough Surfaces [240–242]. The added surface roughening of second-generation photobioreactors enhances biofilm formation and thus increases cell concentration. Nevertheless, this reduces light energy utilization because of the following problems. First, the coating of the SOF is removed, and the fiber core has a higher refractive index than the fiber cladding; thus, light is confined to the core by total internal reflection, so the luminous intensity at the fiber surface depends on the weak evanescent near-field [243]. Second, the wire mesh absorbs and shields against evanescent waves. Furthermore, the wire mesh cannot tolerate an acidic PNSB suspension, resulting in poor stability for long-term operation, and the activity of the underlying biofilm is reduced with biofilm growth owing to substrate and light energy limitations.

To increase the luminous intensity at the fiber surface and the intrinsic roughness of the optical fiber, a new biomaterial (GeO_2-SiO_2-chitosan medium, GSCM) with a high local refractive index due to GeO_2 doping has been proposed, and a new hollow optical fiber (HOF) based on a quartz glass tube with a GSCM coating has been created [241]. The fiber structure is shown in Fig. 15; the length, outer
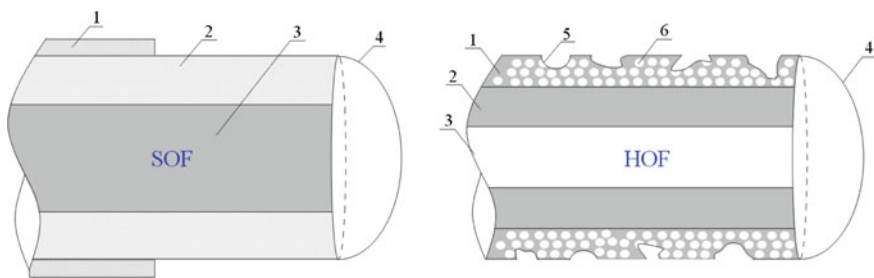
Fig. 15 The structure of the SOF and the HOF (1. coating, 2. cladding, 3. core, 4. hemispherical tip, 5. pit, 6. GeO_2) (adapted from [240], Copyright 2013, with permission from OSA publishing)

diameter, and inner diameter of the SOFs and the HOFs are 160 mm, 6 mm, and 4 mm, respectively.

As shown in Fig. 15, the refractive indices of the fiber core and cladding of the HOFs are 1.000 ± 0.001 and 1.450 ± 0.005, respectively, and the local refractive index of the fiber coating (GeO_2) is 1.985 ± 0.007 at 25 °C. Experimental data show that the surface roughness of the HOFs increases with the increasing GeO_2 content; when the fiber is longer than 30 mm, the luminous intensity of the HOFs increases with the decreasing GeO_2 content. Specifically, HOF doped with 0.1 g of $2GeO_2$-SiO_2 sol shows the highest luminous intensity. Similarly, for HOF doped with 0.1 g of $2GeO_2$-SiO_2 sol, the luminous intensity along the radial direction at an axial distance of 90 mm is also the highest. These results and the proposed light transmission modes confirm that the appropriate doping concentration of GeO_2 can enhance the luminous intensity of a hollow fiber. Although the luminous intensity has been enhanced, an uneven distribution has also been demonstrated at the optical fiber surface. To improve the luminescent properties of the HOF, according to the proposed light transmission modes and obtained experimental data, one can change the size and coverage of GeO_2 at the cladding-coating interface. The coverage of GeO_2 has been further investigated by changing the coating thickness, and the improved structure of the HOF is shown in Fig. 16.

Experimental data show that when the δ_1, δ_2, and L are respectively 100 μm, 50 μm, and 20 mm (δ_1 and δ_2 denote the gradient coating thickness close to the fiber end and fiber incident end; L denotes the uncoated length close to the fiber incident end), the HOF exhibits the highest luminous intensity and uniform light distribution. The luminous intensity of the HOF is 4.5 times higher than that of the SOF at an axial distance of 90 mm. The radial intensity at 20 mm for the HOF is 2.9 times higher than that of the SOF. These results can be attributed to the density distribution of GeO_2 as well as the increase in surface roughness with increasing fiber length; thus, the transmitted scattered intensity increases at the fiber surface.
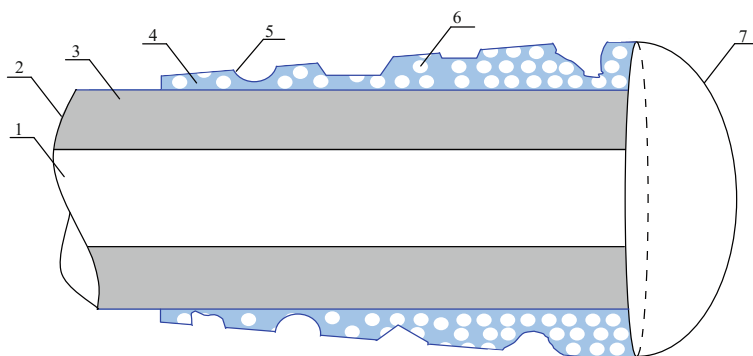
Fig. 16 Structure of the improved GSCM-coated HOF (1. core, 2. fiber incident end, 3. cladding, 4. coating, 5. pit, 6. GeO_2, 7. hemispherical tip) (adapted from [241], Copyright 2014, with permission from Elsevier)

The good luminescence properties of HOFs with intrinsic surface roughness have high potential in immobilized cell applications and photobioreactors. Hence, it is vital to develop a BPBR by adsorption of PNSB on GSCM-coated HOFs to enhance hydrogen production. A schematic of such a photobioreactor is shown in Fig. 17.

Figure 17(a) shows a cylindrical photobioreactor fabricated from PMMA with a working volume of 125 mL and seven GSCM-coated HOFs. The length, outer diameter, and inner diameter of the HOFs are 160 mm, 6 mm, and 4 mm, respectively. The refractive indices of the fiber core and cladding are 1.000 ± 0.001 and 1.450 ± 0.005, respectively, and the local refractive index of the fiber coating (GeO_2) is 1.985 ± 0.007 at 25 °C. The average luminous intensity at the fiber surface is 55 $\mu W/cm^2$ (the average luminous intensity at normal SOF and uncoated HOF surfaces are 11 $\mu W/cm^2$ and 12 $\mu W/cm^2$, respectively). The light source was a tungsten filament lamp (150 W; 580–595 nm). The inset of Fig. 17a shows the distribution of the fibers in the photobioreactor. Two T-type thermocouples were distributed in the photobioreactor to detect the internal temperatures of the inlet and outlet. The photobioreactor was covered with aluminum foil to avoid the impact of outside light. Before PNSB were inoculated with 10% inoculum, the photobioreactor body was sterilized with formalin and then thoroughly washed with deionized water.

The BPBR is operated in two stages. During the first stage, the medium is recycled with a flow rate of 70 mL/h to avoid the loss of activated PNSB cells in the circulating solution; this stage lasts about 1 day. In addition, 50 mL of the medium
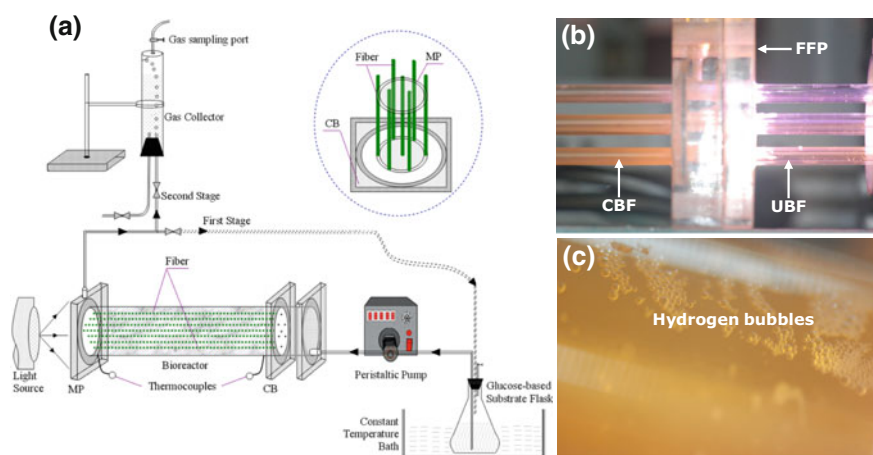
Fig. 17 Experimental apparatus, and picture of the support materials (hollow optical fibers) and produced hydrogen bubbles (adapted from [241], Copyright 2014, with permission from Elsevier, and [244]); a Schematic of experimental apparatus (mounting plate: MP, cross baffle: CB); b The picture of the support materials (CBF: coated biofilm fiber, FFP: fiber fixed plate, UBF: uncoated biofilm fiber); c The picture of the produced hydrogen bubbles by PNSB biofilm on the hollow optical fiber

is discharged and 50 mL of 55 mM fresh nutrient medium is fed into the photobioreactor every day. In this stage, the biofilm dry weights are measured every 2 days. The startup stage of this photobioreactor is about 8 days based on the biofilm dry weight remaining constant, after which continuous operation can be performed. In the second stage, the BPBR becomes an open loop system. The evolved biogas and effluent liquid are discharged from the outlet and flow into a gas-liquid separator (the medium flow was kept at 70 mL/h). The biogas produced is collected by water displacement to determine the volume and density of H_2.

Experimental data show that the GSCM-coated HOF shows high biocompatibility, significantly enhancing biofilm biomass, improving biofilm activity, and increasing H_2 production. This proposed photobioreactor yields fairly stable long-term performance with a hydrogen production rate of 2.65 mmol/L/h, which is 1.56 and 1.51 times higher than those of photobioreactors with uncoated HOF and with fibers having roughened surfaces obtained by wrapping them in wire mesh, respectively.

The high hydrogen production performance of the GSCM-coated HOFs can be explained as follows. First, the presence of nutrients and the high luminous intensity induce the rapid adsorption of PNSB cells on the surface. Second, the appropriate surface grooves increase the contact area of the cells and protect adhered cells from desorption under the flow conditions; because the pits prolong the residence time of the culture medium, the cells on the surface can make better use of the medium. Third, during the biofilm growth period, the roughness provides many capillary channels to increase mass transfer between the substrate and product, and the solid medium in the GSCM coating can supply the nutrition that maintains cell growth and reproduction. Fourth, good penetration depth of light at the fiber surface improves the light conditions of the biofilm. These favorable conditions can lead to high hydrogen production. Excellent light distribution, cell adhesion capacity, and hydrogen production demonstrate the effectiveness of using GSCM-coated HOFs for biochemical reactions, immobilized cell applications, and large-scale photohydrogen production.

7.5 Other Types of Biofilm Photobioreactors

In addition to the above-mentioned three main types, various other biofilm photobioreactors have been used for photofermentation, including an upflow anaerobic sludge blanket photobioreactor [245], a granule-based continuous stirred tank photobioreactor [246], fixed or packed bed photobioreactors [153, 247], anaerobic fluidized bed photobioreactors [248], and a tricking biofilter [249]. These immobilization technologies are mainly based on granulation or biofilm attachment processes. Biofilm support materials with high transparency in the above-mentioned photobioreactors include PMMA, glass beads, and optical fibers. To improve PNSB biofilm development and hydrogen production for photofermentation, a novel photothermal biomaterial, designated GeO_2-SiO_2-Chitosan-Medium-LaB_6
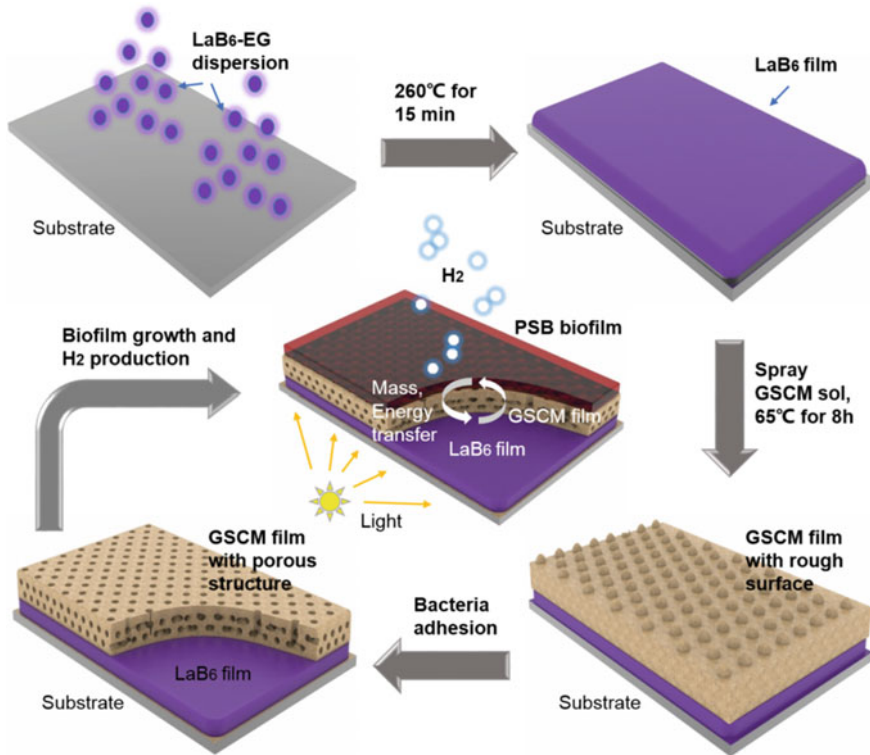
Fig. 18 Schematic representation of the fabrication of the GSCML film and photohydrogen production process of PNSB biofilm on the GSCML film surface (adapted from [250], Copyright 2017, with permission from Elsevier)

(GSCML), has been developed [250]. A schematic representation of preparation process and functional mechanism is shown in Fig. 18.

The GSCML biomaterial employs spectral beam splitting technology to increase the overall utilization of the incident light, in which LaB_6 nanoparticles (NPs) mainly absorb light at approximately 380–510 and 660–780 nm and convert it into heat energy; the transmitted light is around 590 nm for PNSB growth. Experimental data show that the temperature increase and the luminous intensity of the light transmitted through the prepared biomaterial is controlled by adjusting the LaB_6 NP content. The average biofilm growth rate and hydrogen production rate on this material are 0.05 mg/cm^2/d and 2.92 mmol/h/m^2, which are 3.4 and 4.1 times higher than those of the glass slide, respectively.

In summary, in the last few decades, many biofilm photobioreactors and support materials for hydrogen production using photofermentation have been developed. The main aim of this is to increase the light and heat energy efficiency, decrease the time of biofilm formation and energy consumption, enhance substrate and product transfer, optimize the distribution of light and heat, and promote biofilm activity.

Constantly updating these materials can further promote the hydrogen production rate and stability.

8 Fluid Flow and Mass Transfer in a Photobioreactor

To attain a better understanding of the reaction mechanism and the effects of operational factors on photohydrogen production performance, numerous experimental studies have been carried out. Due to the time consumption of experiments and the limitations of even high-end measuring equipment, up to now it has been difficult to understand mass transport phenomena using only experimental studies. Therefore, theoretical studies are necessary to investigate the reaction dynamic mechanisms, and to analyze and predict the characteristics of bioreactors.

At present, some representative mathematical models that have been used to simulate pollutant biodegradation and mass transport in bioreactors have achieved success. Banerjee et al. [251] presented a mathematical model to analyze the mass transfer limitations in phenol biodegradation using *Pseudomonas putida* immobilized in calcium alginate beads. Notably, both internal and external mass transfer limitations and substrate inhibition kinetics of the process were considered. Das et al. [252] studied three different configuration bioreactors for continuous hydrogen production to derive kinetic models, taking into account the effect of external mass transfer resistance on the biodegradation rate. Palazzi et al. [253] developed a kinetic model in a continuous bioreactor for hydrogen production and studied the effect of both residence time and inlet glucose concentration on the hydrogen production rate. Tepe and Dursun [254] developed a new mass transfer correlation and analyzed the combined effect of external mass transfer with biochemical reactions on phenol removal in a packed bed reactor. These models consider only the biochemical reaction kinetics of the substrate degradation and hydrogen production. However, Liao et al. [247] developed a model to investigate two-phase flow and mass transport coupled with biochemical reactions, and predicted the substrate utilization and hydrogen production in an immobilized-cell packed bed photobioreactor. The modeling results of glucose consumption efficiency and hydrogen production rate are in good agreement with the experimental data. Additionally, the effects of parameters, including illumination intensity, temperature, pH, and flow rate of the influent substrate, have been investigated with this model, and the distributions of glucose concentration and influent substrate flow rates have also been successfully predicted. These studies are generally based on macro-scale models that have proven to be very successful for describing biochemical reaction kinetics in photobioreactors. However, these models are based on the continuum hypothesis and need to solve complex nonlinear partial differential equations. This presents difficulties in dealing with micro-scale problems and in treating complex boundaries.

In recent decades, a novel mesoscopic numerical algorithm, named lattice Boltzmann method (LBM), has emerged and received extensive attention. Different

from conventional analytical methods, the LBM is based on kinetic theory and has some distinctive advantages, including simple formulation, natural parallel-computing, and ease in handling complex boundaries [255, 256]. The fundamental idea of LBM is to establish a simplified kinetic model for particle distribution functions, and then the macroscopic properties can be determined via these distribution functions. Since its emergence, LBM has been successfully applied to many fields, such as hydrodynamics [257–259], heat and mass transfer [260–262], multicomponent and multiphase flow [263–265], micro-flow [261, 266, 267], flow in porous media [268–270], and chemical reactions [270–272]. Accordingly, LBM has been used to study reactions in photobioreactors, particularly coupled with hydrodynamics and mass transfer.

8.1 Lattice Boltzmann Method (LBM)

LBM simulates hydrodynamics and mass transport phenomena by tracking the evolution of distribution functions. These distribution functions are governed by the lattice Boltzmann equation (LBE), and a Bhatnagar-Gross-Krook (BGK) model [273, 274] is used, which is a specific numerical scheme of the Boltzmann equation with single-relaxation-time approximation by discretizing the time and space.

For the bioreaction coupled with hydrodynamics and mass transfer, two sets of distribution functions $f_i(\mathbf{x}, t)$ and $g_{i,\sigma}(\mathbf{x}, t)$ are used, relating to flow field and concentration field of the σ-species, respectively. LBEs can be expressed as:

$$f_i(\mathbf{x} + \mathbf{e}_i \delta_t, t + \delta_t) - f_i(\mathbf{x}, t) = -\tau_v^{-1}(f_i(\mathbf{x}, t) - f_i^{eq}(\mathbf{x}, t)) + \delta_t F_i \qquad (13)$$

$$g_{i,\sigma}(\mathbf{x} + \mathbf{e}_i \delta_t, t + \delta_t) - g_{i,\sigma}(\mathbf{x}, t) = -\tau_\sigma^{-1}\left(g_{i,\sigma}(\mathbf{x}, t) - g_{i,\sigma}^{eq}(\mathbf{x}, t)\right) + J_{i,\sigma} \delta_t r_\sigma \qquad (14)$$

where, δ_t is the time step, τ_v and τ_σ are the single relaxation times of particles corresponding to $f_i(\mathbf{x}, t)$ and $g_{i,\sigma}(\mathbf{x}, t)$, respectively, $\mathbf{e}_i$ is the discrete particle velocity along ith, direction, F_i, and r_σ are the force and reaction source, f_i^{eq} and $g_{i,\sigma}^{eq}$ denote the equilibrium distribution function of the ith discrete velocity corresponding to f_i and $g_{i,\sigma}$, and they can be expressed in general as shown in Eqs. (15)–(16) [275]:

$$f_i^{eq} = w_i \rho \left[1 + \frac{3\mathbf{e}_i \cdot \mathbf{u}}{c^2} + \frac{9(\mathbf{e}_i \cdot \mathbf{u})^2}{2c^4} - \frac{3\mathbf{u}^2}{2c^2}\right] \qquad (15)$$

$$g_{i,\sigma}^{eq} = c_\sigma \left(J_{i,\sigma} + K_i \frac{\mathbf{e}_i \cdot \mathbf{u}}{c^2}\right) \qquad (16)$$

where, c is the lattice velocity, $c = \delta_x/\delta_t$, δ_x is the lattice space, and w_i is the weight coefficient. $J_{i,\sigma}$ and K_i are specially chosen constants, and the rest fraction J_0 can be chosen from 0 to 1.

For flow fields, two-dimensional nine-velocity (D2Q9) and three-dimensional fifteen-velocity (D3Q15) models are widely used for 2D and 3D problems, and the discretized velocity space in these models is presented in Fig. 19. For D2Q9 model,

$$\omega_i = \begin{cases} 4/9, i = 0 \\ 1/9, i = 1-4 \\ 1/36, i = 5-7 \end{cases}, \quad \text{and} \quad \mathbf{e} = c\begin{bmatrix} 0 & 1 & 0 & -1 & 0 & 1 & -1 & -1 & 1 \\ 0 & 0 & 1 & 0 & -1 & 1 & 1 & -1 & -1 \end{bmatrix}.$$

For D3Q15 model, $\omega_i = \begin{cases} 2/9, i = 0 \\ 1/9, i = 1-6 \\ 1/72, i = 7-14 \end{cases}$, and

$$\mathbf{e} = c\begin{bmatrix} 0 & 1 & -1 & 0 & 0 & 0 & 0 & 1 & -1 & 1 & -1 & 1 & -1 & -1 & 1 \\ 0 & 0 & 0 & 1 & -1 & 0 & 0 & 1 & -1 & 1 & -1 & -1 & 1 & 1 & -1 \\ 0 & 0 & 0 & 0 & 0 & 1 & -1 & 1 & -1 & -1 & 1 & 1 & -1 & 1 & -1 \end{bmatrix}.$$

For concentration fields, the LBM has 5 directions for the 2D model and 7 directions for the 3D model, which is different from models with 9 directions and 15 directions but without any real loss of accuracy [271, 275].

On a macro-scale, the fluid density ρ, velocity $\mathbf{u}$, and concentration of σ-species c_σ are evaluated in terms of particle distribution functions, Eqs. (17)–(19):

$$\rho = \sum f_i(\mathbf{x}, t) \tag{17}$$

$$\rho\mathbf{u} = \sum \mathbf{e}_i f_i(\mathbf{x}, t) \tag{18}$$

$$c_\sigma = \sum g_{i,\sigma}(\mathbf{x}, t) \tag{19}$$
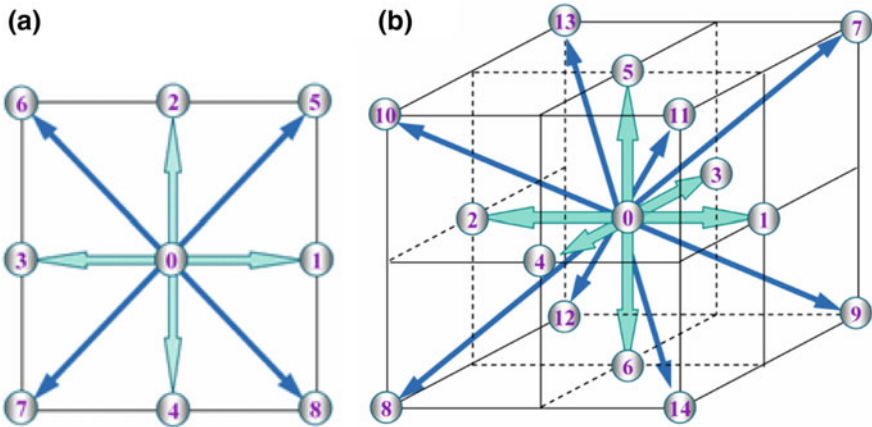
Fig. 19 Discretized velocity space of the **a** D2Q9 and **b** D3Q15 models (adapted from [276])

By performing the Chapman-Enskog expansion on Eqs. (13) and (14) in the incompressible limit $Ma = |\mathbf{u}|/c_s$, both the Navier-Stocks equation and mass transfer equation can be recovered as [277, 278]:

$$\begin{cases} \nabla \cdot \mathbf{u} = 0 \\ \partial_t \mathbf{u} + \nabla \mathbf{u}\mathbf{u} = -\nabla p + \nu\nabla^2\mathbf{u} \end{cases} \qquad (20)$$

$$\partial_t c_\sigma + \mathbf{u}\nabla c_\sigma - D_\sigma\nabla^2 c_\sigma = r_\sigma \qquad (21)$$

where, the pressure p satisfies the state equation $p = \rho c_s^2$, and the viscosity and diffusivity are represented as $\nu = \delta_t c_s^2(\tau - 1/2)$ [279] and $D_\sigma = \delta_t c^2 C_Q(1 - J_0)$ $(\tau_\sigma - 1/2)$[275].

8.2 Flow and Mass Transfer in Membrane Bioreactors

Recently, biofilms as an immobilization technique have been applied to photofermentation bioreactors to elevate the PNSB concentration [280, 281]. During operation, driven by Brownian movement and fluid motion, the bacteria first move towards the carriers and then attach on their surface. Finally, a layer of biofilm forms on the carrier's surface by bonding the bacteria with EPS. It should be noted that both bacterial attachment and biofilm formation are significantly influenced by the influent flow conditions and the mass transport of substrates and products in bioreactors. Therefore, flow and mass transfer combined with reactions in membrane photobioreactors have been investigated to improve hydrogen production with the help of LBM. Prior to simulations, the simplifying assumptions are set as follows:

(1) A steady-state uniform biofilm is formed on the surface of particles, and the biochemical reaction only occurs on the surface of the particles as the thickness of the biofilm (about 100 μm) is much less than the particles' diameter.
(2) The flow and reaction system are implemented under a steady state, and the biochemical reaction operates at the optimum temperature and pH.
(3) The released heat derived from the bioreaction is small enough and can be ignored.
(4) The hydrogen generated in the packed bed is assumed to completely dissolve in the solution, while the physical parameters of substrate and hydrogen are invariable.

The substrate consumption rate r_1 (glucose as the substrate) and hydrogen generation rate r_2 by PNSB (R. palustris CQK 01) in the biofilm are expressed by [282]:

$$r_1 = \frac{1}{Y_{x/s}} \frac{\mu_{\max} c_1 C_x}{k_s + c_1} + m C_x, r_2 = \alpha \frac{1}{Y_{x/s}} \frac{\mu_{\max} c_1 C_x}{k_s + c_1} + \beta C_x \qquad (22)$$

where, C_x is the initial cell density, $Y_{x/s}$ is the cell yield, k_s is the Monod constant, β is the reaction kinetic constant for hydrogen production, c_1 is the local substrate concentration, μ_{max} denotes the maximum specific growth rate (h^{-1}), m is the maintenance coefficient (h^{-1}), and α is the reaction kinetic constant for hydrogen production at a given reaction condition (h^{-1}).

The physical model is schematically illustrated in Fig. 20, where two typical accumulation modes, the face-centered and body-centered cubic structures, are adopted to pack the particles in the bioreactor. The organic wastewater stream with inlet velocity U_0 and inlet substrate concentration C_0 flows around the packed particles covered by a layer of PNSB biofilm on the surface. The boundary conditions are given by:

Inlet boundary conditions: $U = U_0$, $C = C_0$.
Around boundary conditions: $U = 0$, $\frac{\partial C}{\partial \mathbf{n}} = 0$.
Outlet boundary conditions: $\frac{\partial \mathbf{U}}{\partial X} = 0$, $\frac{\partial C}{\partial X} = 0$.

A 3D LBM as described in 7.6.1 is applied to simulate the biochemical reaction in the reactor. In the LBM simulation, a non-equilibrium extrapolation method [283] with second-order accuracy is employed to the curved boundary of the particle. For consistency, a non-equilibrium extrapolation method for straight boundary condition is used for inlet and wall boundaries. The hydrogen production

Fig. 20 Schema of the bioreactor filled with **a** face-centered and **b** body-centered cubic structure packed particles with surface bioreaction (adapted from [282], Copyright 2017, with permission from Elsevier)
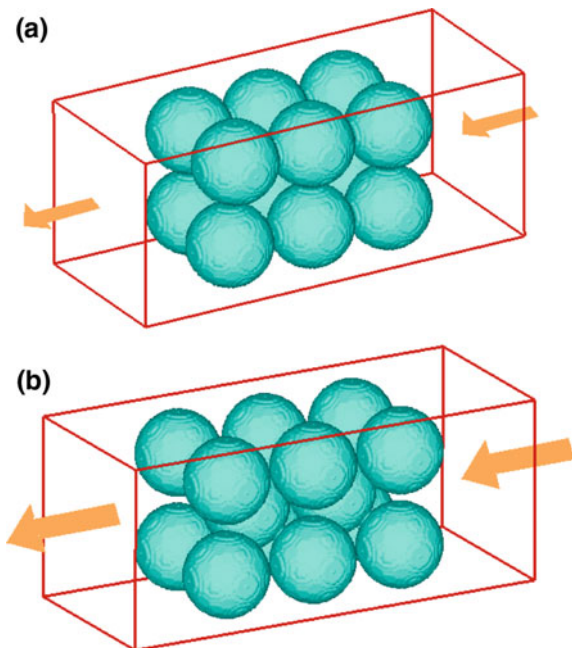
performance is assessed by hydrogen yield r (g/g) and the average substrate consumption efficiency $\bar{\eta}$, which are defined as shown in Eq. (23):

$$r = \frac{\left((CU)_{out} - (CU)_{in}\right)_{hydrogen}}{\left((CU)_{in} - (CU)_{out}\right)_{substrate}}, \bar{\eta} = \left(\frac{(CU)_{in} - (CU)_{out}}{(CU)_{in}} / n\right)\bigg|_{substrate} \times 100\% \quad (23)$$

where, n is the number of the particles.

The fluid flow characteristics are investigated for bioreactors with different particle accumulation modes. Figure 21 present the streamlines in the bioreactor filled with particles in face-centered and body-centered cubic structures at Re = 0.2. All of the streamlines go through the bioreactor smoothly without any vortices, indicating a stable laminar flow around the packed particles in the two accumulation modes. Comparing the two modes, one can notice that the fluid velocity is lower and more uniform in the body-centered cubic structure, which is due to the space between the particles being larger in the body-centered cubic structure, with the rear particles not completely in the wake flow region of the front particles, giving rise to lower velocity and less influence from each other. Additionally, the average drag coefficients on the particle surfaces under different conditions are evaluated in Table 12. An increase in Re number leads to a significant decrease in the average drag coefficient. Compared with face-centered cubic structures, the average drag coefficient is slightly reduced by approximately 0.4% for body-centered cubic structures due to the higher porosity and lower velocity.
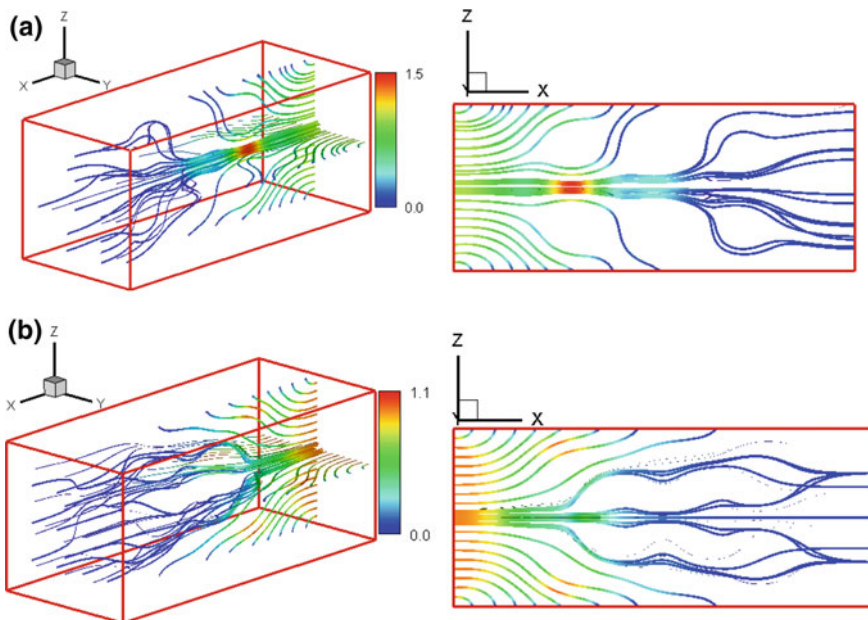
Fig. 21 Streamlines for flow around packed particles with **a** face-centered and **b** body-centered cubic structure at Re = 0.2 (adapted from [282], Copyright 2017, with permission from Elsevier)

Table 12 Effects of particle accumulation mode and Re number on the drag coefficient (adapted from [282], Copyright 2017, with permission from Elsevier)

Re	0.06	0.2	0.6
$\overline{C_D}$			
Face-centered cubic structure	876.17	263.24	88.11
Body-centered cubic structure	872.64	262.16	87.74

The fluid flow can affect the concentration field and the hydrogen performance. Figure 22 presents the concentration fields of the product in the bioreactor at various Re numbers. For both face-centered and body-centered cubic structures,
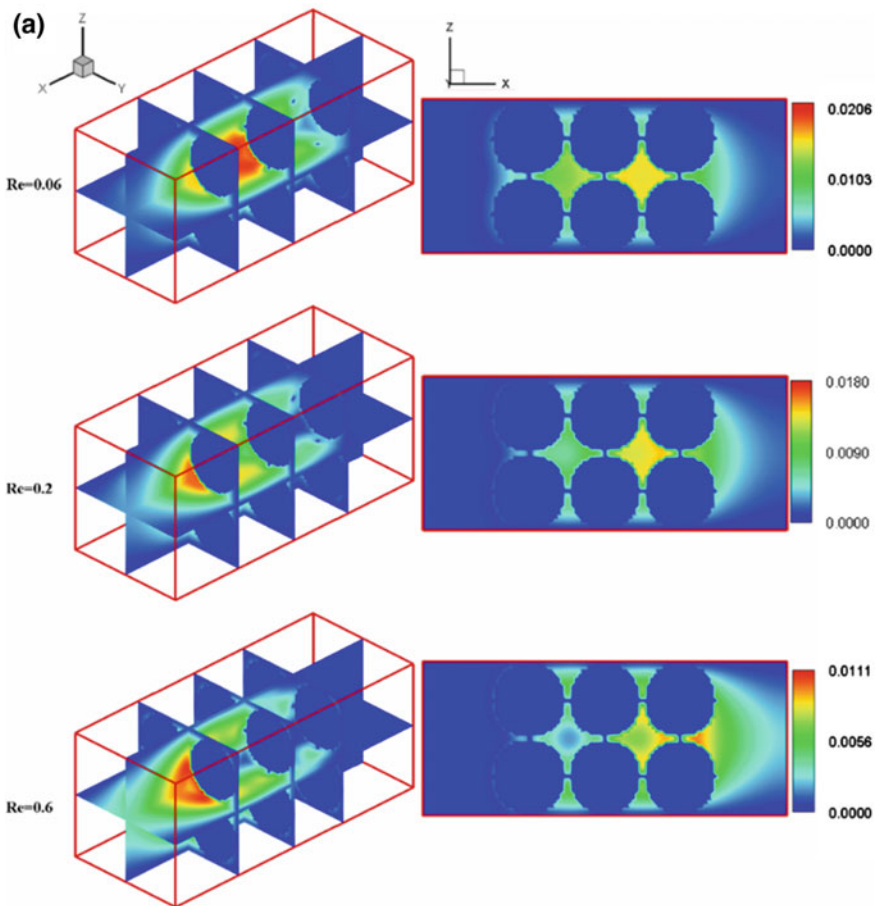
Fig. 22 Product concentration fields in bioreactors with **a** face-centered and **b** body-centered cubic structure at various Re numbers (adapted from [282], Copyright 2017, with permission from Elsevier)
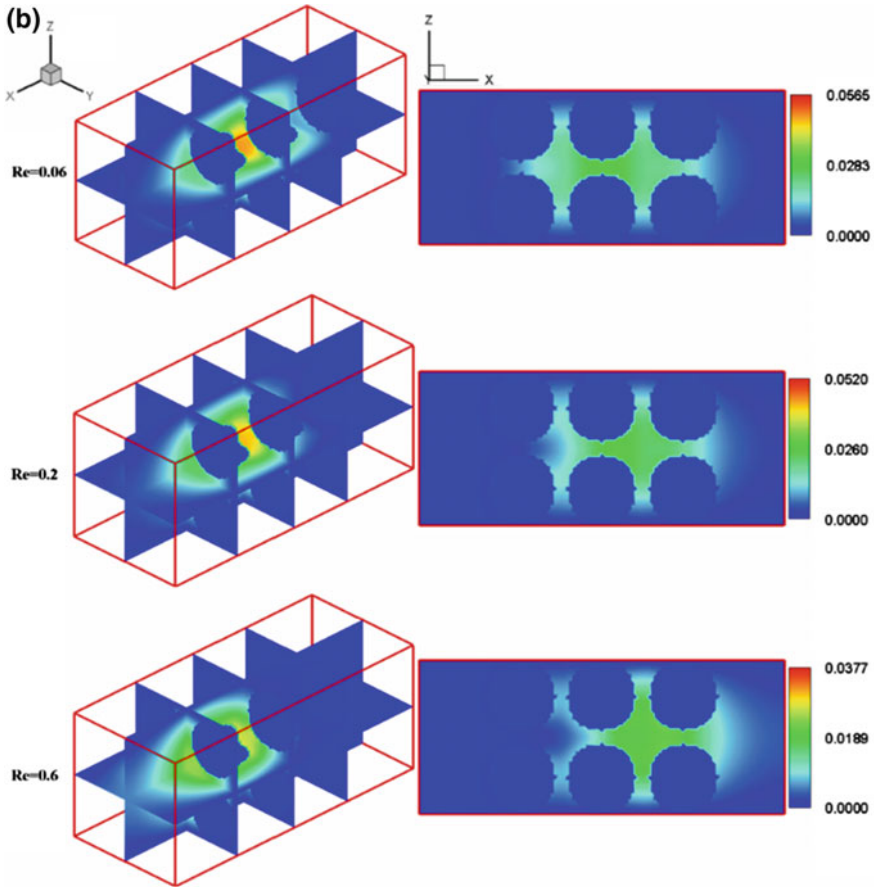
Fig. 22 (continued)

a higher Re number results in lower product concentration in the bioreactor. This implies that the faster product transfer and shorter HRT take over the improved substrate load at a higher Re number, leading to the lower product concentration in the bioreactor. However, the product concentration is evidently higher in body-centered cubic structures. This should be due to the weak influence from the wake flow of the front particles on the rear particles, and then fresh medium with high substrate concentration is delivered into the biofilm for degradation by PNSB. Meanwhile, more particles provide larger reaction surfaces. Therefore, more products can be generated, and the concentration becomes higher. The effects of influent solution velocity on performances of photobioreactors are presented in Fig. 23. The average substrate consumption efficiency and hydrogen yield in any case decrease with the increasing Re number. The average substrate consumption efficiency and hydrogen yield are higher for bioreactions in packed particles with

Fig. 23 Effect of Re number on **a** average substrate consumption efficiency and **b** hydrogen yield for solution around packed particles (adapted from [282], Copyright 2017, with permission from Elsevier)
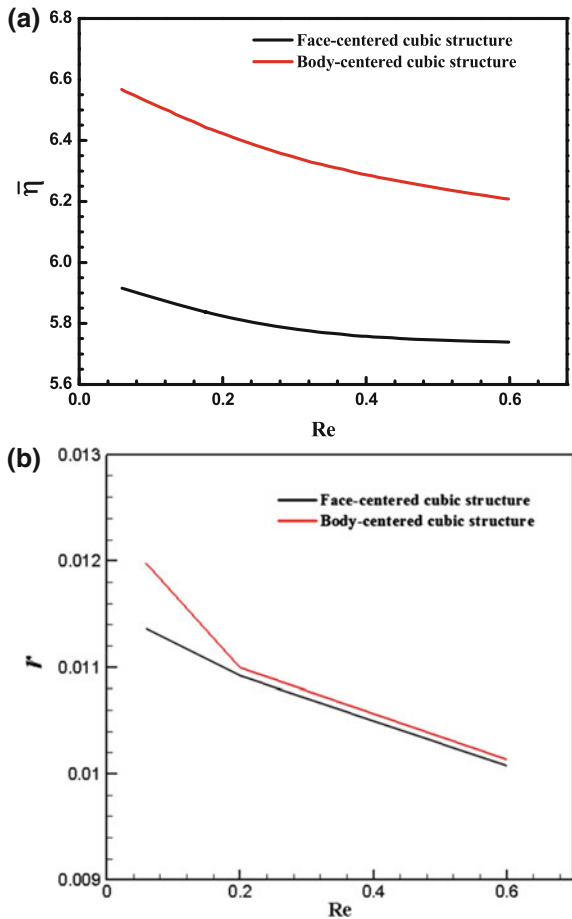
the body-centered cubic structures than for face-centered cubic structures. These results indicate that choosing the accumulation of body-centered cubic structures is beneficial for flow and mass transfer as well as bioreaction. The effect of illumination intensity on hydrogen performance has also been investigated and is shown in Fig. 24. As the illumination intensity increases to 6 klux, the microorganism metabolic activity and effective conversion of light energy are enhanced, and thus the product concentration and hydrogen production performance peak. However, with further increases in illumination intensity, photoinhibition leads to decreases of product concentration and hydrogen production. Furthermore, the accumulation of body-centered cubic structures exhibits a better hydrogen production performance as well as a lower average drag coefficient compared with the face-centered cubic structures. Accordingly, the simulation provides guidance to the design of photobioreactors for efficient hydrogen production.

Fig. 24 Effects of
illumination intensity on
a average substrate
consumption efficiency and
b hydrogen yield of
photobioreactors (adapted
from [282], Copyright 2017,
with permission from
Elsevier)
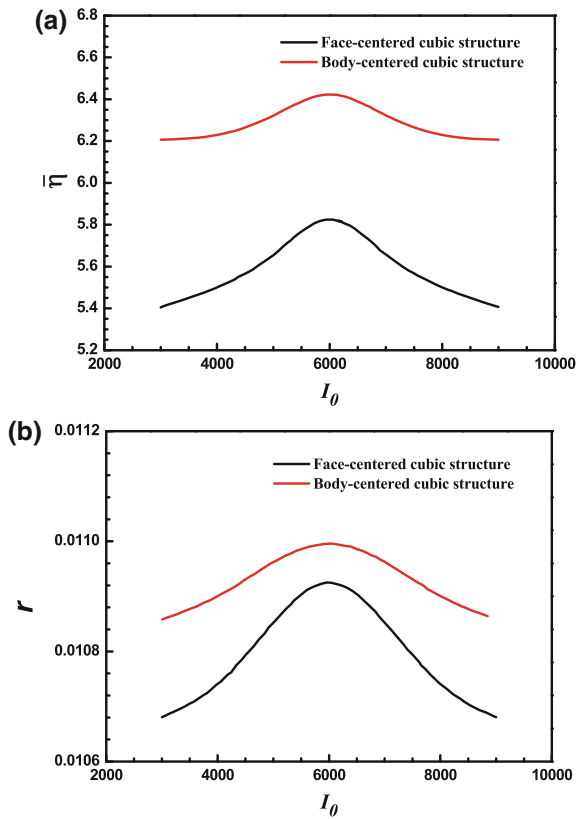
8.3 Flow and Mass Transfer in Bioreactors with Immobilized Granules

Gel granulation immobilization technology is also promising owing to its high biomass content, feasibility of high fluid velocity without suffering cell wash-out, and ease of operation [280]. To improve the hydrogen production performance of granule-packed photobioreactors, intensive investigations of mass and light transfer through the granules as well as the effect of granule structure are urgently needed. LB models for flow in porous media on the representative elementary volume (REV) scale and pore scale have been used to investigate the flow and mass transfer in bioreactors.

Simulation of Flow and Mass transfer in Bioreactors at REV-scale

A LBM model for porous media on the REV-scale by Guo [284] was used to simulate the substrate solution through porous granule-immobilized PNSB cells for biohydrogen production. The model can simulate the porous flow over a wide range

and treat as a variable porosity without invoking any additional boundary conditions. In this model, the force term F_i in Eq. (24) is given by [284]:

$$F_i = w_i \rho \left(1 - \frac{1}{2\tau_v}\right) \left[\frac{\mathbf{e}_i \cdot \mathbf{F}}{c_s^2} + \frac{\mathbf{uF} : \left(\mathbf{e}_i \mathbf{e}_i - c_s^2 \mathbf{I}\right)}{\varepsilon c_s^4}\right] \tag{24}$$

In place of Eq. (25), the equilibrium distribution function $f_i^{eq}(\mathbf{x}, t)$ is defined by:

$$f_i^{eq} = w_i \rho \left[1 + \frac{\mathbf{e}_i \cdot \mathbf{u}}{c_s^2} + \frac{\mathbf{uu} : \left(\mathbf{e}_i \mathbf{e}_i - c_s^2 \mathbf{I}\right)}{2\varepsilon c_s^4}\right] \tag{25}$$

where, ε is the porosity of the porous media, and $\mathbf{F}$ is the total body force.

Different from Eq. (18), the macroscopic velocity $\mathbf{u}$ is calculated by [284]:

$$\mathbf{u} = \frac{\mathbf{v}}{a_0 + \sqrt{a_0^2 + a_1 |\mathbf{v}|}} \tag{26}$$

where, $\mathbf{v}$, a_0, and a_1 are defined as in the previous study [284].

Figure 25 schematically illustrates a simulation in which substrate solution with velocity U_0 and concentration C_0 flows through a porous granule with diameter D and a specific porosity. The substrate is degraded, and simultaneously hydrogen is generated via biochemical reactions of PNSB cells immobilized in the porous granules.

In the simulation, a multi-block strategy for LBM [286] is implemented to improve the computational efficiency, dividing the computational domain into three parts as seen in Fig. 25. For the sake of accuracy, the fine grid and coarse meshes are set as $N_x \times N_y = 201 \times 41$ and $N_x \times N_y = 101 \times 15$, respectively. Both the top and bottom boundary conditions are set as $U = 1.0$, $C_1 = 1.0$, $C_2 = 0.0$, and the free outflow boundary condition is set at the outlet.
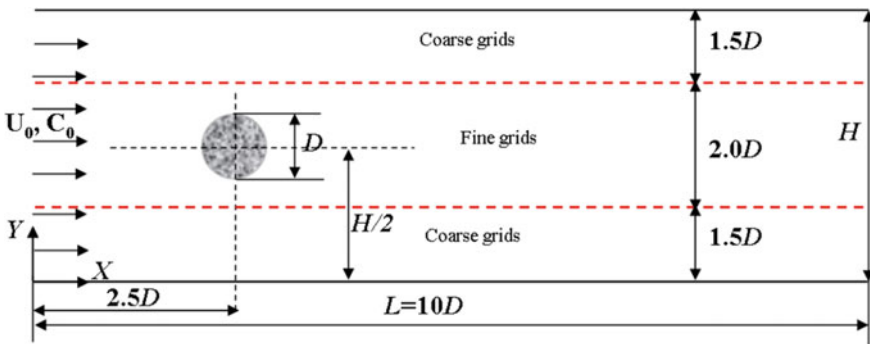
Fig. 25 The geometric configuration for substrate solution through a porous granule immobilized PSB-cell (adapted from [285], Copyright 2013, with permission from Elsevier)

The effects of operational conditions have been investigated. Figure 26 presents the streamlines and concentration fields of substrate and product for various Re numbers at $\varepsilon = 0.1$, $Da = 0.001$, and $I_0 = 6$ klux, as well as the hydrogen performance. As the Re number is very low (<1), the streamlines for various Re numbers are almost identical. However, the differences in concentration fields are evident in Fig. 26b. It is also notable that the substrate concentration is high, while the product concentration is low under a large Re number. This is because more substrate load is delivered into the granules when the fluid penetrates with a high
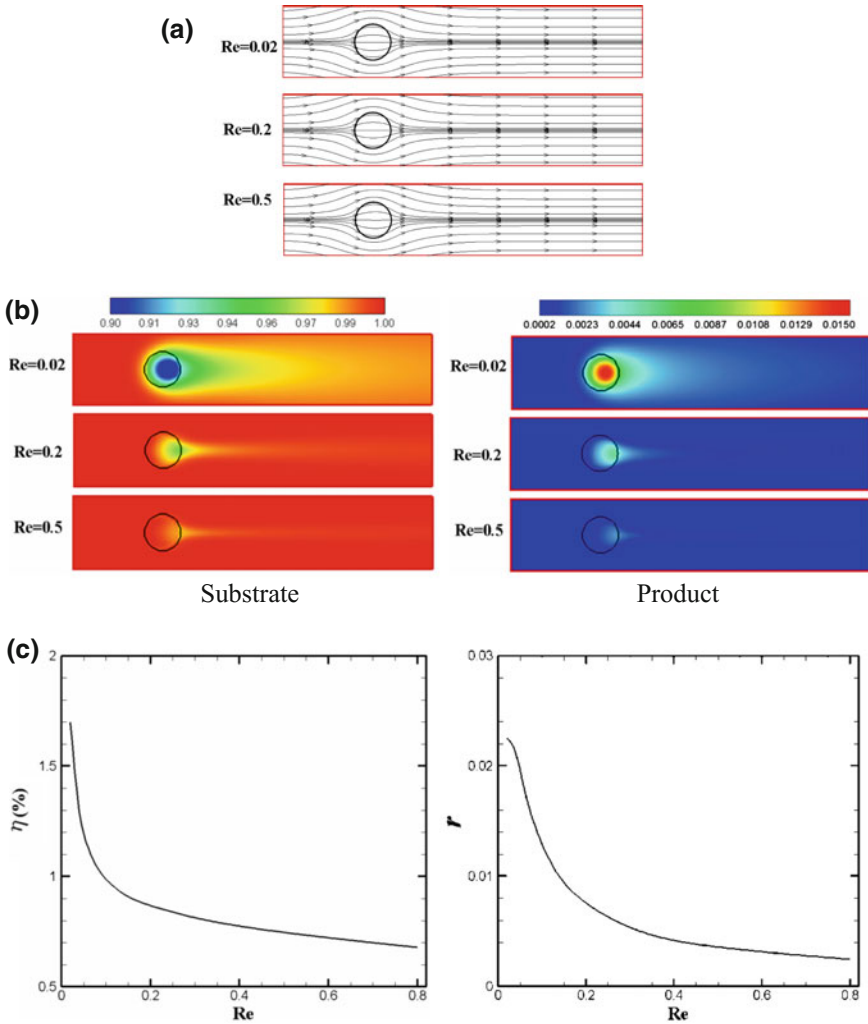
Fig. 26 The effects of Re number on **a** streamlines, **b** concentration fields of substrate and product, and **c** hydrogen production performance (adapted from [285], Copyright 2013, with permission from Elsevier)

velocity. However, the high velocity significantly shortens HRT even though mass transport is improved. This leads to insufficient bioreaction, hence the reduced substrate consumption capacity. It can be seen in Fig. 26c that hydrogen yield r and consumption efficiency η both decrease with the increasing Re number. The effect of illumination intensity is also presented in Fig. 27. It shows that both the hydrogen yield and consumption efficiency achieve the highest values under an illumination intensity of 6 klux. Below the threshold (6 klux), the increase in I_0 leads to the enhancement of microorganism metabolic activity and effective conversion of light energy. However, once I_0 increases over the threshold, the appearance of photoinhibition limits the enzyme activity and the conversion of light energy subsides.

Fig. 27 The effects of illumination intensity on hydrogen production performance (adapted from [285], Copyright 2013, with permission from Elsevier)
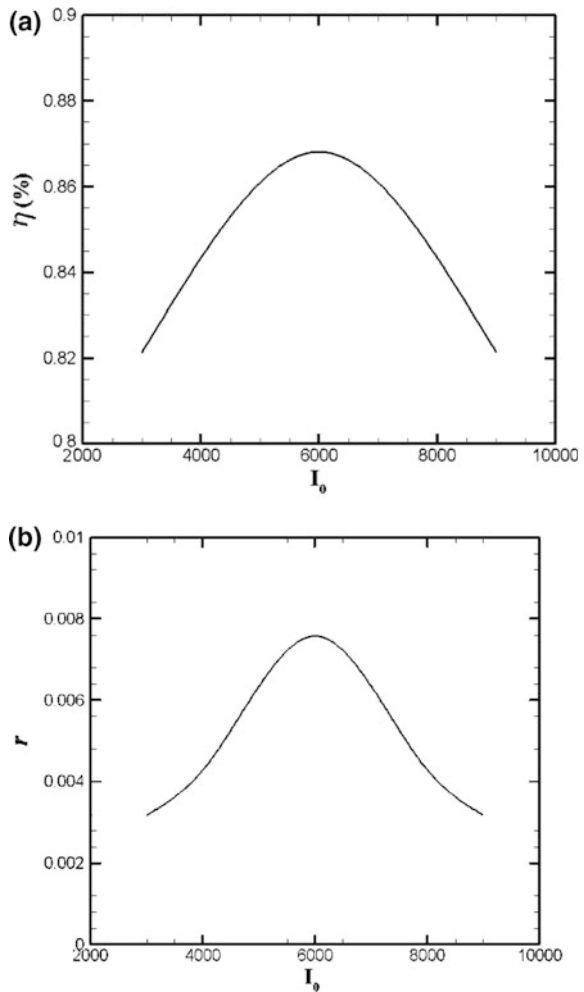
Besides the operational conditions, the characteristics of porous granules will affect flow and mass transfer in the granules, as well as the biohydrogen production performance. Hence, the physical parameters of porous granules have been investigated. The permeability, represented by the *Darcy* (*Da*) number, is an important parameter to assess the ability of porous granules to transmit fluid. Figure 28 describes the velocity and concentration fields, as well as hydrogen production performance for various *Da* numbers at $\varepsilon = 0.1$, Re = 0.2, and $I_0 = 6$ klux. It is noted from Fig. 28a that the curvature of the streamlines sharply shrinks with the increasing *Da* number owing to increasing penetrability. It can also be seen in Fig. 28b that a larger *Da* number leads to higher substrate concentration and
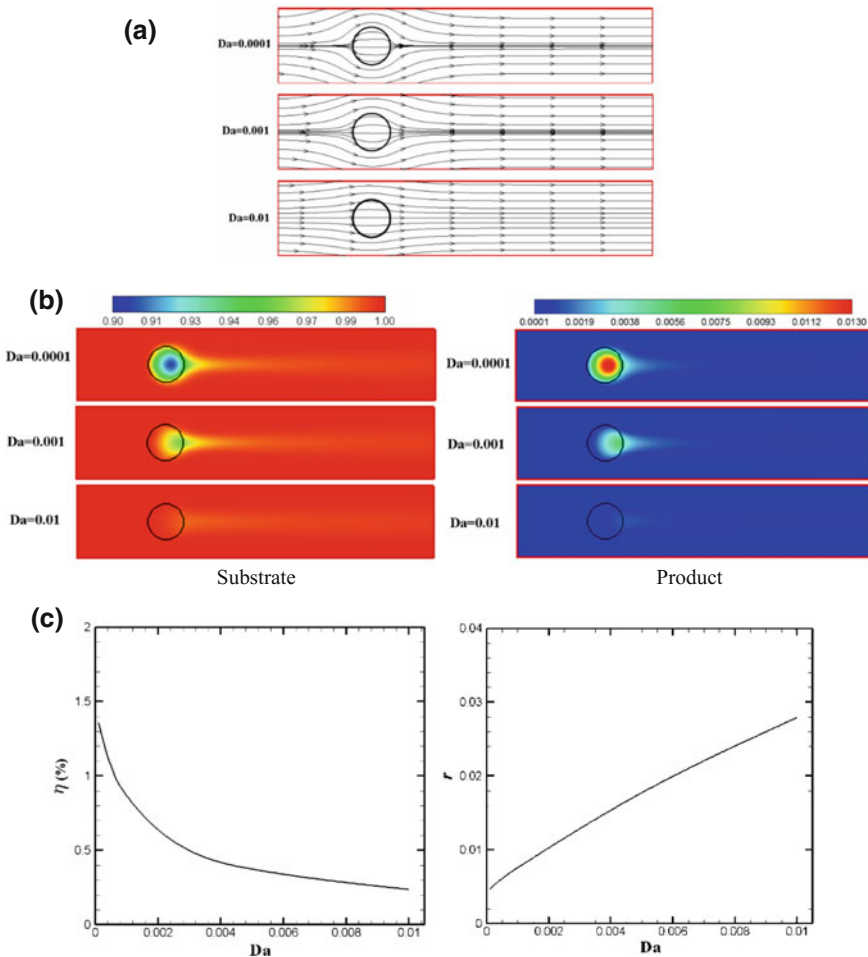
Fig. 28 The effects of *Da* number on **a** streamlines, **b** concentration fields of substrate and product, and **c** hydrogen production performance (adapted from [285], Copyright 2013, with permission from Elsevier)

lower hydrogen concentration. This is because the high velocity inside the granule under the large Da accelerates the mass transport between the bulk flow and porous granule, and simultaneously shortens the HRT for the bioreaction of PNSB. Figure 28c shows that hydrogen yield increases while consumption efficiency decreases with the increasing Da. This can be understood by the mass transfer being enhanced by the increasing Da, which supplies sufficient substrate for degradation by PNSB cells, and thus hydrogen yield increases. However, the short HRT for large Da decreases the substrate degradation, hence leading to a decrease in consumption efficiency. In addition, the porosity of granules is another important parameter that affects hydrogen production performance. Figure 29 presents the hydrogen production performance for various porosities at Re = 0.2, Da = 0.001,

Fig. 29 The effect of porosity on **a** substrate consumption efficiency and **b** hydrogen yield (adapted from [285], Copyright 2013, with permission from Elsevier)
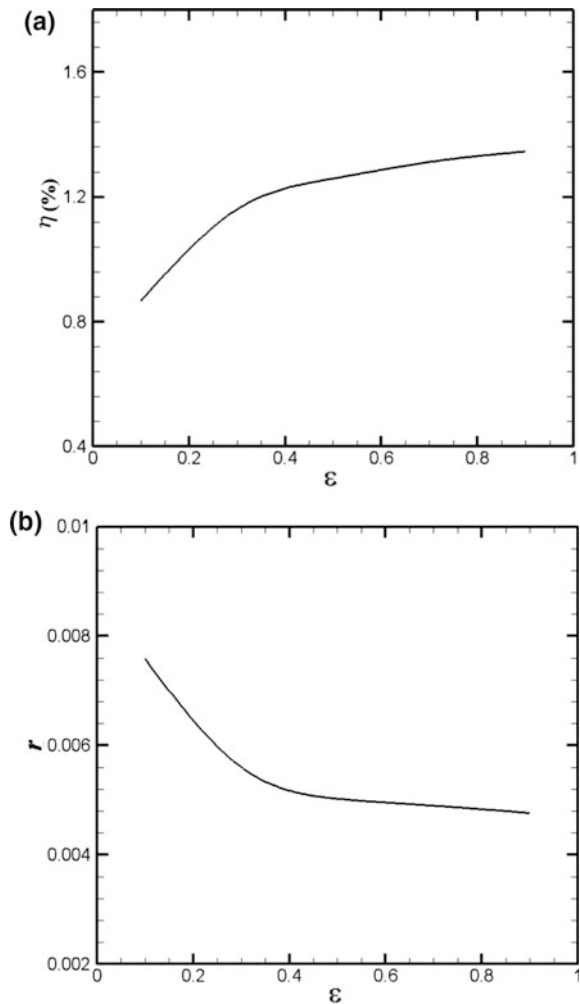
and $I_0 = 6$ klux, showing that the consumption efficiency increases while hydrogen yield decreases with the increasing ε, but the increment in consumption efficiency and decrement in hydrogen yield become smaller, and they tend to stabilize when the porosity is over 0.5. These simulation results provide a theoretical basis for experimental studies.

Simulation of Flow and Mass Transfer in Bioreactors at Pore-scale

Immobilized granules can be considered as porous media with immobilized PNSB cells, and hence the detailed pore structure has a great effect on the flow and mass transfer in a bioreactor as well as hydrogen production. Therefore, a 3D LBM is used to study porous media on the pore-scale. The porous structure of immobilized granules is generated by a quartet structure generation set (QSGS) method [287], which is closely associated with LBM and can generate porous media with different properties. It is worth mentioning, in contrast to traditional models for porous media, the flow and mass transfer can be simulated accurately in every pore using the QSGS method coupled with the LBM.

Figure 30 presents a schematic of a bioreactor with porous granule-immobilized PNSB cells, which is the same scenario of the photobioreactor in the previous study
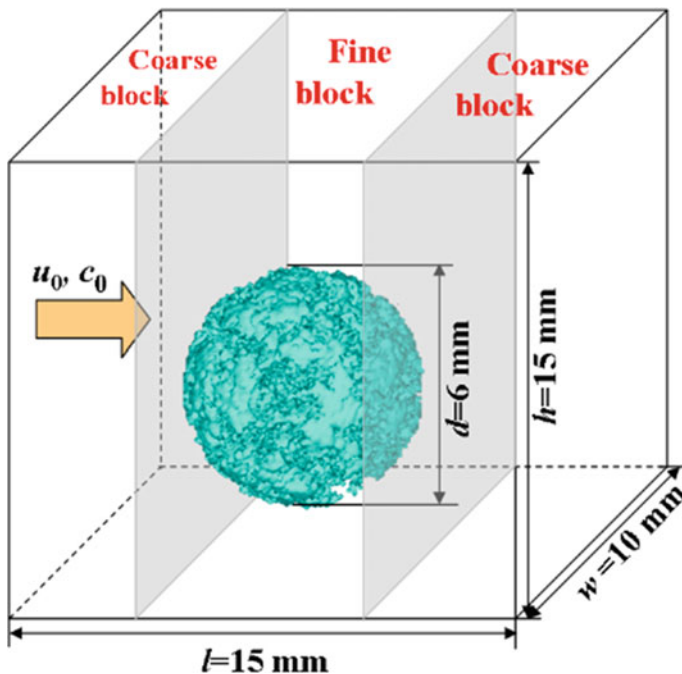
Fig. 30 Schematic of bioreactor with a porous granule immobilized PSB-cell (adapted from [288], Copyright 2017, with permission from Elsevier)

[280]. The substrate solution flows through the porous granule-immobilized PNSB cells for photobiohydrogen production.

To improve the computational efficiency, LBM is coupled with a multi-block model [289], and the computational domain is divided into three parts as seen in
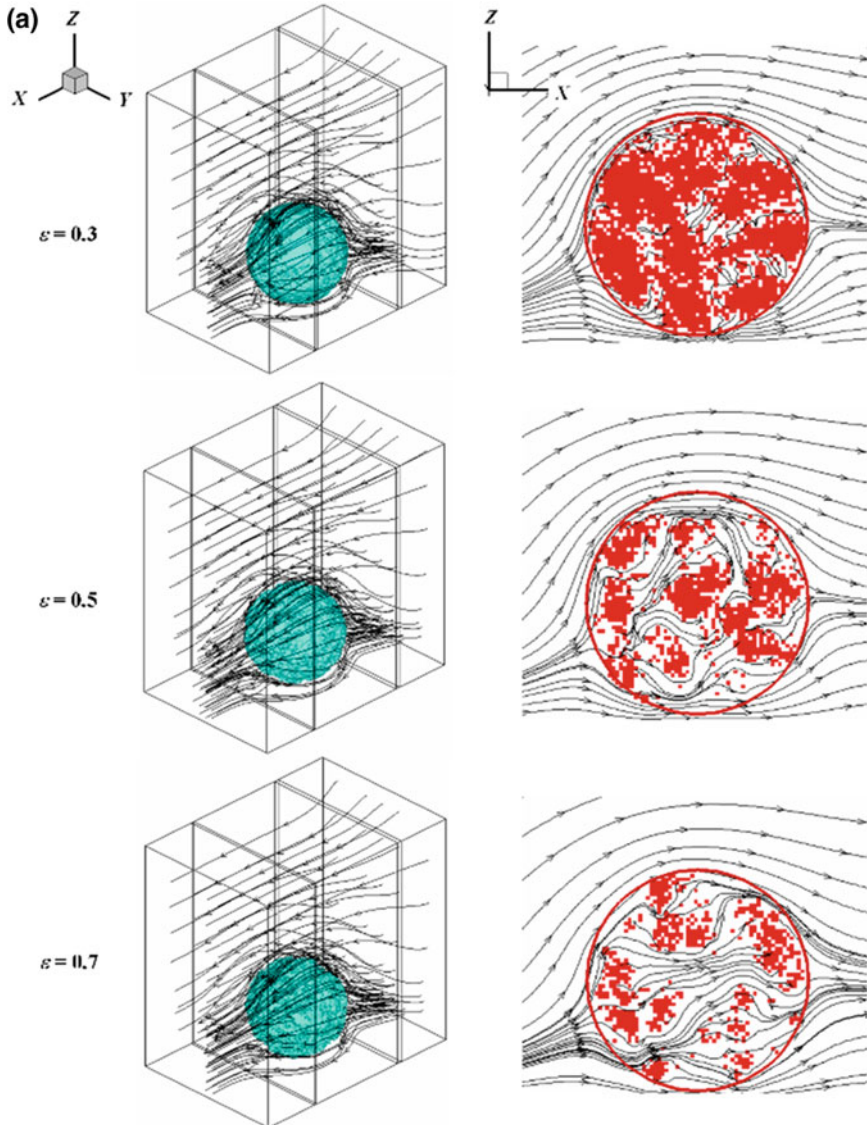
Fig. 31 Streamlines and concentration fields of product around the porous granule immobilized PSB-cell with various porosities (adapted from [288], Copyright 2017, with permission from Elsevier)
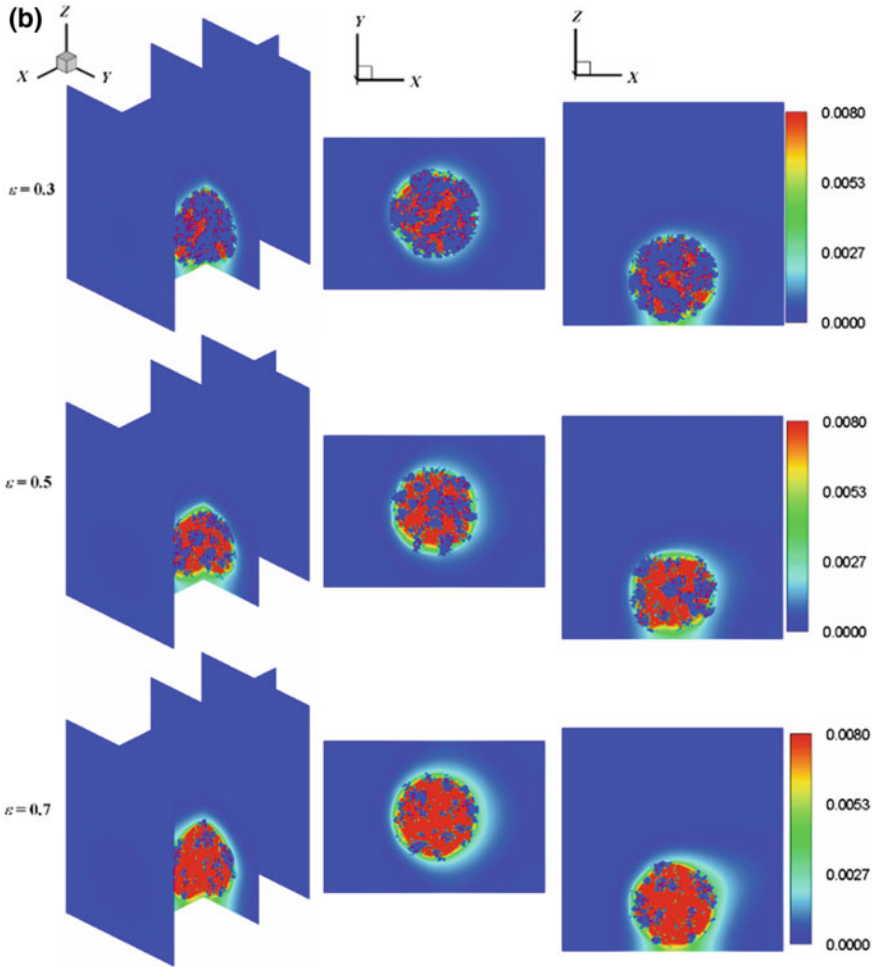
Fig. 31 (continued)

Fig. 30. The grid density of the fine block is set as $D/\delta_{x,f} = 60$, and the grid density of the coarse block is set as $D/\delta_{x,c} = 30$, where $\delta_{x,f}$ and $\delta_{x,c}$ are the lattice space of the fine and coarse blocks. The inlet boundary conditions are set as $U = U_0$, $C = C_0$. The around wall boundary conditions are all set as $U = U_0$, $\frac{\partial C}{\partial n} = 0$. The free outflow boundary condition is set at the outlet.

Figure 31 presents streamlines and concentration fields of products in bioreactors filled with granules with various porosities at Re = 0.05. With increasing porosity of the immobilized granules, the curvature of streamlines flowing into the granules decreases and the streamlines inside the granules are smoothed as seen in Fig. 31a. This can be understood by the resistance between the main flow and the porous granules decreasing with the increasing porosity, and hence, facilitating

fluid flow into the granules and decreasing the streamline curvature. Meanwhile, the fluid suffers fewer constraints from the porous structure with larger porosity and holds a larger flow area, giving rise to smooth fluid flow through the porous granules. It can be seen in Fig. 31b that the product concentration obviously increases both inside the granules and in the bulk flow with increasing granule porosity. The easy delivery of the substrate into immobilized granules with high porosity is beneficial. Meanwhile, increases in the bioreaction surface and light transmissivity of granules with high porosity are also helpful for hydrogen production.

The hydrogen production performance of the bioreactor has been assessed for various immobilized granules as seen in Fig. 32. With increasing porosity, the substrate consumption efficiency increases, while the hydrogen yield slightly

Fig. 32 Effect of porosity on the hydrogen product performance in the bioreactor with a porous granule immobilized PSB-cell (adapted from [288], Copyright 2017, with permission from Elsevier)
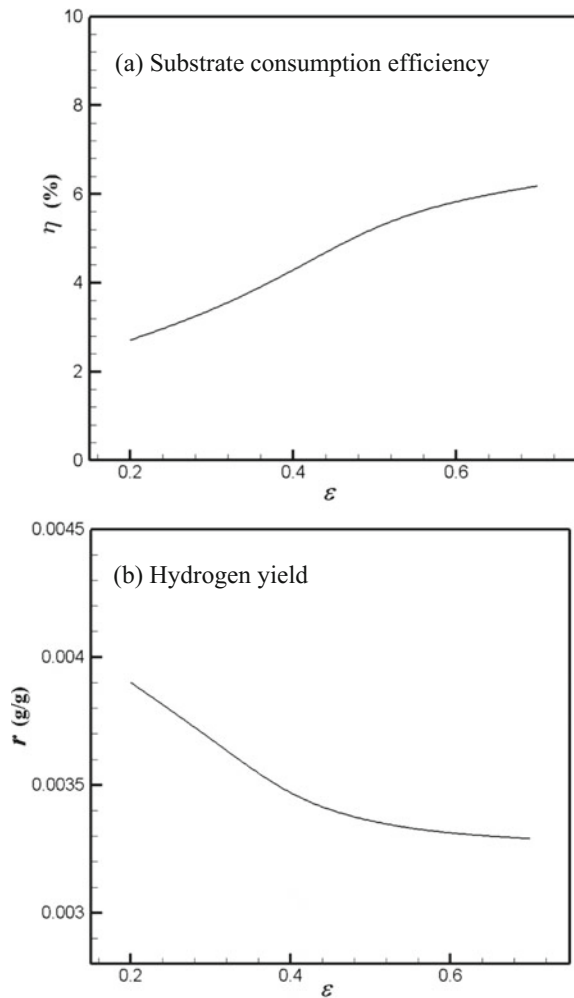
Table 13 Comparison of the hydrogen production performance in a bioreactor between LB numerical results and experimental results at $\varepsilon = 0.3$ (adapted from [288], Copyright 2017, with permission from Elsevier)

	LB numerical results	Experimental results	Error (%)
η (%)	3.40	3.21	5.9
r (g/g)	0.00368	0.00389	5.4

decreases, and they tend to be stable when $\varepsilon > 0.5$. Moreover, the hydrogen production performance obtained by LB numerical simulations for immobilized granules with a porosity of 0.3 is compared with experimental results [149] as shown in Table 13. It shows that the relative error of substrate consumption efficiency between LB results and experimental results is about 5.9%, and that of hydrogen yield is about 5.4%, implying good agreement. This demonstrates that pore-scale LBM simulations coupled with QSGS can simulate photohydrogen production in bioreactors with porous immobilized granules.

9　Conclusion

Photofermentation by PNSB can effectively degrade organic components of waste streams, such as industrial wastes, agricultural wastes, and wastewaters, while producing hydrogen. This process effects a high substrate utilization efficiency with a high hydrogen yield when simple substrates, such as sugars and VFAs, are employed. For high molecular weight biomasses, such as lignocelluloses, an extra pre-treatment step is necessary to produce low molecular weight organic molecules and to improve hydrogen performance. The key enzymes responsible for hydrogen production in PNSB, namely nitrogenase and hydrogenase, are very sensitive to gaseous environments as well as ammonium. This requires a well-controlled environment for photofermentation. To achieve high-performance hydrogen production, various photobioreactors B have been developed. Suspension cultures are advantageous for the mass transfer of substrates and metabolic products, while they suffer from poor light transmission and PNSB retention. Alternatively, immobilized cultures, such as biofilm-type reactors, may offer a cost-effective solution. Nevertheless, many thermodynamic challenges, including fluid flow, heat and mass transfer, as well as light transfer in the growth and metabolism of microbes, significantly limit PBR performance. LBM simulations can provide a comprehensive view of fluid flow and mass transfer coupled with biochemical reactions in PBRs. More work should be devoted to developing high-performance PBRs and optimizing their operational parameters to achieve a high hydrogen production performance, and to realize continuous large-scale photofermentative hydrogen production using natural illumination.

References

1. Baêta BE, Lima DR, Filho JG, Adarme OF, Gurgel LV, Aquino SF (2016) Evaluation of hydrogen and methane production from sugarcane bagasse hemicellulose hydrolysates by two-stage anaerobic digestion process. Bioresource Technol 218:436–446
2. Nath K, Das D (2004) Improvement of fermentative hydrogen production: various approaches. Appl Microbiol Biotechnol 65(5):520–529
3. Sittijunda S, Reungsang A (2017) Fermentation of hydrogen, 1,3-propanediol and ethanol from glycerol as affected by organic loading rate using up-flow anaerobic sludge blanket (UASB) reactor. Int J Hydrogen Energ 42(45):27558–27569
4. Hallenbeck PC (2013) Photofermentative biohydrogen production
5. Hallenbeck PC (2009) D. G. Advances in fermentative biohydrogen production: the way forward. Trends Biotechnol 27:287–297
6. Liu Y, Hallenbeck PC (2016) A kinetic study of hydrogen production by a Calvin-Benson-Bassham cycle mutant, PRK (phosphoribulose kinase), of the photosynthetic bacterium *Rhodobacter capsulatus*. Int J Hydrogen Energ 41(26):11081–11089
7. Zhang Q, Wang Y, Zhang Z, Lee DJ, Zhou X, Jing Y et al (2017) Photo-fermentative hydrogen production from crop residue: A mini review. Bioresource Technol 229:222–230
8. Zhang Z, Zhou X, Hu J, Zhang T, Zhu S, Zhang Q (2017) Photo-bioreactor structure and light-heat-mass transfer properties in photo-fermentative bio-hydrogen production system: A mini review. Int J Hydrogen Energ 42(17):12143–12152
9. Shahzad MS, Iqbal QJ, Zhao Q, Chen S (2013) Photo-biohydrogen production potential of *Rhodobacter capsulatus*-PK from wheat straw. Biotechnol Biofuels 6(1):144–156
10. Pott RWM, Howe CJ, Dennis JS (2013) Photofermentation of crude glycerol from biodiesel using *Rhodopseudomonas palustris*: Comparison with organic acids and the identification of inhibitory compounds. Bioresource Technol 130(1):725–730
11. Pott RW, Howe CJ, Dennis JS (2014) The purification of crude glycerol derived from biodiesel manufacture and its use as a substrate by *Rhodopseudomonas palustris* to produce hydrogen. Bioresource Technol 152(1):464–470
12. Seifert K, Waligorska M, Laniecki M (2010) Brewery wastewaters in photobiological hydrogen generation in presence of *Rhodobacter sphaeroides* O.U. 001. Int J Hydrogen. Energ 35(9):4085–4091
13. Seifert K, Waligorska M, Laniecki M (2010) Hydrogen generation in photobiological process from dairy wastewater. Int J Hydrogen Energ 35(18):9624–9629
14. Niel CBV (1944) The culture, general physiology, morphology, and classification of the non-fulfur purple and brown bacteria. Bacteriol Rev 8(1):1–118
15. JF. I. Anoxygenic photosynthetic bacteria. In: Blankenship RE, Madigan MT, Bauer CE, editors. Taxonomy and physiology of purple bacteria and green sulfur bacteria, USA: Kluwer Academic Publishers. 1995
16. Tao Y, He Y, Wu Y, Liu F, Li X, Zong W et al (2008) Characteristics of a new photosynthetic bacterial strain for hydrogen production and its application in wastewater treatment. Int J Hydrogen Energ 33(3):963–973
17. Assawamongkholsiri T, Reungsang A (2015) Photo-fermentational hydrogen production of *Rhodobacter* sp. KKU-PS1 isolated from an UASB reactor. Electron. J Biotechnol 18(3):221–230

18. Laocharoen S, Reungsang A (2014) Isolation, characterization and optimization of photo-hydrogen production conditions by newly isolated *Rhodobacter sphaeroides* KKU-PS5. Int J Hydrogen Energ 39(21):10870–10882

19. Larimer FW, Chain P, Hauser L, Lamerdin J, Malfatti S, Long D et al (2004) Complete genome sequence of the metabolically versatile photosynthetic bacterium *Rhodopseudomonas palustris*. Nat Biotechnol 22(1):55–61

20. Harwood CS (2009) Degradation of aromatic compounds by purple nonsulfur bacteria. Springer, Netherlands

21. Luongo V, Ghimire A, Frunzo L, Fabbricino M, D'Antonio G, Pirozzi F et al (2016) Photofermentative production of hydrogen and poly-β-hydroxybutyrate from dark fermentation products. Bioresource Technol 228:171–175

22. Ghimire A, Valentino S, Frunzo L, Trably E, Escudié R, Pirozzi F et al (2015) Biohydrogen production from food waste by coupling semi-continuous dark-photofermentation and residue post-treatment to anaerobic digestion: A synergy for energy recovery. Int J Hydrogen Energ 40(46):16045–16055

23. Hay JX, Wu TY, Juan JC, Md JJ (2017) Effect of adding brewery wastewater to pulp and paper mill effluent to enhance the photofermentation process: wastewater characteristics, biohydrogen production, overall performance, and kinetic modeling. Environ Sci Pollut Res Int 24(11):1–10

24. Kim DH, Son H, Kim MS (2012) Effect of substrate concentration on continuous photo-fermentative hydrogen production from lactate using *Rhodobacter sphaeroides*. Int J Hydrogen Energ 37(20):15483–15488

25. Kim MS, Kim DH, Cha J (2012) JK. L. Effect of carbon and nitrogen sources on photo-fermentative H_2 production associated with nitrogenase, uptake hydrogenase activity, and PHB accumulation in *Rhodobacter sphaeroides* KD131. Bioresource Technol 116(4): 176–183

26. Basak N, Das D (2007) The prospect of purple non-sulfur (PNS) photosynthetic bacteria for hydrogen production: the present state of the art. World J Microb Biot 23(1):31–42

27. Obeid J, Flaus JM, Adrot O, Magnin JP, Willison JC (2010) State estimation of a batch hydrogen production process using the photosynthetic bacteria *Rhodobacter capsulatus*. Int J Hydrog Energy 35(19):10719–10724

28. Keskin T, Hallenbeck PC (2012) Hydrogen production from sugar industry wastes using single-stage photofermentation. Bioresour Technol 112(4):131–136

29. Androga DD, Sevinç P, Koku H, Yücel M, Gündüz U, Eroglu I (2014) Optimization of temperature and light intensity for improved photofermentative hydrogen production using *Rhodobacter capsulatus* DSM 1710. Int J Hydrog Energy 39(6):2472–2480

30. Liu BF, Jin YR, Cui QF, Xie GJ, Wu YN, Ren NQ (2015) Photo-fermentation hydrogen production by *Rhodopseudomonas* sp. nov. strain A7 isolated fromthe sludge in a bioreactor. Int J Hydrog Energy 40(28):8661–8668

31. Bianchi L, Mannelli F, Viti C, Adessi A, Philippis RD (2010) Hydrogen-producing purple non-sulfur bacteria isolated from the trophic lake Averno (Naples, Italy). Int J Hydrog Energy 35(22):12216–12223

32. Carlozzi P, Buccioni A, Minieri S, Pushparaj B, Piccardi R, Ena A et al (2010) Production of bio-fuels (hydrogen and lipids) through a photofermentation process. Bioresour Technol 101 (9):3115–3120

33. Cheng J, Su H, Zhou J, Song W, Cen K (2011) Hydrogen production by mixed bacteria through dark and photo fermentation. Int J Hydrog Energy 36(1):450–457

34. Shi XY, Yu HQ (2006) Continuous production of hydrogen from mixed volatile fatty acids with *Rhodopseudomonas capsulata*. Int J Hydrog Energy 31(12):1641–1647

35. Hosseini SS, Aghbashlo M, Tabatabaei M, Younesi H, Najafpour G (2015) Exergy analysis of biohydrogen production from various carbon sources via anaerobic photosynthetic bacteria (*Rhodospirillum rubrum*). Energy 93:730–739

36. Cai J, Wang G (2012) Hydrogen production by a marine photosynthetic bacterium, *Rhodovulum sulfidophilum* P5, isolated from a shrimp pond. Int J Hydrog Energy 37(20): 15070–15080

37. Sasikala K, Ramana CV, Rao PR (1991) Environmental regulation for optimal biomass yield and photoproduction of hydrogen by *Rhodobacter sphaeroides* O.U. 001. Int J Hydrog Energy 16(9):597–601

38. Miyake J, Wakayama T, Schnackenberg J, Arai T, Asada Y (1999) Simulation of the daily sunlight illumination pattern for bacterial photo-hydrogen production. J Biosci Bioeng 88(6):659–663

39. Adessi A, Torzillo G, Baccetti E, Philippis RD (2012) Sustained outdoor H_2 production with *Rhodopseudomonas palustris* cultures in a 50-L tubular photobioreactor. Int J Hydrog Energy 37(10):8840–8849

40. Imhoff JF, Hiraishi A, Süling J (2005) Anoxygenic phototrophic purple bacteria. In: Brenner DJ, Krieg NR, Staley JT, Garrity GM (eds) Bergey's manual of systematic bacteriology. Springer, New York

41. Muzziotti D, Adessi A, Faraloni C, Torzillo G, De PR (2016) H_2 production in *Rhodopseudomonas palustris* as a way to cope with high light intensities. Res Microbiol 167(5):350–356

42. Yang H, Jing Z, Wang X, Feng J, Wei Y, Guo L (2014) A newly isolated *Rhodobacter sphaeroides* HY01 with high hydrogen production performance. Int J Hydrog Energy 39(19):10051–10060

43. Budiman PM, Wu TY, Ramanan RN, Jahim JM (2015) Improvement of biohydrogen production through combined reuses of palm oil mill effluent together with pulp and paper mill effluent in photofermentation. Energy Fuel 29(9):5816–5824

44. Hay JXW, Wu TY, Ng BJ, Juan JC, Jahim JM (2016) Reusing pulp and paper mill effluent as a bioresource to produce biohydrogen through ultrasonicated *Rhodobacter sphaeroides*. Energy Convers Manage 113:273–280

45. Budiman PM, Wu TY, Ramanan RN, Jahim JM (2017) Improving photofermentative biohydrogen production by using intermittent ultrasonication and combined industrial effluents from palm oil, pulp and paper mills. Energy Convers Manage 132:110–118

46. Budiman PM, Wu TY, Ramanan RN, Md JJ (2017) Reusing colored industrial wastewaters in a photofermentation for enhancing biohydrogen production by using ultrasound stimulated *Rhodobacter sphaeroides*. Environ Sci Pollut Res Int 24(19):15870–15881

47. Montiel CV, Le BS, Revah S, Morales M (2017) Effect of light-dark cycles on hydrogen and poly-β-hydroxybutyrate production by a photoheterotrophic culture and *Rhodobacter capsulatus* using a dark fermentation effluent as substrate. Bioresour Technol 226:238–246

48. Chen X, Lv Y, Liu Y, Ren R, Zhao J (2017) The hydrogen production characteristics of mixed photoheterotrophic culture. Int J Hydrog Energy 42(8):4840–4847

49. Sun MLY, Liu Y (2015) A new hydrogen-producing strain and its characterization of hydrogen production. Appl Biochem Biotechnol 177:1676–1689

50. Phankhamla P, Sawaengkaew J, Buasri P, Mahakhan P (2014) Biohydrogen production by a novel thermotolerant photosynthetic bacterium *Rhodopseudomonas pentothenatexigens* strain KKU-SN1/1. Int J Hydrog Energy 39(28):15424–15432

51. Chen CY, Liu CH, Lo YC, Chang JS (2011) Perspectives on cultivation strategies and photobioreactor designs for photo-fermentative hydrogen production. Bioresource Technol 102(18):8484–8492

52. Gest H, Kamen MD (1982) Photoproduction of molecular hydrogen by *Rhodospirillum rubrum*. Science 109:558–559

53. Miyake J, Tomizuka N, Kamibayashi A (1982) Prolonged photo-hydrogen production by *Rhodospirillum rubrum*. J Ferment Technol 60:199–203

54. Barbosa MJ, Rocha JM, Tramper J, Wijffels RH (2001) Acetate as a carbon source for hydrogen production by photosynthetic bacteria. J Biotechnol 85(1):25–33

55. Han H, Liu B, Yang H, Shen J (2012) Effect of carbon sources on the photobiological production of hydrogen using *Rhodobacter sphaeroides* RV. Int J Hydrogen Energ 37(17): 12167–12174

56. Mohan SV, Mohanakrishna GSS (2011) Biohydrogen production from industrial effluents. In: Pandey A, Larroche C, Ricke SC, Dussap CG, Gnansounou E (eds) Biofuels: alternative feedstocks and conversion processes. Elsevier, USA

57. Ghosh D, Tourigny A, Hallenbeck PC (2012) Near stoichiometric reforming of biodiesel derived crude glycerol to hydrogen by photofermentation. Int J Hydrog Energy 37(3):2273–2277

58. Chen CY, Yeh KL, Lo YC, Wang HM, Chang JS (2010) Engineering strategies for the enhanced photo-H_2 production using effluents of dark fermentation processes as substrate. Int J Hydrog Energy 35(24):13356–13364

59. Su H, Cheng J, Zhou J, Song W, Cen K (2010) Hydrogen production from water hyacinth through dark- and photo- fermentation. Int J Hydrog Energy 35(17):8929–8937

60. Özgür E, Uyar B, Öztürk Y, Yücel M, Gündüz U, Eroğlu I (2010) Biohydrogen production by *Rhodobacter capsulatus* on acetate at fluctuating temperatures. Resour Conserv Recycl 54(5):310–314

61. Mishra P, Thakur S, Singh L, Wahid ZA, Sakinah M (2016) Enhanced hydrogen production from palm oil mill effluent using two stage sequential dark and photo fermentation. Int J Hydrog Energy 41(41):18431–18440

62. Nasr M, Tawfik A, Ookawara S, Suzuki M, Kumari S, Bux F (2015) Continuous biohydrogen production from starch wastewater via sequential dark-photo fermentation with emphasize on maghemite nanoparticles. J Ind Eng Chem 21(1):500–506

63. Chookaew T, O-Thong S, Prasertsan P (2015) Biohydrogen production from crude glycerol by two stage of dark and photo fermentation. Int J Hydrog Energy 40(24):7433–8

64. Cheng J, Ding L, Ao X, Lin R, Li Y, Zhou J et al (2015) Hydrogen production using amino acids obtained by protein degradation in waste biomass by combined dark- and photo-fermentation. Bioresour Technol 179:13–19

65. Yang H, Shi B, Ma H, Guo L (2015) Enhanced hydrogen production from cornstalk by dark- and photo-fermentation with diluted alkali-cellulase two-step hydrolysis. Int J Hydrog Energy 40(36):12193–12200

66. Rai PK, Asthana RK, Singh SP (2014) Optimization of photo-hydrogen production based on cheese whey spent medium. Int J Hydrog Energy 39(14):7597–7603

67. Afsar N, Özgür E, Gürgan M, Akköse S, Yücel M, Gündüz U et al (2011) Hydrogen productivity of photosynthetic bacteria on dark fermenter effluent of potato steam peels hydrolysate. Int J Hydrog Energy 36(1):432–438

68. Zong WM, Yu RS, Zhang P, Fan MZ, Zhou ZH (2009) Efficient hydrogen gas production from cassava and food waste by a two-step process of dark fermentation and photo-fermentation. Biomass Bioenergy 33(10):1458–1463

69. Argun H, Kargi F, Kapdan IK (2009) Hydrogen production by combined dark and light fermentation of ground wheat solution. Int J Hydrog Energy 34(10):4305–4311

70. Hitit ZY, Lazaro CZ, Hallenbeck PC (2016) Single stage hydrogen production from cellulose through photo-fermentation by a co-culture of *Cellulomonas fimi* and *Rhodopseudomonas palustris*. Int J Hydrog Energy 42(10):6556–6566

71. Xie GJ, Feng LB, Ren NQ, Ding J, Liu C, Xing DF et al (2010) Control strategies for hydrogen production through co-culture of *Ethanoligenens harbinense* B49 and immobilized *Rhodopseudomonas faecalis* RLD-53. Int J Hydrog Energy 35(5):1929–1935

72. Liu BF, Ren NQ, Tang J, Ding J, Liu WZ, Xu JF et al (2010) Bio-hydrogen production by mixed culture of photo- and dark-fermentation bacteria. Int J Hydrog Energy 35(7):2858–2862

73. Smil V (2004) The transformation of world food production. In: Haber F, Bosch C (eds) Enriching the Earth. The MIT Press, Cambridge

74. Gloe A, Pfennig N Jr, Brockmann H, Trowitzsch W (1975) A new bacteriochlorophyll from brown-colored *Chlorobiaceae*. Arch Microbiol 102(1):103–9

75. Eady RR (1996) Structure—function relationships of alternative nitrogenases. Chem Rev 96(7):3013–3030
76. Hu Y, Lee CC, Ribbe MW (2012) Vanadium nitrogenase: a two-hit wonder? Dalton Trans 41:1118–1127
77. Tan JW, Thong KL, Arumugam ND, Cheah WL, Lai YW, Chua KH et al (2009) Development of a PCR assay for the detection of and genes in indigenous photosynthetic bacteria. Int J Hydrog Energy 34(17):7538–7541
78. Burgess BK, Lowe DJ (1996) Mechanism of molybdenum nitrogenase. Chem Rev 96(7):2983–3012
79. Igarashi RY, Seefeldt LC (2003) Nitrogen fixation: The mechanism of the mo-dependent nitrogenase. Crit Rev Biochem Mol Biol 38(4):351–384
80. Hu Y, Ribbe MW (2013) Nitrogenase assembly. Biochim Biophys Acta 1827(8–9):1112–1122
81. Seefeldt LC, Yang ZY, Duval S, Dean DR (2013) Nitrogenase reduction of carbon-containing compounds. Biochim Biophys Acta 1827(8–9):1102–1111
82. Akkerman I, Janssen M, Rocha J, Wijffels RH (2002) Photobiological hydrogen production: photochemical efficiency and bioreactor design. Int J Hydrog Energy 27(11–12):1195–1208
83. Redwood MD, Paterson-Beedle M, Macaskie LE (2009) Integrating dark and light bio-hydrogen production strategies: Towards the hydrogen economy. Rev Environ Sci Biotechnol 8(2):149–185
84. Vignais PM, Colbeau A, Willison JC, Jouanneau Y (1985) Hydrogenase, nitrogenase, and hydrogen metabolism in the photosynthetic bacteria. Adv Microb Physiol 26(10):155–234
85. Hillmer P, Gest H (1977) H_2 metabolism in the photosynthetic bacterium *Rhodopseudomonas capsulata*: Production and utilization of H_2 by resting cells. J Bacteriol 129(2):732–739
86. Chen CY, Saratale GD, Lee CM, Chen PC, Chang JS (2008) Phototrophic hydrogen production in photobioreactors coupled with solar-energy-excited optical fibers. Int J Hydrog Energy 33(23):6886–6895
87. Schneider K, Gollan U, Dröttboom M, Selsemeier-Voigt S, Müller A (1997) Comparative biochemical characterization of the iron-only nitrogenase and the molybdenum nitrogenase from *Rhodobacter capsulatus*. Eur J Biochem 244(3):789–800
88. Oda Y, Samanta SK, Rey FE, Wu L, Liu X, Yan T et al (2005) Functional genomic analysis of three nitrogenase isozymes in the photosynthetic bacterium *Rhodopseudomonas palustris*. J Bacteriol 187(22):7784–7794
89. Meyer J (2007) [FeFe] hydrogenases and their evolution: a genomic perspective. Cell Mol Life Sci 64(9):1063–1084
90. Cammack R, Frey MRR (2001) Hydrogen as a fuel. In: Shimas S, Thauer RK (eds) A third type of hydrogenase catalyzing H_2 activation. Taylor & Francis, London
91. Shima S, Thauer RK (2007) A third type of hydrogenase catalyzing H_2 activation. Chem Rec 7(1):37–46
92. Koku H, Eroğlu İ, Gündüz U, Yücel M, Türker L (2002) Aspects of the metabolism of hydrogen production by *Rhodobacter sphaeroides*. Int J Hydrog Energy 27(11–12):1315–1329
93. Donghoon K, Misun K, Pandey A, Lee DJ, Chang JS, Guwy AJ (2011) Hydrogenases for biological hydrogen production. Bioresour Technol 102(18):8423–8431
94. Goldet G, Brandmayr C, Stripp ST, Happe T, Cavazza C, Fontecilla-Camps JC et al (2009) Electrochemical kinetic investigations of the reactions of [FeFe]-hydrogenases with carbon monoxide and oxygen: comparing the importance of gas tunnels and active-site electronic/redox effects. J Am Chem Soc 131(41):14979–14989
95. Hexter SV, Grey F, Happe T, Climent V, Armstrong FA (2012) Electrocatalytic mechanism of reversible hydrogen cycling by enzymes and distinctions between the major classes of hydrogenases. Proc Natl Acad Sci 109(29):11516–11521
96. Vignais PM, Billoud B, Meyer J (2001) Classification and phylogeny of hydrogenases1. FEMS Microbiol Rev 25(4):455–501

97. Wakayama TJM (2001) Hydrogen from biomass. In: Miyake J, Matsunaga T, San Pietro A (eds) Biohydrogen II: an approach to environmentally acceptable technology. Oxford, Pergamon

98. Sasikala K, Ramana CV, Rao PR, Subrahmanyam M (1990) Effect of gas phase on the photoproduction of hydrogen and substrate conversion efficiency in the photosynthetic bacterium *Rhodobacter sphaeroides* O.U. 001. Int J Hydrog Energy 15(11):795–797

99. Willison JC, Madern D, Vignais PM (1984) Increased photoproduction of hydrogen by non-autotrophic mutants of *Rhodopseudomonas capsulata*. Biochem J 219(2):593–600

100. Jahn A, Keuntje B, Dörffler M, Klipp W, Oelze J (1994) Optimizing photoheterotrophic H_2 production by *Rhodobacter capsulatus* upon interposon mutagenesis in the hupl gene. Appl Microbiol Biotechnol 40(5):687–690

101. Zorin NA, Lissolo T, Colbeau A, Vignais PM (1996) Increased hydrogen photoproduction by *Rhodobactor capsulatus* strain deficient in uptake hydrogenase. J Mar Biotechnol 4(1): 28–33

102. Öztürk Y, Yücel M, Daldal F, Mandacı S, Gündüz U, Türker L et al (2006) Hydrogen production by using *Rhodobacter capsulatus* mutants with genetically modified electron transfer chains. Int J Hydrog Energy 31(11):1545–1552

103. Chen CY, Chang JS (2006) Enhancing phototropic hydrogen production by solid-carrier assisted fermentation and internal optical-fiber illumination. Process Biochem 41(9):2041–2049

104. Fang HHP, Liu H, Zhang T (2005) Phototrophic hydrogen production from acetate and butyrate in wastewater. Int J Hydrog Energy 30(7):785–793

105. Sagnak R, Kargi F (2011) Photo-fermentative hydrogen gas production from dark fermentation effluent of acid hydrolyzed wheat starch with periodic feeding. Int J Hydrog Energy 36(7):4348–4353

106. Ozmihci S, Kargi F (2010) Bio-hydrogen production by photo-fermentation of dark fermentation effluent with intermittent feeding and effluent removal. Int J Hydrog Energy 35(13):6674–6680

107. Lo YC, Chen CY, Lee CM, Chang JS (2011) Photo fermentative hydrogen production using dominant components (acetate, lactate, and butyrate) in dark fermentation effluents. Int J Hydrog Energy 36(21):14059–14068

108. Pintucci C, Giovannelli A, Traversi ML, Ena A, Padovani G, Carlozzi P (2013) Fresh olive mill waste deprived of polyphenols as feedstock for hydrogen photo-production by means of *Rhodopseudomonas palustris* 42OL. Renew Energy 51(2):358–363

109. Morsy FM (2017) Synergistic dark and photo-fermentation continuous system for hydrogen production from molasses by *Clostridium acetobutylicum* ATCC 824 and *Rhodobacter capsulatus* DSM 1710. J Photochem Photobiol B 169(1):1–6

110. Koku H, Eroğlu İ, Gündüz U, Yücel M, Türker L (2003) Kinetics of biological hydrogen production by the photosynthetic bacterium *Rhodobacter sphaeroides* O.U. 001. Int J Hydrog Energy 28(4):381–388

111. Eroglu N, Aslan K, Gündüz U, Yücel M, Türker L (1999) Substrate consumption rates for hydrogen production by *Rhodobacter sphaeroides* in a column photobioreactor. J Biotechnol 70(1):103–113

112. Oh YK, Seol EH, Kim MS, Park S (2004) Photoproduction of hydrogen from acetate by a chemoheterotrophic bacterium *Rhodopseudomonas palustris* P4. Int J Hydrog Energy 29(11):1115–1121

113. Abo-Hashesh M, Desaunay N, Hallenbeck PC (2013) High yield single stage conversion of glucose to hydrogen by photofermentation with continuous cultures of *Rhodobacter capsulatus* JP91. Bioresour Technol 128(128C):513–517

114. Lee JZ, Klaus DM, Maness PC, Spear JR (2007) The effect of butyrate concentration on hydrogen production via photofermentation for use in a Martian habitat resource recovery process. Int J Hydrog Energy 32(15):3301–3307

115. Chen CY, Lu WB, Wu JF, Chang JS (2007) Enhancing phototrophic hydrogen production of *Rhodopseudomonas palustris* via statistical experimental design. Int J Hydrog Energy 32(8): 940–949
116. Takabatake H, Suzuki K, Ko IB, Noike T (2004) Characteristics of anaerobic ammonia removal by a mixed culture of hydrogen producing photosynthetic bacteria. Bioresour Technol 95(2):151–158
117. Fascetti E, Todini O (1995) *Rhodobacter sphaeroides* RV cultivation and hydrogen production in a one- and two-stage chemostat. Appl Microbiol Biotechnol 44(3–4):300–305
118. Chen CY, Lee CM, Chang JS (2006) Feasibility study on bioreactor strategies for enhanced photohydrogen production from *Rhodopseudomonas palustris* WP3-5 using optical-fiber-assisted illumination systems. Int J Hydrog Energy 31(15):2345–2355
119. Shi XY, Yu HQ (2005) Optimization of glutamate concentration and pH for H_2 production from volatile fatty acids by *Rhodopseudomonas capsulata*. Lett Appl Microbiol 40(6): 401–406
120. Wu YN, Wen HQ, Zhu JN, Ding J, Ren NQ, Liu BF (2016) Best mode for photo-fermentation hydrogen production: The semi-continuous operation. Int J Hydrog Energy 41(36):16048–16054
121. Assawamongkholsiri T, Plangklang P, Reungsang A (2016) Photofermentaion and lipid accumulation by *Rhodobacter* sp. KKU-PS1 using malic acid as a substrate. Int J Hydrog Energy 41(15):6259–6270
122. Liu B, Jin Y, Wang Z, Xing D, Ma C, Ding J et al (2017) Enhanced photo-fermentative hydrogen production of *Rhodopseudomonas* sp. nov. strain A7 by the addition of TiO_2, ZnO and SiC nanoparticles. Int J Hydrog Energy 42:18279–18287
123. Zhang Y, Yang H, Guo L (2016) Enhancing photo-fermentative hydrogen production performance of *Rhodobacter capsulatus* by disrupting methylmalonate-semialdehyde dehydrogenase gene. Int J Hydrog Energy 41(1):190–197
124. Subudhi S, Mogal SK, Kumar NR, Nayak T, Lal B, Velankar H et al (2016) Photo fermentative hydrogen production by a new strain; *Rhodobacter sphaeroides* CNT 2A, isolated from pond sediment. Int J Hydrog Energy 41(32):13979–13985
125. Wen HQ, Du J, Xing DF, Ding J, Ren NQ, Liu BF (2017) Enhanced photo-fermentative hydrogen production of *Rhodopseudomonas* sp. nov. strain A7 by biofilm reactor. Int J Hydrog Energy 42:18288–94
126. Zagrodnik R (2016) M Ł. Hydrogen production from starch by co-culture of *Clostridium acetobutylicum* and *Rhodobacter sphaeroides* in one step hybrid dark- and photofermentation in repeated fed-batch reactor. Bioresour Technol 224:298–306
127. Zagrodnik R, Łaniecki M (2017) The effect of pH on cooperation between dark- and photo-fermentative bacteria in a co-culture process for hydrogen production from starch. Int J Hydrog Energy 42(5):2878–2888
128. Hu J, Zhang Q, Jing Y, Lee DJ (2016) Photosynthetic hydrogen production from enzyme-hydrolyzed micro-grinded maize straws. Int J Hydrog Energy 41(46):21665–21669
129. Shi XY, Yu HQ (2005) Response surface analysis on the effect of cell concentration and light intensity on hydrogen production by *Rhodopseudomonas capsulata*. Process Biochem 40(7):2475–2481
130. Bowles LK, Ellefson WL (1985) Effects of butanol on *Clostridium acetobutylicum*. Appl Environ Microbiol 50(5):1165–1170
131. Lazaro CZ, Varesche MBA, Silva EL (2015) Effect of inoculum concentration, pH, light intensity and lighting regime on hydrogen production by phototrophic microbial consortium. Renew Energy 75:1–7
132. Krahn E, Schneider K, Müller A (1996) Comparative characterization of H_2 production by the conventional Mo nitrogenase and the alternative "iron-only" nitrogenase of *Rhodobacter capsulatus* hup—mutants. Appl Microbiol Biotechnol 46(3):285–290
133. Yu KM, Lee CM (2003) The study of limiting factor for the photo-hydrogen production with purple non-sulfate bacterium. National Chung Hsing University, Taiwan

134. Prashanthi Y, Garimella S, Kudle KR, Merugu R (2014) Effect of light intensity and metal ions on the production of hydrogen by the purple non sulphur bacterium *Rhodospeudomonas palustris* KU003. Int J Res Environ Sci Tech 4:61–64

135. Afşar N, Özgür E, Gürgan M, Vrije Td, Yücel M, Gündüz U et al (2006) Hydrogen production by *R. Capsulatus* on dark fermenter effluent of potato steam peel hydrolysate. Chem Eng Trans 18:385–90

136. Eroglu E, Melis A (2011) Photobiological hydrogen production: recent advances and state of the art. Bioresour Technol 102(18):8403–8413

137. Kars G, Gündüz U, Yücel M, Türker L, Eroglu İ (2006) Hydrogen production and transcriptional analysis of nifD, nifK and hupS genes in *Rhodobacter sphaeroides* O.U.001 grown in media with different concentrations of molybdenum and iron. Int J Hydrog Energy 31(11):1536–1544

138. Ludden PW, Roberts GP (1995) The biochemistry and genetics of nitrogen fixation by photosynthetic bacteria. In: Blankenship BE, Madigan MT, Bauer CE (eds) Anoxygenic photosynthetic bacteria. Kluwer Academic Publishers, Dordrecht

139. Zhu H, Fang HHP, Zhang T, Beaudette LA (2007) Effect of ferrous ion on photo heterotrophic hydrogen production by *Rhodobacter sphaeroides*. Int J Hydrog Energy 32(17):4112–4118

140. Han H, Jia Q, Liu B, Yang H, Shen J (2013) Optimization of photosynthetic hydrogen production from acetate by *Rhodobacter sphaeroides* RV. Int J Hydrog Energy 38(29): 12886–12890

141. Rai PK, Singh SP, Asthana RK, Singh S (2014) Biohydrogen production from sugarcane bagasse by integrating dark- and photo-fermentation. Bioresour Technol 152(1):140–146

142. Klasson KT, Lundbäck KMO, Clausen EC, Gaddy JL (1993) Kinetics of light limited growth and biological hydrogen production from carbon monoxide and water by *Rhodospirillum rubrum*. J Biotechnol 29(1–2):177–188

143. Kim NJ, Lee JK, Lee CG (2004) Pigment reduction to improve photosynthetic productivity of *Rhodobacter sphaeroides*. J Microbiol Biotechnol 14(3):442–449

144. Zhang C, Zhu X, Liao Q, Wang Y, Li J, Ding Y et al (2010) Performance of a groove-type photobioreactor for hydrogen production by immobilized photosynthetic bacteria. Int J Hydrog Energy 35(11):5284–52923

145. Kim MS, Baek JS (2006) JK. L. Comparison of H$_2$ accumulation by *Rhodobacter sphaeroides* KD131 and its uptake hydrogenase and PHB synthase deficient mutant. Int J Hydrog Energy 31:121–127

146. Hallenbeck PC, Liu Y (2016) Recent advances in hydrogen production by photosynthetic bacteria. Int J Hydrog Energy 41(7):4446–4454

147. Krujatz F, Helbig K, Haufe N, Thierfelder S, Bley T, Weber J (2015) Hydrogen production by *Rhodobacter sphaeroides* DSM 158 under intense irradiation. Bioresour Technol 175:82–90

148. Argun H, Kargi F (2010) Effects of light source, intensity and lighting regime on bio-hydrogen production from ground wheat starch by combined dark and photo-fermentations. Int J Hydrog Energy 35(4):1604–1612

149. Tian X, Liao Q, Liu W, Wang Y, Zhu X, Li J et al (2009) Photo-hydrogen production rate of a PVA-boric acid gel granule containing immobilized photosynthetic bacteria cells. Int J Hydrog Energy 34(11):4708–4717

150. Kawagoshi Y, Oki Y, Nakano I, Fujimoto A, Takahashi H (2010) Biohydrogen production by isolated halotolerant photosynthetic bacteria using long-wavelength light-emitting diode (LW-LED). Int J Hydrog Energy 35(24):13365–13369

151. Stevens P, Vertonghen C, Vos PD, Ley JD (1984) The effect of temperature and light intensity on hydrogen gas production by different *Rhodopseudomonas capsulata* strains. Biotechnol Lett 6(5):277–282

152. Cai J, Wang G (2014) Photo-biological hydrogen production by an acid tolerant mutant of *Rhodovulum sulfidophilum* P5 generated by transposon mutagenesis. Bioresource Technol 154:254–259

153. Wang YZ, Liao Q, Zhu X, Tian X, Zhang C (2010) Characteristics of hydrogen production and substrate consumption of *Rhodopseudomonas palustris* CQK 01 in an immobilized-cell photobioreactor. Bioresour Technol 101(11):4034–4041

154. Basak N, Jana AK, Das D (2014) Optimization of molecular hydrogen production by *Rhodobacter sphaeroides O*.U.001 in the annular photobioreactor using response surface methodology. Int J Hydrog Energy 39(23):11889–11901

155. Sasikala CH, Ramana CHV, Rao PR (1995) Regulation of simultaneous hydrogen photoproduction during growth by pH and glutamate in *Rhodobacter sphaeroides* O.U. 001. Int J Hydrog Energy 20(2):123–126

156. De Philippis R, Ena A, Guastini M, Sili C, Vincenzini M (1992) Factors affecting poly-β-hydroxybutyrate accumulation in cyanobacteria and in purple non-sulfur bacteria. FEMS Microbiol Lett 103(2–4):187–194

157. Melnicki MR, Bianchi L, Philippis RD, Melis A (2008) Hydrogen production during stationary phase in purple photosynthetic bacteria. Int J Hydrog Energy 33(22):6525–6534

158. Ooshima H, Takakuwa S, Katsuda T, Okuda M, Shirasawa T, Azuma M et al (1998) Production of hydrogen by a hydrogenase-deficient mutant of *Rhodobacter capsulatus*. J Ferment Bioeng 85(5):470–475

159. Han H, Jia Q, Liu B, Yang H, Shen J (2013) Fermentative hydrogen production from acetate using *Rhodobacter sphaeroides* RV. Int J Hydrog Energy 38(25):10773–10778

160. Zhu H, Suzuki T, Tsygankov AA, Asada Y, Miyake J (1999) Hydrogen production from tofu wastewater by *Rhodobacter sphaeroides* immobilized in agar gels. Int J Hydrog Energy 24(4):305–310

161. Zhu H, Ueda S, Asada Y, Miyake J (2002) Hydrogen production as a novel process of wastewater treatment—studies on tofu wastewater with entrapped *R. sphaeroides* and mutagenesis. Int J Hydrog Energy 27(11):1349–1357

162. Anam K, Habibi MS, Harwati TU, Susilaningsih D (2012) Photofermentative hydrogen production using *Rhodobium marinum* from bagasse and soy sauce wastewater. Int J Hydrog Energy 37(20):15436–15442

163. Jamil Z, Annuar MSM, Ibrahim S, Vikineswary S (2009) Optimization of phototrophic hydrogen production by *Rhodopseudomonas palustris* PBUM001 via statistical experimental design. Int J Hydrog Energy 34(17):7502–7512

164. Budiman PM, Wu TY (2016) Ultrasonication pre-treatment of combined effluents from palm oil, pulp and paper mills for improving photofermentative biohydrogen production. Energy Convers Manage 119:142–150

165. Ghosh D, Sobro IF, Hallenbeck PC (2012) Stoichiometric conversion of biodiesel derived crude glycerol to hydrogen: response surface methodology study of the effects of light intensity and crude glycerol and glutamate concentration. Bioresour Technol 106(106): 154–160

166. Eroğlu İ, Tabanoğlu A, Gündüz U, Eroğlu E, Yücel M (2008) Hydrogen production by *Rhodobacter sphaeroides* O.U.001 in a flat plate solar bioreactor. Int J Hydrog Energy 33(2): 531–541

167. Kars G, Alparslan Ü (2013) Valorization of sugar beet molasses for the production of biohydrogen and 5-aminolevulinic acid by *Rhodobacter sphaeroides* O.U.001 in a biorefinery concept. Int J Hydrog Energy 38(34):14488–14494

168. Yazdani SS, Gonzalez R (2007) Anaerobic fermentation of glycerol: A path to economic viability for the biofuels industry. Curr Opin Biotech 18(3):213–219

169. Reungsang A, Sittijunda S, Angelidaki I (2013) Simultaneous production of hydrogen and ethanol from waste glycerol by *Enterobacter aerogenes* KKU-S1. Int J Hydrog Energy 38(4):1813–1825

170. Yang F, Hanna MA, Sun R (2012) Value-added uses for crude glycerol–a byproduct of biodiesel production. Biotechnol Biofuels 5(13):1–10

171. Sabourin-Provost G, Hallenbeck PC (2009) High yield conversion of a crude glycerol fraction from biodiesel production to hydrogen by photofermentation. Bioresour Technol 100(14):3513–3517

172. Eroğlu E, Eroğlu İ, Gündüz U, Türker L, Yücel M (2006) Biological hydrogen production from olive mill wastewater with two-stage processes. Int J Hydrog Energy 31(11):1527–1535

173. Eroğlu E, Eroğlu İ, Gündüz U, Yücel M (2009) Comparison of physicochemical characteristics and photofermentative hydrogen production potential of wastewaters produced from different olive oil mills in Western-Anatolia. Turkey. Biomass Bioenerg 33(4):706–711

174. Ghosh S, Dairkee UK, Chowdhury R (2017) P. B. Hydrogen from food processing wastes via photofermentation using purple non-sulfur bacteria (PNSB)-A review. Energy Convers Manage 141:299–314

175. Sweet WJ, Burris RH (1981) Inhibition of nitrogenase activity by NH$_4^+$ in *Rhodospirillum rubrum*. J Bacteriol 145(2):824–831

176. Jiang D, Zhuang D, Fu J, Huang Y, Wen K (2012) Bioenergy potential from crop residues in China: Availability and distribution. Renew Sustain Energy Rev 16(3):1377–1382

177. Saratale GD, Chen SD, Lo YC, Saratale RG, Chang JS (2008) Outlook of biohydrogen production from lignocellulosic feedstock using dark fermentation—a review. J Sci Ind Res 67(11):962–979

178. Zhang ZP, Yue JZ, Zhou XH, Jing YY, Jiang DP, Zhang QG (2014) Photo-fermentative bio-hydrogen production from agricultural residue enzymatic hydrolyzate and the enzyme reuse. Bioresources 9(2):2299–2310

179. Pattra S, Sangyoka S, Boonmee M, Reungsang A (2008) Bio-hydrogen production from the fermentation of sugarcane bagasse hydrolysate by *Clostridium butyricum*. Int J Hydrog Energy 33(19):5256–5265

180. Shibata M, Varman M, Tono Y, Miyafuji H, Saka S (2008) Characterization in chemical composition of the oil palm (*Elaeis guineensis*). J Jpn I Energy 87(34):2939–2942

181. Pattanamanee W, Choorit W, Deesan C, Sirisansaneeyakul S, Chisti Y (2012) Photofermentive production of biohydrogen from oil palm waste hydrolysate. Int J Hydrog Energy 37(5):4077–4087

182. Sittijunda S (2015) Biogas production from hydrolysate napier grass by co-digestion with slaughterhouse wastewater using anaerobic mixed cultures. KKU Res J 20:323–336

183. Saxena RC, Adhikari DK, Goyal HB (2009) Biomass-based energy fuel through biochemical routes: A review. Renew Sustain Energy Rev 13(1):167–178

184. Pattra S, Sittijunda S, Reungsang A (2017) Biohydrogen productions from hydrolysate of water hyacinth stem (*Eichhornia crassipes*) using anaerobic mixed cultures. Sains Malays 46(1):51–58

185. Deng J, Xiong T, Wang H, Zheng A, Wang Y (2016) Effects of cellulose, hemicellulose, and lignin on the structure and morphology of porous carbons. ACS Sustain Chem Eng 4(7):3750–3756

186. Sukjun J, Seunghyun K, Illmin C (2015) Comparison of lignin, cellulose, and hemicellulose contents for biofuels utilization among 4 types of lignocellulosic crops. Biomass Bioenerg 83:322–327

187. Jönsson LJ, Martín C (2016) Pretreatment of lignocellulose: Formation of inhibitory by-products and strategies for minimizing their effects. Bioresour Technol 199:103–112

188. Khamtib S, Plangklang P, Reungsang A (2011) Optimization of fermentative hydrogen production from hydrolysate of microwave assisted sulfuric acid pretreated oil palm trunk by hot spring enriched culture. Int J Hydrog Energy 36(21):14204–14216

189. Khamtib S, Reungsang A (2014) Co-digestion of oil palm trunk hydrolysate with slaughterhouse wastewater for thermophilic bio-hydrogen production by *Thermoanaerobacterium thermosaccharolyticm* KKU19. Int J Hydrog Energy 39(13):6872–6880

190. Jiang D, Ge X, Zhang T, Liu H, Zhang Q (2016) Photo-fermentative hydrogen production from enzymatic hydrolysate of corn stalk pith with a photosynthetic consortium. Int J Hydrog Energy 41(38):16778–16785

191. Lu C, Zhang Z, Zhou X, Hu J, Ge X, Xia C et al (2017) Effect of substrate concentration on hydrogen production by photo-fermentation in the pilot-scale baffled bioreactor. Bioresource Technol 247:1173–1176

192. Kapdan IK, Kargi F, Oztekin R, Argun H (2009) Bio-hydrogen production from acid hydrolyzed wheat starch by photo-fermentation using different *Rhodobacter sp*. Int J Hydrog Energy 34(5):2201–2207

193. Jiang D, Zhang Y, Lu C, Sun T, Zhang B, Zhang Q (2015) Dynamics of biomass straw enzymolysis and photosynthetic characteristics of biological hydrogen production. Trans Chin Soc Agri Mach 46(5):196–201

194. Sargsyan H, Gabrielyan L, Trchounian A (2016) The distillers grains with solubles as a perspective substrate for obtaining biomass and producing bio-hydrogen by *Rhodobacter sphaeroides*. Biomass Bioenerg 90:90–94

195. Zhang Z, Wang Y, Hu J, Wu Q, Zhang Q (2015) Influence of mixing method and hydraulic retention time on hydrogen production through photo-fermentation with mixed strains. Int J Hydrog Energy 40(20):6521–6529

196. Lu C, Zhang Z, Ge X, Wang Y, Zhou X, You X et al (2016) Bio-hydrogen production from apple waste by photosynthetic bacteria HAU-M1. Int J Hydrog Energy 41(31):13399–13407

197. Liu H, Stephen Grot A (2005) † BEL. Electrochemically assisted microbial production of hydrogen from acetate. Environ Sci Technol 39(11):4317–4320

198. Lin R, Cheng J, Yang Z, Ding L, Zhang J, Zhou J et al (2016) Enhanced energy recovery from cassava ethanol wastewater through sequential dark hydrogen, photo hydrogen and methane fermentation combined with ammonium removal. Bioresour Technol 214:686–691

199. Fißler J, Schirra C, Kohring G-W, Giffhorn F (1994) Hydrogen production from aromatic acids by *Rhodopseudomonas palustris*. Appl Microbiol Biotechnol 41(4):395–399

200. Foster AE, Forrester K, Gottlieb DJ, Barton GW, Romagnoli JA, Bradstock KF (2004) Large-scale expansion of cytomegalovirus-specific cytotoxic T cells in suspension culture. Biotechnol Bioeng 85(2):138–146

201. zur Nieden NI, Cormier JT, Rancourt DE, Kallos MS (2007) Embryonic stem cells remain highly pluripotent following long term expansion as aggregates in suspension bioreactors. J Biotechnol 129(3):421–432

202. Carmelo JG, Fernandesplatzgummer A, Cabral JM, Da SC (2014) Scalable ex vivo expansion of human mesenchymal stem/stromal cells in microcarrier-based stirred culture systems. Methods Mol Biol 1283:147–159

203. Lee SY, Lee HJ, Park JM, Jin HL, Park JS, Shin HS et al (2010) Bacterial hydrogen production in recombinant *Escherichia coli* harboring a HupSL hydrogenase isolated from *Rhodobacter sphaeroides* under anaerobic dark culture. Int J Hydrog Energy 35(3):1112–1116

204. Wu XD, Rongsheng R, Du ZY, Liu YH (2012) Current status and prospects of biodiesel production from microalgae. Energies 5(8):2667–2682

205. Boran E, Özgür E, Yücel M, Gündüz U, Eroglu I (2012) Biohydrogen production by *Rhodobacter capsulatus* hup—mutant in pilot solar tubular photobioreactor. Int J Hydrog Energy 37(21):16437–16445

206. Uyar B (2016) Bioreactor design for photofermentative hydrogen production. Bioprocess Biosyst Eng 39(9):1–10

207. Zhong N, Liao Q, Zhu X, Zhao M (2015) Fiber-optic differential absorption sensor for accurately monitoring biomass in a photobioreactor. Appl Opt 54(2):228–235

208. Markov SA, Weaver PF, Seibert M (1997) Spiral tubular bioreactors for hydrogen production by photosynthetic microorganisms. Humana Press

209. Tawfik A, Elbery H, Kumari S, Bux F (2014) Use of mixed culture bacteria for photofermentive hydrogen of dark fermentation effluent. Bioresource Technol 168(3):119–126

210. Scoma A, Giannelli L, Faraloni C, Torzillo G (2012) Outdoor H_2 production in a 50-L tubular photobioreactor by means of a sulfur-deprived culture of the microalga *Chlamydomonas reinhardtii*. J Biotechnol 157(4):620–627

211. Adessi A, Philippis RD (2014) Photobioreactor design and illumination systems for H$_2$ production with anoxygenic photosynthetic bacteria: a review. Int J Hydrog Energy 39(7): 3127–3141
212. Singh RN, Sharma S (2012) Development of suitable photobioreactor for algae production —a review. Renew Sust Energy Rev 16(4):2347–2353
213. Muller-Feuga A, Pruvost J, Guédes RL, Déan LL, Legentilhomme P, Legrand J (2003) Swirling flow implementation in a photobioreactor for batch and continuous cultures of porphyridium cruentum. Biotechnol Bioeng 84(5):544–551
214. Krujatz F, Illing R, Krautwer T, Liao J, Helbig K, Goy K et al (2015) Light-field-characterization in a continuous hydrogen-producing photobioreactor by optical simulation and computational fluid dynamics. Biotechnol Bioeng 112(12):2439–2449
215. Wang YZ, Liao Q, Zhu X, Chen R, Guo CL, Zhou J (2013) Bioconversion characteristics of *Rhodopseudomonas palustris* CQK 01 entrapped in a photobioreactor for hydrogen production. Bioresource Technol 135(2):331–338
216. Sierra E, Acién FG, Fernández JM, García JL, González C, Molina E (2008) Characterization of a flat plate photobioreactor for the production of microalgae. Chem Eng J 138(1):136–147
217. Gilbert JJ, Ray S, Das D (2011) Hydrogen production using *Rhodobacter sphaeroides* (O.U. 001) in a flat panel rocking photobioreactor. Int J Hydrog Energy 36(5):3434–3441
218. Lehr F, Posten C (2009) Closed photo-bioreactors as tools for biofuel production. Curr Opin Biotech 20(3):280–285
219. Miyake J, Miyake M, Asada Y (1999) Biotechnological hydrogen production "research for efficient light energy conversion". Prog Ind Microbiol 35(1–3):89–101
220. Hallenbeck PC, Benemann JR (2002) Biological hydrogen production; fundamentals and limiting processes. Int J Hydrog Energy 27(11):1185–1193
221. Chen CY, Yeh KL, Aisyah R, Lee DJ, Chang JS (2011) Cultivation, photobioreactor design and harvesting of microalgae for biodiesel production: A critical review. Bioresource Technol 102(1):71–81
222. Tanisho S, Ishiwata Y (1995) Continuous hydrogen production from molasses by fermentation using urethane foam as a support of flocks. Int J Hydrog Energy 20(7):541–545
223. Otsuki T, Uchiyama S, Fujiki K, Fukunaga S (1998) Hydrogen production by a floating-type photobioreactor. Springer, US
224. Kondo T, Wakayama T, Miyake J (2006) Efficient hydrogen production using a multi-layered photobioreactor and a photosynthetic bacterium mutant with reduced pigment. Int J Hydrog Energy 31(11):1522–1526
225. Qu XF, Wang YZ, Zhu X, Liao Q, Li J, Ding YD et al (2011) Bubble behavior and photo-hydrogen production performance of photosynthetic bacteria in microchannel photobioreactor. Int J Hydrog Energy 36(21):14111–14119
226. Xie GJ, Liu BF, Ding J, Ren HY, Xing DF, Ren NQ (2011) Hydrogen production by photo-fermentative bacteria immobilized on fluidized bio-carrier. Int J Hydrogen Energ 36(21):13991–13996
227. Zhong N, Liao Q, Zhu X, Chen R (2014) A fiber-optic sensor for accurately monitoring biofilm growth in a hydrogen production photobioreactor. Anal Chem 86(8):3994–4001
228. Liao Q, Zhong NB, Zhu X, Chen R, Wang YZ, Lee DJ (2013) Enhancement of hydrogen production by adsorption of *Rhodoseudomonas palustris* CQK 01 on a new support material. Int J Hydrog Energy 38(35):15730–15737
229. Lu L, Xing D, Ren N, Logan BE (2012) Syntrophic interactions drive the hydrogen production from glucose at low temperature in microbial electrolysis cells. Bioresource Technol 124(3):68–76
230. Liao Q, Wang YJ, Wang YZ, Zhu X, Tian X, Li J (2010) Formation and hydrogen production of photosynthetic bacterial biofilm under various illumination conditions. Bioresource Technol 101(14):5315–5324
231. Walker JT, Marsh PD (2004) A review of biofilms and their role in microbial contamination of dental unit water systems (DUWS). Int Biodeter Biodegr 54(3):87–98

232. Carlén A, Nikdel K, Wennerberg A, Holmberg K, Olsson J (2001) Surface characteristics and in vitro biofilm formation on glass ionomer and composite resin. Biomaterials 22(5): 481–487

233. Whitehead KA, Verran J (2007) The effect of surface properties and application method on the retention of *Pseudomonas aeruginosa* on uncoated and titanium-coated stainless steel. Int Biodeter Biodegr 60(2):74–80

234. Scheuerman TR, Camper AK, Hamilton MA (1998) Effects of substratum topography on bacterial adhesion. J Colloid Interface Sci 208(1):23–33

235. Ginsburg MA, Karamanev D (2007) Experimental study of the immobilization of *Acidithiobacillus ferrooxidans* on carbon based supports. Biochem Eng J 36(3):294–300

236. Diskin S, Cao Z, Leffler H, Panjwani N (2011) Performance of continuous hydrogen production in annular fiber-illuminating biofilm reactor. Ciesc J 62(11):3248–3255

237. Zhang C, Chen R, Wang Y, Wang Y, Zhang Q (2014) Effect of mass transfer on performance of substrate degradation within annular fiber-illuminating biofilm reactor for continuous hydrogen production. Energy Procedia 61:1455–1459

238. Zhang C (2010) Characteristics of mass transfer and hydrogen production in biofilm photobioreactor with photosynthetic bacteria (In Chinese). Chongqing University, China

239. Guo CL, Zhu X, Liao Q, Wang YZ, Chen R, Lee DJ (2011) Enhancement of photo-hydrogen production in a biofilm photobioreactor using optical fiber with additional rough surface. Bioresource Technol 102(18):8507–8513

240. Zhong N, Liao Q, Chen R, Zhu X, Wang Y (2013) GeO$_2$-SiO$_2$-chitosan-medium-coated hollow optical fiber for cell immobilization. Opt Lett 38(16):3115–3118

241. Qiang L, Zhong NB, Xun Z, Rong C (2014) High-performance biofilm photobioreactor based on a GeO$_2$ –SiO$_2$ –chitosan-medium-coated hollow optical fiber. Int J Hydrog Energy 39(19):10016–10027

242. Liao Q, Zhong N, Zhu X, Huang Y, Chen R (2015) Enhancement of hydrogen production by optimization of biofilm growth in a photobioreactor. Int J Hydrog Energy 40(14):4741–4751

243. Jain A, Yang AHJ, Erickson D (2012) Gel-based optical waveguides with live cell encapsulation and integrated microfluidics. Opt Lett 37(9):1472–1474

244. Zhang N (2013) A study on surface modification for enhancing hydrogen production of PSB biofilm and an on-line measurement system based on fiber-optic sensors (In Chinese). Chongqing University, China

245. Zhao QB, Yu HQ (2008) Fermentative H$_2$ production in an upflow anaerobic sludge blanket reactor at various pH values. Bioresource Technol 99(5):1353–1358

246. Mizuno O, Dinsdale R, Hawkes FR, Hawkes DL, Noike T (2000) Enhancement of hydrogen production from glucose by nitrogen gas sparging. Bioresource Technol 73(1):59–65

247. Liao Q, Liu DM, Ye DD, Zhu X, Lee DJ (2011) Mathematical modeling of two-phase flow and transport in an immobilized-cell photobioreactor. Int J Hydrog Energy 36(21):13939–13948

248. Wu SY, Lin CJ (2003) Hydrogen production with immobilized sewage sludge in three-phase fluidized-bed bioreactors. Biotechnol Prog 19(3):828–832

249. Ahn Y, Park EJ, Oh YK, Park S, Webster G, Weightman AJ (2005) Biofilm microbial community of a thermophilic trickling biofilter used for continuous biohydrogen production. FEMS Microbiol Lett 249(1):31–38

250. Li Y, Zhong N, Liao Q, Fu Q, Huang Y, Zhu X et al (2017) A biomaterial doped with LaB$_6$ nanoparticles as photothermal media for enhancing biofilm growth and hydrogen production in photosynthetic bacteria. Int J Hydrog Energy 42(9):5793–5803

251. Banerjee I, Modak JM, Bandopadhyay K, Das D, Maiti BR (2001) Mathematical model for evaluation of mass transfer limitations in phenol biodegradation by immobilized *Pseudomonas putida*. J Biotechnol 87(3):211–223

252. Das D, Badri PK, Kumar N, Bhattacharya P (2002) Simulation and modeling of continuous H$_2$ production process by *Enterobacter cloacae* IIT-BT 08 using different bioreactor configuration. Enzyme Microb Technol 31(6):867–875

253. Palazzi E, Perego P, Fabiano B (2002) Mathematical modelling and optimization of hydrogen continuous production in a fixed bed bioreactor. Chem Eng Sci 57(18):3819–3830
254. Tepe O, Dursun AY (2008) Combined effects of external mass transfer and biodegradation rates on removal of phenol by immobilized *Ralstonia eutropha* in a packed bed reactor. J Hazard Mater 151(1):9–16
255. Succi S (2001) The lattice Boltzmann equation—for fluid dynamics and beyond. Clarendon Press
256. Sukop MC, Thorne DTJ (2007) Lattice Boltzmann modeling: an introduction for geoscientists and engineers. Springer Publishing Company, Incorporated
257. Chen S, Doolen GD (2012) Lattice Boltzmann method for fluid flows. Annu Rev Fluid Mech 30(1):329–364
258. He X, Doolen G (1997) Lattice Boltzmann method on curvilinear coordinates system: Flow around a circular cylinder. J Comput Phys 134(2):306–315
259. Hölzer A, Sommerfeld M (2009) Lattice Boltzmann simulations to determine drag, lift and torque acting on non-spherical particles. Comput Fluids 38(3):572–589
260. Zhao LG, Zhao TS (2005) A lattice Boltzmann model for convection heat transfer in porous media. Numer Heat Transf Part B 47(2):157–177
261. Tian ZW, Zou C, Liu HJ, Guo ZL, Liu ZH, Zheng CG (2007) Lattice Boltzmann scheme for simulating thermal micro-flow. Phys A 385(1):59–68
262. Verma N, Mewes D, Luke A (2010) Lattice Boltzmann study of velocity, temperature, and concentration in micro-reactors. Int J Heat Mass Transf 53(15):3175–3185
263. Biferale L, Perlekar P, Sbragaglia M, Toschi F (2012) Convection in multiphase fluid flows using lattice Boltzmann methods. Phys Rev Lett 108(10):104502–104506
264. Kim SH, Pitsch H, Boyd ID (2009) Lattice Boltzmann modeling of multicomponent diffusion in narrow channels. Phys Rev E 79(1):6702–6712
265. Onishi J, Chen Y, Ohashi H (2006) Dynamic simulation of multi-component viscoelastic fluids using the lattice Boltzmann method. Phys A 362(1):84–92
266. Keblinski P, Phillpot SR, Choi SUS, Eastman JA (2002) Mechanisms of heat flow in suspensions of nano-sized particles (nanofluids). Int J Heat Mass Transf 45(4):855–863
267. Wang X, Chen B, Wu J (2007) A semianalytical solution of periodical electro-osmosis in a rectangular microchannel. Phys Fluids 19(12):127101–127109
268. Gao Y, Zhang X, Rama P, Liu Y, Chen R, Ostadi H et al (2012) Calculating the anisotropic permeability of porous media using the lattice Boltzmann method and X-ray computed tomography. TranspPorous Med 92(2):457–472
269. Verma N, Mewes D (2009) Lattice Boltzmann methods for simulation of micro and macrotransport in a packed bed of porous adsorbents under non-isothermal condition. Comput Math Appl 58(5):1003–1014
270. Yamamoto K, Takada N, Misawa M (2005) Combustion simulation with lattice Boltzmann method in a three-dimensional porous structure. P Combust Inst 30(1):1509–1515
271. Sullivan SP, Gladden LF, Johns ML (2006) 3D chemical reactor LB simulations. Math Comput Simul 72(2–6):206–211
272. Yu H, Luo LS, Girimaji S (2012) Scalar mixing and chemical reaction simulations using lattice Boltzmann method. Int J Comput Eng Sci 3(1):73–88
273. Flekkøy EG (1993) Lattice Bhatnagar-Gross-Krook models for miscible fluids. Phys Rev E 47(6):4247–4257
274. Qian YH, D'Humires D, Lallemand P (2007) Lattice BGK Models for Navier-Stokes equation. Europhys Lett 17(6):479–484
275. Sullivan SP, Sani FM, Johns ML, Gladden LF (2005) Simulation of packed bed reactors using lattice Boltzmann methods. Chem Eng Sci 60(12):3405–3418
276. Yang Y (2013) Lattice Boltzmann simulation of flow and mass transfer in porous media with photo bioreaction (In Chinese). Chonqqing University, China
277. He X, Luo LS (1997) A priori derivation of the lattice Boltzmann equation. Phys Rev E 55(6):6333–6336

278. He X, Luo LS (1997) Theory of the lattice Boltzmann method: From the Boltzmann equation to the lattice Boltzmann equation. Phys Rev E 56(6):6811–6817
279. Guo Z, Shi B, Wang N (2000) Lattice BGK model for incompressible Navier-Stokes equation. Academic Press Professional, Inc.
280. Lin CN, Wu SY, Chang JS (2006) Fermentative hydrogen production with a draft tube fluidized bed reactor containing silicone-gel-immobilized anaerobic sludge. Int J Hydrog Energy 31(15):2200–2210
281. Zhang ZP, Show KY, Tay JH, Liang DT, Lee DJ (2008) Biohydrogen production with anaerobic fluidized bed reactors—a comparison of biofilm-based and granule-based systems. Int J Hydrog Energy 33(5):1559–1564
282. Liao Q, Yang YX, Zhu X, Chen R, Fu Q (2017) A simulation on flow and mass transfer in a packed bed photobioreactor for hydrogen production. Int J Heat Mass Tran 109:1132–1142
283. Guo Z, Zheng C, Shi B (2002) An extrapolation method for boundary conditions in lattice Boltzmann method. Phys Fluids 14(6):2007–2010
284. Guo Z, Zhao TS (2002) Lattice Boltzmann model for incompressible flows through porous media. Phys Rev E 66(3):6304–6314
285. Liao Q, Yang YX, Zhu X, Chen R (2013) Lattice Boltzmann simulation of substrate solution through aporous granule immobilized PSB-cell for biohydrogen production. Int J Hydrog Energy 38(35):15700–15709
286. Yu D, Mei R, Wei S (2010) A multi-block lattice Boltzmann method for viscous fluid flows. Int J Numer Meth Fl 39(2):99–120
287. Wang M, Wang J, Pan N, Chen S (2007) Mesoscopic predictions of the effective thermal conductivity for microscale random porous media. Phys Rev E 75(3):6702–6712
288. Liao Q, Yang Y, Zhu X, Chen R, Fu Q (2017) Pore-scale lattice Boltzmann simulation of flow and mass transfer in bioreactor with an immobilized granule for biohydrogen production. Chin Sci Bull 62(1):22–30
289. Yu D, Girimaji SS (2006) Multi-block Lattice Boltzmann method: Extension to 3D and validation in turbulence. Phys A 362(1):118–124

Chapter 8
Fermentative Alcohol Production

Mariano Martín, Antonio Sánchez and John M. Woodley

Nomenclature

a	Specific area (m^{-1})
a′	Horizontal diameter of the bubble (m)
A	Contact area (m^2)
A_r	Instantaneous area of the bubble (m^2)
A_{ref}	Bubble surface area as a rigid body (m^2)
b′	Vertical diameter of the bubble (m)
b	Bubble cup half height (m)
c	Concentration (mol L^{-1})
c_A	Concentration of species A (mol L^{-1})
C	Bubble cup half length (m)
C*	Saturation concentration (kg m^{-3})
C_D	Drag coefficient
C_i	Constants
D_i	Diffusion coefficient of component i (m^2 s^{-1})
d_{32}	Sauter meandiameter (m)
d_b	Initial bubble diameter (m)
d_{eq}	Equivalent bubble diameter (m)
d_{max}	Maximum stable bubble diameter (m)
D_{AB}	Molecular diffusivity of A in B (m^2 s^{-1})
eff	Fouling coefficients
E	2C/2b as defined in Fig. 7
Et	Ethanol concentration (g dm^{-3})
Et^*	Saturation concentration of ethanol (g dm^{-3})
Fl_G	Aeration number $Fl_G = \dfrac{Q_c}{NT^3}$

M. Martín (✉) · A. Sánchez
Departamento de Ingeniería Química y textil, University of Salamanca,
Plz. Caídos 1–5, 37008 Salamanca, Spain
e-mail: mariano.m3@usal.es

J. M. Woodley
Department of Chemical and Biochemical Engineering, Technical University of Denmark,
Søltofts Plads 229 2800 Kgs. Lyngby, Copenhagen, Denmark

Fr	Froude number $\text{Fr} = \dfrac{TN^2}{g}$
g	Gravity constant, 9.8 m s^{-2}
G	Glucose concentration (g dm^{-3})
Gr	Grashof number $\text{Gr} = \dfrac{d_b^3 \rho \cdot \Delta\rho \cdot g}{\mu \cdot D_{AB}}$
h$_i$	Film resistance inside the vessel (J m^{-2} K^{-1})
h$_e$	Film resistance of the fluid (J m^{-2} K^{-1})
k	Film resistance of the jacket (J m^{-2} K^{-1})
k$_L$	Liquid film resistance (m s^{-1})
$k_{H,i}$	Henry coefficient of component I (mol l^{-1} atm^{-1})
K_s	Substrate concentration corresponding to 1/2 μ_{max} (g dm^{-3})
K_I	Inhibition equilibrium constant (mol l^{-1})
K_{mj}	Concentration of the metabolite, where the rate is equal to half of Vmax and j is the number of corresponding reactions (mM)
K_{isj}	Inhibition constant for the substrate, where j is number of corresponding reactions (mM)
K_{iij}	Inhibition constant for the inhibitor, where j is the number of corresponding reactions (mM)
K_{aj}	Activation constant for the activator, where j is the number of corresponding reactions (mM)
k$_G$	Gas phase resistance to mass transfer (m s^{-1})
K	Global phase resistance to mass transfer (m s^{-1})
k$_i$	Interphase resistance to mass transfer (m s^{-1})
k$_L$a	Volumetric mass transfer coefficient (s^{-1})
k$_f$	Conductivity (J s^{-1} m^{-1} K^{-1})
K$_s$	The half velocity constant (M)
m	Maintenance utilization (h^{-1})
N$_i$	Molar flux (mol m^{-2} s^{-1})
N	Impeller speed (s^{-1})
Nu	Nusselt number $Nu = \dfrac{h \cdot L}{k_f}$
P	Product (Ethanol) concentration (g dm^{-3})
P	Impeller power (W)
P$_g$	Aerated power (W)
P$_o$	Power number $P_o = \dfrac{P}{T^5 N^3 \rho}$
P_m	Ethanol concentration above which cells do not grow (g dm^{-3})
P'_m	Ethanol concentration above which cells do not produce ethanol (g dm^{-3})
Pe	Peclet number $\text{Pe} = \dfrac{U_B \cdot d_b}{D_{AB}}$
Pr	Prandtl number $\text{Pr} = \dfrac{Cp \cdot \mu}{k}$
Q$_c$	Gas flow rate (m^3 s^{-1})
Q	Pumping capacity (Eq. 1)
q	Specific rate of substrate utilization (g dm^{-3} h^{-1})
q$_{max}$	Maximum specific rate of substrate utilization (g dm^{-3} h^{-1})

R	Bubble radius (m)
R_g	Constant of the gases (Pa m^3 mol^{-1} K^{-1})
RPD	Gasification factor P_g/P
r_S	Overall reaction rate(mol l^{-1} s^{-1})
r_g	Rate of cell growth (g dm^{-3} h^{-1})
r_d	Rate of cell death (g dm^{-3} h^{-1})
r_{sm}	Rate of substrate consumption for maintenance (g dm^{-3} h^{-1})
Re	Reynolds number Re $= \dfrac{T^2 N \rho}{\mu}$
S	Substrate concentration (g dm^{-3})
s	Element replacement rate (s^{-1})
Sc	Schmidt number Sc $= \dfrac{\mu}{\rho \cdot D_{AB}}$
Sh	Sherwood number Sh $= \dfrac{k_L d_b}{D_{AB}}$
t	Time (s)
T	Impeller diameter (m)
T_i	Impeller blades width (m)
T	Temperature (K)
U	Global heat transfer coefficient (J m^{-2} K^{-1})
U_B	Terminal rising velocity of the bubbles (m s^{-1})
V_{max}	Maximum reaction velocity (mol l^{-1} s^{-1})
V	Volume (dm^3)
x	Width of the wall (m)
X	Biomass concentration or xylose concentration (g dm^{-3})
Y_i	Yield coefficient
$Y_{X/S}$	Biomass yield from substrate
$Y_{Et/X}$	Ethanol yield from biomass
u_G	Superficial gas velocity (m s^{-1})
V	Liquid volume (m^3)
w	Blade speed (m s^{-1})
We	Weber number We $= \dfrac{\rho N^2 T^3}{\sigma}$
x_A	Molar fraction of species A
z	Vertical coordinate (m)
z_b	Film thickness (m)

Greek Symbols

α, β, α', β', α'', β'' and δ	Empirical coefficients
α	Fraction of molecules hitting the surface
α_i	Fraction of the bubble surface
β_i	Mass transfer coefficient (m s^{-1})
β, δ	Empirical coefficients
β	Inhibition constant
δ_o	Boundary layer thickness (m)

ε	Dissipated energy (W kg^{-1})
ε_G	Gas hold up
ρ	Liquid density (kg m^{-3})
ρ_G	Gas density (kg m^{-3})
ρ_i	Reaction rate of component i (mol l^{-1} h^{-1})
μ	Liquid viscosity (Pa s)
σ	Surface tension (N m^{-1})
ε_G	Gas hold up
η	Turbulence characteristic length (m)
ν	Kinematic liquid viscosity (m^2 s^{-1})
γ	Stress (N m^{-2})
μ_{max}	Maximum specific growth rate of the biomass (h^{-1})
μ	Specific growth rate of the biomass (g dm^{-3} h^{-1})
μ_w	Water viscosity (Pa s)
γ	Inhibition constant
υ_i	Specific productivities of component i

1   Introduction

Bioethanol production is typically focused on the use of sugar to obtain ethanol via anaerobic fermentation. This has been the main path used by most first and second generation bioethanol plants all over the world. However, this particular case only covers one example of units and mechanisms for the production of alcohols intended as fuels. A broader view of the problem presents two different feedstocks, not only sugar but also syngas. The principles for the fermentation of both resources are similar, although, while sugar fermentation is a single phase reaction, liquid, where a solution of water and ethanol is produced in jacketed stirred tank reactors, the use of syngas expands the complexity into gas-liquid type bioreactors. These two phase reactors are governed by the mass transfer between the gas, the raw materials, and the liquid, where the ethanol will be obtained. This fact provides a further degree of freedom in terms of reactor design, not only stirred tanks but also bubble columns can be used. This alternative has its supporters but it has not been fully deployed. Furthermore, ethanol is not the only fermentative alcohol of choice as a biofuel, and lately, biobutanol has gained particular interest. In order to cover the basics for the design of the units used for such processes, we have divided this chapter into the principles and the applications. Section 2 presents the hydrodynamics of the units as well as mass transfer rate limitations in the case of gas-liquid systems; the energy transfer required to cool an exothermic reaction and the kinetic mechanisms. Section 3 presents examples for bioethanol and biobutanol production. The kinetics of the production of alcohols from syngas or glucose is based on the Monod model that evaluates the growth of microorganisms such as *Sacharomices cerevisiae, Zymonas Mobilis*, etc. While the basic model is quite

simple, the fact that alcohols inhibit that growth requires the addition of terms to account for that inhibition in the models.

2   Reactor Design Principles

This section is divided into single phase reactors (ignoring the presence of solids), and gas-liquid reactors for application in the fermentation of sugars and syngas, respectively. This classification allows presentation of the main features of the design of such units from the hydrodynamic, as well as mass/heat transfer perspective considering the dispersion of syngas in the fermentation broth.

2.1   Liquid Systems

Within this subsection the units devoted to the fermentation of sugars are presented. This is the base case for aerated stirred tanks that will be presented in Sect. 2.2. We consider the internal hydrodynamics as well as the power input responsible for the fluid circulation in the tanks. We follow this with a discussion about heat removal. Aerobic fermentations are exothermic, and since they operate at near ambient temperature, 32–38 °C, this makes heat transfer an important challenge to be addressed.

2.1.1   Hydrodynamics

The internal flow pattern in a stirred tank is generated by the geometry, the baffles and the impeller (or agitator) used. While the geometry is often standard, and the baffles follow certain rules-of-thumb in terms of allocation and size [1], there are a number of impellers available such as Rushton turbines, pitched blade turbines, propellers and anchors. The typical classification considers those which generate an axial flow (e.g. pitched turbines), and those which generate a radial flow (e.g., Rushton turbines). Figure 1 shows the geometry of a number of commercial impellers typically used in industry [2].

Mixing within the tanks consists of bringing into contact high velocity streams inside the tank with stagnant regions of fluid so that stresses are generated on the contact surface. This mechanism develops turbulent eddies that will be incorporated in the general flow. High turbulent velocity is required for an effective mixing operation. The stream generated by the impeller must generate enough liquid flow in order to move the whole bulk liquid, while at the same time generate kinetic energy to balance the shear stress, and enough velocity so that dead volumes are minimized. Thus, the quality of mixing in a tank can be quantified using two parameters—the mixing time and the pumping capacity. The mixing time refers to
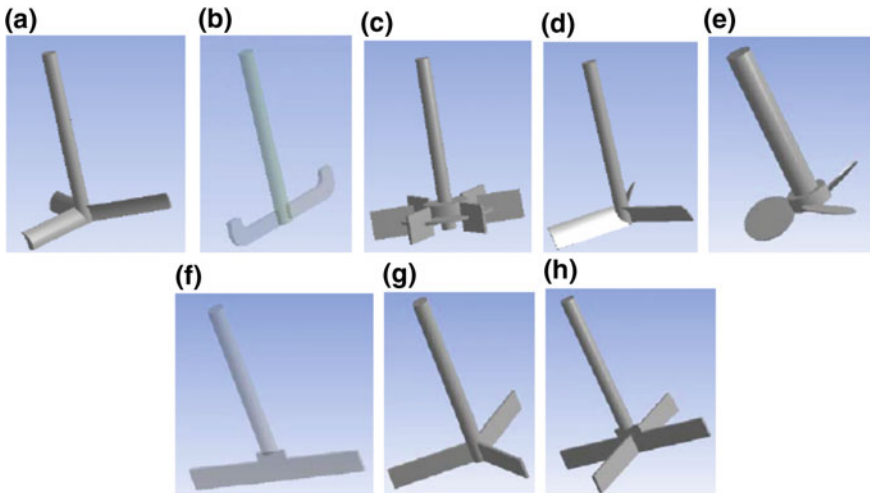
Fig. 1 Impellers geometry **a** pitched curved blade turbine; **b** anchor type turbine; **c** Rushton turbine; **d** pitched curved blade turbine; **e** propeller; **f** two bladed turbine; **g** three bladed turbine; **h** four blade turbine

the time it takes to reach 90–95% of homogeneous concentration in a tank [3]. It is proportional to the circulation time in the tank given by the liquid volume divided by the flow velocity, which is proportional to $N \cdot T^3$, where N is the impeller speed and T its diameter. As a result, according to Gogate et al., the mixing time is inversely proportional to the impeller speed [4]. With respect to the pumping capacity, it is assumed that the impeller behaves as a pump that moves the fluid across the tank. Equation (1) shows the expression for pumping capacity [5]:

$$Q = N_Q \cdot N \cdot T^3 \tag{1}$$

where N_Q is the dimensionless discharge coefficient.

Since the impeller acts as a pump, the power provided can be computed from an analysis of the forces acting on the impeller blades as it rotates inside a liquid with a relative velocity w [6]. The dynamic pressure exerted on the blade can be written as $\frac{1}{2}\rho w^2$, while the theoretical force is obtained by multiplying this pressure by the blade area, A. So, the theoretical force is written as $F_t = \frac{1}{2}\rho w^2 A$. The actual force on the blade is related to the theoretical force by a drag coefficient C_D, so that the force becomes:

$$F_a = \frac{1}{2}\rho w^2 A C_D \tag{2}$$

A definition of power is obtained multiplying force by velocity, therefore giving an expression for power:

$$P = C_D \frac{1}{2} \rho w^3 A \tag{3}$$

For a paddle agitator, the frontal area A is a combination of the length of the blade and its width. Both are functions of the impeller diameter, T; thus $A \propto T^2$. Since velocity is a function of impeller diameter and speed of rotation, then $w \propto NT$. Combining these relations gives the following description of power:

$$P \propto N^3 T^5 \tag{4}$$

An experimentally proved law derived from dimensional analysis, called the "propeller law", states that the theoretical power requirement of the agitator is given by:

$$P = \rho N^3 T^5 \tag{5}$$

And the actual power, P, transmitted by the agitator is related to Eq. (5) through a coefficient, P_o.

$$P = P_o \rho N^3 T^5 \tag{6}$$

Typically P_o is termed the Power Number. The power consumed in a tank is usually calculated from the torque needed to move the fluid inside. In this way, the power transmitted by an agitator given by Eq. (6) can be related to the applied torque, M_r, [6], as follows:

$$P = 2\pi N M_r = P_o \rho N^3 T^5 \tag{7}$$

However, by means of dimensional analysis it has been proved that the power an impeller provides depends on the geometrical characteristics of the system as well as on dimensionless numbers like the Power Number, the Reynolds Number and the Froude Number (Fig. 2).

The Power Number, defined by Eq. (6), accounts for the friction forces, so it is a measure of the resistance of the liquid to move. It is proportional to the ratio between the resistance force acting on the area of the blade and the inertial force. The inertial force is related to the momentum transfer due to the global movement of the fluid. For baffled reactors, the Power Number is constant. Although from Eq. (5) it could be inferred that the number of blades should increase the power proportionately, the wake influence of upstream blades is similar to a sheltering effect and consequently the power only increases in proportion to the number of blades raised to a power in the range of 0.5–0.8. Thus, if more blades are added, the blades are subject to a diminishing local normal velocity.

The Froude Number (Fr = $\frac{TN^2}{g}$), where T is impeller diameter, g is gravity and N the revolutions per minute accounts for the relationship between the inertial force

Fig. 2 Scheme for a jacketed
stirred tank reactor
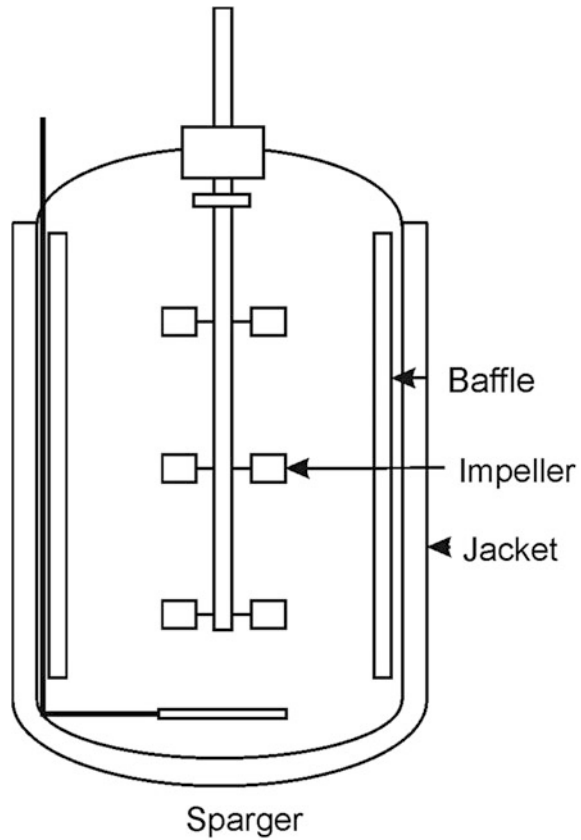
and the gravity per unit area acting on the fluid. It has an important effect when
waves are developed on the liquid surface in the form of vortices.

The Reynolds Number (Re $= \frac{T^2 N \rho}{\mu}$), where ρ and μ are fluid density and vis-
cosity, respectively, represents the ratio between the kinetic forces and the resis-
tance forces. It also describes the flow regime in the tank [7].

2.1.2 Heat Transfer

The energy generated in any reaction or bio-reaction must be dissipated to maintain
isothermal operation avoiding damages to the microorganisms. The heat transfer is
computed using the standard design equation for heat exchangers as follows:

$$Q = U \cdot A \cdot \Delta T \tag{8}$$

where Q is the heat load, A is the contact area, ΔT the temperature gradient and U,
the global heat transfer coefficient. U is computed considering the film resistance

inside the vessel, h_i, as well as the film resistance of the jacket, k, and the fluid, h_e [8]. x is the width of the wall and eff are the fouling coefficients.

$$\frac{1}{U} = \frac{1}{h_i} + \text{eff}_{\text{interior}} + \frac{x}{k} + \text{eff}_{\text{exterior}} + \frac{1}{h_e} \qquad (9)$$

The internal heat transfer resistance is computed using Eq. (10) for Rushton turbines [8], where k_f is the conductivity, D_a is the diffusion and Pr is the Prandtl number and μ_w is water viscosity as a reference.

$$h_i = \frac{k_f}{D_a} \cdot 0.74 \cdot \text{Re}^{0.67} \cdot \overset{0.33}{\text{Pr}} \left(\frac{\mu}{\mu_w}\right)^{0.14} \qquad (10)$$

Likewise, the heat transfer resistance from cooling water flowing inside the jacket can be computed in a similar way as follows:

$$h_e = \frac{k_f}{D_e} \cdot 0.023 \cdot \text{Re}^{0.8} \cdot \overset{0.33}{\text{Pr}} \left(\frac{\mu}{\mu_w}\right)^{0.25} \qquad (11)$$

D_e is the diffusion coefficient.

2.2 Gas-Liquid Systems

The second main system for the production of alcohols is the fermentation of syngas. This system includes another phase, a gas phase, that must be dispersed in the liquid to provide the feed to the microbial cells. The gas from the bubbles gets dissolved into the liquid phase and is consumed by the cells, which metabolize it to produce ethanol. There are two main bioreactor designs possible for such a fermentation, bubble columns and stirred tank reactors. The former are tanks in which the gas flow injected generates the mixing and the flow pattern inside. The latter are just a modification of the units described for the previous case. A sparger is added to inject the gas phase into the liquid, see Fig. 2. The flow dynamics of gassed stirred tanks depends on both, the stirring and the gas flow.

2.2.1 Hydrodynamics: Gas-Liquid Contact Equipment

- **Bubble Columns**

The hydrodynamics inside a bubble column is generated by the gas injected through the dispersion device. The flow pattern developed depends on the flow rate but also on the bubble size, as well as on the geometry of the equipment and on the
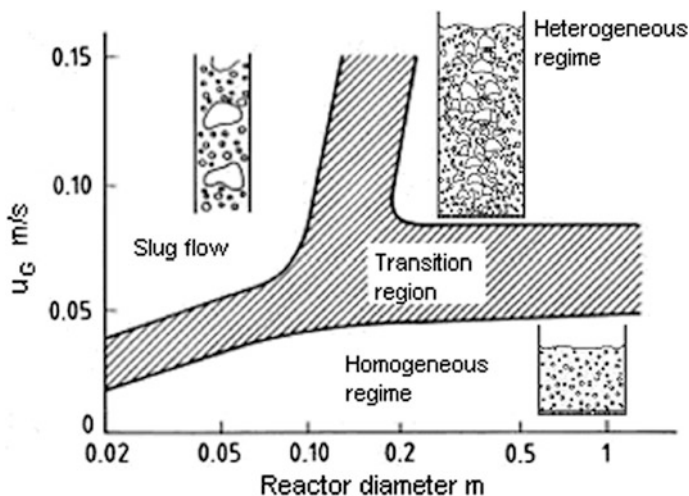
Fig. 3 Flow regimes in a bubble column (Adapted from [9, 10])

physical properties of the liquid. Consequently, three flow regimes are typically found, see Fig. 3. The *homogeneous flow regime* is characterized by a narrow bubble size distribution. The bubbles are distributed across the reactor uniformly. This regime holds up to flow rates of 0.03 m/s, or even as high as 0.08 m/s, depending on the sparger type. As the flow rate increases, the uniform distribution of gas bubbles disappears as turbulent flow develops. This second regime is referred to as the *heterogeneous* or *churn-turbulent flow regime* where a bimodal distribution of bubbles is created. Large bubbles or agglomerates of bubbles form and travel upward at high velocity together with small bubbles which are actually transported downward in a zone close to the column wall. In small diameter bubble columns, like the ones used at laboratory scale, a third regime can be identified, termed slug flow. Slug flow occurs at large flow rates and generates large bubbles that are stabilized at the column wall. Figure 3 shows the three regimes as a function of the superficial gas velocity and the diameter of the column [9, 10].

The bubble dispersion, characterized by equivalent diameter d_{eq}, generated can be characterized by the contact area, a, and the gas hold up, ε_G. The gas hold up refers to the volume of gas within the reactor. Both variables are linked as follows [11]:

$$a = \frac{6\varepsilon_G}{d_{eq}} \qquad (12)$$

The area of the gas-liquid interface is one of the most important process parameters at high reaction rates (e.g., when a bubble column is employed as an absorber). Therefore, the interfacial area becomes a crucial factor in equipment

Fig. 4 Equivalent diameter calculations (Eq. 13)
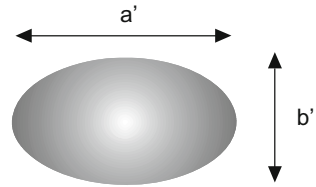
sizing. Like gas hold-up, interfacial area depends on the geometry, the operating conditions, and the gas-liquid system. Mixing deforms the bubbles up to their breaking point, determining the distribution. The equivalent diameter is calculated considering the bubbles as ellipsoids, Fig. 4:

$$d_{eqi} = \left(a'^2 \cdot b'\right)^{(1/3)} \tag{13}$$

The Sauter mean diameter is defined as the ratio between the volume and the surface area and can be computed as follows:

$$d_{32} = \frac{\sum n_i d_{eqi}^3}{\sum n_i d_{eqi}^2} \tag{14}$$

where n_i is the number of bubbles with an equivalent diameter d_{eqi}.

- **Stirred Tank Reactors**

Aside from the use of bubble columns, stirred tanks can also be used for gas-liquid dispersion and mixing. In this case the gas dispersion is generated by combining the gas flow together with the flow pattern generated by the impeller. The two variables that characterize the flow are the dissipated power in the fluid and the gas hold-up. The gas phase affects the mixing and the power consumed. The flow developed by the impeller pushes the bubbles and guides them throughout the tank, against the natural rising tendency of the bubbles (on account of their lower density). This can lead to a great accumulation of gas below the impeller, which will result in hydrodynamic instabilities. In reality, any impeller capable of maintaining the power input in the absence of aeration when the gas phase is introduced will be more stable and its scale-up also be easier. Therefore, each impeller has a particular effect on the gas phase and so the result of the presence of the gas phase on the power input depends on the impeller. For example, it is reported by Vogel and Todaro that Rushton turbines and down flow blades show a reduction in the power input as a result of the gas flow rate [12]. However, concave blades maintain up to 70% of the unaerated power. The equation to compute the aerated power in a gas-liquid system is a modification from the one developed for single phase stirred tanks as follows:

$$P = P_o(RPD)\rho N^3 T^5 \tag{15}$$

where RPD is the relative demand (or the gasification factor) also defined as the ratio between the aerated and the unaerated power input (P_g/P). According to Vogel and Todaro this term depends on the shape of the blades, the gas flow rate, the impeller speed and its diameter [12]. Typical values for the RPD coefficient for Rushton turbines are 0.4, while in the case of concave parabolic blades, it is almost 0.9. If the blades are semi-circular the value is around 0.7. However, when high power is needed, disk turbines with more than 6 blades are used. Turbines with up to 16 blades also result in RPD values around 0.4.

In order to determine the (P_g/P) ratio, empirical correlations based on dimensional analysis have been developed relating the geometrical characteristics of a given impeller to the actual power input. The studied variables have been the stirrer speed, N, the diameter of the stirrer, T, the liquid properties such as density, ρ viscosity, μ, and surface tension, σ, the gas flow, Q. The correlations depend also on dimensionless numbers like the Flow Number of the Weber number [13].The Flow Number, Fl_G, accounts for the effect of the gas phase on the agitation and is defined by Eq. (16) where Q_c is the gas flow rate.

$$Fl_G = \frac{Q_c}{NT^3} \tag{16}$$

For a Rushton turbine, the correlation developed by Hughmark [14], is given by Eq. (17), where V is the volume of the mixture and T_i a blade width:

$$\frac{P_g}{P} = 0.1 \cdot \left(\frac{N^2 T^4}{g T_i V^{2/3}}\right)^{-1/5} \cdot \left(\frac{Q_c}{NV}\right)^{-1/4} \tag{17}$$

Alternatively, Michel and Millar proposed another correlation, Eq. (18) [4]:

$$P_g = 0.783 \left(\frac{P_o^2 NT^3}{Q_c^{0.56}}\right)^{0.459} \tag{18}$$

Finally, design books also present the following Eq. (19):

$$\frac{P_g}{P} = 1 - 1.26 \cdot \frac{Q_c}{NT^3} \tag{19}$$

Although alcohol production will take place in fermentation broth (essentially water), the rheology of the liquid also affects the power input. For instance, pseudoplastic fluids consume less power within a certain range of Reynolds number. Next to the impeller the high velocity gradients result in a small apparent viscosity close to the impeller that increases as the distance from the impeller increases. Thus, the liquid can be in a laminar regime consuming low power.

   The power provided by the impeller together with the gas flow rate are responsible for the bubble dispersion and the flow regime, see Fig. 5 [6]. We distinguish three main regimes:

(1) Flooding: The impeller is overwhelmed by the gas and the real contact is poor.
(2) Before loading bubbles rise with little effect from the impeller.
(3) Loading: The impeller can disperse the gas phase through the upper part of the tank.
(4) Complete dispersion: Bubbles are scattered throughout the tank and the gas phase is recycled to the impeller.

   In the case of high gas flow rates, the gas phase can remain next to the impeller reducing the power input given by the impeller [15].

   Bubble dispersions are characterized by their mean bubble size, ε_G, as well as the specific area. They all play an important role in mass transfer processes since they determine the residence time as well as the contact between the two phases.

   The theoretical study of the bubble mean diameter in a gas liquid dispersion has traditionally been analysed according to the Kolmogorov's theory of isotropic turbulence. The maximum stable diameter, d_{max}, for a bubble or a drop is a function of the Weber Number (We) of the system [16].

$$d_{max} = C_1 \cdot We^{-0.6} = C_2 \cdot \varepsilon^{-0.4} = C_3 \cdot N^{-1.2} \tag{20}$$

   It is widely accepted that the dispersed energy, ε, corresponds to the power input per unit mass, in all the equations proposed above [17]. Thus, Eq. (20) can be rearranged as follows:

$$d_{max} = C_4 \frac{\sigma^{3/5}}{\rho^{3/5} \varepsilon^{2/5}} \tag{21}$$

where C_i are constants.

   The Sauter mean diameter, d_{32}, is considered to be proportional to the maximum stable diameter [16, 18]. Therefore, we can compute d_{32} as follows:

Fig. 5   Flow regimes inside an aerated stirred tank

Higher N →
← Larger Q
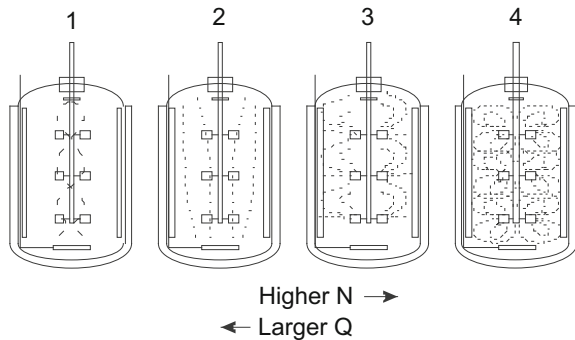
$$d_{32} = C_5 \frac{\sigma^{3/5}}{\rho^{3/5}\varepsilon^{2/5}} \tag{22}$$

However, Eq. (22) does not include the effect of the gas phase within the tank. Therefore, it was included as in Eq. (23) by Calderbank [18].

$$d_{32} = C_6 \frac{\sigma^{3/5}}{\rho^{3/5}\varepsilon^{2/5}} \varepsilon_G^{1/2} \tag{23}$$

In contrast, if the bubble size is not controlled by the bubble break-up process, the Sauter mean diameter is proportional to the minimum diameter of the bubbles in the dispersion [16]. Therefore,

$$d_{32} = C_7 \cdot \varepsilon^{-0.25} \tag{24}$$

In the equations above, the coefficients C_i are functions of the dispersion device and the impeller type. Thus, to simplify the theoretical considerations, an empirical formula is commonly used, where k_d is an adjustable parameter:

$$d_{32} = k_d \cdot \left(\frac{P_g}{V}\right)^\delta \tag{25}$$

This equation has been obtained as the solution to a population balance assuming turbulent break-up of the bubbles whose stability is determined by the surface tension [19]. Several correlations are available in the literature. For example, Bouaifi proposed Eq. (26) for the air-water physical system [20]:

$$d_{32} = 10.1 \times 10^{-3} \cdot \left(\frac{P_g}{V}\right)^{-0.20} \tag{26}$$

The relative volume of gas in the tank is given by the gas hold-up. The empirical equations for the gas hold-up are of the following form [20]:

$$\varepsilon_G = C_1 \left(\frac{P_g}{V}\right)^{\alpha'} u_G^{\beta'} \tag{27}$$

where u_G is the superficial gas velocity. The equation given by Shulka et al. [21] is:

$$\varepsilon_G = C_2 \left[\frac{P_g}{V}(1-\varepsilon_G)\right]^{\alpha''} u_G^{\beta''} \tag{28}$$

Although more complex correlations have also been developed to include the particular hydrodynamics generated by the impeller (e.g., Kudrewizki and Rabe

[22]), it is also possible to adjust Eq. (28). For Rushton turbines, Gogate et al. [4] presented the following correlation:

$$\varepsilon_G = 0.21 \left[\frac{P_g}{V} (1 - \varepsilon_G) \right]^{0.27} u_G^{0.65} \qquad (29)$$

Using the gas hold-up, we compute the superficial contact area (in a similar way to bubble columns), Eq. (12). Alternatively a theoretical correlation has been proposed based on Kolmogorov's theory, by Calderbank [18]:

$$a = 1.44 \left[\frac{(P_g/V)^{0.4} \cdot \rho^{0.2}}{\sigma^{0.6}} \right] \left(\frac{u_G}{U_B} \right)^{0.5} \qquad (30)$$

where, U_B is the terminal rising velocity of the bubbles.

2.2.2 Mass Transfer Principles

The gas phase injected into the reactor carries the reactants. The microorganisms are in the liquid phase and the gas must be transported to them. Thus, three stages are to be considered as resistances to the mass transfer, specifically, mass transfer in the gas phase, the mass transfer at the interphase and the mass transfer in the liquid side. The resistances to the mass transfer are also dependent on the hydrodynamics of each phase.

Two film theory: Whitman in 1923 proposed the first attempt to represent the mass transfer between two fluid phases [23]. In his theory, he assumed that there is a laminar layer on each side of the interface between two fluids, while fluid turbulence occurs in the bulk of the phases as can be seen in Fig. 6. In the bulk region, the resistance to mass transfer is negligible due to turbulent eddies and the chaotic movement of the molecules. However, the mass transfer through the laminar film is due to molecular diffusion. As a result, the concentration gradient is linear in the laminar film and zero in the bulk of the phases.

Furthermore, the mass transfer is supposed to be in equilibrium at the interface. As a result, this theory can only be applied in case the concentration gradients are quickly developed compared to the transfer time. Then, using subscript L for the liquid phase, G for the gas phase, B for the fluid bulk and i for the interface, the rate of mass transfer of component A, N_A, is given by:

$$N_A = k_L(c_{LB} - c_{Li}) = k_G(c_{Gi} - c_{GB}) = K(c_{LB} - c_{GB}) \qquad (31)$$

where c_{jk} is the concentration of the solute in phase j, k_i and K are the resistances to the mass transfer in the liquid (L), gas (G) phases and the global one. So that:

Fig. 6 Two-film theory
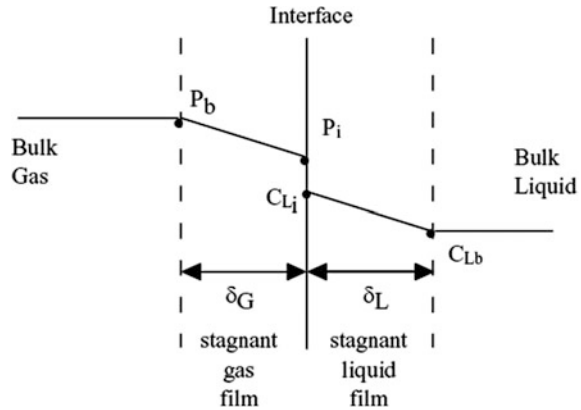
$$\frac{1}{K} = \frac{1}{k_L} + \frac{1}{k_G} \tag{32}$$

k_j (j = L, G) depends on the film thickness as well as on the transport properties. The flow determines the film thickness and it is one on the uncertainties of the theory due to the complexity of characterization.

In case the boundary layer is a turbulent, non-slip surface, both molecular and eddy diffusion must be considered, although the latter is bigger and thus presents a negligible resistance [24].

Even though the two film theory considers that there is an equilibrium at the interface and no diffusional resistance, in liquids containing surfactants the diffusional resistance exists, since surfactants locate at the interface. Furthermore, solute diffusion sometimes causes interfacial turbulence unrelated to the flowing liquid mass. This tends to increase the mass transfer rate. Thus, for completion it is considered that the interface is another resistance to the mass transfer and Eq. (33) becomes:

$$N_A = k_L(c_{LB} - c_{Li}) = k_i(c_{Li} - c_{Gi}) = k_G(c_{Gi} - c_{GB}) = K(c_{LB} - c_{GB}) \tag{33}$$

$$\frac{1}{K} = \frac{1}{k_L} + \frac{1}{k_i} + \frac{1}{k_G} \tag{34}$$

Sherwood et al. [24] determined k_i as the maximum mass transfer rate from a gas surface.

$$\frac{1}{k_i} = \frac{(2\pi R_g T)^{1/2}}{1.006\alpha} \tag{35}$$

α is the fraction of gas molecules colliding with the interface that remains at the liquid phase. $\alpha = 1$ for water, as well as for many simple fluids, and R_g is the gas constant.

It has been experimentally proven that, in gas-liquid processes, the main resistance is usually the resistance of the liquid phase (k_L). Therefore, from now on we present the theory behind predicting k_L. Briefly we discuss three theories:

Penetration theory. Higbie in 1935 developed his theory based on the short contact time between the fluids, resulting in the fact that the concentration gradient does not have the opportunity to reach steady-state [25]. Higbie explained that for a bubble rising through a liquid that absorbs gas, a fluid particle b, initially located on top of the bubble, remains in contact with the gas phase for a time, t, during which the bubble rises a height equal to its diameter. The liquid slips down the bubble. When the contact time is short and the gas diffusion in the liquid phase is slow, solute molecules in solution can never reach a depth equal to z_r, which corresponds to an eddy thickness. Therefore, from the solute point of view the film thickness, z_b is basically infinite [25].

The molar flux of A can be written as:

$$N_A = x_A \cdot (N_A + N_B) - cD_{AB}\nabla x_A \tag{36}$$

where D_{AB} is the diffusion of A into B and x_A is the molar fraction. The unidimensional continuity equation for A is:

$$\frac{\partial c_A}{\partial t} = -\frac{\partial N_{Az}}{\partial z} \tag{37}$$

Combining Eqs. (36) and (37) leads to:

$$N_{Az} = -cD_{AB}\frac{\partial x_A}{\partial z} - x_A\left(\frac{cD_{AB}}{1-x_{Ao}}\right)\frac{\partial x_A}{\partial z}\bigg|_{z=0} \tag{38}$$

Substituting into Eq. (36)

$$\frac{\partial x_A}{\partial t} = D_{AB}\frac{\partial^2 x_A}{\partial z^2} + \frac{D_{AB}}{1-x_{Ao}}\frac{\partial x_A}{\partial z}\bigg|_{z=0}\frac{\partial x_A}{\partial z} \tag{39}$$

The equation is solved using:

$$t = 0, x_A = 0; z = 0, x_A = x_{Ao}; z = \infty, x_A = 0 \tag{40}$$

$$k_L = K\sqrt{\frac{D_{AB}}{\pi t}} \tag{41}$$

Physically, this theory states that the liquid eddies are consecutively retained and released from the gas-liquid interface, defining in this way the contact time of the phases [26].

Surface renewal theory: Danckwerts in 1951 pointed out that Higbies's theory (that considers a constant contact time for the turbulent eddies of the liquid at the

gas surface), was a particular case of a more general situation in which eddies are exposed to different time intervals [27]. In reality, the gas-liquid interface is made up of a large number of surface elements with different exposure times. Since solute penetration depends on the exposure time, an average rate must be calculated per unit of surface area by adding the individual values. Danckwerts suggested that surface element replacement was almost independent of the time it had remained at the surface. Hence the fractional replacement rate for the surface elements:

$$N_A = (c_{A,i} - c_{Ao}) \cdot \sqrt{D_{AB} \cdot s} \tag{42}$$

where s is the element replacement rate. From where the mass transfer coefficient k_L is:

$$k_L = \sqrt{D_{AB} \cdot s} \tag{43}$$

So, it was found that k was proportional to $D_{AB}^{0.5}$ [28, 29]. Independently, similar results were obtained by Kishenevsky [30].

Combined theory of surface renewal and film theory: The concept of combined surface renewal and film theory was developed by Dobbins in 1956 [31]. He pointed out that the film theory (which predicted a proportional relationship between k_L and D_{AB}) considered that surface elements are exposed sufficiently such that they generate a steady-state concentration profile in the film. On the other hand, the penetration theory as well as the surface renewal theory, (which predicts a proportionality between k_L and $D_{AB}^{0.5}$) assume that the surface elements are at an infinite depth and, as a result, the diffusing solute will never reach the interior region of constant concentration. The observed dependency collected in the exponent n, depends on the circumstances, and can be explained considering that the surface elements have a finite depth. If z_b is finite:

$$k_L = \sqrt{D_{AB} \cdot s} \coth\left(\sqrt{\frac{s \cdot z_b^2}{D_{AB}}}\right) \tag{44}$$

In this way the exponent n of the diffusivity is within the range of 0.5–1 [28, 29].

Theory for surface stretch: The final theory was developed by Lightfoot and co-workers [32], looking for a trade-off model. They applied the principles of the penetration-surface renewal theory to particular situations where the interfacial surface, through which mass transfer takes place, varies periodically with time. An example of that is an oscillating bubble. A rising bubble oscillates, and if the flow regime inside the bubble column is turbulent, the main mass transfer resistance can be found in the surface layer of changing thickness. A mean volumetric mass transfer coefficient, $k_L a$, with respect to the area is then calculated as:

$$k_L a = \frac{\left(\frac{A_r}{A_{ref}}\right)\sqrt{\frac{D_{AB}}{\pi t}}}{\sqrt{\int_0^{t/t_r}\left(\frac{A_r}{A_{ref}}\right)^2 dt}} \tag{45}$$

where A is the bubble area.

Mass transfer in fluids, **spheres**: In gas-liquid contact equipment, the gas phase is dispersed as bubbles into the liquid phase. In spite of their usually irregular shape, the first approach to study mass transfer from bubbles is to assume that they are spheres. An equation for the mass transfer rate from spheres, whether they are bubbles, drops or solid particles, was proposed by Sherwood et al. in 1975 [24]. For steady-state flow over a submerged spherical particle and considering that only diffusion takes place:

$$\frac{df}{dt} = -D_{AB} \cdot 4\pi r^2 \frac{dc}{dr} \tag{46}$$

where r is the distance from the centre of the particle. Integrating Eq. (46) between limits from the surface, $R = d_b/2$, to infinity:

$$\frac{df}{dt} \cdot \frac{1}{R} = -4 \cdot D_{AB} \cdot \Delta c \tag{47}$$

So that the Sherwood number becomes:

$$Sh = \frac{kd_b}{D_{AB}} \tag{48}$$

where d_b is bubble diameter and k the mass transfer coefficient. And:

$$k \cdot \Delta c = \left(\frac{-1}{A_{ref}}\right)\frac{df}{dt} \tag{49}$$

From Eqs. (47 to 49) it can be calculated that

$$Sh = 2 \tag{50}$$

However, in forced convection the mass transfer rate is reported to be higher than the one predicted by Eq. (50). Therefore, a term related to the contribution of convection is added to the Sherwood number by the Reynolds (Re) and the Schmidt (Sc) numbers to the purely diffusional term as follows:

$$Sh = 2 + C \cdot (Re)^a Sc^{0.33} \tag{51}$$

where the exponent, a, depends on the geometry of the system. However, the exponent of Sc depends on the nature of the diffusional process [33].

Thus, correlations were developed for small and big bubbles as follows as a function of the Grashof, Gr, and Schmidt, Sc, numbers [34]:

$$\text{Big bubbles} \, (d > 2.5 \, \text{mm}) : Sh = 0.42 \cdot (Sc)^{0.5} \cdot (Gr)^{0.33} \tag{52}$$

$$\text{Small bubbles} \, (d < 0.5 \, \text{mm}) : Sh = 2.0 + 0.31 \cdot (Sc \cdot Gr)^{0.33} \tag{53}$$

The liquid film resistance in the interval among big bubbles and small bubbles increases linearly with bubble size according to the experimental results of Calderbank and Moo-Young [34].

Bubble Columns

Experimental results have been fitted to an empirical equation of the form:

$$k_L a = k \cdot u_G^{\beta} \tag{54}$$

Kawase et al. in 1987 proposed that the contact time between phases in Eq. (41) could be considered as the ratio between the length of turbulence, η, and the turbulent velocity, u, defined by the Kolmogorov's theory of isotropic turbulence [35]. Both magnitudes characterize the turbulent flow developed in a stirred tank.

$$\eta = \left(\frac{\nu^3}{\varepsilon}\right)^{1/4} \tag{55}$$

$$u = (\nu \cdot \varepsilon)^{1/4} \tag{56}$$

ν is the kinematic viscosity. The input power per unit mass was determined by $\varepsilon = u_G \cdot g$ [11].

For a Newtonian fluid, combining Eq. (41) and the contact time proposed by Kawase et al. leads to [35]:

$$k_L = \frac{2}{\sqrt{\pi}} \sqrt{D_{AB}} \left(\frac{\varepsilon \rho}{\mu}\right)^{1/4} \tag{57}$$

In the case of a power law fluid, where n and m are the power flow law coefficients:

$$k_L = \frac{2}{\sqrt{\pi}} \sqrt{D_{AB}} \left(\frac{\varepsilon \rho}{m}\right)^{1/(2 \cdot (1+n))} \tag{58}$$

In order to predict, $k_L a$, not only the liquid phase resistance to mass transfer is needed, but also the contact area between the two phases.

Stirred Tank Reactors

The experimental results were fitted to an empirical equation of the form:

$$k_L a = k \cdot \left(\frac{P_g}{V} \right)^{\alpha} \cdot u_G^{\beta} \tag{59}$$

It has been widely used for the study of stirred tanks. In the case of Non-Newtonian fluids, the effective viscosity must also be considered. Modifications to the correlation above can also be found in the scientific literature. However, the various impellers used and the geometric differences between equipment (baffles, configuration of impellers, etc) make it easier to use empirical correlations for each particular system instead of the theories developed to explain and predict $k_L a$, since the effect of the impeller on the bubbles is not considered in any of the available theories.

The first theory to review is that of Barabash and Belevitskaya [36]. The second has already been described above [37], based on Higbies's Theory.

(A) Barabash's theory for stirred tanks

Barabash and Belevitskaya in 1995 studied mass transfer from bubbles and drops in turbulent flow in mechanically agitated systems [36]. The theory is based on the relationship between the flow of the liquid and the turbulence in the vicinity of the dispersed phase.

According to the scientific literature, the effect of the turbulence on the mass transfer rate can be studied from two points of view. The first approach is based on the diffusion equation in stationary state in the interface considering the effect of the turbulence at the proximity to the bubble surface. The second uses the non-constant diffusion model near the interface.

Experimentally, it has been verified that the relaxation time (the lifetime of the boundary at the interface) of the surface layer is lower than that necessary for the surface renewal given by the variable diffusion model. Thus, before the surface renewal occurs, the diffusion boundary layer has already reached steady-state and the mass transfer can be approximated by a stationary model at the interface.

Barabash and Belevitskaya showed that, according to experimental data, it is possible to divide the study of $k_L a$ in a stirred tank into three different regions [36]. For power inputs lower than 0.1 W/kg, the mass transfer rate is defined by that of the bubbles rising through a non-stirred fluid. From 0.1 to 1 W/kg, mass transfer increases with the dissipated energy. For higher values of dissipated energy, the $k_L a$ remains constant.

The authors proposed relations for determining $k_L a$ for each region:

Zone 1: $\varepsilon < 0.1$ W/kg

This region is characterized by low agitation and ε_G lower than 1%.

The mechanism of mass transfer in this region is similar to one in absence of mixing. There is a difference between the mass transfer in the back of the bubble, (β_{rp}), and the front (β_{fp}). For bubbles of 5 mm, the wake of the bubble represents

about 25% of the total surface of the bubble ($\alpha_{rp} = 0.25$) so that k_La can be calculated by summing the superficial areas .

$$\beta_t = \beta_{rp}\alpha_{rp} + \beta_{fp}\left(1 - \alpha_{rp}\right) \tag{60}$$

In order to calculate the value for the frontal region:

$$\beta_{fp} = \frac{0.65 \cdot D_{AB}}{d_b} \sqrt{Re \cdot Sc} \tag{61}$$

For the back part β_s is used.

This region can also be studied from a different approach. Kendoush in 1994 proposed that the bubble shape in these regions was a spherical cap (see Fig. 6) [38]. Using the analogy between heat and mass transfer, in the absence of viscous warming and based on the Higbie theory, he obtained the relationship between the Nusselt, Nu, and the Peclet, Pe, numbers:

$$Nu = Sh = \frac{2}{\sqrt{\pi}} Pe^{0.5} \tag{62}$$

where the eccentricity terms are included as $E = 2C/2b$ (see Fig. 7)

$$Nu = Sh = \frac{2}{\sqrt{\pi}} Pe^{0.5} \left(\frac{3 \cdot E^2 + 4}{E^2 + 4}\right)^{0.5} \tag{63}$$

Fig. 7 Dimensions of a bubble cup
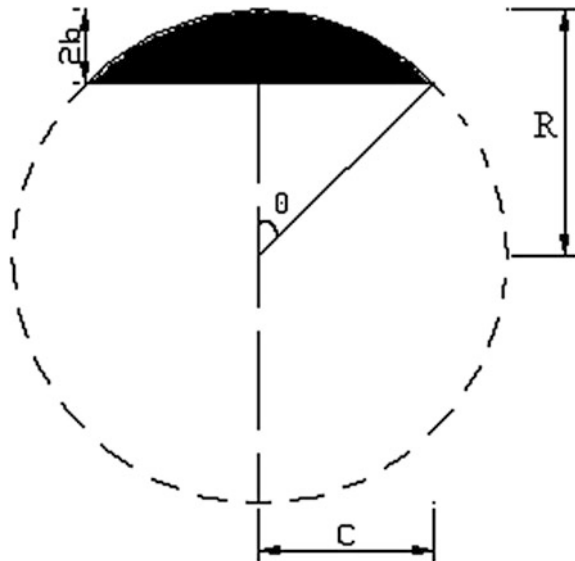
The contribution of both regions to the values of Sh and Nu can be calculated as function of the angle θ.

Zone 2: $0.1 < \varepsilon < 1$ W/kg

Region 2 is characterized by a change in the average energy dissipation rate. This is a complex zone since there is general turbulence surrounding the bubble as long as pulsations cross the boundary layer. It is assumed that the rear part of the bubble occupies 25% of the bubble surface. Turbulent pulsations whose velocities depend on the energy dissipation rate in the wake zone determine the mass transfer coefficient.

For a certain fraction of the frontal surface (α_{fp}) the averaged velocities of the flow around the bubbles determine the mass transfer rates. For the other part of the frontal surface, the pulsation motion, whose intensity depends on the average value of the energy dissipation rate, determines the value of the mass transfer coefficient.

$$\beta_t = 0.25 \cdot \beta_{rp} + \alpha_{fp} \cdot \beta_{fp} + \left(1 - 0.25 - \alpha_{fp}\right)\beta_0 \tag{64}$$

β_0 is given by Eq. (65) and α_{fp} must be calculated experimentally.

Zone 3: $\varepsilon > 1$ W/kg

Stationary state in the boundary layer is assumed as well as the relationships for turbulence damping near the surface being distorted.

$$\beta_s = \frac{0.54 \cdot (\varepsilon \cdot v)^{0.25}}{Sc^{0.5}} \tag{65}$$

(B) Kawase's theory

Kawase and Moo-Young in 1988 derived an expression to determine the $k_L a$ based on Higbie's theory [25, 37]. They used Kolmogorov's isotropic turbulence theory to calculate the exposure or contact time.

When the energy dissipated in the tank is high, the surface renewal is more frequent than for the case of a rising bubble. In this case, the liquid film coefficient depends on the turbulent intensity as energy is dissipated. The exposure time can be determined through the dissipated energy.

The contact time can be calculated using Komogorov's theory as the ratio between the two characteristic parameters of the turbulent eddies, their length, η, and the fluctuation velocity, u. Both depend on the dissipated energy per unit mass, ε, and the kinematic viscosity, v:

$$\eta = \left(\frac{v^3}{\varepsilon}\right)^{1/4} \tag{66}$$

$$u = (v \cdot \varepsilon)^{1/4} \tag{67}$$

For a Newtonian fluid, the liquid film coefficient is:

$$k_L = \frac{2}{\sqrt{\pi}} \sqrt{D_{AB}} \left(\frac{\varepsilon\rho}{\mu}\right)^{1/4} \tag{68}$$

The energy dissipation is that provided by the impeller. If the liquid obeys the power law:

$$k_L = \frac{2}{\sqrt{\pi}} \sqrt{D_{AB}} \left(\frac{\varepsilon\rho}{m}\right)^{1/(2\cdot(1+n))} \tag{69}$$

This is the same theory as for bubble columns but, in this case, the dissipated energy is the power input due to the impellers.

2.3 Kinetic Expressions

Monod kinetics is widely used to model the production of bioproducts. The original specific growth rate was

$$\mu = \mu_{max} \frac{S}{K_s + S} \tag{70}$$

where S is the substrate concentration, μ_{max} is the maximum specific growth rate, and K_s, the half velocity constant. Monod also related the yield coefficient to the specific rate of biomass growth, μ, and the rate of substrate utilization (q):

$$\frac{dx}{ds} = Y_{x/s}, \mu = \frac{Y_{x/s}}{X}, q \cong \frac{1}{Y_{x/s}} \frac{ds}{dt} \tag{71}$$

where X is the cells concentration and Y_i are the yield coefficients. This basic model was modified to account for substrate inhibition, K_i, where q_{max} is the maximum rate of substrate utilization:

$$\mu = \mu_{max} \frac{S}{K_s + S + \frac{S^2}{K_i}} \tag{72}$$

$$q = q_{max} \frac{S}{K_s + S + \frac{S^2}{K_i}} \tag{73}$$

A generalized model type of equation is of the form, where S is the substrate concentration and S_m is the critical inhibition concentration. n and m are constants.

$$q = \frac{q_{max}\left(1 - \frac{S}{S_m}\right)^n}{K_s + S - \left(1 - \frac{S}{S_m}\right)^m} \tag{74}$$

3 Alcohols Production

In this section we present the models for the production of ethanol and biobutanol from sugars and syngas via fermentative processes.

3.1 *Ethanol from Sugars*

3.1.1 First Generation Ethanol

Ethanol production from corn relies on the fermentation of the sugars produced after breaking down the grain structure. The reaction is exothermic, operating at 32–38 °C under a pressure slightly above atmosphere to secure anaerobic conditions. The fermentation time ranges from 24 to 72 h using *Saccharomyces cerevisiae.* A concentration of ethanol in water no greater than 15% can be achieved. Miller and Melick [39] proposed the following mass balance model for the kinetics where X, S and Et are the cells, substrate and Ethanol concentration, r_i, the kinetic rates, Y_i, the yields and V the mixture volume [39]:

$$\begin{cases} Cells \\ V\frac{dX}{dt} = (r_g - r_d)V \\ Substrate \\ V\frac{dS}{dt} = Y_{s/c}(-r_g)V - r_{sm}V \\ Product \\ V\frac{dEt}{dt} = Y_{p/c}(r_g V) \\ Where \\ r_g = \mu_{max}\left(1 - \frac{Et}{Et^*}\right)^{0.52}\frac{SEt}{K_s + S} \\ r_d = k_d X \\ r_{sm} = mX \\ r_p = Y_{p/c}r_g \end{cases} \tag{75}$$

In Fig. 8 the profiles for the cells, the substrate and the ethanol are presented using the values of:

Et* = 93 g/L; n = 0.52; μ_{max} = 0.33 h^{-1}; K_s = 1.7; $Y_{X/S}$ = 0.08 g/g; $Y_{Et/S}$ = 0.45 g/g; $Y_{Et/X}$ = 0.56 g/g; k_d = 0.01 h^{-1}; m = 0.03 g substrate/(g cells h).
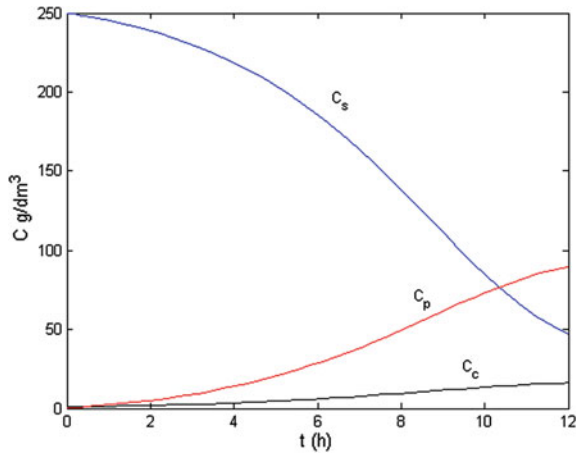
Fig. 8 Species concentration over time

3.1.2 Second Generation Ethanol

It is possible to produce ethanol not only from hexoses but also from pentoses. Second generation ethanol is based on the use of lignocellulosic feedstocks that are composed of a mixture of cellulose, hemicellulose, and lignin. Therefore, the use of both sources of sugars allows a better usage of the crop. However, the fermentation of pentoses is more complex. *Zymomonas mobilis* has been identified as an appropriate microorganism for simultaneously fermenting pentoses and hexoses. Apart from ethanol, other byproducts such as glycerol, succinic acid, acetic acid and lactic acid are also produced. Table 1 shows the reactions and the typical conversions in a second generation bioethanol processes [40].

The reactions to ethanol are exothermic as follows

$$C_6H_{12}O_6 \xrightarrow{\text{yeast}} 2C_2H_5OH + 2CO_2 \quad \Delta H = -84.394 \, \text{kJ} \, \text{mol}^{-1}$$

$$3C_5H_{10}O_5 \xrightarrow{\text{yeast}} 5C_2H_5OH + 5CO_2 \quad \Delta H = -74.986 \, \text{kJ} \, \text{mol}^{-1}$$

The reaction time is about 24 h at 0.12 MPa to avoid entrance of air. The maximum concentration of ethanol in the water is 6–8%. There are a number of models in the literature for the production of ethanol from xylose and glucose. Here we present one given by Krishnan et al. [41]. the modified Monod kinetics is given as follows:

$$\mu = \frac{\mu_m S}{K_s + S + S^2/K_i} \tag{76}$$

Table 1 Reactions and conversions in a second generation bioethanol production

Reaction	Conversion
Glucose $\rightarrow$ 2 Ethanol + 2 CO_2	Glucose 0.92
Glucose + 1.2 NH_3 $\rightarrow$ 6 Z $\cdot$ mobilis + 2.4 H_2O + 0.3 O_2	Glucose 0.04
Glucose + 2 H_2O $\rightarrow$ Glycerol + O_2	Glucose 0.002
Glucose + 2 CO_2 $\rightarrow$ 2 Succinic Acid + O_2	Glucose 0.008
Glucose $\rightarrow$ 3 Acetic Acid	Glucose 0.022
Glucose $\rightarrow$ 2 Lactic Acid	Glucose 0.013
3 Xylose $\rightarrow$ 5 Ethanol + 5 CO_2	Xylose 0.8
Xylose + NH_3 $\rightarrow$ 5 Z $\cdot$ mobilis + 2 H_2O + 0.25 O_2	Xylose 0.03
3 Xylose + 5 H_2O $\rightarrow$ 5 Glycerol + 2.5 O_2	Xylose 0.02
3 Xylose + 5 CO_2 $\rightarrow$ 5 Succinic Acid + 2.5 O_2	Xylose 0.03
2 Xylose $\rightarrow$ 5 Acetic Acid	Xylose 0.01
3 Xylose $\rightarrow$ 5 Lactic Acid	Xylose 0.01

Next, the product, P, inhibition affecting the growth rate, μ, is included as follows:

$$\frac{\mu}{\mu_0} = \left(1 - \left(\frac{P}{P_m}\right)^\beta\right) \tag{77}$$

Thus, the models for the kinetics of the different species involved are as follows, where G represents glucose and X, xylose. The parameters for the fermentation are given in Table 2 [41]. Figure 9 shows the profiles of the main species in the fermentor solving the model given by Eqs. (76)–(79), using the parameters in Table 2.

$$\begin{cases} \text{Cells:} \\ \mu_g = \frac{\mu_{m,g} \cdot S}{K_{s,g} + S + S^2/K_{i,g}} \left(1 - \left(\frac{P}{P_m}\right)^{\beta_g}\right) \\ \mu_x = \frac{\mu_{m,x} \cdot S}{K_{s,x} + S + S^2/K_{i,x}} \left(1 - \left(\frac{P}{P_m}\right)^{\beta_g}\right) \\ \frac{1}{X}\frac{dX}{dt} = \frac{G}{G+X}\mu_g + \frac{X}{G+X}\mu_x \end{cases} \tag{78}$$

$$\begin{cases} \text{Product:} \\ v_{E,g} = \frac{v_{m,g} \cdot S}{K_{s,g} + S + S^2/K_{i,g}} \left(1 - \left(\frac{P}{P_m}\right)^{\gamma_g}\right) \\ v_{E,x} = \frac{v_{m,x} \cdot S}{K_{s,x} + S + S^2/K_{i,x}} \left(1 - \left(\frac{P}{P_m}\right)^{\gamma_x}\right) \\ \frac{1}{X}\frac{dP}{dt} = \left(v_{E,x} + v_{E,g}\right) \end{cases} \text{with} \begin{cases} \mu_{m,g} = 0.152 \cdot X^{-0.461} \\ \mu_{m,x} = 0.075 \cdot X^{-0.438} \\ v_{m,g} = 1.887 \cdot X^{-0.434} \\ v_{m,x} = 0.16 \cdot X^{-0.233} \end{cases}$$
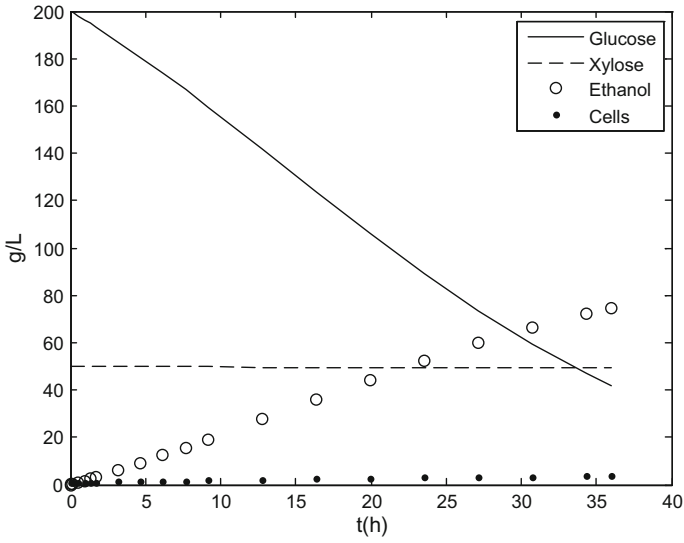
Fig. 9 Ethanol production from hexoses and pentoses [42]

Table 2 Kinetic parameters for fermentation

Parameter	Glucose fermentation	Xylose fermentation
μ_m (h^{-1})	0.662	0.190
ν_m (h^{-1})	2.005	0.250
K_S (g/L)	0.565	3.400
K_S' (g/L)	1.342	3.400
K_i (g/L)	283.700	18.100
K_i' (g/L)	4890.000	81.300
P_m (g/L)	95.4 for P $\leq$ 95.4 g/L	
	129.9 for 95.4 $\leq$ P $\leq$ 129 g/L	59.040
P_m' (g/L)	103 for P $\leq$ 103 g/L	
	136.4 for 103 $\leq$ P $\leq$ 136.4 g/L	60.200
β	1.29 for P $\leq$ 95.4 g/L	
	0.25 for 95.4 $\leq$ P $\leq$ 129 g/L	1.036
γ	1.42 for P $\leq$ 95.4 g/L	0.608
m (h^{-1})	0.097	0.067
$Y_{P/S}$ (g/g)	0.470	0.400
$Y_{X/S}$ (g/g)	0.115	0.162

$$\begin{cases} \text{Sustrate:} \\ -\frac{dS}{dt} = \frac{1}{Y_{X/S}}\frac{dX}{dt} + mX = \frac{1}{Y_{P/S}}\frac{dP}{dt} \\ -\frac{dS}{dt} = \frac{1}{Y_{P/S}}\frac{dP}{dt} \\ -\frac{dxylo}{dt} = \frac{1}{Y_{P/S}}\left(v_{E,x}X\right) \\ -\frac{dglu}{dt} = \frac{1}{Y_{P/S}}\left(v_{E,g}X\right) \end{cases} \quad (79)$$

3.2 Ethanol from Syngas

Second generation ethanol can also be based on gaseous feedstocks. Syngas, a mixture of CO and H_2, can be used in the well-known Fischer-Tropsch reaction, followed by a catalytic synthesis to produce a mixture of alcohols. Alternatively, syngas can also be fermented. The groups of microorganisms that can synthesize valuable products from syngas are known as acetogens. They ferment the gas through the reductive acetyl-CoA pathway with acetate as their main product. Among them we can find the most well studied examples such as *Acetobacterium woodii*, *Alkalibaculumbacchi*, *Butyribacterium methylotrophicum*, *Clostridium aceticum*, *Clostridium ljungdahlii*, *Clostridium thermoaceticum*, *Clostridium auto-ethanogenum*, *Clostridium ragsdalei* and *Clostridium carboxidivorans* [43–45].

This fermentation also takes place at 32–38 °C and pH 4–6, also under anaerobic conditions. It is an exothermic reaction that follows the stoichiometry below. The conversion of the H_2 (or CO since H_2:CO = 1) is about 70%. The unconverted gas can be used as a fuel or cleaned and recycled [46].

$$3CO + 3H_2 \rightarrow C_2H_5OH + CO_2$$
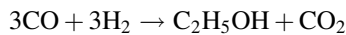
For the reaction to operate, inhibitor species from the raw syngas must be removed such as H_2S, NH_3(and even O_2), which are common in small amounts in the output from gasification plants. The use of pressure swing absorption, with alkali absorbents (such as monoethanolamine, MEA) are typically used to clean up the gas [46]. Once in the reactor, the first key limitation in the fermentation of syngas is the maximum concentration of ethanol. The best current practice claims a maximum concentration of ethanol in the reactor of 5% [47]. Due to this well-established problem, new systems are in development to adsorb ethanol from the water during the synthesis reducing the concentration so that the bacteria can produce more ethanol [48], using in-situ product removal technologies [49].

Until recently, another issue when generating ethanol from syngas has been the production of the by-product acetic acid. In the nineties, it was already possible to obtain high selectivity towards ethanol [50, 51]. BRI and Coskata industries have recently reported that their bacteria are capable of producing only ethanol [52]. In the scientific literature there are several models presenting the kinetics of ethanol production from syngas. For example, Chen et al. present a

Table 3 Stoichiometry of growth and product formation by *C. ljungdahlii* ($v_{i,j}$)

	CO (mol L^{-1})	CO$_2$ (mol L^{-1})	H$_2$ (mol L^{-1})	Biomass (X) (mol L^{-1})	Acetate (mol L^{-1})	Et (mol L^{-1})	
Biomass growth on CO	$-1/Y_1$	$0.5/Y_1 - 0.0175$		1	$0.25/Y_1 - 0.5$		(1)
Biomass growth on CO$_2$ and H$_2$		$-(0.5/Y_2 - 0.0175)$	$-1/Y_2$	1	$0.25/Y_2 - 0.5$		(2)
Ethanol production from CO	$-1/Y_3$	$0.67/Y_4$				1	(3)
Ethanol production from CO$_2$ and H$_2$		$-0.33/Y_4$	$-1/Y_4$			1	(4)
Conversion of acetate into ethanol CO	$-2/Y_5$	$2/Y_5$			$-1/Y_5$	1	(5)
Conversion of acetate into ethanol H$_2$			$-2/Y_6$		$-1/Y_6$	1	(6)

simple model based on the rate of CO consumption [53]. In this section we present the model by Vandecasteele [54] for completeness divided into bio-conversion reactions and the balance to the gas phase. Table 3 shows the stoichiometry of the fermentation:

The kinetics of the reactions above are given as follows:

$$
\begin{cases}
\rho_1 = \mu_1^{\max} \dfrac{C_{CO}}{K_{CO} + C_{CO} + \frac{c_{CO}^2}{K_{I,CO}}} \cdot \dfrac{K_{I,UA}}{K_{I,UA} + C_{UA}} X \\[2ex]
\rho_2 = \mu_2^{\max} \dfrac{C_{CO_2}}{K_{CO_2} + C_{CO_2}} \cdot \dfrac{C_{H_2}}{K_{H_2} + C_{H_2}} \cdot \dfrac{K_{I,CO}^{hy}}{K_{I,CO}^{hy} + C_{CO}} \cdot \dfrac{K_{I,UA}}{K_{I,UA} + C_{UA}} X \\[2ex]
\rho_3 = \mu_3^{\max} \dfrac{C_{CO}}{K_{CO} + C_{CO} + \frac{c_{CO}^2}{K_{I,CO}}} \cdot \dfrac{C_{UA}}{K_{UA} + C_{UA}} X \\[2ex]
\rho_4 = \mu_4^{\max} \dfrac{C_{CO_2}}{K_{CO_2} + C_{CO_2}} \cdot \dfrac{C_{H_2}}{K_{H_2} + C_{H_2}} \cdot \dfrac{K_{I,CO}^{hy}}{K_{I,CO}^{hy} + C_{CO}} \cdot \dfrac{C_{UA}}{K_{UA} + C_{UA}} X \\[2ex]
\rho_5 = \mu_5^{\max} \dfrac{C_{CO}}{K_{CO} + C_{CO} + \frac{c_{CO}^2}{K_{I,CO}}} \cdot \dfrac{C_{UA}}{K_{UA}^{ac} + C_{UA}} X \\[2ex]
\rho_6 = \mu_6^{\max} \dfrac{C_{H_2}}{K_{H_2} + C_{H_2}} \cdot \dfrac{C_{UA}}{K_{UA}^{ac} + C_{UA}} \cdot \dfrac{K_{I,CO}^{hy}}{K_{I,CO}^{hy} + C_{CO}} X
\end{cases}
\tag{80}
$$

See Table 4 for the definition of the terms and the constants involved in the rates above.

Gas phase mass balances (i is the component as in Table 4). It is assumed that the gas is fed to the volume above the liquid, V_G, for simplicity in the model development. That volume is assumed to be constant so, we can compute the partial pressure of the gases assuming ideal behavior and no reaction in the gas phase, no evaporation of water or ethanol:

Table 4 Values for the constants in the mass balances and kinetic rates

Symbol	Description	Value	Unit
Yield coefficients			
Y_1	Cell yield of carbon monoxide	0.0257	Mol cell (mol $CO)^{-1}$
Y_2	Cell yield to hydrogen	0.0068	Mol cell (mol $H_2)^{-1}$
Y_3	Ethanol yield to carbon monoxide	0.167	Mol ethanol (mol $CO)^{-1}$
Y_4	Ethanol yield of hydrogen	0.167	Mol ethanol (mol $H_2)^{-1}$
Y_5	Ethanol yield of acetate (CO)	1	Mol ethanol (mol acetate)$^{-1}$
Y_6	Ethanol yield of acetate (H_2)	1	Mol ethanol (mol acetate)$^{-1}$
Parameters			
μ_1^{max}	Maximum specific growth rate from CO	0.195	Mol cell (mol cell)$^{-1}$ h^{-1}
		0.022	
		0.04	
μ_2^{max}	Maximum specific growth rate from CO_2 and H_2	0.042	Mol cell (mol cell)$^{-1}$ h^{-1}
μ_3^{max}	Maximum specific ethanol production from CO	0.39	Mol ethanol (mol cell)$^{-1}$ h^{-1}
μ_4^{max}	Maximum specific ethanol production from CO_2 and H_2	0.39	Mol ethanol (mol cell)$^{-1}$ h^{-1}
μ_5^{max}	Maximum specific acetate conversion rate from CO	0.39	Mol ethanol (mol cell)$^{-1}$ h^{-1}
μ_6^{max}	Maximum specific ethanol production from CO_2 and H_2	0.39	Mol ethanol (mol cell)$^{-1}$ h^{-1}
K_{CO}	CO saturation constant	0.000078	M
		0.00069	
K_{CO_2}	CO_2 saturation constant	0.00022	M
K_{H2}	H_2 saturation constant	0.00022	M
		0.0003	
K_{UA}	UA saturation constant for ethanol production	0.0005	M
K_{UA}^{ac}	UA saturation constant for acetate conversion	0.0005	M
$K_{I,CO}$	CO inhibition constant	0.002	M
		0.00048	
$K_{I,CO}^{ky}$	CO inhibition constant for hydrogenate	0.000000007	M
$K_{I,UA}$	UA inhibition constant	0.00062	M
X_{Max}	Maximum biomass concentration before total sporulation	0.0009631	M
α	Inhibition coefficient	1	

$$\begin{cases} \frac{d(V_G \cdot C_{G,i})}{dt} = -k_L a_i (C^*_{L,i} - C_{L,i}) V_L \\ n_G = V_G \sum_i C_{G,i} \\ p = \frac{n_G RT}{V_G} \\ p_i = \frac{V_G C_{G,i}}{n_G} p \end{cases} \quad (81)$$

Liquid phase mass balances

$$\begin{cases} \frac{d(V_L \cdot C_{L,i})}{dt} = -k_L a_i (C^*_{L,i} - C_{L,i}) V_L + r_i V_L \\ r_i = \sum_{i=1}^{6} v_{i,j} \rho_j \\ \frac{d(C_{L,i})}{dt} = -k_L a_i (C^*_{L,i} - C_{L,i}) + r_i \\ V_L = cte \end{cases} \quad (82)$$

Taking into account that there is no physical transport of biomass and products

$$\begin{cases} \frac{dC_X}{dt} = r_X = (\mu_{X1} + \mu_{X2}) X \\ \frac{dC_A}{dt} = r_A = \left[\left(\frac{0.25}{Y_{X1}} - 0.5 \right) (\mu_{X1} + \mu_{X2}) - \frac{\mu_{e3}}{Y_{e3}} - \frac{\mu_{e4}}{Y_{e4}} \right] X \\ \frac{dC_E}{dt} = r_E = [(\mu_{e1} + \mu_{e2} + \mu_{e3} + \mu_{e4})] X \end{cases} \quad (83)$$

The conversion rates of carbon monoxide, carbon dioxide and hydrogen can be calculated by the summation of the products of the reaction rates and their respective stoichiometric coefficients:

$$\begin{cases} \frac{dC_{CO}}{dt} = r_{CO} = \left[-\frac{\mu_{X1}}{Y_{X1}} - \frac{\mu_{e1}}{Y_{e1}} - \frac{2\mu_{e3}}{Y_{e3}} \right] X \\ \frac{dC_{CO_2}}{dt} = r_{CO_2} = \left[\left(\frac{0.5}{Y_{X1}} - 0.0175 \right) (\mu_{X1}) - \left(\frac{0.5}{Y_{X2}} - 0.0175 \right) (\mu_{X2}) + \frac{0.67 \mu_{e1}}{Y_{e1}} - \frac{0.33 \mu_{e2}}{Y_{e2}} + \frac{2\mu_{e3}}{Y_{e3}} \right] X \\ \frac{dC_{H_2}}{dt} = r_{H_2} = \left[-\frac{\mu_{X2}}{Y_{X2}} - \frac{\mu_{e2}}{Y_{e2}} - \frac{2\mu_{e4}}{Y_{e4}} \right] X \end{cases}$$

$$(84)$$

The liquid mass balances of the gaseous substrates and nitrogen gas are as follows.

$$\begin{cases} \frac{dC_{L,CO}}{dt} = k_L a_{CO} \cdot (C^*_{L,CO} - C_{L,CO}) + r_{CO} \\ \frac{dC_{L,CO_2}}{dt} = k_L a_{CO_2} \cdot (C^*_{L,CO_2} - C_{L,CO_2}) + r_{CO_2} \\ \frac{dC_{L,H_2}}{dt} = k_L a_{H_2} \cdot (C^*_{L,H_2} - C_{L,H_2}) + r_{H_2} \\ \frac{dC_{L,N_2}}{dt} = k_L a_{N_2} \cdot (C^*_{L,N_2} - C_{L,N_2}) \end{cases} \quad (85)$$

To compute the saturation concentrations, C^*, we assume Henry's Law, see Table 5.

Table 5 Henry's coefficients (k_H)

Components	Value (mol L^{-1} atm^{-1})
CO	8.30×10^{-4}
CO$_2$	2.45×10^{-2}
H$_2$	7.32×10^{-4}
N$_2$	5.48×10^{-4}

$$C^*_{L,i} = p_i \cdot k_{H,i} \tag{86}$$

While the mass transfer coefficient was corrected from the one experimentally determined for CO_2 using Higbies's theory

$$k_L a_i = k_L a_{CO_2} \sqrt{\frac{D_i}{D_{CO_2}}} \tag{87}$$

3.3 Biobutanol

Most of the work in the scientific literature about biofuel production is focused on the production of bioethanol as the alcohol of choice. However, biobutanol is an interesting alternative, not least because it has better properties. For years it has been produced following the so-called ABE (acetone-butanol-ethanol) fermentation. The production of the three products simultaneously results in a low yield of butanol, reducing the economic attractiveness of the system. Only recently Malmierca et al. [55] have developed a process based on an AB fermentation where by integrating fermentation with pervaporation, a high yield of butanol is produced [55]. Additionally, the product stream contains solely acetone and butanol. In this section we present the mechanism and kinetics of typical ABE fermentations from glucose and xylose. There are several models in the literature but among the most complete is the one by Shinto et al. [56], Raganati et al. [57]. We refer to the original paper for further explanation of the model due to the large number of intermediates involved in the kinetics such as fructose-6-phosphate (F6P), glyceraldehyde-3-phosphate (G3P), acetyl-CoA (AcoA), butyryl-CoA (BCoA),acetoacetyl-CoA (AACoA), xylulose-5-phosphate (X5P), sedoheptulose-7-phosphate (S7P), erythrose-4-phosphate (E4P),ribose-5-phosphate(R5P). K_i are half live velocities and V_i are the specific growth rates. F is a binary term that inactivates that part of the model and is equal to 1 if the xylose concentration is over 1 mM and 0 otherwise:

$$
\begin{cases}
r_1 = \dfrac{V_{\max 1}[Glucose][Biomass]}{K_{m1} + K_{m1}([Glucose]/K_{is1})^2 + [Glucose](1 + [Butanol]/K_{ii1})} F \\[2mm]
r_2 = \dfrac{V_{\max 2}[F6P][Biomass]}{K_{m2} + [F6P]} F \\[2mm]
r_3 = \dfrac{V_{\max 3}[G3P][Biomass]}{K_{m3} + [G3P]} F \\[2mm]
r_4 = \dfrac{V_{\max 4}[Lactate][Biomass]}{K_{m4} + [Lactate]} F \\[2mm]
r_5 = \dfrac{V_{\max 5}[Pyruvate][Biomass]}{K_{m5} + [Pyruvate]} F \\[2mm]
r_6 = \dfrac{V_{\max 6}[Pyruvate][Biomass]}{K_{m6} + [Pyruvate]} F \\[2mm]
r_7 = \dfrac{V_{\max 7}[Acetate][Biomass]}{K_{m7} + [Acetate]} F \\[2mm]
r_8 = V_{\max 8} \left(\dfrac{1}{1 + (K_{m8A}/[Acetate])}\right)\left(\dfrac{1}{1 + (K_{m8B}/[AACoA])}\right)[Biomass] \\[2mm]
r_9 = \dfrac{V_{\max 9}[ACoA][Biomass]}{K_{m9} + [ACoA]} F \\[2mm]
r_{10} = \dfrac{V_{\max 10}[ACoA][Biomass]}{K_{m10} + [ACoA]} F \\[2mm]
r_{11} = \dfrac{V_{\max 11}[ACoA][Biomass]}{K_{m11} + [ACoA]} F \\[2mm]
r_{12} = \dfrac{V_{\max 12}[ACoA][Biomass]}{K_{m12}(1 + [Butanol]/K_{ii12}) + [ACoA](1 + [Butanol]/K_{ii12})} \\[2mm]
r_{13} = k_{13}[Biomass] \\[2mm]
r_{14} = \dfrac{V_{\max 14}[AACoA][Biomass]}{K_{m14} + [AACoA]} F \\[2mm]
r_{15} = V_{\max 15} \left(\dfrac{1}{1 + (K_{m15A}/[Butyrate])}\right)\left(\dfrac{1}{1 + (K_{m15B}/[AACoA])}\right)[Biomass] \\[2mm]
r_{16} = \dfrac{V_{\max 16}[Acetoacetate][Biomass]}{K_{m16} + [Acetoacetate]} \\[2mm]
r_{17} = \dfrac{V_{\max 17}[Butyrate][Biomass]}{K_{m17} + [Butyrate]} F \\[2mm]
r_{18} = \dfrac{V_{\max 18}[BCoA][Biomass]}{K_{m18} + [BCoA]} F \\[2mm]
r_{19} = \dfrac{V_{\max 19}[BCoA][Biomass]}{K_{m19} + [BCoA]} F \\[2mm]
r_{20_X} = \dfrac{V_{\max 20}[Xylose][Biomass]}{K_{m20}(1 + [Xylose]/K_{is20}) + [Xylose](1 + [Butanol]/K_{ii20})} F \\[2mm]
r_{21_X} = \dfrac{V_{\max 21}[X5P][Biomass]}{K_{m14} + [X5P]} \\[2mm]
r_{22_X} = \dfrac{V_{\max 22}[R5P][Biomass]}{K_{m22} + [R5P]} \\[2mm]
r_{23_X} = V_{\max 23} \left(\dfrac{1}{1 + (K_{m23A}/[R5P])}\right)\left(\dfrac{1}{1 + (K_{m23B}/[X5P])}\right)[Biomass] \\[2mm]
r_{24_X} = V_{\max 24} \left(\dfrac{1}{1 + (K_{m24A}/[S7P])}\right)\left(\dfrac{1}{1 + (K_{m24B}/[G3P])}\right)[Biomass] \\[2mm]
r_{25_X} = V_{\max 25} \left(\dfrac{1}{1 + (K_{m25A}/[X5P])}\right)\left(\dfrac{1}{1 + (K_{m25B}/[E4P])}\right)[Biomass]
\end{cases}
\tag{88}
$$

$$
\begin{cases}
\frac{d[Glucose]}{dt} = -r_1 \\
\frac{d[F6P]}{dt} = r_1 - r_2 \\
\frac{d[G3P]}{dt} = r_2 - r_3 \\
\frac{d[Pyruvate]}{dt} = r_3 + r_4 - r_5 - r_6 \\
\frac{d[Lactate]}{dt} = r_5 - r_4 \\
\frac{d[ACoA]}{dt} = r_6 + r_7 + r_8 - r_9 - r_{10} - r_{11} - r_{12} \\
\frac{d[Biomass]}{dt} = r_{12} - r_{13} \\
\frac{d[Acetate]}{dt} = r_9 - r_7 - r_8 \\
\frac{d[Ethanol]}{dt} = r_{11} \\
\frac{d[AACoA]}{dt} = r_{10} - r_8 - r_{14} - r_{15} \\
\frac{d[Acetoacetate]}{dt} = r_8 + r_{15} - r_{16} \\
\frac{d[BCoA]}{dt} = r_{14} + r_{15} + r_{17} - r_{18} - r_{19} \\
\frac{d[Butyrate]}{dt} = r_{18} - r_{15} - r_{17} \\
\frac{d[Acetone]}{dt} = r_{16} \\
\frac{d[CO_2]}{dt} = r_6 + r_{16} \\
\frac{d[Butanol]}{dt} = r_{19} \\
\frac{d[Xylose]}{dt} = -r_{20_X} \\
\frac{d[X5P]}{dt} = r_{20_X} + r_{22_X} - r_{21_X} \\
\frac{d[R5P]}{dt} = r_{21_X} - r_{22_X} - r_{23_X} \\
\frac{d[S7P]}{dt} = r_{23_X} - r_{24_X} \\
\frac{d[E4P]}{dt} = r_{24_X} - r_{25_X} \\
\frac{d[F6P]}{dt} = r_{24_X} + r_{25_X} + r_{2_X} \\
\frac{d[G3P]}{dt} = r_{2_X} + r_{25_X} - r_{3_X} - r_{24_X}
\end{cases}
\tag{89}
$$

Table 6 shows the coefficients for the previous equations.

4 Conclusions

In this chapter we have provided an overview of the principles and the design of fermenters devoted to the production of alcohols such as ethanol and butanol. We cover the production of first generation ethanol from glucose, second generation ethanol either from sugars, glucose and xylose, or syngas and finally butanol via ABE fermentation from sugars. The chapter presents the hydrodynamics of the tanks, single phase and multiphase gas-liquid type tanks, the heat and mass transfer characteristics as well as the kinetic expressions. Finally, a sample kinetics of each of the above mentioned cases is presented. Single phase bioreactors are typically used for sugar based alcohols production. The presence of the alcohols in the mixture inhibits the reaction and therefore the kinetics is complex following Monod models.

Table 6 Coefficients for butanol production kinetics

Reaction	K (h^{-1})	V$_{Max}$ (h^{-1})	K$_m$ (mM)	K$_{is}$ (mM)	K$_{ii}$ (mM)	K$_a$ (mM)	K$_{mA}$ (mM)	K$_{mB}$ (mM)
R1		3.2	46.0	55.6	67.5			
R2		40.0	10.0					
R3		120	26.5					
R4		7.50	177					
R5		9.70	500					
R6		180	1.50					
R7		0.30	50.0					
R8		19.0					40.0	70.0
R9		26.5	51.0					
R10		20.0	1.00					
R11		7.45	30.0					
R12		8.10	1.10		23.0			
R13	0.017							
R14		10.0	5.20					
R15		80.0					15.0	50.0
R16		12.0	10.0					
R17		35.0	4.90			2.20		
R18		100	6.10					
R19		3.15	5.00		67.5	2.20		
R20		1.09	0.026	0.126	0.014			
R21		0.83	0.026	0.126	0.014			
R22		45.0					0.05	0.0025
R23		45.0					0.05	0.0025
R24		45.0					0.05	0.0025
R25		65.0					0.05	0.0025

Alternatively, syngas can be fermented to ethanol. These reactors are two phase ones where the mass transfer from the gas to the liquid is the limiting stage. Hydrodynamics are responsible for the contact between the reactants and the liquid and several reactor designs are available, from bubble columns to CSTR's.

References

1. Walas SM (1990) Chemical process equipment. Selection and design. Butterworth-Heinemann, Boston
2. Martín M, Montes FJ, Galán MA (2008) Bubbling process in stirred tank reactors I: agitator effect on bubble size, formation and rising. Chem Eng Sci 63:3212–3222
3. Nienow AW (1997) On impeller circulation and mixing effectiveness in the turbulent flow regime. Chem Eng Sci 52(15):2557–2565

4. Gogate PR, Beenackers AACM, Pandit AB (2000) Multiple-impeller systems with a special emphasis on bioreactors: a critical review. Biochem Eng J 6:109–144
5. Joshi JB, Pandit AB, Sharma MM (1982) Mechanically agitated gas-liquid reactors. Chem Eng Sci 37(6):813–844
6. Harnby N, Edwards MF, Nienow AW (1992) Mixing in the process industries, 2nd edn. Butterworth-Heinemann, Oxford
7. McCabe WL, Smith JC, Harriot P (1985) Unit operations of chemical engineering. McGraw-Hill Book Company, Singapore
8. Sinnott RK (1999) In: Coulson, Richardson (eds) Chemical engineering, 3rd edn. Butterworth Heinemann, Singapore
9. Zehner P, Kraume M (2000) Bubble columns. Ullmann's encyclopedia of industrial chemistry (Online)
10. Krishna R (2000) A scale up strategy for a commercial scale bubble column slurry reactor Fischer-Tropsch synthesis. Oil Gas Sci Tech 55(4):359–393
11. Shimizu K, Takada S, Minekawa K, Kawase Y (2000) Phenomenological model for bubble column reactors prediction of gas hold-ups and volumetric mass transfer coefficients. Chem Eng Sci 78:21–28
12. Vogel HC, Todaro CL (1996) Fermentation and biochemical engineering handbook: principles, process design and equipment, Chapter 5. Noyes Publications, New Jersey
13. Hassan ITM, Robinson CW (1977) Stirred-tank mechanical power requirement and has holdup in aerated aqueous phases. AIChE J 23:48–56
14. Hughmark GA (1980) Power requirements and interfacial area in gas liquid turbine agitated systems. Ind Eng Chem Proc Des Dev 19:638–641
15. Paul EL, Atiemo OVA, Kresta SM (2004) Handbook of industrial mixing. Wiley-Interscience, New York
16. Pacek AW, Man CC, Nienow AW (1998) On the sauter mean diameter and size distributions in turbulent liquid/liquid dispersions in a stirred vessel. Chem Eng Sci 53:2005–2011
17. Alves SS, Maia CI, Vasconcelos JMT (2002) Experimental and modeling study of gas dispersion in a double turbine stirred tank. Chem Eng Sci 57:487–496
18. Calderbank PH (1958) The interfacial area in gas liquid contacting with mechanical agitation. Trans Inst Chem Eng 36:443–463
19. Galindo E, Pacek AW, Nienow AW (2000) Study of drop and bubble sizes in a simulated mycelial fermentation broth of up to four phases. Biotechnol Bioeng 69(2):213–227
20. Bouaifi M, Hebrard G, Bastoul D, Roustan M (2001) A comparative study of gas hold up, bubble size, interfacial area and mass transfer coefficients in stirred gas liquid reactors and bubble columns. Chem Eng Process 40:97–111
21. Shukla VB, Veera UP, Kulkarni PR, Pandit AB (2001) Scale up of biotransformation process in stirred tank reactor using dual impeller bioreactor. Biochem Eng J 8:19–29
22. Kudrewizki F, Rabe P (1986) Model of the dissipation of mechanical energy in gassed stirred tanks. Chem Eng Sci 41:2247–2252
23. Whitman WG (1923) The two-film theory of absorption. Chem Met Eng 29:146–148
24. Sherwood TK, Pingford RL, Wilke CR (1975) Mass transfer. Chemical Engineering Series. McGraw Hill, New York
25. Higbie R (1935) The rate of absorption of a pure gas into a still liquid during a short time of exposure. Trans Am Ins Chem Eng 31:365–389
26. Miller DN (1974) Scale-up of agitated vessels gas-liquid mass transfer. AIChE J 20(3):445–453
27. Danckwerts PV (1951) Significance of liquid-film coefficients in gas absorption. Ind Eng Chem 43:1460–1467
28. Treybal RE (1990) Operaciones de transferencia de masa, Chapter 3, 2nd edn. McGraw Hill, México
29. Skelland AHP (1974) Diffusional mass transfer. Wiley, New York

30. Kafarov V (1975) Fundamentals of mass transfer: gas liquid, Vapour-Liquid and liquid-liquid systems. Mir Publishers, Moscow
31. Dobbins WE (1956) The nature of the oxygen transfer coefficient in aeration systems. Biological treatment of sewage and industrial wastes, 1, 2-1. Reinhold, New York, pp 141–148
32. Angelo JB, Lightfoot EN, Howard DW (1966) Generalization of the penetration theory for surface stretch: application to forming and oscillating drops. AIChE J 12:751–760
33. Davies JT (1972) Turbulence phenomena. Academia Press, New York, pp 143–144
34. Calderbank PH, Moo-Young MB (1961) The continuous phase heat and mass transfer properties of dispersions. Chem Eng Sci 16:39–54
35. Kawase Y, Halard B, Moo-Young M (1987) Theoretical prediction of volumetric mass transfer coefficients in bubble columns for Newtonian and non-Newtonian fluids. Chem Eng Sci 42:1609–1617
36. Barabash VM, Belevitskaya MA (1995) Mass transfer from bubbles and drops in mechanically agitated apparatuses. Theor Found Chem Eng 29(4):333–342
37. Kawase Y, Moo-Young M (1988) Volumetric mass transfer coefficients in aerated stirred tank reactors with Newtonian and non-Newtonian media. Chem Eng Res Des 66:284–288
38. Kendoush AA (1994) Theory of convective heat and mass transfer to spherical cap bubbles. AIChE J 40(9):1440–1448
39. Miller R, Melick M (1987) Chem Eng 113
40. Aden A, Foust T (2009) Techno economic analysis of the dilute sulfuric acid and enzymatic hydrolysis process for the conversion of corn stover to ethanol. Cellulose 16(4):535–545
41. Krishnan MS, Ho NWY, Tsa GT (1999) Fermentation kinetics of ethanol production from glucose and xylose by recombinant *Saccharomyces* 1400 (pLNH33). Appl Biochem Biotech 77–79:373–388
42. Martín M (2016) Industrial chemical process analysis and design. Elsevier, Oxford
43. Munasinghe PC, Khanal SK (2011) Biomass-derived syngas fermentation into biofuels. Biofuels 101(13):79–98
44. Mohammadi M, Najafpour GD, Younesi H, Lahijani P, Uzir MH, Mohamed AR (2011) Bioconversion of synthesis gas to second generation biofuels: a review. Renew Sustain Energy Rev 15(9):4255–4273
45. Madigan MT, Martinko JM, Stahl DA (2012) Biology of microorganisms, 13th edn. Benjamin Cummings
46. Martín M, Grossmann IE (2011) Energy optimization of bioethanol production via gasification of switchgrass. AIChE J 57(12):3408–3428
47. Van Kasteren JMN, Dizdarevic D, Van der Waall WR, Guo J, Verberne R (2005) Bio-ethanol from bio-syngas. Technical Report. Technische Universiteit Eindhoven (TU/e), Telos &Ingenia Consultants & Engineers No 0456372-R02
48. Nielsen DR, Prather KJ (2009) Adsorption of second generation biofuels using polymer resins with in situ product recovery (ISPR) applications. In: AIChE Annual meeting 2009, Paper 564f, Nashville
49. Woodley JM, Bisschops M, Straathof AJJ, Ottens M (2009) Future directions of in-situ product removal (ISPR). J Chem Technol Biotechnol 83(2):121–123
50. Klasson KT, Ackerson MD, Clausen EC, Gaday JL (1991) Bioreactor design for synthesis gas fermentations. Fuel 70(5):605–614
51. Clausen EC, Gaddy JL (2009) Ethanol from biomass by gasification/fermentation. http://www.anl.gov/PCS/acsfuel/preprint%20archive/Files/38_3_CHICAGO_08-93_0855.pdf. Accessed 20 April 2017
52. Bruce WF, President, The co-production of ethanol and electricity from carbon-based wastes, BRI Energy
53. Chen J, Gomez JA, Höffner K, Barton PI, Henson MA (2015) Metabolic modeling of synthesis gas fermentation in bubble column reactors. Biotechnol Biofuels 8(89):1–12
54. Vandecasteele J (2016) Experimental and modelling study of pure-culture syngas fermentation for biofuels production. MSc Universiteit Gent

55. Malmierca S, Díez-Antoínez R, Paniagua AI, Martín M (2017) Technoeconomic study of AB biobutanol production. Part 2: process design. Ind Eng Chem Res 56(6):1525–1533
56. Shinto H, Tashiro Y, Kobayashi G, Sekiguchi T, Hanai T, Kuriya Y, Okamoto M, Sonomoto K (2008) Kinetic study of substrate dependency for higher butanol production in acetone-butanol-ethanol fermentation. Process Biochem 43:1452–1461
57. Raganati F, Procentese A, Olivieri G, Götz P, Salatino P, Marzocchella A (2015) Kinetic study of butanol production from various sugars by *Clostridium acetobutylicum* using a dynamic model. Biochem Eng J 99:156–166

Chapter 9
Biofuels from Microbial Lipids

Kit Wayne Chew, Shir Reen Chia, Pau Loke Show, Tau Chuan Ling and Jo-shu Chang

1 Introduction

The continuous use of fossil fuels has led to the tremendous increase in atmospheric CO_2 and associated global warming trends and other related environmental issues. These issues have clearly exaggerated energy security, alongside soaring oil prices and climate change. With the increase use of petroleum or fossil fuel based hydrocarbons for energy supply, the gap between demand of crude oil and supply from indigenous sources is expected to increase over the years [1]. This has created the need for energy alternatives that would reduce the dependence on fossil fuels. Besides that, fuels derived from renewable sources are undoubtedly one of the top alternatives to divert from the reliance of petroleum fuels [2, 3]. Renewable and non-polluting biomass energy has received increasing attention from industries as well as academic community.

Biofuels like biodiesel can be produced from feedstock such as canola oil, palm oil, soybean oil, rapeseed oil and sunflower oil. Soybean and rapeseed are common feedstocks for biofuel production in America and Europe, respectively. Countries like Malaysia and Thailand have a surplus of palm crops and can generate large

K. W. Chew · P. L. Show (✉)
Faculty of Engineering, Department of Chemical and Environmental Engineering,
University of Nottingham Malaysia Campus, Jalan Broga, 43500 Semenyih,
Selangor Darul Ehsan, Malaysia
e-mail: PauLoke.Show@nottingham.edu.my; showpauloke@gmail.com

S. R. Chia
Faculty of Engineering, Department of Mechanical Engineering,
University of Malaya, 50603 Kuala Lumpur, Malaysia

T. C. Ling
Institute of Biological Sciences, University of Malaya, 50603 Kuala Lumpur, Malaysia

J. Chang
Department of Chemical Engineering, National Cheng Kung University, 701 Tainan, Taiwan

amounts of palm oil for biodiesel production [4, 5]. Many vegetable oil can be converted to renewable fuels, they are favorable due to their environmental benefits and sustainability. The esters from vegetable oils are good substitutes for diesel as they do not require any modification in the current automobile engine design and contain high energetic yields [6]. Fatty acids with longer chain length can also produce biodiesel with high cetane number and reduced nitrogen oxide emissions. It is possible to improve the properties of biodiesel through genetic engineering, where modification of the parent oil could lead to an enriched fuel with certain fatty acids for improved fuel properties.

The development of biofuels with dedicated energy drops like Jatropha and soybean have raised many controversies, including land use changes and competition with food crops for agricultural resources. Biodiesel derived from oilseed or animal fats is currently not able to meet the realistic demand as they can cover only a small fraction of the transport fuel requirements. The infeasibility of these sources become more apparent as large areas of land is needed for the production of oilseed crops and animal feed [7, 8]. Therefore, it is essential to search for new feedstocks which are economically competitive, renewable and can be produced in large quantities without complicated processing. Moreover, the feedstock should provide environmental benefits over fossil fuel sources and do not compete with food crops production. Microbial lipids satisfy these criteria as they can be produced cost-effectively and hence, they have generated interest due to their ability to lessen the global crude oil and greenhouse gas crisis. Lipids are ubiquitous in all living organisms, which form the permeable membranes of cells and organelles as a lipid bilayer. The cultivation of lipid rich microorganisms could be independent from climatic constraints and can valorize industrial wastes by using them as substrates [9]. However, the broad commercialization of microorganisms-derived biofuel is yet to be accomplished due to techno-economic constraints in the downstream processing and mass cultivation [10].

Microalgae can be considered as the ideal feedstock for the production of biodiesel for the following reasons [3, 7, 8, 10]:

i. Microalgae are unicellular with simple nutritional requirements, they grow easily in varied climatic conditions and habitats, thus providing a high biodiversity.

ii. They have high photosynthetic efficiency compared to terrestrial plants, and certain microalgae are able to tolerate very high concentrations of CO_2 and can be used for carbon sequestration. The carbon footprint in biofuel production can be reduced.

iii. Microalgae can assimilate nutrients like nitrogen and phosphorus from wastewater, hence wastewater can be used for biomass production and concomitant bioremediation.

iv. Microalgae can adsorb heavy metals in solution, and can be used for heavy metal removal and reduce environmental pollution.

v. Microalgae are rich in high value compounds like polyunsaturated fatty acids, pigments, and proteins that has applications in pharmaceutical and nutraceutical industries.

vi. Microalgal biomass has diverse applications in human health and nutrition, aquaculture feed, animal feed and with the energy rich compounds like carbohydrates and lipids, they can be used as a sustainable feedstock for biofuel production.

Substantial efforts have been taken for the development of high density cultivation processes in commercializing microalgal biomass production. Two examples of these processes are (i) Utilizing the metabolic potential of microalage and (ii) innovative cultivation systems designed for high cell density cultivation of microalgae. The metabolic pathways depend on the requirement of light and carbon sources for growth and cell division and can be divided into three types, namely photoautotrophy, heterotrophy and mixotrophy [11]. Photoautotrophy is the simplest cultivation system with sunlight and CO_2, generally uses an open pond system and is relatively simple to operate with low cost. Heterotrophic cultivation can utilize a wide source of organic carbon to reduce the overall cost of biofuel produced. For the cultivation systems design, the choice between an open or closed style plays a major role in affecting the efficiency of large scale biofuel production. Open ponds systems can simulate the growth environment in its natural behavior while closed system like photobioreactor which are constructed specifically for the cultivation processes provide uniform and optimal growth conditions for the culture.

Many oleaginous species have the ability to metabolize pentoses, revealing the potential of producing triacylglycerol (TAG) from lignocellulosic biomass and other cheap materials [12]. The cost of microbial oil production may be currently higher compared to vegetable oil, however, the techno-economics of the production processes can be significantly improved with various methods. The costs of biofuel production can be reduced with further developments in using lignocellulose-based carbohydrates as a feedstock. Besides that, the utilization of the by-product from the microorganisms' cultivation for value-added products may also improve the economic potential. Optimization of the operating processes could help attain higher lipid productivity and better cellular lipid content [13].

2   Microbial Lipids as a Potential Resource for Biofuels

The potential feedstocks that may be used as raw materials for biofuel production has been widely extended due to the recent technological advantages in the related areas. Microorganisms, because of their ubiquitous nature, is a potential source for a variety of valuable compounds that can serve as feedstock for biofuel production (Table 1). Microorganisms offer numerous benefits in the environmental, economic and energy security outlook when used for the production of biofuels (Fig. 1).

Table 1 Types of biofuels and the sources and manufacturing process [15–20]

Biofuel	Types of fuel	Sources	Microorganisms sources	Manufacturing process
Biodiesel	Fatty acid methyl esters (FAME)	Microbial lipids, animal fats, vegetable oils	Microalgae, fungi, bacteria, yeast, *Escherichia coli*	Transesterification, heterotrophic fermentation
Biogas	Methane	Cow and pig manure	Methanogenic bacteria	Anaerobic digestion
Biohydrogen	Hydrogen	Water	*Cyanobacterium*	Bio-photolysis
		Cellulose, xylan, pectin	*Caldicellulosiruptor saccharolyticus*	Heterotrophic fermentation
Bio-alcohols	Methanol	Methanol, isobutene	Methanogenic bacteria	Acid catalysis
	Ethanol	Enzymatically hydrolysed starch	Yeast, *Saccharomyces cerevisiae*	Homoacedogenic fermentation
	Propanol	Starch rich wastes	*E. coli*	Anaerobic fermentation
	Butanol	Starch rich wastes	Bacteria, *Clostridium acetobutylicum*	Anaerobic fermentation
Bio-hydrocarbons	n-Alkanes	Sugars and organic acids	*Vibrio furnissii*	Heterotrophic fermentation
	Alkenes	Branched chain fatty acids	*Micrococcus* sp.	Head-to-head condensation

The cultivation of microbes for a desirable product is an age old process and all the techniques have been established for major industrial microorganisms like *E. coli*, the ethanol fermenting yeast *Saccharomyces* and the anaerobic *Clostridia* for Acetone-butanol-ethanol (ABE) fermentation. They can be cultivated with relatively less labor, regardless of the climate or season, can be easily scaled up and contains much higher yield of lipids compared to plants [14]. Using microorganisms to produce biofuels will also not compromise the production food and other products derived from crops. Oleaginous microorganisms, that mainly comprises of bacteria, algae, yeast and molds, are defined as microbes with lipid content exceeding 20% of the cellular biomass content. Lipids produced by oleaginous microorganisms have fatty acid compositions which are similar to that of vegetable oils and this shows great potential for biofuels production.

2.1 Sources of Microbial Lipids from Oleaginous Microorganisms

Oleaginous microorganisms belonging to different families such as algae, bacteria, yeast and fungi are able to generate neutral lipids under certain cultivation conditions. Of these, eukaryotic microorganisms like yeasts and microalgae can
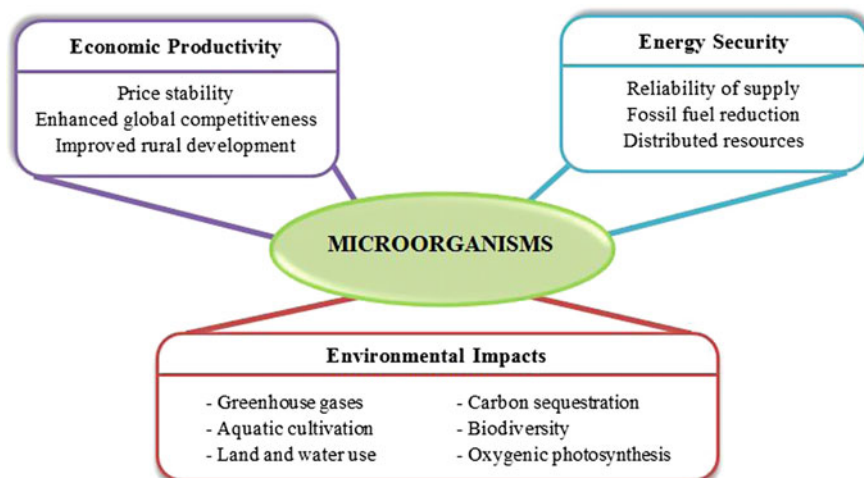
Fig. 1 Benefits of oleaginous microorganisms for the production of biofuels

synthesize and store triacylglycerol (TAG) in their cell when subjected to nutrient derivation in the form of nitrogen limitation. In microalgae, under nitrogen limiting conditions and the continued availability of carbon, cell growth is arrested because of the limited availability of nitrogen for the synthesis of proteins that are responsible for cell division. And nitrogen deprivation leads to the activation of deaminases that particularly act on AMP. Reduction in the cellular and mitochondrial AMP can result in the reduced activity of isocitrate dehydrogenase, and hence citric acid is accumulated, which is then exported to cytosol and converted to acetyl CoA [21]. Acetyl CoA is the major precursor of fatty acid synthesis and hence in nitrogen limiting conditions the metabolized carbon is continuously funneled into lipid synthesis in eukaryotic oleaginous microorganisms. Since lipids are the most reduced forms of carbon, they also need an uninterrupted supply of reducing equivalents like nicotinamide adenine dinucleotide phosphate (NADPH). For the synthesis of one mole of a C18 fatty acid, 16 mol of NADPH is required [22]. The required NADPH is continuously supplied by the TCA cycle via the activity of the malic enzyme or the pentose phosphate pathway [23]. The lipids thus stored serve as an energy source or as precursors of fatty acid synthesis required for cell growth and metabolism after rejuvenation. Hence eukaryotic oleaginous microorganisms are capable of accumulating neutral lipids or TAGs from 40–80% of their biomass [21]. Bacteria generally accumulate polyhydroxy alkonates as lipid reserves and polyhydroxy butyrate is the major PHA to be synthesized and stored and is also mainly studied in the bacteria *Bacillus*. Certain bacteria like *Mycobacterium* sp., *Rhodococcus* sp., *Streptomyces* sp., *Acinetobacter* sp., *Nocardia* sp., *Gordonia* sp., *Micromonospora* sp., and *Dietzia* sp. are capable of accumulating TAGs or neutral lipids [24]. Neutral lipids or TAG accumulation in bacteria is modulated by enhanced activities of phosphatidate phosphatase

Table 2 Oil content of various microorganisms [29, 30]

Microorganisms	Oil content (% dry weight)
Microalgae	
Botryococcus braunii	25–75
Chlorella sp.	28–32
Crypthecodinium cohnii	20
Cylindrotheca sp.	16–37
Dunaliella primolecta	23
Isochrysis sp.	25–33
Monallanthus salina	>20
Nannochloris sp.	20–35
Nannochloropsis sp.	31–68
Neochloris oleoabundans	35–54
Nitzschia sp.	45–47
Phaeodactylum tricornutum	20–30
Schizochytrium sp.	50–77
Tetraselmis sueica	15–23
Fungi	
Aspergillus oryzae	57
Mortierella isabellina	86
Humicola lanuginosa	75
Mortierella vinacea	66
Bacterium	
Arthrobacter sp.	>40
Acinetobacter calcoaceticus	27–38
Rhodococcus opacus	24–25
Bacillus alcalophilus	18–24
Yeast	
Candida curvata	58
Cryptococcus albidus	65
Lipomyces starkeyi	64
Rhodotorula glutinis	72

(PAP) and AcylCoA:Diacyglycerol acyltransferase (DGAT) that converts the fatty acid palmitic acid to TAG, and with reduced β-oxidation of fatty acids by the activity of the transcriptional regulator FadR [25]. Table 2 indicates that bacteria have lower lipid content (20–40% of dry biomass) compared to the other microorganisms. Nevertheless, bacteria have a very high growth rate, such that it can achieve a huge biomass production in about 12–24 h, and the culturing method for bacteria growth is relatively simple. Most bacteria are not oil producers, though there are some types of bacteria which can synthesize high amounts of fatty acids (up to 70% of the cellular dry weight) from simple carbon sources [26]. The extraction of complicated lipoids from bacteria is difficult and hence less significance is placed on the use of oleaginous bacteria as a raw material for the

production of biofuels. With the extended knowledge of lipid accumulation in both prokaryotes and eukaryotes, it is believed that algal lipids has the highest chance to be the alternative biodiesel source compared to yeasts and bacteria, because of their economic production potential and increased accumulation of TAGs, next only to oleaginous yeasts whose production costs should be sustained by alternative cheap carbon sources [27]. Microalgae can grow very rapidly and many of its species contain high amount of oil. This oil content may exceed 80% of its dry biomass weight and its biomass doubling time during exponential growth can be as short as 3.5 h [28]. The oleaginous microalgae and yeasts can grow and accumulate significant amounts of lipids and their maximum achievable lipid content can alter immensely among different species and individual strains [29]. Table 2 shows the potential microorganism for microbial oil production.

The oil productivity depends on the growth rate of the algal strain and oil content of the biomass. Microalgae with high oil content and productivities are highly sought after for producing biofuels. On the other hand, yeasts and fungi are favorable microorganisms as an alternative oil resource as they typically contain intracellular lipid as high as 70% of their biomass dry weight. Oleaginous yeast *Crptococcus curvatus* is extremely efficient and can accumulate lipids up to 60% on a dry weight basis. Oleaginous yeasts and molds can also accumulate triacylglycerols that are rich in polyunsaturated fatty acids [31]. Certain species of yeasts are known for their ability to produce large quantities of microbial lipids due to their capability to obtain a high dry biomass and high cellular lipid content. Furthermore, a recent report has shown that the filamentous fungus *Mucur circinelloides* has potential as a feedstock for biodiesel production. This microbial lipids showed a high content (>85%) of saponifiable matter and adequate fatty acid content for biodiesel production. High purity of fatty acid methyl esters (FAME) was produced and the direct transformation of fungal biomass to biodiesel without an intermediate lipid extraction step was made possible [32]. This strengthens the potential of oleaginous yeasts and fungi as an alternative for biofuels production. The lipids extracted from oleaginous microorganisms also consists of a wide variation of lipid classes, such as acylglycerides, phospholipids, glycolipids, free fatty acids (FFA), lipoproteins, and sterols. These lipid classes will have different physico-chemical properties which can be observed during extraction [2]. Table 3 shows the content of various lipids in cell biomass from the oleaginous microorganisms.

2.2 Microbial Lipids Production from Renewable and Waste Materials

For cost effective biofuels production with microbial lipids, it is essential to reduce production costs and valorize wastes by recycling resources such as spent cell mass, water and nutrients. Lipids are intracellular products and the technology involved for the production of microbial lipids usually produces significant amounts of cell mass by-products, which contain nutrient, proteins, polysaccharides and other trace

Table 3 Characteristics of lipids from various microorganisms

Microorganisms	Growth conditions	Neutral lipids	Phospholipids	Glycolipids	FFA	References
Microalgae						
Chlorella sorokiniana	Glucose as medium, pH 7.0, 37 °C	78.9–81.6	7.1	–	11.2	[33]
Scenedesmus sp.	Cultivated in soil extract medium, 24 °C	81.3–82.3	6.1–6.7	10.9–12.6	–	[34]
Nitzschia laevis	Lewin's marine diatom medium, pH 8.5, 23 °C	78.6	11.6	8.1	–	[35]
Nannochloropsis sp.	Not specified: Purchased from Seambiotic, Tel Aviv, Israel	14.5	12.59	11.99	5.9	[36]
Schizochytrium limacinum SR-21	Grown in 5-L stirred tank with glycerol as carbon source	78.2	0.8	0.07	0.7	[36]
Chlorella vulgaria	Grown in photobioreactor in autotrophic conditions.	57.2	0.28	0.43	30.6	[36]
Scenedesmus sp.	Grown using raceway open ponds with natural field nutrients and local well water	31.5	0.34	0.35	27.4	[36]
Chlamydomonas	Photobioreactor with TAP medium, pH 7.4	51.3	0.64	9.02	26.8	[36]
Fungi						
Cunninghamella echinulata	Tomato wastes hydrolysate with glucose as medium, pH 6.0, 26 °C	44.5–87.9	1.7–7.7	3.6–14.8	–	[37]
Bacteria						
Rhodococcus opacus	Grown on alkanes, phenylalkanes or non-hydrocarbon substrates	87	1.2	–	5	[38]
Yeast						
Rhodosporidium toruloides Y4	Glucose and $(NH_4)_2SO_4$ medium, pH 6.0, 30 °C, phosphate-limiting concentration	81.0–87.7	4.0–6.6	8.3–12.4	–	[39]
Trichosporon oleaginosus	Glucose and $(NH_4)_2SO_4$ medium, pH 6.0, 30 °C	58.2–62.2	0.27–0.33	–	37.5–41.5	[40]
Rhodosporidium azoricum	Glucose and $(NH_4)_2SO_4$ medium, pH 6.0, 30 °C	98.5–98.7	0.23–0.27	–	1.1–1.2	[40]

elements. Besides that, wastewater contains residual nutrients and elements which can be recycled to increase the efficiency of the microbial lipid technology [30, 41]. Biodiesel production commonly involves three processes which are drying of the biomass, lipid extraction and transesterification. Recently, the use of direct transesterification has been reviewed, as fatty acids in the lipid rich biomass can undergo transesterification without a lipid extraction step. This would result in the reduction of processing time and lessen the solvent needed for biofuel production.

The growth of microorganisms and the production of microbial lipids could also be supported by fermentation material like food waste. Food wastes are unconsumed food and food residues from residential areas or commercial businesses. They contain protein, lipids, lignin, carbohydrate and organic acids, which are promising sources of nutrients for the fermentation process and valuable raw material for various biotechnological products. With the use of yeasts, some low-cost fermentation substrates can be converted into bio-lipids. This indicates that recycling food wastes as a low-cost fermentation substrate for yeast cultivation is feasible for biological lipid production [42]. Furthermore, lignocellulosic materials and organic wastes are suitable carbon sources for producing biofuels due to its high availability and low impact on food prices. The cellulosic biomass will be converted into simple sugars and these sugars are subsequently converted into biofuels. Nonetheless, pre-treatment steps are needed and it may be quite energy intensive as the usage of hazardous chemicals or large amount of enzyme during the hydrolysis step is required. The pre-treatment step is necessary to reduce the recalcitrance of lignocellulosic material and this is done by partially breaking the recalcitrant structure [43].

Cheirsilp and Louhasakul [44] studied the cultivation of oleaginous yeast *Yarrowia lipolytica* with industrial wastes like serum latex, palm oil mill effluent and crude glycerol to evaluate their abilities to grow and synthesize lipid from the wastes. Different types and mixtures of wastes were also analyzed to reduce the nutrients requirements. It was found that the yeasts could grow and produce lipids from various types of wastes, yielding a relatively high amount of lipid (1.6–1.7 g/L) and high lipid content (48–61%) based on their dry cell mass [44]. Furthermore, in a study by Poli et al. [45], two industrial wastes have been tested as the carbon and nitrogen sources for *Y. lipolytica* QU21 cultivation. The wastes are crude glycerol from a biodiesel industry and fresh yeast extract from brewery waste. Enhanced biomass production was observed in crude glycerol waste due to the impurities present. The additional amounts of peptides and proteins provided are beneficial as nitrogen sources for yeasts and yeast was found to adapt, grow and accumulate lipids rapidly on a large variety of wastes [45]. The optimum carbon to nitrogen ratio is also significant to enable cells to initiate lipid storage, and the use of crude glycerol for conversion was attractive for increasing the productivity of biofuels.

Microalgal cultivation in photoheterotrophic mode does not need any added organic carbon source and the carbon is supplied as inorganic CO_2 or soluble carbonates. Industrial exhaust gases or flue gases are rich in CO_2 and can be used as a carbon source for the photoautotrophic cultivation of microalgae. Kao et al. cultivated a *Chlorella* sp. MTF-15 on three different flue gases in both indoor and

outdoor cultures and the growth, biomass and lipid productivities were examined [46]. The microalgal strain could efficiently utilize CO_2, SO_x and NO_x present in the flue gas and a lipid accumulation of up to 35% was observed. Growth rate and lipid production were 0.827/d and 0.961 g/L, respectively [46]. The experiments were performed on site of a steel factory in Taiwan, making carbon capture feasible with microalgal cultures. Similarly, *Scenedesmus obliquus* was grown on flue gas for carbohydrate and lipid accumulation, and maximum biomass production was obtained at 14% flue gas [47]. The growth rate, lipid productivity and carbohydrate productivity were 1/d, 9.9 mg/L/d and 10.3 mg/L/d respectively [47]. Thus, flue gas is a potential source of inorganic carbon for the photoautotrophic cultivation of microalgae. However, in heterotrophic cultivation of microalgae, organic carbon can be assimilated into biomass, resulting in high biomass and lipid productivities. And as a cost cutting measure, various waste resources rich in organic carbon like sugarcane bagasse [48], palm oil mill effluent [49], anaerobic digestate [50], lignocellulosic biomass like rice straw [51] and biodiesel derived crude glycerol [52] has been successfully used for the cultivation of various microalgae. Rice straw was saccharified by the combination of gamma irradiation, alkali treatment and enzyme hydrolysis, which was then used for the cultivation of *Chlorella protothecoides*. A biomass concentration and fatty acid methyl ester concentration of 6.51 g/L and 2.95 g/L respectively [51]. Sugarcane bagasse hydrolysed by combined acid and enzymatic treatment and it was shown that better biomass and lipid productivity was obtained by fed batch fermentation. Biomass and lipid productivity were 24 g/L and 1.19 g/L/d respectively [48]. It was shown that the metabolism of pentoes via the pentose phosphate pathway (PPP) supported lipid production much better than the metabolism of glucose by glycolysis. As discussed earlier, the PPP pathway is a source of NADPH which is much needed for the synthesis of lipids. The utilization of waste materials as a nutrient source for the production of microbial lipids and further production to biofuels is a promising platform for the effective transformation of renewable and waste materials. The combination of different wastes rich in different nutrients can improve the economics of large scale lipid production, and the main success factor lies in the selection of microbial strains with high efficiency for lipid production.

2.3   Factors Affecting Microbial Lipids Production

Microalgae which are capable of producing large amounts of lipids and hydrocarbons are a promising alternative feedstock for the next generation of biofuels. They can be cultivated using relatively cheap resources like sunlight and carbon dioxide (CO_2) from flue gases as mentioned earlier and have higher lipid content with rapid growth rate. However, the lipid accumulation and cell growth in algae under phototrophic conditions are influenced by various factors, which include light intensity, dissolved oxygen concentration, pH, carbon dioxide fraction, presence of organic carbon sources and concentration of nutrients such as iron, nitrogen,

phosphorus and silicon [39, 53, 54]. Apart from that, key parameters such as cellular lipid content, lipid productivity and biomass productivity should be improved to enhance the economic feasibility of algal oil production, though it is apparent that algae species with high oil content tends to grow more slowly, resulting in low rates of oil production [55].

Light is essential for cell growth and the specific cell growth rate increases with increasing photon irradiation flux. The excess photonic energy will dissipate as heat and this may lead to the photo inhibition of cellular functions [56]. To overcome this, proper design of bioreactors are selected to elevate the higher limit of photonic flux. The use of low methanol concentrations could also lead to an improvement of phototrophic growth of algae by increasing photosynthesis and algae respiration rates. This indicates that algae grown in a low light exposure condition will have a higher total lipids content compared to algae exposed to higher light intensity [57]. The CO_2 fraction in sparging gas also plays a major role on the cell growth and lipid accumulation as it affects the medium pH and the availability of bicarbonates as carbon source for the cells. Several studies reported that increasing the CO_2 fraction in sparging air could increase the maximum limit of cell concentration and promote the rapid growth of cells. However, further elevations on the CO_2 fraction completely inhibited cell growth in many cases as the concentration of CO_2 above 5% (v/v) would reduce cell growth [58–60]. This has led to development of pre-adaptation of cells to higher CO_2 conditions and the use of high inoculums levels to overcome the CO_2 toxicity. The use of pure carbon dioxide in the sparging medium had shown unfavorable pH changes and growth inhibition and hence, they were replaced with sparging with ambient air and adjustment of pH for successful cultivation of the algal culture.

The growth of algae was also found to improve at the temperature range of 25–35 °C. Reports have stated that the biomass production increased at temperature of 30 °C, though the lipid content of certain species tends to decrease at higher temperatures [61, 62]. Heterotrophic cultivation using carbon sources was introduced to overcome the difficulty of delivering optimal photonic energy to cells in photoautotrophic growth conditions. High lipid yield and high biomass production were observed when heterotrophic algae were placed in low light conditions and supplied with organic carbon instead of CO_2 [63]. Another type of growth is the mixotrophic growth, which utilizes a mixture of different source of energy and carbon, and undergoes two distinctive processes within the cell: photosynthesis and aerobic respiration. This type of growth resulted in several fold increase of maximum cell density and specific growth rates [11]. The nitrogen and phosphorus limitation in the medium also enhances lipid production in algae cells. Many strains of algae was found to contain higher lipid content when cultivated in low-nitrogen medium [64]. The cessation of cell division may occur as a result of nitrogen depletion, but if carbon metabolism continues, the conversion of carbon to lipid will divert as described previously [65]. Apart from that, the nature of nitrogen sources may also affect the algae cell growth and lipid productivity [66]. This is likely to cause variation in the total fatty acid content in algae while the biochemical composition of algae is influenced greatly by the growth phase.

Certain oleaginous fungi can accumulate as much as 80% of their biomass as lipids. The lipids in fungi are mainly affected by the carbon source, temperature, pH, nitrogen source and agitation. Molds are often cultivated as they produce high concentrations of γ-linolenic acid (GLA) and arachidonic acid (AA), which is favorable for the production of biofuels [67]. High oil yields could be obtained with prolonged fermentation times, which are common in single cell oil fermentation processes. Prolonged fermentation are carried out under nitrogen limitation, redirecting the carbon flux of metabolic pathways towards lipid accumulation [68]. In *Cunninghamella echinulata* and *Mortierella isabellina*, the fatty acid content of the microbial oil produced was not significantly affected by the carbon source used, however, the production of these fatty acids in the cells is associated with the age of the mycelia. The highest fraction of these fatty acids can be found in young mycelia, while fully grown mycelia showed lower content as the cells have aged [69]. However in general, the type of carbon source can strongly affect the production and fatty acids content in lipids of fungi. The use of various carbon sources may result in variation in the lipid and GLA content. Since each carbon source would be utilized as a substrate by a different metabolic pathway, the resultant metabolites will contribute to the variations in fatty acids content.

Oleaginous yeasts has a TAG fraction which is similar to that of plant oils, they also have a high oil content and fast growth rate. Yeast can grow on various carbon sources like glucose, mannose, glycerol, xylose, arabinose and other agriculture residues. Most oleaginous yeast accumulate lipids up to 40% of their dry weight and it can increase up to 70% under nutrient-limiting conditions [65]. Many studies were conducted on the use of glycerol as a carbon source, resulting in highs yields and enhanced lipid production. However, different yeast strains might have higher potential of lipid accumulation in different mediums. The supply of excess carbon sources as well as the limiting of certain nutrients in a medium can also help increase the lipid production. Lipid production in yeast is strongly influenced by the aeration, carbon to nitrogen ratio, temperature, pH and inorganic salts [70]. At high temperatures, the cellular lipid content and production can be high with low degree of fatty acid unsaturation, and the composition of the fatty acids might vary as a result of the increased temperature. Moreover, a higher carbon to nitrogen ratio yields higher lipid content [71]. Many strains of yeast requires a high carbon to nitrogen ratio to accumulate large amount of lipids.

Bacteria can exhibit high cell growth rates under simple cultivation methods. Their cellular composition and structure vary depending on the microorganism and the carbon source used. Actinomycete group of bacteria are able to accumulate high amounts of intracellular fatty acids of up to 70% of the cell dry weight from simple carbon sources like glucose under growth-limiting conditions [29, 72]. The accumulation takes place usually at the stationary phase of growth, which is when the proteins are not being synthesized. However, not all bacteria can accumulate large amount of fatty acids, they usually produce complex lipids for energy storage and stored them as insoluble inclusions in the cytoplasm when excess carbon sources are available [73].

3 Conversion of Microbial Lipids to Biofuels

Recently, microbial lipids-derived biofuels are found to contain equivalent qualities with derivatives of fossil fuels. Biofuels are produced from microbial lipids through different conversion processes. Some conventional processes to produce biofuels are transesterification, esterification and anaerobic digestion. These processes are optimized to obtain the maximum yield of biofuel from microbial lipids through manipulating the operating parameters. In order to achieve high yields of biofuels, the lipid accumulation in the feedstock is the key factor. Microbial lipids within the oleaginous microorganisms are categorized as wax esters (WEs), free fatty acid (FFA), TAG and polyhydroxyalkanoates (PHAs). WEs are esters that consist of long chain fatty alcohol and fatty acid. The special properties of WEs resulted in diverse applications of WEs such as lubricants, polishes, coatings and printing inks. However, TAG and PHAs are the favorable lipids in biodiesel production compared to WEs. This is due to the need of the conversion of lipids into a less viscous form to be used in common internal combustion engines. FFA has always been a concern in biodiesel production. The presence of FFA during the conversion process leads to the formation of soap. Therefore, pretreatment has to be performed for removing or reducing the existence of FFA in biofuel production.

In the biofuel production process, the transesterification of TAG will form fatty acid alkyl esters (FAAE) and the esterification of PHAs will form hydroxyalkanoate methyl esters (HAMEs), which could serve as fuel additives as well. Transesterification is a process of reacting triglyceride, which is found in microbial lipid, with an alcohol to produce esters (biodiesel) and glycerol as the products. The common alcohols used are methanol and ethanol that will lead to the formation of fatty acid methyl esters (FAME) and fatty acid ethyl esters (FAEE), respectively. On the other hand, the esterification process will lead to the formation of esters and water by reactions of the alcohol with an acid. The formation of HAMEs can be obtained by using methanol in the esterification of PHAs. Besides that, the anaerobic digestion is an established process applied for biogas production from wastewater or sludge. The biofuels recovery from wastewater and sludge under anaerobic condition are favorable as the bacteria will breakdown the organic matter in the wastewater or sludge to produce biogas.

Microbial lipids extracted from oleaginous microorganisms are converted into biofuels through two types of conversion processes: one-step process or multi-stage process. In one-step process, energy intensive cell disruption and lipid extraction steps are usually avoided and the biomass is directly subjected to the fuel production process. This process often is more beneficial in the economic perspective, as the process duration is shorter and reduces the use of harsh chemicals resulting in less environmental impact. Hence, one-step process tends to be a more environmental friendly conversion process compared to multi-stage process. However, the microbial lipid yields, quality of biofuel and overall lipid productivity have to be considered in order to obtain comparable final products from conventional methods. Multi-stage process is performed by converting microbial lipids to biofuels in two

or more processes simultaneously or sequentially, converting microbial lipids to biofuels. The advantages and disadvantages between single stage and multi-stage conversion process are yet to be weighed out by researchers for the optimum biofuel production method.

3.1 Technologies for Converting Microbial Lipids to Biodiesel

Biodiesel is a "drop-in" type of biofuel that can be utilized in most of the automotive industry without changing the standard diesel engines. The conventional process in biodiesel production is to perform the extraction of accumulated microbial lipids within the feedstocks followed by the transesterification process. The products of transesterification, namely FAMEs and FAEEs, are known as biodiesel as well. Additional of a catalyst is required in transesterification besides an alcohol. The transesterification process includes catalytic transesterification and enzymatic transesterification. The difference between these transesterification processes is the use of catalysts. The common transesterification catalyst for catalytic transesterification is chemicals such as acid or a base while the catalyst for enzymatic transesterification is the biological catalyst lipase [74, 75]. The conventional process for biofuel production by using catalytic transesterification is shown in Fig. 2.

The catalyst used in the process could be either homogenous or heterogeneous catalysts. Transesterification reaction is shown as Eq. 1:

$$
\begin{array}{llll}
CH_2-O-CO-R_1 & & CH_2-OH & R-O-CO-R_1 \\
\quad | & \text{(catalyst)} & \quad | & \\
CH-O-CO-R_2 \quad + \quad 3ROH \quad \longrightarrow & CH-OH & R-O-CO-R_2 \\
\quad | & & \quad | & \\
CH_2-O-CO-R_3 & & CH_2-OH & R-O-CO-R_3 \\
\text{(Triglyceride)} & \text{(Alcohol)} & \text{(Glycerol)} & \text{(Mixture of fatty acid esters)}
\end{array}
$$

$$(1)$$
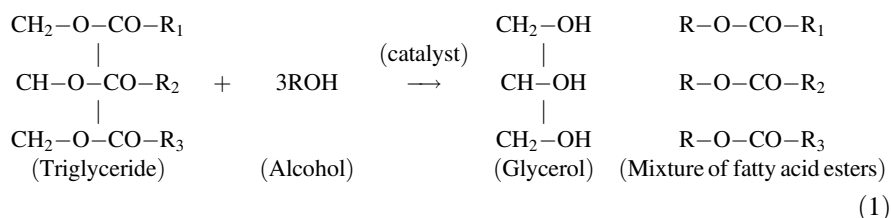
Among the types of transesterification processes mentioned above, base catalyzed transesterification is an established process and is widely used in the industrial production of biodiesel. Strong base chemicals such as sodium hydroxide (NaOH) and potassium hydroxide (KOH) are common catalysts for base catalyzed transesterification [77]. This is due to the relatively low cost of raw materials and high biodiesel productivities [78]. In addition, a comparable yield of biodiesel with conventional petroleum-based diesel could be obtained from base catalyzed transesterification within a few hours [79]. The short duration of catalyzed reaction, high conversion yield, requirement of low operating temperature and pressure (i.e. ambient pressure and low temperature) have made base catalyzed transesterification the most economical process in biodiesel production. However, the microbial lipids that contain high composition of FFA will be required to undergo a pre-treatment

Triglyceride

↓

Pretreatment

↓

Alcohol Recovery and Product Separation

↓

Alkaline Transesterification

↓

Product Separation from Saponified Components

↓

Water Washing

↓

Drying

↓

Biodiesel
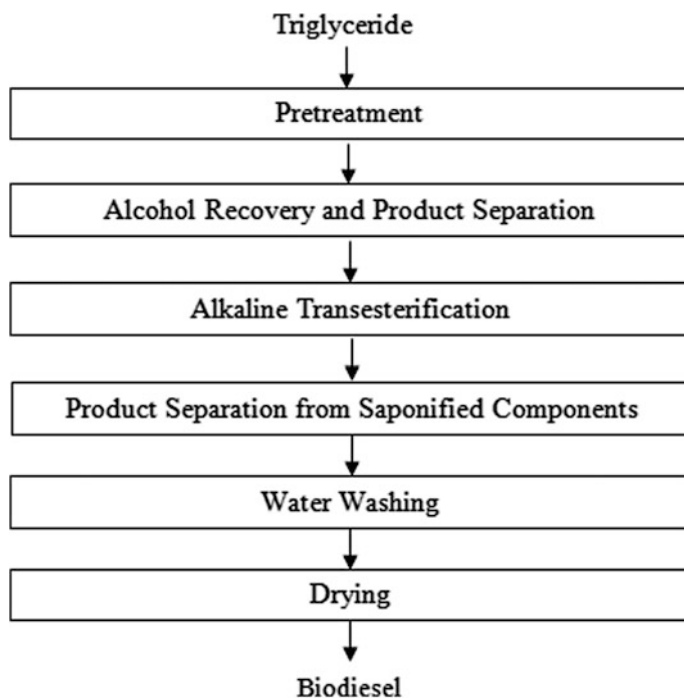
Fig. 2 Conventional process for biofuel production by catalyzed transesterification [76]

process before proceeding to transesterification. This is to avoid the saponification reaction that occurs when FFA reacts with NaOH as shown in Eq. 2:

$$
\underset{\text{(FFA)}}{R_1-COOH} + \underset{\text{(Sodium hydroxide)}}{NaOH} \longrightarrow \underset{\text{(Soap)}}{R_1COONa} + \underset{\text{(Water)}}{H_2O} \quad (2)
$$
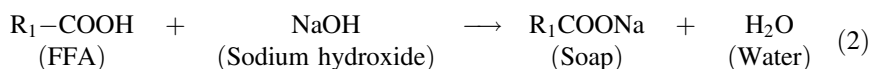
This reaction is not favorable as the yield of esters will decrease with the increase in soap formation and the soap formed will inhibit the separation of esters and glycerol [80]. Furthermore, this reaction also lowers the efficiency of catalyst due to competitive and futile binding of FFA with the catalyst. This resulted in the requirement of higher amount of catalyst and thus, a higher operation cost. Besides FFA, water within the microbial lipid or water formed from the saponification reaction is another concern in transesterification. The water molecules tend to hydrolyze the triglyceride into diglycerides and FFA by hydrolysis. The removal of glycerol, catalyst and impurities such as soap are essential after transesterification process to obtain biodiesel. The saponification compounds contain alkaline metal which may result in the higher ash content in biodiesel and cause problems in the engines. The deactivation of the catalytic converter or the corrosion of motor may occur due to the alkaline metal [78].

When the FFA content in lipid is higher than 1%, acid catalyzed transesterification is used to overcome the wasteful saponification reaction [78]. This type of transesterification has been intensively studied for the benefits of avoiding soap formation and possessing feedstock with residual moisture. The moisture remaining in low cost feedstock is acceptable in acid catalyzed transesterification and the final product would be clear of impurities [81]. The disadvantages of acid catalyzed transesterification are longer reaction time and the requirement of higher molar ratio of catalyst to oil. The operating conditions of acid catalyzed transesterification are more critical than base catalyzed transesterification. Operating cost are usually higher as the highly corrosive catalysts utilized during the process will damage the reactor. A large amount of wastewater will be generated to neutralize the remaining acid catalysts in the system as well. Therefore, most of the biodiesel productions in industries convert lipids into biodiesel by base catalyzed transesterification. So for acid catalyzed process, intensive studies were performed to overcome the barriers. Some strong common acids such as sulfuric acid, hydrochloride acid, and boron trifluoride were used. Most of the studies conducted have utilized methanol with the presence of catalysts (acid or base) with high yields of biodiesel, in the range of 80–98% purity can be obtained as the end product [32, 82, 83]. However, lower productivity of biodiesel could be observed for microbial lipids from certain feedstock, which range from 49 to 66% purity [84, 85]. The choice of catalysts is important as the biodiesel yield vary with the type of catalyst used as studied by Vicente et al. [32]. At the same time, higher operating temperature for the acid catalyzed transesterification is favored compared to low operating temperature, which results in lower ester yield from the microbial lipids [32].

The products from transesterification, FAMEs or FAEE, are analyzed by gas chromatography with flame ionization detector. The temperature of flame ionization detector is controlled at a high temperature of around 250–260 °C during the analysis [86, 87]. The used catalysts may be recycled for next conversion process in order to reduce the operating cost. Besides, the conversion process from lipid to biodiesel, especially for microalgae-based biodiesel, is found to be influenced significantly by several factors such as catalyst loading, types of catalyst, temperature and stirring rate [86]. The reaction time for transesterification of microalgal lipids might vary, ranging from 1 to 48 h, and is different in each study [32, 83, 86, 88]. The biodiesel products are separated from glycerin by allowing the biodiesel to settle down for at least 24 h and biodiesel forms the top layer with glycerin at the bottom. The glycerin is drained off to obtain biodiesel by decantation. For purification, biodiesel is washed by warm distilled water and dried before calculating their exact percentage extracted from the microbial lipids. Biodiesel is dried with anhydrous $CaCl_2$ and heated at 50 °C. After that, the volume of clean dry biodiesel is determined and prepared for analysis.

3.2 Alternative Pathways for the Conversion of Microbial Lipids to Biofuels

The conventional methods in producing biofuel by microbial lipids were explained in detail in the Sect. 3.1. The usage of enzymes as catalysts in transesterification have been considered and studied. Extensive investigations have also been performed by using lipase as the catalyst in transesterification. Lipase is a common enzyme that is produced by all living organisms and a good choice for transesterification. The compatibility of lipase with various raw materials and reusability have showed that it has high potential as a catalyst in transesterification [89]. Lipase as biocatalysts has overcome the difficulty faced by acid and based transesterification, which is the high energy consumption for multi-step purification and wastewater treatment in order to obtain the final product [90]. However, certain drawbacks are observed by using lipase as catalyst. For example, the reaction rate of enzyme catalyzed transesterification is slower compared to acid or base catalyzed transesterification. In addition, the cost of enzyme is comparatively higher than the cost of common acid or base. The usage of enzyme will directly increase the operating cost of whole process.

Most of the lipase utilized as biocatalysts are obtained from microbes, which have comparatively higher yield than the lipase extracted from animal and plants. Lipase to be used as catalysts are available in three forms: extracellular lipase, intracellular lipase and immobilized lipase. Extracellular lipase is the lipase extracted or purified from microbial fermentation broths and these are hydrolytic enzymes secreted by the cells. Microbial lipase is normally produced through submerged fermentation or solid state fermentation. The increased market price of microbial lipase is high due to the need of a high degree of purity that is required as a biocatalyst. Furthermore, the high cost of purification of enzymes is one of the difficulties in commercializing enzymatic transesterification. The purification steps depend on the source of the lipase and the structure [90]. The intracellular lipase used in the transesterification process is the metabolic or cytosolic lipase present inside the cells. Whole cell biocatalysts are microbial cells that are used as catalyst in transesterification. This method is relatively inexpensive compared to pure enzymes and the additional enzyme extraction steps has been eliminated. In order to increase the reaction rate of transesterification, immobilized lipase was introduced. Instead of free enzyme, whole microbial cells with intracellular lipase are immobilized in porous biomass particles and can be directly used as a biocatalyst [90].

The wet biomass of *Chlorella vulgaris* ESP-31 with 63% lipid content was successfully converted to biodiesel by transesterification with immobilized *Burkholderia* lipase [91]. The wet microalgal biomass without lipid extraction (70% water content) showed better results than lipid extracts, with a biodiesel conversion efficiency of 97.3% and the lipase could be reused for six continuous cycles [91]. And it was shown that for direct transesterification of wet microalgal biomass with lipases, the lipid content of the biomass determines the biodiesel conversion efficiency and hence a microalgal biomass with high lipid content is preferable [86].

The oleaginous yeast *Rhodosporidium toruloides* was cultivated in detoxified sugarcane bagasse hydrolysate with a lipid content of 52.5%. When the lipids were extracted and subjected to transesterification with commercial lipases in a tert-butanol system, biodiesel yield of 88.4% was observed [74]. The immobilization of lipase in iron-nanoparticles could help in easy removal of lipases after the reaction with a magnet and it was found that the reaction efficiency remains unchanged for at least 4 cycles [86]. In the transesterification of microalgal lipids from *Tetraselmis* sp., enzyme catalyzed transesterification achieved 5 folds higher biodiesel conversion yield compared to alkali catalyzed transesterification [92].

The alcoholysis process which uses methanol to produce biodiesel is also known as methanolysis. This process is commonly used in plastic recycling by converting polyesters into monomers. The direct methanolysis method is more advantageous than conventional methods as oil extraction and cell disruption can be eliminated prior to methanolysis. The study of Thliveros et al. [79] investigated the microbial biodiesel production with different types of methanolysis: direct base catalyzed methanolysis, direct acid catalyzed methanolysis and a conventional method with cell disruption, oil extraction and acid-catalyzed esterification. Among these methods, highest yield of FAME was obtained with direct base-catalyzed methanolysis compared to the others and lowest yield of FAME was produced in the conventional method [79]. Methanolysis is performed under atmospheric pressure with temperatures ranging from 40 to 70 °C. Vigorous stirring of the mixture is required to dissolve the base or acid catalyst completely in methanol. In direct methanolysis, the dried microbial biomass is added after thorough mixing of methanol and catalyst.

3.3 Improved Pathways for the Conversion of Microbial Lipids

The conventional biodiesel production with pre-treatment to extract microbial lipid prior to transesterification have been investigated in numerous studies. Yet, biodiesel produced by conventional transesterification requires longer time and it is a multi-step process. Direct transesterification of the biomass is an excellent option for efficient conversion of microbial lipids to biodiesel. Direct transesterification is a simplified and improved pathway in yielding biodiesel. Direct transesterification is similar to direct methanolysis, where the microbial lipids still inside the whole microbes are directly converted into biodiesel without lipid extraction. Figure 3 shows the flowchart of both direct and indirect transesterification.

The microalga *Nannochloropsis* sp. CCMP1776 was cultivated outdoors in tubular photobioreactors and the lipid content was 50% and the dried biomass had a moisture content of about 8–10%. This biomass was subjected to direct transesterification with supercritical methanol (250 °C, 8% w/v methanol, 25 min) and microwave assisted transesterification. Biodiesel conversion efficiency and FAME
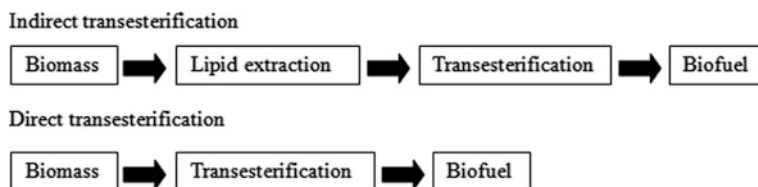
Fig. 3 Flowchart of direct and indirect transesterification process of biofuels [44]

yield was higher in supercritical methanol method with FAME yield of 84.5% and the biodiesel obtained was stable and pure. With the microwave assisted method, 80.3% FAME was obtained, but the energy consumed was considerably less, it was only 250 kJ compared to 600 kJ in supercritical methanol. So, for large scale purposes, microwave assisted transesterification could be a viable option [93]. The wet biomass of the oleaginous yeast *C. curvatus* with a total lipid content of 42% was subjected to microwave assisted direct transesterification with methanol and KOH as a catalyst. The reaction conditions as optimized by statistical design are as follows: methanol biomass ratio of 50:1, 5% KOH, 80% water, 2 min reaction time and stirring at 966 rpm. The biodiesel yield reached 92% after two rounds of reaction with 63.88% FAME content [94]. Cheirsilp and Louhasakul's (2013) study has investigated the transesterification of yeast lipid into fatty acid methyl ester (FAME) [44]. The cells were subjected to conventional acid catalyzed transesterification, transesterification with dried biomass and direct transesterification of wet biomass. The production of FAME is found to be highest for direct transesterification with high methanol molar ratio (167:1 and 209:1) in 1 h reaction but the reverse reaction of FAME to monoglyceride was observed at 6 h reaction time. However, at high methanol molar ratio, the highest amount of FAME was produced with transesterification of dried biomass at the reaction time of 6 h without any reverse reaction. These methods have proved to be more efficient than the conventional methods (lipid extraction followed by transesterification) and have showed great potential in cost reduction of biodiesel production. Table 4 shows the transesterification of various lipids.

4 Life-Cycle Assessment

Life-cycle assessment (LCA) is a systematic framework for evaluating the implications of products, processes and activities involved in the production of a particular product towards environmental damages. LCA uses specific metrics through life-cycle impact assessment that can be assessed to determine the effect on the environment. The development towards life-cycle based metrics for biofuel policies also extends the sustainability criteria to non-greenhouse gas related projects and is a very effective tool to compare alternative energy routes in terms of environmental

Table 4 Transesterification of various lipids

Lipid extraction process	Source (Microalgae)	Biodiesel yield (%)	Remarks	References
Direct transesterication using immobilized lipase	*Chlorella vulgaris*	63.2	Higher biodiesel conversion can be achieved with higher lipid content, lower biocatalyst loading and better lipase recycle efficiency	[86]
Enzymatic transesterification using immobilized lipase	*Chlorella vulgaris*	58.3	Direct conversion of wet microalgae to biodiesel reduces the processing cost	[91]
Lipase catalysed transesterification	*Tetraselmis* sp.	29.6	Lipase catalysed reactions offer more compatibility and reusability of enzymes	[92]
Direct transesterifcaiton	*Chlorella pyrenoidosa*	7.8–8.4	Single-stage reaction, less time consuming and less loss during extraction	[95]
Direct transesterification	*Schizochytrium limacinum*	66.3	Single-stage method led to higher yield of crude biodiesel	[96]
Direct transesterification with sequential wet extraction	*Chlamydomonas* sp.	99	Higher catalyst loading is needed in direct transesterification but higher biodiesel yield can be obtained	[97]
Simultaneous cooling and microwave heating transesterification	*Nannochloropsis* sp; *Tetraselmis* sp.	83.3 77.1	Consumes less energy for higher biodiesel productivity	[98]
Microwave-assisted transesterification	*Chlorella pyrenoidosa*	86.7	Hexane extraction after microwave treatment ensures that polar pigments are not extraction into the crude biodiesel	[99]
Extractive-transesterification under microwave irradiation	*Chlorella* sp.	96.2	Microwave extraction method shortens transesterification time and lowers solvents requirements	[100]
Alkaline in situ transesterification	*Chlorella vulgaris*	77.6	Higher yield achieve using alkaline catalyst instead of acid catalyst	[101]

Table 4 (continued)

Lipid extraction process	Source (Microalgae)	Biodiesel yield (%)	Remarks	References
Two-step in situ transesterification	*Chlorella sorokiniana*	65.2[a]; 94.9[b]	[a]H_2SO_4 + KOH catalyst [b]Amberlyst-15 recyclable catalyst	[102]
Micro-mixer reactor transesterification	*Chaetoceros* sp.; *Chlorella vulgaris*; *Nannochloropsis*	98.1	Yield optimized by altering types of reactor, volume ratio and reaction time	[103]
Supercritical in situ transesterification	*Chlorella protothecoides*	89	Catalyst is not required and higher tolerance for feedstocks containing water and fatty acids	[104]

impact and indirect natural sources costs towards various services and commodities. LCA has been widely conducted to estimate the life-cycle impact of various biofuels produced from different feedstocks. It includes the entire life cycle of the fuel production process from the collection of feedstock to the combustion of biofuels. Life cycle assessment has shown that first generation biofuels, which are fuels derived from sources such as sugar, starch, animal fats and vegetable oil, provided little to no benefit regarding greenhouse gas (GHG) reductions compared to petroleum fuels. It was expected that second generation biofuels, which are fuels derived from non-food feedstock such as lignocellulosic materials, would be able to achieve better GHG reductions as well as avoid sustainability issues. However, great variability and uncertainty has been displayed by the LCA of this second generation biofuels, hence creating an inconclusive analysis [105].

Oleaginous microorganisms such as microalgae have high growth rates and photosynthetic efficiencies, which makes it potentially advantageous over conventional terrestrial biofuel feedstock. In addition, algae has high lipid content and can use non-arable land for cultivation. Microalgae cultivation has been compared with conventional crops from a life-cycle perspective, the results indicated that conventional crops had lower environmental impacts, greenhouse gas emissions, water and energy use [106]. Algae performed more favorably in the aspects of total land area used and eutrophication potential. Studies on crops such as canola, corn or switchgrass resulted in less GHG emissions compared to that of algae. This suggests that algae requires more fossil-based carbon to produce the equivalent amount of bioenergy. However, significant developments are being made in algae cultivation to increase the feasibility of biofuel production. The direct nutrient discharge from algae ponds and the resultant eutrophication improved as engineered ponds were used and this allows better runoff control compared to that of terrestrial cultivation. It is essential to establish and maintain the infrastructure for algae

cultivation and conversion as the efficient land use for algae cultivation will be beneficial for the transportation energy system [107].

Besides that, life-cycle assessment on the effects of nitrogen supply and oil extraction technologies showed promising results in the fossil energy ratio of algal biofuel production. The life-cycle fossil energy ratio describes the ratio of energy output to fossil energy consumption [108]. This factor is important for life-cycle analysis to evaluate the depletion of non-renewable resource as well as in terms of pollution to the environment. It was found that nitrogen deficiency successfully elevated the oil content and productivity of algae. Moreover, the extraction of oil directly from wet algae with subcritical solvents can efficiently enhance the life-cycle fossil energy ratio of algal biomass compared to extraction from dried biomass. Several other factors which affect the life cycle fossil energy ratio includes the esterification efficiency, heat value or calorific value of algae, ratio of algal residue and algae cultivation water recycling rate. Different life-cycle stages of the utilization of algal biomass for the production of biofuels are presented in Fig. 4: Life-cycle stages of bioethanol, biomethane and biodiesel production from algal biomass. The cultivation of microalgae requires considerable amount of freshwater, hence, this leads the necessity for the quantification of water footprint and nutrient usage for microalgae biofuel production. It was shown that using seawater or wastewater with recycling for the cultivation of microalgae could significantly reduce the freshwater usage by as much as 90% [109, 110]. The usage of nutrients such as phosphorus, potassium, nitrogen, magnesium and sulfur can also be reduced by approximately 55% with harvest water recycling.

A comparative LCA study of algal biodiesel production was carried out by Lardon et al. to assess the energetic balance and potential environmental impacts of the whole process chain, from biomass production to biodiesel combustion. Two different culture conditions (nominal fertilizing and nitrogen starvation) and two extraction methods (dry and wet) were analyzed and the best scenario was
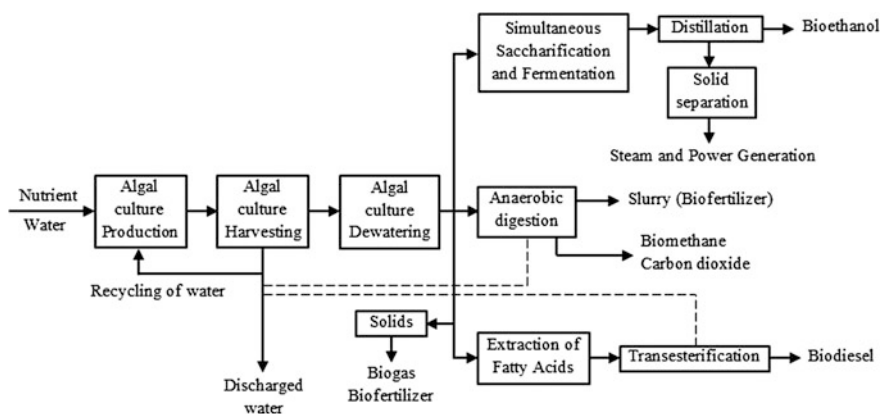
Fig. 4 Life-cycle stages of bioethanol, biomethane and biodiesel production from algal biomass

compared with first generation biodiesel [111]. All the equipment for cultivation showed high energetic consumption. However, it is worth noting that both fertilizers and energetic requirements were lower for the low nitrogen culture condition. The use of wet oil extraction also reduced the energy requirements but had lower extraction efficiency. Several factors were selected from a whole set of impacts to evaluate the potential effects on human health, ecosystem quality and resource usage. The production steps were categorized into several groups to examine the contribution of the process chain to different impacts, where each impact is standardized with the worst situation for evaluation. It was found that a low nitrogen condition with wet extraction method always showed lower impacts. Besides that, the comparison of algal biodiesel with other fuels showed very low impacts for eutrophication, land use and human toxicity effects, which can be attributed to better control of fertilizers as well as the absence of pesticides [111]. Nevertheless, algal biodiesel was not deemed favorable in terms of global warming, ozone depletion and mineral resources as it requires large amount of heat and electricity.

Growing algae using carbon dioxide flue gases from various power stations has also been regarded as a possible GHG capture mechanism. However, this mechanism does not gain any carbon credits as the algae-derived fuel would eventually be burnt and the captured carbon would return to the atmosphere. The carbon credit arises from the fact that biofuel availability replaces the utilization of fossil fuels. Similar case can be observed for electricity production, such that carbon credits are obtained from the use of algal biomass instead of coal or gas for electricity production [112]. A study by Jorquera et al. [113] showed that the energy return of algae grown using ponds was greater than unity while algae grown using photo-bioreactors were less than unity. A higher ratio of illuminated area to cultivation volume was needed for photo-bioreactor systems compared to open ponds, but in order to generate the same amount of biomass, an area twice as large as the photo-bioreactor was needed for the pond system. The water consumption in the pond was also about 16 times higher than that required for the photo-bioreactor [113]. Furthermore, the commercial scale production of algal biofuel needs much consideration in terms of economic aspects. At present, the economical complication of producing biofuels shows greater uncertainty than the GHG emissions. To make algal fuels profitable, a higher production rate is necessary as a lower production rate would result in an expensive final product and would not be cost competitive with fossil fuels. This situation should relatively improve with the technological advances in algal biofuels production and the rise of crude oil price due to its continuous depletion.

The improvements made on oil extraction techniques could directly impact the sustainability of biofuel production, where almost 90% of the process energy is reserved for lipid extraction. For example, the drying of biomass for lipid recovery can be improved with alternative methods that are less energy consuming. A more secure control on the energy consumption could very well reduce numerous impacts and this will lead to better overall environment performance compared to other

biofuels. With additional research on the optimization of growth conditions for oleaginous microorganisms, along with industrial scale research, biofuels from microbial lipids could be produced with low capital costs and eventually commercialized.

5 Challenges and Future Perspectives

Many of the recent investments in green fuels are steering the market attention towards the production of algal biofuels and development of outstanding production systems. The major requirements for producing biofuels from microbial lipids is the large-scale cultivation and harvesting systems, and the challenge rests on the ability to reduce the cost per unit area. Apart from that, a large amount of land is needed to grow oil crops and this may lead to the clearing of rainforests for the purpose of monoculture plantations [114]. Besides that, the strong interest in sustainable biofuel production requires industrial processes to exploit new genetically modified microbial strains with enhanced photosynthetic efficiency, increased growth rate and biomass production. Other desirable features in microalgal biofuel system would be: increased oil content and productivity and enhanced temperature tolerance aiding in outdoor cultivation. Microalgal biotechnology has improved greatly in the recent past and well defined genetic tools for gene silencing and heterologous protein expression are available for model microalgae. These are the upstream processes in arriving at a particularly robust strain with high biomass and lipid productivity. Cultivation of the strain under optimal conditions, with efficient process control and aided by process engineering strategies will greatly enhance the biomass production potential. Valorization of wastes like flue gases, wastewater or carbon rich waste and lignocellulosic biomass can be applied for the photoautotrophic or heterotrophic cultivation of microalgae, thereby cutting cultivation costs.

Further efforts on oil rich microbial biomass production should concentrate on the cost reduction for small and large scale systems as the feasibility of producing viable biofuels is dependent on the efficiency, cost structure and ease of scale up [115]. Biofuels from microbial lipids could play a major role in the future energy systems and this will be realized through a defined set of technology breakthroughs, based on the development of the optimum utilization of algal biomass for commercial biofuel production. Moreover, the life cycle assessment of algal biofuels concerning the environment benefits and impacts should be used for as a guide for decisions on the operation and technology sides. Lastly, the possibilities of producing high-value co-products from the biomass residues after the extraction of microbial lipid should be considered. These biomass residues can be used in different applications like food, medicine, agriculture and this could well save raw material costs, reduce waste amount as well as GHG emissions. The utilization of wastes and residues from the microorganisms will contribute tremendously to the sustainability and market competitiveness of the biofuel industry.

6 Conclusion

In conclusion, the biofuels from microbial lipids have shown great potential as a replacement for petroleum-based fuels. The nature of lipids varies in each microbe, like yeasts, molds, bacteria and microalgae and they can serve as feedstock for the production of different biofuels. Microbial lipids can be obtained with existing infrastructure which will greatly improve the economics of biofuel production and reduce the dependency on fossil fuels. The feedstock for biofuel production should be chosen with prudence, which can be produced economically with high lipid content. The lipid content of the microbial biomass is affected by the nutritional status of the medium and is also modified by certain environmental stress. The current technologies discussed in this chapter will provide sufficient information to design a biofuel production facility which is comparable to petroleum based fuels in an economic perspective. The limitation of nitrogen and the choice of oil extraction methods for algae cultivation have significantly lowered the eutrophication potential of the effluent as described in the life cycle assessment. Challenges in commercializing microbial lipids based biofuels such as high production cost, large-scale cultivation and harvesting systems are being overcome in order to commercialize biofuel production.

References

1. Khan SA, Rashmi Hussain MZ, Prasad S, Banerjee UC (2009) Prospects of biodiesel production from microalgae in India. Renew Sustain Energy Rev 13(9):2361–2372
2. Dong T, Knoshaug EP, Pienkos PT, Laurens LML (2016) Lipid recovery from wet oleaginous microbial biomass for biofuel production: a critical review. Appl Energy 177:879–895
3. Brennan L, Owende P (2010) Biofuels from microalgae—a review of technologies for production, processing, and extractions of biofuels and co-products. Renew Sustain Energy Rev 14(2):557–577
4. Srivastava PK, Verma M (2008) Methyl ester of karanja oil as an alternative renewable source energy. Fuel 87(8):1673–1677
5. Sarin R, Sharma M, Sinharay S, Malhotra RK (2007) Jatropha-Palm biodiesel blends: an optimum mix for Asia. Fuel 86(10):1365–1371
6. Pinto AC, Guarieiro LLN, Rezende MJC, Ribeiro NM, Torres EA, Lopes WA, De Pereira PAP, De Andrade JB (2005) Biodiesel: an overview. J Braz Chem Soc 16(6B): 1313–1330
7. Chisti Y (2008) Biodiesel from microalgae beats bioethanol. Trends Biotechnol 26:126–131
8. Chisti Y (2007) Biodiesel from microalgae. Biotechnol Adv 25(3):294–306
9. Li Q, Du W, Liu D (2008) Perspectives of microbial oils for biodiesel production. Appl Microbiol Biotechnol 80(5):749–756
10. Wu X, Ruan R, Du Z, Liu Y (2012) Current status and prospects of biodiesel production from microalgae. Energies 5(8):2667–2682
11. Chojnacka K, Noworyta A (2004) Evaluation of *Spirulina* sp. growth in photoautotrophic, heterotrophic and mixotrophic cultures. Enzyme Microb Technol 34(5):461–465

12. Papanikolaou S, Chevalot I, Komaitis M, Marc I, Aggelis G (2002) Single cell oil production by Yarrowia lipolytica growing on an industrial derivative of animal fat in batch cultures. Appl Microbiol Biotechnol 58(3):308–312

13. Chang YH, Chang KS, Lee CF, Hsu CL, Huang CW, Der Jang H (2015) Microbial lipid production by oleaginous yeast *Cryptococcus* sp. in the batch cultures using corncob hydrolysate as carbon source. Biomass Bioenergy 72:95–103

14. Rittmann BE (2008) Opportunities for renewable bioenergy using microorganisms. Biotechnol Bioeng 100(2):203–212

15. Muniraj IK, Uthandi SK, Hu Z, Xiao L, Zhan X (2015) Microbial lipid production from renewable and waste materials for second-generation biodiesel feedstock. Environ Technol Rev 2515:1–16

16. Wackett LP (2011) Engineering microbes to produce biofuels. Curr Opin Biotechnol 22:388–393

17. Wackett LP (2008) Microbial-based motor fuels: science and technology. Microb Biotechnol 1(3):211–225

18. Zhang F, Rodriguez S, Keasling JD (2011) Metabolic engineering of microbial pathways for advanced biofuels production. Curr Opin Biotechnol 22(6):775–783

19. Peralta-Yahya PP, Keasling JD (2010) Advanced biofuel production in microbes. Biotechnol J 5(2):147–162

20. Antoni D, Zverlov VV, Schwarz WH (2007) Biofuels from microbes. Appl Microbiol Biotechnol 77(1):23–35

21. Ratledge C (2004) Fatty acid biosynthesis in microorganisms being used for single cell oil production. Biochimie 86(11):807–815

22. Ochsenreither K, Glück C, Stressler T, Fischer L, Syldatk C (2016) Production strategies and applications of microbial single cell oils. Front Microbiol 7:1539

23. Ratledge C, Wynn J (2005) Microbial production of oils and fats. Food Biotechnol Second. https://doi.org/10.1201/9781420027976.ch1.17

24. Wältermann M, Steinbüchel A (2005) Neutral lipid bodies in prokaryotes: recent insights into structure, formation, and relationship to eukaryotic lipid depots. J Bacteriol 187 (11):3607–3619

25. Kosa M, Ragauskas AJ (2011) Lipids from heterotrophic microbes: advances in metabolism research. Trends Biotechnol 29(2):53–61

26. Alvarez HM, Steinbüchel A (2002) Triacylglycerols in prokaryotic microorganisms. Appl Microbiol Biotechnol 60(4):367–376

27. Ratledge C, Cohen Z (2008) Microbial and algal oils: Do they have a future for biodiesel or as commodity oils? Lipid Technol 20(7):155–160

28. Spolaore P, Joannis-Cassan C, Duran E, Isambert A (2006) Commercial applications of microalgae. J Biosci Bioeng 101(2):87–96

29. Meng X, Yang J, Xu X, Zhang L, Nie Q, Xian M (2009) Biodiesel production from oleaginous microorganisms. Renew Energy 34(1):1–5

30. Subramaniam R, Dufreche S, Zappi M, Bajpai R (2010) Microbial lipids from renewable resources: production and characterization. J Ind Microbiol Biotechnol 37(12):1271–1287

31. Kavadia A, Komaitis M, Chevalot I, Blanchard F, Marc I, Aggelis G (2001) Lipid and γ-linolenic acid accumulation in strains of zygomycetes growing on glucose. J Am Oil Chem Soc 78(4):341–346

32. Vicente G, Bautista LF, Rodríguez R, Gutiérrez FJ, Sádaba I, Ruiz-Vázquez RM, Torres-Martínez S, Garre V (2009) Biodiesel production from biomass of an oleaginous fungus. Biochem Eng J 48(1):22–27

33. Zheng Y, Li T, Yu X, Bates PD, Dong T, Chen S (2013) High-density fed-batch culture of a thermotolerant microalga chlorella sorokiniana for biofuel production. Appl Energy 108:281–287

34. Yang F, Long L, Sun X, Wu H, Li T, Xiang W (2014) Optimization of medium using response surface methodology for lipid production by *Scenedesmus* sp. Mar Drugs 12 (3):1245–1257

35. Chen GQ, Jiang Y, Chen F (2007) Fatty acid and lipid class composition of the eicosapentaenoic acid-producing microalga, Nitzschia laevis. Food Chem 104(4):1580–1585

36. Yao L, Gerde JA, Lee S-L, Wang T, Harrata KA (2015) Microalgae lipid characterization. J Agric Food Chem 63(6):1773–1787

37. Fakas S, Galiotou-Panayotou M, Papanikolaou S, Komaitis M, Aggelis G (2007) Compositional shifts in lipid fractions during lipid turnover in *Cunninghamella echinulata*. Enzyme Microb Technol 40(5):1321–1327

38. Alvarez HM, Mayer F, Fabritius D, Steinbüchel A (1996) Formation of intracytoplasmic lipid inclusions by *Rhodococcus opacus* strain PD630. Arch Microbiol 165(6):377–386

39. Wu S, Hu C, Jin G, Zhao X, Zhao ZK (2010) Phosphate-limitation mediated lipid production by Rhodosporidium toruloides. Bioresour Technol 101(15):6124–6129

40. Huang X, Shen Y, Luo H, Liu J, Liu J (2018) Enhancement of extracellular lipid production by oleaginous yeast through preculture and sequencing batch culture strategy with acetic acid. Bioresour Technol 247:395–401

41. Yang X, Jin G, Gong Z, Shen H, Bai F, Zhao ZK (2015) Recycling microbial lipid production wastes to cultivate oleaginous yeasts. Bioresour Technol 175:91–96

42. Zeng Y, Bian D, Xie Y, Jiang X, Li X, Li P, Zhang Y, Xie T (2016) Utilization of food waste hydrolysate for microbial lipid and protein production by *Rhodosporidium toruloides* Y2. J Chem Technol Biotechnol

43. Martínez EJ, Raghavan V, González-Andrés F, Gómez X (2015) New biofuel alternatives: integrating waste management and single cell oil production. Int J Mol Sci 16(5):9385–9405

44. Cheirsilp B, Louhasakul Y (2013) Industrial wastes as a promising renewable source for production of microbial lipid and direct transesterification of the lipid into biodiesel. Bioresour Technol 142:329–337

45. Poli JS, da Silva MAN, Siqueira EP, Pasa VMD, Rosa CA, Valente P (2014) Microbial lipid produced by Yarrowia lipolytica QU21 using industrial waste: A potential feedstock for biodiesel production. Bioresour Technol 161:320–326

46. Kao C-Y, Chen T-Y, Chang Y-B, Chiu T-W, Lin H-Y, Chen C-D, Chang J-S, Lin C-S (2014) Utilization of carbon dioxide in industrial flue gases for the cultivation of microalga *Chlorella* sp. Bioresour Technol 166:485–493

47. Ji M-K, Yun H-S, Hwang J-H, Salama E-S, Jeon B-H, Choi J (2017) Effect of flue gas CO_2 on the growth, carbohydrate and fatty acid composition of a green microalga *Scenedesmus obliquus* for biofuel production. Environ Technol 38(16):2085–2092

48. Mu J, Li S, Chen D, Xu H, Han F, Feng B, Li Y (2015) Enhanced biomass and oil production from sugarcane bagasse hydrolysate (SBH) by heterotrophic oleaginous microalga *Chlorella protothecoides*. Bioresour Technol 185:99–105

49. Resdi R, Lim JS, Kamyab H, Lee CT, Hashim H, Mohamad N, Ho WS (2016) Review of microalgae growth in palm oil mill effluent for lipid production. Clean Technol Environ Policy 18(8):2347–2361

50. Zuliani L, Frison N, Jelic A, Fatone F, Bolzonella D, Ballottari M (2016) Microalgae cultivation on anaerobic digestate of municipal wastewater, sewage sludge and agro-waste. Int J Mol Sci 17(10):1692

51. Joe M-H, Kim J-Y, Lim S, Kim D-H, Bai S, Park H, Lee SG, Han SJ, Choi J (2015) Microalgal lipid production using the hydrolysates of rice straw pretreated with gamma irradiation and alkali solution. Biotechnol Biofuels 8:125

52. Chen Y-H, Walker TH (2011) Biomass and lipid production of heterotrophic microalgae *Chlorella protothecoides* by using biodiesel-derived crude glycerol. Biotechnol Lett 33 (10):1973

53. Griffiths MJ, Harrison STL (2009) Lipid productivity as a key characteristic for choosing algal species for biodiesel production. J Appl Phycol 21(5):493–507

54. Wan M, Jin X, Xia J, Rosenberg JN, Yu G, Nie Z, Oyler GA, Betenbaugh MJ (2014) The effect of iron on growth, lipid accumulation, and gene expression profile of the freshwater microalga Chlorella sorokiniana. Appl Microbiol Biotechnol 98(22):9473–9481

55. Lv JM, Cheng LH, Xu XH, Zhang L, Chen HL (2010) Enhanced lipid production of *Chlorella vulgaris* by adjustment of cultivation conditions. Bioresour Technol 101 (17):6797–6804

56. Luo HP, Al-Dahhan MH (2004) Analyzing and modeling of photobioreactors by combining first principles of physiology and hydrodynamics. Biotechnol Bioeng 85(4):382–393

57. Khotimchenko SV, Yakovleva IM (2005) Lipid composition of the red alga *Tichocarpus crinitus* exposed to different levels of photon irradiance. Phytochemistry 66(1):73–79

58. Yoo Chan, Jun So-Young, Lee Jae-Yon, Chi-Yong Ahn H-MO (2010) Selection of microalgae for lipid production under high levels carbon dioxide. Elsevier Ltd 101:S71–S74

59. Chiu SY, Kao CY, Tsai MT, Ong SC, Chen CH, Lin CS (2009) Lipid accumulation and CO2 utilization of *Nannochloropsis oculata* in response to CO2 aeration. Bioresour Technol 100(2):833–838

60. de Morais MG, Costa JAV (2007) Biofixation of carbon dioxide by *Spirulina* sp. and *Scenedesmus obliquus* cultivated in a three-stage serial tubular photobioreactor. J Biotechnol 129(3):439–445

61. Pahl SL, Lewis DM, King KD, Chen F (2012) Heterotrophic growth and nutritional aspects of the diatom *Cyclotella cryptica* (Bacillariophyceae): Effect of nitrogen source and concentration. J Appl Phycol 24(2):301–307

62. Converti A, Casazza AA, Ortiz EY, Perego P, Del Borghi M (2009) Effect of temperature and nitrogen concentration on the growth and lipid content of *Nannochloropsis oculata* and *Chlorella vulgaris* for biodiesel production. Chem Eng Process Process Intensif 48(6):1146–1151

63. Xu H, Miao X, Wu Q (2006) High quality biodiesel production from a microalga *Chlorella prototothecoides* by heterotrophic growth in fermenters. J Biotechnol 126(4):499–507

64. Dean AP, Sigee DC, Estrada B, Pittman JK (2010) Using FTIR spectroscopy for rapid determination of lipid accumulation in response to nitrogen limitation in freshwater microalgae. Bioresour Technol 101(12):4499–4507

65. Beopoulos A, Cescut J, Haddouche R, Uribelarrea JL, Molina-Jouve C, Nicaud JM (2009) Yarrowia lipolytica as a model for bio-oil production. Prog Lipid Res 48(6):375–387

66. Rodolfi L, Zittelli GC, Bassi N, Padovani G, Biondi N, Bonini G, Tredici MR (2009) Microalgae for oil: strain selection, induction of lipid synthesis and outdoor mass cultivation in a low-cost photobioreactor. Biotechnol Bioeng 102(1):100–112

67. Rasheva T, Kujumdzieva A, Hallet JN (1997) Lipid production by *Monascus purpureus* albino strain. J Biotechnol 56(3):217–224

68. Wynn JP, Hamid AA, Li Y, Ratledge C (2001) Biochemical events leading to the diversion of carbon into storage lipids in the oleaginous fungi *Mucor circinelloides* and *Mortierella alpina*. Microbiology 147(10):2857–2864

69. Fakas S, Papanikolaou S, Batsos A, Galiotou-Panayotou M, Mallouchos A, Aggelis G (2009) Evaluating renewable carbon sources as substrates for single cell oil production by *Cunninghamella echinulata* and *Mortierella isabellina*. Biomass Bioenergy 33(4):573–580

70. Papanikolaou S, Galiotou-Panayotou M, Chevalot I, Komaitis M, Marc I, Aggelis G (2006) Influence of glucose and saturated free-fatty acid mixtures on citric acid and lipid production by *Yarrowia lipolytica*. Curr Microbiol 52(2):134–142

71. Angerbauer C, Siebenhofer M, Mittelbach M, Guebitz GM (2008) Conversion of sewage sludge into lipids by Lipomyces starkeyi for biodiesel production. Bioresour Technol 99 (8):3051–3056

72. Kalscheuer R, Stölting T, Steinbüchel A (2006) Microdiesel: *Escherichia coli* engineered for fuel production. Microbiology 152(9):2529–2536

73. Zabeti N, Bonin P, Volkman JK, Guasco S, Rontani JF (2010) Fatty acid composition of bacterial strains associated with living cells of the haptophyte Emiliania huxleyi. Org Geochem 41(7):627–636

74. Zhao X, Peng F, Du W, Liu C, Liu D (2012) Effects of some inhibitors on the growth and lipid accumulation of oleaginous yeast *Rhodosporidium toruloides* and preparation of

biodiesel by enzymatic transesterification of the lipid. Bioprocess Biosyst Eng 35(6):993–1004

75. Wahlen BD, Morgan MR, McCurdy AT, Willis RM, Morgan MD, Dye DJ, Bugbee B, Wood BD, Seefeldt LC (2013) Biodiesel from microalgae, yeast, and bacteria: engine performance and exhaust emissions. Energy Fuels 27(1):220–228

76. Sawangkeaw R, Bunyakiat K, Ngamprasertsith S (2010) A review of laboratory-scale research on lipid conversion to biodiesel with supercritical methanol (2001–2009). J Supercrit Fluids 55(1):1–13

77. Karatay SE, Dönmez G (2011) Microbial oil production from thermophile cyanobacteria for biodiesel production. Appl Energy 88(11):3632–3635

78. Hidalgo P, Toro C, Ciudad G, Navia R (2013) Advances in direct transesterification of microalgal biomass for biodiesel production. Rev Environ Sci Biotechnol 12(2):179–199

79. Thliveros P, Uçkun Kiran E, Webb C (2014) Microbial biodiesel production by direct methanolysis of oleaginous biomass. Bioresour Technol 157:181–187

80. Leung DYC, Wu X, Leung MKH (2010) A review on biodiesel production using catalyzed transesterification. Appl Energy 87(4):1083–1095

81. Zhao L, Liu DXW (2007) Effect of several factors on peracetic acid pretreatment of sugarcane bagasse for enzymatic hydrolysis. J Chem Technol Biotechnol 82:1115–1121

82. Dai C-C, Tao J, Xie F, Dai Y-J, Zhao M (2007) Biodiesel generation from oleaginous yeast *Rhodotorula glutinis* with xylose assimilating capacity. African J Biotechnol 6(18):2130–2134

83. Awolu OO, Layokun SK (2013) Optimization of two-step transesterification production of biodiesel from neem (*Azadirachta indica*) oil. Int J Energy Environ Eng 4(1):39

84. Liu G-Q, Lin Q-L, Jin X-C, Wang X-L, Zhao Y (2010) Screening and fermentation optimization of microbial lipid-producing molds from forest soils. African J Microbiol Res 4:1462–1468

85. Amirsadeghi M, Shields-menard S, French WT, Hernandez R (2015) Lipid production by *Rhodotorula glutinis* from pulp and paper wastewater for biodiesel production. J Sustain Bioenergy Syst 5:114–125

86. Tran DT, Chen CL, Chang JS (2013) Effect of solvents and oil content on direct transesterification of wet oil-bearing microalgal biomass of *Chlorella vulgaris* ESP-31 for biodiesel synthesis using immobilized lipase as the biocatalyst. Bioresour Technol 135:213–221

87. Revellame E, Hernandez R, French W, Holmes W, Alley E (2010) Biodiesel from activated sludge through in situ transesterification. J Chem Technol Biotechnol 85(5):614–620

88. Montero-rodríguez D, Andrade RFS, Lima RA, Silva GKB, Rubio-ribeaux D, Silva TA, Hélvia WC (2016) Conversion of agro-industrial wastes by *Serratia marcescens* UCP/WFCC 1549 into lipids suitable for biodiesel. Production 49:307–312

89. Fjerbaek L, Christensen KV, Norddahl B (2009) A review of the current state of biodiesel production using enzymatic transesterification. Biotechnol Bioeng 102(5):1298–1315

90. Ghaly AE, Dave D, Brooks MS, Budge S (2010) Production of biodiesel by enzymatic transesterification: review. Am J Biochem Biotechnol 6(2):54–76

91. Tran D-T, Yeh K-L, Chen C-L, Chang J-S (2012) Enzymatic transesterification of microalgal oil from *Chlorella vulgaris* ESP-31 for biodiesel synthesis using immobilized Burkholderia lipase. Bioresour Technol 108:119–127

92. Teo CL, Jamaluddin H, Zain NAM, Idris A (2014) Biodiesel production via lipase catalysed transesterification of microalgae lipids from Tetraselmis sp. Renew Energy 68:1–5

93. Patil PD, Gude VG, Mannarswamy A, Cooke P, Nirmalakhandan N, Lammers P, Deng S (2012) Comparison of direct transesterification of algal biomass under supercritical methanol and microwave irradiation conditions. Fuel 97:822–831

94. Cui Y, Liang Y (2014) Direct transesterification of wet *Cryptococcus curvatus* cells to biodiesel through use of microwave irradiation. Appl Energy 119:438–444

95. D'Oca MGM, Viêgas CV, Lemões JS, Miyasaki EK, Morón-Villarreyes JA, Primel EG, Abreu PC (2011) Production of FAMEs from several microalgal lipidic extracts and direct transesterification of the *Chlorella pyrenoidosa*. Biomass Bioenerg 35(4):1533–1538

96. Johnson MB, Wen Z (2009) Production of Biodiesel Fuel from the Microalga *Schizochytrium limacinum* by Direct Transesterification of Algal Biomass. Energy Fuels 23(10):5179–5183

97. Chen C-L, Huang C-C, Ho K-C, Hsiao P-X, Wu M-S, Chang J-S (2015) Biodiesel production from wet microalgae feedstock using sequential wet extraction/transesterification and direct transesterification processes. Bioresour Technol 194:179–186

98. Chee Loong T, Idris A (2014) Rapid alkali catalyzed transesterification of microalgae lipids to biodiesel using simultaneous cooling and microwave heating and its optimization. Bioresour Technol 174:311–315

99. Cheng J, Huang R, Li T, Zhou J, Cen K (2014) Biodiesel from wet microalgae: extraction with hexane after the microwave-assisted transesterification of lipids. Bioresour Technol 170:69–75

100. Martinez-Guerra E, Gude VG, Mondala A, Holmes W, Hernandez R (2014) Extractive-transesterification of algal lipids under microwave irradiation with hexane as solvent. Bioresour Technol 156:240–247

101. Velasquez-Orta SB, Lee JGM, Harvey A (2012) Alkaline in situ transesterification of *Chlorella vulgaris*. Fuel 94:544–550

102. Dong T, Wang J, Miao C, Zheng Y, Chen S (2013) Two-step in situ biodiesel production from microalgae with high free fatty acid content. Bioresour Technol 136:8–15

103. Liu J, Chu Y, Cao X, Zhao Y, Xie H, Xue S (2015) Rapid transesterification of micro-amount of lipids from microalgae via a micro-mixer reactor. Biotechnol Biofuels 8 (1):229

104. Levine RB, Bollas A, Savage PE (2013) Process improvements for the supercritical in situ transesterification of carbonized algal biomass. Bioresour Technol 136:556–564

105. Kendall A, Yuan J (2013) Comparing life cycle assessments of different biofuel options. Curr Opin Chem Biol 17(3):439–443

106. Clarens AF, Resurreccion EP, White MA, Colosi LM (2010) Environmental life cycle comparison of algae to other bioenergy feedstocks. Environ Sci Technol 44:1813–1819

107. Clarens AF, Nassau H, Resurreccion EP, White MA, Colosi LM (2011) Environmental impacts of algae-derived biodiesel and bioelectricity for transportation. Environ Sci Technol 45(17):7554–7560

108. Jian H, Jing Y, Peidong Z (2015) Life cycle analysis on fossil energy ratio of algal biodiesel: Effects of nitrogen deficiency and oil extraction technology. Sci World J. https://doi.org/10.1155/2015/920968

109. Yang J, Xu M, Zhang X, Hu Q, Sommerfeld M, Chen Y (2011) Life-cycle analysis on biodiesel production from microalgae: water footprint and nutrients balance. Bioresour Technol 102(1):159–165

110. Singh A, Olsen SI (2011) A critical review of biochemical conversion, sustainability and life cycle assessment of algal biofuels. Appl Energy 88(10):3548–3555

111. Lardon L, Helias A, Sialve B, Steyer J-P, Bernard O (2009) Life-cycle assessment of biodiesel production from microalgae. Environ Sci Technol 43:6475–6481

112. Campbell PK, Beer T, Batten D (2011) Life cycle assessment of biodiesel production from microalgae in ponds. Bioresour Technol 102:50–56

113. Jorquera O, Kiperstok A, Sales EA, Embiruçu M, Ghirardi ML (2010) Comparative energy life-cycle analyses of microalgal biomass production in open ponds and photobioreactors. Bioresour Technol 101(4):1406–1413

114. Huang D, Zhou H, Lin L (2011) Biodiesel: an alternative to conventional fuel. Energy Procedia 16:1874–1885

115. Mata TM, Martins AA, Caetano NS (2010) Microalgae for biodiesel production and other applications: a review. Renew Sustain Energy Rev 14(1):217–232

Part IV
Bioreactors for Microbial Electrochemical Systems

Chapter 10
Electricity from Microbial Fuel Cells

Jun Li, Wei Yang, Biao Zhang, Dingding Ye, Xun Zhu and Qiang Liao

1 Introduction

The development and implementation of renewable energy resources is an effective approach to cope with global energy and pollution issues. Microbial fuel cell (MFC) technology has the promise to produce electrical energy and treat wastewater simultaneously because it converts the chemical energy contained in wastewater to electricity using electrochemically active bacteria (EAB) [1]. A schematic diagram of an MFC is shown in Fig. 1. In a typical MFC, electrons are produced from the degradation of organic matter by the metabolism of an EAB biofilm attached to the anode. The electrons are then transferred to the cathode through an external circuit where they are combined with protons and finally electron acceptors (e.g., oxygen) to close the circuit [2]. Unlike the combustion process, the oxidation and reduction reactions occur on the anode and cathode separately, requiring anaerobic anode conditions to keep the EAB from oxygen or any other terminal acceptors for electricity generation [3]. When acetate and oxygen are used as reactants (fuels) the electrode reactions at pH 7 are as follows:

Anode reaction:

$$CH_3COO^- + 4H_2O \rightarrow 2HCO_3^- + 9H^+ + 8e^- \quad E_a^0 = -0.300$$

J. Li (✉) · W. Yang · B. Zhang · D. Ye · X. Zhu · Q. Liao
Key Laboratory of Low-Grade Energy Utilization Technologies and Systems,
Chongqing University, Chongqing 400030, China
e-mail: lijun@cqu.edu.cn

J. Li · W. Yang · B. Zhang · D. Ye · X. Zhu · Q. Liao
Institute of Engineering Thermophysics, Chongqing University,
Chongqing 400030, China

Fig. 1 Schematic diagram of an MFC

Cathode reaction:

$$2O_2 + 8e^- + 8H^+ \rightarrow 4H_2O \quad E_c^0 = 0.805 \, V$$

Overall reaction:

$$CH_3COO^- + 2O_2 \rightarrow 2HCO_3^- + H^+ \quad E^0 = 1.105 \, V$$

Based on the reaction above, the substrate is decomposed into bicarbonate and oxygen is reduced to water. When wastewater is fed into MFCs, the organic/inorganic matters can be degraded, providing wastewater treatment and energy recovery in the form of electricity.

Many efforts have been made to improve the capacity of MFC technology for waste treatment and power generation. Many organic matters such as acetate, glucose, butyrate, and lactate (Table 1), have been used as substrates for MFCs and this has demonstrated the feasibility of recovering electricity from different organic matters [4]. To simulate and verify the in situ treatment of MFC technology, some prototypes have been tested using brewery wastewater, landfill wastewater, and starch processing wastewater under continuous or batch feed conditions (Table 1). Liu et al. reported an MFC capable of producing electricity from domestic wastewater. The MFC generated a maximum power output of 26 mW/m² while

Table 1 Different substrates used in microbial fuel cells (MFCs)

Type of substrate	Concentration	Source inoculum	Type of MFC (with electrode surface area and/or cell volume)	References
Glucose	6.7 mM	Mixed bacterial culture maintained on sodium acetate for 1 year	One-chamber air-cathode MFC (12 mL) with non wet proofed carbon cloth as anode (2 cm^2) and wet proofed carbon cloth as cathode (7 cm^2)	[7]
Acetate	1 g/L	Pre-acclimated bacteria from MFC	Cube shaped one-chamber MFC with graphite fiber brush anode (7170 m^2/m^3 brush volume)	[8]
Lactate	18 mM	Pure culture of *S. oneidensis* MR-1	Two-chambered MFC with graphite felt electrode (20 cm^2)	[9]
Domestic wastewater	600 mg/L	Anaerobic sludge	Two-chambered mediator-less MFC with plain graphite electrode (50 cm^2)	[10]
Brewery wastewater	2240 mg/L	Full strength brewery wastewater	One-chamber air-cathode MFC with non-wet proofed carbon cloth as anode (7 cm^2) and wet proofed carbon cloth containing Pt as cathode	[11]
Beer brewery wastewater	600 mg/L	Anaerobic mixed consortia	One-chamber air-cathode MFC with carbon fibers as anode	[12]
Starch processing wastewater	4852 mg/L COD	Starch processing wastewater	One-chamber air-cathode MFC with carbon paper anode (25 cm^2)	[13]
Landfill leachate	6000 mg/L	Leachate and sludge	Two-chambered MFC with carbon veil electrode (30 cm^2)	[14]
Azo dye with glucose	300 mg/L	Mixture of aerobic and anaerobic sludge	One-chamber air-cathode MFC with carbon paper anode (36 cm^2)	[15]
Synthetic wastewater	510 mg/L	Anaerobic culture from a preexisting MFC	Dual chamber MFC with stainless tell as anode (170 cm^2) and graphite rods as cathode (150 cm^2)	[16]

removing 80% of the chemical oxygen demand (COD) in the wastewater [2]. Many studies have focused on MFC scale-up and practical applications. MFC studies have typically been conducted in reactors with small volumes ranging from several

microliters to liters. These reactors are suitable for obtaining basic information but for practical wastewater treatment, the goal is to develop a scalable technology for large-scale implementation. The first large-scale MFC test was performed at Foster's brewery in Yatala by the Advanced Water Management Center at the University of Queensland. This study used a reactor consisting of 12 modules, each 3 m high, with a total volume of approximately 1 m^3 [5]. The goal is for the electricity recovered from wastewater to at least partially cover the cost of the wastewater treatment process. To date, the electrical power production has been increased by five- to sixfolds and improvements continue to be made [5]. Novel approaches have been reported to improve MFC performance, either by optimizing the MFC structure or exploring cost-efficient and high performance electrode materials. To improve the cathode performance while reducing cost, a stainless steel mesh-based (SSM) cathode and inexpensive carbon catalysts were proposed to replace the conventional expensive platinum-based (Pt) system for MFC applications [6].

Although significant improvements have been achieved, challenges remain in scale-up and practical applications. A major obstacle for MFC application is the low amount of electricity generation. This is mainly affected by four factors: (1) the biofilm's activity to oxidize the substrate of the anode, (2) the low efficiency of the electron transfer between the biofilm and the anode, (3) the slow oxygen reduction reaction (ORR) at the cathode, and (4) the high internal ohmic resistance. Many methods have been tested to enhance MFC performance. These include: exploiting three-dimensional (3D) open porous anode materials, preparing novel ORR catalysts, and optimizing the reactor architecture. Another major limitation is the high fabrication cost of MFCs. In typical MFCs, the most commonly used ORR catalyst is platinum and its alloys. The anode materials are carbon cloth or carbon paper. The costs for both of these materials are high, especially for large-scale wastewater treatment applications. In addition, the procedure for fabricating electrodes is complex and labor intensive; this also increases the cost of MFCs. For example, the MFC cathode is usually prepared by brushing or spraying catalyst inks onto the supporting carbon materials, leading to an additional cost in MFC applications [6, 17]. These problems are being addressed by research on high-efficiency materials and optimized MFC electrode designs. The goal is the development of a scalable technology for treating different types of wastewater and simultaneous energy recovery.

This chapter (1) details the fundamental principles of MFCs, (2) reviews the electrode materials and construction methods, (3) provides an overview of MFC architecture, (4) discusses the MFC stack and the feasibility in practical power generation, and (5) reviews the various applications of MFC technology.

2 Fundamental Principles of MFCs

2.1 Voltage and Current

A working MFC usually produces an operating voltage (U) of ~ 0.5 V, which is a function of external resistance (R_{ex}) and current (I). The relationship is as follows:

$$U = IR_{ex} \tag{1}$$

Therefore, the current can be calculated from the measured voltage drop across the external resistance as $I = U/R_{ex}$. The highest voltage, which is produced in an open-circuit condition, is open-circuit voltage (OCV).

The theoretical maximum voltage (reversible voltage) that can be generated from an MFC is limited by thermodynamics, which can be predicted by the Nernst equation:

$$E_{mef} = \mathrm{E}^0 - \frac{RT}{nF} \ln \frac{[\text{products}]^{\mathrm{p}}}{[\text{reactants}]^{\mathrm{r}}} \tag{2}$$

where E_{mef} is the maximum electromotive force, E^0 is the standard cell electromotive force, R is the gas constant (8.31447 J/mol K), T is the absolute temperature (K), n is the transferred electron number, and F = 96,485 C/mol is the Faraday's constant. According to the International Union of Pure and Applied Chemistry (IUPAC) convention, all of the reaction equations are expressed in the direction of a reduction reaction, so that the production and reactants are the reduced and oxidized species respectively. $E°$ is calculated based on hydrogen under standard conditions (at 298 K, chemical concentration of 1 M for liquid and 1 bar for gases), which is defined as $E° (H_2) = 0$, referred to as the normal hydrogen electrode (NHE).

Based on these principles, the electrode potential and voltage generation can be determined. In an MFC system, the bacteria need to be operated in neutral pH conditions. The ORR reaction can be described as:

$$1/2 O_2 + 2H^+ + 2e^- \rightarrow H_2O,\ E^0(O_2) = 1.229\ \text{V}$$
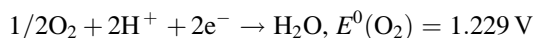
Then, the cathode potential (E_c) at pH = 7 can be calculated as [18]:

$$E_c = E^0 - \frac{RT}{nF} \ln \frac{1}{[O_2]^{1/2}[H^+]^2}$$

$$E_c = 1.229\ \text{V} - \frac{(8.31\ \text{J/mol K})(298.15\ \text{K})}{(2)(96,485\ \text{C/mol})} \ln \frac{1}{[0.2\ \text{mol/L}]^{1/2}[10^{-7}\ \text{mol/L}]^2}$$

$$= 0.805\ \text{V}$$

For an MFC using acetate as the substrate, the HCO_3^-/Ac can be expressed as:

$$2HCO_3^- + 9H^+ + 8e^- \rightarrow 4H_2O + CH_3COO^-$$
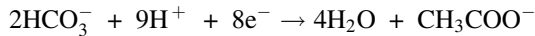
For acetate E^0 (acetate) = 0.187 V, with a concentration of 1 g/L, a neutral pH = 7 and a bicarbonate concentration of HCO_3^- = 5 mM, the anode potential (E_a) can be calculated as [18]:

$$E_a = E^0 - \frac{RT}{nF} \ln \frac{[CH_3COO^-]}{[HCO_3^-]^2[H^+]^9}$$

$$E_a = 0.187\,V - \frac{\left(\frac{8.31J}{mol} \cdot K\right)(298.15\,K)}{(8)\left(96,485\frac{C}{mol}\right)} \ln \frac{1}{\left[0.005\frac{mol}{L}\right]^2\left[10^{-7}\frac{mol}{L}\right]^9} = -0.300V$$

The highest cell voltage that can be generated from an MFC is the difference between the anode and cathode potentials:

$$E = E_c - E_a \tag{3}$$

Therefore, an MFC using acetate as the substrate and oxygen as the terminal electron acceptor can obtain a maximum voltage output of 0.805 V – (–0.300 V) = 1.105 V. However, in practical applications, the voltage output of the air-cathode MFCs is much lower than this value. This can be attributed to two aspects: the first is the voltage loss caused by activation losses, ohmic losses, and mass transfer losses during the operation. The second is the inefficient ORR through a two-electron pathway (E_c = 0.328 V), compared to a four-electron pathway (E_c = 0.805 V).

2.2   Electricity Generation and Energy Recovery

In an MFC, power is calculated from the measured voltage and current across the external load as:

$$P = IU \tag{4}$$

The current produced by an MFC can be obtained by measuring the voltage drop across the external resistor using $I = U/R_{ex}$, thus, the power can be expressed as a function of U and R_{ex}:

$$P = \frac{U^2}{R_{ex}} \tag{5}$$

Based on the equation $I = U/R_{ex}$, power also can be expressed in terms of the calculated current as:

$$P = I^2 R_{ex} \tag{6}$$

2.2.1   Power Density

To evaluate the power output generated from an MFC with a specific architecture, the power density can be calculated based on the electrode surface area or the reactor volume. Thus the power density can be categorized into surface specific power density and volumetric power density.

Surface specific power density is the power output normalized by the electrode surface area:

$$P_a = \frac{U^2}{A_a R_{ex}} \text{ or } P_c = \frac{U^2}{A_c R_{ex}} \tag{7}$$

where P_a and P_c are the power density based on the anode and cathode surface area, respectively. A_a and A_c are the effective areas of the anode and cathode, which can be the specific surface area or geometric area. In an MFC with a membrane or separator, power density can also be calculated based on the membrane/separator area (A_m). Volumetric power density, used to evaluate the power output of a whole MFC system, is the power output normalized by the reactor volume. Volumetric power density can be expressed as:

$$P_V = \frac{U^2}{V R_{ex}} \tag{8}$$

where P_V is the volumetric power density (W/m^3) and V is the volume of the reactor (m^3).

2.2.2   Energy Recovery

The goal of MFC technology is to recover the energy contained in the wastewater. To evaluate the recovery efficiency of electrons from wastewater, coulombic efficiency (CE) is commonly used and it is defined as the fraction of coulombs recovered versus the total energy contained in the wastewater:

$$CE = \frac{\text{Coulombs recovered}}{\text{Total coulombs in substrate}} \tag{9}$$

Coulombs can be calculated by integrating the current with the time; therefore, CE can be expressed as:

$$CE = \frac{M \int_0^t I dt}{FeV\Delta C} \tag{10}$$

where M is the molecular weight of substrate (g/mol), V is the volume of the liquid in the anode chamber (m^3), and ΔC is the substrate concentration (mol/L) change over a fed-batch cycle (t).

For an MFC system using complex substrates, CE can be obtained using COD as the measure of substrate concentration:

$$CE = \frac{8 \int_0^t I dt}{FV\Delta COD} \tag{11}$$

where 8 is a constant for the COD, based on the molecular weight of oxygen (32 g/mol), and 4 is the electron transfer number per mol of oxygen.

2.3 Polarization and Power Density Curves

The polarization curve is a plot of current density versus voltage, which can be obtained by varying the external resistance while recording the current density and voltage values at each resistance (Fig. 2a). A typical polarization curve of an MFC is shown in Fig. 2b. The power density curve, as a function of current density, is usually shown along with the polarization curve. It is also commonly observed that
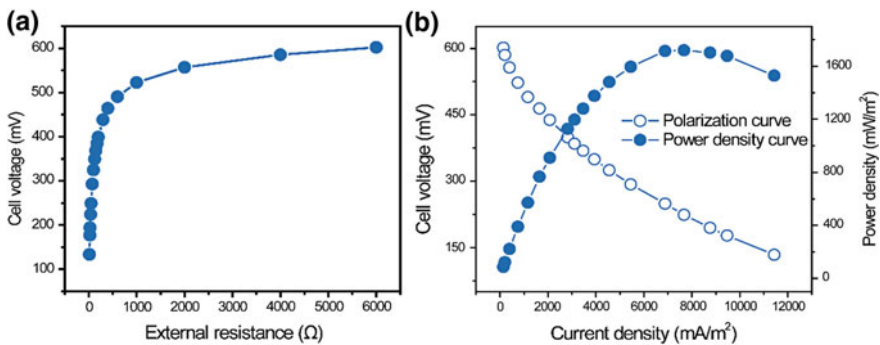
Fig. 2 Cell voltage as a function of external resistances (**a**), polarization curve, and power density curve of an MFC (**b**)
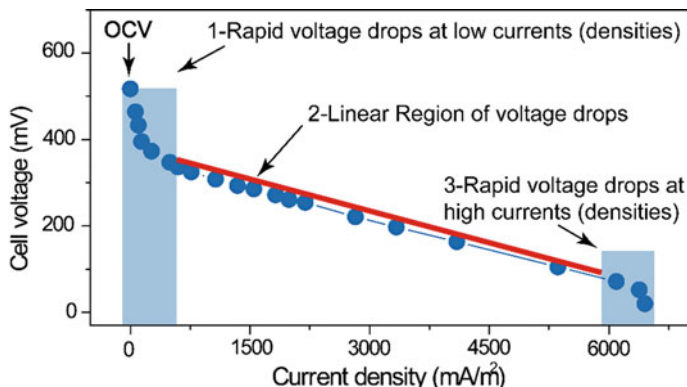
Fig. 3 Characteristics of a polarization curve, showing three types of voltage losses

a peak, called the maximum power density, appears at high current densities in the power density curve.

The OCV and the operation voltage of an MFC are always lower than the reversible voltage predicted by the Nernst equation. To analyze the voltage losses, the polarization curve can be divided into three regions: (1) a rapid voltage drop at low current densities; (2) a nearly linear decrease in voltage at medium current densities; and (3) a rapid voltage drop at high current densities (Fig. 3). The voltage losses are the result of electrode overpotentials, which are current dependent (overpotentials change with current densities). Electrode overpotentials are thought to arise from basic losses corresponding to three regions: (1) activation losses; (2) ohmic losses; and (3) mass transport losses.

(1) Activation losses are the energy losses incurred for driving the oxidation or reduction reactions, and for transferring electrons from the bacteria to the anode surface by the conductive nanowire, mediator, or terminal cytochrome on the cell surface [18]. Enhancing the electron transfer between anode and bacteria, using highly efficient cathode catalysts, and improving the anode biofilm metabolism activity for substrate oxidation would reduce the activation losses.

(2) Ohmic losses arise from the resistance of ion conduction in the solution and membrane and the flow of electrons through the electrodes and wires as well as their connection points. The ohmic losses can be reduced by decreasing the electrode spacing, removing the membrane or using a membrane with a high ion conductivity, increasing the solution conductivity, improving the electrode conductivity, and ensuring a good connection between the electrodes and connection wires.

(3) Mass transport losses arise from the insufficient transport of species to/from the electrode. At the anode, ensuring a sufficient substrate supply and proton removal is an effective approach for reducing mass transport losses. The limited proton removal within the biofilm can be a problem as it lowers the local pH of

biofilm and adversely affects the biofilm activity. Similarly, the limited proton supply for the ORR at the cathode can also increase the pH, which can lower the cathode potential and decrease the cathode performance.

2.4 Electrochemical Analysis

2.4.1 Electrochemical Impedance Spectroscopy (EIS)

EIS is commonly used for quantifying the internal resistance of MFCs. Generally, EIS tests are performed on a potentiostat by applying a sinusoidal signal with small amplitude on the working electrode. By changing the sinusoidal signal frequency over a wide range (typically from 100 kHz to 0.01 Hz), impedance spectra can be obtained for the MFC system. A Nyquist curve is plotted using the impedance spectra as the real impedance (Z_{re}) versus imaginary impedance (Z_{im}), as shown in Fig. 4. To obtain more detailed information about the component of the internal resistance, the impedance spectra usually needs to be fitted using an equivalent circuit by EIS software.

2.4.2 Voltammetry

Voltammetry is typically used to determine the redox potential of redox active matter. The information can be used to evaluate electrochemical activity of the biofilm and cathode catalysts. There are two types of voltammetry: linear sweep

Fig. 4 Nyquist plots of an activated carbon cathode in a single-chamber MFC
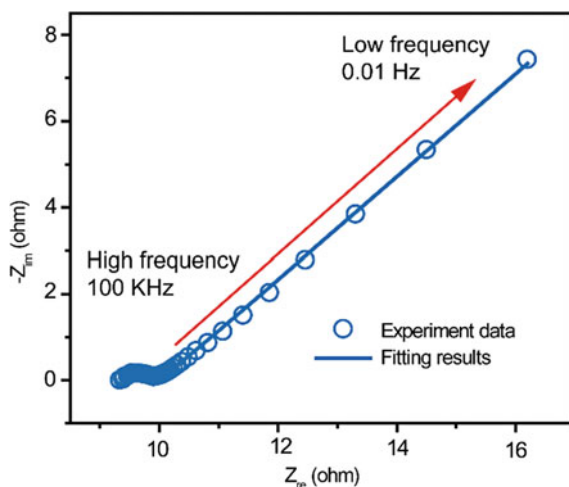
Fig. 5 Cyclic voltammetry of the anode of an MFC under turnover conditions
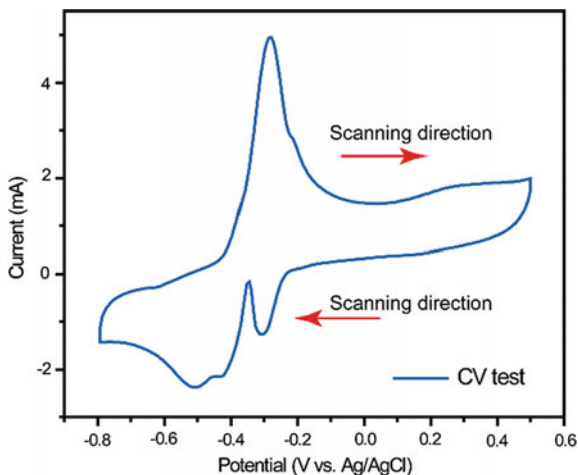
voltammetry (LSV) and cycle voltammetry (CV). In LSV tests, the potential of the working electrodes (anode or cathode) varies at a certain scan rate in one direction. For CV tests, the scan is conducted in one direction first and then continued in the reverse direction until the potential is returned to the start value (Fig. 5). In an MFC system, CV is the most commonly used method to determine the presence of electron shuttles or mediators produced by bacteria under non-turnover conditions and to determine the oxidation current of anode biofilm under turnover conditions. LSV is mainly applied to record the current response of the cathode under different potentials for the evaluation of the electrocatalytic activity of the ORR (Figs. 6 and 7).
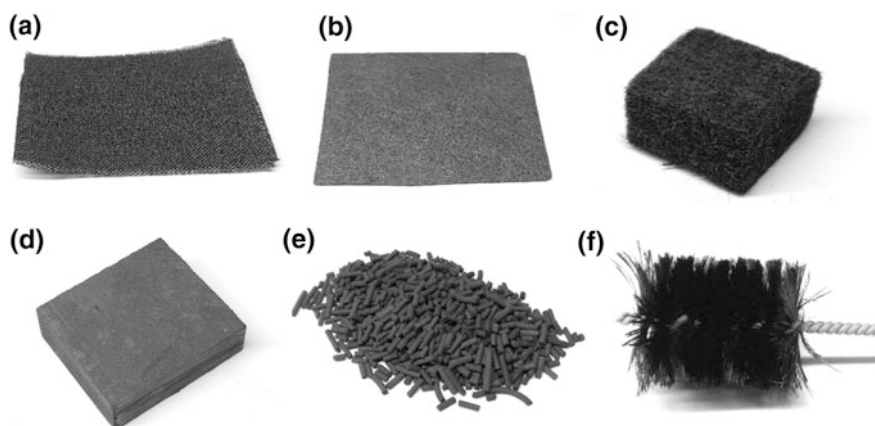
Fig. 6 Common anode materials used in MFCs: a carbon cloth, b carbon paper, c carbon felt, d graphite plate, e granular carbons, and f carbon brush
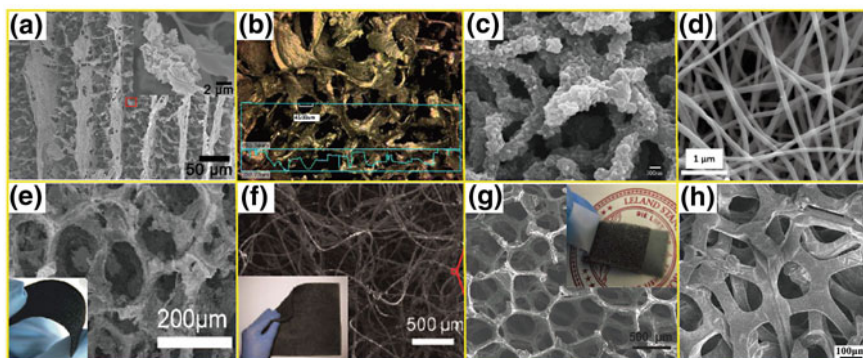
Fig. 7 3D porous anode derived from nanomaterials: **a** chitosan/vacuum-stripped graphene scaffolds (adapted and reprinted from [19], Copyright 2012, with permission from American Chemical Society), **b** 3D chitosan–carbon nanotube scaffolds (adapted and reprinted from [20], Copyright 2011, with permission from Elsevier), **c** CNT/PANI nanocomposite (adapted and reprinted from [21], Copyright 2007, with permission from Elsevier), **d** porous carbon nanofiber aerogel (adapted and reprinted from [22], Copyright 2016, with permission from Wiley), **e** graphene-coated nickel foam (adapted and reprinted from [23], Copyright 2013, with permission from Royal Society of Chemistry), **f** 3D carbon nanotube-textile (adapted and reprinted from [24], Copyright 2011, with permission from American Chemical Society), **g** graphene-sponge (adapted and reprinted from [25], Copyright 2012, with permission from Royal Society of Chemistry), and **h** polyaniline hybridized three-dimensional graphene (adapted and reprinted from [26], Copyright 2012, with permission from American Chemical Society)

3 Electrode and Separator Materials of MFCs

As discussed in Sect. 2.3, the power generation of an MFC depends on the rate of substrate degradation, bacterial growth and respiration rate on the anode, circuit resistance, ion mass transfer in the electrolyte, mass transfer of the cathode electron acceptor, reduction rate of the cathode electron acceptor, and the operating conditions. Different electrode and separator materials vary in their physical and chemical properties (e.g., surface area, electric conductivity, and chemical stability), thus they also vary in their impacts on biofilm establishment, bacterial metabolism, ohmic resistance, and the rate of electrode reactions. Therefore, it is of interest to develop low-cost, high performance anode, cathode, and separator materials to promote the performance of MFCs.

3.1 Anode Materials

The anode is where the electroactive biofilm establishes and the bioelectrochemical reaction occurs. Therefore, anode materials play a significant role in MFC performance. An ideal anode would have high conductivity, high specific surface area or

porosity, low cost, biocompatibility, and good stability. Several metal materials, such as stainless steel, titanium, copper, nickel, and gold, and carbon materials, such as carbon cloth/paper, carbon graphite brush, and biomass-derived porous carbon, have been used for the anode of MFCs [6, 27–29]. Among these materials, the carbonaceous anodes are regarded as the most cost-effective and promising for the large-scale application of the MFCs.

3.1.1   Traditional Carbon Materials

Carbon materials (e.g., carbon cloth/paper, graphite plate/granules/rod, carbon mesh, carbon felt, reticulated vitreous carbon, and graphite brush) are widely used as anode materials because of their high conductivity and biocompatibility [6, 30–34]. Carbon cloth/paper is a planar, porous, but fragile and expensive, material so it is mainly used in lab-scale testing. Carbon felt and reticulated vitreous carbon are also porous materials and therefore can provide many inner spaces for bacteria growth and channels for substrate supply and proton removal. Unfortunately, the low electrical conductivity of carbon felt leads to high ohmic resistance, and the cost of reticulated vitreous carbon is too high for wastewater treatment use. Granular activated carbon (GAC) is also used as the anode because of its good biocompatibility and low cost [35]. Generally, GAC is usually used in packing-bed anodes, which produce low anode electrical conductivity. Additionally, the specific surface area of the GAC-based anode is quite high, but the surface area accessible to bacteria acclimation is relatively low because most of the pores in GAC are small pores with a diameter < 50 nm. The graphite brush electrode is one of the most promising anodes for practical application of MFC technology. The MFC using the graphite brush had a maximum power density of 2400 mW/m^2, which was about 4 times higher than using carbon paper (600 mW/m^2) [8]. A graphite brush is prepared by folding and twisting a titanium wire to form a succession of regular loophole openings in which graphite fiber bundles are crimped to form a spiral structure [36, 37]. The central titanium metal guarantees high electrical conductivity. The micro-scale diameter of graphite fibers ($\sim$7 μm) provides a highly open porous structure for bacterial acclimation. Graphite brushes have been extensively used as MFC anodes and ongoing investigations are focused on reducing the overall cost.

3.1.2   3D Porous Anode Base on Carbon Nanomaterials

To improve the anode performance, 3D materials with large surface areas are emerging as alternatives for the anode. A variety of 3D nanomaterial-based anodes, such as chitosan/vacuum-stripped graphene scaffold, 3D chitosan–carbon nanotube scaffolds, polyaniline hybridized 3D graphene, carbon nanotube (CNT)/polyaniline (PANI) nanocomposite, PANI/graphene-coated nickel foams, 3D carbon nanotube-textiles, porous carbon nanofiber aerogels, graphene-sponges, and

graphene-coated nickel foams have been studied as MFC anodes [19–26]. Katuri et al. fabricated a multiwall carbon nanotube (MWCNT)/chitosan 3D composite anode by ice segregation-induced self-assembly (ISISA). A maximum current density of 24.5 A/m^2 was achieved at 0 V versus Ag/AgCl for 200 h [38]. Chitosan/vacuum-stripped graphene scaffold and 3D chitosan–carbon nanotube scaffolds prepared using ISISA also exhibited a great advantage over carbon cloth or felt. Vacuum-stripped graphene powder randomly embedded on the chitosan layers increased the surface roughness of the layers and provided a larger graphene surface area for bacteria adhesion. In addition, due to the presence of meso/micropores in the anode, a large internal surface area was accessible to endogenous mediators for the electron transfer between bacteria and anode, leading to increased biofilm activity. An MFC using these anodes achieved 78 times higher power output than with the conventional carbon cloth [19]. These 3D porous nanomaterials-based anodes generally possess a hierarchical porous structure that benefits efficient diffusion of electron mediators and substrate as well as bacterial adhesion in the interior of the 3D electrode. They show great potential for use in MFCs.

3.1.3 Biomass Derived Materials

Many types of biomass, such as chestnut shells, pomelo peels, natural loofah sponges, and bamboo, have been used as precursors for the fabrication of the MFC anodes (Fig. 8) [39–42]. In general, the inherent pore structure of the biomass can evolve into macropores during carbonization at a temperature above 800 °C. The macropores are usually cross-linked, favoring a rather high conductivity and a high performance anode. For example, Chen et al. used sponge-like pomelo peels as the precursor for the anode. The MFC using the reticulated carbon foam derived from pomelo peels achieved a maximum current density of 4.0 mA/cm^2 [39], which was 2.5 times higher than that of graphite felt. Zhang et al. reported that carbonized dry bamboo branches can be directly used as the high performance anode for biofilm establishment because the obtained electrode maintained the inherent structure of bamboo, which is a hollow tube with an inner diameter of 2 mm and highly ordered 15–100-µm macropores [41]. A chestnut shell-derived porous carbon anode has also been tested. An MFC with this anode achieved a maximum power density (23.6 W/m^3) 2.3 times higher than carbon cloth anode (10.4 W/m^3) [42]. Anodes derived from corn stems, king mushrooms, and wild mushrooms have been reported by Karthikeyan et al. [43]. Lu et al. reported a high-performance flexible anode derived from carbonized silk cocoons. Due to their hierarchical 3D, pseudographitic microstructure, good biocompatibility, and high capacitance, an MFC equipped with the carbonized silk cocoon anodes provided ∼2.5-fold maximum power density greater than that of carbon cloth anodes [44]. The use of natural and recyclable materials can greatly reduce the cost of electrode materials and improve anode performance. These materials provide a potential avenue for MFC
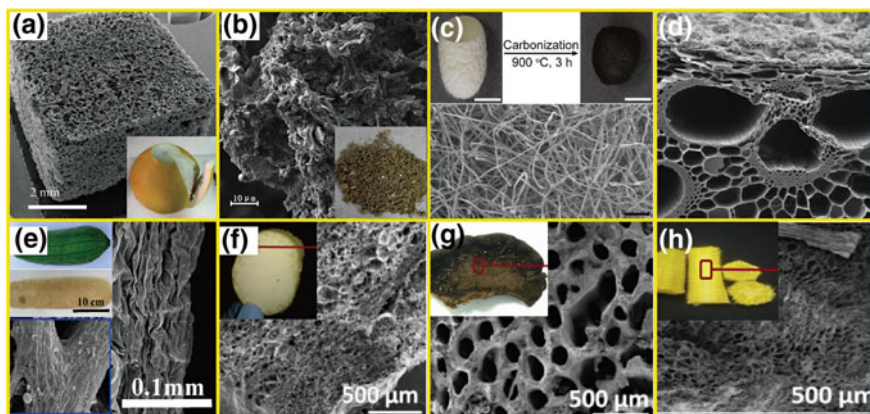
Fig. 8 3D porous anode materials derived from biomass: **a** pomelo peel (adapted and reprinted from [39], Copyright 2012, with permission from Royal Society of Chemistry), **b** chestnut shell (adapted and reprinted from [42], Copyright 2018, with permission from Elsevier), **c** silk cocoon (adapted and reprinted from [44], Copyright 2017, with permission from Elsevier), **d** bamboo (adapted and reprinted from [41], Copyright 2014, with permission from Elsevier), **e** natural loofah sponge (adapted and reprinted from [40], Copyright 2013, with permission from American Chemical Society), **f** king mushroom, **g** wild mushroom (adapted and reprinted from [43], Copyright 2015, with permission from Elsevier), and **h** corn stem (adapted and reprinted from [43], Copyright 2015, with permission from Elsevier)

commercialization. However, the structure of these materials is difficult to control and reproduce thus limiting their application in MFCs.

3.1.4 Modification of the Anode Materials

Modification of anode materials can improve MFC performance by increasing the bacterial affinity for the anode surface, by providing an extra supporting and conductive surface, or by facilitating the extracellular electron transfer (EET) between bacteria and the electrode. The modification methods can be classified into the following types: (1) decorating with carbon nanomaterials, (2) modification using a conducting polymer, and (3) chemical/electrochemical anode modifications.

The widely used nanomaterials for anode modifications are CNTs, carbon nanospheres, and graphene. CNTs are cylindrically-shaped carbon materials with a large surface area and these promote microbial adhesion and electron transfer between the bacteria and anode surface. Ren et al. reported that an anode with horizontally aligned spin-spray layer-by-layer CNT showed a smaller sheet resistance and induced a thicker biofilm than the unmodified samples. A maximum power density of 3320 ± 40 W m^{-3} was obtained by using the anode in a miniaturized MFC. This value was more than 8.5 times greater than values reported by prior-art MFCs using 2D and 3D nanostructured electrodes [45]. Similarly,

nitrogen-doped CNT not only facilitated EET from the c-cytochrome located on the outer membrane of the bacteria to the electrode but also enhanced the contact area between the bacteria and the electrode [46]. Graphene is a unique carbon nano-material with 2D lattice made of sp^2-hybridized carbon atoms. Graphene has great application potential in MFCs. Decorating the electrode with graphene can create an electrically conductive surface similar to that of CNT-coated materials while considerably reducing the electrode cost. A graphene-modified anode improved the power density and the energy conversion efficiency by 2.7 and 3 times, respectively [47]. Zhang et al. also demonstrated that the graphene-modified SSM anode produced a maximum power density of 2668 mW/m^2, which was 18 times larger than the unmodified SSM anode [48].

Conducting polymers, such as polyaniline and polypyrrole, have been widely used to modify the electrode due to their high conductivity and durability in MFC-relevant conditions. Polyaniline carries positive charges in neutral environments; therefore, it is attractive for enhancing the adhesion of the negatively charged bacteria. A polyaniline-coated anode reduced the start-up time of MFCs from 140 to 78 h by enhancing bacterial cell attachment [49]. The conducting polymer facilitated the EET between the bacteria and the anode. For example, a anode modified by polypyrrole/graphene oxide composites using electro-polymerization delivered an 8 times higher maximum power density than the unmodified anode in MFCs [50]. Gnana Kumar et al. reported that a reduced graphene oxide/polypyrrole composite-modified carbon cloth anode achieved a 3 times higher maximum power density than that of unmodified carbon cloth, due to the increased electron transfer efficiency and the increased contact area between the bacteria and the anode [51].

With chemical and electrochemical modifications, functional groups can be introduced onto the electrode surfaces, leading to a change in the physicochemical properties of the electrodes and creating a larger electrocatalytically active area, increased surface charges on the electrode, and a faster EET rate. Chemical and electrochemical modifications of the anode are effective methods for improving the anode performance due to the enhanced bacterial cell attachment and the facilitated EET rate from the bacteria to the anode surface. Chemical modification of the anode is usually carried out by directly soaking the electrode in strong acid or treating the carbon materials in ammonia at 600–800 °C [52–54]. Cheng et al. achieved a 48% increase in power production and a 50% decrease in the start-up time by treating the carbon cloth in ammonia at 700 °C [54]. However, chemical modification usually requires toxic chemicals and high temperatures, both of which increase the cost of MFCs. Anode modification can also be achieved by electrochemical oxidation in different electrolytes, such as NH_4NO_3, $(NH_4)_2SO_4$ and HNO_3/H_2SO_4 [55, 56]. Zhang et al. found that electrolyzing the carbon cloth in nitric acid followed by soaking in aqueous ammonia could produce a 58% higher maximum power density compared to the untreated control [55].

3.2 Separators

3.2.1 Ion Exchange Membrane

In the double-chamber MFCs (DCMFCs), the membrane is usually used to separate the anode and cathode chamber. This prevents the crossover of oxygen and substrate while allowing ion transfer between the anode and cathode chamber. The major types of membranes used in MFCs include cation exchange membranes (CEM), anion exchange membranes (AEM), and the polymer/composite membranes. Many CEMs, including Nafion, Hyflons, Zirfons, and Ultrexs CMI 7000, are used in DCMFCs. Nafions are the most commonly used CEM in MFCs because of their good proton conductivity resulting from the negatively charged hydrophilic sulfonate groups attached to the hydrophobic fluorocarbon backbone [57]. Usually, a thinner membrane has lower ohmic resistance and produces higher performance. For example, an MFC with a thinner Nafion 112 membrane had a higher power density of 31.32 mW/m^2 than one using a thicker Nafion 117 membrane (9.95 mW/m^2). Pant et al. investigated the effect of membrane types on MFC performance and found that an MFC with Ultrexs CMI 7000 had a comparable performance to that with the Nafion membrane [58], but had a lower oxygen mass transfer coefficient (2.8×10^{-4} cm/s) compared to one with Zirfons (1.9×10^{-3} cm/s) [59]. AEMs, such as AFN, AM-1, and ACS, are also widely used in MFCs. AFN had the lowest membrane resistance among these AEMs, resulting in the increased production of electricity [60]. However, AM-1 and ACS have a lower oxygen mass transfer coefficient compared with AFN. Polymer/composite membranes, such as sulfonated polyether ether ketone (SPEEK) membranes and disulfonated poly (arylene ether sulfone) (BPSH) membranes, are also used as alternatives to the Nafion membrane in MFCs. A high proton conductivity and a low oxygen mass transfer coefficient of the SPEEK membrane can be obtained by sulfonating the native PEEK membranes [61]. Leong et al. found that MFCs with a BPSH membrane had a higher performance than those with Nafion. This was due to the lower ohmic resistance and the lower extent of biofouling of the membrane resulting from the higher proton conductivity and the higher hydrophilicity of the BPSH membrane [60]. Although these ion exchange membranes can effectively prevent the crossover of oxygen and the substrate, their main problem is the pH imbalance created between the anode and cathode chambers. This is caused by the limited cation or anion transfer across the membranes, resulting in anode chamber acidification and cathode chamber alkalization [62, 63]. Anode chamber acidification and cathode alkalization leads to the inhibition of microbial activity, deterioration of the cathode catalyst activity, and a reduction in whole cell performance.

3.2.2 Other Porous Membranes or Separators

To overcome the ion exchange membrane problems, such as pH imbalance between the anode and cathode chambers, high costs, and high internal resistance, different porous membranes or separators have been proposed. Ultrafiltration membranes, microfiltration membranes, nylon and glass fiber filters, J-cloths, and polyether sulfone resin have been studied as separators for MFCs [64–67]. Fan et al. used J-cloth as the separator on the water-facing side of the air-cathode of an MFC. The CE was significantly improved from 35 to 71% due to the significant reduction of oxygen diffusion in the presence of the J-cloth [68]. Separators with a large pore size typically produce higher performance due to lower internal resistance. For example, Zhang et al. used nylon filters with different pore sizes as separators in MFCs. The power generation increased from 769 ± 65 to 941 ± 47 mW/m^2 when the pore size increased from 10 to 160 mm [67]. Porous membranes usually have a low internal resistance, compared to the ion exchange membranes, due to the porous structure. This structure benefits the ion transfer between the anode and the cathode. Therefore, the use of these porous membranes or separators can effectively prevent the diffusion of oxygen from the cathode to the anode, improve the CE, and alleviate the pH imbalance.

3.3 Cathode Materials

The design and fabrication of the cathode is a major challenge for MFC applications. To achieve high performance, aqueous cathodes using soluble electron acceptors with a high electrode potential (such as, potassium ferricyanide, and potassium peroxodisulfate) have been widely used [69, 70]. However, the electron acceptors must be replaced after depletion. This would create an additional cost for the treatment of wastewater and secondary pollution. Therefore, the air-cathode that uses oxygen as the electron acceptor is considered as the most promising cathode for practical applications due to the high electrode potential and the ready availability of oxygen. The main components of an air-cathode include ORR catalysts (to reduce the ORR overpotential), ionomer binders (to facilitate proton conduction in catalyst layers (CLs), and to tightly deposit the ORR catalysts), a hydrophobic layer (to permit air supply to the ORR catalysts and to prevent water leakage), and electrode supports (to provide mechanical support to CLs and to collect the electrons).

3.3.1 ORR Catalysts

In lab-scale MFCs, Pt is considered to be the most active catalyst for ORR. To achieve acceptable performance, the Pt loading of a typical MFC air-cathode needs to be ~ 0.5 mg cm^{-2} [71]. This would significantly increase the cost of
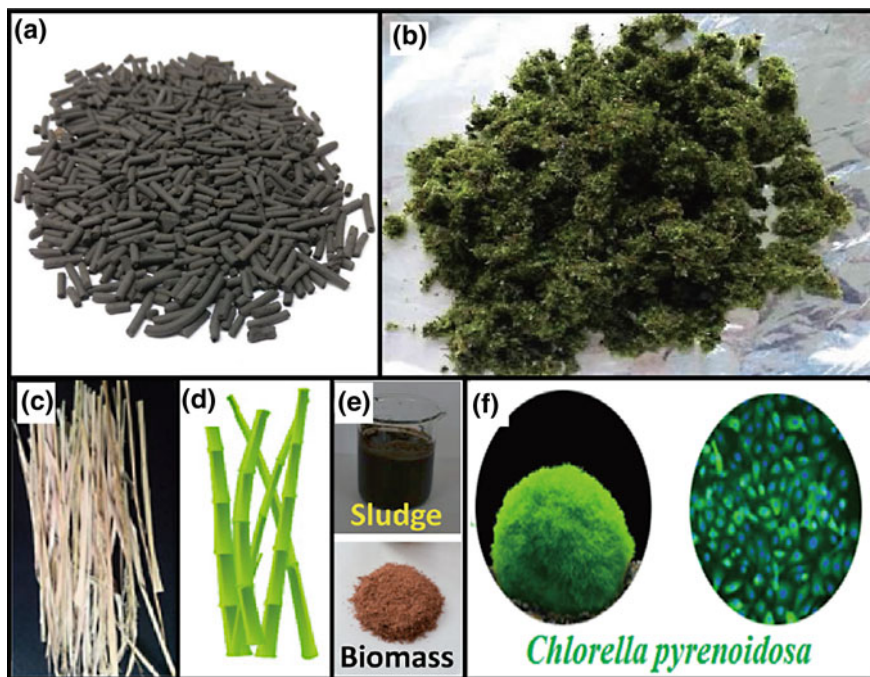
Fig. 9 Carbonaceous air-cathode catalysts derived from biomass: **a** activated carbon, **b** plant moss (adapted and reprinted from [75], Copyright 2016, with permission from Elsevier), **c** rice straw (adapted and reprinted from [76], Copyright 2015, with permission from Royal Society of Chemistry), **d** bamboo branches (adapted and reprinted from [73], Copyright 2017, with permission from Elsevier), **e** mixture of sludge and coconut shell derived powders (adapted and reprinted from [82], Copyright 2015, with permission from Royal Society of Chemistry), and **f** *Chlorella pyrenoidosa* (adapted and reprinted from [80], Copyright 2017, with permission from Elsevier)

commercial-scale MFCs. Carbon materials, such as activated carbon (AC) and biomass-derived carbons, exhibit comparable or higher ORR activity compared to Pt [72, 73]. Watson et al. reported that an air-cathode using the coal-derived AC catalyst had a higher performance than Pt/C. Watson et al. also compared the ORR activity of the catalysts with those derived from peat, coconut shell, hardwood, and phenolic resin, and found that the ORR activity of the catalysts was dependent on the precursors [74]. Since then, various types of plant biomass (plant moss, rice straw, bamboo, sludge, and microalgae) (Fig. 9), have been proposed as precursors for the carbonaceous ORR catalysts [73, 75, 76]. Sun et al. prepared a cornstalk-derived nitrogen-doped carbonaceous catalyst to facilitate ORR and obtained a maximum power density of 1122 ± 32 mW/m^2 in MFCs [77]. Zhou et al. synthesized a self-assembled carbon nanoparticle-coated porous ORR catalyst from plant moss and achieved a maximum power density of 703 ± 16 mW/m^2 (Fig. 9b) [75]. In addition to plant biomass, animal biomass, such as eggs, blood,

bones, urea, and animal liver, have also been used as precursors for ORR catalysts. Wang et al. synthesized non-precious tremella-like mesoporous carbon as the ORR catalyst using carbonized egg white as the carbon source [78]. Wu et al. developed an ORR catalyst based on co-doped mesoporous carbon microspheres from the ecofriendly biomass of eggs without the introduction of extrinsic dopants [79]. Microalgae, such as *Chlorella* spp., with a high nitrogen content between 4–8% have been proposed as the precursor for a cost-efficient ORR catalyst in MFCs. The catalyst derived from *Chlorella pyrenoidosa* can achieve a higher power generation (>2000 mW/m^2) than with Pt/C (Fig. 9f) [80]. Sludge that is usually regarded as an unwanted byproduct of wastewater treatment was also used as the precursor for the ORR catalyst due to high N and metal levels. Deng et al. found that N, P, and Fe heteroatom-doped hierarchical carbon catalysts with honeycomb-like interconnected macro-mesoporous frameworks can be obtained by direct pyrolysis of livestock sewage sludge. A maximum power density of 1273 ± 3 mW/m^2 can be obtained when this catalyst is applied in MFCs, and this power density is comparable to that of commercial Pt/C (1294 ± 2 mW/m^2) [81].

3.3.2 Binders

Nafion is commonly used as the binder for the ORR catalyst due to its high proton conductivity. Nevertheless, the high cost of Nafion restricts large-scale use. Several less expensive polymers, such as polytetrafluoroethylene (PTFE), polydimethylsiloxane (PDMS) and polyvinylidene fluoride (PVDF), could be alternatives to Nafion. For example, Dong et al. reported that the air-cathode using AC as the ORR catalyst and PTFE as the binder showed a higher performance than that using Nafion because of the improved oxygen supply [83]. The CL preparation process using PTFE as the binder can have a significant impact on MFC performance. A 35% higher performance was obtained by avoiding sintering during CL preparation compared to the use of sintering because sintering reduced the pore area and the porosity of CL and led to a deteriorated oxygen supply to the CL [84]. Yang et al. proposed an easy way to manufacture inexpensive air-cathodes using PVDF as the binder. The PVDF-based cathode was feasible in MFC operation because a cheap, but high-performance MFCs can be achieved [85]. The binder content in the air-cathode has an optimum value. High binder loading can increase the ohmic resistance of the electrode because binders are usually an electrical insulator, while a low binder loading can lead to the detachment of catalyst powder from the catalyst layer [86]. In addition, the binders are usually hydrophobic and can obstruct H$^+$ and OH$^-$ supply towards the CL, contributing to an additional cathodic potential loss of the air-cathode in MFCs [87, 88].

3.3.3   Electrode Supports

Carbon cloth/paper (Fig. 10a) is widely used in both anode and air-cathode fabrication. The common electrode supports for the cathode are carbon cloth/paper and graphite paper, on which the catalyst ink is coated on the water-facing side and the waterproofed layer is applied on the air-facing side [89]. However, the friability and the high cost of carbon cloth/paper and graphite paper hampers large-scale application for wastewater treatment. Recently, nickel foam, nickel mesh, and stainless steel mesh (Fig. 10b–d) have been reported as alternatives to carbon cloth/paper due to their high electrical conductivity and their high stability in MFC-relevant conditions. Zhang et al. proposed a method to prepare air-cathodes by pressing CL onto nickel mesh, which was used as a cathode support and current collector, avoiding the need for carbon cloth and reducing the cost [72]. Cheng and Wu studied the use of nickel foam as the current collector in air-cathode preparation. Their results indicated that the nickel foam cathode could be used in scaling up the MFC system [86]. With high corrosion resistance and electrical conductivity, metallic nickel remains a metal material that is too expensive for large-scale applications. To reduce the cost of cathode fabrication, Dong et al. reported SSM as
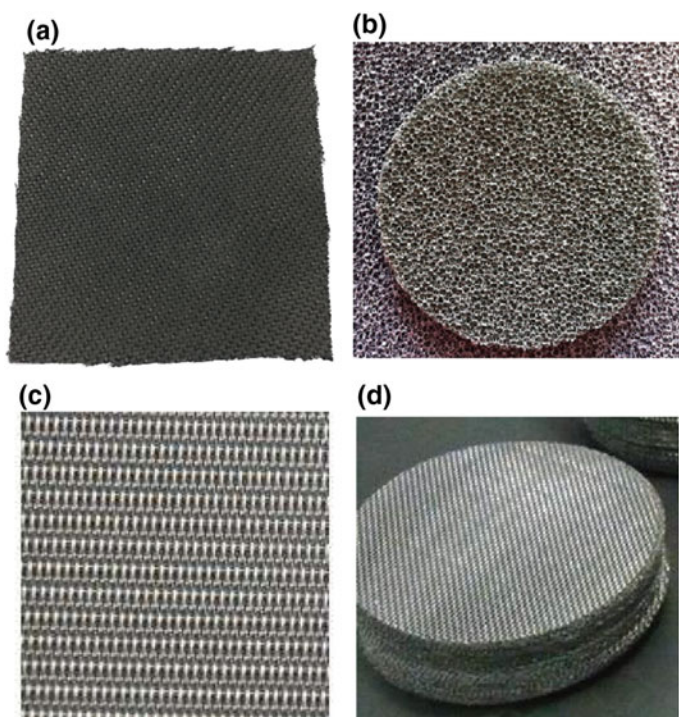
Fig. 10 Air-cathode supports or current collector in MFCs: **a** carbon cloth, **b** nickel foam, **c** nickel mesh, and **d** stainless steel mesh

an alternative to nickel foam and mesh in the cathode [6]. Usually, SSM is corrosion resistant, with high electrical conductivity, and low cost, being overall superior to nickel mesh/foam. The SSM can be directly used as a cathode support and current collector by pressing CL and a gas diffusion layer (GDL) on its two sides, respectively. Li et al. optimized the opening size of SSM in an AC air-cathode and reported that a cathode using SSM with 40 M had a better performance due to the lower internal resistance [90]. So far, SSM remains one of the most widely used cathode supports for the air-cathode of MFCs.

4   MFC Architecture

4.1   Double- and Single-Chamber MFCs

Various MFC architecture has been reported and the majority of it fall into the categories of cubic, cylindrical, H-cell, and plate- and tube-shaped reactors. Based on different working principles, the MFC can be categorized into paper-based MFCs, microfluidic MFCs, plant MFCs, and sediment MFCs. Although there are many kinds of MFC designs intended for scale-up and practical application, MFCs can be classified into DCMFCs and single-chamber MFCs (SCMFCs) depending on whether an ion exchange membrane is used. The advantages of SCMFCs are reduced setup costs due to the absence of an ion exchange membrane and the direct usage of freely available oxygen in the air as electron acceptors. The drawbacks of SCMFCs are the decreased CE that results from oxygen crossover from the cathode to the anode and a low power density caused by the thermodynamic and kinetic constraints of ORR in the cathode. The ion exchange membrane in DCMFCs reduces oxygen crossover to the anode and, thus, leads to enhanced CE of the MFCs. However, the pH imbalance between the anode and cathode chamber, which is caused by the limited proton transfer across the proton exchange membrane, results in anode chamber acidification, which leads to the inhibition of microbial activity and reduced performance.

4.1.1   DCMFCs

DCMFCs are composed of anode and cathode chambers separated by an ion exchange membrane, which prevents the mixing of anolytes and catholytes (as described in Sect. 3.2). This feature allows the use of an immersed cathode in MFC. For example, Zhang et al. developed a plate-shaped DCMFC using potassium ferricyanide as the cathode electron acceptor (Fig. 11b) [70]. Many immersed cathodes using soluble electron acceptors with high redox potentials, such as persulfate, permanganate, triiodide, and hydrogen peroxide, have been proposed for
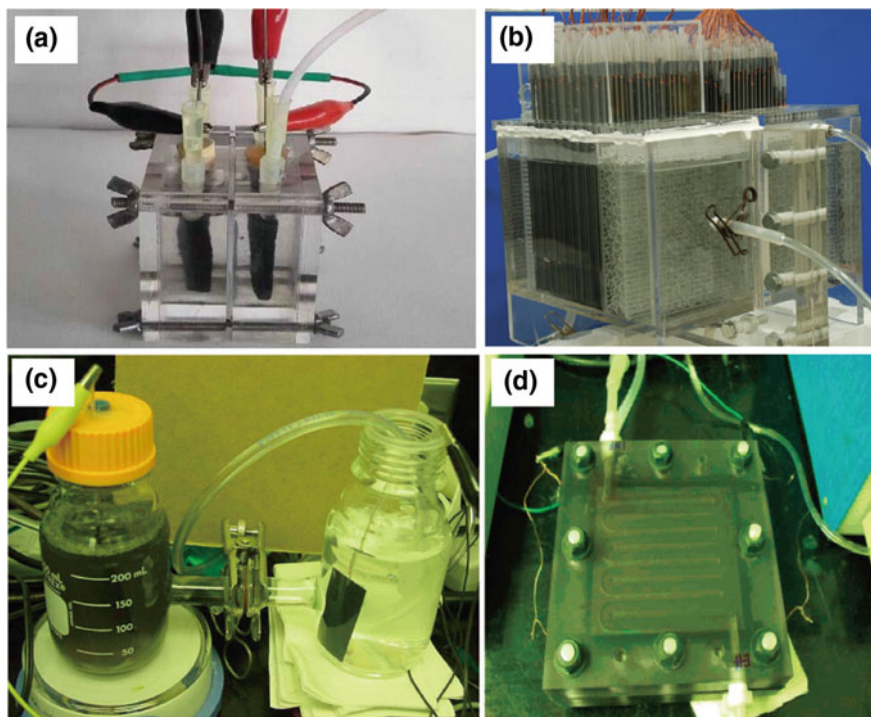
Fig. 11 Pictures of DCMFCs: **a** cubic MFC (adapted and reprinted from [94], Copyright 2015, with permission from Royal Society of Chemistry), **b** liter-scale MFC (adapted and reprinted from [32], Copyright 2013, with permission from Elsevier), **c** bottle-based H-shape MFC (adapted and reprinted from [95], Copyright 2005, with permission from Elsevier), and **d** plate MFC (adapted and reprinted from [96], Copyright 2004, with permission from American Chemical Society)

the DCMFC cathode [69, 91–93]. However, these electron acceptors are not regenerative in ambient conditions and need to be replaced after they are depleted.

The use of membranes in DCMFCs can also limit the oxygen diffusion from cathode to anode. A significant increase in CE occurs compared to SCMFCs since the membrane suppresses the oxygen crossover from the cathode to the anode chamber and thus decreases the aerobic substrate degradation. Existence of an ion exchange membrane allows for very small electrode spacing, and can significantly reduce the ohmic resistance of the MFC and improve MFC performance. Zhang et al. designed a plate MFC in which the anode and cathode were pressed onto the two sides of a cation exchange membrane, respectively (Fig. 11d) [70]. However, other cation species in the anolytes usually have a significantly higher concentration than protons, making the flux of proton transport considerably lower compared to the transport of other cations. This causes acidification of the anode chamber and decreased anode performance.

4.1.2 SCMFCs

SCMFCs eliminate the membrane between the anode and the cathode and enable a simple design and a lower fabrication cost. A SCMFC only contains a single chamber coupled with a porous air-cathode exposed to the atmosphere. This eliminates the requirement of aeration in the cathode chamber. In a SCMF, protons are transferred from the anode to the porous air-cathode through the electrolyte by diffusion. Liu et al. reported the first SCMFC consisting of an anode placed inside a plastic cylindrical chamber and a cathode assembled outside (Fig. 12a) [97]. Cheng et al. designed a single-chamber MFC with a cylindrical structure. The air-cathode made of carbon cloth and Pt/C was wrapped around the cylindrical reactor [98]. The proton transfer resistance in SCMFCs is much lower than that of DCMFCs due to the absence of the ion exchange membrane. However, compared to DCMFCs, the oxygen diffusion from the cathode to the anode is higher in SCMFCs, leading to a larger amount of aerobic degradation of the substrate. A considerable amount of substrate is consumed by bacterial growth on the anode, rather than electricity generation, and this leads to a lower CE. For example, Liu et al. reported that a DCMFC can achieve a CE value of 40–55%, while a CE value of only 9–12% is possible for a SCMFC [97].
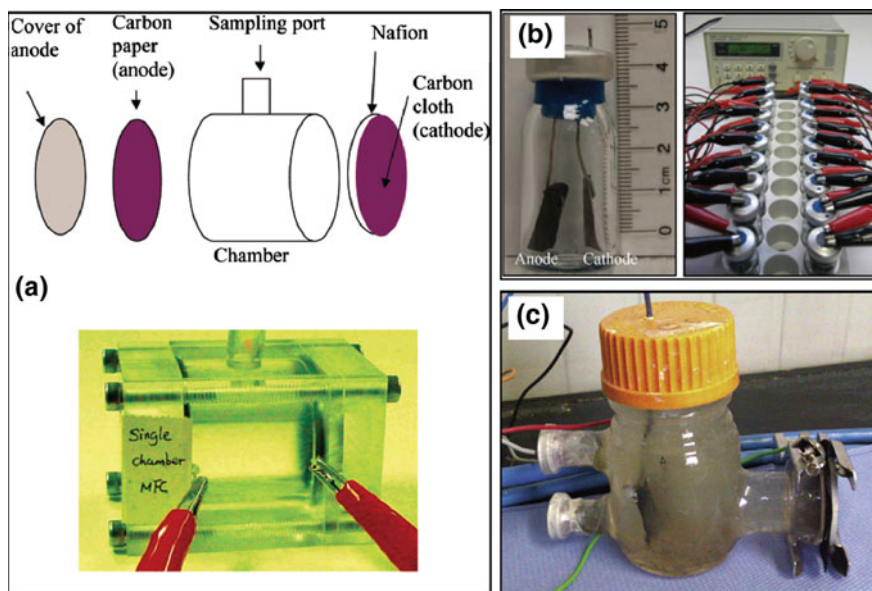
Fig. 12 Single-chamber MFCs: **a** structure of a cubic single-chamber MFC (adapted and reprinted from [97], Copyright 2004, with permission from American Chemical Society), **b** bottle-based single-chamber MFC (adapted and reprinted from [99], Copyright 2011, with permission from Elsevier) and **c** bottle-based single-chamber MFC (adapted and reprinted from [100], Copyright 2013, with permission from Elsevier)

4.2 Air-Cathode MFCs

4.2.1 Designs of Air-Cathode MFCs

Air-cathode MFCs are considered to be promising architecture for scaling-up because the cathode is directly exposed to the air and it does not require additional energy to supply oxygen. The air-cathode can be integrated in flat plate, cubic, and tubular MFCs. Air-cathode MFCs with plate and cubic architecture typically consist of rectangular anode chambers, and the air-cathode is assembled on the side opposite the anode. Compared with the cubic design, the flat plate MFC has a lower ohmic resistance because the design minimizes the spacing between the anode and the cathode [101]. Tubular structures are also widely used to design air-cathode MFCs. The tubular MFC is typically composed an anode surrounded by a porous separator and the cathode is wrapped outside the separator. The separator is used to avoid an electrical short-circuit between the anode and cathode and to maximize the CE. Perforated cylindrical materials, such as polyvinyl chloride or polypropylene tubes, are usually used as the mechanical support [102, 103]. The tubular architecture is optimal for scaling-up, since it enables sufficient substrate supply, product removal, and continuous operation [104]. During scale-up, this architecture could be enlarged by simply extending the tube in the axial direction. In addition, when it is operated in continuous-feed mode, tubular MFCs only need a simple manifold to distribute water into various reactors.

4.2.2 Air-Cathode Fabrication

To achieve acceptable cathode performance, a good air-cathode should provide a large amount of triple-phase boundaries (TPB) with oxygen, protons, and electrons simultaneously present. In order to provide sufficient TPBs, the air-cathode usually consists of several layers, including the CL, the hydrophobic layer, the GDL, and the carbon paper/cloth support. The fabrication method for the air-cathode has a great influence on the physical and chemical properties of these layers, and therefore greatly affects the performance of the air-cathode. The approaches used to prepare the air-cathode of MFCs can be classified as follows:

Carbon Cloth/Paper Based Cathode Using Spray/Brushing Methods

Spray/brushing is a common method for the fabrication of air-cathodes. It usually involves sequentially preparing the hydrophobic layer or GDL on the air-facing side of the carbon material support and the CL on the water-facing side of the carbon material support. The hydrophobic layer, or GDL, is made by spraying 15–60 wt% PTFE suspension onto the carbon material supports to facilitate the air supply and to prevent water leakage from the reactor [71]. Cheng et al. prepared an air-cathode

by brushing the Pt catalyst and a mixture of carbon black and 30% wt. PTFE solution onto water-facing and air-facing sides of the carbon cloth serving as the CL and the hydrophobic layer, respectively. Cheng el al. studied the effects of the number of hydrophobic layers on the performance of the air-cathode. An increase in the cathode potential of 117 mV and a CE increase of 171% were achieved with four hydrophobic layers, respectively [105]. A sintering temperature, ranging from 340 to 370 °C, is needed during the cathode fabrication process to achieve a uniform PTFE distribution. This causes significant changes in the physicochemical properties of the ORR catalysts and in the pore structures of the GDL and CL. Therefore, other fluoropolymers, such as PVDF with low melting points (melting point 177 °C), have been used to form the hydrophobic layer. Qiu et al. used PVDF to prepare the hydrophobic layer of the air-cathode and showed that the PVDF based air-cathode outperformed the PTFE air-cathode [106]. To minimize the ohmic resistance between the CL and carbon material supports, GDLs are usually added between the CL and carbon material supports by directly spraying the mixture of carbon black and PTFE suspension onto the carbon material supports. Santoro et al. found that the presence of the GDL substantially reduced the water loss and biofilm infiltration into the CL, thus enhancing the MFC performance [107].

Cold- and Rolling-Press Method

To meet the requirements of a large cathode size and ease of fabrication for commercialization, Zhang et al. proposed the cold press method for cathode fabrication [72]. In this method, a mixture of catalyst/PTFE and carbon black/PTFE was pasted on both sides of a nickel mesh current collector and cold-pressed at a pressure of 150 bar. Dong et al. proposed a rolling-press method for preparing the MFC air-cathode using SSM as the current collector. In this method, the CL and GDL were first prepared by rolling-press and then they were rolled onto the SSM. The rolling-press method is an accurate, labor-saving fabrication process and it can produce an air-cathode with high ORR activity [6]. SSM properties, such as opening size and density, can have a great influence on cathode performance because they affect the oxygen transfer, ion transfer, and electrical conductivity of the cathode [90]. Besides the properties of the SSM, the pressing conditions also influence the cathode performance because the porosity and electrical conductivity of the CL is closely related to the pressing pressure and temperature. For example, Zhang et al. found that the CL prepared under a lower pressure induced a higher total pore volume of the GDL and the CL and thus resulted in higher performance [108]. In order to increase the pore volume of the GDL and CL, the addition of a pore former is also a feasible way for increasing MFC performance. Liu et al. attempted to increase the porosity of the air-cathode by mixing the ACs with pore formers (NH_4HCO_3). They found that the improved porosity induced by the pore formers produced a higher exchange current density of ORR due to the extended TPBs [109]. Another factor affecting cathode performance is catalyst loading.

Yang et al. found that increasing the AC catalyst loading at levels of up to 27 mg/cm^2 improved the performance of the air-cathode due to the increased ORR active sites. However, a further increase in the catalyst loading from 27 to 62 mg/cm^2 only had a minor impact on cathode performance [110]. This was because the beneficial effects of increasing the catalyst loading were overwhelmed by the increased electrical resistance and oxygen diffusion resistance of the CL, resulting from the increased catalyst loading.

Self-assembly or Self-Standing Electrode

Many efforts have been made to optimize air-cathode fabrication. The process is complex, since it usually involves the preparation of CL and GDL, as well as their assembly on the current collector or electrode support. Therefore, the development of an easy fabrication method for the air-cathode is important for the practical application of MFCs. Several reports have presented methods for fabricating the self-assembly or free-standing cathode for ORR. Yang et al. reported a 3D nitrogen-enriched iron-coordinated CNT sponge cathode by two-stage chemical vapor deposition (Fig. 13a) [111]. The MFC with the prepared cathode delivered a higher power density (20.3 W/m^3) than that of the Pt/C cathode (12.8 W/m^3). Wu et al. developed 3D nitrogen-doped graphene aerogel-supported Fe_3O_4 nanoparticles for ORR through hydrothermal self-assembly and freeze-dry fabrication processes [112]. Although the price of graphene and CNT is still too expensive for using MFCs in wastewater treatment, the approaches provide new ways to prepare the self-assembly or free-standing electrode with low-cost carbon or biomass. Yang et al. proposed that heat-treated bamboo charcoal tubes (BCT), fabricated by directly carbonizing bamboo tubes, can be used as the monolithic air-cathode of MFCs [66]. In the BCT cathode, the carbonized N- and P-doped carbon can be directly used to catalyze the ORR without the involvement of PTFE and/or Nafion binder for CL fabrication. In the air-cathode, the inherent porous and tubular structure derived from BCT (Fig. 13b) can serve as oxygen or proton transfer channels, and the monolithic structure support, respectively. The MFC using the BCT cathode showed a power output (40 W/m^3) that was similar to the MFC using Pt/C.

5   Stacked MFCs

5.1   *Power Generation of MFC Stacks*

The power density of MFCs has increased several orders of magnitude over initial designs due to the optimization of reactor configuration, improvement of operational parameters, use of bacteria with greater electrochemical activity, and the
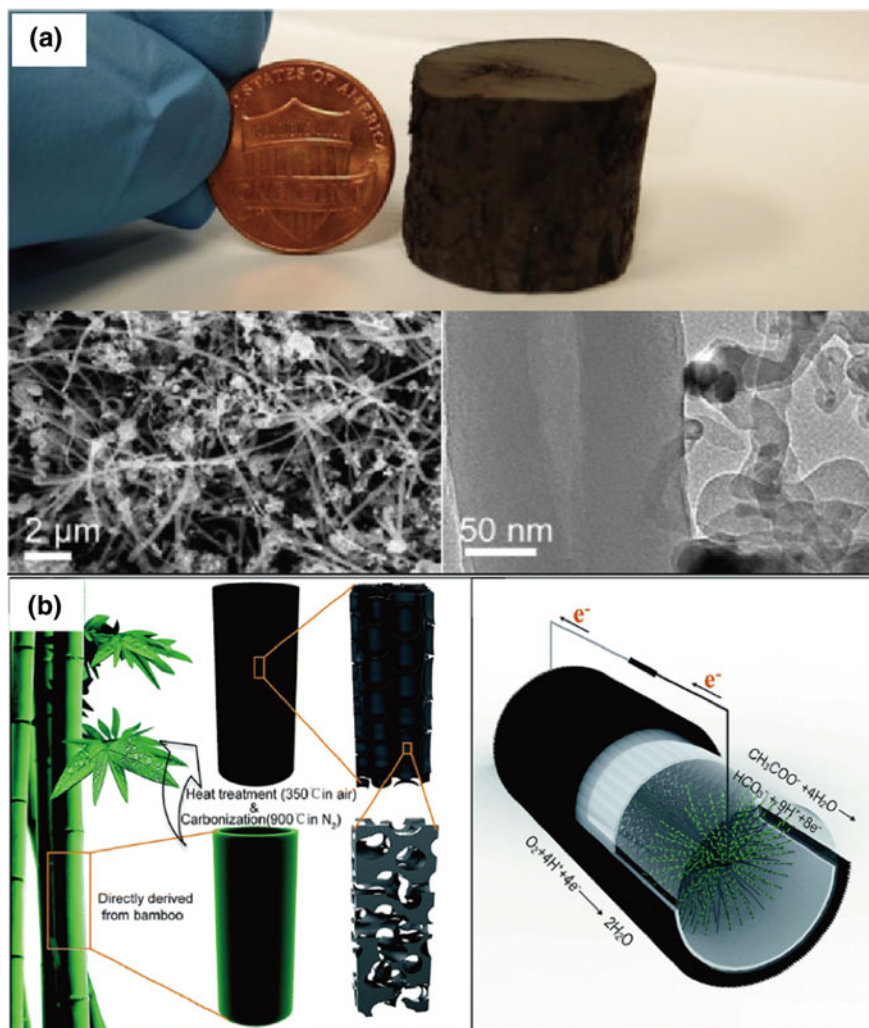
Fig. 13 Monolithic or free-standing cathode used in MFCs. **a** CNT sponge as a self-standing cathode (adapted and reprinted from [111], Copyright 2016, with permission from Elsevier), **b** bamboo charcoal tube derived air-cathode (adapted and reprinted from [66], Copyright 2017, with permission from Royal Society of Chemistry)

application of novel electrode materials. However, the practical application of MFCs remains limited by low voltage output. For example, the theoretical voltage output of MFC is ~ 1.1 V when oxygen and sodium acetate are used as the electron acceptor and the electron donor, respectively, but the practical operating voltage is only ~ 0.5 V. This is much lower than the theoretical value due to the charge transfer, ohmic, and mass transport overpotentials. In addition, the power density of

MFC is decreased with the increase of MFC volume, and it is very difficult to improve the power output by directly scaling up the MFC size. Therefore, stacking multiple MFCs in parallel or series is a promising strategy to realize the enhanced power and current output in practical application.

MFC stacks connected in parallel results in a current equal to the sum of the individual MFCs, while keeping a voltage equal to the average of the individual MFCs. For example, Wu et al. reported that an MFC stack constructed with five MFC units achieved a power density of 50.9 ± 1.7 W/m^3, which was about five times higher than that of the individual MFCs (~ 10 W/m^3) [113]. Aelterman et al. suggested that six individual continuous MFC units in a stacked configuration produced a maximum power output of 258 W/m^3, which was approximately six times higher than that of the individual MFCs [114]. In contrast to MFC stacking in a parallel connection, connecting multiple individual MFCs in series is an efficient way of achieving a high-voltage output. Theoretically, the voltage output from a series stack of MFCs should be the sum of the voltage outputs of the individual MFCs. For example, Gurung et al. showed that two MFCs stacked together in series could produce an OCV that equaled the mathematical sum of the individual MFCs [115].

Attempts have been made to build different MFC stacks using approaches, such as scaling-up by miniaturization and multiplication. Many types of MFC stacks, such as tubular, multi-electrode, cassette-electrode, and baffled MFC stacks, have been proposed to improve electricity generation or wastewater treatment (Fig. 14).

5.2 Limitations of Stacked MFCs

Although MFC stacks have shown to be an efficient approach to enhance the voltage and current output of MFCs, voltage reversal could cause system failure or a significant reduction of power generation in an MFC stack. Voltage reversal, which has usually been observed in series-connected MFC stacks, is a phenomenon where the voltage of an individual MFC in an MFC stack reverses from a positive to a negative value [123]. Voltage reversal in stacked MFCs is the result of non-spontaneous anode/cathode overpotential in a unit MFC that has sluggish anode/cathode kinetics compared to the other unit MFCs. For example, Oh et al. demonstrated that fuel starvation in an active cell, or a lack of power generation in the absence of bacterial activity in a unit cell (abiotic conditions) induced voltage reversal, due to the insufficient voltage of a unit cell compared to other cells [123]. An et al. also showed that the sluggish reaction rate of the anode in the weak MFC was responsible for voltage reversal in an MFC stack [124]. Voltage reversal in stacked MFCs can also be caused by slow cathode kinetics. For example, An et al. demonstrated that the inefficient catalytic activity of the ORR catalyst was the main reason for the voltage reversal in the stacked MFCs. They also showed that the voltage reversal can shift from the cathode to the anode when the anode performance became the limiting factor of the unit MFC [125]. Therefore, voltage
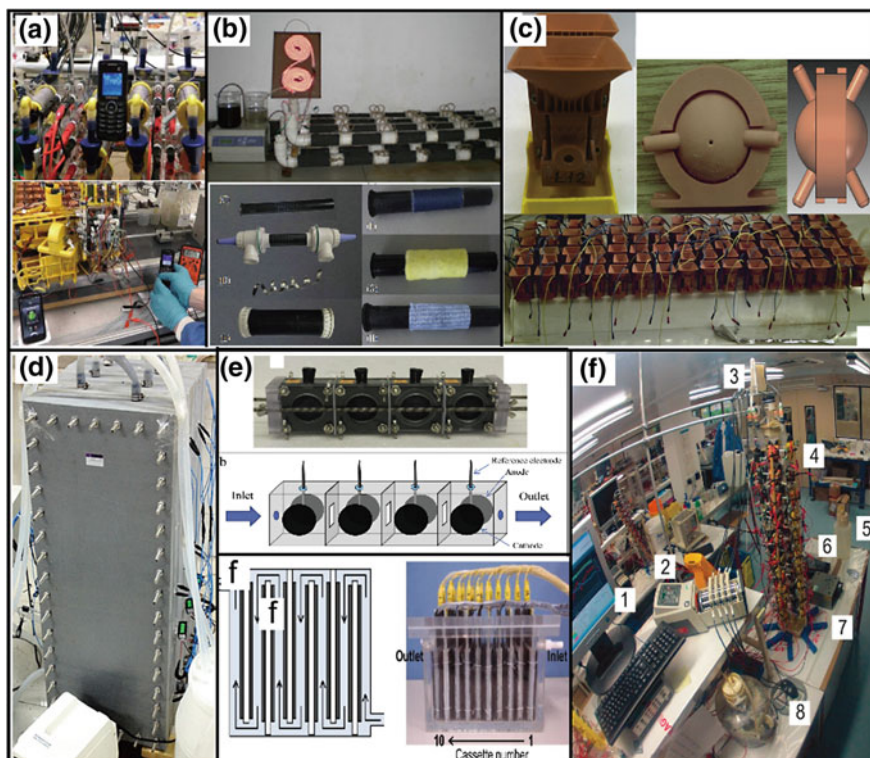
Fig. 14 Different MFC stacks using for power generation and wastewater treatment. **a** MFC stacks using for powering mobile phone (adapted and reprinted from [116], Copyright 2013, with permission from Royal Society of Chemistry), **b** tubular MFC stack (adapted and reprinted from [117, 118], Copyright 2012, Copyright 2016, with permission from Elsevier), **c** MFC stacks for urine utilization (adapted and reprinted from [119], Copyright 2013, with permission from Elsevier), **d** pilot-scale MFC stack (adapted and reprinted from [113], Copyright 2016, with permission from Elsevier), **e** multi-electrode MFC stack (adapted and reprinted from [120], Copyright 2014, with permission from Elsevier), **f** cassette-electrode MFC stack (adapted and reprinted from [121], Copyright 2013, with permission from Elsevier), (g) self-sustainable MFC stack (adapted and reprinted from [122], Copyright 2013, with permission from Royal Society of Chemistry)

reversal is a dynamic phenomenon that occurs in response to the dominant kinetic bottlenecks in the electrode or unit.

To avoid the requirement of a complicated water distribution system to pump substrate individually to different reactors and discharge separately, the MFC stack can be operated under a continuous-flow mode, in which the MFC units are hydraulically connected by substrate flow. However, as the MFC stack was operated with both electrical and hydraulic connections, substrate cross-conduction is usually observed because of the parasitic current flow in the parasitic fuel cell. This results in reduced performance during the MFC operation (Fig. 15). Zhuang and
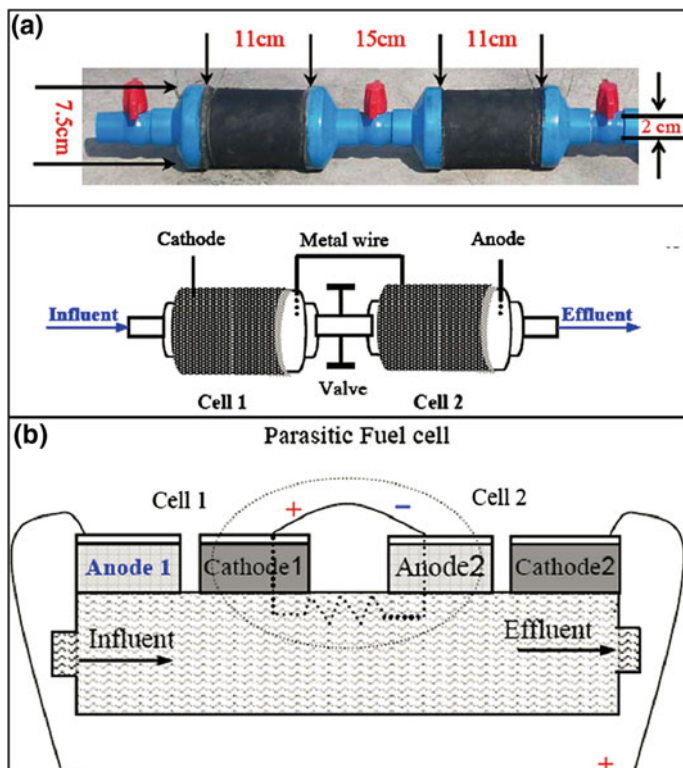
Fig. 15 Illustration of substrate cross-conduction effect between the serially connected MFCs (adapted and reprinted from [104], Copyright 2009, with permission from Elsevier)

Zhou suggested that two hydraulically connected MFCs could result in a 200–300 mV open-circuit voltage loss compared to the electrically isolated MFCs [104].

5.3 Maximizing Power Generation

Voltage reversal is a key factor limiting the power output in electrical series-connected MFCs, and attempts have been made to reduce this problem. One effective method is to keep the current density of the unit MFCs below the critical current density using an additional electrical circuit or device during the power generation (Fig. 16). For example, Wu et al. adopted a DC/DC booster circuit to convert the low DC voltage of the MFCs (0.2–0.4 V) to a more practical electronics range of >3.0 V, instead of stacking MFCs in a series [126]. A maximum power point tracking algorithm proposed by Boghani et al. was used to set the operating point of the MFC to optimize power harvesting [127]. An et al. used a threshold
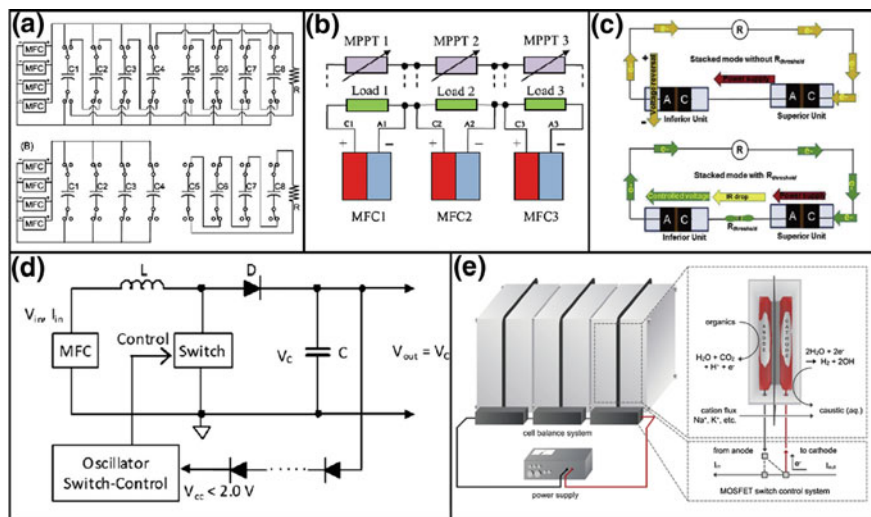
Fig. 16 Different methods to avoid or alleviate voltage reversal in MFC stacks. **a** An electronic circuit containing two sets of multiple capacitors that were alternately charged and discharged (adapted and reprinted from [129], Copyright 2011, with permission from Royal Society of Chemistry), **b** MFC subsystem series connectivity along with maximum power point tracking (adapted and reprinted from [127], Copyright 2014, with permission from Elsevier), **c** a threshold resistance for MFC stack (adapted and reprinted from [128], Copyright 2015, with permission from Elsevier), **d** a low power DC/DC booster circuit (adapted and reprinted from [126], Copyright 2012, with permission from Elsevier), **e** assistance current or voltage for MFC stack (adapted and reprinted from [132], Copyright 2013, with permission from Royal Society of Chemistry)

resistance to limit the operating current density of an MFC stack to a lower level than the critical current density and thus prevent voltage reversal in the MFC stack [128]. However, these methods are usually energy-consuming. To maximize energy harvesting, Kim et al. used an electronic circuit containing two sets of multiple capacitors that were alternately charged in parallel and discharged in series to increase continuous power production [129]. This electronic circuit boosted the voltage of the MFC stack and can be used to power an a microbial electrolysis cell (MEC) without the risk of voltage reversal. Compensating the non-uniformities in power output between the individual MFCs using electronic circuits was also used to prevent voltage reversal. For example, Khaled et al. demonstrated that the cell voltage of MFCs in a stack can be equalized using this balancing method [130]. Similarly, Yang et al. proposed a series-parallel-connected hybrid MFC stack and demonstrated that this connection can promote both the voltage, the current output, and the stable operating time of the stack in comparison to the series and parallel connected stacks by alleviating voltage reversal [131].

In addition, an efficient approach is the application of an external assistance potential or current on the individual MFCs to balance the inequalities and alleviate

the risk of voltage reversal. Andersen et al. reported a cell balance system that controlled the unit cells connected electrically in a series to maintain the cell voltage of individual cells at, or below, a maximum set point to prevent voltage reversal [132]. Kim et al. proposed an assistance-current method to prevent voltage reversal by connecting a supporting electrode in parallel and adjusting the assistance current flowing from the supporting electrode [133].

6 MFC Technologies and Applications

6.1 Wastewater Treatment

MFCs were first proposed for wastewater treatment in 1991. MFCs have tremendous substrate (fuel) versatility [7–9]. They can be operated using various readily bioconvertible organics ranging from pure compounds to complex mixtures in wastewater, such as acetate, glucose, and lactate. Acetate is commonly used as a substrate because of its inertness towards alternative microbial conversion (fermentations and methanogenesis) at room temperatures. Compared to acetate, glucose, lactate, or mixed organic pollutant-fed MFCs have a lower CE value due to the electron loss by competing bacteria. Domestic wastewater, such as brewery, starch processing, dye wastewater, and even landfill leachates, have also been used as substrates in MFCs for simultaneous electricity generation and wastewater treatment [10, 11, 13–16]. Processes that can generate electricity during different wastewater treatments will help to reduce the economic burden of wastewater treatment and provide a green alternative for electricity generation.

6.2 MFC Coupled System

MFCs are usually used as the on-site electrical power source for other microbial energy conversion systems to minimize the use of electricity from the local electrical grid. Wang et al. coupled MFCs with MECs to form an MFC-MEC system to convert the energy contained in wastewater into hydrogen [134]. In the system (Fig. 17a), the electricity produced by MFCs (at $\sim$0.5 V) was used to power MECs (0.110 V in theory, >0.2 V in practice). Therefore, the integration of MFCs and MECs can reduce the need for additional electrical grid energy. Sun et al. combined a single two-chamber MEC (450 mL) with an MFC (225 mL) and achieved a maximum hydrogen production rate of 0.0149 m^3 H$_2$/day [135].

Besides their use for powering MECs, MFCs can also be combined with bioreactors for continuous effluent treatment to achieve maximum substrate utilization [136, 137]. Many soluble fermentation byproducts, such as formate, lactate, propionate, acetate, and butyrate, can be degraded in MFCs. Li et al. investigated
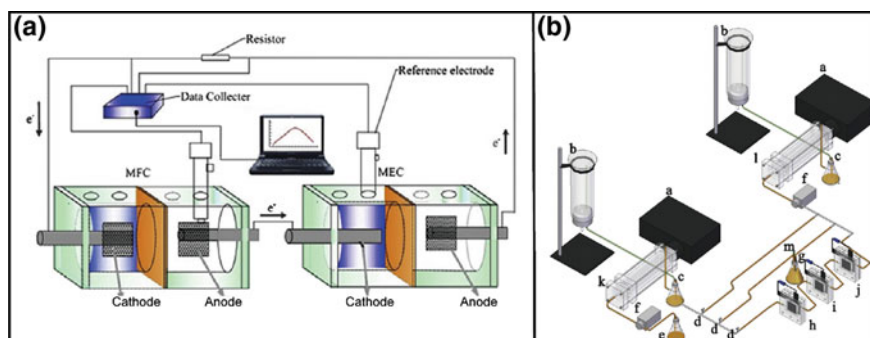
Fig. 17 Common used MFC coupled system. **a** MFC-MEC coupled system (adapted and reprinted from [139], Copyright 2014, with permission from Elsevier), **b** MFC-PBR coupled system (adapted and reprinted from [138], Copyright 2013, with permission from Elsevier)

the feasibility of using MFCs for pH adjustment and inhibitory byproduct removal for photobiohydrogen reactors (PBRs). In this study (Fig. 17b), single-chamber MFCs were connected between two series-connected PBRs. The coupled system achieved a significantly higher hydrogen production rate and substrate utilization due to the beneficial role of MFCs for pH adjustment and inhibitory byproduct removal [138].

6.3 Biosensors

MFCs can be used as biosensors for pollutant analysis and in situ process monitoring. In an MFC-based sensor, the chemical signals are usually the current or electrode potential generated from the substrate oxidation by the electroactive bacteria in the anode. The signals are directly related to factors, such as pH, substrate concentration, and toxin concentration (Fig. 18), and thus can be used to monitor the water quality [140]. The design of the MFC type of biosensor integrates the advantages of the whole-cell biosensor and the self-powered MFC device. This unique design provides featured compact sensor configuration, in which the microorganisms directly generate readable electric signal output without any externally powered transducer. Different types of MFCs have been used as biosensors for different purposes. Compared with other types of MFCs, the SCMFC type of biosensors are the most promising because aeration, recycling, and chemical regeneration of the catholyte is not required during the operation. For example, Lorenzo et al. constructed a biosensor based on the working principles of SCMFCs and demonstrated that the biosensor can be used as a probe for labile organics [141]. According to the application purposes, the MFCs can be designed as biosensors for monitoring biochemical oxygen demand/COD, toxic component
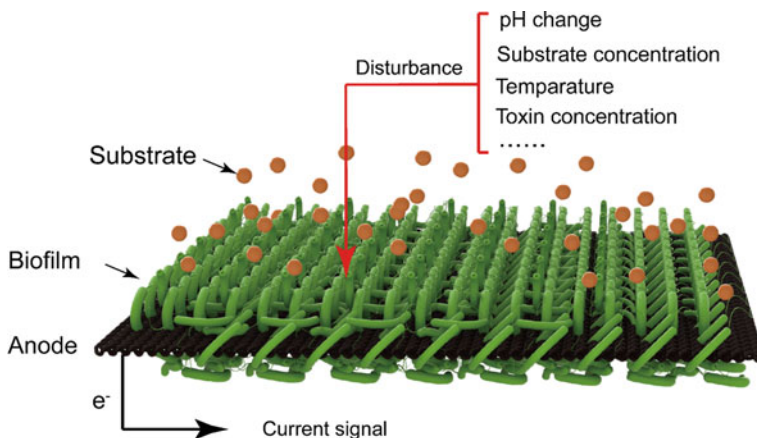
Fig. 18 Schematic of MFC based biosensor

detection, volatile fatty acids and anaerobic digestion processing [140, 142–146]. However, the stability, sensitivity, response time, and detection limit of the biosensor system still need improvement for practical application and to successfully compete with other analytical methods.

7   Outlook

Although MFC technology has been intensively studied as a promising method to achieve sustainable wastewater treatment and electricity generation, many barriers need to be overcome before practical implementation. Among these, fabrication of high-performance and cost-effective anodes and cathodes are the most important challenges. Many alternative anode materials, such as carbon brushes, loofah sponge-derived porous carbon, graphene aerogels, and carbon nanomaterials, have been used in MFCs. These 3D porous electrodes can achieve a higher performance level than carbon cloth/paper because of the greater electrode surface accessible to electroactive bacteria. However, their high price and the complex production process offsets the benefits from the performance improvement. A low-cost and high-performance cathode is equally important for MFC performance. MFCs using carbonaceous materials as the ORR catalysts can deliver similar or greater performance than that of the Pt/C cathode, while the cost can be reduced by at least one order of magnitude. However, fabricating and doping the carbon materials usually requires toxic chemicals, sophisticated preparation routes, and specialized equipment. Preparation of these catalysts can have a negative environmental impact.

Although there has been significant development in MFCs recent years, most of these achievements were based on lab-size MFCs ranging from microliters to milliliters. Therefore, these results cannot be directly applied to large-scale reactors

due to poor understanding of the effects of reactor architecture and operation conditions on MFC performance. In a scaled-up system, water pressure, that is quite low in a lab-scale MFC, can challenge the mechanical strength and the stability of the air-cathode. Additionally, the wastewater usually contains small particles. These may block reactor pipes and limit the substrate supply to the biofilm, leading to a significant decrease of biofilm activity on the anode. Therefore, many efforts are needed to develop or establish an improved MFC system that can be operated in a real wastewater treatment plant.

MFCs represent a proven carbon neutral technology and they can be used for renewable energy production and wastewater treatment. There is a bright and promising future for a wide range of MFC technologies and these are the foundation of a new generation of renewable energy systems.

References

1. Logan BE, Hamelers B, Rozendal R, Schröder U, Keller J, Freguia S, Aelterman P, Verstraete W, Rabaey K (2006) Microbial fuel cells: methodology and technology. Environ Sci Technol 40(17):5181–5192
2. Liu H, Ramnarayanan R, Logan BE (2004) Production of electricity during wastewater treatment using a single chamber microbial fuel cell. Environ Sci Technol 38(7):2281–2285
3. Du Z, Li H, Gu T (2007) A state of the art review on microbial fuel cells: a promising technology for wastewater treatment and bioenergy. Biotechnol Adv 25(5):464–482
4. Pant D, Bogaert GV, Diels L, Diels L (2010) A review of the substrates used in microbial fuel cells (MFCs) for sustainable energy production. Bioresour Technol 101(6):1533–1543
5. Logan BE (2010) Scaling up microbial fuel cells and other bioelectrochemical systems. Appl Microbiol Biot 85(6):1665–1671
6. Dong H, Yu H, Wang X, Zhou Q, Feng J (2012) A novel structure of scalable air-cathode without Nafion and Pt by rolling activated carbon and PTFE as catalyst layer in microbial fuel cells. Water Res 46(17):5777
7. Catal T, Li K, Bermek H, Liu H (2008) Electricity production from twelve monosaccharides using microbial fuel cells. J Power Sources 175(1):196–200
8. Logan B, Cheng S, Watson V, Estadt G (2007) Graphite fiber brush anodes for increased power production in air-cathode microbial fuel cells. Environ Sci Technol 41(9):3341–3346
9. Manohar AK, Mansfeld F (2009) The internal resistance of a microbial fuel cell and its dependence on cell design and operating conditions. Electrochim Acta 54(6):1664–1670
10. Wang X, Feng Y, Ren N, Wang H, Lee H, Li N, Zhao Q (2009) Accelerated start-up of two-chambered microbial fuel cells: effect of anodic positive poised potential. Electrochim Acta 54(3):1109–1114
11. Feng Y, Wang X, Logan BE, Lee H (2008) Brewery wastewater treatment using air-cathode microbial fuel cells. Appl Microbiol Biotechnol 78(5):873–880

12. Wen Q, Wu Y, Cao D, Zhao L, Sun Q (2009) Electricity generation and modeling of microbial fuel cell from continuous beer brewery wastewater. Bioresour Technol 100(18): 4171–4175

13. Lu N, S-g Zhou, Zhuang L, J-t Zhang, J-r Ni (2009) Electricity generation from starch processing wastewater using microbial fuel cell technology. Biochem Eng J 43(3):246–251

14. Greenman J, Gálvez A, Giusti L, Ieropoulos I (2009) Electricity from landfill leachate using microbial fuel cells: comparison with a biological aerated filter. Enzyme Microb Tech 44(2): 112–119

15. Sun J, Y-y Hu, Bi Z, Y-q Cao (2009) Simultaneous decolorization of azo dye and bioelectricity generation using a microfiltration membrane air-cathode single-chamber microbial fuel cell. Bioresour Technol 100(13):3185–3192

16. Jadhav G, Ghangrekar M (2009) Performance of microbial fuel cell subjected to variation in pH, temperature, external load and substrate concentration. Bioresour Technol 100(2): 717–723

17. Chakrapani S, Perozo E (2006) Increased performance of single-chamber microbial fuel cells using an improved cathode structure. Electrochem Commun 8(3):489–494

18. Logan BE (2008) Microbial fuel cells. Wiley

19. He Z, Liu J, Qiao Y, Li CM, Tan TTY (2012) Architecture engineering of hierarchically porous chitosan/vacuum-stripped graphene scaffold as bioanode for high performance microbial fuel cell. Nano Lett 12(9):4738

20. Higgins SR, Foerster D, Cheung A, Lau C, Bretschger O, Minteer SD, Nealson K, Atanassov P, Cooney MJ (2011) Fabrication of macroporous chitosan scaffolds doped with carbon nanotubes and their characterization in microbial fuel cell operation. Enzyme Microb Tech 48(6):458–465

21. Qiao Y, Li CM, Bao S-J, Bao Q-L (2007) Carbon nanotube/polyaniline composite as anode material for microbial fuel cells. J Power Sources 170(1):79–84

22. Manickam SS, Karra U, Huang L, Bui NN, Li B, McCutcheon JR (2013) Activated carbon nanofiber anodes for microbial fuel cells. Carbon 53:19–28

23. Wang H, Wang G, Ling Y, Qian F, Song Y, Lu X, Chen S, Tong Y, Li Y (2013) High power density microbial fuel cell with flexible 3D graphene–nickel foam as anode. Nanoscale 5(21):10283–10290

24. Xie X, Hu L, Pasta M, Wells GF, Kong D, Criddle CS, Cui Y (2011) Three-dimensional carbon nanotube-textile anode for high-performance microbial fuel cells. Nano Lett 11(1): 291–296

25. Xing X, Yu GH, Liu N, Bao ZN, Criddle CS, Yi C (2012) Graphene-sponges as high-performance low-cost anodes for microbial fuel cells. Energy Environ Sci 5(5):6862–6866

26. Yong YC, Dong XC, Chanpark MB, Song H, Chen P (2012) Macroporous and monolithic anode based on polyaniline hybridized three-dimensional graphene for high-performance microbial fuel cells. ACS Nano 6(3):2394

27. ter Heijne A, Hamelers HV, Saakes M, Buisman CJ (2008) Performance of non-porous graphite and titanium-based anodes in microbial fuel cells. Electrochim Acta 53(18):5697–5703

28. Baudler A, Schmidt I, Langner M, Greiner A, Schröder U (2015) Does it have to be carbon? Metal anodes in microbial fuel cells and related bioelectrochemical systems. Energy Environ Sci 8(7):2048–2055

29. Zhang X, Shi J, Liang P, Wei J, Huang X, Zhang C, Logan BE (2013) Power generation by packed-bed air-cathode microbial fuel cells. Bioresour Technol 142:109–114

30. Zhang GD, Zhao QL, Jiao Y, Zhang JN, Jiang JQ, Ren N, Kim BH (2011) Improved performance of microbial fuel cell using combination biocathode of graphite fiber brush and graphite granules. J Power Sources 196(15):6036–6041

31. Zhao F, Rahunen N, Varcoe JR, Chandra A, Avignonerossa C, Thumser AE, Slade RCT (2008) Activated carbon cloth as anode for sulfate removal in a microbial fuel cell. Environ Sci Technol 42(13):4971–4976

32. Zhang L, Li J, Zhu X, Ye D, Liao Q (2013) Anodic current distribution in a liter-scale microbial fuel cell with electrode arrays. Chem Eng J 223(5):623–631

33. Lepage G, Albernaz FO, Perrier G, Merlin G (2012) Characterization of a microbial fuel cell with reticulated carbon foam electrodes. Bioresour Technol 124(337):199–207

34. Yuan Y, Kim SH (2008) Polypyrrole-coated reticulated vitreous carbon as anode in microbial fuel cell for higher energy output. Bull Korean Chem Soc 29(29):168–172

35. Sasaki K, Yasuda K, Nakanishi K, Rakugi H, Isaka Y, Yamato M (2011) Granular activated carbon based microbial fuel cell for simultaneous decolorization of real dye wastewater and electricity generation. New Biotechnol 29(1):32–37

36. Li J, Liu C, Liao Q, Zhu X, Ye D (2013) Improved performance of a tubular microbial fuel cell with a composite anode of graphite fiber brush and graphite granules. Int J Hydrog Energy 38(35):15723–15729

37. Liu C, Li J, Zhu X, Zhang L, Ye D, Brown RK, Liao Q (2013) Effects of brush lengths and fiber loadings on the performance of microbial fuel cells using graphite fiber brush anodes. Int J Hydrog Energy 38(35):15646–15652

38. Katuri K, Ferrer ML, Gutiérrez MC, Jiménez R, del Monte F, Leech D (2011) Three-dimensional microchanelled electrodes in flow-through configuration for bioanode formation and current generation. Energy Environ Sci 4(10):4201–4210

39. Chen S, Liu Q, He G, Zhou Y, Hanif M, Peng X, Wang S, Hou H (2012) Reticulated carbon foam derived from a sponge-like natural product as a high-performance anode in microbial fuel cells. J Mater Chem 22(35):18609–18613

40. Yuan Y, Zhou S, Liu Y, Tang J (2013) Nanostructured macroporous bioanode based on polyaniline-modified natural loofah sponge for high-performance microbial fuel cells. Environ Sci Technol 47(24):14525–14532

41. Zhang J, Li J, Ye D, Zhu X, Liao Q, Zhang B (2014) Tubular bamboo charcoal for anode in microbial fuel cells. J Power Sources 272:277–282

42. Chen Q, Pu W, Hou H, Hu J, Liu B, Li J, Cheng K, Huang L, Yuan X, Yang C (2018) Activated microporous-mesoporous carbon derived from chestnut shell as a sustainable anode material for high performance microbial fuel cells. Bioresour Technol 249:567–573

43. Karthikeyan R, Wang B, Xuan J, Wong JW, Lee PK, Leung MK (2015) Interfacial electron transfer and bioelectrocatalysis of carbonized plant material as effective anode of microbial fuel cell. Electrochim Acta 157:314–323

44. Lu M, Qian Y, Yang C, Huang X, Li H, Xie X, Huang L, Huang W (2016) Nitrogen-enriched pseudographitic anode derived from silk cocoon with tunable flexibility for microbial fuel cells. Nano Energy 32:382–388

45. Ren H, Pyo S, Lee J-I, Park T-J, Gittleson FS, Leung FC, Kim J, Taylor AD, Lee H-S, Chae J (2015) A high power density miniaturized microbial fuel cell having carbon nanotube anodes. J Power Sources 273:823–830

46. Hindatu Y, Annuar M, Gumel A (2017) Mini-review: anode modification for improved performance of microbial fuel cell. Renew Sustain Energy Rev 73:236–248

47. Liu J, Qiao Y, Guo CX, Lim S, Song H, Li CM (2012) Graphene/carbon cloth anode for high-performance mediatorless microbial fuel cells. Bioresour Technol 114:275–280

48. Zhang Y, Mo G, Li X, Zhang W, Zhang J, Ye J, Huang X, Yu C (2011) A graphene modified anode to improve the performance of microbial fuel cells. J Power Sources 196 (13):5402–5407

49. Wang P, Li H, Du Z (2014) Polyaniline synthesis by cyclic voltammetry for anodic modification in microbial fuel cells. Int J Electrochem Sci 9:2038–2046

50. Lv Z, Chen Y, Wei H, Li F, Hu Y, Wei C, Feng C (2013) One-step electrosynthesis of polypyrrole/graphene oxide composites for microbial fuel cell application. Electrochim Acta 111:366–373

51. Gnana Kumar G, Kirubaharan CJ, Udhayakumar S, Ramachandran K, Karthikeyan C, Renganathan R, Nahm KS (2014) Synthesis, structural, and morphological characterizations of reduced graphene oxide-supported polypyrrole anode catalysts for improved microbial fuel cell performances. ACS Sustain Chem Eng 2(10):2283–2290

52. Zhu N, Chen X, Zhang T, Wu P, Li P, Wu J (2011) Improved performance of membrane free single-chamber air-cathode microbial fuel cells with nitric acid and ethylenediamine surface modified activated carbon fiber felt anodes. Bioresour Technol 102(1):422–426

53. Feng Y, Yang Q, Wang X, Logan BE (2010) Treatment of carbon fiber brush anodes for improving power generation in air–cathode microbial fuel cells. J Power Sources 195 (7):1841–1844

54. Cheng S, Logan BE (2007) Ammonia treatment of carbon cloth anodes to enhance power generation of microbial fuel cells. Electrochem Commun 9(3):492–496

55. Zhang J, Li J, Ye D, Zhu X, Liao Q, Zhang B (2014) Enhanced performances of microbial fuel cells using surface-modified carbon cloth anodes: a comparative study. Int J Hydrog Energy 39(33):19148–19155

56. Zhou M, Chi M, Wang H, Jin T (2012) Anode modification by electrochemical oxidation: a new practical method to improve the performance of microbial fuel cells. Biochem Eng J 60:151–155

57. Mauritz KA, Moore RB (2004) State of understanding of Nafion. Chem Rev 104(10):4535–4586

58. Nambiar S, Togo C, Limson J (2009) Application of multi-walled carbon nanotubes to enhance anodic performance of an Enterobacter cloacae-based fuel cell. Afr J Biotechnol 8(24)

59. Pant D, Van Bogaert G, De Smet M, Diels L, Vanbroekhoven K (2010) Use of novel permeable membrane and air cathodes in acetate microbial fuel cells. Electrochim Acta 55 (26):7710–7716

60. Leong JX, Daud WRW, Ghasemi M, Liew KB, Ismail M (2013) Ion exchange membranes as separators in microbial fuel cells for bioenergy conversion: a comprehensive review. Renew Sustain Energy Rev 28:575–587

61. Zaidi SJ, Mikhailenko SD, Robertson G, Guiver M, Kaliaguine S (2000) Proton conducting composite membranes from polyether ether ketone and heteropolyacids for fuel cell applications. J Membr Sci 173(1):17–34

62. Zhang X, Cheng S, Huang X, Logan BE (2010) Improved performance of single-chamber microbial fuel cells through control of membrane deformation. Biosens Bioelectron 25 (7):1825–1828

63. Kazemi S, Fatih K, Mohseni M, Wang H (2012) Investigating separators to improve performance of flat-plate microbial fuel cells. Meeting Abstracts: The Electrochemical Society, pp 3593–3593

64. Kim JR, Cheng S, Oh S-E, Logan BE (2007) Power generation using different cation, anion, and ultrafiltration membranes in microbial fuel cells. Environ Sci Technol 41(3):1004–1009

65. Sun J, Hu Y, Bi Z, Cao Y (2009) Improved performance of air-cathode single-chamber microbial fuel cell for wastewater treatment using microfiltration membranes and multiple sludge inoculation. J Power Sources 187(2):471–479

66. Yang W, Li J, Zhang L, Zhu X, Liao Q (2017) A monolithic air cathode derived from bamboo for microbial fuel cells. RSC Adv 7(45):28469–28475

67. Zhang X, Cheng S, Huang X, Logan BE (2010) The use of nylon and glass fiber filter separators with different pore sizes in air-cathode single-chamber microbial fuel cells. Energy Environ Sci 3(5):659–664

68. Fan Y, Hu H, Liu H (2007) Enhanced Coulombic efficiency and power density of air-cathode microbial fuel cells with an improved cell configuration. J Power Sources 171(2):348–354

69. Li J, Fu Q, Liao Q, Zhu X, D-d Ye, Tian X (2009) Persulfate: a self-activated cathodic electron acceptor for microbial fuel cells. J Power Sources 194(1):269–274

70. Zhang L, Zhu X, Li J, Liao Q, Ye D (2011) Biofilm formation and electricity generation of a microbial fuel cell started up under different external resistances. J Power Sources 196 (15):6029–6035

71. Cheng S, Liu H, Logan BE (2006) Power densities using different cathode catalysts (Pt and CoTMPP) and polymer binders (Nafion and PTFE) in single chamber microbial fuel cells. Environ Sci Technol 40(1):364–369

72. Zhang F, Cheng S, Pant D, Van Bogaert G, Logan BE (2009) Power generation using an activated carbon and metal mesh cathode in a microbial fuel cell. Electrochem Commun 11 (11):2177–2179

73. Yang W, Li J, Ye D, Zhu X, Liao Q (2017) Bamboo charcoal as a cost-effective catalyst for an air-cathode of microbial fuel cells. Electrochim Acta 224:585–592

74. Watson VJ, Nieto Delgado C, Logan BE (2013) Influence of chemical and physical properties of activated carbon powders on oxygen reduction and microbial fuel cell performance. Environ Sci Technol 47(12):6704–6710

75. Zhou L, Fu P, Wen D, Yuan Y, Zhou S (2016) Self-constructed carbon nanoparticles-coated porous biocarbon from plant moss as advanced oxygen reduction catalysts. Appl Catal B-Environ 181:635–643

76. Liu L, Xiong Q, Li C, Feng Y, Chen S (2015) Conversion of straw to nitrogen doped carbon for efficient oxygen reduction catalysts in microbial fuel cells. RSC Adv 5(109):89771–89776

77. Sun Y, Duan Y, Hao L, Xing Z, Dai Y, Li R, Zou J (2016) Cornstalk-derived nitrogen-doped partly graphitized carbon as efficient metal-free catalyst for oxygen reduction reaction in microbial fuel cells. ACS Appl Mater Inter 8(39):25923–25932

78. Wang H, Zhang Z, Yang Y, Wang K, Ji S, Key J, Ma Y, Wang R (2015) A Co-N-doped carbonized egg white as a high-performance, non-precious metal, electrocatalyst for oxygen reduction. J Solid State Electron 19(6):1727–1733

79. Wu H, Geng J, Ge H, Guo Z, Wang Y, Zheng G (2016) Egg-derived mesoporous carbon microspheres as bifunctional oxygen evolution and oxygen reduction electrocatalysts. Adv Energy Mater 6(20)

80. Fan Z, Li J, Zhou Y, Fu Q, Yang W, Zhu X, Liao Q (2017) A green, cheap, high-performance carbonaceous catalyst derived from Chlorella pyrenoidosa for oxygen reduction reaction in microbial fuel cells. Int J Hydrog Energy

81. Deng L, Yuan H, Cai X, Ruan Y, Zhou S, Chen Y, Yuan Y (2016) Honeycomb-like hierarchical carbon derived from livestock sewage sludge as oxygen reduction reaction catalysts in microbial fuel cells. Int J Hydrog Energy 41(47):22328–22336

82. Yuan Y, Liu T, Fu P, Tang J, Zhou S (2015) Conversion of sewage sludge into high-performance bifunctional electrode materials for microbial energy harvesting. J Mater Chem A 3(16):8475–8482

83. Dong H, Yu H, Wang X, Zhou Q, Feng J (2012) A novel structure of scalable air-cathode without Nafion and Pt by rolling activated carbon and PTFE as catalyst layer in microbial fuel cells. Water Res 46(17):5777–5787

84. Dong H, Yu H, Yu H, Gao N, Wang X (2013) Enhanced performance of activated carbon–polytetrafluoroethylene air-cathode by avoidance of sintering on catalyst layer in microbial fuel cells. J Power Sources 232:132–138

85. Yang W, He W, Zhang F, Hickner MA, Logan BE (2014) Single-step fabrication using a phase inversion method of poly (vinylidene fluoride)(PVDF) activated carbon air cathodes for microbial fuel cells. Environ Sci Technol Lett 1(10):416–420

86. Cheng S, Wu J (2013) Air-cathode preparation with activated carbon as catalyst, PTFE as binder and nickel foam as current collector for microbial fuel cells. Bioelectrochemistry 92:22–26

87. Popat SC, Ki D, Rittmann BE, Torres CI (2012) Importance of OH − transport from cathodes in microbial fuel cells. ChemSusChem 5(6):1071–1079

88. Popat SC, Ki D, Young MN, Rittmann BE, Torres CI (2014) Buffer pKa and transport govern the concentration over potential in electrochemical oxygen reduction at neutral pH. ChemElectroChem 1(11):1909–1915

89. Liu H, Cheng S, Logan BE (2005) Production of electricity from acetate or butyrate using a single-chamber microbial fuel cell. Environ Sci Technol 39(2):658–662

90. Li X, Wang X, Zhang Y, Ding N, Zhou Q (2014) Opening size optimization of metal matrix in rolling-pressed activated carbon air–cathode for microbial fuel cells. Appl Energy 123:13–18

91. You S, Zhao Q, Zhang J, Jiang J, Zhao S (2006) A microbial fuel cell using permanganate as the cathodic electron acceptor. J Power Sources 162(2):1409–1415

92. Li J, Fu Q, Zhu X, Liao Q, Zhang L, Wang H (2010) A solar regenerable cathodic electron acceptor for microbial fuel cells. Electrochim Acta 55(7):2332–2337

93. Tartakovsky B, Guiot SR (2006) A comparison of air and hydrogen peroxide oxygenated microbial fuel cell reactors. Biotechnol Progr 22(1):241–246

94. Tang X, Li H, Du Z, Wang W, Ng HY (2015) Conductive polypyrrole hydrogels and carbon nanotubes composite as an anode for microbial fuel cells. Rsc Adv 5(63):50968–50974

95. Min B, Cheng S, Logan BE (2005) Electricity generation using membrane and salt bridge microbial fuel cells. Water Res 39(9):1675–1686

96. Min B, Logan BE (2004) Continuous electricity generation from domestic wastewater and organic substrates in a flat plate microbial fuel cell. Environ Sci Technol 38(21):5809–5814

97. Liu H, Logan BE (2004) Electricity generation using an air-cathode single chamber microbial fuel cell in the presence and absence of a proton exchange membrane. Environ Sci Technol 38(14):4040–4046

98. Cheng S, Logan BE (2011) Increasing power generation for scaling up single-chamber air cathode microbial fuel cells. Bioresour Technol 102(6):4468–4473

99. Call DF, Logan BE (2011) A method for high throughput bioelectrochemical research based on small scale microbial electrolysis cells. Biosens Bioelectron 26(11):4526–4531

100. Cristiani P, Franzetti A, Gandolfi I, Guerrini E, Bestetti G (2013) Bacterial DGGE fingerprints of biofilms on electrodes of membraneless microbial fuel cells. Int Biodeterior Biodegrad 84:211–219

101. Janicek A, Fan Y, Liu H (2014) Design of microbial fuel cells for practical application: a review and analysis of scale-up studies. Biofuels 5(1):79–92

102. Kim JR, Premier GC, Hawkes FR, Dinsdale RM, Guwy AJ (2009) Development of a tubular microbial fuel cell (MFC) employing a membrane electrode assembly cathode. J Power Sources 187(2):393–399

103. Kim JR, Rodríguez J, Hawkes FR, Dinsdale RM, Guwy AJ, Premier GC (2011) Increasing power recovery and organic removal efficiency using extended longitudinal tubular microbial fuel cell (MFC) reactors. Energy Environ Sci 4(2):459–465

104. Zhuang L, Zhou S (2009) Substrate cross-conduction effect on the performance of serially connected microbial fuel cell stack. Electrochem Commun 11(5):937–940

105. Cheng S, Liu H, Logan BE (2006) Increased performance of single-chamber microbial fuel cells using an improved cathode structure. Electrochem Commun 8(3):489–494

106. Qiu Z, Su M, Wei L, Han H, Jia Q, Shen J (2015) Improvement of microbial fuel cell cathodes using cost-effective polyvinylidene fluoride. J Power Sources 273:566–573

107. Santoro C, Agrios A, Pasaogullari U, Li B (2011) Effects of gas diffusion layer (GDL) and micro porous layer (MPL) on cathode performance in microbial fuel cells (MFCs). Int J Hydrog Energy 36(20):13096–13104

108. Zhang Y, Wang X, Li X, Gao N, Wan L, Feng C, Zhou Q (2014) A novel and high performance activated carbon air-cathode with decreased volume density and catalyst layer invasion for microbial fuel cells. RSC Adv 4(80):42577–42580

109. Li D, Qu Y, Liu J, He W, Wang H, Feng Y (2014) Using ammonium bicarbonate as pore former in activated carbon catalyst layer to enhance performance of air cathode microbial fuel cell. J Power Sources 272:909–914

110. Yang W, Logan BE (2016) Engineering a membrane based air cathode for microbial fuel cells via hot pressing and using multi-catalyst layer stacking. Environ Sci: Water Res Technol 2(5):858–863

111. Yang G, Erbay C, S-i Yi, de Figueiredo P, Sadr R, Han A, Yu C (2016) Bifunctional nano-sponges serving as non-precious metal catalysts and self-standing cathodes for high performance fuel cell applications. Nano Energy 22:607–614

112. Wu Z-S, Yang S, Sun Y, Parvez K, Feng X, Müllen K (2012) 3D nitrogen-doped graphene aerogel-supported Fe_3O_4 nanoparticles as efficient electrocatalysts for the oxygen reduction reaction. J Am Chem Soc 134(22):9082–9085

113. Wu S, Li H, Zhou X, Liang P, Zhang X, Jiang Y, Huang X (2016) A novel pilot-scale stacked microbial fuel cell for efficient electricity generation and wastewater treatment. Water Res 98:396–403

114. Aelterman P, Rabaey K, Pham HT, Boon N, Verstraete W (2006) Continuous electricity generation at high voltages and currents using stacked microbial fuel cells. Environ Sci Technol 40(10):3388–3394

115. Gurung A, Oh S-E (2012) The performance of serially and parallelly connected microbial fuel cells. Energy Sources Part A: Recovery Util Environ Effects 34(17):1591–1598

116. Ieropoulos IA, Ledezma P, Stinchcombe A, Papaharalabos G, Melhuish C, Greenman J (2013) Waste to real energy: the first MFC powered mobile phone. Phys Chem Chem Phys 15(37):15312–15316

117. Zhuang L, Zheng Y, Zhou S, Yuan Y, Yuan H, Chen Y (2012) Scalable microbial fuel cell (MFC) stack for continuous real wastewater treatment. Bioresour Technol 106:82–88

118. Yousefi V, Mohebbi-Kalhori D, Samimi A, Salari M (2016) Effect of separator electrode assembly (SEA) design and mode of operation on the performance of continuous tubular microbial fuel cells (MFCs). Int J Hydrog Energy 41(1):597–606

119. Ieropoulos IA, Greenman J, Melhuish C (2013) Miniature microbial fuel cells and stacks for urine utilisation. Int J Hydrog Energy 38(1):492–496

120. Ren L, Ahn Y, Hou H, Zhang F, Logan BE (2014) Electrochemical study of multi-electrode microbial fuel cells under fed-batch and continuous flow conditions. J Power Sources 257:454–460

121. Miyahara M, Hashimoto K, Watanabe K (2013) Use of cassette-electrode microbial fuel cell for wastewater treatment. J Biosci Bioeng 115(2):176–181

122. Ledezma P, Stinchcombe A, Greenman J, Ieropoulos I (2013) The first self-sustainable microbial fuel cell stack. Phys Chem Chem Phys 15(7):2278–2281

123. Oh S-E, Logan BE (2007) Voltage reversal during microbial fuel cell stack operation. J Power Sources 167(1):11–17

124. An J, Lee HS (2014) Occurrence and implications of voltage reversal in stacked microbial fuel cells. ChemSusChem 7(6):1689–1695

125. An J, Kim B, Chang IS, Lee H-S (2015) Shift of voltage reversal in stacked microbial fuel cells. J Power Sources 278:534–539

126. Wu PK, Biffinger JC, Fitzgerald LA, Ringeisen BR (2012) A low power DC/DC booster circuit designed for microbial fuel cells. Process Biochem 47(11):1620–1626

127. Boghani HC, Papaharalabos G, Michie I, Fradler KR, Dinsdale RM, Guwy AJ, Ieropoulos I, Greenman J, Premier GC (2014) Controlling for peak power extraction from microbial fuel cells can increase stack voltage and avoid cell reversal. J Power Sources 269:363–369

128. An J, Sim J, Lee H-S (2015) Control of voltage reversal in serially stacked microbial fuel cells through manipulating current: significance of critical current density. J Power Sources 283:19–23

129. Kim Y, Hatzell MC, Hutchinson AJ, Logan BE (2011) Capturing power at higher voltages from arrays of microbial fuel cells without voltage reversal. Energy Environ Sci 4(11):4662–4667

130. Khaled F, Ondel O, Allard B, Degrenne N (2013) Voltage balancing circuit for energy harvesting from a stack of serially-connected microbial fuel cells. In: 2013 IEEE ECCE Asia Downunder (ECCE Asia). IEEE, pp 392–397

131. Yang W, Li J, Ye D, Zhang L, Zhu X, Liao Q (2016) A hybrid microbial fuel cell stack based on single and double chamber microbial fuel cells for self-sustaining pH control. J Power Sources 306:685–691

132. Andersen SJ, Pikaar I, Freguia S, Lovell BC, Rabaey K, Rozendal RA (2013) Dynamically adaptive control system for bioanodes in serially stacked bioelectrochemical systems. Environ Sci Technol 47(10):5488–5494

133. Kim B, Lee BG, Kim BH, Chang IS (2015) Assistance current effect for prevention of voltage reversal in stacked microbial fuel cell systems. ChemElectroChem 2(5):755–760

134. Wang A, Sun D, Cao G, Wang H, Ren N, Wu W-M, Logan BE (2011) Integrated hydrogen production process from cellulose by combining dark fermentation, microbial fuel cells, and a microbial electrolysis cell. Bioresour Technol 102(5):4137–4143
135. Sun M, Sheng G-P, Zhang L, Xia C-R, Mu Z-X, Liu X-W, Wang H-L, Yu H-Q, Qi R, Yu T (2008) An MEC-MFC-coupled system for biohydrogen production from acetate. Environ Sci Technol 42(21):8095–8100
136. Mohanakrishna G, Mohan SV, Sarma P (2010) Utilizing acid-rich effluents of fermentative hydrogen production process as substrate for harnessing bioelectricity: an integrative approach. Int J Hydrogen Energ 35(8):3440–3449
137. Vazquez-Larios AL, Solorza-Feria O, Vazquez-Huerta G, Esparza-García F, Rinderknecht-Seijas N, Poggi-Varaldo HM (2011) Effects of architectural changes and inoculum type on internal resistance of a microbial fuel cell designed for the treatment of leachates from the dark hydrogenogenic fermentation of organic solid wastes. Int J Hydrog Energy 36(10):6199–6209
138. Li J, Zou W, Xu Z, Ye D, Zhu X, Liao Q (2013) Improved hydrogen production of the downstream bioreactor by coupling single chamber microbial fuel cells between series-connected photosynthetic biohydrogen reactors. Int J Hydrog Energy 38(35): 15613–15619
139. Huang L, Yao B, Wu D, Quan X (2014) Complete cobalt recovery from lithium cobalt oxide in self-driven microbial fuel cell–microbial electrolysis cell systems. J Power Sources 259:54–64
140. Stein NE, Hamelers HV, Buisman CN (2012) The effect of different control mechanisms on the sensitivity and recovery time of a microbial fuel cell based biosensor. Sens Actuators B: Chem 171:816–821
141. Di Lorenzo M, Curtis TP, Head IM, Scott K (2009) A single-chamber microbial fuel cell as a biosensor for wastewaters. Water Res 43(13):3145–3154
142. Stein NE, Hamelers HV, Buisman CN (2010) Stabilizing the baseline current of a microbial fuel cell-based biosensor through over potential control under non-toxic conditions. Bioelectrochemistry 78(1):87–91
143. Kim BH, Chang IS, Gil GC, Park HS, Kim HJ (2003) Novel BOD (biological oxygen demand) sensor using mediator-less microbial fuel cell. Biotechnol Lett 25(7):541–545
144. Donovan C, Dewan A, Heo D, Beyenal H (2008) Batteryless, wireless sensor powered by a sediment microbial fuel cell. Environ Sci Technol 42(22):8591–8596
145. Stein NE, Hamelers HM, van Straten G, Keesman KJ (2012) On-line detection of toxic components using a microbial fuel cell-based biosensor. J Process Control 22(9):1755–1761
146. Kaur A, Kim JR, Michie I, Dinsdale RM, Guwy AJ, Premier GC (2013) Microbial fuel cell type biosensor for specific volatile fatty acids using acclimated bacterial communities. Biosens Bioelectron 47:50–55

Chapter 11
Biofuel Production from Bioelectrochemical Systems

Zhuo Li, Qian Fu, Hajime Kobayashi and Shuai Xiao

1 Introduction

Environmental pollution and the global energy crisis call for new renewable technologies to support a more sustainable society. Microbial electrolysis cells (MECs) and microbial electrosynthesis cells can degrade organic matter and pollutants in wastewater; when producing biofuels, they offer promising renewable energy technologies for carbon dioxide (CO_2) reduction and wastewater treatment. In the two bioelectrochemical systems, hydrogen and methane (CH_4) can be easily produced by applying a voltage of 0.2–0.6 V, and other value-added products, such as acetate, ethanol, hydrogen peroxide, and formic acid, also can be produced at low overpotentials [1–3]. Many challenges still face these bioelectrochemical systems, such as the low production rate of biofuels, hydrogen re-oxidation, and the difficult separation of liquid products. In this chapter, we review the recent progress in electrodes and reactor configurations, electrode materials, electron transfer mechanism, and applications of the two systems.

Z. Li · Q. Fu (✉) · S. Xiao
Key Laboratory of Low-grade Energy Utilization Technologies and Systems,
Chongqing University, Ministry of Education, Chongqing 400044, China
e-mail: fuqian@cqu.edu.cn

Z. Li · Q. Fu · S. Xiao
Institute of Engineering Thermophysics, Chongqing University,
Chongqing 400044, China

H. Kobayashi (✉)
Department of Systems Innovation, Graduate School of Engineering,
The University of Tokyo, Tokyo 113-8656, Japan
e-mail: kobayashi@frcer.t.u-tokyo.ac.jp

2   Hydrogen Production from MECs

2.1   Working Principle of MECs

Similar to a typical dual-chamber microbial fuel cell (MFC), a typical MEC reactor consists of an anode and a cathode chamber, which are separated by an ion exchange membrane. On the anode, exoelectrogenic microorganisms (such as the *Geobacter* and *Shewanella* species) colonize on the surface and oxidize organic substrates (such as acetate and glucose in wastewater) to produce electrons and protons. The generated electrons transfer to the anode via direct or indirect electron transfer and pass through the circuit to the cathode. On the cathode, the electrons combine with the protons permeating from the anode chamber to produce hydrogen. During this operation, both the anode and cathode chambers are maintained at anaerobic conditions (Fig. 1).

Unlike the reactions in a MFC, the reaction in an MEC cannot spontaneously occur because of its irreversibility. According to the Nernst equation, under typical biological conditions (T = 25 °C, p = 1 bar, and pH 7.0), the standard potential of H^+/H_2 (the cathode reaction) can be calculated as shown in the following equations:

$$2H^+ + 2e^- \rightarrow H_2 \tag{1}$$

$$E_{cat} = -\frac{RT}{2F} \ln \left(\frac{p_{H_2}}{[H^+]^2} \right) \tag{2}$$

where p_{H_2} is the partial pressure of hydrogen, $F = 96,485$ (C/mol; the Faraday constant), T is the temperature, and R is the ideal gas constant. Under standard biological conditions, the cathode potential is equal to −0.414 V versus the standard hydrogen electrode (SHE). The potential of the bioanode in an MEC, which uses acetate as an electron donor, can be calculated using the following equations:
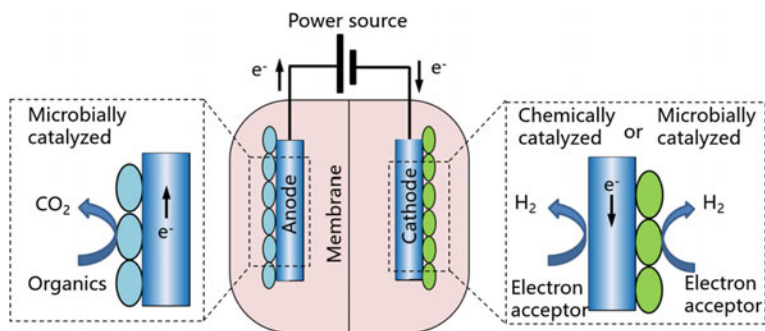
Fig. 1   The working principle of microbial electrolysis cell

$$CH_3COO^- + 4H_2O \rightarrow 2HCO_3^- + 9H^+ + 8e^- \tag{3}$$
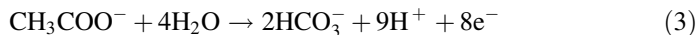
$$E_{an} = E_{an}^0 - \frac{RT}{8F} \ln \left(\frac{[CH_3COO^-]}{[HCO_3^-]^2[H^+]^9} \right) \tag{4}$$

Under standard biological conditions, the anode potential is equal to -0.279 V versus SHE. Therefore, the voltage required for the operation of an MEC is $E_{eq} = (-0.414 \text{ V}) - (-0.279 \text{ V}) = -0.14$ V.

In dark fermentation, various organic acids (such as acetate) are considered as end-products, which cannot be degraded by microorganisms [4, 5]. Notably, these end products can be degraded by the bioanodes of MECs. For a reaction that occurs spontaneously, the Gibbs free energy (ΔG_r) must be negative, but the conversion of such end-products to hydrogen yields a positive ΔG_r in dark fermentation. In MECs, acetate and protons are commonly used as the electron donor and electron acceptor, respectively. Under biological conditions, the reaction equation and Gibbs free energy ($\Delta Gr''$) of acetate oxidation to hydrogen are as follows [4]:

$$CH_3COO^- + 4H_2O \rightarrow 2HCO_3^- + H^+ + 4H_2, \ \Delta Gr'' = +104.6 \text{ kJ/mol} \tag{5}$$
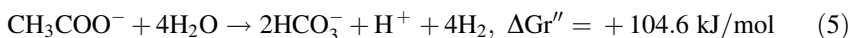
The positive Gibbs free energy means that acetate cannot be spontaneously fermented to hydrogen in the MECs, and thus additional energy has to be added to MECs to realize the reaction. According to thermodynamics, the applied voltage needs to be larger than $\Delta Gr''/nF$, where n is the amount of electrons involved in the reaction (for hydrogen production, n = 2), and F is the Faraday constant. The voltage calculated from thermodynamics is referred as the equilibrium voltage, E_{eq}. For MECs that use acetate as the electron donor under standard biological conditions, the voltage is

$$E_{eq} = -\Delta Gr''/nF = -104.6 \times 10^3/4 \times 2/96485 = -0.14 \text{ V} \tag{6}$$

where the negative sign indicates that the reaction is not spontaneous.

In practice, a voltage between 0.2 and 0.6 V is required for an efficient hydrogen production rate because of the overpotentials on the electrodes, ohmic losses, and concentration losses in the systems. Yet, the input voltage is still substantially lower than the voltage necessary for conventional water electrolysis (in practice, greater than 1.6 V) [6].

2.2 MEC Systems

2.2.1 Configuration

Various MEC configurations have been proposed for high-efficiency hydrogen production [4, 7]. Generally, MEC configurations can be classified into dual-chamber and single-chamber reactors. In the dual-chamber reactors, the anode and cathode chambers are divided by a separator (mainly ion exchange membranes), by which the anodic and cathodic reactions cannot be affected by each other. The dual-chamber can minimize hydrogen re-oxidation by microorganisms in the anode chamber [8] and can prevent the mixing of hydrogen generated in the cathode chamber and the CO_2 generated in the anode chamber. The H-type reactor is a typical dual-chamber reactor that has been widely used in MEC experiments [4, 9, 10]. This kind of reactor has a high internal resistance because of the large distance between the anode and cathode and the small size of the separating membrane [10], and these issues largely limit the performance of MECs. There are various approaches to enhancing the hydrogen production performance of H-type MECs, such as increasing the size of the membrane relative to the electrode-projected surface areas [5, 11], using a high surface area electrode [12, 13], and reducing the distance between the anode and cathode [14]. For example, Cheng et al. clamped an anion exchange membrane (AEM) between the anode (30 mm in diameter, 20 mm long; 14 ml) and cathode chambers (30 mm in diameter, 40 mm long; 28 ml), and obtained a hydrogen production rate of 1.1 m^3-H_2 m^{-3} d^{-1} at an applied voltage of 0.6 V [5]. Liu et al. used graphite granules as the anode and a graphite rod that was inserted into the granules as an electron conductor, significantly increasing the surface area of the anode [15]. Because higher anode surfaces are suitable for the attachment of microorganisms on the anode, a higher MEC performance was obtained by using this anode in contrast to that in a plain carbon cloth anode. Inspired by the membrane-electrode-assembly in proton exchange membrane fuel cells (PEMFCs), Rozendal et al. proposed an MEC reactor using the membrane-electrode-assembly module, in which the anode and cathode are pressed onto the two sides of the ion exchange membrane. Using the membrane-electrode-assembly module, the distance between the anode and cathode are significantly reduced, thereby resulting in a higher hydrogen production performance [11].

The cation exchange membrane (CEM) and AEM are commonly used separators between the anode and cathode chamber in MECs. Cations (such as Na^+, K^+, and NH_4^+) and anions (such as OH^-) can pass through the CEM and AEM, respectively. However, when the CEM (especially a Nafion membrane) is used in an MEC, cation species (such as Na^+, K^+, and NH_4^+) other than protons are responsible for the positive charge transport through the membrane because of their much higher concentration than the protons in the cathodic liquid (pH 7.0). As a result, the protons consumed at the cathode cannot be replenished by the protons generated at the anode, leading to a pH increase in the cathode chamber and a pH decrease in

the anode chamber, leading to a loss of voltage according to the Nernst equation. To deal with this problem, Tartakovsky et al. proposed using a J-cloth, a material without electrical conductivity, as the separator in the MECs [14]. Cations and anions can both pass through a J-cloth, resulting in equal pHs in the anode and cathode. A bipolar membrane, which consists of a cation-selective layer and an anion-selective layer, also has been used, because it can dissociate water to H^+ and OH^- under a reverse bias direct current field, thereby controlling the pH of the anodic and cathodic liquid [16, 17].

No matter what kind of separators are used, the existence of separators between the anode and cathode chamber can increase the ohmic resistance. Therefore, a configuration without separators (i.e., single-chamber reactors) was proposed to reduce the ohmic resistance and increase the performance of MECs [11, 15, 18, 19]. Call et al. reported the first single-chamber reactor for hydrogen production in an MEC and achieved a hydrogen production rate of 3.12 ± 0.02 m^3-H_2 m^{-3} d^{-1} at an applied voltage of 0.8 V [18]. Although it has been reported that hydrogen can be re-oxidized by anode-respiring bacteria [8], Call and Logan [18] demonstrated that it was possible to achieve a high hydrogen recovery and production rate in single-chamber MECs, potentially reducing the costs of MECs and enabling the construction of simpler designs. This process, however, resulted in other negative impacts because it eliminated the ion exchange membranes, such as hydrogen consumption by methanogens [20, 21] and the gas mixing of the CO_2 that was produced by the bioanodes. For example, Cusick et al. constructed a pilot-scale MEC that was inoculated with winery wastewater and reported that CH_4 was the main gas product that resulted from the long operation cycles [21]. Therefore, the primary challenge of developing a single-chamber MEC is to avoid CH_4 production, especially when complex inoculum are used.

2.2.2 Electrodes Materials and Cathode Catalysts

Carbon materials are commonly used as electrode materials in MECs. On the anode, the catalytic reactions are essentially the same as those in the MFC anodes. Thus, the materials used as anodes in MFCs also can be used as anode materials in MECs. For example, carbon cloth, carbon paper, graphite felt, graphite granules, and carbon brushes are commonly used as anode materials in MECs [12].

Carbon materials are commonly used also as the cathode materials in MECs. The reaction rate is relatively slow on plain carbon electrodes because of the high overpotentials. To reduce the overpotentials, metal catalysts, such as platinum (Pt), nickel (Ni), and stainless steel, are often used at the cathodes. Among them, Pt is the most investigated catalyst because of its low overpotential (0.05 V at 15 A m^{-2}) for hydrogen evolution under optimized conditions (at a pH of 6.2 for the phosphate buffer) [12, 22]. Cheng and Logan [5] constructed the first MEC reactor that used Pt (0.5 mg cm^{-2}) as the catalyst on the cathode and obtained a hydrogen production rate of 1.1 m^3-H_2 m^{-3} d^{-1} at an applied voltage of 0.6 V. Call and Logan [18, 23] used a Pt catalyst on a carbon cloth in a single-chamber MEC and obtained

hydrogen production rates of 3.12 ± 0.02 m^3 m^{-3} of reactor liquid volume per day at an applied voltage of 0.8 V with a hydrogen recovery of 96%.

The application of Pt in cathode catalysts is largely limited due to its high cost, however. In addition, Pt can be easily poisoned by sulfide, which is a common constituent of wastewater [4, 23]. Further studies found that nickel (Ni) alloys and stainless steel (SS) were promising catalysts because of their availability, low overpotentials, and stability in wastewater [23]. Selembo et al. [24] investigated the influence of different SS and Ni alloys on the hydrogen production rate in MECs. They showed that stainless steel A286 was superior to Pt sheet metal in terms of its cathodic hydrogen recovery (61 vs. 47%), overall energy recovery (46 vs. 35%), and maximum volumetric hydrogen production rate (1.5 vs. 0.68 m^3 m^{-3} d^{-1}) at an applied voltage of 0.9 V. Although Ni 625 was better than other Ni alloys, it did not perform as well as stainless steel A625. They also reported that the performance of stainless steel and Ni cathodes could be further increased by electrodepositing a nickel oxide layer onto the sheet metal, although the performance of the nickel oxide cathodes decreased over time because of a reduction in the stability of the oxides. To further improve the hydrogen production rate, three-dimensional (3D) materials were also used as cathode materials because of their high specific surface area. Many nonprecious materials were used as 3D cathodes. Call et al. [25] showed that a stainless steel brush cathode, 2.5 cm long and 2.5 cm in diameter with a specific surface area of 810 m^2 m^{-3}, achieved a hydrogen production rate and efficiencies similar to those achieved with a Pt-catalyzed carbon cloth. The hydrogen production rate of the stainless steel brush was 1.7 ± 0.1 m^3-H$_2$ m^{-3} at an applied voltage of 0.6 V. Zhang et al. [26] studied the effect of the stainless steel mesh size on the performance of MECs. They showed that a stainless steel mesh with a relatively thick wire size (0.02 cm), a medium pore size (0.02 cm), and a specific surface area of 66 m^2 m^{-3} had the best performance with a hydrogen production rate of 2.1 ± 0.3 m^3-H$_2$ m^{-3} and hydrogen recovery of $98 \pm 4\%$ at an applied voltage of 0.9 V.

Graphene and carbon nanotubes (CNTs), materials with a good conductivity and excellent performance for the modification of bioanodes in MFCs, also were used in the MEC cathodes. A 3D hybrid of layered MoS$_2$/nitrogen-doped graphene nanosheet aerogels were used as cathode catalysts in MECs [27]. A high current density of 0.36 mA cm^{-2} and a hydrogen production rate of 0.19 m^3-H$_2$ m^{-3} d^{-1} was achieved at a 0.8 V bias. Hou et al. suggested that the outstanding performance of the hybrid cathode benefited from its 3D conductive networks, porous structure, and strong synergic effects between the MoS$_2$ nanosheets and N-gas. Cai et al. [28] constructed a cathode using 3D self-assembly Ni foam-graphene in MECs. In this study, improved electrochemical activity and effective mass diffusion were achieved after coating the Ni foam with graphene. The average hydrogen production rate was comparable to that of the Pt/C (1.32 ± 0.07 m^3-H$_2$ m^{-3} d^{-1}) catalyst at an applied voltage of 0.8 V. Dai et al. synthesized a series of nano-Mg(OH)$_2$/graphene composites via the hydrothermal method [29]. The cathode with this composite exhibited good stability, and its current density was comparable to that of the Pt/C cathode. CNTs, widely used in super-capacitors and MFCs, also can be

used as a base material to synthesize nanoparticles as cathode catalysts in MECs. Wang et al. [30] used a CNT-based electrode as an alternative to Pt in a single chamber MEC and achieved a hydrogen production rate of 1.42 $m^3 \, m^{-3} \, day^{-1}$ with a current density of 192 A m^{-3} at an applied voltage of 0.9 V. Furthermore, conductive polymers, which have been used in various electrochemical devices [31, 32], also have attracted significant attention for their applications in MECs. For example, polyaniline was used to modify the cathode with multi-walled CNTs [33], and a hydrogen production rate of 1.04 $m^3 \, m^{-3} \, day^{-1}$ and current density of 163 A m^{-3} were achieved.

2.3   Biocathode Catalyzing H₂ Evolution in MECs

2.3.1   Development of Biocathodes

Inspired by the electricity generation using exoelectrogenic microorganisms on bioanodes, researchers proposed to use microorganisms as the catalysts on the cathode to produce hydrogen in MECs. Rozendal et al. reported on the first biocathode that was capable of catalyzing hydrogen evolution in MECs. The biocathode was achieved through a three-phase biocathode startup procedure, which turned an acetate- and hydrogen-oxidizing bioanode into a hydrogen-producing biocathode by reversing the electrode's polarity [34]. Compared to the plan graphite felt, the hydrogen production rate of the biocathode significantly increased. Jeremiasse et al. demonstrated the proof-of-concept of an MEC in which both the anode and cathode reaction were catalyzed by microorganisms. At an applied voltage of 0.5 V and a cathode potential of −0.7 V versus SHE, a maximum current density of 1.4 A m^{-2} and 3.3 A m^{-2} were achieved, respectively. In contrast, a control cathode (graphite felt without a biofilm) only showed a current density of 0.3 A m^{-2} at a potential of −0.7 V versus SHE [35].

Biocathodes still have room for improvement when compared with the current density generated by the cathodes with metal catalysts. For example, current densities in the range of 4–10 A m^{-2} are typically achieved when Pt is used on the cathode, whereas it was only around 1.2 A m^{-2} with a biocathode at a cathode potential of −0.7 V versus SHE [34]. However, the biocathode possesses other attractive advantages, as it is inexpensive, not easily poisoned by wastewater, and capable of self-regeneration.

Various methods have been proposed to modify the cathode surface to further improve the hydrogen production rate of biocathodes. For example, CNTs, graphene, and polymers have been used to modify biocathodes [36, 37]. Polyaniline was reported to improve the electrode's bioaffinity and electron transfer [38]. Carbon nanotubes were found to reinforce the electrochemical activity of the electrode. Chen et al. [36] used polyaniline and CNTs to modify a biocathode and achieved a hydrogen production rate of 0.67 $m^3 \, m^{-3} \, day^{-1}$ at an applied voltage of 0.9 V. They reported that some electrode characteristics, such as the number of

active positions [39], ability of electron transfer [38, 40], and specific surface area [41], could be improved by using polyaniline and multi-walled CNTs. Graphene [37] was also used to promote the performance of the hydrogen production of biocathodes. Su et al. constructed a biocathode modified by graphene and assessed the performance of this biocathode under different cathode potentials [37]. At a cathode potential of −0.9 V versus SHE, the hydrogen production rate of the modified biocathode achieved 2.49 ± 0.23 m^3 m^{-3} day^{-1}, which was about three times higher than that of the unmodified biocathode. In their research, the hydrogen production performance of the modified biocathode was similar to that of the cathode that was catalyzed by Pt and superior to that of the stainless steel mesh cathode at −0.9 V versus SHE. In addition to the surface modification of the cathode, the employment of microorganisms with better catalytic properties also improved performance. Fu et al. [42] used thermophilic microorganisms to develop a hydrogen producing biocathode with the advantages of thermophilic microorganisms, such as a higher reaction activity and greater durability [43, 44]. At a potential of −0.8 V versus SHE, the thermophilic biocathode achieved a current density of 1.28 ± 0.15 A m^{-2} and a hydrogen production rate of 376.5 ± 73.42 mmol m^{-2} day^{-1} at 55 °C, which were around 10 times higher than those same values achieved with noninoculated electrodes.

Notably, in MECs with biocathodes, hydrogen can be further converted to CH_4 by methanogens, which were commonly enriched with hydrogen and CO_2 [20, 21, 45]. To improve the hydrogen production rate in MECs, several approaches have been used to inhibit the growth of methanogens. For example, biocathodes have been exposed to air to inhibit the growth of methanogens [18]. A specific inhibitor for methanogens also has been applied [46].

2.3.2   Microbial Ecosystem of Biocathodes

Microorganisms adhering on cathode surfaces can catalyze hydrogen production, but it is still not well understood how those microorganisms catalyze the reaction. To understand the working principle of a biocathode, Croese et al. analyzed the microbial community of a mixed culture biocathode [47]. They reported that the bacterial population consisted of 46% *Proteobacteria*, 25% *Firmicutes*, 17% *Bacteroidetes*, and 12% other phyla. They also found that the *Desulfovibrio* species were the dominant microorganisms at the biocathode. Fu et al. analyzed the bacterial community of a thermophilic biocathode [42] and found that *Firmicutes* was the dominant phylum (77.4%), followed by *Coprothermobacter* (19.8%).

Few studies have examined the electron transfer manners of microorganisms adhering on cathodes. It has been hypothesized that the electron transfer between the electrode and the microorganisms may be possible reverse reactions of those in the bioanodes, as some similarities were found between anodic bacteria and cathodic bacteria. For example, the genomes of the *Desulfovibrio* species encode several c-type cytochromes and multicopper proteins, which show homologies to the proteins involved in the electron donation in the *Geobacter* species (a main

bacteria species in bioanodes). Similar to the pilin-like appendages that were reported to be electron transfer structures in the *Geobacter* sp., the *D. vulgaris* flagellar appendages are involved in a physical association during syntrophic growth with other microbes and also might be involved in the adherence to electrodes. These similarities suggest that the mechanism of extracellular electron transfer by the *Desulfovibrio* species could be, at least partly, similar to the electron transfer mechanisms at the bioanodes [47].

2.4 Development and Application of MECs

2.4.1 MFC-MEC Coupled Systems

In theory, an applied voltage of 0.14 V is required to drive the production of hydrogen in MECs [4]. In practice, a voltage of 0.6 V or more is required for high-efficiency hydrogen production because of the overpotentials [4, 18]. Notably, the open circuit voltage of a typical MFC can reach as high as 0.8 V [48]; thus, a high-efficiency hydrogen production may be achieved by using an MFC to power an MEC, creating an MFC-MEC coupled system. In this system, hydrogen can be harvested from substrates, and no external power supply is required. Min et al. reported the first demonstration of an MFC-MEC coupled system, which combined a single-chamber MFC with an air cathode and a dual-chamber MEC. Using acetate (0.1 g L^{-1}) as the electron donor in both the MFC and MEC, the hydrogen production rate of the system reached $2.2 \pm 0.2 \text{ mL L}^{-1} \text{ d}^{-1}$. The cathodic hydrogen recovery and overall systemic Columbic efficiency were 88%–96% and 28%–33%, respectively. The overall systemic hydrogen peak production was 1.21 mol-H_2/mol-acetate [49]. Performance of the coupled system was further investigated under different configurations: When the resistor changed from 10 Ω to 10 kΩ, the results showed that the hydrogen production rate varied in the range of 2.9 ± 0.2– $0.2 \pm 0.0 \text{ mL L}^{-1} \text{ d}^{-1}$. The hydrogen production rate increased significantly when the MFCs were connected in a series, whereas it slightly decreased when the MFCs were connected in parallel [50].

2.4.2 Photo-Microbial Coupled System

As an environmentally friendly approach to generating hydrogen, the direct utilization of renewable energy (such as solar) is an obvious but still challenging choice. A dye-sensitized solar cell (DSSC)-driven MEC system was reported in the literature [51–54], where an external solar cell taking the place of the electrical bias was coupled with an MEC device to supply the required additional energy. Furthermore, a solar-powered MEC system integrating the microbial anode and semiconductor photocathode (such as Cu_2O [55], TiO_2 [56]) has been shown to

generate hydrogen effectively. It can minimize the material preparation and device fabrication costs of a DSSC-driven MEC.

2.4.3 MEC-Fermentation Coupled Systems

Because of the thermodynamic limitations (refer to Sect. 2.1), many organic compounds produced by dark fermentation cannot be further degraded into hydrogen via fermentation [4, 5]. An MEC can be coupled with fermentation to further degrade these dead-end products. For example, Lu et al. fed a single-chamber MEC with the effluent that was produced in an ethanol-type fermentation reactor. The MEC achieved a hydrogen production rate of 1.41 ± 0.08 m^3 L^{-3} d^{-1} at an applied voltage of 0.6 V, much higher than that (0.70 m^3 L^{-3} d^{-1}) of the fermentation reactor [57]. MECs also were used to degrade the fermentation effluent of recalcitrant substrates, such as lignocellulose and cellobiose. Lalaurette et al. achieved a hydrogen production rate of 0.96 ± 0.16 L L^{-1} d^{-1} (cellobiose) and 1.00 ± 0.19 L L^{-1} d^{-1} (lignocellulose), respectively, when the MECs were fed with the fermentation effluent of lignocellulose and cellobiose [58]. Yan et al. fed MFCs with the fermentation effluent of xylose and corncob hydrolysate. When a current was generated, the MFCs were used as MECs to produce hydrogen. The hydrogen production rates of 41.7 and 23.3 mmol per mol-acetate were achieved with the xylose and corncob hydrolysate effluent, respectively [59]. The fermentation effluents of cellulose [60] and glycerol [61] were also used as electron donors in MECs.

2.4.4 MECs for Wastewater Treatment

It has been reported that 7.6 kJ L^{-1} energy was obtained from domestic wastewater [62], indicating that wastewater contains abundant energy. Both MFCs and MECs were used to recover energy from wastewater. MECs have some advantages over MFCs from both an economic and environmental perspective [63, 64]. Several MEC reactors were designed for wastewater treatment. Ditzig et al. [65] designed the first MEC that used domestic wastewater as the substrate. A double-chamber reactor was used to treat domestic wastewater at the anode chamber with applied voltages of 0.2–0.6 V. The MEC was operated in the fed-batch mode and removed COD almost completely (87–100%). The hydrogen yield (ca. 10% of the theoretical value) was low because of the low conversion of the substrate and hydrogen loss.

Laboratory results at the pilot scale must be used to assess the practical application of MECs and to estimate the durability of their critical components, such as the electrodes and membranes. Cusick et al. constructed the first pilot-scale MEC to treat actual wastewater from a winery plant [21]. The MEC was a 1,000 L-volume single-chamber reactor that used graphite fiber brushes as anodes and SS mesh as cathodes. The MEC achieved a hydrogen production rate of 0.2 L L^{-1} d^{-1} and an

average soluble COD removal of 62%. The produced gas, however, was mainly composed of CH_4 (86%) and CO_2, with trace amounts of hydrogen, because the produced hydrogen was further converted to CH_4 by methanogens. Heidrich et al. [66] constructed a 120 L-volume MEC system, which consisted of six independent MEC modules using a stainless steel cathode and low-cost microporous membrane for domestic wastewater treatment. The MEC system produced virtually pure hydrogen gas ($100 \pm 6.4\%$) for more than 3 months with an average COD removal efficiency of 34% and hydrogen production rate of 0.015 L L^{-1} d^{-1}.

Additionally, as the cathode potential of MECs can be controlled with the electricity supply, recalcitrant pollutants (such as nitrobenzene and 4-chlorophenol) can be reduced as electron acceptors at the cathodes. Compared with conventional electrochemical reduction, the removal of these pollutants in MECs consumes much less energy. Furthermore, electroactive microorganisms on the anode or cathode could greatly lower the overpotential of the electrochemical reactions, leading to higher removal efficiencies and rates.

3 Methane Production from Electromethanogenesis

3.1 Working Principle of Electromethanogensis

In practice, MECs are usually inoculated with wastewater and sludge, as electrochemically active microorganisms are enriched in these environments. Coincidently, methanogens are also often enriched in wastewater and sludge, resulting in the production of CH_4 (rather than hydrogen) in MECs using biocathodes [21, 67, 68]. Although several approaches have been employed to inhibit the growth of methanogens in MECs [46], most of these approaches are ineffective or energy intensive. However, the production of CH_4 in bioelectrochemical systems possesses several advantages over hydrogen production. The storage requirements for CH_4 are not as restrictive as those for hydrogen. Moreover, CH_4 can be more easily integrated into the existing infrastructure. Furthermore, the standard potential of CO_2/CH_4 is higher than that of H^+/H_2 under neutral conditions, suggesting that bioelectrochemical CH_4 production is potentially more energy saving than hydrogen production in MECs.

Electromethanogensis (EM), a derivative of MEC, is a promising technology that can convert electric energy and CO_2 into CH_4 using microorganisms as biocatalysts. The configuration and working principle of EM are similar to that of MECs. Generally speaking, electrochemically active microorganisms adhering on the anode oxidize organic matter and transfer electrons to the anode. The electrons pass through the external circuit to the cathode with the assistance of a power source. On the cathode, microorganisms (mainly methanogens) attached on the surface utilize electrons from the cathode to reduce CO_2 to CH_4.
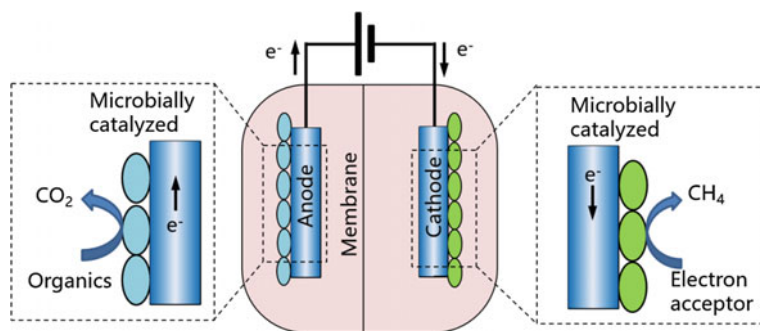
Fig. 2 The working principle of electromethanogenesis

According to the Nernst equation, under neutral conditions, the standard potential of acetate/CO_2 (a typical anode reaction) and CO_2/CH_4 (cathode reaction) is -0.28 V and -0.24 V versus SHE, respectively. Thus, in theory, a CH_4-producing bioelectrochemical systems (BES) can be a spontaneous system based on a thermodynamic analysis. In practice, because of the overpotentials, ohmic losses, and concentration losses, a voltage of 0.6 V or more is required for efficient CH_4 production (Fig. 2).

3.2 Development of Electromethanogensis

Park et al. reported on CH_4 production in a bioelectrochemical system for the first time and showed that methanogens could accept electrons through hydrogen or reduced neutral red to convert CO_2 to CH_4 [69]. In the following years, after hydrogen-producing biocathodes were first reported [34], researchers found that the produced hydrogen could be further converted into CH_4 by the hydrogenotrophic methanogens existing in the reactor. Cusick et al. developed a pilot-scale MEC using winery wastewater [21]. They found that the hydrogen produced at the cathodes was converted into CH_4. The conditions in the reactor that enriched the exoelectrogens and hydrogenogens were also suitable to promote the growth of the methanogens. Clauwaert et al. used an abiotic cathode of an MEC to produce hydrogen, which was further converted into CH_4 via anaerobic digestion in an external reactor [70]. Clauwaert and Verstraete were the first to use a biocathode to generate CH_4 as the main product in a single-chamber BES [45]. In these studies, hydrogen-mediated electron transfer from the cathode to the methanogens played the role of an electron shuttle. In other words, hydrogen was first produced on the biocathode and quickly consumed for hydrogenotrophic methanogenesis. As the heating value of hydrogen is much higher than that of CH_4, it was considered somewhat a pity to convert hydrogen to CH_4.

To avoid intermediate chemical transitions and to achieve a direct bioelectrochemical conversion of CO_2 to CH_4 at a biocathode, Cheng et al. used a two-chamber BES with CO_2 as the sole electron acceptor at the cathode. Although no significant hydrogen production was detected in this study, microbial- or abiotic-generated hydrogen may have acted as a mediating component between the cathode and methanogens [71]. Because of a relatively high cathode potential, the CH_4 production rate was much lower than that of a BES in which hydrogen mediated the electron transfer from the electrode to the methanogens [72]. Villano et al. indicated that bioelectrochemical CH_4 production can occur via both direct electron transfer and the intermediate production of hydrogen gas [73]. Fu et al. acclimated a biocathode that could produce CH_4 at a potential of -0.35 V versus SHE, suggesting that methanogens could directly accept electrons from the cathode surface without generating hydrogen.

3.3 Mechanisms of Electron Transfer from the Electrode to the Methanogens

Two major pathways have been proposed for the electron transfer from the electrodes to the methanogenic archaea (methanogen): Direct and indirect (mediated) electron transfer (Fig. 3; Pathways I and II) [73–76]. Until recently, however, these models could not be examined conclusively because of their experimental set-ups.

In most studies, environmental samples (such as anaerobic sludge and bioreactor effluents) were used as the inoculums [71, 72, 77, 78]. Thus, the resulting biocathodes generally contained multiple species of undefined metabolic abilities. It therefore was difficult to examine the roles of each microbial species on electromethanogenesis and the biocathode ecosystem. Moreover, ferredoxin and coenzyme F420, the central electron carriers of methanogens, have midpoint potentials in the range of -0.36 to -0.42 V versus SHE, which overlap with the redox potential of the small intermediates (such as hydrogen, -0.41 V vs. SHE, at a neutral pH) [79, 80]. Thus, the cathode potentials are negative enough to enable the
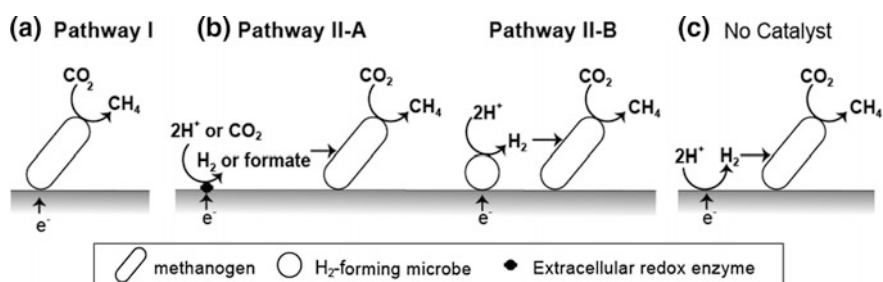
Fig. 3 Electrons are transferred from the electrode to the methanogens via the direct electron transfer (Pathway I) and indirect electron transfer (Pathway II)

direct electron transfer to the redox-active components of the methanogens, and they can also facilitate the intermediate formations, making the discrimination of the electron-transfer pathways difficult.

Recently, several studies on electromethanogenic systems using defined species provided key insights into the electron transfer mechanisms by addressing the contributions of each pathway, as well as the role of each microbial species [81–84]. In this section, we describe the current knowledge about the electron transfer mechanisms at the electromethanogenic biocathode, particularly focusing on these studies.

3.3.1 Pathway I: Direct Electron Transfer from the Electrode to the Methanogens

Beese-Vasbender et al. reported electromethanogenesis by a pure culture of a biocathode inoculated with the strain IM1 [81]. The strain IM1 is an iron-corroding hydrogenotrophic methanogen closely related to *Methanobacterium* [85]. The authors employed a dual-compartment bioelectrochemical cell in which two bioreactors were connected via a salt bridge, and therefore, possible interferences from the anode side (such as the contamination of microbes, organic substrates, or reactive oxygen species from the anode compartments) to the cathode were minimized (Fig. 4).

A pure culture of the strain IM1 was inoculated onto a pre-sterilized cathode and incubated at the set potential of -0.4 V versus SHE. The IM1-inoculated biocathode started to produce CH_4 at 12 days postinoculation. The CH_4 production rate increased simultaneously with the increase in the current density and reached 3.5 mmol m^{-2} day^{-1} with a columbic efficiency of about 80% at 23 days postincubation. No appreciable CH_4 production or increase in the current density were observed at the cathode inoculated with *Methanococcus maripaludis* (another hydrogenotrophic methanogen) or the noninoculated control, suggesting that the strain IM1 had the ability of catalyzing electromethanogenesis at the cathode.
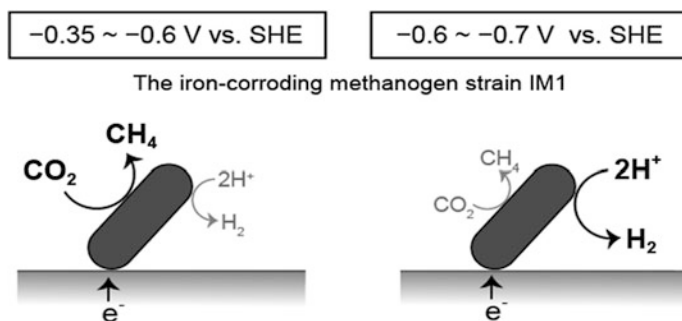
Fig. 4 Electron transfer manner of the iron-corroding methanogen strain IM1

Cyclic voltammetry with the IM1-inoculated biocathode showed that the cathodic current increased when the cathode potential was lowered, indicating a facilitated electron transfer to the redox active components closely attached to the electrode's surface. On the cathode's surface, the strain IM1 cells were directly attached to the electrode's surface and relatively sparsely distributed. No obvious biofilm was observed, implying that soluble electron mediators (such as hydrogen) or conductive pili were likely not involved in the electron transfer from the electrode to the strain IM1. Taken together, these observations strongly suggest that the methanogens alone can take up electrons from the cathode's surface.

The CH_4 and current production by the IM1-inoculated biocathode showed a dependence on the set potential. At potentials around −0.3 V versus SHE, the CH_4 and current production rates were attenuated to the same level as the noninoculated cathode. At the potentials from −0.4 to −0.6 V versus SHE, the CH_4 production rate remained at similar levels, while the cathodic current density was increased as the cathode potential was lowered. However, at potentials more negative than −0.6 V versus SHE, the cathodic current density further increased and was accompanied by hydrogen evolution. The CH_4 formation rate was, on the contrary, significantly reduced. This hydrogen evolution (rather than methanogenesis) at lower potentials was likely due to the limited capacity of the enzyme system for methanogenesis and can be a protective mechanism of the strain IM1: By shuttling excess electrons to hydrogen evolution (i.e., hydrogenases), the strain IM1 can avoid the accumulation of negative charges close to the cell and maintain the electrochemical gradient across the cell membrane.

To understand the mechanism underlying the direct-electron transfer from an electrode to the strain IM1, it is crucial to identify the cell-surface-associated redox active component(s) of the methanogen, which serves as the entrance point of the electrons. As the strain IM1 is not genetically tractable, the detailed bioelectrochemical characterization of the outer surface of the cell in combination with proteomic approaches can provide further insights.

3.3.2   Pathway II: Indirect Electron Transfer Mediated via Diffusible Intermediates

Pathway II-A: Intermediate Formations Catalyzed by Extracellular Enzymes

At low redox potentials, diffusible molecules (such as hydrogen and formate) can be electrochemically formed on the electrode's surface. Such intermediates can be consumed rapidly by hydrogenotrophic methanogens [86], thereby mediating the electron transfer between the electrode and methanogen. Although the formation of these intermediates is thermodynamically favored at low potentials, the rates of these reactions at carbon electrodes (without catalysts) are too slow in comparison with the CH_4 formation rates at biocathodes [71, 73].

Recently, it has been suggested that the formation of intermediates can be catalyzed by extracellular redox enzymes, which are released from microbial cells and
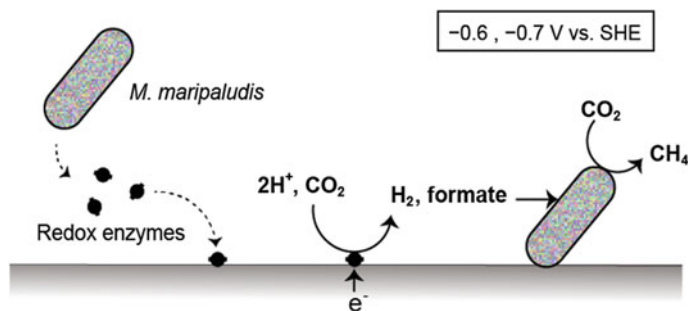
Fig. 5 Formation of intermediates can be catalyzed by extracellular redox enzymes

adsorbed on the cathode's surface [82] (Fig. 5). Lohner et al. examined a cathode that was inoculated with a pure culture of *M. maripaludis* [84]. *M. maripaludis* is a hydrogenotrophic methanogen and genetically tractable [87, 88]. At a set potential of −0.6 V versus SHE, the *M. maripaludis* (the wild-type)-inoculated cathode produced CH_4 at a rate of ca. 11.4 mmol m^{-2} day^{-1} with a columbic efficiency of 70–80%. CH_4 formation was not detected in the absence of the low cathode potential (−0.6 V vs. SHE) or the inoculum. At the abiotic electrode, molecular hydrogen was produced at a rate of 1.2 mmol m^{-2} day^{-1}, which was too low to account for the CH_4 production at the inoculated cathode. When a cathode was inoculated with the *M. maripaludis* strain MM1284, a mutant in which all genes encoding hydrogenases were knocked out, CH_4 was produced at the cathode potential of −0.6 V versus SHE. However, the CH_4 production rate was largely attenuated (ca. 10% of that of the wild-type-inoculated cathode). In the presence of 2-bromoethanesulfonate, a specific inhibitor of methylcoenzyme *M. reductase* (the key enzyme in the last step in methanogenesis) [89], the wild-type-inoculated cathode produced hydrogen and formate, whereas the cathode inoculated with the strain MM1284 produced only formate, suggesting that the hydrogenase(s) derived from *M. maripaludis* was responsible for the hydrogen formation.

Strikingly, the cell-free spent medium of the *M. maripaludis* culture could catalyze the formation of hydrogen as well as formate at a noninoculated cathode poised at −0.6 V versus SHE [82]. The rates of hydrogen and formate formation were sufficient to explain the CH_4 production rates at the inoculated cathode. The catalytic activity of the cell-free spent media was heat- and proteinase-sensitive, indicating that the enzymes were catalyzing these reactions. Moreover, the formation of formate (but not hydrogen) was facilitated by the cell-free spent medium of the mutant MM1284, suggesting that extracellular hydrogenase(s) released from *M. maripaludis* cells is responsible for the hydrogen formation. Furthermore, the current consumption at the cathode with the cell-free spent medium was higher than that in the control, even after several weeks of operation and medium exchanges, suggesting that the extracellular enzymes were relatively stable and tightly adsorbed onto the electrode.

These observations indicated that redox enzymes, such as hydrogenases and presumably formate dehydrogenases, are released from the cells of *M. maripaludis* and can utilize electrons from the cathode's surface, catalyzing the formation of intermediates (such as hydrogen and formate, respectively), which are rapidly consumed by the methanogens for methanogenesis (Fig. 5). The enzymes can be released from the cells by loss of the cellular integrity, which can be caused by nutrient starvation, physical stress (such as shearing by stirring), osmotic stress, and exposure to low redox potentials.

To complement these studies, proteomic approaches, as well as the bioelectrochemical characterization of the purified redox enzymes at an electrode, might be useful to further understand this pathway. It has been reported that the cell components of nonviable microorganisms (i.e., cell debris) can catalyze hydrogen formation at a cathode [90]. Thus, redox enzymes derived from microbes other than methanogens could contribute to the catalytic ability of the biocathode.

Pathway II-B: Intermediate Formations Catalyzed by Microorganisms

At the mixed-culture biocathode, it is also possible that microorganisms (for example, bacteria other than methanogens) can take up electrons from the electrode, catalyzing the formation of diffusible intermediates (such as hydrogen), which are in turn utilized by methanogens for methanogenesis (Fig. 6). Previous studies have shown that bacteria can produce hydrogen at the cathode [42, 47, 91–93]. Thus, if present, methanogens can utilize the produced hydrogen for methanogenesis.

Deutzmann and Spormann examined a biocathode inoculated with a synthetic co-culture of the Fe(0)-corroding sulfate-reducing strain IS4 [85] and *M. maripaludis* [83] (Fig. 6). A cathode was first inoculated with a pure culture of the strain IS4. The IS4-inoculated cathode produced hydrogen upon the depletion of sulfate. At a poised potential of −0.4 V versus SHE, the hydrogen formation rate was of 96–120 mmol m^{-2} day^{-1}. When the cathode potential was lowered to −0.5 V versus SHE (below the thermodynamic equilibrium potential of hydrogen formation), the hydrogen formation rate was significantly increased to 960–1680 mmol m^{-2} day^{-1}. At −0.6 V versus SHE, however, hydrogen formation was not further enhanced. The coulombic efficiencies of the hydrogen formation were

Fig. 6 A synthetic co-culture of the Fe(0)-corroding sulfate-reducing strain IS4 and *M. maripaludis*
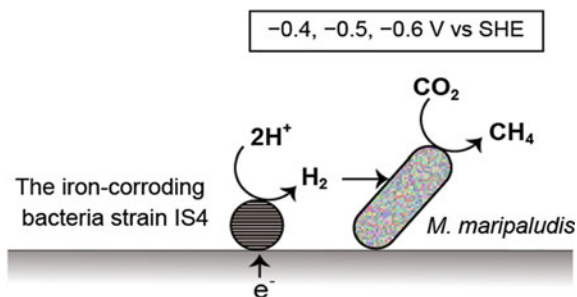
90–110% at the potentials examined (−0.4, −0.5, and −0.6 V vs. SHE). Cyclic voltammetry indicated that the hydrogen formation was reversible, and the overpotential for the reaction was significantly reduced to a practically unnoteworthy level (less than 5 mV). Thus, these observations indicated that the strain IS4 could effectively catalyze hydrogen formation by using electrons from the cathode.

The hydrogen-producing biocathode was further inoculated with a pure culture of *M. maripaludis*, resulting in the formation of CH_4. At −0.4 V versus SHE, the co-culture-inoculated biocathode produced CH_4 at a rate 24–33.6 mmol m^{-2} day^{-1}. No accumulation of hydrogen was detected, indicating the produced hydrogen was rapidly consumed during methanogenesis. Moreover, the inoculation of the methanogens resulted in a small increase in the current consumption, which was likely due to this effective removal of hydrogen. When the cathode potential was lowered to −0.5 V (or −0.6 V) versus SHE, the CH_4 formation rate became 144–216 mmol m^{-2} day^{-1} (or 144–288 mmol m^{-2} day^{-1}), responding to the potential changes with the responses of the hydrogen formation rate by the IS4-inoculated biocathode. Cyclic voltammetry showed that the electrochemical reaction at the co-culture-inoculated biocathode was irreversible, and no catalytic current was produced at potentials more positive than the thermodynamic equilibrium potential for proton reduction, further indicating the high efficiency of the interspecies hydrogen transfer. Moreover, the overpotential for electromethanogenesis by the co-culture biocathode was 4.2 V lower than that of the cathode inoculated with the *M. maripaludis* pure culture. Collectively, these observations indicate that a co-culture of strain IS4 and *M. maripaludis* can effectively catalyze methanogenesis at the cathode via multiple steps: The hydrogen formation uses cathodic electrons (by the strain IS4), and then the interspecies hydrogen transfer occurs, followed by hydrogenotrophic methanogenesis (by *M. maripaludis*).

In comparison with other defined-culture systems, the co-culture-inoculated biocathode showed a higher ability for catalyzing electromethanogenesis: At −0.4 V versus SHE, the methanogenesis rates were about one order of magnitude higher than those of the cathode inoculated with the methanogen strain IM1 (Pathway I). At −0.6 V versus SHE, the methanogenesis rates were about 20 times higher than those of the cathode inoculated with the pure culture of *M. maripaludis* (Pathway II-B). Thus, it has been proposed that such a co-culture system is a promising candidate for the industrial application of electromethanogenesis. To date, however, the mechanistic basis for the electron uptake by the hydrogen-forming microbes remains unknown. It would be useful to elucidate the mechanism of hydrogen formation at the biocathodes using genetically tractable model microbes (such as the *Shewanella* and *Geobacter* species). It has been reported that the *Geobacter* species transfer electrons to an electrode (anode) via nanowires and cytochromes [94–96]. Similarly, in *Shewanella oneidensis*, nanowire-like appendages (the outer membrane and periplasmic extensions) together with the outer membrane multi-heme cytochromes (MtrC and OmcA) transfer electrons from the bacteria to an anode [97–99]. It has been suggested that those components are also likely involved in the uptake of electrons from a cathode [100], whereas some components are required only for the electron uptake from the cathode [101].

3.4 Microbial Ecosystem at the Electromethanogenic Biocathodes

As described earlier, most studies on electromethanogenic biocathodes have been carried out using mixed microbial cultures. However, little is known about the microbial ecosystems developed on biocathodes. Although the microbial compositions of the acclimated biocathodes are rarely documented, it has been reported that hydrogenotrophic methanogens are commonly detected as the dominant archaea in biocathode microbiotas. The roles of the methanogens and other microorganisms in the biocathode's ecosystem can be speculated on based on the proposed electron-transfer mechanisms described earlier. It is likely that electromethanogenesis via all of the pathways can operate, depending on the cathode potential. Hydrogenotrophic methanogens with and without the ability to take up electrons from the cathode play central roles (Fig. 7).

Methanobacterium and, to a lesser extent, *Methanobrevibacter*, have previously been found to be the predominant genera in most of electromethanogenic biocathode microbiotas. Cheng et al. constructed a biocathode using the effluent of an existing bioanode as the inoculum [71]. The biocathode community was dominated by a methanogen closely related to *Methanobacterium palustre*, accounting for 86% of the total number of cells. In Marshall et al., a biocathode was developed by inoculating brewery wastewater sludge and incubating it at the set potential of −0.59 V versus SHE [77, 102]. The microbial community of the biocathode mainly consisted of methanogens related to *Methanobacterium* sp. (>93% in abundance) and *Methanobrevibacter* (∼5%). Similarly, *Methanobacterium* and *Methanobrevibacter* were highly enriched on cathodes inoculated with an anaerobic
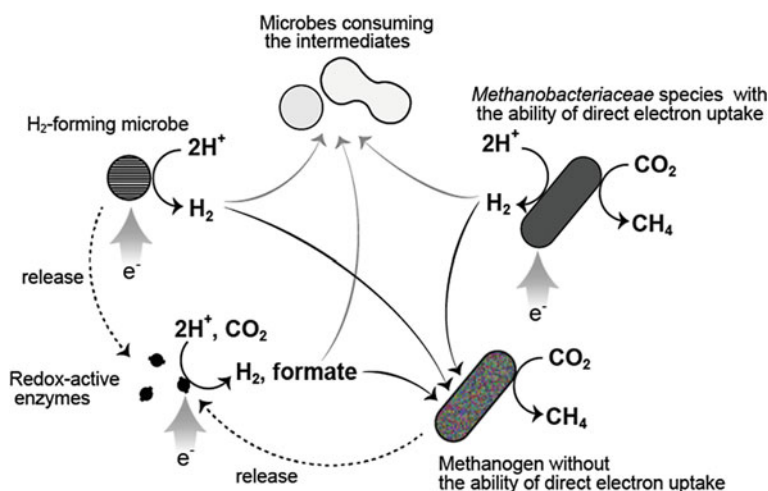
Fig. 7 Roles of methanogens and other microorganisms in the biocathode ecosystem

bog sediment or anaerobic digester sludge [103, 104]. Moreover, Sigert et al. extensively investigated the microbial compositions of biocathodes made from 10 different materials (carbon brushes, plain graphite blocks, blocks coated with carbon black and Pt, stainless steel, nickel, ferrihydrite, magnetite, iron sulfide, and molybdenum disulfide) [78]. The cathodes were inoculated with anaerobic digester sludge and incubated at a set potential of -0.6 V versus SHE. The archaeal communities of all biocathodes, except those coated with Pt (a highly efficient hydrogen-forming catalyst), were dominated by *Methanobacterium* (a median of 97% in abundance of all archaea). In the Pt-coated cathode, the archaeal community was dominated by *Methanobrevibacter*. These two hydrogenotrophic genera were significantly enriched at the biocathodes, whereas the inoculum had contained primarily the genus *Methanosaeta*. The abundance of *Methanobacterium* and *Methanobrevibacter* in the cathode microbiotas increased 500-fold and 10,000-fold, respectively, after five fed-batch cycles. Moreover, because of the decrease in the numbers of bacteria on the cathode, the relative abundance of archaea in the total population increased 10-fold. These observations suggest that the genus *Methanobacterium* was primarily responsible for CH_4 production in those systems when cathodes lack efficient chemical catalysts for hydrogen formation. Additionally, in thermophilic biocathodes, which were inoculated with thermophiles derived from the formation water of a petroleum reservoir, the archaeal community mainly consisted of a thermophilic hydrogenotrophic methanogens closely related to *Methanothermobacter thermautotrophicus* [72, 105]. These genera, *Methanobacterium*, *Methanobrevibacter*, and *Methanothermobacter*, are close relatives and belong to the same family of *Methanobacteriaceae* of the *Methanobacteriales* order. It is unclear why, however, hydrogenotrophic methanogens of *Methanobacteraceae* are enriched in electromethanogenic biocathodes. Recently, it has been shown that direct interspecies electron transfer mediates the syntrophic interactions between electron-donating and -accepting microorganisms [106–109]. Several studies have indicated that acetoclastic methanogens, the *Methanosaeta* and *Methanosarcina* species, can accept electrons from their syntrophic partners (such as the *Geobacter* species). *Methanosaeta* and *Methanosarcina* belong to the order *Methanosarcinales*, all members of which have a broad substrate spectrum and contain cytochromes (although hydrogenotrophic methanogens lack cytochrome) [110]. Thus, it is possible that membrane-bound cytochromes may mediate the electron uptake. Yet, no acetoclastic methanogen has been shown to be predominant in electromethanogenic biocathodes. This is likely because acetoclastic methanogens generally have considerably higher threshold concentrations for hydrogen than hydrogenotrophic methanogens (which lack cytochromes), resulting in the inability of the acetoclastic methanogens to compete with the hydrogenotrophic methanogens for hydrogen [110]. Moreover, the ability to utilize formate is restricted to hydrogenotrophic methanogens [110]. Thus, the formation of hydrogen and formate as intermediates (Pathway II) can be a problem for acetoclastic methanogens with a high hydrogen threshold (>10 Pa) when they are in competition with other organisms (including hydrogenotrophic methanogens) with lower hydrogen thresholds (<10 Pa) in the biocathode microbiota.

However, the members of four orders, *Methanobacteriales*, *Methanopyrales*, *Methanococcales* (including the *Methanococcus* genus), and *Methanomicrobiales*, are all hydrogenotrophic methanogens lacking cytochromes. Those methanogens share low hydrogen thresholds, and some of them can also utilize formate for methanogenesis. Yet, hydrogenotrophic methanogens (including *M. maripaludis*) other than *Methanobacteriaceae* have rarely been detected as the predominant species at biocathodes [111]. Thus, it remains to be determined whether *Methanobacteriaceae* species have an advantage over other hydrogenotrophic methanogens in biocathode ecosystems. Because the strain IM1, which is closely related to *Methanobacterium*, can solely catalyze electromethanogenesis, it is tempting to speculate that some methanogens belonging to the *Methanobacteriaceae* family have the specialized ability to take up electrons from the electrodes. To this end, comparative genomic analysis between the members of the *Methanobacteriaceae* family (including the strain IM1) and other methanogens might provide insight into the genes responsible for such a specialized function. Yet this determination may be difficult to make, as no genetic system is currently available for *Methanobacteraceae* species.

Generally, wide varieties of anaerobic bacteria have been detected in biocathode microbiotas [71, 72, 77, 78, 102, 105, 111]. No dominant species, however, has been commonly identified for bacteria. In the study described previously, Sigert et al. showed a lack of bacterial clusters in the principal component analysis and the lack of a correlation between the bacterial cell numbers and biocathode performance, suggesting that specific bacteria were not directly involved in electromethanogenesis [78]. Because bacterial species still remain on the biocathodes after long-term operation (albeit in a lower abundance), they may play some role(s) in catalyzing electromethanogenesis or may have an advantage in biocathode ecosystems. Presumably, the bacteria or the redox enzymes released from them can catalyze the intermediate formations by taking up cathodic electrons. Because the methanogen strain IM1 not only catalyzed electromethanogenesis, but also promoted hydrogen formation at lower potentials [81], it is also possible that bacteria consume the produced hydrogen (as well as CH_4) for their metabolism. As studied in oxygen-reducing biocathodes [112], metagenomic approaches (including transcriptomic and proteomic analyses) may be useful to gain insight into the functions of each type of bacteria in biocathode ecosystems.

4   Remarks and Perspectives

Over the past 10 years, alternative fuels produced in bioelectrochemical systems have been intensively investigated. Among these alternative fuels, the hydrogen produced via MECs and CH_4 produced via electromethanogenesis are considered to be the most promising renewable fuels because of their high heating value and easy separation. However, many scientific, economic, and technical challenges still hinder the commercial application of these systems [113–115]. For example, until

now, there has been no research about the electron transfer characteristics in the cathode biofilm or about novel reactor configurations designed for microbial electrosynthesis cells. Further research is required to improve the application of bioelectrochemical systems. Researchers should focus on the bacterial communities on the biocathode, electron transfer manner from the cathode to the microorganisms, and the topography of the electrodes.

References

1. Pant D, Singh A, Van Bogaert G, Irving Olsen S, Singh Nigam P, Diels L, Vanbroekhoven K (2012) Bioelectrochemical systems (BES) for sustainable energy production and product recovery from organic wastes and industrial wastewaters. RSC Adv 2(4):1248–1263
2. Kumar G, Saratale RG, Kadier A, Sivagurunathan P, Zhen G, Kim SH, Saratale GD (2017) A review on bio-electrochemical systems (BESs) for the syngas and value added biochemicals production. Chemosphere 177:84–92
3. Jadhav DA, Ghosh Ray S, Ghangrekar MM (2017) Third generation in bio-electrochemical system research—a systematic review on mechanisms for recovery of valuable by-products from wastewater. Renew Sustain Energy Rev 76:1022–1031
4. Logan BE, Call D, Cheng S, Hamelers HV, Sleutels TH, Jeremiasse AW, Rozendal RA (2008) Microbial electrolysis cells for high yield hydrogen gas production from organic matter. Environ Sci Technol 42(23):8630–8640
5. Cheng S, Logan BE (2007) Sustainable and efficient biohydrogen production via electrohydrogenesis. Proc Natl Acad Sci USA 104(47):18871–18873
6. Harnisch F, Schroder U (2010) From MFC to MXC: chemical and biological cathodes and their potential for microbial bioelectrochemical systems. Chem Soc Rev 39(11):4433–4448
7. Escapa A, Mateos R, Martínez EJ, Blanes J (2016) Microbial electrolysis cells: an emerging technology for wastewater treatment and energy recovery. From laboratory to pilot plant and beyond. Renew Sustain Energy Rev 55:942–956
8. Lee HS, Rittmann BE (2010) Significance of biological hydrogen oxidation in a continuous single-chamber microbial electrolysis cell. Environ Sci Technol 44(3):948–954
9. Liu H, Grot S, Logan BE (2005) Electrochemically assisted microbial production of hydrogen from acetate. Environ Sci Technol 39(11):4317–4320
10. Logan BE, Hamelers B, Rozendal R, Schröder U, Keller J, Freguia S, Aelterman P, Verstraete W, Rabaey K (2006) Microbial fuel cells: methodology and technology. Environ Sci Technol 40(17):5181–5192
11. Rozendal RA, Hamelers HV, Molenkamp RJ, Buisman CJ (2007) Performance of single chamber biocatalyzed electrolysis with different types of ion exchange membranes. Water Res 41(9):1984–1994
12. Kundu A, Sahu JN, Redzwan G, Hashim MA (2013) An overview of cathode material and catalysts suitable for generating hydrogen in microbial electrolysis cell. Int J Hydrogen Energy 38(4):1745–1757
13. Siegert M, Yates MD, Call DF, Zhu XP, Spormann A, Logan BE (2014) Comparison of nonprecious metal cathode materials for methane production by electromethanogenesis. Acs Sustain Chem Eng 2(4):910–917

14. Tartakovsky B, Manuel M, Wang H, Guiot S (2009) High rate membrane-less microbial electrolysis cell for continuous hydrogen production. Int J Hydrogen Energy 34(2):672–677

15. Liu J, Zhang F, He W, Yang W, Feng Y, Logan BE (2014) A microbial fluidized electrode electrolysis cell (MFEEC) for enhanced hydrogen production. J Power Sources 271:530–533

16. Rozendal RA, Sleutels TH, Hamelers HV, Buisman CJ (2008) Effect of the type of ion exchange membrane on performance, ion transport, and pH in biocatalyzed electrolysis of wastewater. Water Sci Technol 57(11):1757–1762

17. Chen M, Zhang F, Zhang Y, Zeng RJ (2013) Alkali production from bipolar membrane electrodialysis powered by microbial fuel cell and application for biogas upgrading. Appl Energ 103(1):428–434

18. Call D, Logan BE (2008) Hydrogen production in a single chamber microbial electrolysis cell lacking a membrane. Environ Sci Technol 42(9):3401–3406

19. Hu H, Fan Y, Liu H (2008) Hydrogen production using single-chamber membrane-free microbial electrolysis cells. Water Res 42(15):4172–4178

20. Logan BE (2010) Scaling up microbial fuel cells and other bioelectrochemical systems. Appl Microbiol Biotechnol 85(6):1665–1671

21. Cusick RD, Bryan B, Parker DS, Merrill MD, Mehanna M, Kiely PD, Liu G, Logan BE (2011) Performance of a pilot-scale continuous flow microbial electrolysis cell fed winery wastewater. Appl Microbiol Biotechnol 89(6):2053–2063

22. Jeremiasse AW, Hamelers HV, Kleijn JM, Buisman CJ (2009) Use of biocompatible buffers to reduce the concentration overpotential for hydrogen evolution. Environ Sci Technol 43 (17):6882–6887

23. Holladay JD, Hu J, King DL, Wang Y (2009) An overview of hydrogen production technologies. Catal Today 139(4):244–260

24. Selembo PA, Merrill MD, Logan BE (2009) The use of stainless steel and nickel alloys as low-cost cathodes in microbial electrolysis cells. J Power Sources 190(2):271–278

25. Call DF, Merrill MD, Logan BE (2009) High surface area stainless steel brushes as cathodes in microbial electrolysis cells. Environ Sci Technol 43(6):2179–2183

26. Zhang Y, Merrill MD, Logan BE (2010) The use and optimization of stainless steel mesh cathodes in microbial electrolysis cells. Int J Hydrogen Energy 35(21):12020–12028

27. Hou Y, Zhang B, Wen Z, Cui S, Guo X, He Z, Chen J (2014) A 3D hybrid of layered MoS2/nitrogen-doped graphene nanosheet aerogels: an effective catalyst for hydrogen evolution in microbial electrolysis cells. J Mater Chem A 2(34):13795–13800

28. Cai W, Liu W, Han J, Wang A (2016) Enhanced hydrogen production in microbial electrolysis cell with 3D self-assembly nickel foam-graphene cathode. Biosens Bioelectron 80:118–122

29. Dai H, Yang H, Xian L, Xuan J, Liang Z (2016) Electrochemical evaluation of nano-Mg (OH) 2/graphene as a catalyst for hydrogen evolution in microbial electrolysis cell. Fuel 174:251–256

30. Wang L, Chen Y, Huang Q, Feng Y, Zhu S, Shen S (2012) Hydrogen production with carbon nanotubes based cathode catalysts in microbial electrolysis cells. J Chem Technol Biotechnol 87(8):1150–1156

31. Winther-Jensen B, Fraser K, Ong C, Forsyth M, Macfarlane DR (2010) Conducting polymer composite materials for hydrogen generation. Adv Mater 22(15):1727–1730

32. Snook GA, Kao P, Best AS (2011) Conducting-polymer-based supercapacitor devices and electrodes. J Power Sources 196(1):1–12

33. Yang Q, Jiang Y, Xu Y, Qiu Y, Chen Y, Zhu S, Shen S (2015) Hydrogen production with polyaniline/multi-walled carbon nanotube cathode catalysts in microbial electrolysis cells. J Chem Technol Biotechnol 90(7):1263–1269

34. Rozendal RA, Jeremiasse AW, Hamelers HVM, Buisman CJN (2008) Hydrogen production with a microbial biocathode. Environ Sci Technol 42(2):629–634

35. Jeremiasse AW, Hamelers HV, Buisman CJ (2010) Microbial electrolysis cell with a microbial biocathode. Bioelectrochemistry 78(1):39–43

36. Chen YW, Yuan X, Chen LL, Li PW, Zhu SM, Shen SB (2015) Microbial electrolysis cells with polyaniline/multi-walled carbon nanotube-modified biocathodes. Energy 88:377–384

37. Su M, Wei L, Qiu Z, Jia Q, Shen J (2015) A graphene modified biocathode for enhancing hydrogen production. RSC Adv 5(41):32609–32614

38. Lai B, Tang XH, Li HR, Du ZW, Liu XW, Zhang Q (2011) Power production enhancement with a polyaniline modified anode in microbial fuel cells. Biosens Bioelectron 28(1):373–377

39. Yuan Y, Zhou S, Li Z (2010) Polypyrrole/carbon black composite as a novel oxygen reduction catalyst for microbial fuel cells. J Power Sources 195(11):3490–3493

40. Yong Y, Bo Z, Jeon Y, Zhong S, Zhou S, Kim S (2011) Iron phthalocyanine supported on amino-functionalized multi-walled carbon nanotube as an alternative cathodic oxygen catalyst in microbial fuel cells. Bioresour Technol 102(10):5849–5854

41. Mehdinia A, Dejaloud M, Jabbari A (2013) Nanostructured polyaniline-coated anode for improving microbial fuel cell power output. Chem Pap 67(8):1096–1102

42. Fu Q, Kobayashi H, Kuramochi Y, Xu J, Wakayama T, Maeda H, Sato K (2013) Bioelectrochemical analyses of a thermophilic biocathode catalyzing sustainable hydrogen production. Int J Hydrogen Energy 38(35):15638–15645

43. Kato T, Haruki M, Imanaka T, Morikawa M, Kanaya S (2001) Isolation and characterization of long-chain-alkane degrading bacillus thermoleovorans from deep subterranean petroleum reservoirs. J Biosci Bioeng 91(1):64–70

44. Niehaus F, Bertoldo C, Kähler M, Antranikian G (1999) Extremophiles as a source of novel enzymes for industrial application. Appl Microbiol Biotechnol 51(6):711–729

45. Clauwaert P, Verstraete W (2009) Methanogenesis in membraneless microbial electrolysis cells. Appl Microbiol Biotechnol 82(5):829–836

46. Zhang J, Bai Y, Fan Y, Hou H (2016) Improved bio-hydrogen production from glucose by adding a specific methane inhibitor to microbial electrolysis cells with a double anode arrangement. J Biosci Bioeng 122(4):488–493

47. Croese E, Pereira MA, Euverink GJW, Stams AJM, Geelhoed JS (2011) Analysis of the microbial community of the biocathode of a hydrogen-producing microbial electrolysis cell. Appl Microbiol Biotechnol 92(5):1083–1093

48. Liu H, Cheng S, Logan BE (2005) Production of electricity from acetate or butyrate using a single-chamber microbial fuel cell. Environ Sci Technol 39(2):658–662

49. Min S, Sheng GP, Lei Z, Xia CR, Mu ZX, Liu XW, Wang HL, Yu HQ, Rong Q, Tao Y (2008) An MEC-MFC-coupled system for biohydrogen production from acetate. Environ Sci Technol 42(21):8095–8100

50. Sun M, Sheng GP, Mu ZX, Liu XW, Chen YZ, Wang HL, Yu HQ (2009) Manipulating the hydrogen production from acetate in a microbial electrolysis cell–microbial fuel cell-coupled system. J Power Sources 191(2):338–343

51. Ajayi FF, Kim KY, Chae KJ, Choi MJ, Chang IS, Kim IS (2010) Optimization studies of bio-hydrogen production in a coupled microbial electrolysis-dye sensitized solar cell system. Photochem Photobiol Sci Official J Eur Photochem Assoc Eur Soc Photobiol 9(3):349–356

52. Ajayi FF, Kim KY, Chae KJ, Choi MJ, Kim SY, Chang IS, Kim IS (2009) Study of hydrogen production in light assisted microbial electrolysis cell operated with dye sensitized solar cell. Int J Hydrogen Energy 34(23):9297–9304

53. Chae KJ, Choi MJ, Kim KY, Ajayi FF, Chang IS, Kim IS (2009) A solar-powered microbial electrolysis cell with a platinum catalyst-free cathode to produce hydrogen. Environ Sci Technol 43(24):9525–9530

54. Jeon Y, Kim S (2016) Persistent hydrogen production by the photo-assisted microbial electrolysis cell using a p-type polyaniline nanofiber cathode. Chemsuschem 9(23):3276–3279

55. Fang Q, Wang G, Li Y (2010) Solar-driven microbial photoelectrochemical cells with a nanowire photocathode. Nano Lett 10(11):4686–4691

56. He YR, Yan FF, Yu HQ, Yuan SJ, Tong ZH, Sheng GP (2014) Hydrogen production in a light-driven photoelectrochemical cell. Appl Energy 113(1):164–168

57. Lu L, Ren N, Xing D, Logan BE (2009) Hydrogen production with effluent from an ethanol–H 2 -coproducing fermentation reactor using a single-chamber microbial electrolysis cell. Biosens Bioelectron 24(10):3055–3060
58. Lalaurette E, Thammannagowda S, Mohagheghi A, Maness P-C, Logan BE (2009) Hydrogen production from cellulose in a two-stage process combining fermentation and electrohydrogenesis. Int J Hydrogen Energy 34(15):6201–6210
59. Yan D, Yang X, Yuan W (2015) Electricity and H2 generation from hemicellulose by sequential fermentation and microbial fuel/electrolysis cell. J Power Sources 289:26–33
60. Wang A, Sun D, Cao G, Wang H, Ren N, Wu WM, Logan BE (2011) Integrated hydrogen production process from cellulose by combining dark fermentation, microbial fuel cells, and a microbial electrolysis cell. Bioresource Technol 102(5):4137–4143
61. Selembo PA, Perez JM, Lloyd WA, Logan BE (2009) High hydrogen production from glycerol or glucose by electrohydrogenesis using microbial electrolysis cells. Int J Hydrogen Energy 34(13):5373–5381
62. Heidrich ES, Curtis TP, Dolfing J (2011) Determination of the internal chemical energy of wastewater. Environ Sci Technol 45(2):827–832
63. Sleutels TH, Ter HA, Buisman CJ, Hamelers HV (2012) Bioelectrochemical systems: an outlook for practical applications. Chemsuschem 5(6):1012–1019
64. Zhang Y, Angelidaki I (2014) Microbial electrolysis cells turning to be versatile technology: recent advances and future challenges. Water Res 56:11–25
65. Ditzig J, Liu H, Logan BE (2007) Production of hydrogen from domestic wastewater using a bioelectrochemically assisted microbial reactor (BEAMR). Int J Hydrogen Energy 32 (13):2296–2304
66. Heidrich ES, Dolfing J, Scott K, Edwards SR, Jones C, Curtis TP (2013) Production of hydrogen from domestic wastewater in a pilot-scale microbial electrolysis cell. Appl Microbiol Biot 97(15):6979–6989
67. Blasco-Gomez R, Batlle-Vilanova P, Villano M, Balaguer MD, Colprim J, Puig S (2017) On the edge of research and technological application: a critical review of electromethanogenesis. Int J Mol Sci 18(4):874–906
68. Moreno R, San-Martín MI, Escapa A, Morán A (2016) Domestic wastewater treatment in parallel with methane production in a microbial electrolysis cell. Renew Energy 93:442–448
69. Park DH, Laivenieks M, Guettler MV, Jain MK, Zeikus JG (1999) Microbial utilization of electrically reduced neutral red as the sole electron donor for growth and metabolite production. Appl Environ Microb 65(7):2912–2917
70. Clauwaert P, Tolêdo R, Van dHD, Crab R, Verstraete W, Hu H, Udert KM, Rabaey K (2008) Combining biocatalyzed electrolysis with anaerobic digestion. Water Sci Technol 57 (4):575–579
71. Cheng SA, Xing DF, Call DF, Logan BE (2009) Direct biological conversion of electrical current into methane by electromethanogenesis. Environ Sci Technol 43(10):3953–3958
72. Fu Q, Kuramochi Y, Fukushima N, Maeda H, Sato K, Kobayashi H (2015) Bioelectrochemical analyses of the development of a thermophilic biocathode catalyzing electromethanogenesis. Environ Sci Technol 49(2):1225–1232
73. Villano M, Aulenta F, Ciucci C, Ferri T, Giuliano A, Majone M (2010) Bioelectrochemical reduction of CO$_{(2)}$ to CH$_{(4)}$ via direct and indirect extracellular electron transfer by a hydrogenophilic methanogenic culture. Bioresour Technol 101(9):3085–3090
74. Choi O, Sang BI (2016) Extracellular electron transfer from cathode to microbes: application for biofuel production. Biotechnol Biofuels 9:11
75. Rosenbaum M, Aulenta F, Villano M, Angenent LT (2011) Cathodes as electron donors for microbial metabolism: which extracellular electron transfer mechanisms are involved? Bioresour Technol 102(1):324–333
76. Geppert F, Liu D, van Eerten-Jansen M, Weidner E, Buisman C, Ter Heijne A (2016) Bioelectrochemical power-to-gas: state of the art and future perspectives. Trends Biotechnol 34(11):879–894

77. Marshall CW, Ross DE, Fichot EB, Norman RS, May HD (2012) Electrosynthesis of commodity chemicals by an autotrophic microbial community. Appl Environ Microb 78 (23):8412–8420

78. Siegert M, Yates MD, Spormann AM, Logan BE (2015) Methanobacterium dominates biocathodic archaeal communities in methanogenic microbial electrolysis cells. Acs Sustain Chem Eng 3(7):1668–1676

79. Hedderich R, Whitman WB (2006) Physiology and biochemistry of the methane-producing archaea. In: Prokaryotes: a handbook on the biology of bacteria, 3rd edn, vol 2, pp 1050–1079

80. Hedderich R (2004) Energy-converting [NiFe] hydrogenases from archaea and extremophiles: Ancestors of complex I. J Bioenergy Biomembr 36(1):65–75

81. Beese-Vasbender PF, Grote JP, Garrelfs J, Stratmann M, Mayrhofer KJ (2015) Selective microbial electrosynthesis of methane by a pure culture of a marine lithoautotrophic archaeon. Bioelectrochemistry 102:50–55

82. Deutzmann JS, Sahin M, Spormann AM (2015) Extracellular enzymes facilitate electron uptake in biocorrosion and bioelectrosynthesis. MBio 6(2)

83. Deutzmann JS, Spormann AM (2017) Enhanced microbial electrosynthesis by using defined co-cultures. ISME J 11(3):704–714

84. Lohner ST, Deutzmann JS, Logan BE, Leigh J, Spormann AM (2014) Hydrogenase-independent uptake and metabolism of electrons by the archaeon *methanococcus maripaludis*. ISME J 8(8):1673–1681

85. Dinh HT, Kuever J, Mussmann M, Hassel AW, Stratmann M, Widdel F (2004) Iron corrosion by novel anaerobic microorganisms. Nature 427(6977):829–832

86. Ferry JG (2010) How to make a living by exhaling methane. Annu Rev Microbiol 64:453–473

87. Jones WJ, Paynter MJB, Gupta R (1983) Characterization of *Methanococcus-Maripaludis* Sp-Nov, a new methanogen isolated from salt-marsh sediment. Arch Microbiol 135(2):91–97

88. Tumbula DL, Whitman WB (1999) Genetics of Methanococcus: possibilities for functional genomics in archaea. Mol Microbiol 33(1):1–7

89. Smith MR (1983) Reversal of 2-bromoethanesulfonate inhibition of methanogenesis in Methanosarcina sp. J Bacteriol 156(2):516–523

90. Yates MD, Siegert M, Logan BE (2014) Hydrogen evolution catalyzed by viable and non-viable cells on biocathodes. Int J Hydrogen Energy 39(30):16841–16851

91. Geelhoed JS, Hamelers HVM, Stams AJM (2010) Electricity-mediated biological hydrogen production. Curr Opin Microbiol 13(3):307–315

92. Aulenta F, Catapano L, Snip L, Villano M, Majone M (2012) Linking bacterial metabolism to graphite cathodes: electrochemical insights into the H2-producing capability of *Desulfovibrio* sp. Chemsuschem 5(6):1080–1085

93. Jafary T, Daud WRW, Ghasemi M, Kim BH, Jahim JM, Ismail M, Lim SS (2015) Biocathode in microbial electrolysis cell; present status and future prospects. Renew Sustain Energy Rev 47:23–33

94. Reguera G, McCarthy KD, Mehta T, Nicoll JS, Tuominen MT, Lovley DR (2005) Extracellular electron transfer via microbial nanowires. Nature 435(7045):1098–1101

95. Vargas M, Malvankar NS, Tremblay PL, Leang C, Smith JA, Patel P, Snoeyenbos-West O, Nevin KP, Lovley DR (2013) Aromatic amino acids required for pili conductivity and long-range extracellular electron transport in Geobacter sulfurreducens. MBio 4(2)

96. Tremblay PL, Summers ZM, Glaven RH, Nevin KP, Zengler K, Barrett CL, Qiu Y, Palsson BO, Lovley DR (2011) A c-type cytochrome and a transcriptional regulator responsible for enhanced extracellular electron transfer in Geobacter sulfurreducens revealed by adaptive evolution. Appl Environ Microb 13(1):13–23

97. Okamoto A, Nakamura R, Hashimoto K (2011) In-vivo identification of direct electron transfer from Shewanella oneidensis MR-1 to electrodes via outer-membrane OmcA-MtrCAB protein complexes. Electrochim Acta 56(16):5526–5531

98. Gorby YA, Yanina S, McLean JS, Rosso KM, Moyles D, Dohnalkova A, Beveridge TJ, Chang IS, Kim BH, Kim KS, Culley DE, Reed SB, Romine MF, Saffarini DA, Hill EA, Shi L,

Elias DA, Kennedy DW, Pinchuk G, Watanabe K, Ishii S, Logan B, Nealson KH, Fredrickson JK (2006) Electrically conductive bacterial nanowires produced by Shewanella oneidensis strain MR-1 and other microorganisms. Proc Natl Acad Sci USA 103(30):11358–11363

99. Pirbadian S, Barchinger SE, Leung KM, Byun HS, Jangir Y, Bouhenni RA, Reed SB, Romine MF, Saffarini DA, Shi L, Gorby YA, Golbeck JH, El-Naggar MY (2014) Shewanella oneidensis MR-1 nanowires are outer membrane and periplasmic extensions of the extracellular electron transport components. Proc Natl Acad Sci USA 111(35):12883–12888

100. Ross DE, Flynn JM, Baron DB, Gralnick JA, Bond DR (2011) Towards electrosynthesis in Shewanella: energetics of reversing the mtr pathway for reductive metabolism. PLoS One 6(2)

101. Strycharz SM, Glaven RH, Coppi MV, Gannon SM, Perpetua LA, Liu A, Nevin KP, Lovley DR (2011) Gene expression and deletion analysis of mechanisms for electron transfer from electrodes to Geobacter sulfurreducens. Bioelectrochemistry 80(2):142–150

102. Van Eerten-Jansen MC, Veldhoen AB, Plugge CM, Stams AJ, Buisman CJ, Ter Heijne A (2013) Microbial community analysis of a methane-producing biocathode in a bioelectrochemical system. Archaea 2013

103. Lee HS, Torres CI, Parameswaran P, Rittmann BE (2009) Fate of H2 in an upflow single-chamber microbial electrolysis cell using a metal-catalyst-free cathode. Environ Sci Technol 43(20):7971–7976

104. Siegert M, Li XF, Yates MD, Logan BE (2014) The presence of hydrogenotrophic methanogens in the inoculum improves methane gas production in microbial electrolysis cells. Front Microbiol 5:778

105. Kobayashi H, Nagashima A, Kouyama M, Fu Q, Ikarashi M, Maeda H, Sato K (2017) High-pressure thermophilic electromethanogenic system producing methane at 5 MPa, 55 ° C. J Biosci Bioeng 124(3):327–332

106. Rotaru AE, Shrestha PM, Liu F, Markovaite B, Chen S, Nevin KP, Lovley DR (2014) Direct interspecies electron transfer between Geobacter metallireducens and Methanosarcina barkeri. Appl Environ Microb 80(15):4599–4605

107. Summers ZM, Fogarty HE, Leang C, Franks AE, Malvankar NS, Lovley DR (2010) Direct exchange of electrons within aggregates of an evolved syntrophic coculture of anaerobic bacteria. Science 330(6009):1413–1415

108. Kato S, Hashimoto K, Watanabe K (2012) Microbial interspecies electron transfer via electric currents through conductive minerals. Proc Natl Acad Sci USA 109(25):10042–10046

109. Kato S, Hashimoto K, Watanabe K (2012) Methanogenesis facilitated by electric syntrophy via (semi)conductive iron-oxide minerals. Environ Microbiol 14(7):1646–1654

110. Thauer RK, Kaster AK, Seedorf H, Buckel W, Hedderich R (2008) Methanogenic archaea: ecologically relevant differences in energy conservation. Nat Rev Microbiol 6(8):579–591

111. Kobayashi H, Saito N, Fu Q, Kawaguchi H, Vilcaez J, Wakayama T, Maeda H, Sato K (2013) Bio-electrochemical property and phylogenetic diversity of microbial communities associated with bioelectrodes of an electromethanogenic reactor. J Biosci Bioeng 116(1):114–117

112. Desmond-Le Quemener E, Rimboud M, Bridier A, Madigou C, Erable B, Bergel A, Bouchez T (2016) Biocathodes reducing oxygen at high potential select biofilms dominated by Ectothiorhodospiraceae populations harboring a specific association of genes. Bioresour Technol 214:55–62

113. Rabaey K, Rozendal RA (2010) Microbial electrosynthesis - revisiting the electrical route for microbial production. Nat Rev Microbiol 8(10):706–716

114. Rabaey K, Girguis P, Nielsen LK (2011) Metabolic and practical considerations on microbial electrosynthesis. Curr Opin Microbiol 22(3):371–377

115. Lovley DR, Nevin KP (2011) A shift in the current: new applications and concepts for microbe-electrode electron exchange. Curr Opin Microbiol 22(3):441–448

Index

© Springer Nature Singapore Pte Ltd. 2018

Q. Liao et al. (eds.), *Bioreactors for Microbial Biomass and Energy Conversion*,

Green Energy and Technology, https://doi.org/10.1007/978-981-10-7677-0

463